UC San Diego
UC San Diego Electronic Theses and Dissertations

Title
Conformational Control: A Strategy to Increase Kinase Inhibitor Selectivity

Permalink
https://escholarship.org/uc/item/2849m7cp

Author
Toenjes, Sean

Publication Date
2020

Peer reviewed|Thesis/dissertation

eScholarship.org
Powered by the California Digital Library
University of California

UNIVERSITY OF CALIFORNIA SAN DIEGO

SAN DIEGO STATE UNIVERSITY

Conformational Control: A Strategy to Increase Kinase Inhibitor Selectivity

A dissertation submitted in partial satisfaction of the requirements for the degree

Doctor in Philosophy

in

Chemistry

by

Sean Toenjes

Committee in Charge:

University of California San Diego

Professor Daniel Donoghue
Professor Joseph O'Connor
Professor Jean Wang

San Diego State University

Professor Jeffrey Gustafson, Chair
Professor B. Mikael Bergdahl

2020

Copyright

Sean Toenjes, 2020

All Rights Reserved

This dissertation of Sean Toenjes is approved, and is acceptable in quality and form for publication on microfilm and electronically:

Chair

University of California San Diego

San Diego State University

2020

Dedication

This dissertation is dedicated to my parents, Thomas and Theresa Toenjes, for their endless love and support.

Table of Contents

Signature Page iii
Dedication iv
Table of Contents v
List of Figures vii
List of Tables ix
List of Schemes x
Acknowledgements xi
Vita xiv
Abstract of the Dissertation xvii
Chapter 1: Introduction 1
  1.1 Copyright 1
  1.2 Atropisomerism in Drug Discovery 1
  1.3 Atropisomerism as a Selectivity Filter in Drug Design 11
  1.4 Opportunities, Challenges and Future Perspective 14
  1.5 Acknowledgments 19
Chapter 2: Leveraging Atropisomerism to Obtain a Selective Inhibitor of RET Kinase with Secondary Activities towards EGFR Mutants 20
  2.1 Copyright 20
  2.2 Introduction 20
  2.3 Discovery of (R_a)-3 as a Highly Potent and Selective Inhibitor of RET. 25
  2.4 Selectivity of Atropisomeric (R_a)-2.16 Caused by Restriction of Accessible Conformations 32
  2.5 Cellular Activity of (R_a)-2.16 40
  2.6 Conclusion 43
  2.7 Acknowledgements 44
Chapter 3: Controlling Ibrutinib's Conformations to Obtain Selective BTK Inhibitors 46
  3.1 Introduction 46
  3.2 BTK on the PP/PPY Conformational Binding Map 47
  3.3 Development of Atropisomerically Stable Analogs of Ibrutinib 49
  3.4 Acknowledgments 58
Chapter 4: Extension of Conformational Control to New Targets and Inhibitor Scaffolds 59
  4.1 Introduction 59
  4.2 Revisiting the PP/PPY Conformational Binding Map 59
  4.3 Expansion of Conformational Control to the Pyridone Scaffold 63
  4.4 Expansion of Conformational Control to the Diaryl Amine Scaffold 67

4.5 Acknowledgments 75

Chapter 5: Accessing Atropisomerically Enriched Compounds 76
  5.1 Copyright 76
  5.2 Introduction 76
  5.3 Enantioselective Synthesis of Pyrrolopyrimidine Scaffolds through Cation-directed Nucleophilic Aromatic Substitution 77
  5.4 Towards a Catalytic Atroposelective Synthesis of Diaryl Ethers via C(sp^2)-H Alkylation Using Nitroalkanes 82
  5.5 Catalytic Atroposelective Synthesis of N-Aryl Quinoid Compounds 88
  5.6 Acknowledgements 94

Appendix 95
  A.1 Chapter 2 Experimental Section 95
  A.2 Chapter 3 Experimental Section 272

References 335

List of Figures

Figure 1.2.1. Examples of atropisomeric scaffolds. 2

Figure 1.2.2. Conformational energy profile of an atropisomerically stable PPY inhibitor.......... 3

Figure 1.2.3. Atropisomerically stable FDA-approved small molecule drugs. 5

Figure 1.2.4. Class 2 and 3 atropisomeric compounds from the medicinal chemistry literature. .. 6

Figure 1.2.5. A) FDA-approved class 1 atropisomeric drugs. B) FDA-approved pro-atropisomeric drugs.......... 10

Figure 1.3.1. *In vitro* and *in silico* data for (R_a)-1.1, (R_a)-1.1 and 1.25 13

Figure 1.4.1. Rigidification of two axes to increase selectivity for BMS's BTK inhibitor.......... 17

Figure 2.2.1. Atropisomerism in drug discovery. 22

Figure 2.2.2. FDA-approved small-molecule kinase inhibitors.......... 24

Figure 2.3.1. Docking studies on RET and in vitro results for select inhibitors.......... 28

Figure 2.3.2. Partial kinome profiling of (R_a)-2.9 and NA-PP1[a] 29

Figure 2.4.1. Graphical comparison of RET selectivity for (R_a)-2.16 and 2.20 sorted by fold selectivity. 33

Figure 2.4.2. Docking studies of (R_a)-2.16 34

Figure 2.4.3. Conformational binding map of PP/PPY ligands. 36

Figure 2.4.4. Molecular Dynamic simulations of (R_a)-2.16, 2.20, and PP1 (2.21) in RET, SRC and EGFR T790M.......... 38

Figure 2.5.1. Breast cancer cell line experiments with (S_a)-2.16 and (R_a)-2.16. 41

Figure 3.1.1. Atropisomerism and examples of flexible, atropisomeric FDA-approved drugs. .. 47

Figure 3.2.1. PP/PPY Conformational Binding Map.......... 48

Figure 3.3.1. Rigidification strategy of Ibrutinib with two conformationally locking groups. 49

Figure 3.3.2. Conformation-activity analysis of Ibrutinib, (R_a)-3.1, and (R_a)-3.2. 52

Figure 3.3.3. PDB structural analysis of PP or PPY ligands superimposed with CEP's of Ibrutinib and conformationally-tuned series of BTK inhibitors. 54

Figure 4.2.1. Conformational map of PPY and PP ligands found in PDB. 60

Figure 4.2.2. Conformational map of proposed selective inhibitors. 61

Figure 4.3.2. Conformational binding map of *N*-aryl pyridones. 63

Figure 4.3.3. Conformational binding map of *N*-aryl pyridones with protein targets. 65

Figure 4.4.1. PDB ligand binding analysis for diaryl amines. 68
Figure 4.4.2. Conformational binding map of an unsubstituted diaryl amine (4.4). 69
Figure 4.4.3. Conformational binding map of a *N*-aryl-2-pyrimidine scaffold (4.5). 70
Figure 4.4.4. Conformational binding map of a *N*-aryl-pyridine scaffold (4.6). 72
Figure 4.4.5. Conformational binding map of a 2-methyl diaryl amine scaffold (4.7). 73
Figure 4.4.6. Conformational binding map of a 2-nitro diaryl amine scaffold (4.8). 74
Figure 5.3.1. An overview of the potential of atroposelective S_NAr in drug discovery. 77
Figure 5.3.2. The substrate scope of PPYs. 79
Figure 5.3.3. Post enantioinduction modifications. 80
Figure 5.3.4. Evaluation of enantioenriched PPYs across SRC and BRK kinases 81
Figure 5.4.1. Examples of Diaryl Ethers, previous asymmetric synthesis, and our atroposelective organocatalytic synthesis on diaryl ethers. 83
Figure 5.4.2. Proposed mechanism for the nucleophilic methylation. 85
Figure 5.4.3. Conformational analysis and absolute configuration assignment 86
Figure 5.4.4. Dihedral-angle contour diagram. 87
Figure 5.5.1. Atropisomerism in Diarylamines and related scaffolds. 89
Figure 5.5.2. *N*-Aryl quinoids as a diaryl amine surrogate with one chiral axis. 90
Figure 5.5.3. Mechanism of Racemization. 91
Figure 5.5.4. Conformational energy plot for 5.12. 92
Figure 5.5.5. Proposed transition state with substrate, catalyst and *N*-bromophthalimide. 93

List of Tables

Table 2.3.1. *In vitro* inhibition of compounds 1.1, 1.25, 2.1 – 2.20 27

Table 2.4.1. Selectivity of Inhibitors[a] 33

Table 2.4.2 Inhibitor activity on WT EGFR and mutants[a] 39

Table 2.5.1 Anti-proliferative effects of inhibitors on RET-driven cell lines and controls.[a] 40

Table 2.5.2 Anti-proliferative effects of inhibitors on EGFR-driven cell lines and controls.[a] 42

Table 3.3.1 Kinase inhibition data for Ibrutinib, 3.1 and 3.2.. 51

Table 3.3.2 Kinase inhibition data for 3.3 - 3.8 53

Table 3.3.3. Kinase inhibition data for 3.10 - 3.12 57

List of Schemes

Scheme 2.3.1. Condensed synthetic routes for compounds 2.1 – 2.20. 31
Scheme 3.3.1. Synthesis of pyrrolopyrimidine analogs 3.1 – 3.6. 50
Scheme 3.3.2. Synthesis of pyrazolopyrimidine analogs 3.7 – 3.9. 56
Scheme 3.3.3. Synthesis of amide-linked pyridine boronic esters for inhibitors 3.10 – 3.12. 57

Acknowledgements

I would like to thank many incredible people. First, my family. You guys have been my support system from day one, encouraging me every step along the way. To my fiancée, Anna – your constant love and support throughout my time in graduate school is something I will always be grateful for. Your patience for my long workdays, the number of "you'll never guess how this cancer works" dinner conversations, and all the ACS memorabilia in our small apartment does not go unnoticed. I eagerly look forward to ~~June 2020~~ Summer 2021 for our big day.

I was fortunate to join the Gustafson lab that had a productive and innovative environment set by the senior PhD students at the time, Dr. Chris Nalbandian and Dr. Sean Maddox. I thank Sean for my fundamental understanding of organic chemistry and showing me the drive needed to be a successful graduate student. To the squad, Andrew, Mariel, Ryan, Zach and Ashley, you guys made lab life better. I can't imagine grad school without pint nights, poké(mon) walks, ChemHub, chiral solvent discussions, and boba sales. Andrew, here's to many more years of atrop(X)isomers. To the Gustafson Lab's first post-docs, Dr. Sagar and Dr. Della, thank you for your mentorship. To the army of undergraduates I worked with (for), this dissertation is a result of you guys. To the new crew, Mariam, Beeta and Bahar, I am excited to what the future holds for you guys and the lab. And finally, to Professor Gustafson, I couldn't ask for a better scientific mentor. Your focus and curiosity across all sciences is motivating and something I strive to match. My PhD work is simply a manifestation of your idea - thank you for trusting me with it and giving me the insight and flexibility to develop it into its current state.

To my scientific collaborators. Javi and Toni, your willingness to train a messy organic chemist how to culture cells (among many other techniques) bridged a critical gap between chemistry and biology. Your commitment to your research is inspiring and I will always be thankful for the time you have given me. Professor Hecht, thank you for opening the door to *in silico* studies – this helped shape our overall strategy and provided me with an invaluable tool for future endeavors.

I am grateful to be financially supported by SDSU scholarships, University Graduate Fellowship, and NIGMS grant R35GM124637 (PI: Gustafson).

Chapter 1 is in part a reformatted reprint of the following perspective, with permission from Future Science Ltd.: Toenjes, S.; Gustafson, J. Atropisomerism in Medicinal Chemistry: Challenges and Opportunities. *Future Med. Chem.* **2018**, *10,* 409-422. The dissertation author reviewed the literature and was a co-author of this material. Support of this work by the National Institute of General Medical Sciences is acknowledged (R35GM124637).

Chapter 2 is a reformatted reprint of the following research article, with permission from American Chemical Society: Toenjes, S.; Garcia, V.; Maddox, S.; Dawson, G.; Ortiz, M.; Piedrafita, F.; Gustafson, J. Leveraging Atropisomerism to Obtain Selective Inhibitors of RET Kinase with Secondary Activities towards EGFR Mutants. *ACS Chem. Biol.* **2019**, *14*, 1930-1939. The dissertation author was the primary researcher and co-author of this material. Support of this work by the National Institute of General Medical Sciences is acknowledged (R35GM124637).

Chapter 3 is a manuscript draft awaiting final experiments before submission: Toenjes, S.; Albright, S.; Hazin, R.; Gustafson, J. Controlling Ibrutinib's conformations to impart Selectivity. *Bioorg. Med. Chem. Lett.* **2020** *Manuscript in preparation*. The dissertation author was the primary researcher and author of this material. Support of this work by the National Institute of General Medical Sciences is acknowledged (R35GM124637).

Chapter 4 contains material that may be used in a future publication. The following are coauthors for this project: Toenjes, S.; Garcia, V.; Basilaia, M.; Heydari, Be.; Heydari, Ba.;

Vaidya, S.; Gustafson, J. Extension of Conformational Control to New Targets and Inhibitor Scaffolds. The dissertation author was the primary researcher and author of this material. Support of this work by the National Institute of General Medical Sciences is acknowledged (R35GM124637).

Chapter 5 is a compilation of highlighted sections from three different manuscripts with permission from each manuscript's journal: Cardenas, M.; Toenjes, S**.**; Nalbandian, C.; Gustafson, J. Enantioselective Synthesis of Pyrrolopyrimidine Scaffolds through Cation-directed Nucleophilic Aromatic Substitution. *Org. Lett.* **2018**, *20,* 2037-2041*,* Dinh, A.; Noorbehesht, R.; Toenjes, S.; Jackson, A.; Saputra, M.; Maddox, S.; Gustafson, J. Towards a Catalytic Atroposelective Synthesis of Diaryl Ethers via C(sp^2)-H Alkylation Using Nitroalkanes. *Synlett* **2018**, *29,* 2155-2160, and Vaidya, S.; Toenjes, S.; Yamamoto, N.; Maddox, S.; Gustafson, J. Catalytic Atroposelective Synthesis of N-Aryl Quinoid Compounds. *J. Am. Chem. Soc.* **2020**, *142*, 2198-2203. The dissertation author was a supplemental researcher and coauthor for each of these manuscripts. Support of this work by the National Institute of General Medical Sciences is acknowledged (R35GM124637).

Vita

Education

2007-2008	Harper Community College
2008-2011	B.S. Chemistry, University of Illinois at Urbana-Champaign
2015-2020	Ph.D. Chemistry, University of California San Diego and San Diego State University

Publications

Michaels, H.; Ortiz, M.; Molina, B.; **Toenjes, S.**; Davis, J.; Hecht, D.; Gustafson, J.; Nefzi, A.; Marconi, G.; Piedrafita, F. Discovery of Cyclic Guanidine-linked Sulfonamides as Inhibitors of LMTK3 Kinase. *Bioorg. Med. Chem. Lett.* **2020**, *30,* 1-6.

Vaidya, S.; **Toenjes, S.**; Yamamoto, N.; Maddox, S.; Gustafson, J. Catalytic Atroposelective Synthesis of N-Aryl Quinoid Compounds. *J. Am. Chem. Soc.* **2020**, *142*, 2198-2203.

Toenjes, S.; Garcia, V.; Maddox, S.; Dawson, G.; Ortiz, M.; Piedrafita, F.; Gustafson, J. Leveraging Atropisomerism to Obtain Selective Inhibitors of RET Kinase with Secondary Activities towards EGFR Mutants. *ACS Chem. Biol.* **2019**, *14*, 1930-1939.

Dinh, A.; Noorbehesht, R.; **Toenjes, S.**; Jackson, A.; Saputra, M.; Maddox, S.; Gustafson, J. Towards a Catalytic Atroposelective Synthesis of Diaryl Ethers via C(sp^2)-H Alkylation Using Nitroalkanes. *Synlett* **2018**, *29,* 2155-2160.

Cardenas, M.; **Toenjes, S.**; Nalbandian, C.; Gustafson, J. Enantioselective Synthesis of Pyrrolopyrimidine Scaffolds through Cation-directed Nucleophilic Aromatic Substitution. *Org. Lett.* **2018**, *20,* 2037-2041.

Toenjes, S.; Gustafson, J. Atropisomerism in Medicinal Chemistry: Challenges and Opportunities. *Future Med. Chem.* **2018**, *10,* 409-422.

Nalbandian, C.; Miller, E.; **Toenjes, S.**; Gustafson, J. A Conjugate Lewis base-Brønsted acid Catalyst for the Sulfenylation of Nitrogen Containing Heterocycles under Mild Conditions. *Chem. Commun.* **2017**, *53*, 1494-1497.

Manuscripts in Preparation

Toenjes, S.; Albright, S.; Hazin, R.; Gustafson, J. Controlling Ibrutinib's conformations to impart Selectivity. *Bioorg. Med. Chem. Lett.* **2020** *Manuscript in preparation*.

Patents

Gustafson, J.; Smith, D.; Hecht, D.; Marquez, I.; **Toenjes, S**. Atropisomerism For Increased Kinase Inhibitor Selectivity. U.S. Patent 10,550,124 (B2) filed Feb. 12, 2018 and issued Feb. 4, 2020 (priority Aug. 13, 2015).

Gustafson, J.; **Toenjes, S**.; Maddox, S. Atropisomerism For Enhanced Kinase Inhibitor Selectivity. U.S. PCT Pub. WO 2018/237134 (A1) filed Jun. 21, 2018 and published 27 Dec. 2018 (priority Jun. 23, 2017).

Gustafson, J.; **Toenjes, S**.; Albright, S.; Hazin, R. Controlling Conformational Space of Ibrutinib to Obtain a More Selective BTK Inhibitor. U.S. Prov. App. 62/866,507 filed Jun. 25, 2019.

Awards and Fellowships

2019-2020	James & Mary Crouch Memorial Scholarship
2019-2020	Tom Ragan Memorial Endowed Fellowship
2018-2019	SDSU Annual Ph.D. Research Award
2018-2019	Wilmia Tyler Trott Memorial Scholarship
2017-2019	Harry E. Hamber Memorial Scholarship
2017-2019	University Graduate Fellowship

Abstract of the Dissertation

Conformational Control of Kinase Inhibitors to Increase Target Selectivity

by

Sean Toenjes

Doctor of Philosophy in Chemistry

University of California San Diego, 2020

San Diego State University, 2020

Professor Jeffrey Gustafson, Chair

Atropisomerism is a dynamic type of axial chirality that is ubiquitous in medicinal chemistry. Majority of drugs (83% of FDA-approved kinase inhibitors) possess an unstable atropisomeric axis, allowing these compounds to access the majority of dihedral conformations around the bond axis. While they engage their targeted protein within a narrow range of these conformations, the remaining available conformations can interact with other proteins leading to off-target inhibition causing unwanted side-effects. The Gustafson lab hypothesized that the

selectivity of an atropisomerically unstable, promiscuous inhibitor could be increased by preorganizing it into the conformation preferred by oncogenic targets and preventing bond rotation to bind off-target proteins. Chapter 1 reviews examples of atropisomerism in drug discovery including my colleague's proof-of-concept paper on leveraging atropisomerism to increase selectivity of pyrrolopyrimidine-based inhibitors (PPYs). My PhD research begins in Chapter 2 where we optimized the atropisomeric PPYs for potency and selectivity, resulting in a therapeutically relevant inhibitor towards RET and mutant EGFR kinases. Along the way, we discovered the increases in inhibitor selectivity was due to the narrowing of accessible low-energy conformations. This led to the development of conformational binding maps that were used to predict a kinase's preferred binding conformation and guide the design of new covalent inhibitors for BTK kinase (Chapter 3). During this work we encountered unintended structural perturbations when incorporating an atropisomeric locking substituent, which led to the design of a stereochemically unstable, yet conformationally-tuned, selective BTK inhibitor. Chapter 4 presents other PPY preorganization strategies to target unique ligand binding regions as well as the development of conformational binding maps for pyridones and diaryl amines drug scaffolds. Chapter 5 discusses various catalytic atropisomeric methodologies to access enantiopure inhibitor scaffolds of PPYs, diaryl ethers and diaryl amines. Together, restricting accessible conformational space via stable atropisomerism or other tuning methods has catalyzed the development of novel, selective therapeutics and should serve as a long-standing strategy in drug design.

Chapter 1: Introduction

1.1 Copyright

Chapter 1 is in part a reformatted reprint with permission from *Future Med. Chem.* **2018**, *10,* 409-422. Copyright 2018 Future Science Ltd.

1.2 Atropisomerism in Drug Discovery

The implications of chirality on the biological activity of a drug has long been appreciated, in part due to examples such as thalidomide where severe complications were caused by one enantiomer of a racemic or rapidly racemizing mixture. Atropisomerism is a type of chirality that arises from differential substitution about a bond, typically between two sp^2 hybridized atoms. Atropisomerism arises in many common scaffolds in drug discovery including biaryls, diaryl ethers, diaryl amines, benzamides, and anilides (Figure 1.2.1A). Atropisomerism differs from other instances of chirality in that racemization can occur spontaneously via bond rotation, rather than the process of bond breaking and bond making needed for the racemization of other instances of chirality. Atropisomeric small molecules can thus span the gamut of stereochemical stability with examples that are exceedingly stable when there is a large degree of hindrance to rotation about the chiral axis, as with BINOL (Figure 1.2.1B) which has a half-life of racemization at room temperature ($t_{1/2\ (\mathrm{rt})}$) of ~2 million years. Conversely, when there is little hindrance to rotation about the chiral axis, atropisomers can racemize freely, as is the case with myriad pharmaceuticals and chemical probes. Indeed, a cursory analysis of ~1900 small molecule drugs in the FDA Drug Bank reveals that ~15% of FDA approved small molecules contain at least one atropisomeric axis, with the vast majority existing as rapidly interconverting atropisomers.[1] Furthermore, an additional

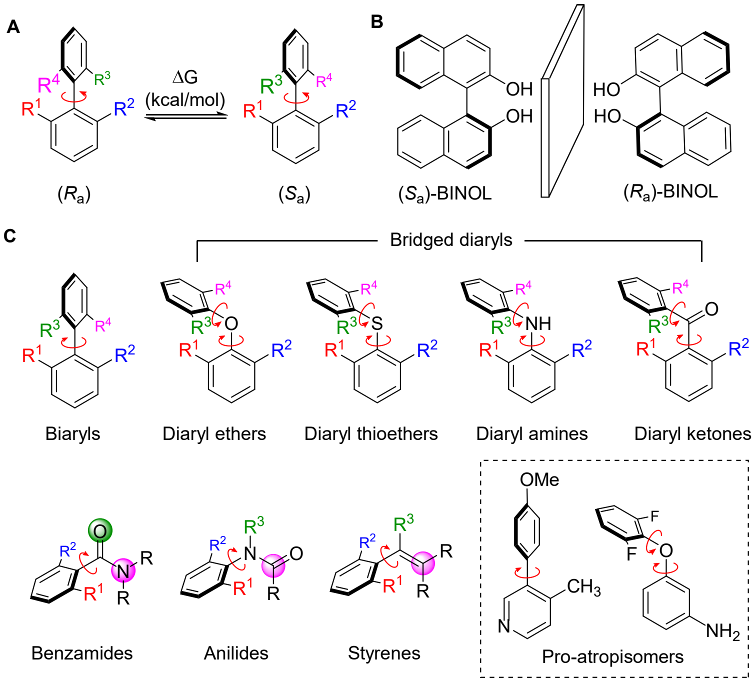
A
ΔG
(kcal/mol)
(Ra)
(Sa)
B
(Sa)-BINOL
(Ra)-BINOL
OH
HO
C
Bridged diaryls
Biaryls
Diaryl ethers
Diaryl thioethers
Diaryl amines
Diaryl ketones
Benzamides
Anilides
Styrenes
OMe
CH3
NH2
Pro-atropisomers

Figure 1.2.1. Examples of atropisomeric scaffolds.

~10% of structures are 'pro-atropisomeric', meaning simple modifications about the axis can break the symmetry and render these drugs atropisomeric. The prevalence of atropisomerism in drug discovery has been increasing over the last decade. Indeed, if you bias the analysis to FDA approved small molecule drugs since 2011, ~30% of small molecule drugs contain an axis of chirality, with another 16% being pro-atropisomeric. Perhaps unsurprisingly, certain classes of inhibitors are made up almost exclusively of scaffolds that display atropisomerism, for example 83% (39/47 as of April 2019) of FDA-approved kinase inhibitors possess at least one rapidly interconverting axis of atropisomerism.[2]

The current 'industry standard' approach is to avoid stable atropisomerism when possible, and to treat rapidly interconverting atropisomers as achiral.[3,4] Despite this, rapidly interconverting atropisomers typically interact with their target protein in an atropisomer selective fashion, and it has become increasingly appreciated that each possible atropisomeric conformation of a molecule can possess different drug-properties and target profiles.[5] In this chapter, we discuss the current state of atropisomerism in drug discovery as well as challenges and opportunities moving forward. We place emphasis on how rapidly interconverting atropisomers shouldn't be readily dismissed as achiral and in many cases the synthesis of atropisomerically stable analogs can improve different properties of a lead compound and therefore is a worthwhile endeavor to include in structural optimization campaigns.

The stereochemical stability of an atropisomeric lead compound is of utmost importance when considering how to further develop it. Figure 1.2.2 displays a conformational energy profile (CEP) that measures relative energies as its chiral axis is rotated (M06-2X/6-31+G(d)//RB3LYP/6-31G(d); RB3LYP/6-31G(d) thermal corrections).[6] Atropisomers will have two different planar conformations that represent local energy maximums, with the planar conformation that possesses the lower $\Delta G^{\ddagger}$ defining the stereochemical stability (±180° in the case of **1.1** in Figure 1.2.2). LaPlante and coworkers have computationally surveyed several industrial screening decks for potentially atropisomeric compounds, leading them to classify atropisomers into three categories based on the amount of energy needed for the chiral axis to racemize via rotation.[3,7] Class 1 atropisomers possess barriers to rotation around the chiral axis of less than 20 kcal/mol and racemize on the minute or faster time scale at room temperature; class 2 atropisomers possess a

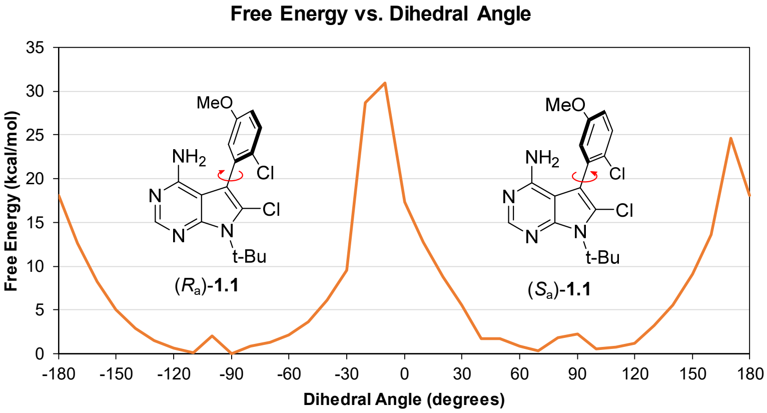

Figure 1.2.2. Conformational energy profile of an atropisomerically stable PPY inhibitor.

barrier to rotation between 20-28 kcal/mol and racemize on the hour to month time scale at room temperature; and class 3 atropisomers possess a barrier to rotation greater than 28 kcal/mol and racemize on the year or greater timescale at room temperature. Stereochemically stable class 3 atropisomers (which possess a racemization ($t_{1/2\ (37^{\circ}\mathrm{C})}$) > 6 months) have found their way into the everyday vernacular of chemistry with ligands such as BINAP being widely viewed as privileged chiral scaffolds for catalysis, and natural products such as vancomycin representing important and indispensable therapeutics. As class 3 atropisomers are stable for prolonged periods at physiological conditions they are typically treated in a manner similar to point chiral molecules. Conversely, stereochemically unstable class 1 atropisomers are perhaps the most common manifestation of atropisomerism in medicinal chemistry, however the 'latent' chirality of such molecules is often disregarded, and these compounds are typically treated as 'achiral'. Class 2 atropisomers, represent a conundrum in drug discovery as they racemize on an intermediate time scale that can cause complications when characterizing the activities of each atropisomer in early stage development. In fact, a seminal review has characterized class 2 atropisomerism as 'a lurking menace' and suggests avoiding intermediate atropisomerism when at all possible.[4]

There is a growing body of literature illustrating the impacts of axial chirality on the activities of a compound. A key point that has become apparent from this work is that stable atropisomers (class 3) often have markedly divergent activities. For example, it has become clear that in many cases the majority of activity (towards a desired target) belongs to one atropisomer, while the other atropisomer contributes very little.[5] These differences are embodied by three notable small molecule atropisomeric FDA-approved drugs telenzepine (**1.2**), colchicine (**1.3**), and lesinurad (**1.4**) (Figure 1.2.3). The most discussed example of an atropisomeric FDA-approved

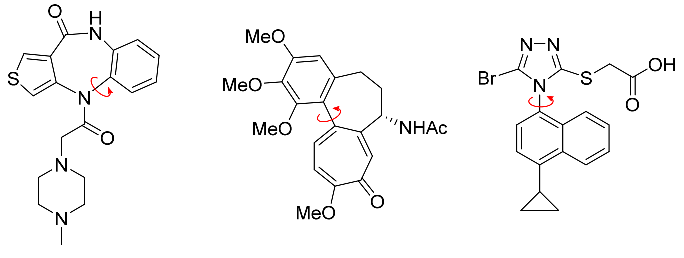

Telenzepine (**1.2**) Colchicine (**1.3**) Lesinurad (**1.4**)

Figure 1.2.3. Atropisomerically stable FDA-approved small molecule drugs.

drug in the literature is perhaps the anti-muscarinic telenzepine which possesses a $t_{(1/2)}$ to racemization at 20°C of approximately 1000 years, and a 500 fold difference in potency between atropisomers.[4,8] (R_a,7S)-Colchicine, which inhibits microtubule polymerization, is an example of an FDA approved atropisomeric natural product whose enantiomer is notably (~40-fold) less cytotoxic. Colchicine is also interesting from a fundamental perspective as the atropisomeric axis is constrained in a medium sized 7-membered ring, leading to a significantly lower than expected barrier to rotation due to a phenomena related to Bringmann's 'Lactone effect'.[9,10] Despite this, colchicine behaves as a class 3 atropisomer due to an instance of point chirality (the acetamide at the 7 position) that significantly stabilizes one diastereomer over the other, effectively rendering (R_a,7S)-colchicine indefinitely atropisomerically stable.[11] It should be noted that removal of the 7-acetamido group results in an atropisomer with a barrier to rotation of ~22 kcal/mol that racemizes on the minute to hour time scale.[12] Finally, lesinurad, a hURAT1 inhibitor approved for the treatment of gout was discovered to exist as a mixture of stable atropisomers after initial approval, with the (S_a)-atropisomer proving to be a 3x more potent hURAT1 inhibitor.[13] It is also worth noting that the atropisomers displayed markedly different pharmacokinetic profiles, underscoring another factor that should be taken into account when dealing with an atropisomer drug candidate.

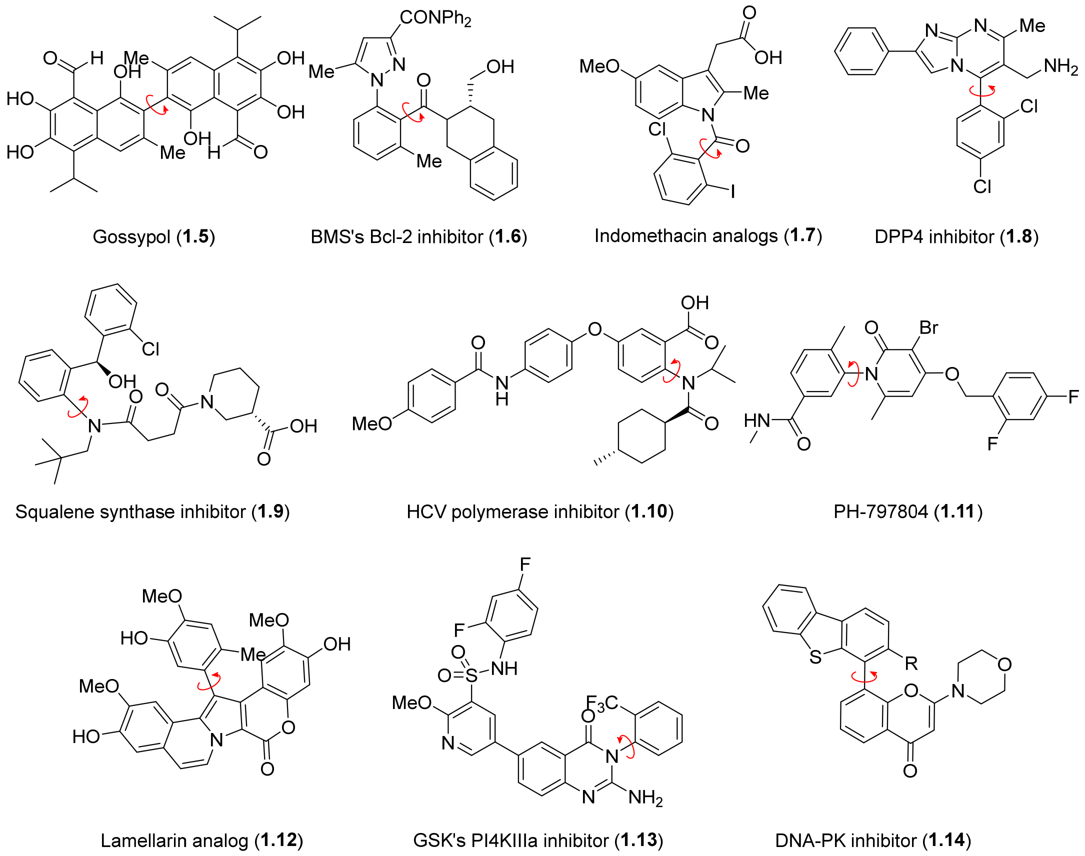
O
H
Me
OH
HO
HO
OH
OH
Me
OH
H
O
CONPh2
Me
N
N
N
O
OH
Me
MeO
O
OH
Me
N
Cl
O
I
N
N
N
Me
N
NH2
Cl
Cl
Cl
OH
O
O
N
N
OH
O
OH
O
O
O
N
H
MeO
N
O
Br
O
N
O
F
HN
O
F
MeO
HO
MeO
Me
OH
MeO
HO
N
O
O
F
F
O
O=S
NH
MeO
N
F3C
O
N
N
NH2
S
R
O
N
O
O

Gossypol (**1.5**) BMS's Bcl-2 inhibitor (**1.6**) Indomethacin analogs (**1.7**) DPP4 inhibitor (**1.8**)

Squalene synthase inhibitor (**1.9**) HCV polymerase inhibitor (**1.10**) PH-797804 (**1.11**)

Lamellarin analog (**1.12**) GSK's PI4KIIIa inhibitor (**1.13**) DNA-PK inhibitor (**1.14**)

Figure 1.2.4. Class 2 and 3 atropisomeric compounds from the medicinal chemistry literature.

There have also been many recent examples in the medicinal chemistry literature of experimental atropisomeric compounds (Figure 1.2.4). The natural product gossypol (**1.5**) and its derivatives have been studied extensively as Bcl-2 inhibitors with the (R_a)-atropisomer possessing the bulk of the desired anti-cancer activities.[14,15] The divergent activities of gossypol's atropisomers was also highlighted in a study where gossypol was studied as a male contraceptive in which the (R_a)-atropisomer sterilized 3 of 5 hamsters while the (S_a)-atropisomer displayed no such activity.[16] It is worth noting that gossypol is an example of an atropisomeric natural product that is produced in nature with a moderate degree of enantiopurity that varies from source to source.[17] Another example of an atropisomerically stable Bcl-2 inhibitor (**1.6**) was reported by a team at BMS in 2009.[18,19] In these studies, a series of atropisomeric Bcl-2 inhibitors with varying barriers to racemization were synthesized and evaluated. As with colchicine, the atropisomeric axis of the lead BMS compound was not stereochemically stable on its own, however a point chiral center in the molecule stabilizes the Bcl-2 active atropisomer relative to other diastereomers, resulting in an equilibration at room temperature to a mixture that is primarily the active atropisomer. Nonetheless, the BMS team was able to separate each atropisomer and found that the (R_a)-atropisomer inhibited Bcl-2 up to 30-fold more than the (S_a)-atropisomer. The observed activity for the (S_a)-atropisomer was attributed to interconversion to the (R_a)-atropisomer over the course of the experiment.

Another seminal demonstration of differential activities among atropisomers was published in 2011 by Takahashi and Natsugari wherein they synthesized atropisomeric analogs (**1.7**) of the COX1/2 inhibitor indomethacin finding only the (R_a)-atropisomer possessed any observable COX1 inhibition [20]. While these derivatives were an order of magnitude less potent than indomethacin itself, they displayed no observable activity towards COX2. Another example was disclosed by a BMS team in the context of a suite of serine dipeptidyl peptidase IV (DPP4) inhibitors containing a biaryl axis (**1.8**).[21] During the initial structural optimization they found DPP4 exhibited preferences for *ortho* substitution on an aryl ring, resulting in their top compounds existing as stable atropisomers. After separation, the (S_a)-atropisomers of the two leading compounds were 74-fold and 27-fold more active towards DPP4 than the (R_a)-atropisomer. Ichikawa happened upon atropisomerism in a different fashion, as his group's potent squalene synthase inhibitor (SSI) (**1.9**), unintentionally, existed as an interconverting mixture of atropisomers.[22] X-ray co-crystallography displayed only the (S, R_a)-diastereomer bound. Evaluation of subsequent atropisomerically stable analogs *in vitro* confirmed the X-ray crystallography data, showing SSI's preference for the (R_a)-atropisomer was up to 130-fold greater than (*S*a)-atropisomer depending on the substrate. In a similar scenario as Ichikawa, LaPlante and coworkers designed a hepatitis C viral (HCV) polymerase inhibitor (**1.10**) with a racemization half-life of 69 minutes (class 2 atropisomer).[23] They found that while the (*R*a)-atropisomer inhibited HCV NS5B polymerase the (*S*a)-atropisomer inhibited an HIV matrix protein, representing one of the first examples that a non-relevant atropisomer can lead to undesired off-target effects.

Finally, as mentioned earlier, kinase inhibitors are heavily biased towards atropisomeric scaffolds. As such, there have been several instances of atropisomerically stable compounds in the field of kinase inhibition. For example, a team at Pfizer found a lead p38 inhibitor to be a class 3 atropisomer. Upon separating the atropisomers they discovered the (*S*a)-atropisomer (PH-797804) (**1.11**) to be 100-fold more potent towards p38 than the (*R*a)-atropisomer. Yoshida has synthesized analogs of the kinase inhibiting natural product lamellarin (**1.12**), and serendipitously found them to be atropisomerically stable, with one atropisomer being consistently less potent, but arguably more selective, across a panel of 8 kinases.[24] Yoshida's work represents another early example that suggests atropisomerically pure compounds may possess improved target selectivities. A team at GSK has recently disclosed an inhibitor of type III phosphatidylinositol 4-kinase alpha (PI4KIIα) (**1.13**) as a potential HCV therapeutic.[25] After extensive optimization they arrived to an atropisomerically stable lead molecule of which they found the (Sa)-atropisomer to be one order of magnitude more potent towards PI4KIIIα. Finally, Cano and colleagues saw similar potency trends after restricting rotation about an axis of a known DNA-PK inhibitor (**1.14**) through addition of alkyl groups adjacent to a biaryl axis.[26] For each analog, the (-)-atropisomers was 80 to 100-fold more potent than the (+)-atropisomers. Put together, these examples suggest that leveraging atropisomer conformation via the synthesis of atropisomerically pure compounds can lead to more potent compounds (compared to racemic mixtures), by ensuring that the compound is preorganized into the desired active conformation for a given target.

Class 1 atropisomers have become increasingly prevalent in drug discovery (Figure 1.2.5). As mentioned in the introduction, ~30% of FDA-approved small molecule drugs since 2011 possess at least one interconverting axis of chirality. As early stage medicinal chemistry is currently biased towards reaction classes (i.e. cross-coupling, amide formation, S_NAr) that often yield atropisomeric molecules, pharmaceutical compound collections are becoming increasingly inundated with rapidly interconverting atropisomerism, thus one may expect that the prevalence of atropisomers in drug discovery will only continue to increase over the foreseeable future.[27,28]

Examples of marketed drugs that exist as rapidly interconverting atropisomers include the heterobiaryls, dabrafenib (**1.15**) and sildenafil (**1.16**) and the anilide eszopiclone (**1.17**). While these drugs are treated as achiral, examination of co-crystal structures reveal that they bind their respective targets in an atroposelective manner. For example, both atropisomeric axes of dabrafenib are found to interact with its primary target BRAF in the (S_a)-atropisomeric conformation[29]; sildenafil is found to bind phosphodiesterase 5 (PDE5) in the (S_a)-atropisomeric conformation[30]; and eszopiclone is found to interact with the GABA Type A receptor in the (R_a)-atropisomer conformation.[31] Furthermore, an additional 15% of FDA approved small molecules such as the selective estrogen receptor modulator bazedoxifene (**1.22**), the type 1 angiotensin receptor inhibitor valsartan (**1.23**), and the COX inhibitor indomethacin (**1.24**) are 'pro-atropisomeric' (pro-chiral), wherein simple modification about the axis can break symmetry and render them atropisomeric.

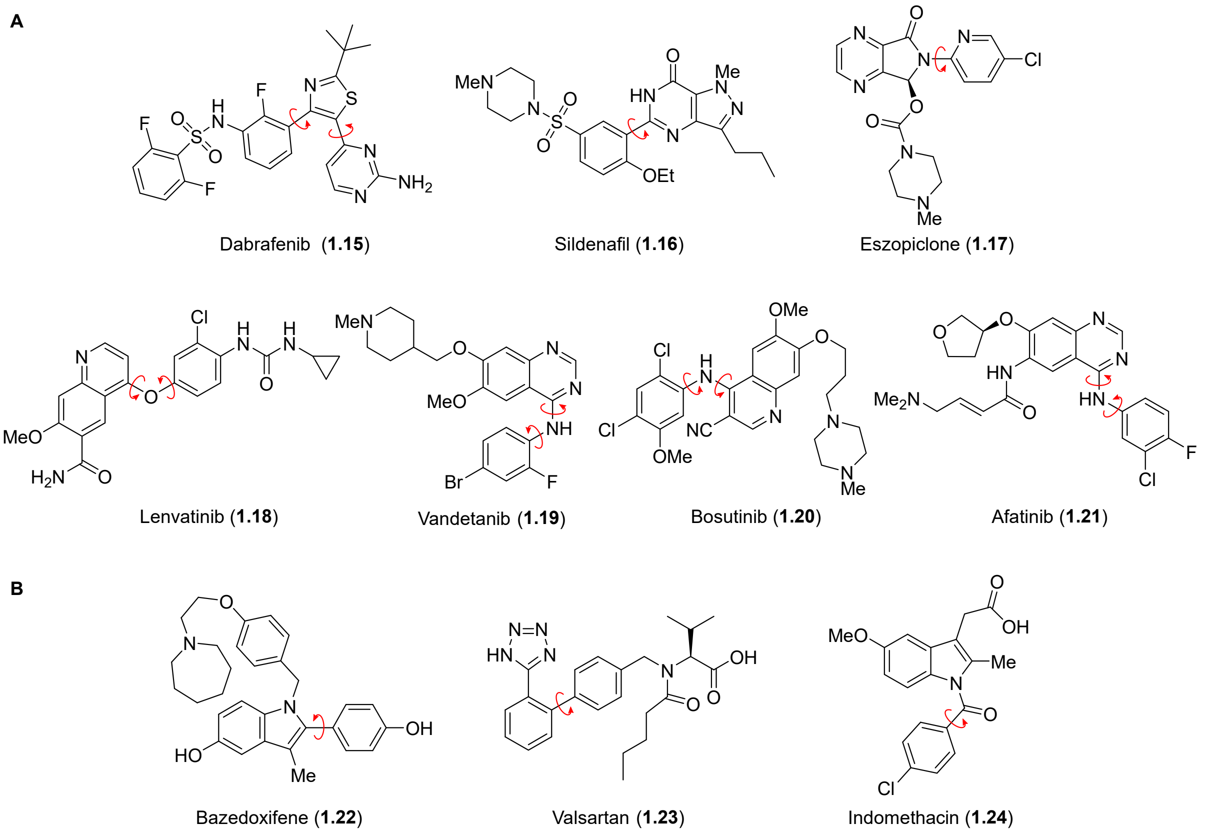
A
Dabrafenib (1.15)
Sildenafil (1.16)
Eszopiclone (1.17)
Lenvatinib (1.18)
Vandetanib (1.19)
Bosutinib (1.20)
Afatinib (1.21)
B
Bazedoxifene (1.22)
Valsartan (1.23)
Indomethacin (1.24)

Figure 1.2.5. A) FDA-approved class 1 atropisomeric drugs. B) FDA-approved pro-atropisomeric drugs

While a large number of rapidly interconverting atropisomers are scaffolds such as biaryls or heterobiaryls that are readily recognized as potentially atropisomeric, there are also numerous instances of scaffolds whose atropisomerism is often overlooked. For example, diaryl ethers are often not considered to be atropisomeric as they possess lower stereochemical stabilities than biaryls, however there have been reports in the literature with diaryl ethers possessing barriers to racemization greater than 28 kcal/mol (See Chapter 5).[32–35] Lenvatinib (**1.18**), is an example of a rapidly interconverting diaryl ether based kinase inhibitor that is a near pan inhibitor of the VEGFR, EGFR, FGFR, PDGFR, and RET families of kinases and also possesses low nM activities towards certain members of the ABL, SRC, and Ephrin families.[36] A recent crystal structure of lenvatinib bound to VEGFR2 with both axes of the diaryl ether in the (S_a)-atropisomeric conformation has been recently published, offering evidence that diaryl ethers do bind their target in an atropisomer specific fashion.[37]

Diaryl amines are another non-traditional atropisomeric scaffold that are prevalent throughout drug discovery, particularly among kinase inhibitors, with the FDA-approved vandetanib (**1.19**), bosutinib (**1.20**) and afatinib (**1.21**) representing examples that exist as rapidly interconverting atropisomers. The atropisomerism of diaryl amines has been largely ignored save work by the Gustafson Lab (Chapter 4 and 5) and the Kawabata Lab where each group separately accessed a series of atropisomerically stable diaryl amines and found the strength of an intramolecular H-bond to be crucial to stereochemical stability of examples that had relatively small 'conformational' locking groups.[38–40] Beyond this, relatively little is known about the factors that render a diaryl amine atropisomerically stable. Nonetheless, co-crystal structures of vandetanib (bound to RET)[41], bosutinib (bound to ABL)[42] and afatinib (bound to EGFR)[43] have each been recently published, with each compound bound to their respective targets in the (S_a, S_a)-atropisomer conformation.

1.3 Atropisomerism as a Selectivity Filter in Drug Design

Rapidly interconverting atropisomers are typically treated as achiral compounds, however in reality at any given moment these molecules exist as racemic mixture of interconverting enantiomers, not too dissimilar from how the infamous point-chiral drug thalidomide exists.[44] Furthermore, as demonstrated in the previous section, such compounds will likely interact with their respective biological targets in an atropisomer specific manner, with the non-relevant atropisomer contributing little to the desired activities.[5] The documented differential biology among atropisomers can result in the non-relevant atropisomer possessing undesired off-target activities that can lead to side effects in patients or muddle experimental results. Inspired by this, the Gustafson Lab initially hypothesized that atropisomerism may be leveraged as a design element to increase the target selectivity of promiscuous small molecules that possess a rapidly interconverting axis of atropisomerism.[6] In other words, atropisomerically pure and stable analogs of known promiscuous rapidly interconverting atropisomers would possess increased target selectivities via removal of any off-target activities associated with the non-relevant atropisomer.

While one may argue that the equilibrium between interconverting atropisomers may be biased by one protein target effecting an *'in situ* dynamic kinetic resolution' therefore removing the non-relevant atropisomer, this can be offset if a second target prefers the other atropisomer and biases the equilibrium in the opposite direction. In a biological system the compound will be exposed to perhaps hundreds of proteins that possess affinity for either atropisomer, thus it is likely there will be significant amounts of both atropisomers, and thus effects from the activities of both atropisomers would be expected. When the interconverting atropisomer is rigidified, no equilibrium is at play and the situation is perhaps simplified.

It is appreciated that target selectivity is an important factor in drug development. This has proven one of the most difficult issues in the development of small-molecule kinase inhibitors.[45–47] Aberrant kinase activity is involved in many different diseases, focusing research efforts towards the development of small-molecule kinase inhibitors, resulting in an expanding number of FDA-approved kinase inhibitors based therapeutics.[48,49] A large degree of active site conservation throughout the kinome has led to most kinase inhibitors to possess promiscuous activities towards many kinases.[46,50] This polypharmacology can lead to unwanted, often severe, side effects thus largely hindering efforts towards kinase inhibitor based therapeutics.[51–53] Kinase inhibitors are also commonly used as chemical probes to study the underpinnings of cellular processes and diseases, however these studies are often convoluted due to a lack of kinase inhibitor selectivity.[45,46,54] In recent years, chemists have designed 'selectivity filters' that take advantage of uncommon features of a kinase to modulate the selectivity of kinase inhibitors.[55–59] While these approaches have led to selective kinase inhibitors, and FDA-approved therapeutics, a general selectivity filter has remained unobtainable.[56,60] As selectivity is an unsolved problem for kinase inhibitors, and atropisomerism is ubiquitous in kinase inhibitors, this field was an ideal arena to study the effects of atropisomerism on target selectivity. My colleagues initially chose to study the pyrrolopyrimidine (PPY) scaffold, a common class of multi-kinase inhibitors that are related to the better-known pyrazolopyrimidine ligands (*i.e.* PP1).[61] They synthesized and separated atropisomerically stable PPY analogs (**1.1** in Figure 1.2.6) via HPLC on a chiral stationary phase. After assigning each compound's stereochemical conformation through small molecule X-ray crystallography and circular dichroism, they subjected each atropisomer, and a rapidly

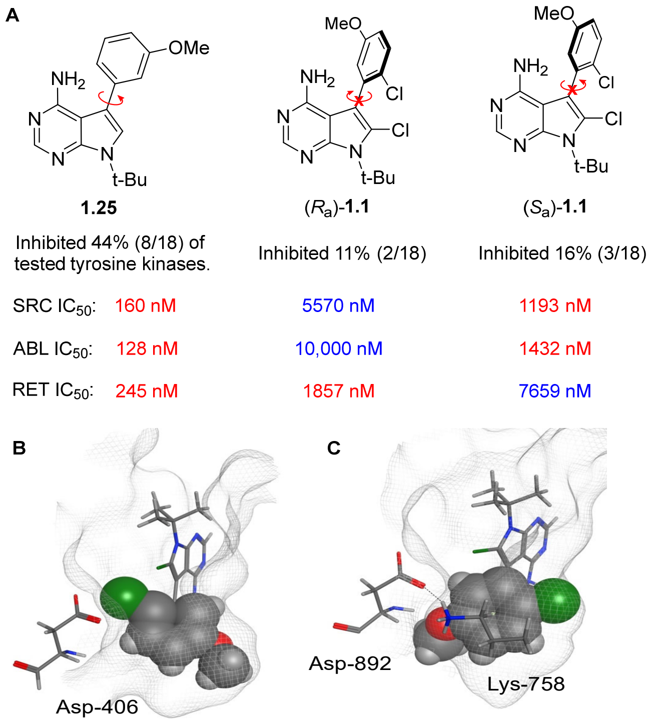
A
OMe
NH2
N
N
N
t-Bu
1.25
Inhibited 44% (8/18) of tested tyrosine kinases.
MeO
Cl
Cl
(Ra)-1.1
Inhibited 11% (2/18)
(Sa)-1.1
Inhibited 16% (3/18)
SRC IC50: 160 nM 5570 nM 1193 nM
ABL IC50: 128 nM 10,000 nM 1432 nM
RET IC50: 245 nM 1857 nM 7659 nM
B
Asp-406
C
Asp-892
Lys-758

Figure 1.3.1. *In vitro* and *in silico* data for (R_a)-**1.1**, (R_a)-**1.1** and **1.25**

A) *In vitro* activity of rapidly interconverting 1.25 and atropisomerically stable (R_a)-1.1 and (S_a)-1.1. B) (S_a)-1.1 docked into SRC (PDB 1YOL). C) (R_a)-1.1 docked into RET (PDB 2IVV).

interconverting control (**1.25**) to a panel of kinases. The atropisomeric analogs displayed increased selectivity compared to **1.25** across the panel with each atropisomer inhibiting different kinases, albeit at the expense of potency (SRC, RET, and ABL (Figure 1.3.1A)). For example, (*R*a)-**1.1** inhibited RET kinase, but possessed reduced potency towards ABL and SRC. Conversely, the (*S*a)-**1.1** configuration was less potent towards RET, while maintaining activity towards SRC and ABL. This data represented one of the first intentional demonstrations that members of highly conserved protein families such as kinases can prefer different atropisomer conformations of the same inhibitor, and that this can be harnessed to modulate inhibitor promiscuity.

To obtain a better understanding of the observed effects they turned to molecular modeling where each atropisomer of **1.1** in was docked in RET and SRC. In SRC (PDB 1YOL), **1.1** bound active site making the key hydrogen bonds with the hinge region and aryl ring orientated in the (*S*a)-conformation (Figure 1.3.1B). Subsequent docked poses suggest that SRC's preference for (*S*a)-**1.1** over (*R*a)-**1.1** may be caused by steric clashes between the methoxy group on (*R*a)-**1.1** and the hydrophobic binding pocket of SRC. Conversely, docking 1.1 in RET (PDB 2IVV) showed the preferred binding mode of **1.1** was with the aryl-chlorine ring in the (*R*a)-conformation (Figure 1.3.1C). The majority of RET's preference for (*R*a)-**1.1** over (*S*a)-**1.1** appears to be caused by destabilizing steric interactions between the aryl chloride in (*S*a)-**1.1** and Asp892. These experiments illustrate that the inherent atropisomer preference can be predicted *in silico***,** thus representing a tool that we used in the following chapters to assess of the prospect of using atropisomerism as a selectivity filter to a target kinase a priori.

1.4 Opportunities, Challenges and Future Perspective

We feel that the proof of concept data from the Gustafson lab coupled with the discussed literature examples illustrate that control of atropisomeric conformation can be used as a strategy to modulate the selectivity profile of small molecules. As rapidly interconverting atropisomerism is ubiquitous in drug discovery, controlling this chemical property has the potential to represent a general and useful strategy for medicinal chemists. It is enticing to draw a relation between leveraging atropisomerism and the 'magic methyl' effect, as in many cases the magic methyl effect has been found to be caused by conformational effects that bias against planar and near planar conformations, while still maintaining access to both possible atropisomeric conformations.[62,63] Atropisomerically stable compounds take this a step further by completely precluding the other atropisomer and further biasing against more planar conformations.

Perhaps the most well-known method of small-molecule conformational preorganization of small molecules is macrocyclization, a classic and indispensable strategy in drug discovery that is applicable to any flexible scaffold.[64–66] While there have been numerous success stories, macrocyclization based strategies often require significantly more complex syntheses and often result in unintended structural consequences that can lead to a loss of all desired activities. Employing atropisomerism (when possible), on the other hand, represents a more facile process where small substitutions adjacent to an axis are replaced by larger ones (i.e. an H replaced with a Cl). This will result in syntheses that are comparable in complexity to that of the parent molecule and a lessened risk of undesired structural perturbations. These minimal additions allow for further structural optimization using traditional methods while still staying within the framework of 'drug likeness'. Furthermore, an analysis of Figure 1.2.2 shows atropisomerically stable compounds typically retain ~80° conformational flexibility (low energy conformations) about the chiral axis, perhaps lessening the risk of completely ablating the activity towards a target. While this might lessen risk, it also leads to a minimal reduction of any entropic penalty of binding compared to macrocyclization, especially coupled with the fact that only one bond (the chiral axis) is being rigidified.

More broadly, as atropisomerism is becoming more prevalent throughout drug discovery there are likely to be increasing opportunities to exploit atropisomer conformation to modulate the potency, selectivity and perhaps even pharmacokinetics of a lead molecules across many classes of proteins. While the outlook is certainly bright there are several challenges that need to be overcome when dealing with atropisomerism in drug development. We will discuss these challenges in the upcoming paragraphs.

First, when designing an atropisomerically stable analog one must take appropriate precautions to ensure that the analog is sufficiently stereochemically stable as to avoid racemization (atropisomer interconversion) under physiological conditions. Some recent guidelines set forth by LaPlante state that a candidate should have a high enough barrier to rotation (27.3 kcal/mol) such that it racemizes <0.5% after 24 hours *in vivo.*[7] Computational tools that prediction of barriers to rotation (before synthesis) will also be quite useful.[3] In addition, as more systems are experimentally studied there will be an increased number of data sets of barrier to rotations across sets of pharmaceutically relevant scaffolds which will result in an improved institutional knowledge on what will sufficiently rigidify a specific atropisomeric scaffold. The data sets combined with predictive calculations provide valuable tools when dealing with atropisomeric scaffolds that are less well studied such as diaryl ethers[33] (Chapter 5) and diaryl amines (Chapter 4 and 5).[38,39] Generally, halogen, alkyl, amino, and thiol substitutions will be broadly useful as conformational locking substitutions, whereas sp^2 groups, hydroxyl and fluoro substitutions will likely only be useful in certain systems that already possess a fairly large barrier.[67] Finally, as demonstrated with the natural product colchicine, the addition of a point chiral center also represents a potential strategy to rigidify a rapidly interconverting axis by biasing the axis in the thermodynamically most stable diastereomer. While enticing, such a strategy will likely require a great deal of serendipity to generate the sought after diastereomer. It should also be noted that the diastereomeric ratio can very well be condition dependent and can change over time, representing an added layer of complexity that must be addressed.

One drawback of our previous work was the loss of potency observed for atropisomeric PPY analogs. While incorporating 'conformational locking' substitutions may lead to decreased potency in some cases, any loss of potency can likely be mitigated by the careful choice of 'conformational locking groups' and consideration of other factors, for example potency may be regained elsewhere in the context of a larger structural optimization effort if necessary. Support for this assertion will be demonstrated in Chapters 2 and 3 but can be observed from work outside the Gustafson Lab, where a BMS group developed an atropisomerically stable a reversible BTK inhibitor, BMS-986142 (**1.27**, Figure 1.4.1).[68] In this work they took a lead compound (**1.26**) that possessed two rapidly interconverting axes of atropisomerism and found notable increases in potency (up to 20-fold between atropisomers for each axis) and selectivity towards BTK (**1.27**).

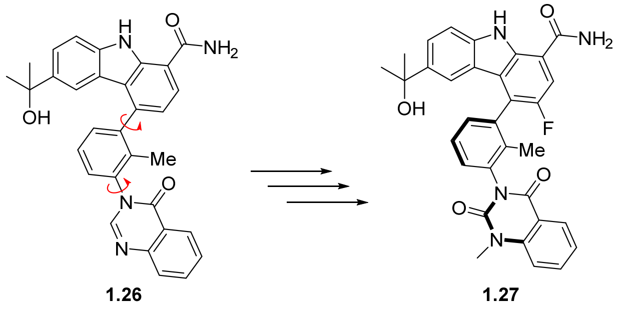

1.26

BTK IC$_{50}$: 2.6 nM
Promiscuous
2 rapidly interconverting axes

1.27

BTK IC$_{50}$: 1.0 nM
Improved BTK selectivity
2 atropisomerically stable axes

Figure 1.4.1. Rigidification of two axes to increase selectivity for BMS's BTK inhibitor.

While most of the examples discussed in the previous sections were largely serendipitous discoveries, moving forward, it is needed to be demonstrated that the control of atropisomerism can be applied to a lead compound *de novo*. Thus, another potential challenge is how to determine when rigidifying an axis of atropisomerism is a viable strategy to improve a target selectivity. In an ideal situation one would obtain co-crystal structures of the lead compound towards the desired target, as well as its off-targets, and observe differential atropisomeric binding, however this is not feasible in most situations. A more realistic approach might be to computationally dock the lead compound across a directed panel of proteins that includes the target and off-targets, as we used in our previous work (Figure 1.3.1) and more recent work (Chapters 2 and 3). If these studies predict that the lead compound will interact with the panel in an atropisomerically differential fashion, then it would be worthwhile to evaluate some atropisomerically stable analogs. This level of inquiry mirrors that of other selectivity filters such as covalently targeting non-conserved cysteines in a kinase active site.[55]

Accessing atropisomerically stable compounds in an enantiopure fashion is another major challenge facing stable atropisomers in drug development. Most of the examples above, including our work, rely on chromatographic separation to obtain atropisomers. While appropriate for early stage medicinal chemistry, this is inefficient from a material throughput perspective when only one atropisomer is needed and the non-relevant atropisomer (half of the material) will go to waste or, theoretically, be subjected to additional cycles of racemization and separation. Either way this becomes a hindrance when handed off to process chemistry, or when extensive structural optimization is needed, requiring the synthesis and separation of many atropisomeric analogs. While advances in large scale analytical separations and resolutions would certainly improve this situation, the ultimate solution will likely also need to include the development of new atroposelective methodologies, such as the ones discussed in Chapter 5, that can be employed on many of the common atropisomeric scaffolds in drug discovery. While there has been seminal examples in the literature over the past decade, the field of atroposelective synthesis is much less studied than that of point chirality, with the majority of atroposelective examples being studied on biaryls.[9,69,78,70–77] As controlling atropisomer conformation becomes a more prevalent strategy in drug discovery we expect there to be increasing need and opportunities for the development of innovative new atroposelective methodologies and expect that the field will be up for the challenge.

1.5 Acknowledgments

Chapter 1 is in part a reformatted reprint of the following manuscript, with permission from Future Science Ltd.: Toenjes, S.; Gustafson, J. Atropisomerism in Medicinal Chemistry: Challenges and Opportunities. *Future Med. Chem.* **2018**, *10,* 409-422. The dissertation author reviewed the literature and co-wrote the manuscript.

Chapter 2: Leveraging Atropisomerism to Obtain a Selective Inhibitor of RET Kinase with Secondary Activities towards EGFR Mutants

2.1 Copyright

Chapter 2 is reformatted reprint with permission from *ACS Chem. Biol.* **2019**, *14*, 1930-1939. Copyright 2019 American Chemical Society.

2.2 Introduction

There are over 500 protein kinases in the human genome, many of which play key roles in regulating various cellular processes.[47] Aberrant kinase activity has been implicated in a myriad of diseases and is a common contributing factor to many cancers.[79] As such, small molecule inhibitors of kinase activity have been robustly pursued over the past two decades, revolutionizing the manner by which many cancers are treated.[80] Despite these monumental achievements, obtaining highly selective kinase inhibitors remains a challenge[81,82] due to the high degree of active site conservation among kinases. The lack of an inhibitor's kinase specificity often leads to adverse events that can limit their safety, efficacy and usefulness as chemical probes.[45]

Recently, chemists have begun to implement 'selectivity filters' that allow for rapid improvements in selectivity by taking advantage of unique features of a kinase's active site, such as covalently targeting relatively non-conserved cysteines.[56–58] While such methods have led to the development of several important drugs, these approaches are not broadly applicable as they rely on relatively rare features of specific kinases that are susceptible to resistance via mutation.[83,84] As such, there remains a dire need for new broadly applicable strategies in medicinal chemistry that allow for efficient enhancement of selectivity and potency of pharmaceutical leads with relatively simple modifications.

These challenges are exemplified by RET, a receptor tyrosine kinase whose aberrant activity has been implicated in numerous cancers.[85] Activating RET point mutations[86,87] contribute to medullary thyroid cancers, RET fusions are common in papillary thyroid cancers and nonsmall-cell-lung cancers[88–91], and overexpression of wild-type (WT) RET is observed in endocrine resistant luminal breast cancers.[92] Current small molecule therapeutics used in treating RET driven diseases, such as vandetanib, are associated with grade 3 & 4 adverse effects[93,94] including thyroid malfunction[95], hypertension[96], QTc prolongation[97], and severe dermatological issues.[98] These undesirable effects are attributed to the inhibition of kinases other than RET, such as VEGFR2 and EGFR.[99,100] Consequently, recent efforts have focused on RET kinase inhibitors that inhibit fewer off-target kinases. Two inhibitors with improved RET selectivity, BLU-667 and LOXO-292, display improved safety and efficacy in phase I trials.[101] While promising, these compounds still exhibit low nM binding affinities towards troublesome off-target kinases (i.e BLU-667 possesses a K_i of 16 nM against VEGFR2).

EGFR represents another target in which inhibitor selectivity is of great importance, in this case for EGFR mutants over WT EGFR. EGFR mutants are a long-standing target in NSCLC, however 1st generation EGFR inhibitors are often met by acquired resistance, typically caused by T790M gatekeeper mutation. To overcome this mutation, Gray and others have targeted the cysteine 797 residue of EGFR[102], yielding 3rd generation EGFR inhibitors, Osimeritinib[103], WZ4002[102], and CO-1686.[104] Recently, a 3rd mutation in EGFR, C797S (most commonly appearing as a triple mutant with L858R and T790M), has been discovered that leads to resistance to 3rd generation inhibitors, spurring the need for development of 4th generation EGFR inhibitors that target C797S harboring mutants.[84,105,106] While several innovative strategies, including allosteric inhibition[107,108] and targeting additional neighboring binding pockets[109–111] and residues[112–115], have yielded inhibitors that function *in vitro*, these molecules either possess significant WT EGFR activity, resulting in well-characterized side effects, or have minimal cellular activity as a single agent. As such, there remains a dire need for a WT EGFR-sparing inhibitor that possesses activities against EGFR mutants, particularly the L858R/T790M/C797S triple mutant.

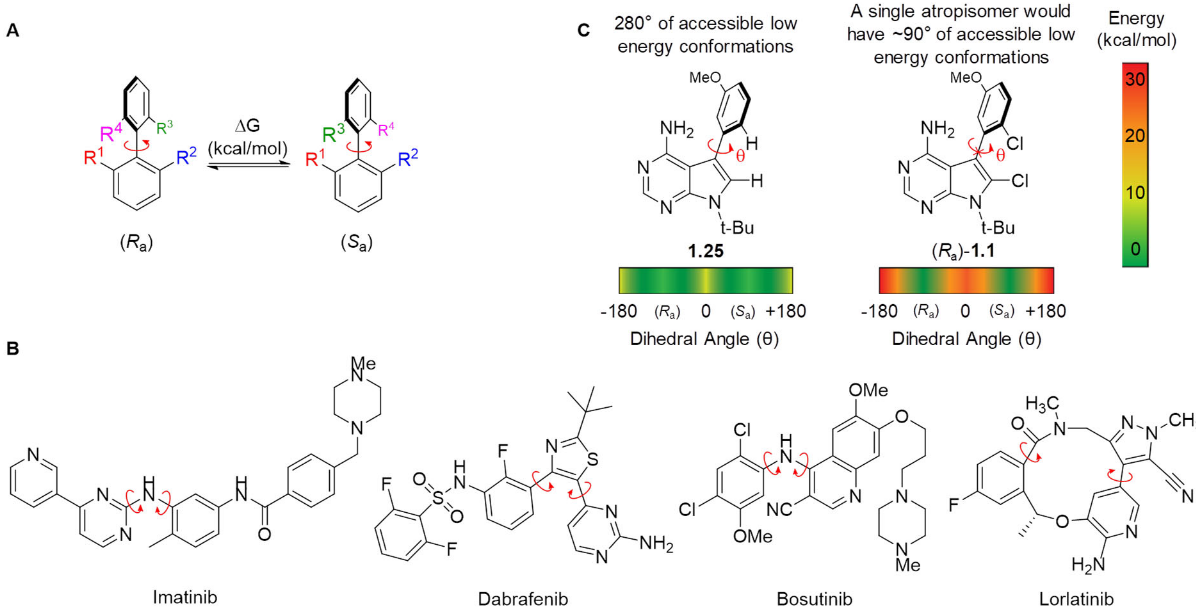
A
R1
R2
R3
R4
ΔG
(kcal/mol)
(Ra)
(Sa)
C
280° of accessible low energy conformations
A single atropisomer would have ~90° of accessible low energy conformations
Energy (kcal/mol)
30
20
10
0
MeO
NH2
N
H
θ
t-Bu
Cl
1.25
(Ra)-1.1
-180 (Ra) 0 (Sa) +180
Dihedral Angle (θ)
-180 (Ra) 0 (Sa) +180
Dihedral Angle (θ)
B
Imatinib
Dabrafenib
Bosutinib
Lorlatinib

Figure 2.2.1. Atropisomerism in drug discovery.

A) Bond rotation leads to racemization of atropisomers. B) Examples of atropisomerism in FDA-approved kinase inhibitors. C) Limited access to dihedral angles as a consequence of atropisomerism.

As discussed extensively in Chapter 1, atropisomerism is a stereochemical phenomenon that arises due to asymmetry about a bond, most typically a sp^2-sp^2 axis such as that in a nonsymmetrical biaryl (Figure 2.2.1). As racemization can occur spontaneously via bond rotation, atropisomers can span the gamut of stereochemical stability, ranging from rapidly racemizing

(Class 1) to stable enantiomers (Class 3).[3,7] Over the past several decades class 1 atropisomerism has become ubiquitous in modern drug discovery, perhaps due to the increased use of reactions that can form atropisomeric axes.[27,28] Indeed, at the time of this writing, over 83% of FDA-approved small molecule kinase inhibitors exist as class 1 atropisomers (Figure 2.2.1 and 2.2.2). The current 'industry standard' approach is to treat class 3 atropisomers as stable enantiomers, avoid class 2 atropisomers, and to treat rapidly interconverting class 1 atropisomers as achiral. While class 1 atropisomers do not display the hallmarks of chirality at room temperature, most interconverting atropisomeric compounds interact with their target as a single atropisomer with the other accessible atropisomer contributing little to the desired activities.[116]

The Gustafson Lab previously hypothesized (Chapter 1) that the target selectivity of a promiscuous lead compound could be improved through preorganizing the inhibitor into the atropisomeric conformation preferred by the targeted kinase by precluding any off-target inhibition contributed by the other atropisomer.[6] My colleagues executed a proof of concept experiment wherein they synthesized and tested atropisomerically stable analogs of a promiscuous, rapidly interconverting pyrrolopyrimidine (PPY) kinase inhibitor. While an order of magnitude less potent than the parent interconverting compound, each atropisomer displayed modulated selectivity across a panel of kinases. In this chapter's work, we describe studies that have led to a highly potent and selective atropisomeric inhibitor of RET kinase that possesses promising activities in models of RET-driven cancer. An analysis to determine the origins of the observed gains in selectivity and potency suggest that the bulk of improvement in selectivity is not a direct consequence of precluding the other atropisomer, but rather of constraining the accessible range of dihedral angles about the atropisomeric axis (Figure 2.2.1C), an outcome that is akin to the 'magic methyl effect'.[63]

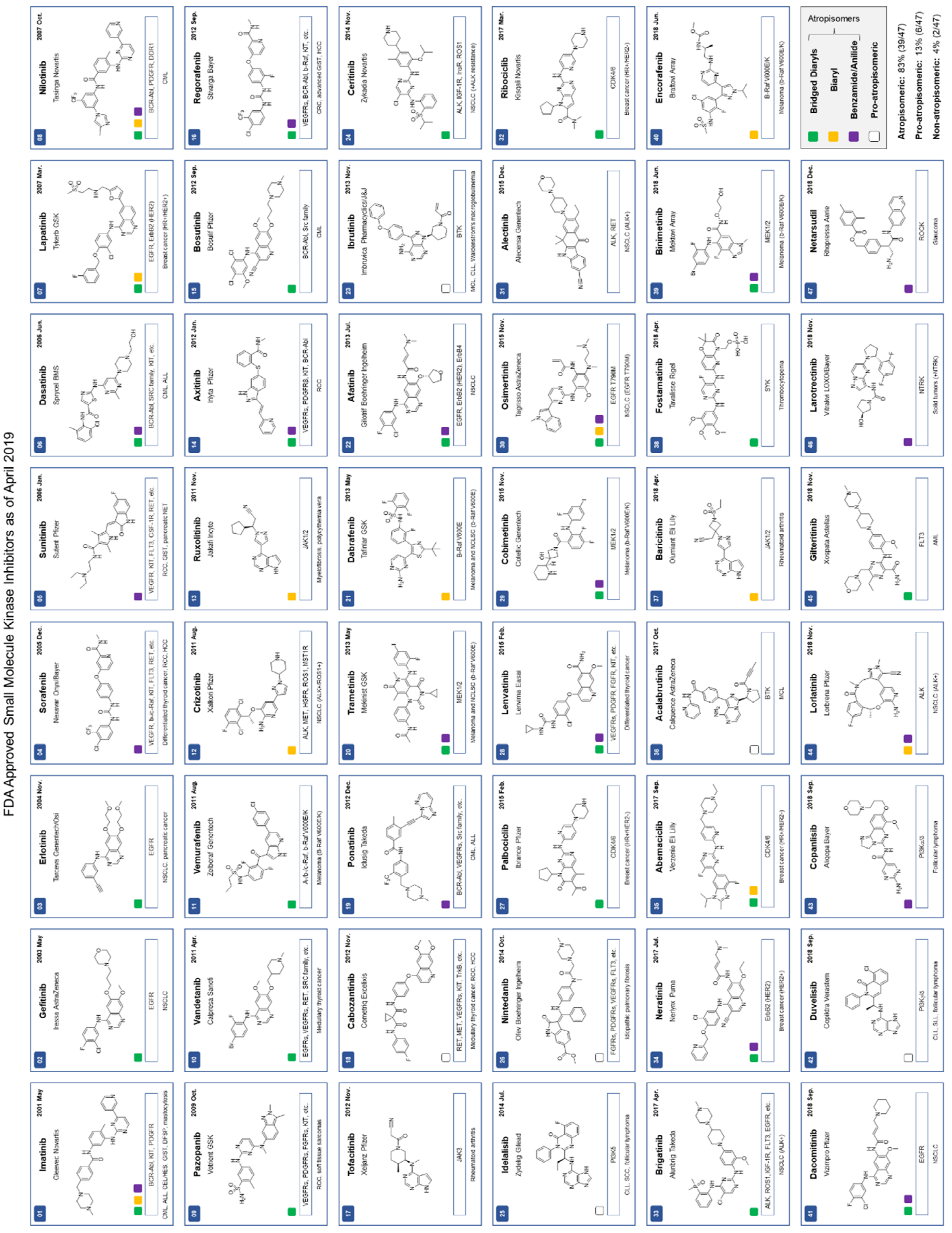
FDA Approved Small Molecule Kinase Inhibitors as of April 2019
01 Imatinib Gleevec Novartis 2001 May
BCR-Abl, KIT, PDGFR
CML, ALL, CEL/HES, GIST, DFSP, mastocytosis
02 Gefitinib Iressa AstraZeneca 2003 May
EGFR
NSCLC
03 Erlotinib Tarceva Genentech/Osi 2004 Nov.
EGFR
NSCLC, pancreatic cancer
04 Sorafenib Nexavar Onyx/Bayer 2005 Dec.
VEGFR, b-/c-Raf, KIT, FLT3, RET, etc.
Differentiated thyroid cancer, RCC, HCC
05 Sunitinib Sutent Pfizer 2006 Jan.
VEGFR, KIT, FLT3, CSF-1R, RET, etc.
RCC, GIST, pancreatic NET
06 Dasatinib Sprycel BMS 2006 Jun.
BCR-Abl, SRC family, KIT, etc.
CML, ALL
07 Lapatinib Tykerb GSK 2007 Mar.
EGFR, ErbB2 (HER2)
Breast cancer (HR+/HER2+)
08 Nilotinib Tasinga Novartis 2007 Oct.
BCR-Abl, PDGFR, DDR1
CML
09 Pazopanib Votrient GSK 2009 Oct.
VEGFRs, PDGFRs, FGFRs, KIT, etc.
RCC, soft tissue sarcomas
10 Vandetanib Calprosa Sanofi 2011 Apr.
EGFRs, VEGFRs, RET, SRC family, etc.
Medullary thyroid cancer
11 Vemurafenib Zelboraf Genentech 2011 Aug.
A-/b-/c-Raf, b-Raf V600E/K
Melanoma (B-Raf V600E/K)
12 Crizotinib Xalkori Pfizer 2011 Aug.
ALK, MET, HGFR, ROS1, MST1R
NSCLC (ALK+/ROS1+)
13 Ruxolitinib Jakafi Incyte 2011 Nov.
JAK1/2
Myelofibrosis, polycythemia vera
14 Axitinib Inlyta Pfizer 2012 Jan.
VEGFRs, PDGFRβ, KIT, BCR-Abl
RCC
15 Bosutinib Bosulif Pfizer 2012 Sep.
BCR-Abl, Src family
CML
16 Regorafenib Stivarga Bayer 2012 Sep.
VEGFRs, BCR-Abl, b-Raf, KIT, etc.
CRC, advanced GIST, HCC
17 Tofacitinib Xeljanz Pfizer 2012 Nov.
JAK3
Rheumatoid arthritis
18 Cabozantinib Cometriq Exelixis 2012 Nov.
RET, MET, VEGFRs, KIT, TrkB, etc.
Medullary thyroid cancer, RCC, HCC
19 Ponatinib Iclusig Takeda 2012 Dec.
BCR-Abl, VEGFRs, Src family, etc.
CML, ALL
20 Trametinib Mekinist GSK 2013 May
MEK1/2
Melanoma and NCLSC (b-Raf V600E)
21 Dabrafenib Tafinlar GSK 2013 May
B-Raf V600E
Melanoma and NCLSC (b-Raf V600E)
22 Afatinib Gilotrif Boehringer Ingelheim 2013 Jul.
EGFR, ErbB2 (HER2), ErbB4
NSCLC
23 Ibrutinib Imbruvica Pharmacyclics/J&J 2013 Nov.
BTK
MCL, CLL, Waldenstrom's macroglobulinemia
24 Ceritinib Zykadia Novartis 2014 Nov.
ALK, IGF-1R, InsR, ROS1
NSCLC (+ALK resistance)
25 Idelalisib Zydelig Gilead 2014 Jul.
PI3Kδ
CLL, SCC, follicular lymphoma
26 Nintedanib Ofev Boehringer Ingelheim 2014 Oct.
FGFRs, PDGFRs, VEGFRs, FLT3, etc.
Idiopathic pulmonary fibrosis
27 Palbociclib Ibrance Pfizer 2015 Feb.
CDK4/6
Breast cancer (HR+/HER2-)
28 Lenvatinib Lenvima Easai 2015 Feb.
VEGFRs, PDGFR, FGFR, KIT, etc.
Differentiated thyroid cancer
29 Cobimetinib Cotellic Genentech 2015 Nov.
MEK1/2
Melanoma (b-Raf V600E/K)
30 Osimertinib Tagrisso AstraZeneca 2015 Nov.
EGFR T790M
NSCLC (EGFR T790M)
31 Alectinib Alecensa Genentech 2015 Dec.
ALK, RET
NSCLC (ALK+)
32 Ribociclib Kisqali Novartis 2017 Mar.
CDK4/6
Breast cancer (HR+/HER2-)
33 Brigatinib Alunbrig Takeda 2017 Apr.
ALK, ROS1, IGF-1R, FLT3, EGFR, etc.
NSCLC (ALK+)
34 Neratinib Nerlynx Puma 2017 Jul.
ErbB2 (HER2)
Breast cancer (HER2+)
35 Abemaciclib Verzenio Eli Lilly 2017 Sep.
CDK4/6
Breast cancer (HR+/HER2-)
36 Acalabrutinib Calquence AstraZeneca 2017 Oct.
BTK
MCL
37 Baricitinib Olumiant Eli Lilly 2018 Apr.
JAK1/2
Rheumatoid arthritis
38 Fostamatinib Tavalisse Rigel 2018 Apr.
SYK
Thrombocytopenia
39 Binimetinib Mektovi Array 2018 Jun.
MEK1/2
Melanoma (b-Raf V600E/K)
40 Encorafenib Braftovi Array 2018 Jun.
B-Raf V600E/K
Melanoma (b-Raf V600E/K)
41 Dacomitinib Vizimpro Pfizer 2018 Sep.
EGFR
NSCLC
42 Duvelisib Copiktra Verastem 2018 Sep.
PI3Kγ/δ
CLL, SLL, follicular lymphoma
43 Copanlisib Aliqopa Bayer 2018 Sep.
PI3Kα/δ
Follicular lymphoma
44 Lorlatinib Lorbrena Pfizer 2018 Nov.
ALK
NSCLC (ALK+)
45 Gilteritinib Xospata Astellas 2018 Nov.
FLT3
AML
46 Larotrectinib Vitrakvi LOXO/Bayer 2018 Nov.
NTRK
Solid tumors (+NTRK)
47 Netarsudil Rhopressa Aerie 2018 Dec.
ROCK
Glaucoma
Atropisomers
🟩 Bridged Diaryls
🟨 Biaryl
🟪 Benzamide/Anilide
☐ Pro-atropisomeric
Atropisomeric: 83% (39/47)
Pro-atropisomeric: 13% (6/47)
Non-atropisomeric: 4% (2/47)

Figure 2.2.2. FDA-approved small-molecule kinase inhibitors

We then evaluated our lead compounds against kinases that were predicted to bind ligands in a similar conformational window to that of RET, discovering that the lead RET inhibitor also possessed low nanomolar inhibitory activities towards EGFR mutants including the 3rd generation EGFR inhibitor-resistant L858R/T790M/C797S mutant, while sparing WT EGFR.

2.3 Discovery of (*R*$_a$)-3 as a Highly Potent and Selective Inhibitor of RET.

To form actionable SAR hypotheses to improve the potency and selectivity of the previous lead, Chapter 1's (*R*$_a$)-**1.1**, towards RET, we performed a series of *in silico* docking studies on various PPY inhibitors into a crystallographic model of RET (PDB 2IVV). Analysis of several docking poses suggested that the electronics of both aromatic rings (core pyrrolopyrimidine and aryl rings) of the inhibitors could influence affinity towards RET. Beginning with adjustments on the aryl ring, we synthesized **2.1** which possess a more electron neutral methyl in place of the chlorine at the *ortho*-aryl position in **1.1.** We measured **2.1**'s activity against RET using an ADP-Glo kinase inhibition assay (Table 2.3.1) finding no significant difference in affinity with the adjusted aryl ring electronics ((*R*$_a$)**-2.1** 1581 nM vs (*R*$_a$)**-1.1** 1857 nM RET IC$_{50}$). Next, moving the electron donating methoxy substituent to the *para* position in compound (*R*$_a$)-**2.2** showed little improvement in potency towards RET maintained potency (1871 nM RET IC$_{50}$) compared to (*R*$_a$)**-1.1**, however there was little difference observed between the atropisomers ((*R*$_a$)-**2.2** 1871 nM vs (*S*$_a$)-**2.2** 2998 nM RET IC$_{50}$). This is likely because the methoxy group was moved to a pseudo-symmetrical position of the ring, removing any potential atroposelective interactions it may have with RET's binding pocket. As the parent rapidly interconverting analog, **1.25**, possessed 10x selectivity RET over VEGFR2, but no selectivity for RET over SRC, the initial set of atropisomerically stable compounds (**2.1** – **2.8**) were also evaluated against SRC. Notably, the RET/SRC selectivity trends observed for **1.1** (3x RET/SRC) were either conserved in **2.1** (3x

RET/SRC) or slightly improved in **2.2** (5x RET/SRC), with the (*R*a)-atropisomer of each favoring RET. Next, we synthesized a PPY with a tri-substituted aryl ring (**2.3**) in which the (*R*a)-atropisomer lost potency towards RET yet **2.3**'s (*S*a)-atropisomer increased affinity towards SRC.

With the lack of significant improvement during the aryl ring optimization, we next focused on optimizing the PPY electronics. The initial docking studies predicted that (*R*a)**-1.1**'s 10x loss in potency towards RET compared to rapidly interconverting parent compound (**1.25**) was due to the weakening of a key hydrogen-bonding interaction between the pyrimidine and the kinase hinge region. Analysis of the docked poses suggested that this likely caused by the electron withdrawing chlorine attenuating the ability of *N*-5 to accept a hydrogen-bond (Figure 2.3.1A). Based on this, we synthesized **2.4** which possesses an electron donating methyl at the *C*-2 position, resulting in a significant increase in potency in kinase inhibition assays (Figure 2.3.1B). Surprisingly, compound **2.4** represented a case where each atropisomer's potency was increased toward their respective kinases, (*R*a) for RET and (*S*a) for SRC. **2.4** demonstrates that the strategy of using atropisomerism has the potential to be applied a variety of kinases using both atropisomers. Again, we coupled a more electron rich aryl ring, with the *C*-2 methyl core pyrrolopyrimidine (**2.5**) and saw no discernable difference between the chloro and methyl groups at the *ortho* position ((*R*a)**-2.5** 731 nM vs (*R*a)**-2.4** 699 nM RET IC_{50}).

We next synthesized and tested **2.6**, containing a bromine group at this position, which demonstrated affinity towards RET affinity comparable to that of *C*-2 chlorine in (*R*a)**-2.1** (1543 nM vs 1857 nM RET IC_{50}), providing evidence that it is the methyl's electronics influencing affinity rather than its size and lipophilicity. Extension of the alkyl group off the *C*-2 position as with methylene amine **2.8** proved nearly indistinguishable with methyl substitution in **2.7** ((*R*a)**-2.7** 450 nM vs (*R*a)**-2.8** 773 nM RET IC_{50}).

Table 2.3.1. *In vitro* inhibition of compounds **1.1**, **1.25**, **2.1** – **2.20**

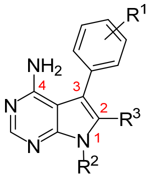

Compound	R^1	R^3	R^2	RET IC_{50}	SRC IC_{50}
1.25	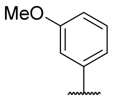	H	*t*-Bu	128	151
(R_a)-**1.1**	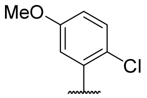	Cl	*t*-Bu	1857	5570
(S_a)-**1.1**		Cl	*t*-Bu	7659	1193
(R_a)-**2.1**	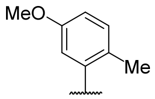	Cl	*t*-Bu	1581	4547
(S_a)-**2.1**		Cl	*t*-Bu	2243	4089
(R_a)-**2.2**	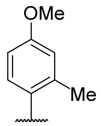	Cl	*t*-Bu	1871	>10000
(S_a)-**2.2**		Cl	*t*-Bu	2998	>10000
(R_a)-**2.3**	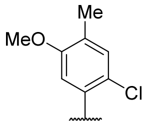	Cl	*t*-Bu	7066	>10000
(S_a)-**2.3**		Cl	*t*-Bu	4806	918
(R_a)-**2.4**	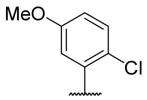	Me	*i*-Pr	699	1330
(S_a)-**2.4**		Me	*i*-Pr	2268	406
(R_a)-**2.5**	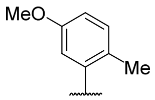	Me	*t*-Bu	731	6374
(S_a)-**2.5**		Me	*t*-Bu	2497	4104
(R_a)-**2.6**	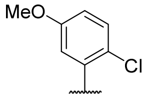	Br	*t*-Bu	1543	>10000
(S_a)-**2.6**		Br	*t*-Bu	8100	>10000
(R_a)-**2.7**	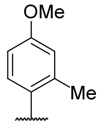	Me	*t*-Bu	450	3321
(S_a)-**2.7**		Me	*t*-Bu	918	4749
(R_a)-**2.8**	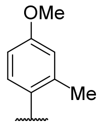	$MeNH_2$	*t*-Bu	773	5286
(S_a)-**2.8**		$MeNH_2$	*t*-Bu	9067	>10000

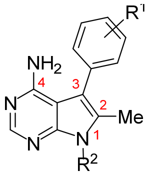

Compound	R^1	R^2	RET IC_{50}	SRC IC_{50}	VEGFR2 IC_{50}
(R_a)-**2.9**	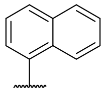	*i*-Pr	34	1366	938
(S_a)-**2.9**		*i*-Pr	8811	>10000	>10000
(R_a)-**2.10**	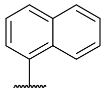	*t*-Bu	282	5572	5484
(S_a)-**2.10**		*t*-Bu	9565	>10000	>10000
(R_a)-**2.11**	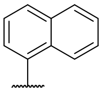	piperidine	189	2362	2823
(S_a)-**2.11**		piperidine	4449	>10000	>10000
(R_a)-**2.12**	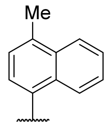	*i*-Pr	150	1650	601
(S_a)-**2.12**		*i*-Pr	2865	4560	>10000
(R_a)-**2.13**	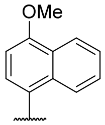	*i*-Pr	350	>10000	522
(S_a)-**2.13**		*i*-Pr	>10000	>10000	>10000
(R_a)-**2.14**	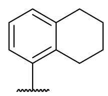	*t*-Bu	>10000	>10000	>10000
(S_a)-**2.14**		*t*-Bu	>10000	>10000	>10000
2.15[c]	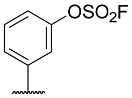	*t*-Bu	1140	>10000	>10000
(R_a)-**2.16**	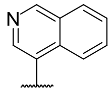	*t*-Bu	8	316	1031
(S_a)-**2.16**		*t*-Bu	282	7451	>10000
(R_a)-**2.17**	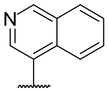	*i*-Pr	5	69	230
(S_a)-**2.17**		*i*-Pr	43	1073	853
(R_a)-**2.18**	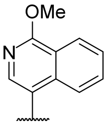	*i*-Pr	200	>10000	522
(S_a)-**2.18**		*i*-Pr	3533	9038	2351
(R_a)-**2.19**[b]	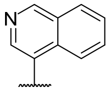	*i*-Pr	38	1421	413
(S_a)-**2.19**[b]		*i*-Pr	>10000	>10000	>10000
2.20[c]	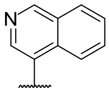	*t*-Bu	24	34	670

IC_{50}'s are reported in nM and were measured in duplicate using ADP-Glo assay (Promega). [b] C-2 position contains cyclopropyl. [c] C-2 position contains hydrogen.

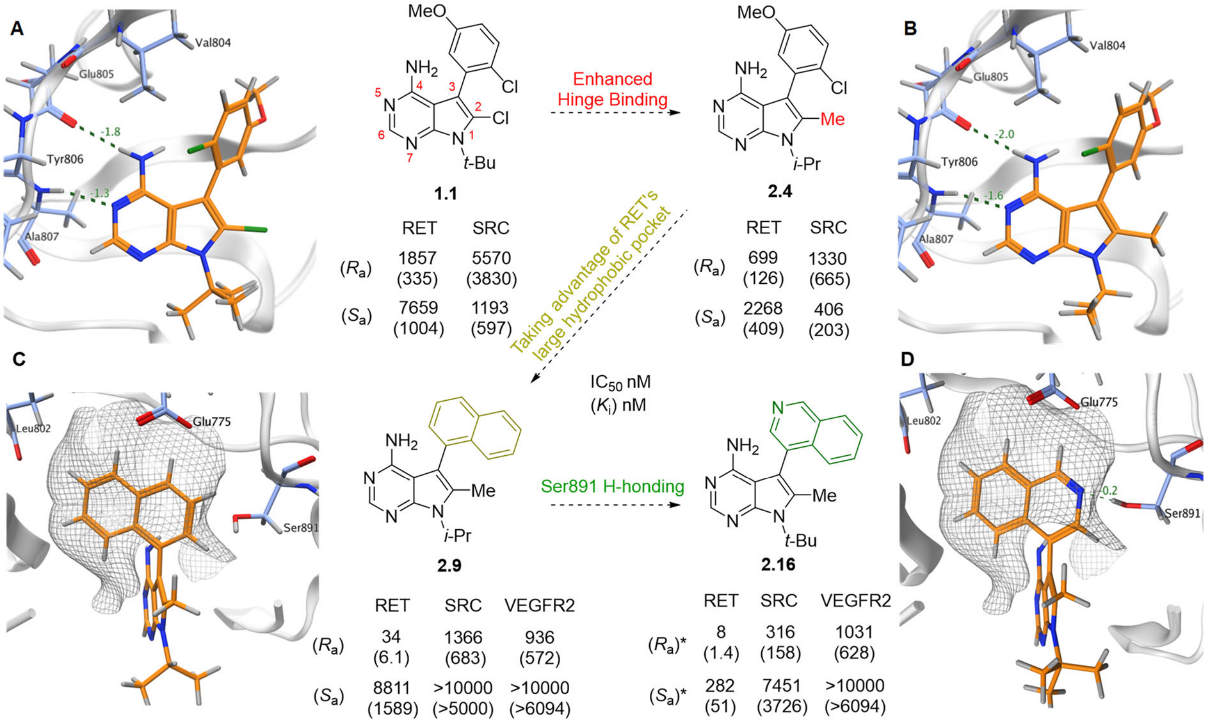
A
Val804
Glu805
Tyr806
Ala807
-1.8
-1.3
MeO
NH2
Cl
Cl
t-Bu
1.1
RET SRC
(Ra) 1857 (335) 5570 (3830)
(Sa) 7659 (1004) 1193 (597)
Enhanced Hinge Binding
MeO
NH2
Cl
Me
i-Pr
2.4
RET SRC
(Ra) 699 (126) 1330 (665)
(Sa) 2268 (409) 406 (203)
B
Val804
Glu805
Tyr806
Ala807
-2.0
-1.6
Taking advantage of RET's large hydrophobic pocket
IC50 nM
(Ki) nM
C
Leu802
Glu775
Ser891
NH2
Me
i-Pr
2.9
RET SRC VEGFR2
(Ra) 34 (6.1) 1366 (683) 936 (572)
(Sa) 8811 (1589) >10000 (>5000) >10000 (>6094)
Ser891 H-honding
NH2
Me
t-Bu
2.16
RET SRC VEGFR2
(Ra)* 8 (1.4) 316 (158) 1031 (628)
(Sa)* 282 (51) 7451 (3726) >10000 (>6094)
D
Leu802
Glu775
Ser891
-0.2

Figure 2.3.1. Docking studies on RET and in vitro results for select inhibitors.

A) (*R*a)-**1.1** docked in RET (front view). B) (*R*a)-**2.4** docked in RET (front view). C) (*R*a)-**2.9** (orange) docked in RET (side). D) (*R*a)-**2.16** (orange) docked in RET (side).

Comparison of the active sites of RET and other kinases suggested that the hydrophobic pocket beyond RET's Val804 gatekeeper residue could better accommodate extended aryl groups when the axis is in the (*R*a)-conformation. To test this hypothesis, we synthesized and evaluated PPYs that possessed polycyclic aromatic groups, finding that naphthyl-containing (*R*a)-**2.9** (Figure 2.3.1C) displayed significantly improved RET inhibition (RET IC_{50} of 34 nM (K_i of 6.1 nM)) and enhanced selectivity over SRC and VEGFR2 (112x and 94x, respectively; comparison of selectivity is based on K_i as it is independent of kinases' K_M). K_i values were calculated using the K_M of each kinase for ATP in the Cheng-Prusoff equation. Note that **2.9** is nearly a direct atropisomeric analog of the 'allele-specific' tool compound NA-PP1[117], however, we found (*R*a)-**2.9** to be 8-fold more potent towards RET with a modulated selectivity pattern across a panel of 25 kinases known to be inhibited by NA-PP1 (Figure 2.3.2).

Substituting *t*-Bu for *i*-Pr at off the *N*-1 position in compound (*R*a)-**2.10** increased the stereochemical stability to that of a class 3 atropisomer (ΔG of 30 kcal/mol vs 28.8 kcal/mol) but lost >10x potency across all tested kinases. Next, we installed a piperidine off the naphthyl-PPY in (*R*a)-**2.11**, which displayed good but attenuated potency (189 nM RET IC_{50} and selectivity (12x RET/SRC and VEGFR) towards RET. None the less the piperidine can serve as a handle for further optimization or as a site of incorporation of chemical biological motifs for future studies. Adding a group '*para*' to the PPY (**2.12** and **2.13**), showed decreases in RET affinity with IC_{50}'s of 150

	% Inhibition (50 nM)	% Inhibition (1000 nM)
Kinase	(R_a)-**2.9**	NA-PP1
ABL1	16	26
ACVR1B (ALK4)	7	65
BTK	4	49
EGFR (ErbB1)	7	28
EGFR (ErbB1) T790M	11	48
EPHA1	73	93
EPHB2	65	78
FGR	43	71
FLT3	6	13
FRK (PTK5)	41	89
FYN	8	45
HCK	17	59
KDR (VEGFR2)	10	24
LCK	12	52
LYN A	36	82
MAP4K4 (HGK)	52	92
MAP4K5 (KHS1)	12	69
MAPKAPK2	1	-2
MINK1	18	89
PDGFRB (PDGFR beta)	1	12
PTK6 (Brk)	34	98
RET	54	79
RET V804L	2	11
SRC	18	65
YES1	34	54

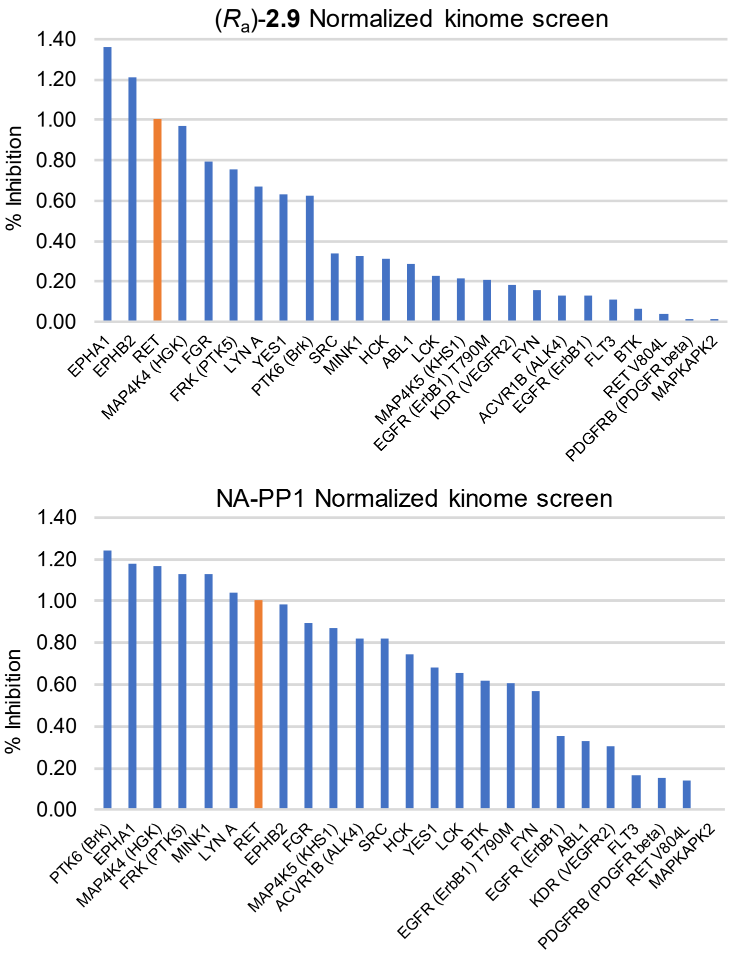

Figure 2.3.2. Partial kinome profiling of (*R*a)-**2.9** and NA-PP1[a]

[a] K_i's Partial kinome profiling of (*R*a)-**2.9** at 50 nM compared with previous literature profiling of NA-PP1 at 1000 nM[117]. Bar charts are normalized to level of RET inhibition for each kinome screen.

nM and 350 nM, respectively. The partially reduced analog 5,6,7,8-tetrahydronaphthalen-1-yl aryl ring of **2.14** proved inactive (>10000 nM RET IC_{50}), suggesting that RET (and other kinases) could not accommodate this bulky of a group in the hydrophobic pocket.

Further analysis of (R_a)-**2.9** docked into the RET active site revealed that there was a relatively non-conserved serine (Ser891) that could potentially be engaged (Figure 2.3.1D). While a fluorosulfate-containing[118] analog (**2.15**) possessed greatly diminished activities, we were able to exploit this serine with quinoline-containing (R_a)-**2.16**, that has an appropriately placed nitrogen to engage Ser891 in hydrogen-bonding. (R_a)-**2.16** inhibits RET with an IC_{50} of 8 nM (K_i=1.4 nM) and exhibits 110x selectivity over SRC and 436x over VEGFR2. Note that (R_a)-**2.16** possesses an *t*-Bu group *N*-1 position to increase the stereochemical stability to that of a class 3 atropisomer. We did synthesize and test the *N*-1 *i*-Pr analog of **2.16**, finding (R_a)-**2.17** had slightly increased potency albeit with a large drop in selectivity towards RET. Again, the potential to extend further into the binding pocket led us to synthesize a *para*-substituted heterocycle (**2.18**) but this extended analog lost significant potency towards RET compared to (R_a)-**2.16**. Adding a cyclopropyl group at the C-2 position in compound (R_a)-**2.19** lead to a loss in potency and selectivity for RET, however demonstrated the ability to incorporate different, bulkier groups, at this position for future inhibitors.

The synthesis of compounds **2.1** – **2.19** followed one of two synthetic routes described in Scheme 2.3.1 (see Appendix A.1 for extended synthesis and compound characterization). For compounds **2.1** – **2.8**, **2.15**, and **2.20**, the iodinated PPY core was synthesized following previous literature procedures. Following a Suzuki-Miyaura coupling with the appropriate aryl boronic acid, the PPY was aminated via S_NAr with NH_4OH in a microwave reactor. The increased electron density in the PPY core allowed for subsequent chlorination and bromination at the *C*-2 position.

Scheme 2.3.1. Condensed synthetic routes for compounds **2.1** – **2.20**.

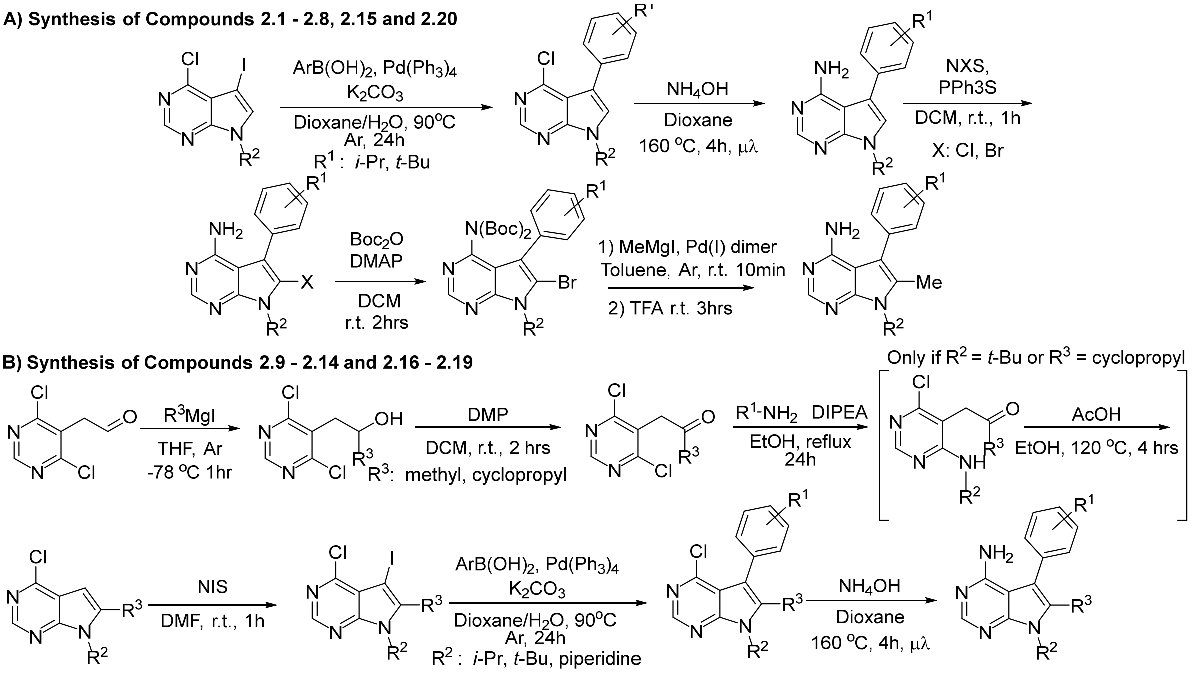
A) Synthesis of Compounds 2.1 - 2.8, 2.15 and 2.20
ArB(OH)2, Pd(Ph3)4
K2CO3
Dioxane/H2O, 90°C
Ar, 24h
R1 : i-Pr, t-Bu
NH4OH
Dioxane
160 °C, 4h, μλ
NXS,
PPh3S
DCM, r.t., 1h
X: Cl, Br
Boc2O
DMAP
DCM
r.t. 2hrs
1) MeMgI, Pd(I) dimer
Toluene, Ar, r.t. 10min
2) TFA r.t. 3hrs
B) Synthesis of Compounds 2.9 - 2.14 and 2.16 - 2.19
R3MgI
THF, Ar
-78 °C 1hr
DMP
DCM, r.t., 2 hrs
R3: methyl, cyclopropyl
R1-NH2 DIPEA
EtOH, reflux
24h
Only if R2 = t-Bu or R3 = cyclopropyl
AcOH
EtOH, 120 °C, 4 hrs
NIS
DMF, r.t., 1h
ArB(OH)2, Pd(Ph3)4
K2CO3
Dioxane/H2O, 90°C
Ar, 24h
R2 : i-Pr, t-Bu, piperidine
NH4OH
Dioxane
160 °C, 4h, μλ

The *C*-2 bromine then served as a site for late-stage functionalization, however due to severe steric hinderance at the *C*-2 position, only Copper-catalyzed cyanation and cutting-edge palladium chemistry proved effective with product isolated in moderate yields.

The synthetic route was optimized mid-project for compounds **2.9** – **2.14** and **2.16** – **2.19** once it was understood that the *C*-2 methyl substituent was critical for affinity, as well as an important sp^3 conformational locking group (Scheme 2.4.1B). The installation of the methyl early in the synthetic route allows for efficient, bulk synthesis of optimized core PPY scaffold. Subsequent late-stage incorporation of 'gate keeper' aryl rings allowed us to generate direct SAR trends for aryl substituents. To begin, the eventual *C*-2 methyl group was added via grignard addition to the pyrimidine aldehyde starting material. This reaction was amenable to other alkyl grignard reagents, such as cyclopropyl magnesium bromide, and can serve as a node to alter substituents at the C-2 position for later generations of PPY inhibitors. After methyl grignard addition, an oxidation with dess-martin periodinane was performed to access the ketone. At this stage, different alkyl amines were added via S_NAr. The less sterically incumbered isopropyl amine and piperidine amine cyclized after addition while the *tert*-butyl amine S_NAr intermediate needed to be purified and subjected to heat and acid to afford the desired cyclized product. Iodination at the PPY's 3-position creates the starting material for cross-coupling reaction with a range of boronic acids. Simple amination at the chlorine position yields the final inhibitors (**2.9** – **2.14** and **2.16** – **2.19**) in a more efficient manner (6 – 7 steps, 5 – 10 % overall yield).

As each synthetic step was performed racemically and/or at elevated temperature, the resulting racemic mixture of atropisomeric inhibitors were separated on a semi-preparative chiral-phase HPLC column to obtain enantiopure inhibitors. Prior to *in vitro* testing, stereochemistry was assigned for the lead compounds by using predictive and measured circular dichroism techniques (see Appendix A.1). It is important to note the chirality of **2.16** – **2.20** were assigned giving priority to steric bulk and is therefore consistent with the (R_a) binding conformations of **2.1** – **2.15**. If the later compounds' chirality were assigned with traditional IUPAC atomic priorities, the nomenclature would be reversed. Due to the dynamic nature of axial chirality, attention was given to the stereochemical stability of isolated enantiomers. Barrier to rotation energies and half-lives to racemization ($t_{1/2}$) were determined for lead compounds using standard methods described in Appendix A.1.

2.4 Selectivity of Atropisomeric (R_a)-2.16 Caused by Restriction of Accessible Conformations

We next evaluated both atropisomers of **2.16** for selectivity by subjecting them to inhibitor profiling across 127 kinases at 300 nM, more than 200x the K_i of (R_a)-**2.16** toward RET (See Appendix A.1). The panel was comprised of kinases known to bind 3-aryl substituted PPYs, kinases with high homology to RET, as well as common oncogenic kinases including RET mutants. At this concentration, 10% of WT kinases in the panel, primarily SRC and ephrin family kinases, were inhibited greater than 90% by (R_a)-**2.16**. To verify these results and gain a better idea of selectivity, we measured the K_i through 10-point titration curves for many of these kinases (Table 2.4.1), as well as EGFR and VEGFR2, two related receptor tyrosine kinases, to which many

Table 2.4.1. Selectivity of Inhibitors[a]

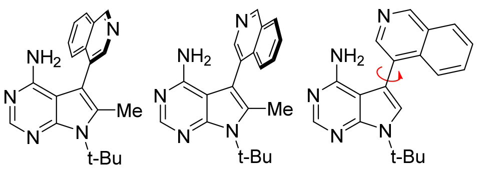

Kinase	(S_a)-**2.16**	(R_a)-**2.16**	*RET/ Kinase*	**2.20**	*RET/ Kinase*
RET K_i (nM):	51	1.4		4	
VEGFR2 K_i (nM):	>5000	628	*(436x)*	408	*(94x)*
ABL K_i (nM):	>5000	22	*(15x)*	26	*(6x)*
SRC K_i (nM):	3726	158	*(110x)*	17	*(4x)*
YES K_i (nM):	>5000	45	*(31x)*	50	*(12x)*
LCK K_i (nM):	>5000	119	*(83x)*	102	*(24x)*
BRK K_i (nM):	>5000	73	*(50x)*	65	*(15x)*
FRK K_i (nM):	1074	13	*(9x)*	13	*(3x)*
EGFR K_i (nM):	>5000	1623	*(1125x)*	721	*(167x)*
MINK K_i (nM):	-	212	*(147x)*	318	*(73x)*
HGK K_i (nM):	-	128	*(89x)*	146	*(34x)*

[a] K_i's are reported in nM and were measured in duplicate

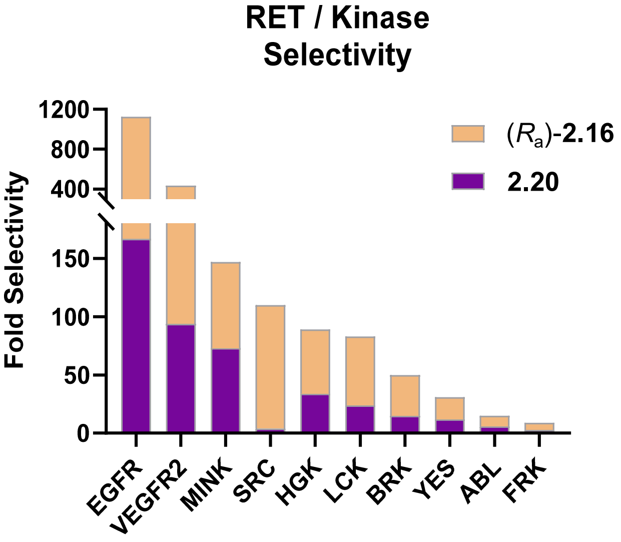

Figure 2.4.1. Graphical comparison of RET selectivity for (R_a)-**2.16** and **2.20** sorted by fold selectivity.

of the side effects of current RET inhibitors are attributed. These studies verified the selectivity of (R_a)-**2.16** as only FRK possessed a K_i within 10x of RET. Overall (R_a)-**2.16** exhibited a 10- to 100-fold preference for RET over the SRC family or similar kinases and exhibited significant selectivity for RET over EGFR and VEGFR2.

(S_a)-**2.16** proved to be significantly less potent against all kinases tested in both studies, suggesting that simply precluding the (S_a)-atropisomer was not the major driving force for increasing RET selectivity. To evaluate if there was an advantage to preorganized atropisomers in this case, we synthesized a rapidly interconverting derivative of (R_a)-**2.16**, (**2.20**, Table 2.4.1 and Figure 2.4.1) and evaluated it against the same panel of kinases, finding **2.20** was both less potent and selective towards RET. Specifically, (R_a)-**2.16** was 7x, 4.5x and 27x more selective than **2.20**

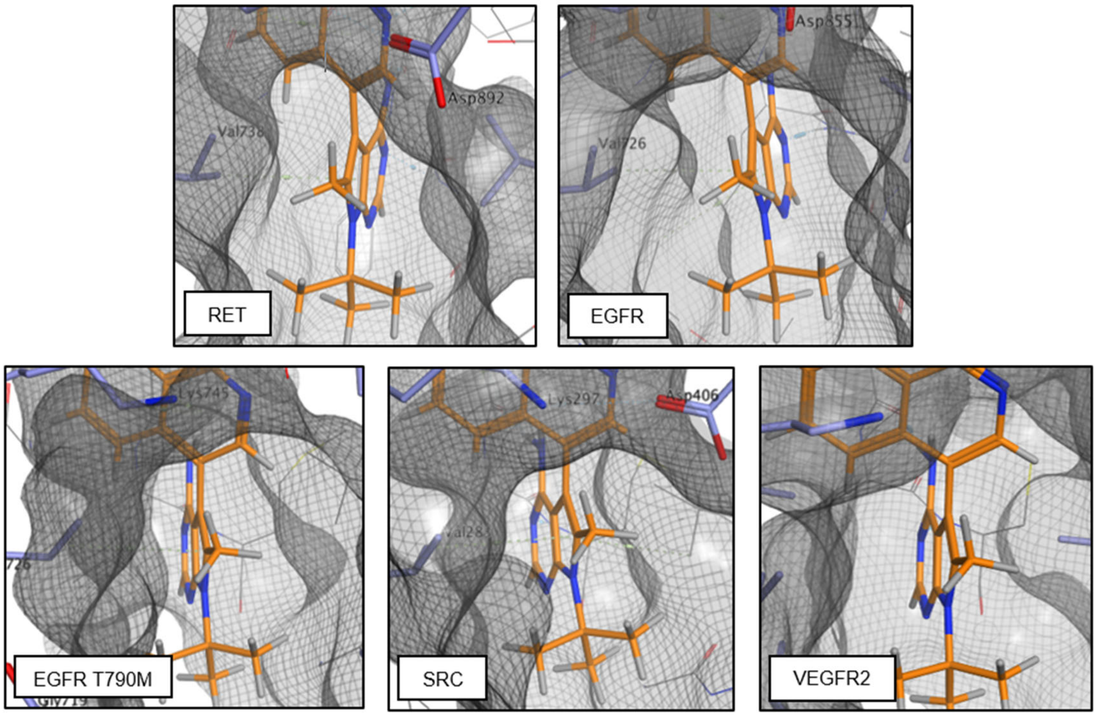

Figure 2.4.2. Docking studies of (R_a)-**2.16**

(R_a)-**2.16** in EGFR (PDB 2GS6), EGFR T790M (PDB 5YU9), RET (PDB 2IVV), SRC (PDB 1YOL), and VEGFR2 (PDB 3WZD). The pictures focused on the *C*-2 methyl group located near the conserved ribose pocket opening.

for RET over EGFR, VEGFR2, and SRC respectively. For the other kinases tested, the enhanced RET selectivity of (R_a)-**2.16** compared to **2.20** is largely due to the increased potency for RET (1.4 nM vs 4 nM RET K_i) as there was little change in the potency for these kinases between (R_a)-**2.16** and **2.20**.

As the *C*-2 methyl in (R_a)-**2.16** is likely oriented near a conserved large ribose pocket (Figure 2.4.2), the observed increases in selectivity towards RET compared to **2.20** are likely due to factors other than the kinases' interactions with the methyl group. Inspired by classic work from Jorgensen on the origins of the 'magic-methyl' effect[63], we hypothesized that the addition of a bulkier methyl group results in a shift of the low energy conformational window about the atropisomeric axis towards more orthogonal conformations. To investigate this further, we calculated the conformational energy profile (CEP)[119] of **2.16**'s and **2.20**'s atropisomeric axes using Guassian16 at the DFT-RB3LYP/6-31G(d) level (Figure 2.4.3). Focusing on the energy profile for the active (R_a)-conformation (which we define as θ = -180° to 0°), (R_a)-**2.16** (green) possesses a narrower low energy conformational window (defined as within 1.36 kcal/mol of the local minimum) of 80° (-130° to -50°). Accessing conformations outside this range would result in an energetic penalty that could correspond to a 10x loss in the inhibitor's kinase affinity. On the other hand, interconverting **2.20** (blue) has a conformational window of 105° about the aryl-aryl axis (-140° to -35°). If you include the (S_a) conformational window, **2.20** can access 210° of conformations within 1.36 kcal/mol.

Calculating the CEP for the often used chemical probe PP1 (**2.21**, a pyrazolopyrimidine ligand, in purple)[61] and generic PPY scaffold **2.22** (orange), each of which possess no *ortho* substituents, revealed these compounds to have significantly different profiles of low energy conformations. PP1 and **2.22** each possessed a low energy window of 90° (180° including the (S_a)-

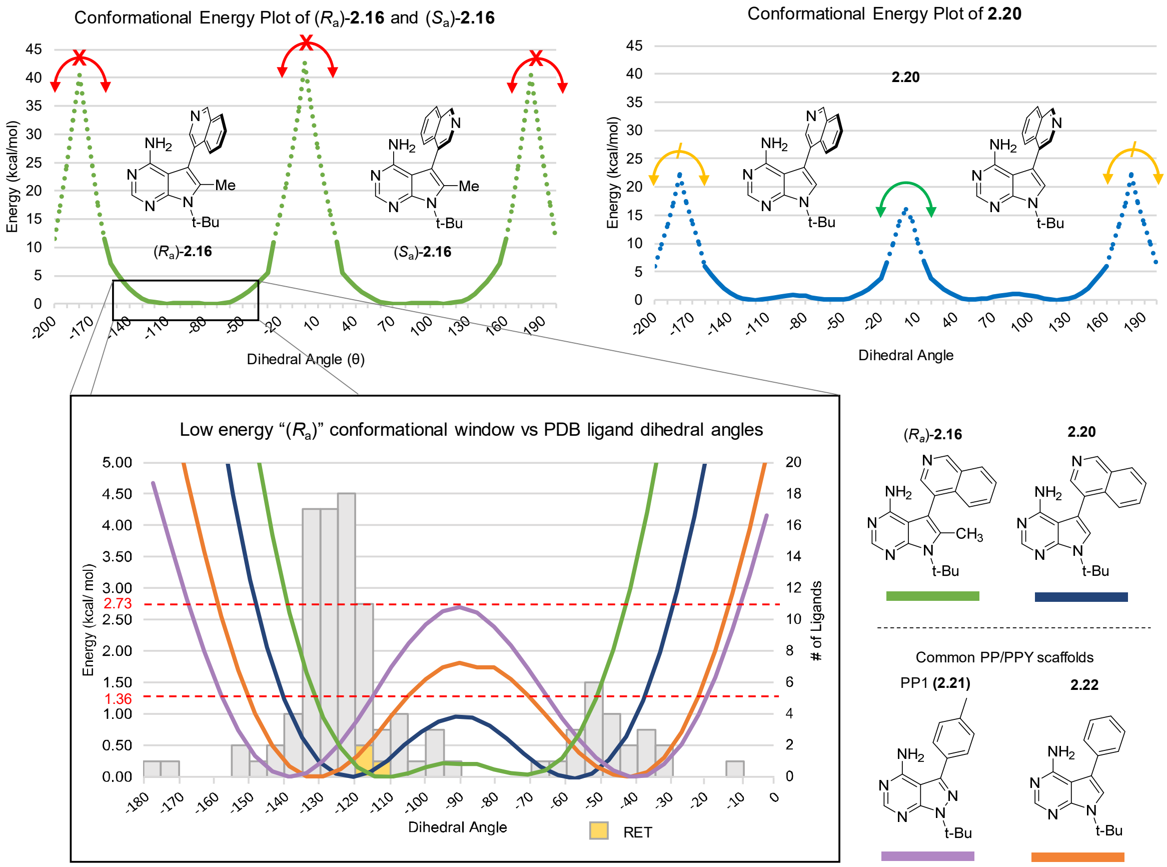

Figure 2.4.3. Conformational binding map of PP/PPY ligands.

Analysis of conformational energy profiles for certain scaffolds superimposed with the dihedral angles of co-crystalized ligands obtained from Protein Data Bank (PDB). Red dotted lines represent the conformational energy at which the inhibitor would lose 10x binding affinity towards its target.

conformations), each broken up into two windows (PP1: -160° to -115° and -65° to -20°; **2.22**: -150° to 105° and -70° to -25°).

We then analyzed the dihedral angles of 109 PPY and PP ligands bound to 29 kinases from x-ray crystal structures deposited at the PDB (See Appendix A.1 for a complete list). 56 ligands possess substitution patterns that render them type 1 atropisomers, with 46/56 exhibiting dihedral angles between -180° and 0° (corresponding to the active conformation of **2.16**), and 10/56 displaying dihedral angles between 0° and 180° (corresponding to the inactive enantiomer). The remaining 53 bound ligands are ‘pro-atropisomeric’. Most ligands bound their targets with dihedral angles between -140° to -105° and -60° to -35°, overlapping well with the low energy conformations of PP1 (**2.21**) and generic PPY ligand **2.22** (Figure 2.4.3). Of the 109 bound ligands, 85% and 91% fell within the low energy window (within 1.36 kcal/mol of local minima) for **2.21** and **2.22** respectively. Accordingly, 91% of the ligands fell within the low energy conformations of **2.20**.

Interestingly, only 60% of the kinase-bound ligands fell within the low energy conformations of (R_a)-**2.16**. While ~20% of the precluded ligands correspond to those of the other atropisomer, the preclusion of the remaining 80% is a result of restricting the range of accessible low energy dihedral angles. Analysis of the three RET structures in the data set revealed that the ligands (PP1 in each case) bound RET (PDB 2IVV, 5FM2, 5FM3) with dihedral angles between -111° and -117° which are at or near the local minimum for (R_a)-**2.16**, and correspond to destabilized conformations (vs the local minima) for the other ligands analyzed. We next reviewed the aforementioned kinase inhibitor profiling experiment for other kinases that bound their respective ligands with similar dihedral angles to that of RET, finding these kinases were significantly inhibited by (R_a)-**2.16** at 300 nM (LYN 80% activity inhibited, LCK 75%, and HCK 74%). To further verify the observations gleaned from the analysis of the crystallographic data, we turned to docking studies followed by molecular dynamic (MD) simulations to predict the preferential binding window of dihedral conformations for a given kinase to its PP or PPY ligand. We performed these MD simulations on kinases for which there is crystallographic data bound to PP or PPY ligands (RET, SRC) using (R_a)-**2.16**, **2.20** and PP1 (Figure 2.4.4). For RET, the predicted binding windows for (R_a)-**2.16**, and to a slightly lesser extent **2.20**, overlap well with both the CEP’s low energy window and the observed dihedral angles observed in the PDB.

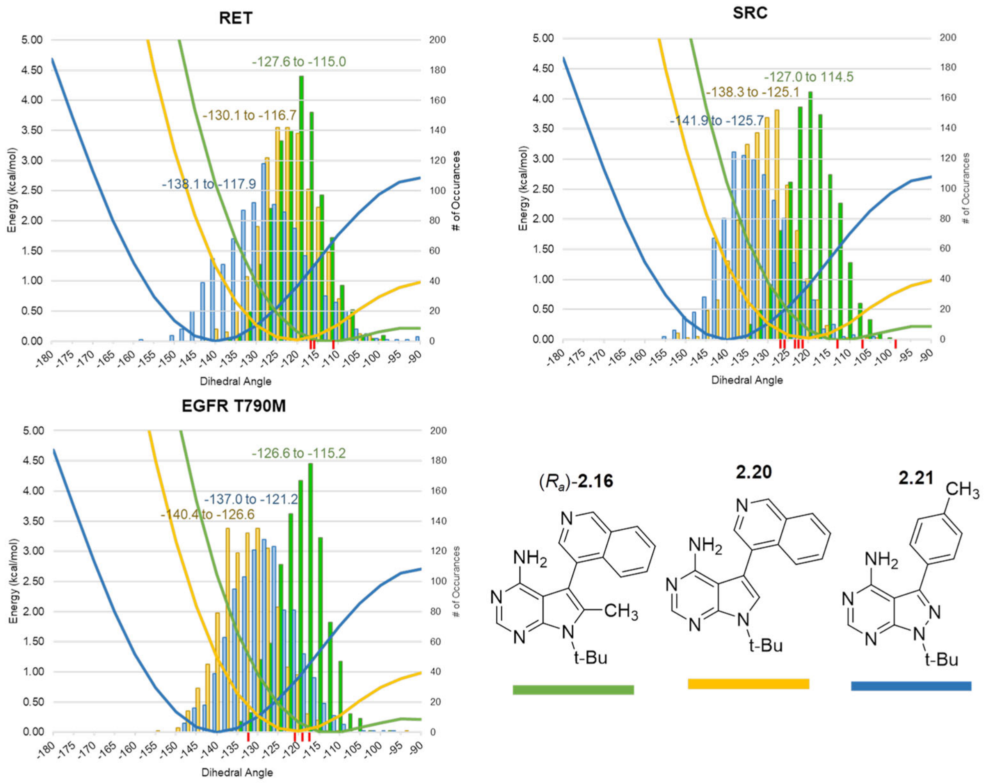

Figure 2.4.4. Molecular Dynamic simulations of (*R*a)-**2.16**, **2.20**, and PP1 (**2.21**) in RET, SRC and EGFR T790M.

Ligands' dihedral angles were recorded every 0.5 ns for 500 ns (1000 total) in RET (PDB 2IVV), SRC (PDB 1YOL), and EGFR T790M (PDB 5YU9). Red marks represent the dihedral angles of PP or PPY ligands co-crystalized with each kinase in PDB

On the other hand, there was poor overlap between the crystallographic data and the predicted binding window of PP1, which binds RET with an attenuated affinity compared to (*R*a)-**2.16** and **2.20** (K_i of 40 nM[120]), perhaps because PP1 is forced to bind RET in a conformation that is greater than 1 kcal/mol higher in energy than its local minima. For SRC, the predicted binding window for **2.20** overlapped almost perfectly with the bulk of dihedral angles observed in the PDB, whereas there is poor overlap between the crystallographic data and the predicted binding windows of (*R*a)-**2.16** and PP1, perhaps explaining why **2.20** possesses 10x higher potency towards SRC than PP1 or (*R*a)-**2.16** (17 nM for **2.20**, 158 nM for (*R*a)-**2.16**, and 170 nM for PP1).

While analyzing ligands' dihedral angles found in PDB, we observed that the T790M mutant of EGFR binds PP ligands (5GTY, 5J9Y, 5J9Z, 5GNK, 5YU9) in a similar range to that of RET, well within the low energy conformational window of (R_a)-**2.16**. Indeed, performing the aforementioned docking and MD studies predicted that T790M EGFR mutants would bind (R_a)-**2.16** and PP1 ligands in a conformational window similar to that of RET, and thus predicts that (R_a)-**2.16** will possess significant affinity towards EGFR T790M harboring mutants. This led us to evaluate (R_a)-**2.16** against a panel of EGFR and its mutants (Table 2.4.2). These studies confirmed that (R_a)-**2.16** possessed little WT EGFR activity (1623 nM K_i) but proved quite potent towards the T790M mutant (16.5 nM). This mutant EGFR activity extended to the L858R mutant (77 nM), double mutant L858R/T790M (15.8 nM), and triple mutant L858R/T790M/C797S (53 nM).

Table 2.4.2 Inhibitor activity on WT EGFR and mutants[a]

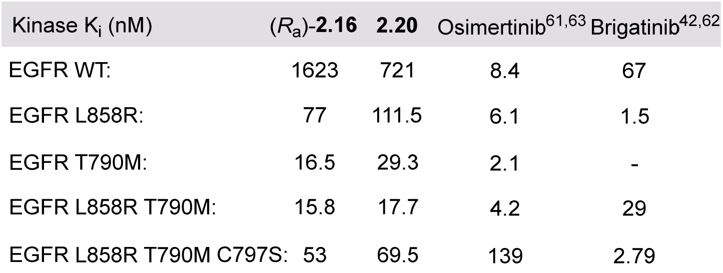

Kinase K_i (nM)	(R_a)-**2.16**	**2.20**	Osimertinib[61,63]	Brigatinib[42,62]
EGFR WT:	1623	721	8.4	67
EGFR L858R:	77	111.5	6.1	1.5
EGFR T790M:	16.5	29.3	2.1	-
EGFR L858R T790M:	15.8	17.7	4.2	29
EGFR L858R T790M C797S:	53	69.5	139	2.79

[a] K_i's are reported in nM and were measured in duplicate

While less potent toward EGFR mutants than to RET, (R_a)-**2.16** compares favorably to the state-of-the-art EGFR inhibitors as it possesses significantly improved mutant over WT selectivity[115,121–123], which could result in an improved toxicological profile. It is also worth noting that a RET fusion (RET-CCDC6) has been implicated as another mechanism of acquired resistance to 3rd generation EGFR inhibitors.[90] Thus, a dual RET/EGFR mutant inhibitor may be of use for patients irrespective of acquisition of the C797S mutation.

2.5 Cellular Activity of (R_{a})-2.16

We next tested both atropisomers of **2.16**, racemizing **2.20**, and vandetanib (the current standard of care RET inhibitor) in cellular models of RET-driven cancers and non-RET-driven control cell lines (Table 2.5.1). (R_{a})-**2.16** inhibited cell growth of all RET-driven cell lines with GI_{50} values of approximately 1 μM, including cells with RET fusions (CCDC6-RET-driven LC-2 NSCLC cells), RET mutants (C634W in TT thyroid cancer cells) and overexpressed WT RET (estrogen deprived MCF7 (ED-MCF7) cells in the presence of 20 nM of RET activating ligand GDNF). As WT RET is dependent on GDNF for activity, we were able to compare the effect of inhibition of RET in ED-MCF7 cells to that of RET inactivation in the same cell line by removal of GDNF model (Figure 2.5.1A). This study revealed that at 3μM, (R_{a})-**2.16** inhibited cell growth of +GDNF ED-MCF7 to a similar level as that of the -GDNF ED-MCF7 control cell line. This suggests that the observed cellular effect at 3μM of (R_{a})-**2.16** recapitulates complete RET inactivation in this.

Table 2.5.1 Anti-proliferative effects of inhibitors on RET-driven cell lines and controls.[a]

Cell line	(R_{a})-**2.16**	(S_{a})-**2.16**	**2.20**	Vandetanib	BLU-667[28]
LC-2/AD (CCDC6-RET)	2.81	>10	4.3	1.47	0.004[b]
TT (RET C634W)	1.45	>10	2.59	1.01	0.015[b]
ED-MCF7 (overexpressed WT RET)	1.15	>10	1.31	0.25	-
BT474 (+ER, PR and HER2)	>10	>10	>10	5.91	>10
H292 (overexpressed WT EGFR)	>10	>10	>10	1.14	>10

[a] Cell growth GI_{50}'s are reported in μM and were measured in triplicate. [b] Data taken from Ref. 28

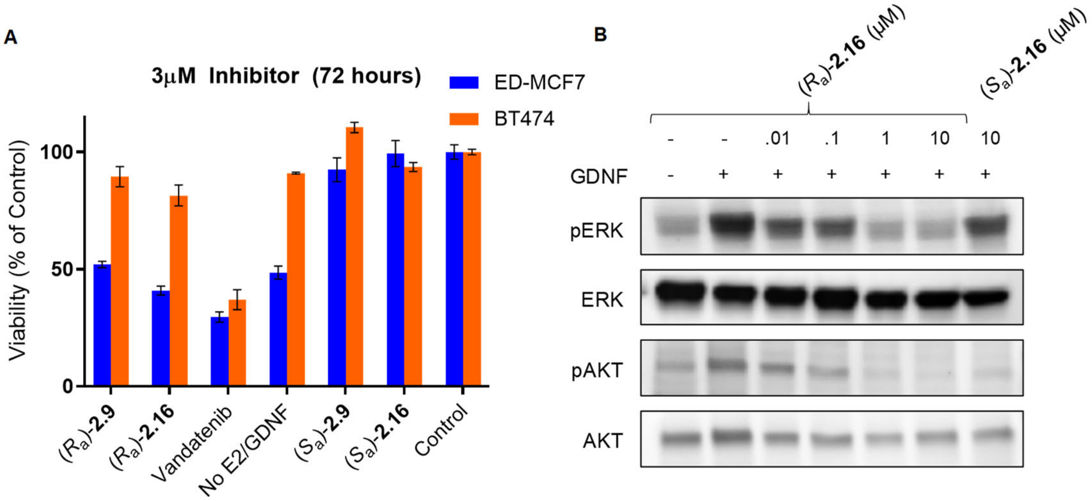

Figure 2.5.1. Breast cancer cell line experiments with (S_{a})-**2.16** and (R_{a})-**2.16**.

A) 72-hour estrogen deprived MCF7 (ED-MCF7) and BT474 cellular viability assays in the presence of 3μM inhibitor or absence of 1nM estradiol (E2) and 20nM GDNF. B) Western blots of varying concentrations of (S_{a})-**2.16** and (R_{a})-**2.16** in estrogen deprived MCF7 cells in the presence or absence of 20nM GDNF after 30min.

To further investigate the downstream effects of (R_{a})-**2.16** on the RET signaling pathway, we measured the level of phosphorylation of the kinases AKT and ERK in ED-MCF7 cells under varying conditions. In the presence of GDNF, complete loss of phosphorylation is observed at 1μM (R_{a})-**2.16** in both AKT and ERK (Figure 2.5.1B). Consistent with the *in vitro* data, (S_{a})-**2.16** had no effect on the cell lines while the racemizing **2.20** was roughly 2x less active than (R_{a})-**2.16**. Importantly, (R_{a})-**2.16** displayed no observable anti-proliferative activity against cell lines (BT474 and H292) that are not driven by RET. On the other hand, vandetanib significantly inhibited the growth of these control cell lines. In light of the -GDNF ED-MCF7 experiment, it is likely that the additional anti-proliferative effects of vandetanib compared to (R_{a})-**2.16** on the RET-driven cell lines is due to off-target kinase inhibition.

Next, we turned to cellular models driven by mutants of EGFR (Table 2.5.2). (R_{a})-**2.16** displayed moderate activity relative to current 3rd generation EGFR inhibitors with a GI$_{50}$ of 4.35

Table 2.5.2 Anti-proliferative effects of inhibitors on EGFR-driven cell lines and controls.^{a}

Cell line	(R_a)-**2.16**	(S_a)-**2.16**	**2.20**	Osimertinib	Brigatinib
H292 (overexpressed WT EGFR)	>10	>10	>10	3.75	2.76
H1975 (EGFR L858R/T790M)	4.3	>10	5.0	0.343	0.890
Ba/F3 (EGFR L858R)	2.27	>10	2.60	0.015	0.385
Ba/F3 (EGFR L858R/T790M)	5.87	>10	8.38	0.064	0.527
Ba/F3 (EGFR L858R/T790M/C797S)	5.42	>10	6.20	3.18	0.882
Ba/F3 (empty vector)	>10	>10	>10	2.76	2.10

^{a}Cell growth GI_{50}'s are reported in µM and were measured in triplicate.

µM in L858R/T790M-driven H1975 cells. Notably, (R_a)-**2.16** did not exhibit any activity (>10µM GI_{50}) towards H292 cells driven by overexpression of WT EGFR while the more promiscuous vandetanib did (1.14 µM GI_{50}), validating the mutant selectivity of (R_a)-**2.16**. To gain a clearer picture of cellular activity of (R_a)-**2.16** against the triple mutant, we generated Ba/F3 cell lines that were dependent upon the phosphorylation activity of mutants L858R, L858R/T790M and L858R/T790M/C797S EGFR. In agreement with our other observations, (R_a)-**2.16** possessed low to mid-single digit µM activities against each EGFR mutant-driven Ba/F3 cell line, while displaying no activity against a control IL-3 dependent Ba/F3 cell line. Brigatinib and Osimertinib displayed improved inhibition of these cell lines, however also displayed significant activities against WT driven H292 and the control IL-3 dependent Ba/F3 cell line, suggesting that a portion of these drug's observed activities are due to inhibition of other kinases. The activity of (R_a)-**2.16** in the triple mutant-driven Ba/F3 cell line is notable as, to the best of our knowledge, it represents the first example of a highly WT EGFR sparing small molecule that displays appreciable activity in this model as a single agent. While further structural optimization is needed to obtain a therapeutic agent and chemical probe for EGFR mutant inhibition, (R_a)-**2.16** represents an exciting lead towards these ends.

2.6 Conclusion

By introducing stable atropisomerism into a promiscuous unstable atropisomeric scaffold, we were able to access a highly potent and selective inhibitor of RET kinase, an emerging oncogenic target. We obtained drastic improvements in potency and selectivity by strategically adding five non-hydrogen atoms to a highly promiscuous kinase inhibitor scaffold (PP1). The lead compound, (*R*a)-**2.16** displays 2-3 orders of magnitude selectivity for RET over EGFR and VEGFR2, kinases whose off-target inhibition leads to well-characterized adverse events in patients. (*R*a)-**2.16** displays good antiproliferative activities in RET-driven models of thyroid cancer, breast cancer, and non-small cell lung cancer, and importantly has no observable effects against cell lines that are not RET-dependent. These studies validate (*R*a)-**2.16** as a chemical probe to study RET's biology, as well as an intriguing lead towards a new generation of selective RET inhibitors.

To better understand the origin of the observed improvements in RET potency and selectivity upon introducing atropisomerism, we performed an analysis of 109 cocrystal structures of kinases bound to PP and PPY scaffolds. Comparing the observed dihedral angles with the predicted conformational energy profiles of (*R*a)-**2.16**, **2.20,** and PP1 suggests that the major driver of selectivity is the narrowing of the low energy conformational window about the atropisomeric axis. In other words, (*R*a)-**2.16** is preorganized into a conformational window optimal for RET, but less optimal for other kinases. As such, the observed effects on selectivity and potency when introducing stable atropisomerism are related to Jorgensen's seminal explanation for the origins of the 'magic methyl effect'. While these effects may not be a direct consequence of atropisomerism, rigidifying the axis to the point of atropisomer stability is likely unavoidable in order to design compounds that favor conformations approaching orthogonality. Furthermore, our analysis did reveal a small but significant number of kinases (20%) preferred ligands that were bound in the (*S*a)-conformation, and off-target inhibition of these kinases would be avoided with an atropisomerically constrained compound. Moreover, if one desires to target any of these 20% of kinases, leveraging atropisomerism would appear to be a promising strategy to obtain selective leads. Note that there are other examples of rigidification of kinase inhibitors to improve the selectivity of an inhibitor independent of atropisomerism.[124]

Extending this analysis to other kinases predicted that EGFR mutants would also prefer to bind PP-type ligands with a conformational window similar to that of RET, leading us to evaluate (*R*a)-**2.16** against a series of EGFR mutants. We found (*R*a)-**2.16** to spare WT EGFR but potently inhibit several EGFR mutants, including the vaunted L858R/T790M/C797S triple mutant. This activity held in cellular models of mutant EGFR driven cancer, including triple mutant dependent Ba/F3 cell lines. While we need to further optimize this scaffold for EGFR mutants, (*R*a)-**2.16** represents, to the best of our knowledge, the first example of a highly mutant selective EGFR inhibitor that displays cellular activity as a single agent towards the triple mutant driven cell line, rendering it a lead towards a 4th generation EGFR therapy for NSCLC.

In conclusion, this work suggests that controlling the accessible dihedral angles of a potentially atropisomeric axis can function as a useful strategy to modulate an inhibitor's selectivity profile. While this hypothesis needs further validation across different atropisomeric scaffolds and target classes, we hope that this work can serve as tool to guide the design and discovery of more selective chemical probes and therapeutics.

2.7 Acknowledgements

Chapter 2 is reformatted reprint with permission from Toenjes, S.; Garcia, V.; Maddox, S.; Dawson, G.; Ortiz, M.; Piedrafita, F.; Gustafson, J. Leveraging Atropisomerism to Obtain

Selective Inhibitors of RET Kinase with Secondary Activities towards EGFR Mutants. *ACS Chem. Biol.* **2019**, *14*, 1930-1939. This work supported by NIH grant R35GM124637 awarded to J. Gustafson. We thank D. Hecht (Southwestern College) for insight and help with the MD simulation studies.

Chapter 3: Controlling Ibrutinib's Conformations to Obtain Selective BTK Inhibitors

3.1 Introduction

Bruton's Tyrosine Kinase (BTK) is a cytoplasmic Tec family kinase involved in controlling immune response through the B-cell receptor (BCR) signaling pathway.[125] Upon association to activated BCR and subsequent phosphorylation by Src family kinases, BTK phosphorylates PLCγ2 to extend BCR's signal downstream to the calcium and MAPK pathways.[126] Aberrant BCR signaling can lead to autoimmune diseases such as rheumatoid arthritis (RA) and systemic lupus erythematosus (SLE) as well as B-cell malignancies such as mantle cell lymphoma (MCL) and chronic lymphocytic leukemia (CLL).[127,128] A number of research groups have shown genetic knockdown or small molecule inhibition of BTK reduces cell growth in lymphoma cell lines and disease severity in RA and SLE mouse models.[129,130] These efforts, primarily in oncology, have led to FDA-approval of three BTK inhibitors, Ibrutinib, Acalabrutinib and Zanubrutinib, for the treatment of patients with MCL (all 3 drugs) and CLL (Ibrutinib and Acalabrutinib).[130–133]

Each of these drugs, along with majority of BTK inhibitors, possess an electrophilic motif to covalently bind BTK's nucleophilic Cys481 residue located near the ATP-binding pocket. While these irreversible inhibitors possess high affinity towards BTK, they typically lack selectivity particularly within the subset of kinases that possess a cysteine residue in a similar region as BTK.[130] Off-target inhibition of these kinases, including ITK, TEC, BLK, EGFR, and JAK3, can lead to adverse events not observed in BTK deficient patients, such as rash, atrial fibrillation and major hemorrhage.[134–136] Due to these issues, immense research efforts have focused on increasing selectivity using traditional medicinal chemistry approaches such as optimizing the inhibitor's gate-keeper aryl or electrophilic handle; yielding more selective drugs like Acalabrutinib. However, more unconventional selectivity filters are needed in drug development to sample different chemical space particularly for BTK inhibitors, a class of inhibitors haunted by promiscuity.

Often overlooked when designing small molecule inhibitors is the 3D spatial orientation of the inhibitor and how it correlates to potency and selectivity. As designed, each generation of BTK inhibitor (and 83% of all FDA-approved kinase inhibitors) possess rotatable bonds between asymmetric aromatic rings, leading to instances of axial chirality known as atropisomerism (Figure 3.1.1). These flexible axes can rotate a full 360°, allowing the inhibitor to adopt a large range of conformations to fit the target's binding pocket. Unfortunately, these molecules can flex to other conformations that can bind off-target kinases critical for healthy biological functions.

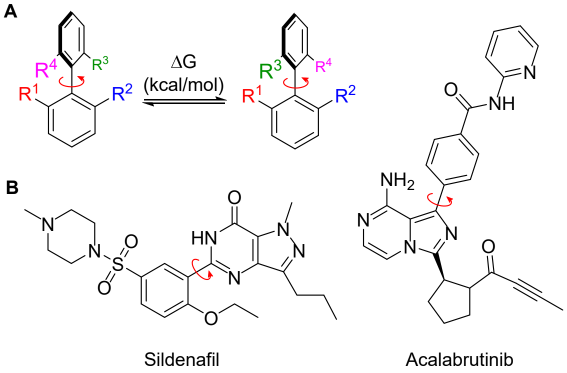

Figure 3.1.1. Atropisomerism and examples of flexible, atropisomeric FDA-approved drugs.

3.2 BTK on the PP/PPY Conformational Binding Map

Chapter 2's work described a strategy of increasing selectivity of flexible pyrrolopyrimidine (PPY) inhibitors by preorganizing them into distinct conformations preferred by two targets, RET and mutant EGFR.[137] To help explain the broad increases in selectivity across the kinome, we generated a map that reveals a kinase's preferred pyrrolopyrimidine (PPY) or pyrazolopyrimidine (PP) binding inhibitor conformation using PDB co-crystal structures (Figure 3.2.1, grey columns). When superimposing the calculated the conformational energy plots (CEPs) of the different inhibitors, we observed the increase in selectivity originates from the narrowing of rigid, atropisomer inhibitor's accessible conformations to a window covering RET and EGFR's preferred binding dihedral angle. Like RET and mutant EGFR, BTK also bound its inhibitors in a similar region around -120° suggesting this strategy of confining an inhibitor's conformational space near orthogonality via stable atropisomerism could be amenable to BTK. In addition, both Ibrutinib and Acalabrutinib possess an atropisomeric PP scaffold, so their structures can serve as a guide for our inhibitor optimization and can be represented in the PP/PPY conformational binding map.

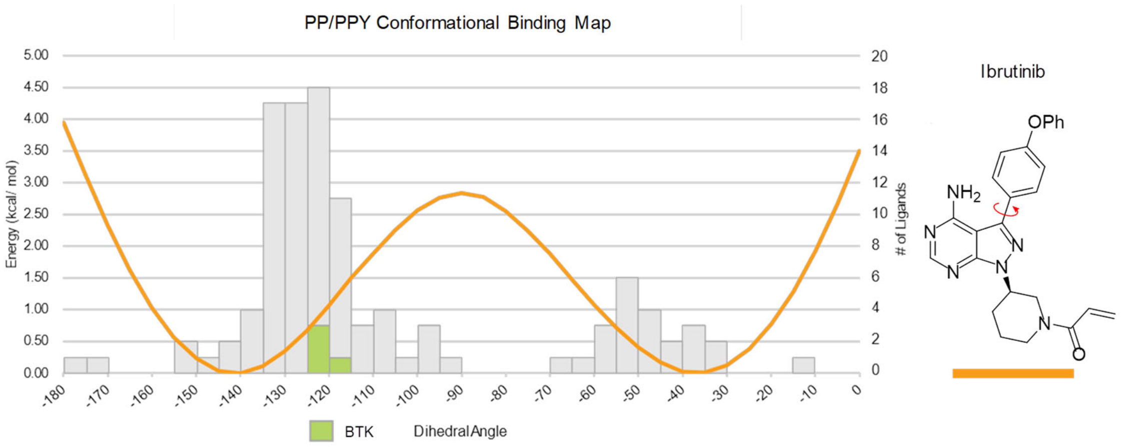

Figure 3.2.1. PP/PPY Conformational Binding Map.

PDB structural analysis of PP or PPY ligands bound to kinases (gray, BTK in green) with Ibrutinib's conformational energy plot superimposed (orange).

3.3 Development of Atropisomerically Stable Analogs of Ibrutinib

In this chapter we develop preorganized analogs of ibrutinib that sample a range of conformational space to extend our strategy to a new target, BTK. During inhibitor optimization, we encountered unintended consequences when incorporating steric bulk to this scaffold and developed ways to circumvent these issues. To begin, we analyzed the binding pockets of four PDB BTK structures co-crystalized with freely rotating, unsubstituted PP/PPY ligands (Figure 3.2.1, green). Two key observations where made: 1) Each ligand bound BTK with its atropisomeric dihedral angle between -123.98° and -119.57° and 2) there is a hydrophobic cavity near each ligands' aryl *ortho* position (Figure 3.3.1). This suggests that BTK would have an atropisomeric preference to bind the (R_a)-atropisomer with a hydrophobic substituent orientated in the -180° - 0° dihedral angle range. We also noticed the PP nitrogen (*N*-2), *ortho* to Ibrutinib atropisomeric axis, is directed towards a conserved space, vacant of BTK amino acids. Incorporation at this site, in combination with an aryl *ortho* substituent, would likely rigidify the axis generating two separable atropisomers each possessing narrower CEP than Ibrutinib's (Figure 3.2.1, orange), with the (R_a)-atropisomer's CEP in range of BTK's -120° preferred dihedral angle. Similar to the lead RET/EGFR mutant inhibitor from Chapter 2, the proposed rigid analog's

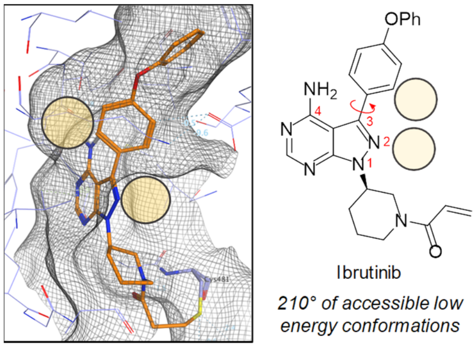

Figure 3.3.1. Rigidification strategy of Ibrutinib with two conformationally locking groups.

selectivity could be enhanced as its unable to access less orthogonal conformations preferred by other kinases.

To incorporate substituents at the 2 position, we moved to the PPY scaffold which contains a functionalizable C-H in place of the PP scaffold's N-electron lone pair. Synthesis of the PPY scaffold begins with subjecting 2-(4,6-dichloropyrimidin-5-yl)acetaldehyde to MeMgI via grignard addition (Scheme 3.3.1). After oxidizing the alcohol to a ketone with dess-martin periodinane, the ketone underwent a cyclodehydration + S$_N$Ar with *N*-boc-protected 3-aminopiperidine at 80°C in DME in the presence of TEA to afford the cyclized pyrrolopyrimidine scaffold with a *C*-2 methyl. For unsubstituted *C*-2 PPYs, *N*-boc-protected 3-aminopiperidine was

Scheme 3.3.1. Synthesis of pyrrolopyrimidine analogs **3.1 – 3.6**.

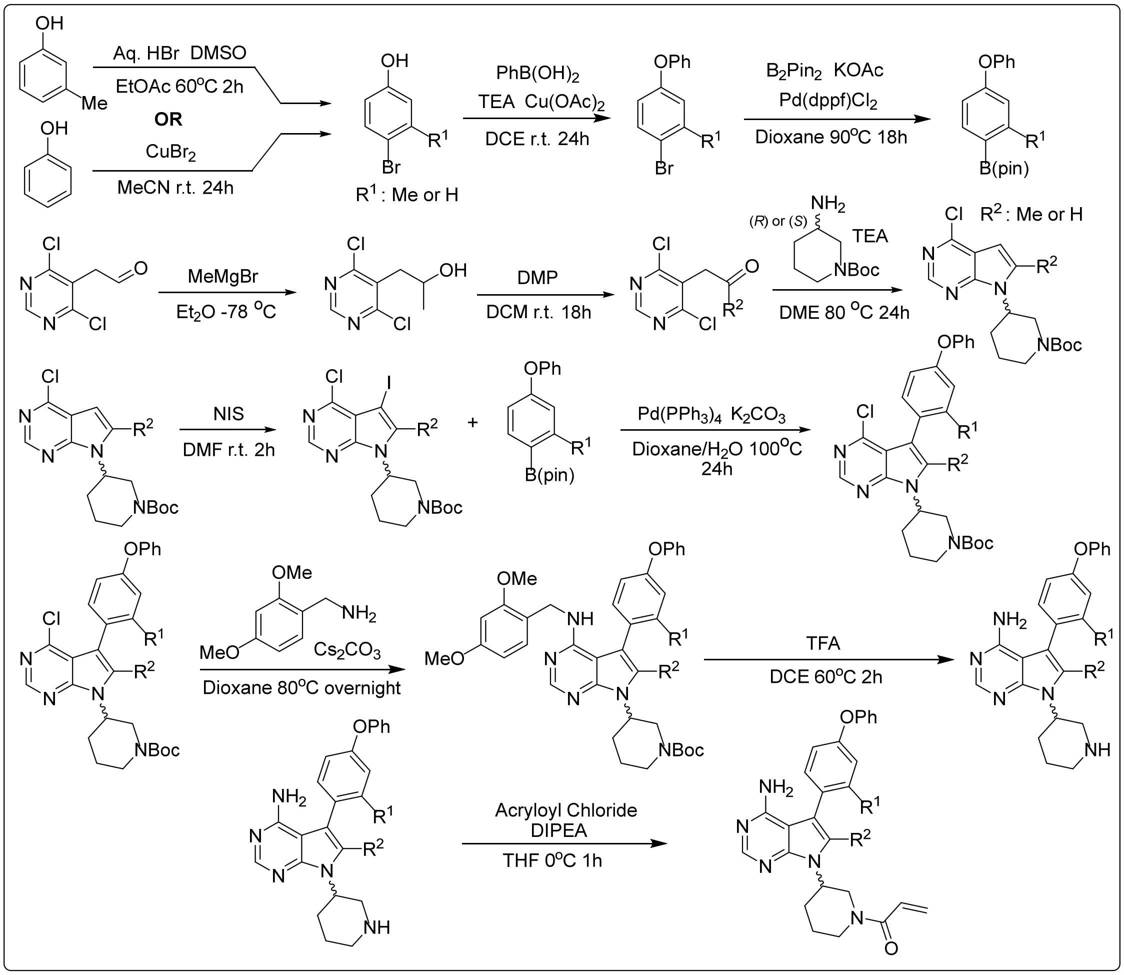

OH
Me
Aq. HBr DMSO
EtOAc 60°C 2h
OR
CuBr2
MeCN r.t. 24h
OH
R1
Br
R1 : Me or H
PhB(OH)2
TEA Cu(OAc)2
DCE r.t. 24h
OPh
B2Pin2 KOAc
Pd(dppf)Cl2
Dioxane 90°C 18h
B(pin)
Cl
N
O
MeMgBr
Et2O -78 °C
OH
DMP
DCM r.t. 18h
R2
NH2
(R) or (S)
TEA
NBoc
DME 80 °C 24h
R2 : Me or H
NIS
DMF r.t. 2h
I
Pd(PPh3)4 K2CO3
Dioxane/H2O 100°C
24h
OMe
MeO
Cs2CO3
Dioxane 80°C overnight
NH
TFA
DCE 60°C 2h
Acryloyl Chloride
DIPEA
THF 0°C 1h

reacted in the same manner with the aldehyde as starting material instead of the ketone. Iodination at *C*-3 followed by Suzuki-Miyaura cross-coupling to corresponding boronic esters, yielded *C*-3 aryl PPYs. The aryl boronic esters were synthesized starting with *para* bromination of *m*-cresol or phenol under conditions listed in Scheme 3.3.1. A Chan Lam reaction with phenyl boronic acid afforded brominated diaryl ethers. Subsequent Miyaura borylation yielded the boronic esters that served as starting materials for the Suzuki-Miyaura cross-coupling step to the PPY. Addition of 2,4-dimethoxy benzylamine at elevated temperatures yielded a di-protected (piperidine *N*-boc and *C*-4 *N*-bzn) PPY containing a nitrogen at the *C*-4 position. Following deprotection with TFA, the crude material was added to acryloyl chloride yielding the final pyrrolopyrimidine inhibitors. If the inhibitor was atropisomerically stable, the racemic mixture was separated by chiral-phase HPLC.

Based on the *in silico* hypotheses, we first synthesized and tested an atropisomerically stable PPY analog of Ibrutinib, **3.1**, possessing two conformationally locking methyl groups *ortho* to the axis (Table 3.3.1). *In vitro* biochemical assays showed (R_a)-atropisomer of **3.1** had higher affinity to BTK than (S_a)-**3.1** (3307 nM vs >10000 nM IC$_{50}$), aligning well with dimensional analysis of the BTK's binding pocket. However, both atropisomers of **3.1** observed a significant (100x) loss in potency compared to the freely rotating Ibrutinib (2.3 nM IC$_{50}$). In attempts to

Table 3.3.1 Kinase inhibition data for Ibrutinib, **3.1** and **3.2**

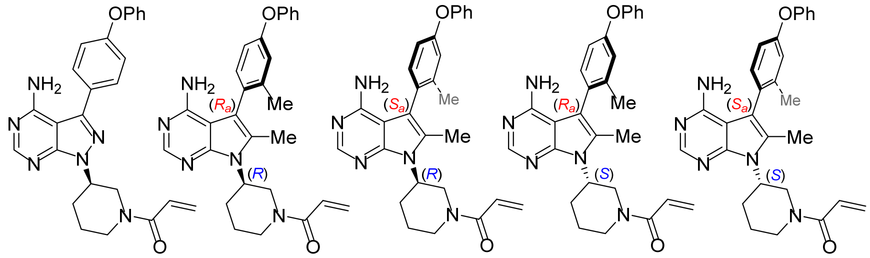

Kinase IC$_{50}$ (nM)	Ibrutinib	(R$_a$)-**3.1**	(S$_a$)-**3.1**	(R$_a$)-**3.2**	(S$_a$)-**3.2**
BTK	2.3	3307	>10000	425	3923
BLK	8.1	1814	9964	187	1732

understand this loss in activity, we turned to molecular docking studies where we docked Ibrutinib and (R_a)-**3.1** into co-crystal structures of BTK (PDB 5P9J, Figure 3.3.2). This revealed that both methyl groups bound without any hindering steric clashes with BTK, however (R_a)-**3.1**'s piperidine chair was rotated 180° to the *endo* conformation, positioning the electrophilic acrylamide in the opposite direction of the nucleophilic Cys841.

To verify this result, we analyzed the relative low energy conformations of Ibrutinib and (R_a)-**3.1** in the absence of BTK using Gaussian16 software. The calculations showed Ibrutinib's lowest energy conformation possessed the PP scaffold in an equatorial position off the (R)-piperidine in an *exo* conformation (away from chair) directing the piperidine's axial C-H's towards the PP scaffold's *N*-2 electron lone pair. In this pose, the acrylamide's β-carbon is extended out from the PP scaffold and 'into the page', mimicking the orientation Ibrutinib engages BTK's Cys481 in co-crystal structures. On the other hand, (R_a)-**3.1** existed at a relative high energy conformation (+4.8 kcal/mol) when its (R)-piperidine is forced into the *exo* conformation due to a

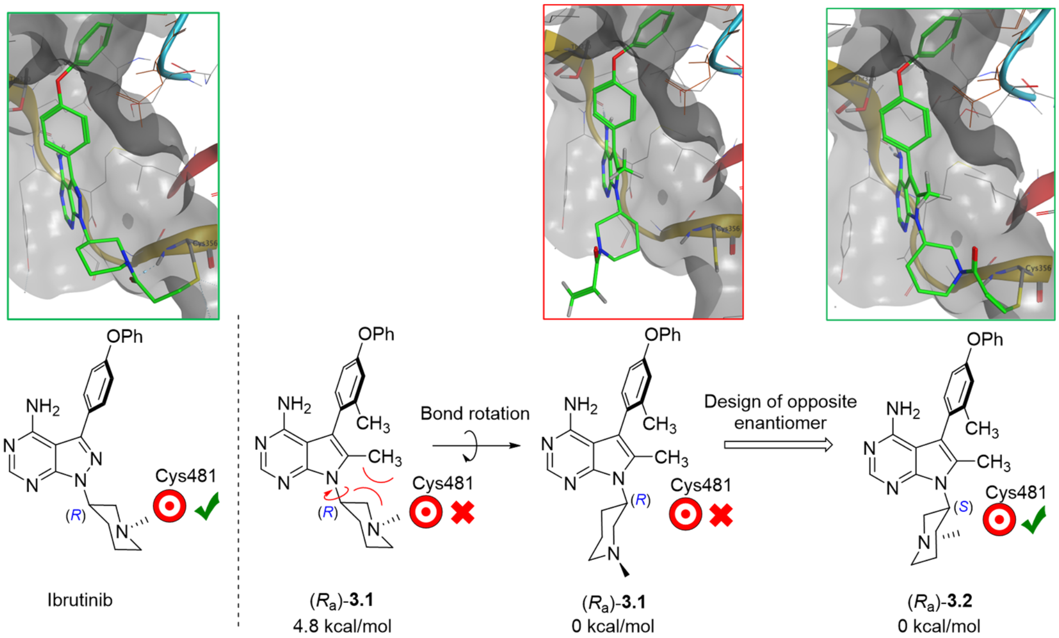

Figure 3.3.2. Conformation-activity analysis of Ibrutinib, (R_a)-**3.1**, and (R_a)-**3.2**.

1,3 diaxial strain between the C-H piperidine hydrogens and the *C*-2 methyl group. This interaction forces the PPY-piperidine bond to rotate 180° away from the methyl group to an *endo* conformation (0 kcal/mol). In this conformation the acrylamide β-carbon is pointed 'out of the page' aligning with conformation seen in the docking studies suggesting (*R*$_a$)-**3.1**'s lowest energy conformation is unable to covalently interact with Cys481 resulting in substantial loss in affinity towards BTK compared to Ibrutinib (2.3 nM vs 3307 nM BTK IC$_{50}$). Because the *C*-2 methyl is necessary for stabilizing the atropisomeric axis, we hypothesized that if (*R*$_a$)-**3.1**'s piperidine *endo* conformation was optimized to orientate acrylamide in the proper direction, we can regain a covalent interaction with BTK. To accomplish this, we synthesized (*R*$_a$)-**3.2** possessing an (*S*)-piperidine, which places the piperidine nitrogen on the opposite side of the chair, demonstrating a 10x improvement in affinity towards BTK over its diastereomer (*R*$_a$)-**3.1** (425 nM vs 3307 nM BTK IC$_{50}$).

While (*R*$_a$)-**3.2**'s acrylamide was positioned in the general vicinity for covalent binding, molecular docking showed (*R*$_a$)-**3.2** had to extend its *endo*-(S)-piperidine into a strained, unfavorable conformation to reach the Cys481 perhaps explaining the lowered BTK affinity compared to Ibrutinib (2.3 nM vs 425 nM BTK IC$_{50}$). To investigate this, we synthesized a series

Table 3.3.2 Kinase inhibition data for **3.3 - 3.8**

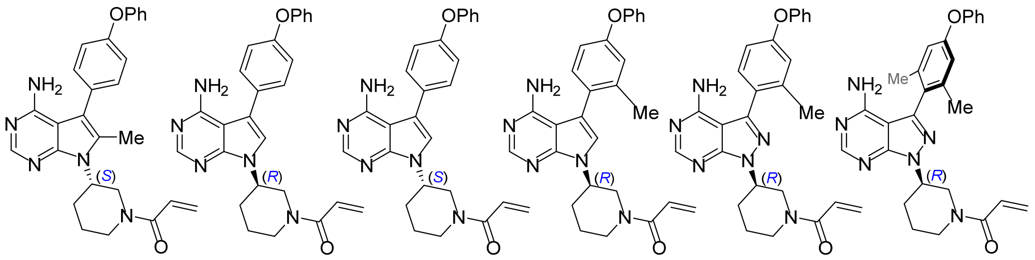

Kinase IC$_{50}$ (nM)	**3.3**	**3.4**	**3.5**	**3.6**	**3.7**	**3.8**
BTK	444	2.7	17.3	6.4	5.5	37.4
BLK	451	9.1	55.9	14.0	8.4	174

of controls beginning with **3.3** where we removed the aryl methyl group from **3.2** (Table 3.3.2). **3.3** showed no improvement of potency towards BTK (444 nM) suggesting the *C*-2 methyl and *endo*-(S)-piperidine combination was cause of decreased BTK affinity and not the rigid atropisomeric axis or aryl methyl group. Synthesizing and testing a pair of PPY controls without any *ortho* substituents (**3.4** and **3.5**) showed 1) there was no discernible difference between the PP and PPY scaffold (**3.4**'s 2.7 nM vs Ibrutinib's 2.3 nM BTK IC_{50}) and 2) when unsubstituted at C-2, the PPY (*R*)-piperidine relaxes to the favorable *exo* conformation to bind BTK's Cys481, similar to Ibrutinib. With no *ortho* substitution, **3.4** and **3.5** possess the same conformational freedom about the atropisomeric axis as Ibrutinib and are likely equally as promiscuous. In attempts to tune low energy conformational window to increase selectivity, we incorporated a methyl group to aryl's *ortho* position in **3.6**, and its PP analog **3.7**. Again, there was minimal differences in BTK

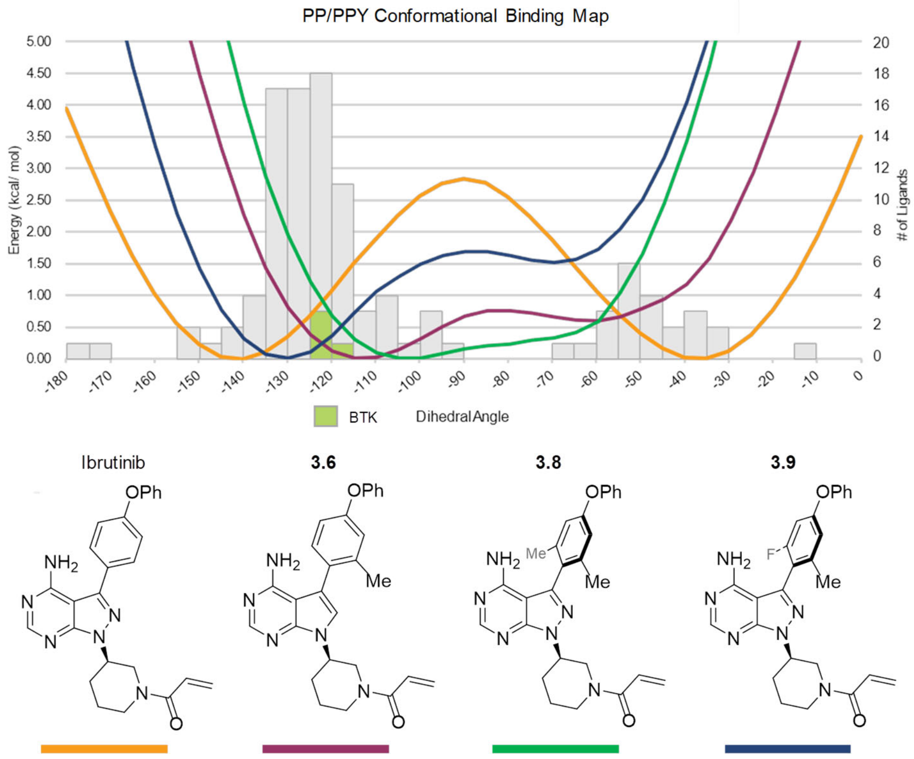

Figure 3.3.3. PDB structural analysis of PP or PPY ligands superimposed with CEP's of Ibrutinib and conformationally-tuned series of BTK inhibitors.

potency between the PPY scaffold (**3.6**) and PP scaffold (**3.7**) (6.4 nM vs 5.5 nM BTK IC_{50}) and each inhibitor maintained similar level of potency to the unsubstituted analog, **3.4** (2.7 nM BTK IC_{50}). While **3.6**'s BTK/BLK selectivity is mediocre (2x), its CEP was narrowed by 40° potentially precluding it from binding other untested kinases (Figure 3.3.3, purple). Future assays will focus on evaluating the new series of inhibitors against broader scope of kinases, including EGFR and Tec family kinases, to better assess selectivity. To try and further narrow **3.6/3.7**'s CEP, we synthesized and tested a 2,6-dimethyl aryl analog (**3.8**) (Figure 3.3.3, green) which lost affinity to BTK compared to **3.7** (5.5 nM vs 37.4 nM), perhaps in part, due to overcorrecting **3.8**'s CEP towards orthogonality (-90°) making it unable to adopt the binding conformation preferred by BTK at -120°. In efforts to re-correct **3.8**'s CEP, we calculated the CEP for a PPY with a 2-fluoro,6-methyl aryl (**3.9**) and found it possessed limited low energy conformational window tuned to BTK's binding range. At the time of writing, **3.9**'s synthetic route has been optimized and an organic chemist will resume its synthesis once SARS-Cov-2 is done wreaking havoc.

The PP scaffold was chosen for **3.8** and **3.9** because of extremely low yields when cross-coupling the iodinated PPY scaffold to sterically hindered 2,6-disubstituted boronic esters. The synthesis of the PP scaffold provided an alternate route where the heterocycle-aryl C-C bond is instead formed through an aryl grignard addition prior to cyclizing the PP scaffold (Scheme 3.3.2). The precursor to the aryl grignard was formed by subjecting the brominated phenol to a Chan Lam coupling with phenyl boronic acid yielding a brominated diaryl ether. This substrate was then was reacted with activated Mg° and added into 4,6-dichloropyrimidine-5-carbaldehyde under inert atmosphere to afford an alcohol intermediate. Following oxidation with dess-martin periodinane, the ketone substrate was reacted with hydrazine monohydrate to effectively cyclize the pyrazolo portion of the PP scaffold. The PP scaffold was then subjected to a mitsunobu reaction with the

Scheme 3.3.2. Synthesis of pyrazolopyrimidine analogs **3.7 – 3.9**.

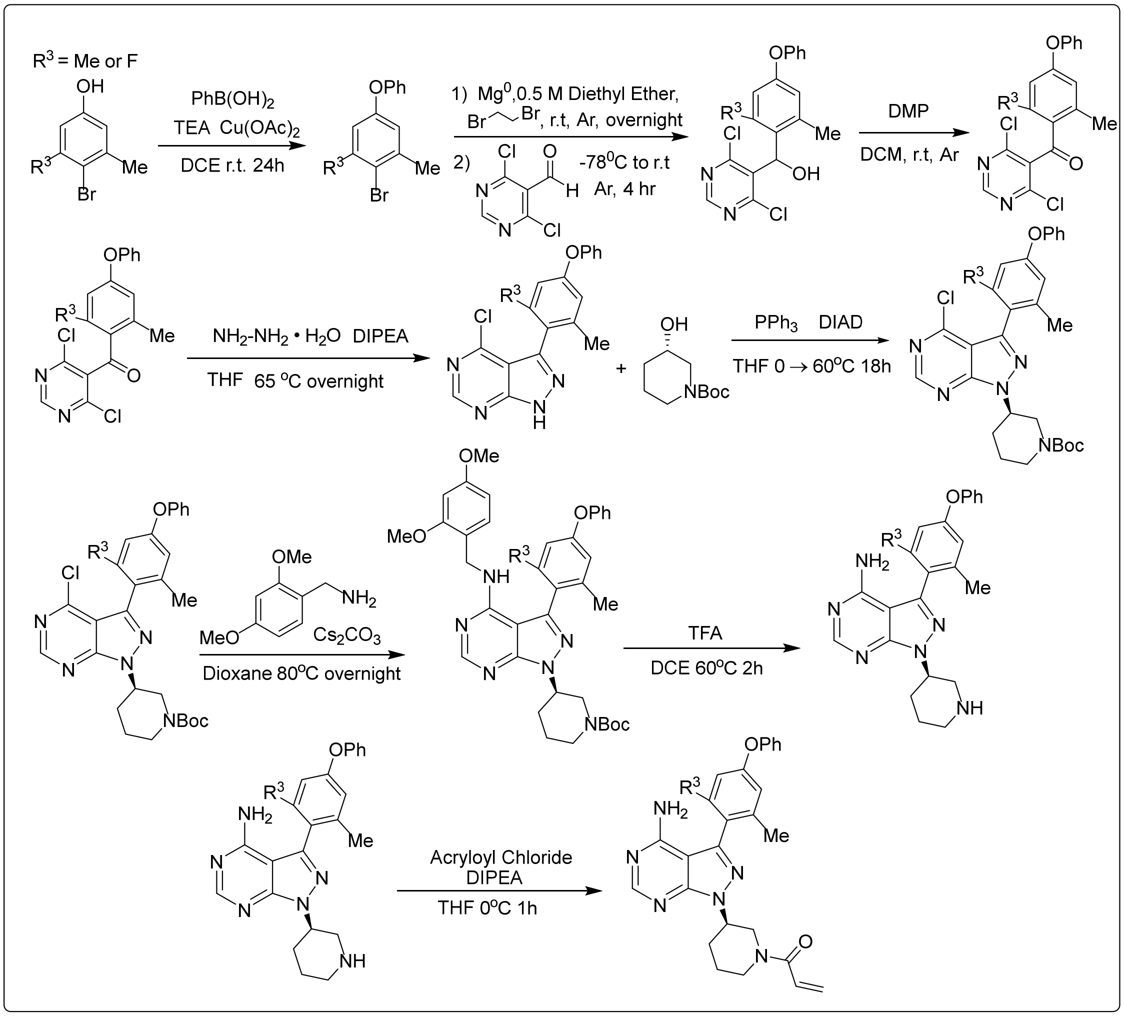
R^3 = Me or F
PhB(OH)$_2$
TEA Cu(OAc)$_2$
DCE r.t. 24h
1) Mg^0,0.5 M Diethyl Ether, Br⌒Br, r.t, Ar, overnight
2) -78^{0}C to r.t Ar, 4 hr
DMP
DCM, r.t, Ar
NH$_2$-NH$_2$ • H$_2$O DIPEA
THF 65 ^{o}C overnight
PPh$_3$ DIAD
THF 0 → 60^{o}C 18h
Cs$_2$CO$_3$
Dioxane 80^{o}C overnight
TFA
DCE 60^{o}C 2h
Acryloyl Chloride
DIPEA
THF 0^{o}C 1h

(*S*)-*N*-boc-protected 3-hydroxypiperidine. Subsequent steps of amination (protected), deprotection and addition of acryloyl chloride were followed according to the previous PPY synthetic route (Scheme 3.3.1).

We next sought to optimize the inhibitor's aryl ether extension towards the interior of BTK's binding pocket. Guided by Acalabrutinib's potent gate-keeper aryl, we synthesized a set of atropisomeric analogs, (*R*a)-**3.10** and (*S*a)-**3.10**, that possessed an optimized amide-linked pyridine at the aryl's *para* position (Scheme 3.3.3) along with (*S*)-piperidine enantiomer and *C*-2 and aryl methyl groups. (*R*a)-**3.10** proved to be quite potent towards BTK compared to its aryl

Table 3.3.3. Kinase inhibition data for **3.10 - 3.12**

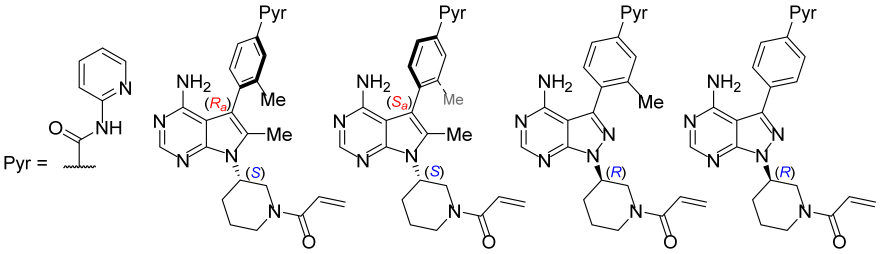

Kinase IC_{50} (nM)	(R_a)-**3.10**	(S_a)-**3.10**	**3.11**	**3.12**
BTK	24.2	21.7	1.12	-
BLK	128	90.4	32.4	-

ether equivalent, (R_a)-**3.2**, (24.2 nM vs 425 nM BTK IC_{50}, Table 3.3.3). Following the trends from the aryl ether set of compounds, we synthesized and tested an optimized analog with an (*R*)-piperidine and no *C*-2 substituent (**3.11**) arriving at our most promising inhibitor yet with a 1.12 nM IC_{50} affinity towards BTK and 30x selectivity over BLK. To understand the extent that **3.11**'s narrowed CEP increased selectivity, we synthesized an unsubstituted analog **3.12**. Unfortunately, assessment of biological activity for **3.12** will have to wait until full-time research at SDSU is permitted

Scheme 3.3.3. Synthesis of amide-linked pyridine boronic esters for inhibitors **3.10 – 3.12**.

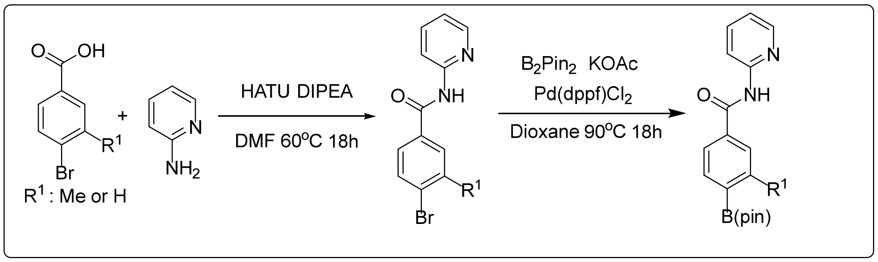

Once the inhibitors are evaluated against a panel of kinases, an accurate assessment of how conformational control correlates to BTK selectivity can be made. Completion of this work will demonstrate how conformational control can be used as an alternative strategy to generate new inhibitor leads for BTK kinase, a prominent target in lymphomas and rheumatoid arthritis.

3.4 Acknowledgments

Chapter 3 is a manuscript draft awaiting final experiments before submission: Toenjes, S.; Albright, S.; Hazin, R.; Gustafson, J. Controlling Ibrutinib's Conformations to Impart Selectivity. *Bioorg. Med. Chem. Lett.* **2020** *Manuscript in preparation*. The dissertation author was the primary researcher and author of this material. Support of this work by the National Institute of General Medical Sciences is acknowledged (R35GM124637).

Chapter 4: Extension of Conformational Control to New Targets and Inhibitor Scaffolds

4.1 Introduction

Chapters 2 and 3 described two examples on how conformational control of an atropisomeric axis can increase inhibitor selectivity of innately promiscuous scaffolds through minimal perturbations. Through this work we developed a conformational binding map for PP and PPY scaffold which we used to design conformational-tuned inhibitors for targets preferring to bind their ligands in an orthogonal manner. In this chapter, we seek to extend our strategy to other targets outside of the orthogonal window by introducing other methods of scaffold preorganization. As there are other privileged yet promiscuous drug scaffolds, we analyzed PDB for inhibitors possessing atropisomeric pyridone and diaryl amine scaffold. The new conformational binding maps allow us to identify variety potential targets, complementary to that of the PP and PPY scaffolds.

4.2 Revisiting the PP/PPY Conformational Binding Map

As discussed in Chapters 2 and 3, we first applied the conformational control strategy to a commonly used drug scaffold, PPY and PP, which serve as cores for the BTK drug Ibrutinib and chemical probes PP1 and NA-PP1. Each of these inhibitors possess severe off-target potencies and require selectivity filter for them to safer drug or accurate tool when studying cell signaling. In short (see full details in Chapter's 2 and 3), co-crystallized bound PPY and PP ligands' atropisomeric dihedral angles were measured and plotted as a bar graph on the conformational binding map in Figure 4.2.1. Next, we superimposed the conformational energy profile (CEP) of a pyrazolopyrimidine inhibitor with a flexible atropisomeric axis (orange) finding its low-energy

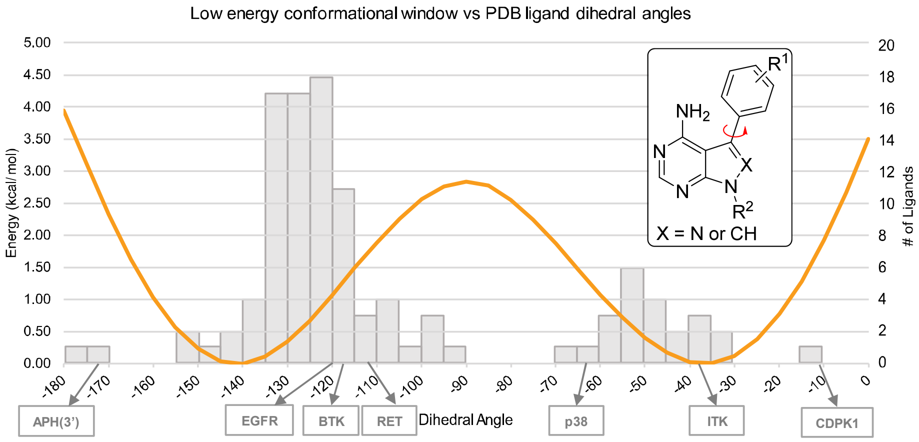

Figure 4.2.1. Conformational map of PPY and PP ligands found in PDB.

conformational window (defined as within 1.36 kcal/mol of the local minima) spans 90° covering a 91% of kinases represented, perhaps explaining the inhibitor's promiscuity.

We propose the design of inhibitors that are restricted to dihedral angles to areas of low binding frequency to obtain highly selective molecule to those kinases for which there are no truly selective inhibitor. In the two previous chapters, we leaned on our background in atropisomerism and began designing atropisomerically stable compounds to target proteins more towards orthogonality. After rounds of optimization, we efficiently generated different inhibitors for RET/mutant EGFR (**4.1** in green) and BTK (**4.2** in pink) shown in Figure 4.2.2.

While these projects produced selective inhibitors for kinases that prefer -120° binding conformation, there are less-populated areas of the conformational binding map where the kinases bind their ligands in a more unique manner. Which suggests we could generate an ultra-selective inhibitor by properly tuning the inhibitor's dihedral angle to match these unique proteins. The following are proposed inhibitor conformations and their respective targets:

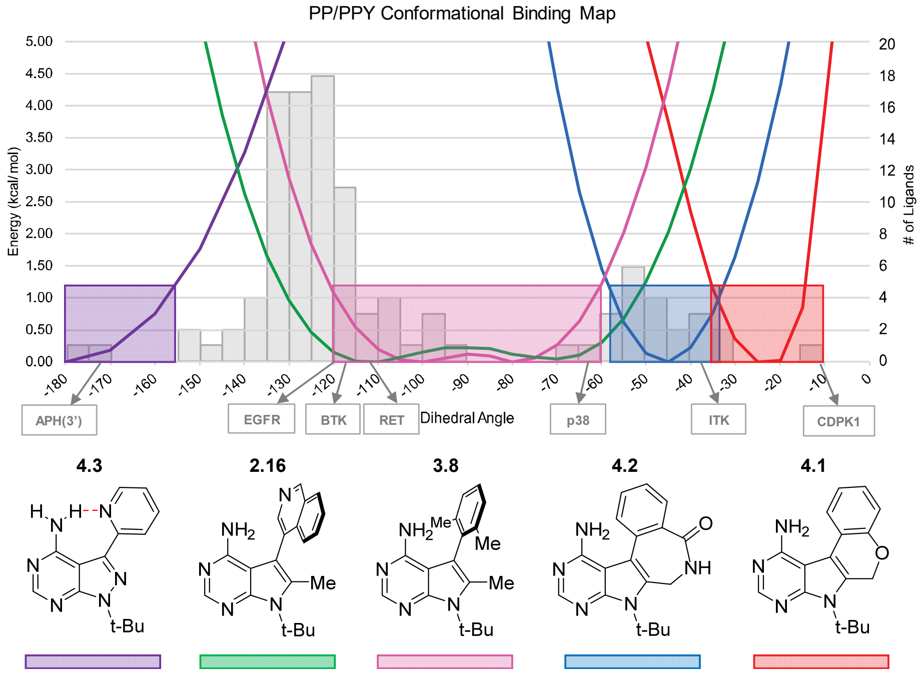

Figure 4.2.2. Conformational map of proposed selective inhibitors.

- CDPK1 kinase at -10° dihedral angle: The less common, planar-like binding modes of PP and PPY are intriguing because, if designed properly, the inhibitor would inhibit very few off-target kinases. In addition, the published PP or PPY ligands bound in these ranges possess enough affinity to obtain co-crystal structures yet their axes are strained into an unfavorable dihedral angle (+3.00 kcal/mol). Simply restructuring the current co-crystallized inhibitor of CDPK1 (bound at -10°) to relieve the axial strain could result in a quick increase in potency. To access this area of the map, we designed an inhibitor (**4.1**) that possesses an aryl ring tethered by a string of atoms causing a narrow low-energy conformational window centered around -20° (red, Figure 4.2.2). The added CH_2 and O atoms, comprising the tether, should not have a big impact on binding affinity or selectivity as they are orientated to a relatively large, conserved area of the pocket where the alpha phosphate of ATP resides. Shortening the tether or reducing the size of the aryl ring to 5 atoms leads to a more planar conformation if needed.

- ITK kinase at -40° dihedral angle: When designing the proposed CDPK1 inhibitor core, we found that lengthening the tether by one atom shifts the low-energy conformation window 25° towards orthogonality yet still maintains a narrow range (**4.2** in blue, Figure 4.2.2). This unexpected result presented an opportunity to target proteins that preferred binding PP or PPY ligands with dihedral angles in the -40° range. The current ITK inhibitors are often plagued by inhibition of TEC kinase family exemplified by Ibrutinib's activity towards BTK (0.5 nM IC_{50}), BLK (8.1 nM IC_{50}) and ITK (10.7 nM IC_{50}). The lengthen tethered scaffold provides an opportunity to preserve favorable TEC family PP scaffold but preorganize it to a conformation that is preferred by only one of the family's kinase, ITK.
- APH(3')-Ia kinase at -175° dihedral angle: At the other end of the map, APH(3')-Ia, was co-crystalized with two different ligands at a near-planar state. When targeting proteins in this range, using sterics or tethered atoms to perturb the atropisomeric axis will not suffice. Instead, we hypothesis taking advantage of intramolecular bonding to create a pseudo-macrocyclic inhibitor that resides in a planar conformation. By exchanging the aryl group for 2-pyrimidine (**4.3** in purple, Figure 4.2.2), the atropisomeric axis is locked into a planar state due to strong intramolecular hydrogen bond with the hinge-binding amine. This unique, straightforward way of preorganization specifically effects only the atropisomeric axis without requiring additional substitution off the inhibitor. Exchanging the aryl ring for pyridine may also enhance biological properties such as metabolic stability and target potency through increased N-H---hinge hydrogen bond strength.

Future studies will also look at the effect of a preorganized atropisomeric axis has on the aryl's *meta* substituents. There are many regions of the protein binding pocket at a suitable distance to be engaged by the aryl's *meta* position. Perhaps the most well-studied is the hydrophobic cleft found in inactive, DFG-out kinases. This could be challenging and more of a boom or bust strategy but nonetheless an avenue worth pursuing to expand our scope to type II class of kinase inhibitors. Another interaction off the aryl's *meta* substituent vector, is the salt bridge of lysine and aspartate of DFG-in conformation. These residues could be targeted using a more planar atropisomeric axis, as in **4.1** – **4.3,** and could represent a therapeutic strategy to increase target potency. Each of these applications potentially allows for another handle to selectivity if kinases' hydrophobic cleft or Lys/Asp salt bridges are positioned at different regions in the binding pocket.

4.3 Expansion of Conformational Control to the Pyridone Scaffold

N-aryl pyridones are another common atropisomeric scaffold found in therapeutics. In fact, there are 110 inhibitors with an *N*-Aryl pyridone scaffold co-crystalized to their respective proteins in the PDB. Measuring the atropisomeric dihedral angles and plotting these ligands (Figure 4.3.2) shows a similar conformational landscape as the PP/PPY scaffolds albeit with a few

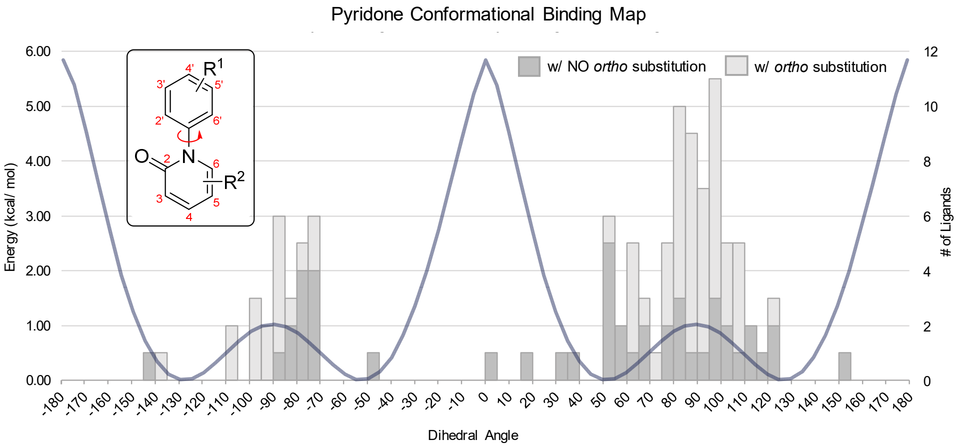

Figure 4.3.2. Conformational binding map of *N*-aryl pyridones.

differences. Because majority of the PP/PPY ligands contained symmetric aryl rings with no *ortho* substituents, their relative dihedral angles were measured in the -180° – 0 ° range and represented on the x-axis of the PP/PPY conformational binding map. Meanwhile 64 out of 110 (58%) *N*-aryl pyridone ligands deposited in PDB possessed at least one *ortho* substituent, allowing us to measure the dihedral angle in with respect to the substituted *ortho* position sampling a full 360° window about the axis. This reveals that proteins binding *N*-aryl pyridone with an asymmetric aryl ring have atropisomeric preference with dihedral angles -180° – 0° representing (R_a) atropisomeric conformations and 0° – +180° representing (S_a) atropisomeric conformations. Axial chiral configuration was assigned giving the carbonyl oxygen priority over substitution (if any) off pyridone's 6 position to provide consistency between substituted analogs.

Also unique to the *N*-aryl pyridone map are the ligand clusters centered around orthogonality (-90° and +90°), different from the dihedral clusters around wider angles (-125° and -55°) in the PP/PPY conformational binding map. This can, in part, be explained by number of *ortho* substituted ligands in the *N*-aryl pyridone dataset, but measuring the CEP of unsubstituted *N*-aryl pyridone (blue) revealed a low-energy window 20° more narrow than an unsubstituted PP/PPY scaffold (± 150° to ± 30° for N-aryl pyridones vs ±160° to ±20° for PP/PPY). Contributing to this observed effect are properties specific to the *N*-aryl pyridone scaffold that increase effective size of *ortho* substituents, specifically its 6-6' ring system and N-C bond. The average angle between the atropisomeric axis and the 6-membered ring's *ortho* substituent is 120°, 6° tighter of an angle found in 5-membered rings (126°) such as PP/PPY's heterocycle. This orientates the *ortho* substituent closer to the axis, forcing earlier and larger steric strain with the adjacent *ortho* substituent as you rotate the atropisomeric axis towards planarity. Similarly, the N-C bonds are generally .08 Å shorter than C-C bonds in this system (1.49 Å vs 1.41 Å), shortening the distance between *ortho* substituents thereby increasing their effect size and relative energies for the planar states. Together, these properties explain the orthogonal clustering of *N*-aryl pyridone ligands and their narrow CEP.

Superimposing the *N*-aryl pyridone's CEP and PDB conformational allows one to identify promising targets for future studies. It must be noted that, unlike the PP/PPY scaffold, the N-aryl pyridone is much smaller fragment and binds in a in a variety of poses and locations in proteins' binding pockets. In order to use the conformational binding map to directly predict effect of a proposed inhibitor's CEP has on target selectivity, the proteins in consideration must bind the pyridone motif in a similar pose (but different dihedral angle) in their binding pocket. This is often the case in kinase families such as TEC or SRC family or certain ligand sub-classes. Nonetheless, the conformational map gives insight to the broader conformational space sampled across all proteins and target specificity will likely increased if a flexible ligand is preorganize into the pose preferred by the protein. The following are potential targets and proposed preorganization strategies to pursue in future studies:

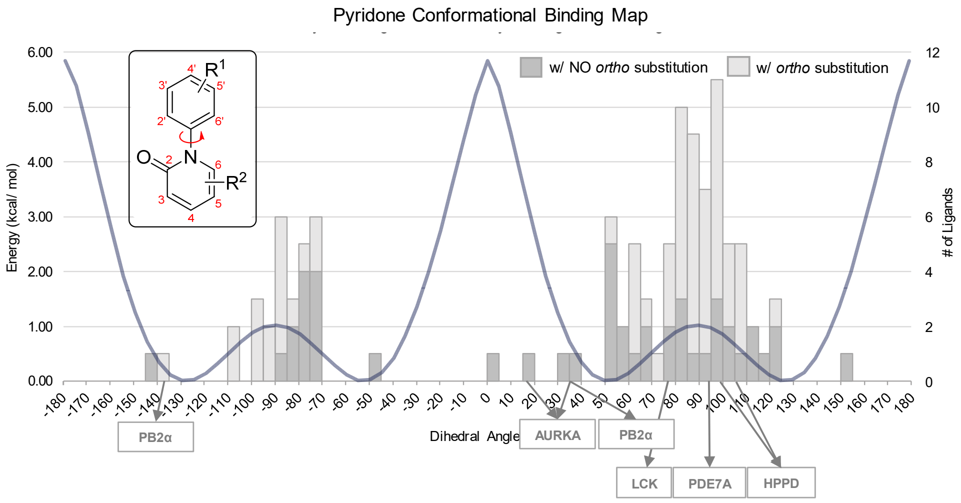

Figure 4.3.3. Conformational binding map of *N*-aryl pyridones with protein targets.

- The N-aryl pyridone conformational binding map revealed two proteins bound their ligands near the limit of their low-energy window: PBP2α (-135° and 32°) and AURKA (19° and 37°). Interestingly, the QLN ligand bound to PBP2α (PDB 6Q9N) possesses an alkene at the pyridone's 6 position, likely shifting its CEP out of range for PBP2a binding causing a loss in affinity. The ligands for PBP2α and AURKA could be optimized towards the more planar binding conformation by incorporating a substituent that can engage in intramolecular hydrogen bonding with the carbonyl oxygen.
- As discussed earlier, many of the ligands contained two *ortho* substituents (including the *ortho* pyridone carbonyl) adopting near-orthogonal conformations existing as class 1 atropisomers. Because these ligands have an atropisomeric preference, we plan to rigidify the axis to class 3 atropisomers by adding one more substituent. Isolating the preferred atropisomer (based on conformational binding map) via chiral-phase HPLC, could potentially remove the off-target binding associated the unwanted atropisomer. Some ligand's atropisomeric axes are already rigid and tetra-substituted but possess symmetry across the aryl ring's 2'-6' positions lending to instances of 'pro-atropisomerism'. While symmetry is strategy to avoid atropisomerism and the need to separate and characterize the enantiomers, we believe, as shown in Chapter 2, there's an added selectivity benefit from embracing atropisomerism and the divergent environments of a protein's binding pocket. The following are proteins co-crystalized with symmetric, tetra-substituted ligands: HPPD (2'-6'-dimethyl aryl at 97° and 105°), LCK (2'-6'-dimethyl aryl at 79°) and PDE7A (2'-6'-difluoro aryl at 93°). Analyzing the differences in residues engaging the 2'-6' aryl substituents will help design asymmetric, stable atropisomers for each protein.

- Lastly, there are families of proteins are biased towards *N*-aryl pyridone scaffolds that show up with more frequency than others. As mentioned previously, having a consistent inhibitor binding pose across a subset of proteins allows one to more accurately correlate ligand dihedral angle to protein specificity as many other variables contributing to activity are held constant. The PDB analysis there are 14 *N*-aryl pyridone ligands bound to the PI3k family and 8 ligands bound to the PDE family. Follow up *in silico* assessment of the minor differences in these family's binding pockets and the design of preorganized ligands can provide a selectivity filter for highly homologous protein families.

4.4 Expansion of Conformational Control to the Diaryl Amine Scaffold

43% (20/47) FDA-approved kinase inhibitors contain a diaryl amine motif yet their structural perturbation has been scarcely studied, perhaps due to the complexity of different conformations that the two aryl groups can exist relative to each other and the N-H bond. Conformational control of this two-axis system represents a great opportunity for drug design but brings challenges different from that of a one-axis system like biaryl PP/PPYs and *N*-aryl pyridone scaffolds. Complete rigidification of diaryl amines into stable atropisomers often requires excessively bulky *ortho* substituents (i.e. *t*-Bu) that will likely hinder binding activity, reducing atropisomeric diaryl amine's therapeutic potential. However, conformational control extends beyond stable atropisomerism and our previous studies (Chapter 3 and Chapter 4.2) show that incorporating medium-sized substituents or H-bond donating/accepting groups adjacent to a ligand's axis can sufficiently perturb the low-energy conformations to increase target selectivity.

An analysis of co-crystalized ligands in the PDB revealed 1076 instances of ligands possessing one diaryl amine scaffold. Due to the quantity of ligands and varying degree of substitutions across the scaffold, dihedral angles were measured in the positive range (0° – +180°)

regardless of substituent priority for the initial analysis presented in this sub-chapter. The ligands are plotted on an X-Y scatter plot, where the ligand's dihedral angle for axis 1 is represented on the x-axis (red) and axis 2 on the y-axis (blue) (Figure 4.4.1). The majority of ligands (53%) bound proteins with both of their aryl groups at or near planar with respect to the N-H bond (axes 1 and 2 within 35° of the map's 'planar' corners). Only 25 out of 1076 ligands (2%) bound with their axes between 35° and 155°, represented in the middle of the plot. The remaining ligands typically bound with one axis planar and other axis non-planar, with distinct clusters around the planar/orthogonal axes combinations (e.g. around (180°, 90°)).

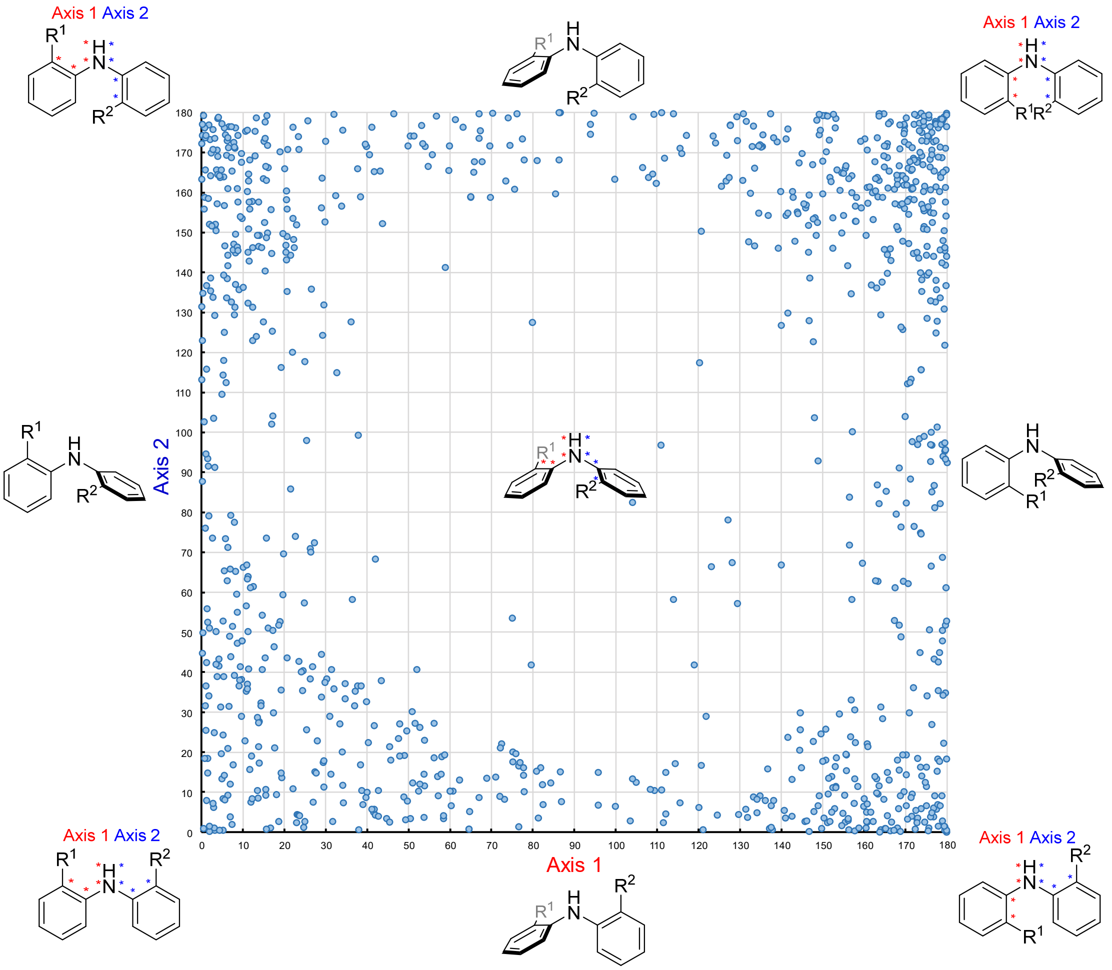

Figure 4.4.1. PDB ligand binding analysis for diaryl amines.

To better understand the diaryl amine ligand's accessible conformational space and provide insight on the PDB analyses' binding patterns, we generated conformational energy plots (CEPs) for different diaryl amine analogs. We first calculated the CEP for a simple unsubstituted diaryl amine with hydrogens *ortho* to the axes (**4.4**), and superimposed it with the PDB analysis (Figure 4.4.2). Because both aromatic rings are symmetric, **4.4**'s CEP is mirrored across axis 2's 90° plane. This allowed us to condense the PDB ligands to match the CEP's boundaries allowing a more focused analysis of **4.4**'s unique conformations. While the PDB ligands represented in this map possess varying substitution, the binding distribution correlates well with the low-energy conformations of **4.4**'s unsubstituted scaffold (majority bind within 2 kcal/mol of **4.4**'s CEP). The low-energy, near-planar conformations are stabilized by shared resonance of the N lone pair to both rings (e.g. 0.2 kcal/mol at (20°, 20°)), however **4.4**'s relative energy increases at a true planar states due to small steric clashing of the *ortho* hydrogens *endo* to the C-N-C bond angle (e.g. 2+ kcal/mol at (0°, 0°)). As either rings rotate towards orthogonality with respect to the N-H bond

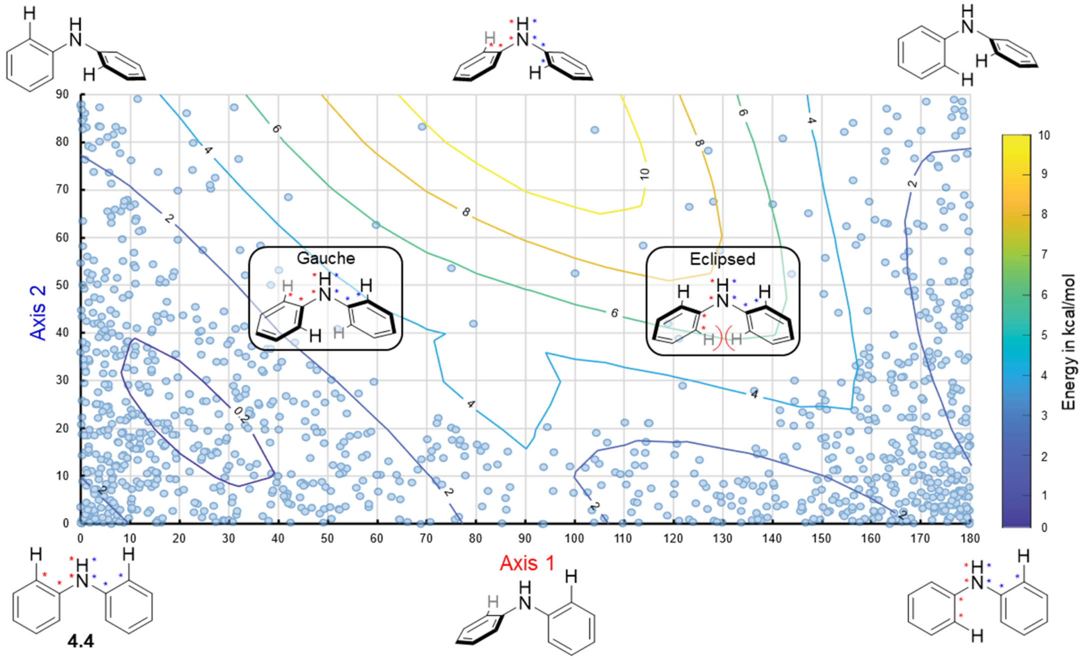

Figure 4.4.2. Conformational binding map of an unsubstituted diaryl amine (**4.4**).

(i.e. 90°), resonance is lost and the overall structure is destabilized. Interestingly, the energy destabilization patterns are different depending on the relative orientation of **4.4**'s aryl groups are to each other. If the aryl axes rotate in the opposite direction relative to each other (0°, 0° to 90°, 90°), the *endo* hydrogens reside in gauche conformation lessening the steric interaction between them. However, as the aryl axes rotate in the same direction (180°, 0° to 90°, 90°), the *endo* hydrogens become eclipsed and encounter a destabilizing steric clash compared to **4.4**'s gauche conformations. Perhaps not surprising, the binding frequency of PDB ligands align well with this observation, where the ligands bound in eclipsed quadrant are sequestered into the planar corner (180°, 0°) as opposed to the more dispersed binding found in the gauche quadrant.

26% of the diaryl amine ligands deposited in PDB possessed an *N*-aryl-2-pyrimidine motif. The calculated CEP of this analog (**4.5**) showed low-energy conformations centered around the planar corners similar to **4.4** (Figure 4.4.3). However, **4.5**'s eclipsed conformations are nearly identical to the gauche conformations, explained by the absence of steric clash between the *endo*

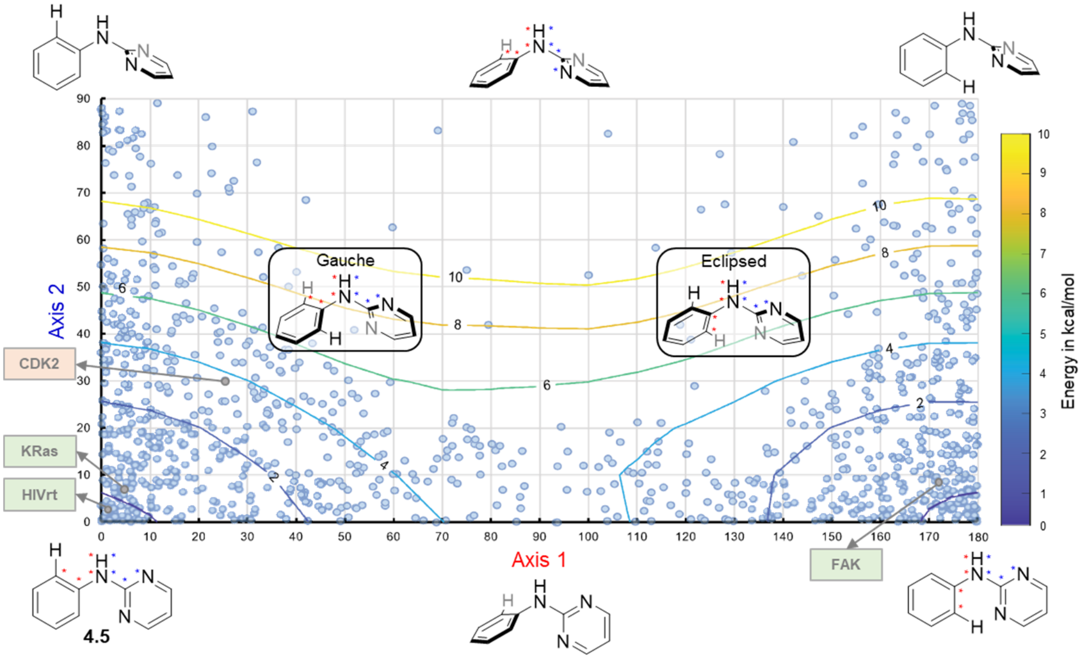

Figure 4.4.3. Conformational binding map of a *N*-aryl-2-pyrimidine scaffold (**4.5**).

aryl hydrogen and pyrimidine fused nitrogen. The gaussian calculations also revealed strong N-pyrimidine double-bond character in **4.5**'s axes 2 planar conformations due the push-pull electronics of N-H and the electron-deficient pyrimidine. This biased resonance towards the pyrimidine explains the large energy gap between the axes' ortho/planar combinations of the aryl and pyrimidine ring (4 kcal/mol at (90°, 0°) vs 10+ kcal/mol at (0°, 90°) and (180°, 90°)). Compared to **4.4**, **4.5** has a decreased overall low-energy area (< 2 kcal/mol) with pockets centered at the planar conformations. This suggests that incorporating a *N*-aryl-2-pyrimidine scaffold in inhibitors that possess substituted scaffolds yet bind their targeted proteins in planar conformations (i.e. HIVrt, KRas, and FAK), could increase target potency as the optimized scaffold binds in a more favorable conformation. Conversely, if a protein binds a *N*-aryl-2-pyrimidine ligand scaffold in a gauche conformation (i.e. CDK2), exchanging its core with **4.4**'s diaryl amine core could result in potency increase for the same reasons.

For the next three calculated analogs, one substituent was changed removing the symmetry of axis 2's ring causing the size of the contour map to double (y-axis extends to 180°). The first analog, *N*-aryl-pyridine (**4.6**), possesses an extended CEP that, unsurprisingly, has similarities with sections of **4.4** and **4.5** (Figure 4.4.4). **4.6**'s quadrants I and II energy profiles match that of **4.4**'s gauche and eclipse conformations, when **4.6** positions the hydrogens in the same *endo* environment. Again, biased by the *ortho* substituents *endo* to the C-N-C angle, **4.6**'s low-energy conformations in quadrants III and IV mimic that of **4.5**'s planar states with an *endo*-fused-

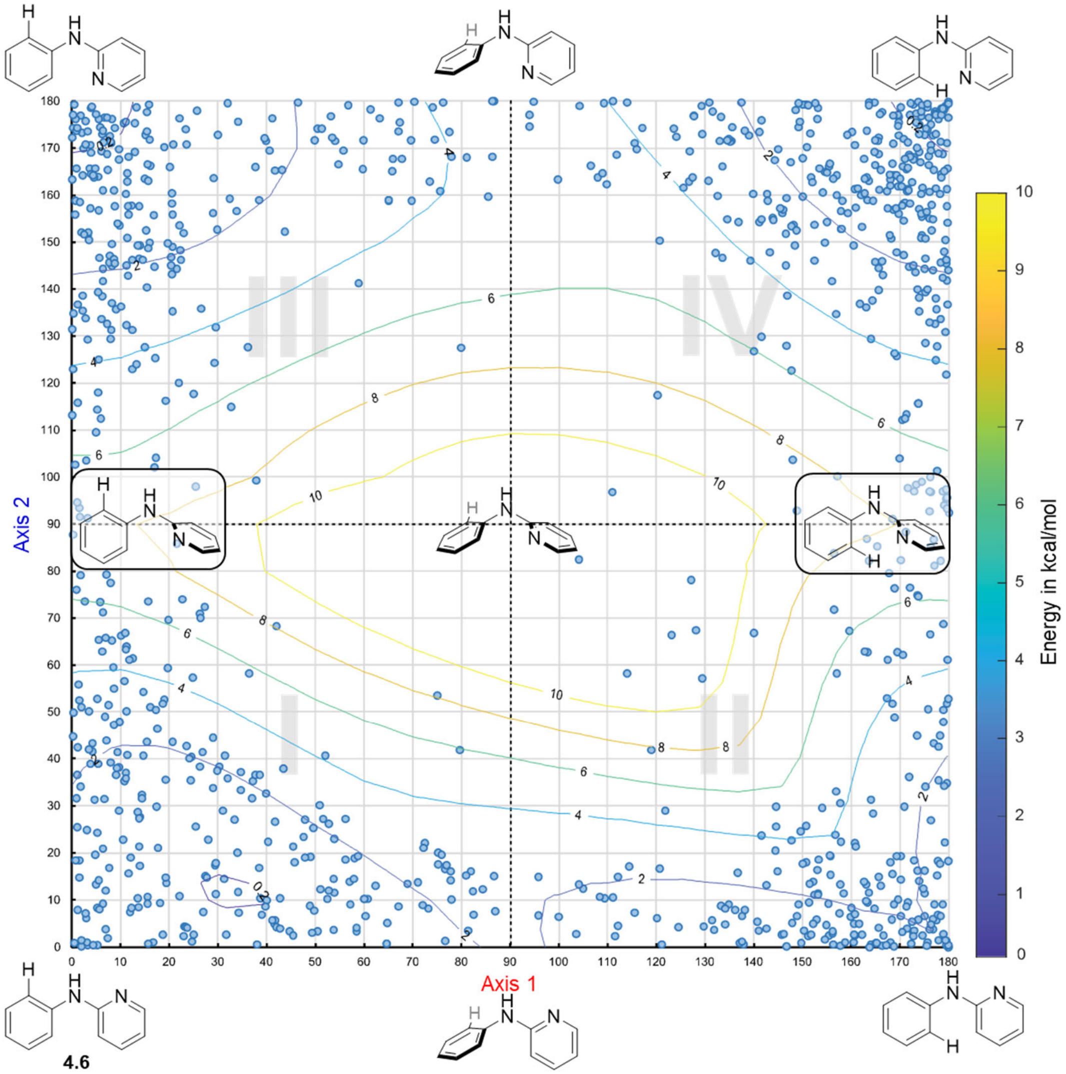

4.6

Figure 4.4.4. Conformational binding map of a *N*-aryl-pyridine scaffold (**4.6**).

nitrogen. All 3 scaffolds discussed thus far access majority of the bound ligand conformations deposited in the PDB, and while they each provide opportunities to increase potency, incorporating them into inhibitors will likely not lead to target specificity.

Next, we calculated the CEP of a diaryl amine possessing an *ortho* methyl group (**4.7**) to analyze how sterics adjacent to an axis will influence the scaffold's low-energy conformations (Figure 4.4.5). The effective size of **4.7**'s methyl group is increased when oriented in the *endo* conformation raising the relative energies up to 10 kcal/mol for the highly populated ligand

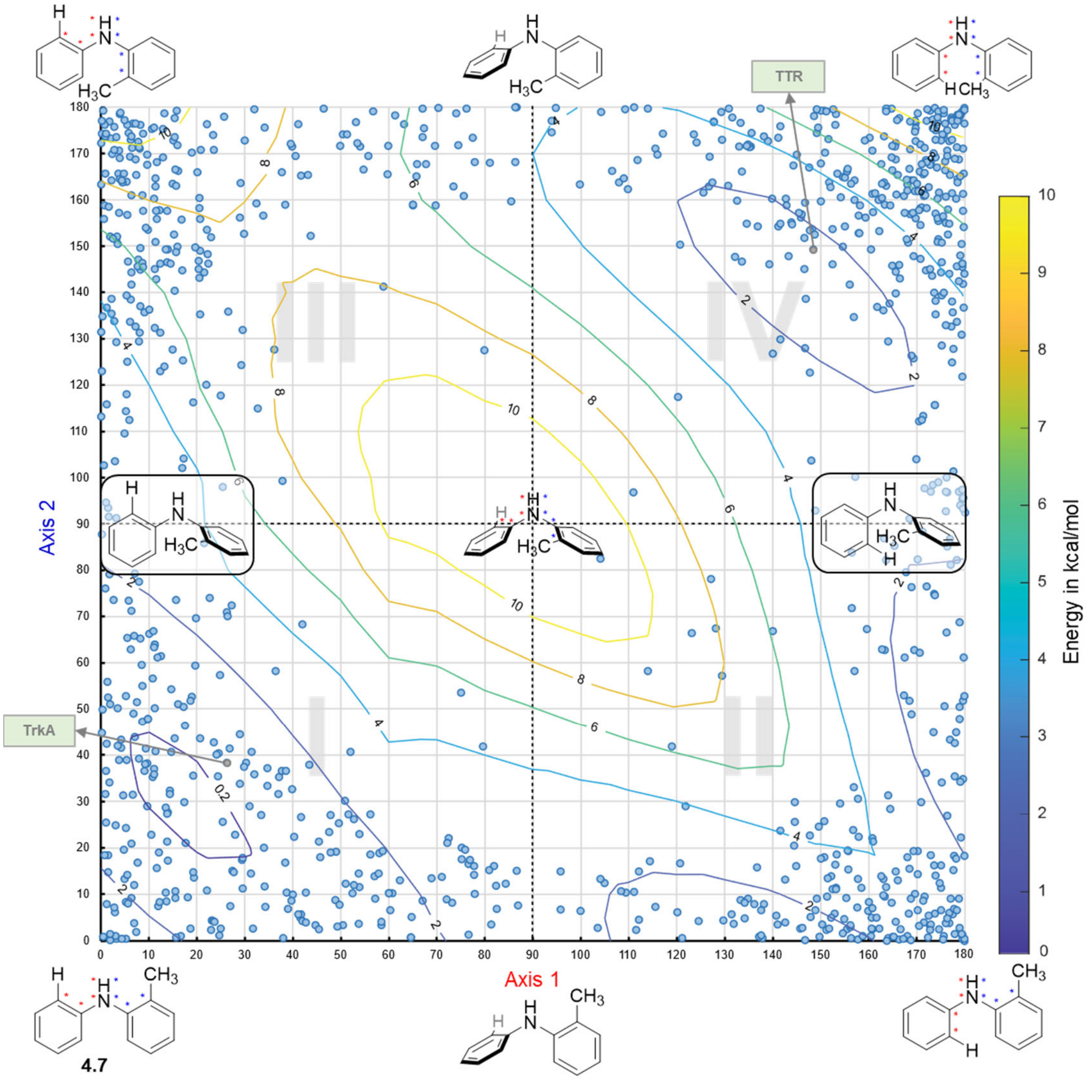

Figure 4.4.5. Conformational binding map of a 2-methyl diaryl amine scaffold (**4.7**).

binding areas in quadrants III and IV. This effectively reduces the total low-energy conformational space and suggests that this scaffold could be used to selectively target proteins that prefer (30°, 30°) and (150°, 150°) binding poeses (i.e. TrkA and TTR). Future binding pocket analysis will confirm whether targeted proteins can accommodate a hydrophobic substituent *exo* to the C-N-C bond angle.

Lastly, we noticed the N-H bond could act as handle to engage in intramolecular H-bonding with an *ortho* lewis-basic substituent similar to **4.3**'s PPY-pyridine intramolecular H-bond in Chapter 4.2. We calculated the CEP of diaryl amine analog with an *ortho* nitro group (**4.8**) which revealed a preference for the axis 1's nitro group to exist in a *exo* planar state, regardless of axis 2's dihedral angle due to the intense H-bonding between the N-H and nitro oxygen (Figure 4.4.6). This enhanced stabilization, creates high relative energy values (10+ kcal/mol) for nearly every conformation with axis's 2 > 60° leaving quadrants III and IV inaccessible to this scaffold. **4.8**'s

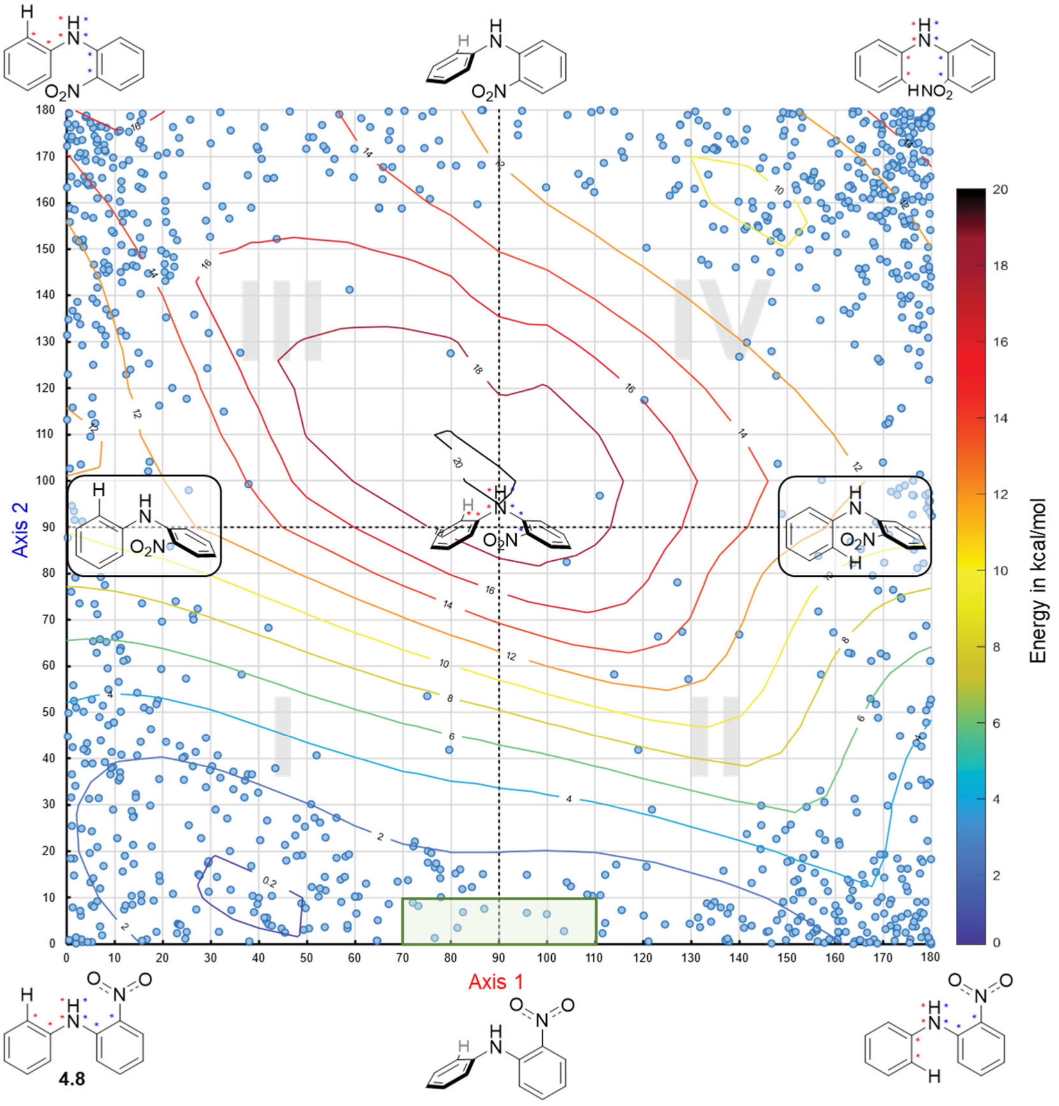

Figure 4.4.6. Conformational binding map of a 2-nitro diaryl amine scaffold (**4.8**).

total low-energy conformational area is similar to that of **4.7** but organized over a different range of proteins. One can imagine combinations of these two scaffolds to target confined areas on the conformational binding map. For example, only 9 proteins bound their diaryl amine ligands with axis 1 (70° to 110°) and axis 2 from (0° to 10°) (green box Figure 4.4.6). Incorporating a second *ortho* substituent on the nitro aryl group should position the low-energy conformational space across this range.

Future work will include designing more complex scaffolds to target regions of low binding frequency and subsequent *in silico* docking against the target and off-target proteins to verify any predicted binding pocket specificity. Select core scaffolds and their controls will be synthesize and tested via *in vitro* assays to assess true target selectivity. Together, this work allows us to expand our strategy of conformation control to a dynamic, two-axes diaryl amine scaffold commonly found in drug discovery.

4.5 Acknowledgments

Chapter 4 contains material that may be used in a future publication. The following are coauthors for this project: Toenjes, S**.**; Garcia, V.; Basilaia, M.; Heydari, Be.; Heydari, Ba.; Vaidya, S.; Gustafson, J. Extension of Conformational Control to New Targets and Inhibitor Scaffolds. The dissertation author was the primary researcher and author of this material. Support of this work by the National Institute of General Medical Sciences is acknowledged (R35GM124637).

Chapter 5: Accessing Atropisomerically Enriched Compounds

5.1 Copyright

Chapter 5 is a compilation of highlighted sections from three different manuscripts with permission from each manuscript's journal: *Org. Lett.* **2018**, *20,* 2037-2041*, Synlett* **2018**, *29,* 2155-2160, and *J. Am. Chem. Soc.* **2020**, *142*, 2198-2203. Copyright 2018 American Chemical Society. Copyright 2018 Thieme. Copyright 2020 American Chemical Society.

5.2 Introduction

As discussed in Chapters 2 and 3, atropisomer confirmation can be leveraged to improve various properties of biologically active small molecules.[68,116,138,139] The ability to obtain atropisomerically pure pharmaceutical scaffolds has been a long-standing challenge, with our group and others currently relying upon traditional chiral resolutions or HPLC separation on a chiral stationary phase.[140,141] This hinders access to small libraries of atropisomerically pure compounds in early stage drug discovery, and also limits access to larger amounts of lead atropisomeric compounds that may be needed for subsequent studies. A catalytic atroposelective route would facilitate such endeavors, yet there are relatively few[69,70,73–75,142] atroposelective methodologies that yield direct access to relevant atropisomeric pharmaceutical scaffolds. This chapter describes projects of which I contributed to but led by my colleagues centered on developing methodologies for the common biaryl PPY scaffold as well as the less-studied two axes systems of diaryl ethers and diaryl amines.

5.3 Enantioselective Synthesis of Pyrrolopyrimidine Scaffolds through Cation-directed Nucleophilic Aromatic Substitution

My colleagues hypothesized that an atroposelective SNAr reaction could be amenable to diverse atropisomer synthesis problems in drug discovery. For example, the PPY inhibitors discussed in Chapters 2 and 3, a PI4KIIIa inhibitor from GSK,[25] and the FDA approved urate transport inhibitor lesinurad,[13] are all atropisomerically stable bioactives whose syntheses can potentially involve a SNAr proximal to the chiral axis.

While there are several recent precedence for enantioselective SNAr,[143–145] my colleagues were inspired by the seminal atroposelective SNAr from the Smith group[77] in which they used chiral quaternary ammonium salts to effect the desymmetrization via SNAr of biaryl pyrimidines. My lab mates, Mariel Cardenas and Chris Nalbandian decided to evaluate whether similar

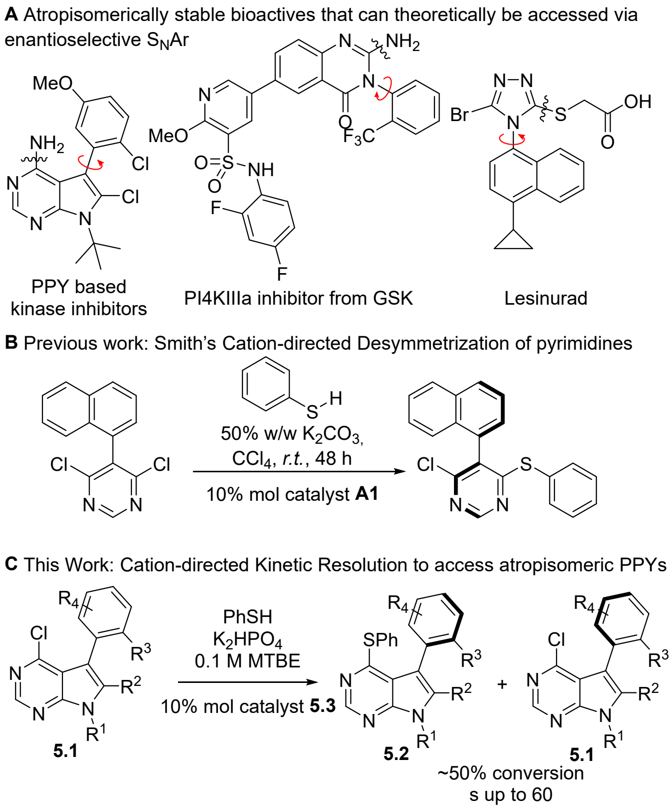

A Atropisomerically stable bioactives that can theoretically be accessed via enantioselective S_NAr
MeO
NH_2
N
N
N
Cl
Cl
PPY based kinase inhibitors
N
MeO
O=S-NH
O
F
F
N
NH_2
N
O
F_3C
PI4KIIIa inhibitor from GSK
N-N
Br
N
S
OH
O
Lesinurad
B Previous work: Smith's Cation-directed Desymmetrization of pyrimidines
S
H
50% w/w K_2CO_3,
CCl_4, *r.t.*, 48 h
10% mol catalyst **A1**
Cl
Cl
N
N
Cl
S
N
N
C This Work: Cation-directed Kinetic Resolution to access atropisomeric PPYs
R_4
Cl
R^3
R^2
N
N
N
R^1
5.1
PhSH
K_2HPO_4
0.1 M MTBE
10% mol catalyst **5.3**
SPh
5.2
+
5.1
~50% conversion
s up to 60

Figure 5.3.1. An overview of the potential of atroposelective SNAr in drug discovery.

chemistry could be applied to the kinetic resolutions of the 3-arylated PPY scaffold. They were particularly intrigued by the use of thiophenol as the nucleophile, as the resulting sulfide product could be transformed to an excellent S_NAr leaving group,[146] allowing for the potential for both the recovered starting material and products to be brought on to the final kinase inhibiting scaffolds in a stereodivergent manner.

They began their studies by evaluating various catalysts and conditions on a racemic PPY **5.1** that possessed a trifluoromethyl group adjacent to the axis of chirality. Smith's optimal biphasic conditions employing a readily available quinine based quaternary ammonium salt proved sluggish (22% conversion), however yielded promising selectivity with an s-factor over 5. My colleagues optimized the reaction conditions at room temperature finding that MTBE facilitated faster conversion while weak base (K_2PHO_4), the quinine's quaternary ammonium benzyl group and counter chlorine anion aided in increased enantioselectivity.

With the optimal reaction conditions in hand, my colleagues next set out to define the substrate scope of this reaction. They found their chemistry was amenable to substrates that had a range of *N*-1 alkyl substituents (R^1, in Figure 5.3.2) with s-factor between 15 and 40. As the goal was to develop an enantioselective methodology that would be amenable to a medicinal chemistry campaign, I joined the team to help synthesize substrates with diverse substitutions at the *C*-3 aryl position and *C*-2 position; two positions that we know from Chapter 2 and 3's work play a major role in modulating kinase inhibitor selectivity. We synthesized a C-3 naphthyl derivative, **5.1**, that when reacted with thiophenol under the optimal conditions yielded **5.2a** with an s-factor of almost 13. **5.2a** is particularly notable as it represents the enantioenriched atropisomeric analog of NA-PP1 (**2.9**) discussed in Chapter 2.[117]

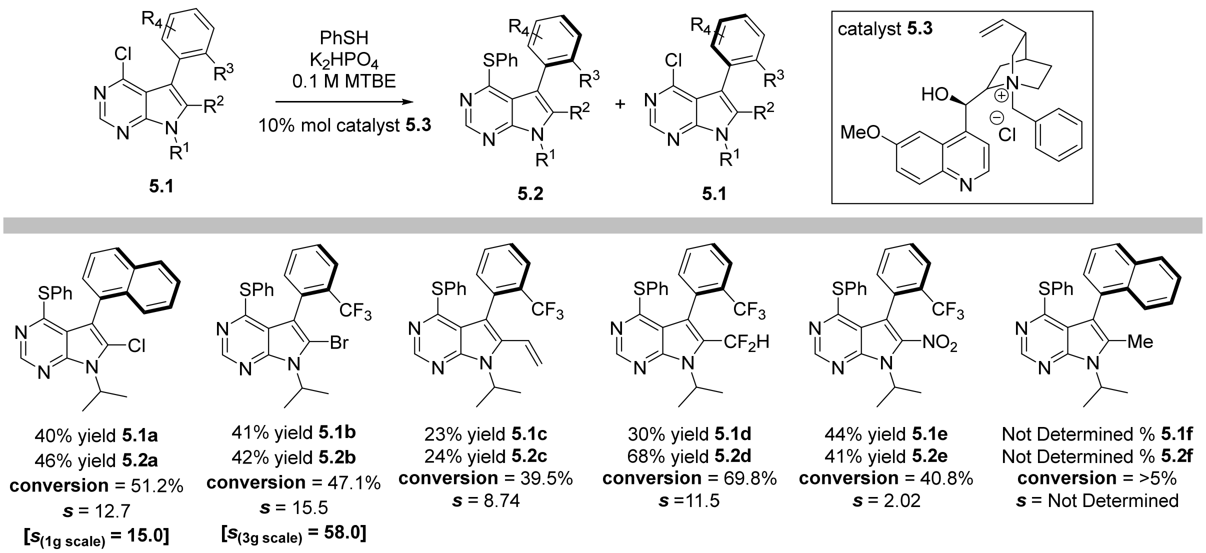
5.1
PhSH
K2HPO4
0.1 M MTBE
10% mol catalyst 5.3
5.2
5.1
catalyst 5.3
40% yield 5.1a
46% yield 5.2a
conversion = 51.2%
s = 12.7
[s(1g scale) = 15.0]
41% yield 5.1b
42% yield 5.2b
conversion = 47.1%
s = 15.5
[s(3g scale) = 58.0]
23% yield 5.1c
24% yield 5.2c
conversion = 39.5%
s = 8.74
30% yield 5.1d
68% yield 5.2d
conversion = 69.8%
s =11.5
44% yield 5.1e
41% yield 5.2e
conversion = 40.8%
s = 2.02
Not Determined % 5.1f
Not Determined % 5.2f
conversion = >5%
s = Not Determined

Figure 5.3.2. The substrate scope of PPYs.

Reactions were performed on a 25 mg scale of **5.1**. Conversion and s-factors were determined using HPLC. Results are reported as an average of at least 3 trials.

Next, we evaluated the effects of changing the substitution of the *C*-2 position of the PPY. This position needs to be substituted to impart stereochemical stability to the system, and can influence protein binding by engaging nearby residues.[57] Of note, tolerable *C*-2 substitutions included bromine **5.1b**, vinyl **5.1c**, and difluoromethyl **5.1d**. However, there seems to be a goldilocks trend where the *C*-2 groups that were too electron withdrawing (e.g. nitro in **5.1e**), yielded poor selectively due to background reaction and too electron rich groups (e.g. methyl in **5.1f**) proved unreactive. These substrates underscore the importance of electronics for the reaction rate and selectivity of SNAr.

We next sought to determine if both the recovered starting materials and products from this kinetic resolution could be brought forward to the final kinase inhibiting PPY scaffold (with NH_2 at *C*-4) without losing enantiopurity. Typical conditions to accomplish this require heating at 140

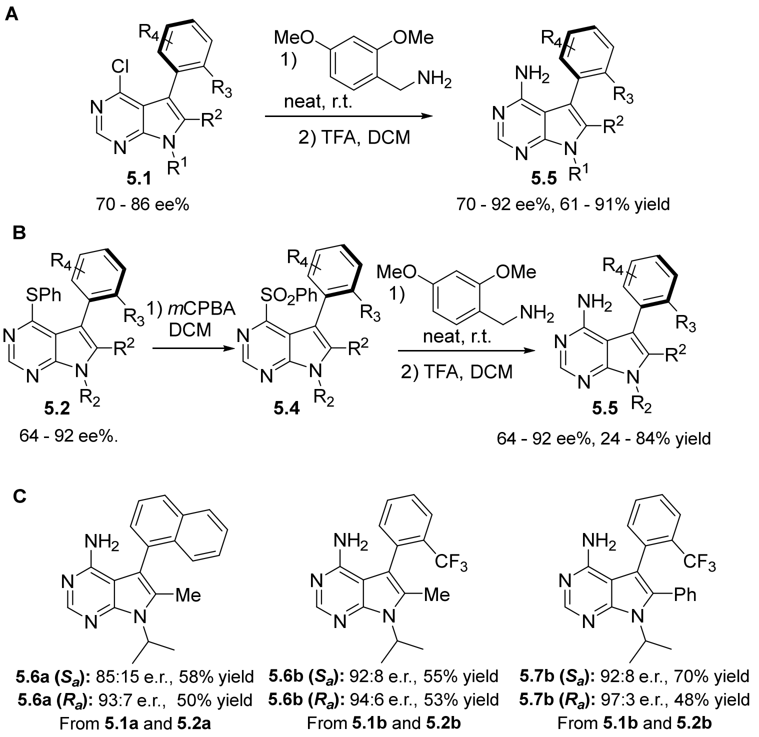
A
5.1
70 - 86 ee%
1)
neat, r.t.
2) TFA, DCM
5.5
70 - 92 ee%, 61 - 91% yield
B
5.2
64 - 92 ee%.
1) mCPBA DCM
5.4
1)
neat, r.t.
2) TFA, DCM
5.5
64 - 92 ee%, 24 - 84% yield
C
5.6a (Sa): 85:15 e.r., 58% yield
5.6a (Ra): 93:7 e.r., 50% yield
From 5.1a and 5.2a
5.6b (Sa): 92:8 e.r., 55% yield
5.6b (Ra): 94:6 e.r., 53% yield
From 5.1b and 5.2b
5.7b (Sa): 92:8 e.r., 70% yield
5.7b (Ra): 97:3 e.r., 48% yield
From 5.1b and 5.2b

Figure 5.3.3. Post enantioinduction modifications.

Transformation of enantioenriched A) starting materials and B) products to *C*-4 aminated kinase inhibitors. C) Modification of the *C*-2 position.

°C with ammonium hydroxide in a sealed tube, which would almost certainly result in complete racemization. While evaluating other options, we found that stirring recovered starting material PPYs (Figure 5.3.3A) in neat 2,4-dimethoxybenzylamine resulted in quantitative aminated product in 24-48 hours. Subsequent treatment of the isolated 2,4-dimethoxy benzyl substituted aniline with trifluoroacetic acid (TFA) over the course of an hour then yielded the biologically active scaffold with no observable degradation in enantiopurity for any of the cases evaluated. We also found we could oxidize the product sulfide to a sulfone (**5.4**) using *m*CPBA (Figure 5.3.3B) which could then be transformed to **5.5** using the route described above with no observable degradation in enantiopurity. It should be noted that in many cases we observed an increase in e.r., most likely because the final products were often isolated via trituration.

As the *C*-2 position was perhaps the most limited position in terms of scope, we determined if this position could be diversified by post kinetic resolution (Figure 5.3.3C). We focused on further functionalizing the final *C*-4 aminated products (**5.5**) as the same chemistry could be used on both enantiomers. To avoid complications arising from the *C*-4 aniline, we boc-protected this functionality in both cases. Protected **5.5a** can also be transformed to a *C*-2 methylated analog (**5.6a**) using Organ's PEPPSI-ipent catalyst[147] with no observed degradation in e.r.. Protected **5.5b** could be readily functionalized to C-2 methylated **5.6b** using cutting edge chemistry from Schoenebeck[148] and *C*-2 arylated **5.7b** using conditions from Buchwald,[149] each in good yields over two steps with no observed racemization. Furthermore, the enantiomeric purity of each enantiomer could be improved via trituration with hexanes/isopropanol.

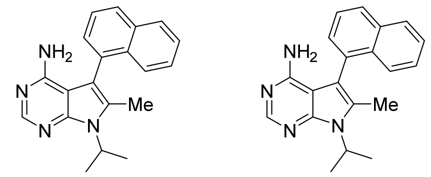

(S_a): 85:15 e.r.
(R_a): 93:7 e.r.

[Enantiopure]

5.6a (S_a): SRC IC_{50} 3257 nM
BRK IC_{50} 97 nM
5.6a (R_a): SRC IC_{50} 814 nM
BRK IC_{50} 23 nM

5.6a (S_a)*: SRC IC_{50} >15000 nM
BRK IC_{50} 1488 nM
5.6a (R_a)*: SRC IC_{50} 1366 nM
BRK IC_{50} 6 nM

Figure 5.3.4. Evaluation of enantioenriched PPYs across SRC and BRK kinases.
IC_{50}'s were determined using Promega's ATP Glo Kinase Inhibition Assay in duplicate.

We finally tested each atropisomer of **5.6a** for inhibitory activity across the kinases SRC and BRK (Breast Tumor Kinase). SRC is a prototypical kinase that is often studied in chemical biology and is implicated in several resistant cancers.[150] BRK inhibitors have recently received interest for targeting breast cancer.[151,152] Enantioenriched **5.6a** proved interesting as the putative (*R*a)-atropisomer displayed low nM activity towards BRK with a 35x preference for BRK over SRC. As both enantioenriched samples of **5.6a** possessed relatively significant amounts of the other enantiomer (7% or 15% as shown in Figure 5.3.4), we next sought to obtain enantiopure samples. While we could modulate the reaction conversion to obtain improved e.r.s, for simplicity we chose to further purify an aliquot of each enantioenriched sample of **5.6a** by HPLC on a chiral stationary phase. Perhaps unsurprisingly, the observed trends for enantioenriched **5.6a** were amplified with enantiopure sample, as (*R*a)-**5.6a** inhibited BRK with an IC_{50} of 6 nM, and SRC with an IC_{50} of 1366 nM. The >225x preference for BRK over SRC is striking and suggests that the (*R*a)-atropisomer of **5.6a** is an intriguing lead towards a selective BRK inhibitor.

Through this work we have developed a S_NAr approach to the kinetic resolution of an important class of kinase inhibitor. The chemistry proved quite robust and has allowed us to access several new enantioenriched PPY analogs. Overall, we show that this chemistry should be quite amenable to furnishing libraries and gram quantities of atropisomer enriched PPYs, which circumvents need for tedious milligram separation of enantiomers with chiral-phase HPLC as done in Chapters 2 and 3. We hope these studies serve as a springboard toward employing atroposelective S_NAr to other pharmaceutically relevant atropisomeric scaffolds.

5.4 Towards a Catalytic Atroposelective Synthesis of Diaryl Ethers via C(sp^2)-H Alkylation Using Nitroalkanes

Diaryl ethers are a type of atropisomer that have been largely over-looked by the enantioselective catalysis community despite their prevalence in natural products, exemplified by the macrocyclic diaryl ethers in vancomycin. Furthermore, atropisomerically unstable diaryl ethers are common motifs in drug discovery (Figure 5.4.1A). Thus far, the literature involving diaryl ethers is highlighted by diastereoselective examples in route to vancomycin[153] and several excellent studies by Clayden and coworkers[33,34,76,154,155] wherein they characterized the stereochemical stabilities of differently substituted diaryl ethers, and developed diastereoselective routes to atropisomeric diaryl ethers (Figure 5.4.1B).

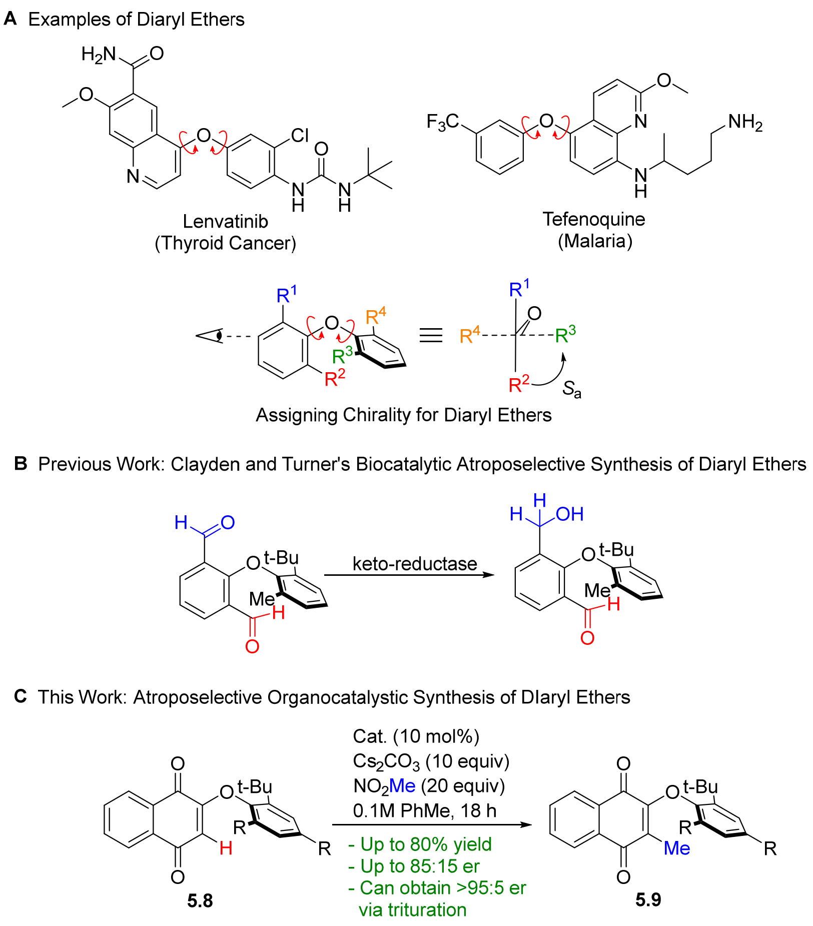
A Examples of Diaryl Ethers
Lenvatinib
(Thyroid Cancer)
Tefenoquine
(Malaria)
Assigning Chirality for Diaryl Ethers
B Previous Work: Clayden and Turner's Biocatalytic Atroposelective Synthesis of Diaryl Ethers
keto-reductase
C This Work: Atroposelective Organocatalystic Synthesis of DIaryl Ethers
Cat. (10 mol%)
Cs2CO3 (10 equiv)
NO2Me (20 equiv)
0.1M PhMe, 18 h
- Up to 80% yield
- Up to 85:15 er
- Can obtain >95:5 er via trituration
5.8
5.9

Figure 5.4.1. Examples of Diaryl Ethers, previous asymmetric synthesis, and our atroposelective organocatalytic synthesis on diaryl ethers.

Other than these groundbreaking examples, work on the catalytic atroposelective synthesis of diaryl ethers has been scarce. Perhaps the major reason for this is that diaryl ethers possess two axes that can complicate reaction development (*i.e.* finding a catalyst that can set both axes) and, in some cases, result in racemization at a lower-than-expected energy via a concerted gearing mechanism.[33] When defining the chirality of diaryl ethers, Clayden and others have made an analogy to atropisomeric biaryl systems, defining chirality based on the orientation of the substituents across both aryl planes when looking down one aryl-ether axis (see Figure 5.4.1A, priority assigned in example according to R group's number).

As there is a lack of enantioselective routes towards atropisomeric diaryl ethers, my colleagues, led by Andrew Dinh, decided to test whether an addition of a nucleophile adjacent to a stereochemically unstable diaryl ether bond could rigidify the 2 axes system in enantioselective fashion (Figure 5.4.1C). They chose to evaluate a naphthoquinone scaffold linked via an ether bond to aryl groups that possessed a large *tert*-butyl group and a 2nd smaller substituent *ortho* to the ether axis, as Clayden has shown that having one large quaternary substituent is often a prerequisite to obtain stereochemically stable diaryl ethers.

While evaluating nucleophiles for the addition into **5.8**, they observed that the use of nitromethane in the presence of excess Cs_2CO_3 and tetrabutylammonium bromide (TBAB) resulted in the isolation of a C(-sp^2)-H methylated product **5.9**, in line with seminal work reported by Mukherjee.[156,157] After much reaction condition and catalyst optimization, they found the addition of 3Å molecular sieves increased yield and exchanging a *tert*-butyl urea-containing quinine quaternary ammonium salt for TBAB resulted in enantioenrichment of **5.9** (*e.r.* 85:15). Andrew and colleagues then expanded the scope of the reaction to other substrates finding ones that possessed electron rich aryl rings resulted in lower yields while electron deficient rings increased yield. Perhaps explained by an increase in electron density on the ether, reducing the electrophilicity of the quinone. Interestingly they found when substituting the aryl ring with one or two phenyl groups, they observed predominantly “nitroethylated” product in similar yields and selectivities. They postulated that these diaryl ether substrates proceed via a quinone methide intermediate based on work from Mukherjee.[156] If this intermediate is sufficiently long lived, then

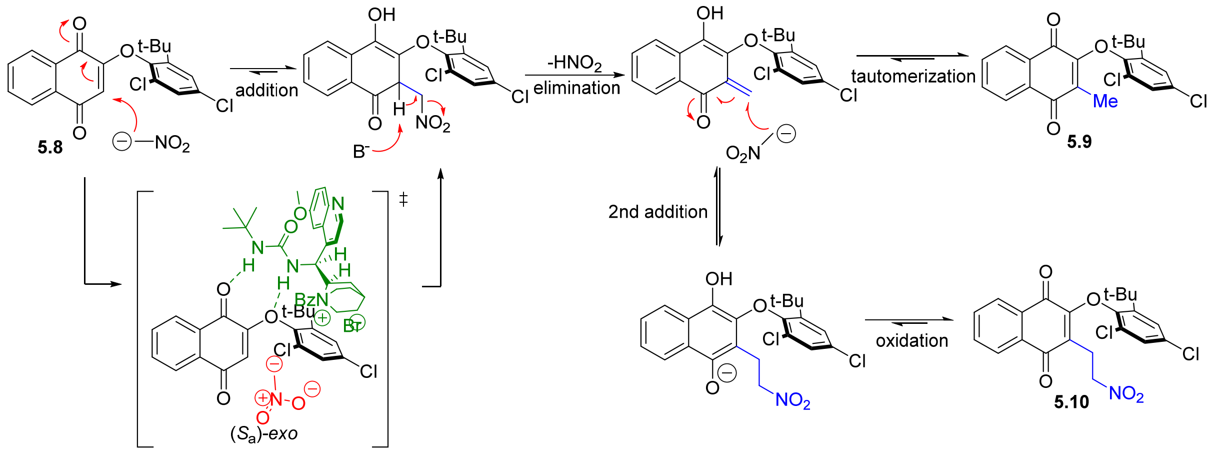

Figure 5.4.2. Proposed mechanism for the nucleophilic methylation.

another equivalent of nitronate anion can add 1,4 into the quinone-methide to yield the "nitroethylated" product **5.10** (Figure 5.4.2).

At this point in the project's timeline, I joined the team to help define the point of stereochemical induction and the mechanism of racemization. As we were unable to obtain suitable crystals, we compared experimental and computational circular dichroism (CD) spectra, a method that is gaining acceptance in the stereochemical community.[158–160] We obtained CD spectra of highly enantioenriched (e.r. > 97:3), as well as enantiopure sample of the opposite enantiomer (e.r. 0:100) separated via HLPC chiral column, of **5.9** and compared it to the weighted computational CD spectra of each enantiomer of **5.9** (Figure 5.4.3A). The predicted CD spectra was greatly influenced by the dihedral angles of both diaryl ether axes. To accurately predict the likely low energy conformations of the molecule, the molecule's CD spectra was predicted at various dihedral angles of both axes and then weighted based on the conformation's relative energy ((S_a)-**5.9** shown in Figure 5.4.3B). This analysis suggests that the major product from the enantioselective reaction is in the (S_a)-configuration with the *ortho* quinone carbonyl *endo* to the aryl ring, or (S_a)-*endo*.

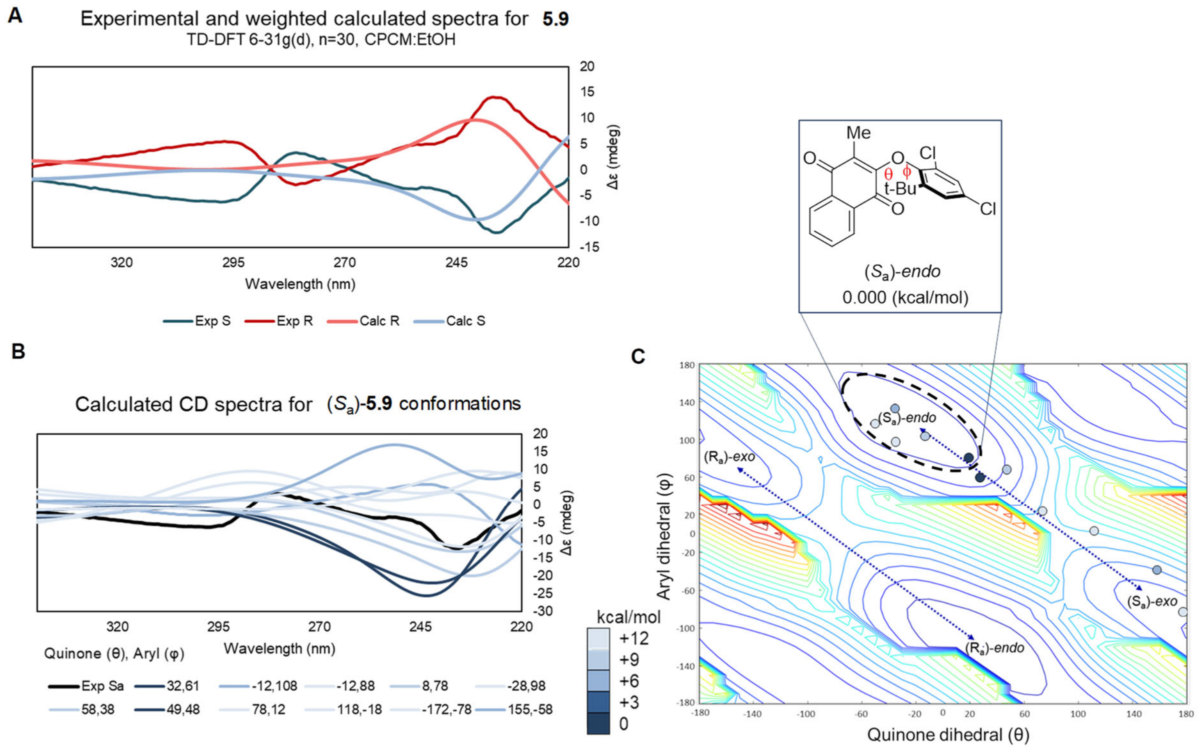

Figure 5.4.3. Conformational analysis and absolute configuration assignment

A) Overlaid experimental and calculated CD spectra for **5.9** (weighted average). B) (S_a)-**5.9** contributing conformation's CD spectra and relative energies used to calculate the predicted CD spectra. C) The MMFF calculated contour plot containing various (S_a)-**5.9** conformations labeled with circles shaded according to their relative calculated energies.

Guided by the computational CD studies, we used the calculated conformation's relative energies to generate hypotheses on which conformations contribute to racemization, catalyst-substrate transition state, and complete mechanism of the reaction. We first noticed the (S_a)-*endo* conformation of **5.9** is predicted to be significantly more stable than the (S_a)-*exo* conformation (Figure 5.4.4). Interestingly, we observed the opposite trend for the starting material **5.8**, with the *exo*-conformation being the more stable. To investigate this further, we generated contour energy maps of the rotational landscape about both axes of the diaryl ether (Seen in Figure 5.4.3 and Figure 5.4.4). In a manner consistent with results from Clayden and co-workers,[33] these maps demonstrate that there is a low energy pathway for interconversion between the *exo* and *endo*

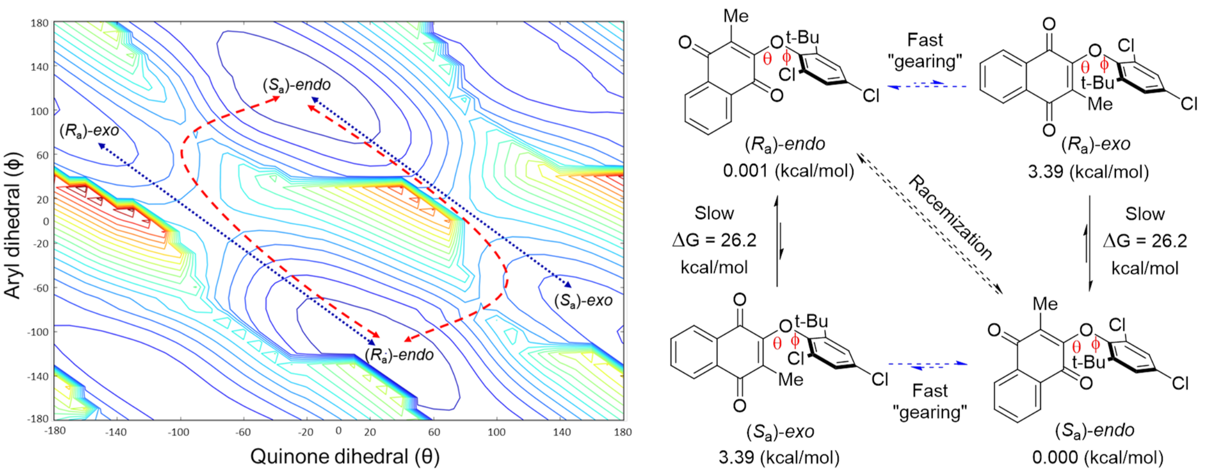
Aryl dihedral (ϕ)
Quinone dihedral (θ)
180
140
100
60
20
0
-20
-60
-100
-140
-180
-180
-140
-100
-60
-20
0
20
60
100
140
180
(S_a)-endo
(R_a)-exo
(S_a)-exo
(R_a)-endo
Me
O
O
O
t-Bu
Cl
Cl
θ
ϕ
Fast
"gearing"
(R_a)-endo
0.001 (kcal/mol)
(R_a)-exo
3.39 (kcal/mol)
Racemization
Slow
ΔG = 26.2
kcal/mol
Slow
ΔG = 26.2
kcal/mol
(S_a)-exo
3.39 (kcal/mol)
Fast
"gearing"
(S_a)-endo
0.000 (kcal/mol)

Figure 5.4.4. Dihedral-angle contour diagram.

This diagram was generated through a force-field molecular model and conveys an energetically favorable pathway towards racemization through a concerted gearing mechanism.

conformations of a given enantiomer that proceeds via a concerted gearing mechanism. Thus, because the *exo* conformation of the starting material is more stable than the *endo*, it is the *exo* that likely be the conformation that interacts with the catalyst. However, addition of the methyl group will lead to an immediate conformational gear shift to the *endo* enantiomers.

Our working model for stereoinduction is shown in the proposed transition state shown in Figure 5.4.2, in which we propose that the urea moiety of the catalyst forms a hydrogen bond with both the ether oxygen and one of the quinone carbonyls of the lower-energy *exo* diaryl ether conformation. From here, the diaryl ether is preorganized into the (S_a)-atropisomer to avoid steric interactions between the *tert*-butyl group and the quinuclidinium that would be present in the (R_a)-atropisomer/catalyst complex. We postulate that the hydrogen bonding activates the diaryl ether toward nucleophilic attack by the nitronate anion and that the molecule subsequently undergoes HNO_2 elimination followed by tautomerism to give the alkylated quinone, or subsequent attack by nitronate followed by oxidation to give the nitroethylated byproduct. At this point, it is likely that both products will rapidly relax to the *endo* conformation, perhaps providing a release mechanism from the catalyst.

We have disclosed the first example of a small-molecule-catalytic synthesis of diaryl ethers. Although the selectivities were moderate to good, the highly enantioenriched ethers could be accessed through trituration. We hope that these studies will serve as a starting point for future efforts towards the enantioselective syntheses of diaryl ethers and related atropisomers.

5.5 Catalytic Atroposelective Synthesis of N-Aryl Quinoid Compounds

As described in Chapter 4, diaryl amines are among the most common potentially atropisomeric chemotypes in medicinal chemistry, with FDA-approved binimetinib, bosutinib and afatinib representing examples of diaryl amines that exist as rapidly interconverting atropisomers (Figure 5.5.1A).[42,56,161] Diarylamines are also interesting from a stereochemical perspective as they possess two contiguous atropisomeric axes which leads to a complex conformational profile as well as a potential gearing mechanism that can lead to lower than expected barriers to racemization.[162,163] Relatively little is known about atropisomerically stable diaryl- amines. Kawabata[38,39] resolved the atropisomers of a series of diarylamines that possessed an intramolecular N-H-N hydrogen bond that preorganized one of the axes into a planar conformation (Figure 5.5.1B), simplifying diarylamines to a single axis system and resulting in compounds that possessed barriers to racemization of up to ~28 kcal/mol, existing as class 2 atropisomers half-life to racemization on the day to month timescale at 37 ºC. More recently, Clayden[162] resolved the atropisomers for diarylamines without an internal H-bond, finding them to only have stereochemical stabilities on the hour time scale at room temperature.

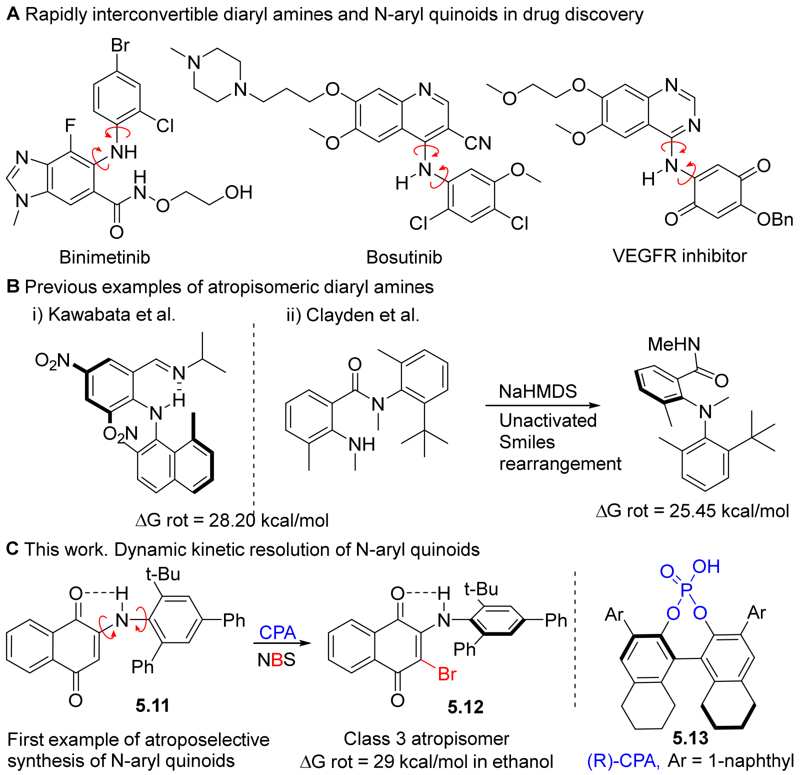
A Rapidly interconvertible diaryl amines and N-aryl quinoids in drug discovery
Br
F
Cl
NH
N
N
H
N
O
OH
O
Binimetinib
N
N
O
N
CN
O
H
N
O
Cl
Cl
Bosutinib
O
O
N
N
O
H
N
O
O
OBn
VEGFR inhibitor
B Previous examples of atropisomeric diaryl amines
i) Kawabata et al.
ii) Clayden et al.
O2N
N
H
N
O2N
ΔG rot = 28.20 kcal/mol
O
N
NH
NaHMDS
Unactivated
Smiles
rearrangement
MeHN
O
N
ΔG rot = 25.45 kcal/mol
C This work. Dynamic kinetic resolution of N-aryl quinoids
t-Bu
O----H
N
Ph
Ph
O
5.11
CPA
NBS
O----H
t-Bu
N
Ph
Ph
Br
O
5.12
O
OH
P
O
O
Ar
Ar
5.13
First example of atroposelective
synthesis of N-aryl quinoids
Class 3 atropisomer
ΔG rot = 29 kcal/mol in ethanol
(R)-CPA, Ar = 1-naphthyl

Figure 5.5.1. Atropisomerism in Diarylamines and related scaffolds.

As instances of stereochemically stable diarylamines have been scarce, there are no published examples of their enantioselective synthesis. Below describes the work of my colleagues and I that have led to the first catalytic atroposelective synthesis of a diarylamine-like scaffold, finding *N*-aryl quinoids that possess a 5-membered intramolecular N-H-O hydrogen bond to exist as stereochemically stable class 3 atropisomers with barriers to racemization approaching and exceeding 30 kcal/mol ($t_{1/2\ (37^{\circ}\ \mathrm{C})}$ > 4.5 years).

Inspired by Kawabata's work, as well as a series of *N*-aryl quinoid-based kinase inhibitors,[81] my colleague, Dr. Sagar Vaidya, synthesized substrate **5.11** which exists as a stereochemically unstable class 1 atropisomer. Computational studies and X-ray crystallographic analysis done by myself and Dr. Nobuyuki Yamamoto suggested that the quinoid-nitrogen axis exists in a planar '*exo*' conformation due to a strong intramolecular N-H-O hydrogen bond. This

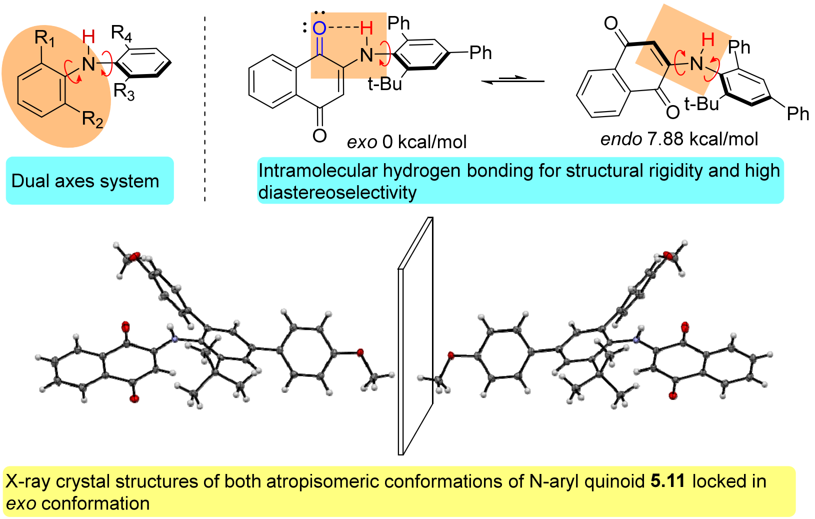
R1
H
R4
N
R3
R2
Dual axes system
O
H
N
Ph
Ph
t-Bu
O
exo 0 kcal/mol
O
H
N
Ph
O
t-Bu
Ph
endo 7.88 kcal/mol
Intramolecular hydrogen bonding for structural rigidity and high diastereoselectivity
X-ray crystal structures of both atropisomeric conformations of N-aryl quinoid 5.11 locked in exo conformation

Figure 5.5.2. *N*-Aryl quinoids as a diaryl amine surrogate with one chiral axis.

scaffold's inherent interaction, simplifies its 2-axis system into a single axis system in a manner analogous to that of Kawabata (Figure 5.5.2). Therefore, we hypothesized that functionalization of the quinoid C-H could lead to stable atropisomerism.

As the amino naphthoquinone moiety could be considered 'enamine-like' and inspired by Akiyama[164–169], Dr. Sagar Vaidya evaluated the electrophilic functionalization of **5.11** using chiral phosphoric acids, observing facile electrophilic halogenation using *N*-halosuccinimides.[170,171] Excitingly, these products (e.g. **5.12**) proved quite stereochemically stable (*vida infra*), confirming that this system may be amenable to atropisomer selective catalysis. While many of these catalysts yielded poor selectivity, a CPA (*R*)-TRIPS analog with 1-naphthyl substitution at the 3,3' position (**5.13**) to be an effective catalyst yielding brominated product **5.12** in 94% yield and an e.r. of 96:4 under optimized conditions.

The chemistry proved to be tolerant of diverse aryl substitutions of the 2,4-positions of the aniline, including electron rich, electron poor and fused ring systems. He also evaluated anilines that possessed groups smaller than *t*-Bu at the 6-position such as isopropyl and trifluoromethyl observing drastic decreases in e.r. to 63:37 and 56:44 respectively, likely due to a low barrier to racemization (measured to be~24 kcal/mol) for these substrates leading to racemization during the course of the reaction.

Racemization studies were also carried out to investigate the stereochemical stability of representative products. Product **5.12** was found to have an average barrier to rotation of 30 kcal/mol at 100 ºC in toluene, ethanol, a 4:1 mixture of EtOH and 0.5M HCl, and mixture of toluene in pH 7.5 in 1 M tris buffer. This data is significant as it suggests that these compounds would be stereochemically stable under biological environments; thus, this work could be a gateway towards the development of atropisomerically stable analogs for the myriad diarylamines in medicinal chemistry.

I was brought on board to help better understand the unexpected high stereochemical stability (30.31 kcal/mol) that was observed for **5.12**. In the X-ray crystal structure of **5.12**, the naphthoquinone-N axis is locked into a planar *exo* orientation due to the aforementioned intramolecular hydrogen bonding. We further explored this by computationally evaluating the relative energy values of other conformations (Figure 5.5.3). Both *exo*, (R_{a}) and *exo,* (S_{a}) conformations (0 kcal/mol) were significantly lower in energy than their respective *endo*

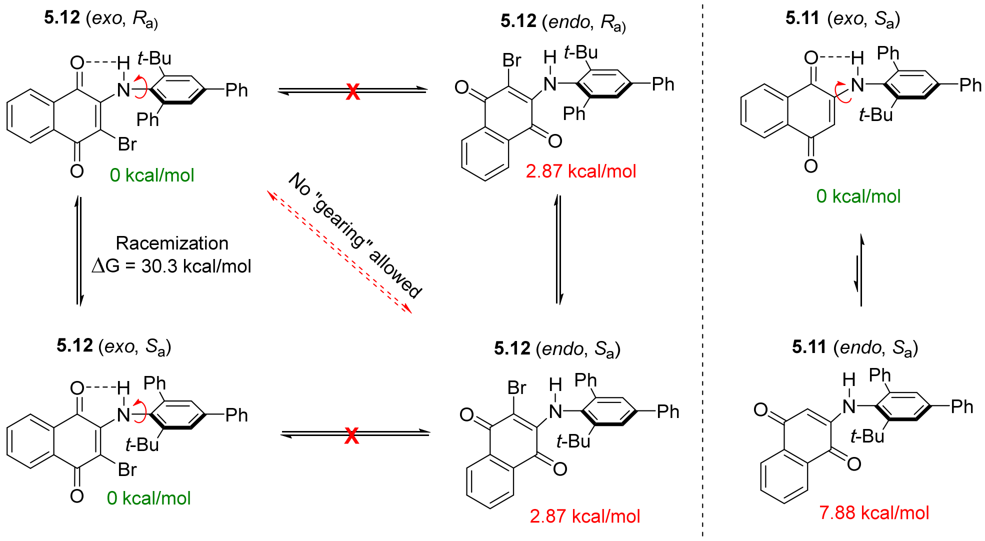
5.12 (*exo*, *R*a)
O---H *t*-Bu
N
Ph
Ph
Br
O
0 kcal/mol
5.12 (*endo*, *R*a)
Br
H *t*-Bu
N
Ph
Ph
O
O
2.87 kcal/mol
5.11 (*exo*, *S*a)
O---H Ph
N
Ph
t-Bu
O
0 kcal/mol
Racemization
ΔG = 30.3 kcal/mol
No "gearing" allowed
5.12 (*exo*, *S*a)
O---H Ph
N
Ph
t-Bu
Br
O
0 kcal/mol
5.12 (*endo*, *S*a)
Br H Ph
N
Ph
t-Bu
O
O
2.87 kcal/mol
5.11 (*endo*, *S*a)
H Ph
N
Ph
t-Bu
O
O
7.88 kcal/mol

Figure 5.5.3. Mechanism of Racemization.

conformations that possessed no intramolecular hydrogen bonding (+2.87 kcal/mol). Previously reported 2 axes systems are able to undergo concerted "gearing" to racemize, like the examples in sub-chapter **5.4**, allowing for a lower energy pathway to racemization (barrier to rotations of 25-27 kcal/mol with similar sized substituents). The strong intramolecular hydrogen bonding likely precludes the gearing mechanism for racemization, requiring a more rigid pathway to racemization that is more analogous to biaryl and benzamide systems. Indeed, computational studies predicted barrier to rotations that agreed with our experimentally determined values when freezing the naphthoquinone-N axis; when the system was allowed to rotate both axes, predicted barriers to rotations were significantly lower than the experimental values (Figure 5.5.4).

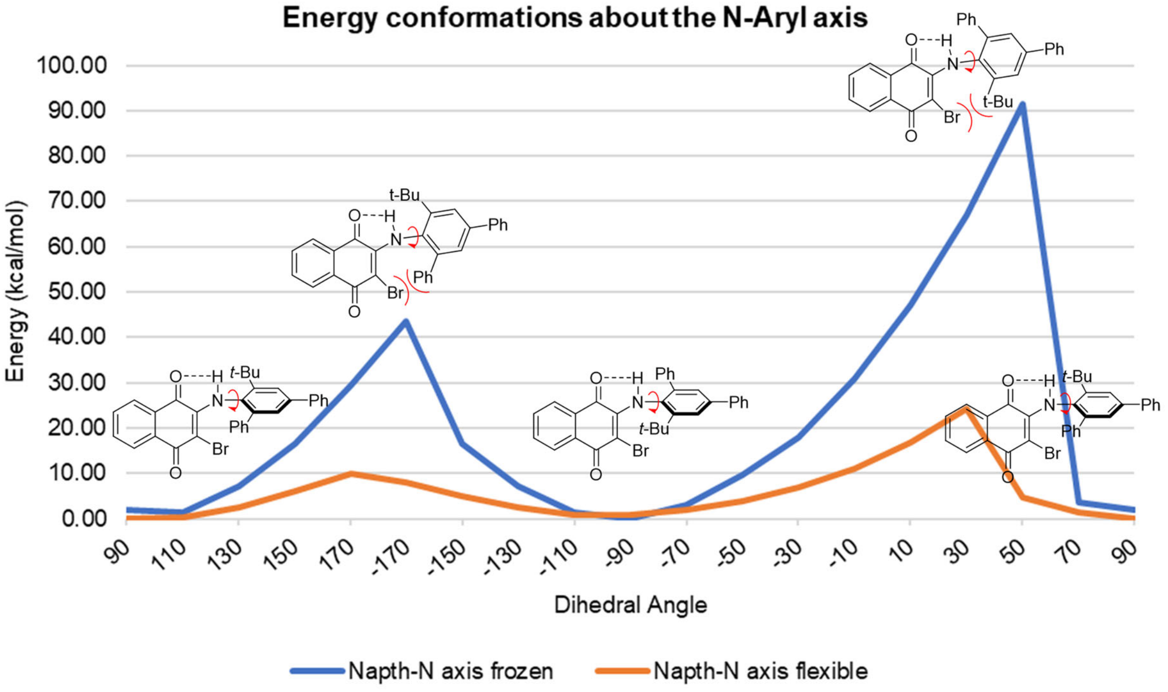

Figure 5.5.4. Conformational energy plot for **5.12**.

Gaussian 09's scan function (B3LYP/6-31(d) in gas phase) was used to predict barrier to rotation of product **5.12** when the Naphthoquinone-N axis is frozen (blue) or when allowed to rotate during minimizations.

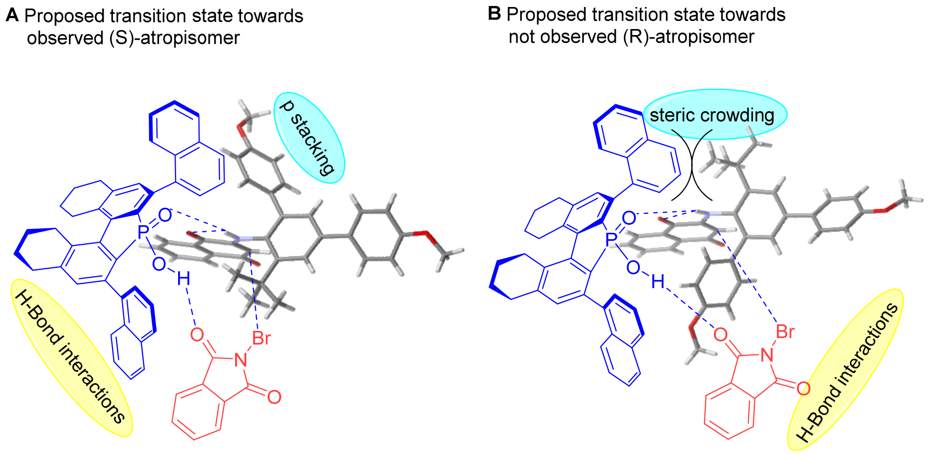

A Proposed transition state towards observed (S)-atropisomer

B Proposed transition state towards not observed (R)-atropisomer

Figure 5.5.5. Proposed transition state with substrate, catalyst and *N*-bromophthalimide.

Based on our data thus far, we propose the mechanism for stereochemical induction depicted in Figure 5.5.5. We postulate the CPA **5.13** engages in hydrogen bonding with the substrates O-H-N network with the starting material **5.11** locked in the *exo* conformation, which is 7.88 kcal/mol more stable than the *endo* conformation (Figure 5.5.3). This H-bonding interaction would be expected to increase the energy level of the HOMO of the enamine-like amino naphthoquinone. The *N*-aryl axis would then be expected to rotate as to orientate the *t*-Bu group away from the catalyst, which would result in this axis being organized into the (S_a) conformation. Notably, the (S_a) conformation would also have the potential for the *ortho* aryl group to participate in pi-stacking with the catalyst naphthyl group, whereas the enantiomeric conformation would not. Finally, the acidic proton from CPA can activate the electrophilic halogenation reagent via H-bonding which will also allow for direction of bromination towards the naphthoquinone site. Upon electrophilic bromination, the axis will be rigidified selectively into the (S_a) configuration

We have described the first catalytic atropisomer selective synthesis of a diarylamine-like scaffold. This chemistry proceeds via phosphoric acid catalyzed halogenation of *N*-aryl quinoids and yields products in upwards of 95:5 e.r. and 90% yield. Surprisingly, we found these products existed as stereochemically stable class-3 atropisomers in protic and aprotic conditions due to a strong intramolecular H-bond that locks one of the axes into a planar conformation. As diarylamines are among the most ubiquitous scaffolds in drug discovery, the chemistry, concepts and principles put forward can extend far beyond this work and be of use for the design and enantioselective synthesis of diverse chiral diarylamine scaffolds with applications in drug discovery and asymmetric synthesis.

5.6 Acknowledgements

Chapter 5 is a compilation of highlighted sections from three different manuscripts with permission from each manuscript's journal: Cardenas, M.; Toenjes, S**.**; Nalbandian, C.; Gustafson, J. Enantioselective Synthesis of Pyrrolopyrimidine Scaffolds through Cation-directed Nucleophilic Aromatic Substitution. *Org. Lett.* **2018**, *20,* 2037-2041*,* Dinh, A.; Noorbehesht, R.; Toenjes, S.; Jackson, A.; Saputra, M.; Maddox, S.; Gustafson, J. Towards a Catalytic Atroposelective Synthesis of Diaryl Ethers via C(sp^2)-H Alkylation Using Nitroalkanes. *Synlett* **2018**, *29,* 2155-2160, and Vaidya, S.; Toenjes, S.; Yamamoto, N.; Maddox, S.; Gustafson, J. Catalytic Atroposelective Synthesis of N-Aryl Quinoid Compounds. *J. Am. Chem. Soc.* **2020**, *142*, 2198-2203. The dissertation author was a supplemental researcher and coauthor for each of these manuscripts. Support of this work by the National Institute of General Medical Sciences is acknowledged (R35GM124637).

Appendix

A.1 Chapter 2 Experimental Section

H and C NMR spectra were recorded on Varian VNMRS 400 MHz, Varian Inova 500 MHz, and Bruker Avance III 600 MHz spectrometers at 25 ºC. All chemical shifts were reported in parts per million (ppm) and were internally referenced to residual protio solvents unless otherwise noted. Spectral data were reported as follows: chemical shift (multiplicity [singlet (s), doublet (d), triplet (t), quartet (q), pentet (p), and multiplet (m)], coupling constants [Hz], integration). Carbon spectra were recorded with complete proton decoupling. Conventional mass spectra were obtained using Advion Expression CMS (APCI and ASAP). All chemicals used in the synthesis of substrates were purchased from Sigma Aldrich, TCI, Frontier Scientific, Acros Organics, Strem, Oakwood, Matrix Scientific, or Fisher Scientific and were used as received without further purification, unless specifically noted. All normal phase flash column chromotagraphy (FCC) was performed using Grade 60 Silca Gel (230-400 mesh) purchased from Fisher Scientific or performed on a Biotage Isolera One with a Biotage SNAP cartridge (KP-SIL- 10-50g). Preparative Thin Layer Chromatography (TLC) plates contained grade 60 silica-gel coated with fluorescent indicator F_{254}. Atropisomerically stable compounds were isolated via chiral HPLC using an Agilent 1100 series HPLC. CHIRALPAK IA column were purchased from Diacel Technologies Corporation. Monowave 400 by Anton Paar was used for all microwave reactions in 10G or 30G reactor vessels.

Cell lines and antibodies. Human cancer cell lines LC-2/AD, TT, MCF7, BT474, H292, H1975 were purchased from the American Type Culture Collection (ATCC) (Manassas, VA, USA). Ba/F3 cell line was purchased from DSMZ (Brunswick, Germany). All cell lines were maintained in the ATCC or DSMZ's recommended culture media at 37 °C with 5% CO_2.

Ba/F3 cell generation. The retroviral pBabe-Puro-EGFR-L858R and EGFR-L858R/T790M plasmids were obtained from the Meyerson Lab (via Addgene). pBabe-Puro backbone plasmid was donated by the Land Lab (via Addgene). The EGFR-L858R/T790M/C797S triple mutant was generated by QuikChange site-directed mutagenesis (Agilent) using pBabe-Puro-EGFR-L858R/T790M as template DNA using the following primers: F-GCAGCTCATGCCCTTCGGCT**C**CCTCCTGGACTATGTCCGG, and C797S R-CCGGACATAGTCCAGGAGG**G**AGCCGAAGGGCATGAGCTGC (where the mutated nucleotide is in bold and underlined). pBabe-Puro constructs were cotransfected in HEK293T cells along with pCL-Eco (via Verma's Lab from Addgene) packaging plasmid. Supernatant containing retroviruses was collected at 24, 48, and 72 hours post transfection, filtered through 0.45 μm filters, and used to infect 1 million Ba/F3 cells in three consecutive days. 48 h after the last infection, infected Ba/F3 cells were selected by culturing for 4 days with 4μg/ml puromycin in RPMI supplemented with 10% FBS and 10 ng/ml IL-3 (R&D Systems). After the 4 days, IL-3 was completely withdrawn and cells were grown in the absence of IL-3 obtain IL-3 independent EGFR signaling-addicted cells.

Antiproliferation assays. LC-2/AD, TT, BT474, H292 and H1975 were seeded in white 384-well culture plates (3000 cells/well). Cells were allowed to attach for 2-4 h and then compounds were added at the indicated concentrations. Ba/F3 cells were seeded at a density of 500/well and treated with varying concentrations of test compounds. Cell viability was determined after 72 h by CellTiter-Glo assay (Promega), and luminescence was measured in a ClarioStar plate reader (BMG Labtech). MCF7 cells were steroid deprived prior to cell proliferation assays by culturing in phenol red-free DMEM containing 10% dextran-coated charcoal treated FBS for three days. Estrogen-deprived MCF7 cells (ED-MCF7) were seeded in 96-well culture plates (4000 cells/well) and growth was stimulated with 1 nM estradiol (E2) and 20 nM GDNF in the absence or in the presence of test compounds. Cell viability was measured using MTT assay (USB) after 3 days of treatment and absorbance was measured at 570 nm. Data were normalized to control groups (0.1% DMSO) and represented by the mean of three independent measurements.

Kinase inhibition assays. Kinases were purchased from Signal Chem and evaluated in ADP-Glo (Promega) assays. 50µM ATP was mixed with 100 µg/ml substrate and added to 1.2ng/µl kinase with varying inhibitor concentrations in kinase buffer (1% DMSO) in a 384-well white plate. The manufacturer's protocol was followed and luminescence was read with a ClarioStar plate reader (BMG Labtech). IC_{50}'s were converted to K_i's using ATP concentration and reported K_M's of tested kinases in the Cheng-Prusoff equation. The partial kinome screen was carried out by Life Technologies' SelectScreen Biochemical Kinase Profiling Service. The inhibitory activity of (R_a)-2.16 and (S_a)-2.16 at 300 nM were evaluated against each kinase using their ATP K_M concentration. Results reported as a percent of inhibition in the tables are the mean of duplicate points. Follow-up EGFR mutant IC_{50} 10-point titrations were evaluated at the K_M of each kinase using the Kinase Profiling service Z-Lyte assay from Life Technology.

Western blots. Estrogen-deprived MCF7 cells (1 million per condition) were serum starved in 0.1% DCC FBS overnight, then treated with serially diluted (R_a)-2.16 (10µM – 10nM) or (S_a)-2.16 (10µM) for 2 hours followed by addition of 20nM GDNF. After 30min, cells were placed on ice, washed with cold PBS and lysed in RIPA lysis buffer. Protein concentration was measured by the BCA Protein Assay Reagent (Thermo Scientific) according to the manufacturer's protocol. Western blot analyses were conducted after separation by SDS-PAGE and transferred to polyvinylidene difluoride membranes. After blocking in 5% BSA with Tris-buffered saline/Tween 20 (TBS-T), membranes were incubated with phospho-Akt (Ser473; R&D, MAB887, 1:500), total

Akt (Cell Signaling Technology, #9272, 1:2000), phospho-ERK (Thr202/Tyr204; Cell Signaling Technology, #9101, 1:1000), or total ERK1/2 (Santa Cruz, sc-154, 1:2000).

Computational methods. *Inhibitor docking*. The x-ray crystal structures of RET (PDB 2IVV), SRC (PDB 1YOL), EGFR (PDB 2GS6), EGFR T790M (PDB 5YU9), VEGFR2 (PDB 3WZD) and BTK (PDB 5P9I) were used for these studies. Each x-ray structure was imported into MOE (Chemical Computing Group). All waters as well as other non-protein, non-ligand, or non-cofactor molecules were removed and the structures were protonated. For each protein, the x-ray conformation of the bound ligand was used to define the binding pocket. Docking experiments were performed with the Dock function in MOE using the Amber12:EHT forcefield2 with parameterized solvation and default parameters and fitness functions. The receptor binding site was allowed minimal flexibility and the ligand was allowed full flexibility with the top ten scoring ('S' score from MOE), non-redundant poses retained. These ten poses were visually inspected and used to optimize next the iteration of inhibitors.

Conformational Energy Plots. All structures were optimized in the gas phase using density functional theory (RB3LYP) with the 6-31G(d) basis set as implemented in the Gaussian 09 suite of programs. The atropisomeric axis dihedral was frozen every 5 degrees while the rest of the structure was minimized and single point energies were recorded. All energies are reported in kcal/mol with respect to the minimized inhibitor.

Molecular dynamic simulations. All molecular dynamics (MD) simulations were carried out using MOE. The top two binding poses of each inhibitor in each kinase from the previously mentioned docking studies were used as initial structures for the (MD) simulation. MOE's QuickPrep was used to add partial charges and minimize structure. The Amber force field was used for protein, ligand and ions. The system was equilibrated with no positional restraints on any atoms for 100 ns under constant volume and followed by 500 ns a production run with snapshots taken every 0.5 ns.

Kinase inhibitors. Compound syntheses and characterizations are reported below.

Supplementary Table 1. Partial kinome screen of (S_a)-**2.16** and (R_a)-**2.16** at 300 nM (in duplicate) against kinases 127 kinases using Life Technologies SelectScreen® Kinase Profiling Services. The average % activity inhibited is listed for each compound against each kinase. Note, the screening concentration (300 nM, 215x the K_i of (R_a)-**2.16**) was chosen to get a better gauge of selectivity.

(S_a)-**2.16**		(R_a)-**2.16**	
Kinase	**%inhibtion**	**Kinase**	**%inhibtion**
ACVR2B	59	ACVR2B	104
RET Y791F	59	RET Y791F	99
EPHA1	40	EPHA1	99
EPHA6	65	EPHA6	98
RET A883F	65	RET A883F	98
EPHB2	37	EPHB2	98
RET	43	RET	97
FGR	57	FGR	97
PTK6 (Brk)	24	PTK6 (Brk)	97
RET S891A	71	RET S891A	97
FRK (PTK5)	70	FRK (PTK5)	96
ABL2 (Arg)	47	ABL2 (Arg)	95
PEAK1	45	PEAK1	93
BMPR1B (ALK6)	30	BMPR1B (ALK6)	91
RET M918T	27	RET M918T	91
CSNK1E (CK1 epsilon)	38	CSNK1E (CK1 epsilon)	90
FYN	27	FYN	90
SRC	18	SRC	89
YES1	36	YES1	89
EGFR (ErbB1) T790M	25	EGFR (ErbB1) T790M	87
RET G691S	30	RET G691S	86
ABL1	27	ABL1	86
BLK	23	BLK	85
EPHA2	19	EPHA2	82
CSF1R (FMS)	16	CSF1R (FMS)	81
LYN A	27	LYN A	80
BMX	19	BMX	78
FGFR1	16	FGFR1	77
BMPR1A (ALK3)	8	BMPR1A (ALK3)	77
FGFR2	18	FGFR2	76
LCK	-5	LCK	75
HCK	9	HCK	74
RIPK2	12	RIPK2	72
MAP4K5 (KHS1)	26	MAP4K5 (KHS1)	68
CSK	12	CSK	68
ACVR1 (ALK2)	13	ACVR1 (ALK2)	67
ACVRL1 (ALK1)	14	ACVRL1 (ALK1)	63
BTK	6	BTK	59
BRAF	22	BRAF	56

Supplementary Table 1 (*continued*).

(S_a)-2.16		**(R_a)-2.16**	
Kinase	**%inhibtion**	**Kinase**	**%inhibtion**
BRAF V599E	23	BRAF V599E	56
EGFR (ErbB1)	-6	EGFR (ErbB1)	53
FGFR4	3	FGFR4	53
ACVR1B (ALK4)	-10	ACVR1B (ALK4)	47
RAF1 (cRAF) Y340D Y341D	17	RAF1 (cRAF) Y340D Y341D	47
MAP4K4 (HGK)	-2	MAP4K4 (HGK)	44
KDR (VEGFR2)	-4	KDR (VEGFR2)	44
MINK1	10	MINK1	37
CDK8/cyclin C	17	CDK8/cyclin C	34
NTRK3 (TRKC)	3	NTRK3 (TRKC)	32
ERN1	17	ERN1	26
PTK2 (FAK)	3	PTK2 (FAK)	20
TGFBR2	-10	TGFBR2	19
MAPK14 (p38 alpha) Direct	-6	MAPK14 (p38 alpha) Direct	18
TYK2	5	TYK2	17
NTRK2 (TRKB)	2	NTRK2 (TRKB)	17
MAP4K2 (GCK)	7	MAP4K2 (GCK)	17
FGFR3	3	FGFR3	16
MAP2K5 (MEK5)	4	MAP2K5 (MEK5)	15
ROS1	4	ROS1	15
FLT4 (VEGFR3)	-6	FLT4 (VEGFR3)	14
MAP4K3 (GLK)	6	MAP4K3 (GLK)	13
MAP3K9 (MLK1)	5	MAP3K9 (MLK1)	12
MAPK10 (JNK3)	-1	MAPK10 (JNK3)	11
MAP2K1 (MEK1)	4	MAP2K1 (MEK1)	11
CDK9/cyclin T1	12	CDK9/cyclin T1	10
DYRK2	2	DYRK2	9
DDR1	-1	DDR1	9
LIMK1	-10	LIMK1	8
RET V804E	5	RET V804E	8
RET V804M	6	RET V804M	8
MAP3K11 (MLK3)	1	MAP3K11 (MLK3)	8
PRKCB1 (PKC beta I)	6	PRKCB1 (PKC beta I)	7
PDGFRB (PDGFR beta)	0	PDGFRB (PDGFR beta)	6
PIK3CB/PIK3R1 (p110 beta/p85 alpha)	5	PIK3CB/PIK3R1 (p110 beta/p85 alpha)	6
PIK3CA/PIK3R1 (p110 alpha/p85 alpha)	6	PIK3CA/PIK3R1 (p110 alpha/p85 alpha)	6
PRKACA (PKA)	-3	PRKACA (PKA)	6
ALK	5	ALK	6
KIT	-4	KIT	6
ERBB2 (HER2)	1	ERBB2 (HER2)	6
CDK4/cyclin D1	8	CDK4/cyclin D1	5
MAPK9 (JNK2)	1	MAPK9 (JNK2)	5
AURKA (Aurora A)	3	AURKA (Aurora A)	5
RET V804L	4	RET V804L	5
BRSK1 (SAD1)	4	BRSK1 (SAD1)	4
MERTK (cMER)	3	MERTK (cMER)	4
BRSK2	6	BRSK2	4
TYRO3 (RSE)	-1	TYRO3 (RSE)	3
CLK1	2	CLK1	3
PDGFRA (PDGFR alpha)	-4	PDGFRA (PDGFR alpha)	3
MAP3K10 (MLK2)	-2	MAP3K10 (MLK2)	3
IGF1R	1	IGF1R	3
SRPK1	2	SRPK1	2

Supplementary Table 1 (*continued*).

(S_a)-**2.16** **Kinase**	**%inhibtion**	(R_a)-**2.16** **Kinase**	**%inhibtion**
CDK13/cyclin K	-4	CDK13/cyclin K	2
FLT1 (VEGFR1)	-2	FLT1 (VEGFR1)	2
PIK3C2A (PI3K-C2 alpha)	-9	PIK3C2A (PI3K-C2 alpha)	2
FRAP1 (mTOR)	2	FRAP1 (mTOR)	1
CDK6/cyclin D1	-4	CDK6/cyclin D1	1
MAP3K19 (YSK4)	1	MAP3K19 (YSK4)	1
MAP3K14 (NIK)	0	MAP3K14 (NIK)	1
PIK3C2G (PI3K-C2 gamma)	-2	PIK3C2G (PI3K-C2 gamma)	1
PRKCA (PKC alpha)	1	PRKCA (PKC alpha)	1
AXL	-1	AXL	0
ROCK2	1	ROCK2	0
DAPK3 (ZIPK)	1	DAPK3 (ZIPK)	0
CDK7/cyclin H/MNAT1	-6	CDK7/cyclin H/MNAT1	0
MAPK8 (JNK1)	0	MAPK8 (JNK1)	0
PRKCI (PKC iota)	6	PRKCI (PKC iota)	-1
SGK (SGK1)	0	SGK (SGK1)	-1
DAPK1	-3	DAPK1	-1
NTRK1 (TRKA)	1	NTRK1 (TRKA)	-2
MAPKAPK2	-1	MAPKAPK2	-2
PIK3CG (p110 gamma)	-19	PIK3CG (p110 gamma)	-2
PAK1	-2	PAK1	-3
AKT1 (PKB alpha)	-3	AKT1 (PKB alpha)	-3
FLT3	-3	FLT3	-4
MAPK1 (ERK2)	-3	MAPK1 (ERK2)	-4
ROCK1	-5	ROCK1	-4
GSK3A (GSK3 alpha)	-4	GSK3A (GSK3 alpha)	-4
PRKCE (PKC epsilon)	1	PRKCE (PKC epsilon)	-4
JAK3	-8	JAK3	-5
MET (cMet)	-6	MET (cMet)	-6
JAK1	-8	JAK1	-7
JAK2	-9	JAK2	-7
TEK (Tie2)	-9	TEK (Tie2)	-8
SYK	-8	SYK	-9
IRAK4	-9	IRAK4	-11
IRAK1	-13	IRAK1	-11

Supplementary Table 2. Low energy conformational energy profiles of **2.16**, **2.20**, PP1 (**2.21**), and **2.22**. All structures were optimized in the gas phase using density functional theory (RB3LYP) with the 6-31G(d) basis set as implemented in the Gaussian 09[172] suite of programs. The indicated dihedral angle was frozen every 5 degrees while the rest of the structure was minimized and energies were recorded. All energies are reported in kcal/mol with respect to the global minimum of each inhibitor.

	2.16	**2.20**	**2.21**	**2.22**
Dihedral Angle	Energy (kcal/mol) (-657804.6 min.)	Energy (kcal/mol) (-633321.9 min.)	Energy (kcal/mol) (-561579.5 min.)	Energy (kcal/mol) (-526703.0 min.)
-180	20.7	14.95	4.68	7.23
-175	17.3	12.47	3.74	6.00
-170	14.61	10.11	2.83	4.76
-165	11.78	7.98	2.01	3.60
-160	9.30	6.10	1.30	2.57
-155	7.16	4.50	0.74	1.70
-150	5.35	3.17	0.34	1.01
-145	3.85	2.09	0.09	0.50
-140	2.62	1.25	0.00	0.17
-135	1.66	0.65	0.07	0.02
-130	0.96	0.27	0.27	0.02
-125	0.47	0.07	0.55	0.13
-120	0.16	0.02	0.91	0.34
-115	0.01	0.10	1.33	0.64
-110	0.00	0.27	1.76	0.98
-105	0.07	0.52	2.13	1.30
-100	0.15	0.74	2.44	1.56
-95	0.22	0.89	2.64	1.75
-90	0.22	0.98	2.71	1.82
-85	0.21	0.97	2.61	1.74
-80	0.12	0.83	2.40	1.74
-75	0.07	0.63	2.10	1.56
-70	0.04	0.39	1.73	1.30
-65	0.11	0.18	1.33	1.01
-60	0.30	0.04	0.94	0.69
-55	0.68	0.00	0.60	0.39
-50	1.25	0.07	0.32	0.17
-45	2.03	0.29	0.11	0.04
-40	3.01	0.67	0.01	0.00
-35	4.22	1.24	0.04	0.08
-30	5.67	2.01	0.21	0.32
-25	7.36	2.98	0.52	0.72
-20	9.30	4.15	0.98	1.29
-15	11.47	5.52	1.59	2.02
-10	13.87	7.09	2.34	2.92
-5	15.7	8.85	3.21	3.96
0	18.4	10.78	4.17	5.12

Supplementary Table 3. Protein Data Bank ligand conformation analysis. Relative angles were used for Figure 2.4.3.

PDB ID	Protein	Chemical ID	Scaffold	Angle	Relative Angle	Aryl substitution	Position
6G6W	PI3Kd	EO5	PPY	142.73	-37.27	sulfonamide	*m*
3FI4	p38	FI4	PP	114.2	-65.8	Cl	*o*
4WG4	CDPK1	UWB	PP	62.11	-117.89	napth	*m*
4U8Z	MST3	3FE	PPY	51.24	-128.76	CN	*m*
4WG3	CDPK1	UWA	PP	50.69	-129.31	napth	*m*
4N4S	ERk2	2H1	PP	48.32	-131.68	Me	*m*
6HJJ	Aurora	G7T	PP	46.34	-133.66	Me	*o*
4W8E	MST3	3JB	PPY	42.94	-137.06	CN	*m*
4GKH	APH(3')-Ia	0J9	PP	34.17	-145.83	napth	*o*
5OP5	CHK1	3FE	PPY	29.16	-150.84	CN	*m*
4IH8	CDPK1	B43	PPY	-10.28	-10.28	OPh	*p*
2WXK	PI3Kd	RW4	PP	-31.21	-31.21	benathiozole	*m*
2WXJ	PI3Kd	RW3	PP	-33.81	-33.81	benathiozole	*m*
4HCU	ITK	13L	PP	-37.1	-37.1	amide	*m*
4HCV	ITK	13J	PP	-39.21	-39.21	amide	*m*
4HCT	ITK	18R	PP	-40.02	-40.02	amide	*m*
5HZN	IGFR1	66A	PPY	-41.17	-41.17	Obz	*m*
3ENE	PI3Kg	NPZ	PP	-45.42	-45.42	napth	*m*
2V4L	PI3Kg	ABJ	PP	-47.76	-47.76	OH	*m*
3EL8	Src	PD5	PP	-48.75	-48.75	anilide	*p*
5HHW	IGFR1	60O	PPY	-49.29	-49.29	O-alkyl	*m*
4CMG	PTR1	UHX	PPY	-50.16	-50.16	OMe	*p*
2WXG	PI3Kd	ZZN	PP	-50.86	-50.86	F	*m*
4CMA	PTR1	M2N	PPY	-52.11	-52.11	H	*p*
4CMC	PTR1	VS8	PPY	-52.29	-52.29	H	*p*
2WXH	PI3Kd	ZZO	PP	-53.93	-53.93	F	*m*
4X7O	PERK	3Z6	PPY	-54.3	-54.3	indoline	*m*
6HJK	Aurora	G7W	PP	-57.19	-57.19	anilide	*p*
4M7I	PERK	27D	PPY	-58.92	-58.92	F	*o*
4G31	PERK	0WH	PPY	-59.27	-59.27	indoline	*m*
4CME	PTR1	KTZ	PPY	-62.33	-62.33	H	*p*
5SWH	Src (V231C)	71D	PPY	-90.5	-90.5	Cl	*p*
4D9U	Rsk2	0JH	PPY	-97.04	-97.04	Me	*p*
5T0P	Src	73A	PPY	-98.38	-98.38	Cl	*p*
2BRO	Chk1	DF2	PPY	-98.54	-98.54	H	*p*
4D9T	Rsk2	0JG	PPY	-102.83	-102.83	Me	*p*
2BRM	Chk1	DFZ	PPY	-106.44	-106.44	H	*p*
3EN5	Src	KS4	PP	-106.94	-106.94	OMe	*m*
3QLF	Src (L317I)	PD5	PP	-108.34	-108.34	anilide	*p*
3SXS	BMX	PP2	PP	-109.29	-109.29	Cl	*p*
2ZV9	Lyn	PP2	PP	-111.27	-111.27	Cl	*p*
5FM3	Ret	PP1	PP	-111.74	-111.74	Me	*p*
3GEQ	Src	PP2	PP	-112.99	-112.99	Cl	*p*
4IFG	CDPK1	1E8	PP	-116.22	-116.22	OPh	*p*
2C0I	Hck	L1G	PP	-116.57	-116.57	OMe	*m*
2IVV	Ret	PP1	PP	-116.87	-116.87	Me	*p*
2C0O	Hck	L2G	PP	-117.02	-117.02	OMe	*m*
5FM2	Ret	PP1	PP	-117.04	-117.04	Me	*p*
5YU9	Egfr (T790M)	1E8	PP	-117.54	-117.54	OPh	*p*
5GNK	Egfr (T790M)	80U	PP	-119.31	-119.31	Cl	*m*
1QPE	Lck	PP2	PP	-119.4	-119.4	Cl	*p*
5P9J	Btk	8E8	PP	-119.57	-119.57	OPh	*p*
4LUE	Hck	VSE	PPY	-119.59	-119.59	OPh	*p*
5ZJ6	Hck	VSE	PPY	-120.13	-120.13	OPh	*p*
5P9I	Btk	1E8	PP	-120.41	-120.41	OPh	*p*
5J9Y	Egfr (T790M)	6HL	PP	-120.67	-120.67	napth	*m*
4CMJ	PTR1	UIH	PPY	-120.74	-120.74	H	*p*
3GEN	Btk	B43	PPY	-121.03	-121.03	OPh	*p*
3EN7	Src	ABJ	PP	-121.4	-121.4	OH	*m*

Supplementary Table 3 (*continued*).

PDB ID	Protein	Chemical ID	Scaffold	Angle	Relative Angle	Aryl substitution	Position
3SX9	CDPK1	BK7	PP	-121.96	-121.96	napth	*m*
3UQF	Src	BK5	PP	-121.97	-121.97	napth	*m*
1QCF	Hck	PP1	PP	-122.62	-122.62	Me	*p*
1YOL	Src	S03	PPY	-122.67	-122.67	OMe	*m*
5TEH	RORg	S56	PPY	-122.82	-122.82	OPh	*p*
3VS6	Hck	VSH	PP	-123.28	-123.28	OMe	*m*
4YHF	Btk	4C9	PP	-123.98	-123.98	OPh	*p*
3VS4	Hck	VSF	PPY	-124.03	-124.03	OPh	*p*
5H0G	Hck	OOU	PPY	-124.26	-124.26	OPh	*p*
3V5T	CDPK1	UW9	PP	-124.27	-124.27	napth	*m*
2C0T	Hck	L3G	PP	-124.47	-124.47	OMe	*m*
4MXA	CDPK1	BK7	PP	-124.95	-124.95	napth	*m*
3T3U	CDPK1	BK6	PP	-125.23	-125.23	napth	*m*
3VRY	Hck	B43	PPY	-125.32	-125.32	OPh	*p*
3V5P	CDPK1	C88	PP	-125.71	-125.71	Me	*m*
4DGG	Src	I76	PP	-125.76	-125.76	napth	*m*
3EN6	Src	KS5	PP	-126.51	-126.51	Isoquinoline	*m*
4CM4	PTR1	4NR	PPY	-127.15	-127.15	F	*p*
3I7C	CDPK1	BK2	PP	-127.29	-127.29	napth	*m*
5H09	Hck	OOO	PPY	-127.63	-127.63	OPh	*p*
5H0E	Hck	OOS	PPY	-127.81	-127.81	OPh	*p*
5H0B	Hck	OOQ	PPY	-127.85	-127.85	OPh	*p*
4K11	Src (T338G)	0J9	PP	-127.97	-127.97	napth	*o*
3VS1	Hck	VSA	PPY	-128.02	-128.02	urea	*p*
3SXF	CDPK1	BK5	PP	-128.31	-128.31	napth	*m*
4CM3	PTR1	KP2	PPY	-128.7	-128.7	H	*p*
3VS0	Hck	VS0	PPY	-128.89	-128.89	anilide	*p*
3V51	CDPK1	I76	PP	-130.14	-130.14	napth	*m*
4TZR	CDPK1	UW2	PP	-130.36	-130.36	Isoquinoline	*m*
3T3V	CDPK1	BK4	PP	-130.37	-130.37	napth	*m*
5H0H	Hck	OOV	PPY	-130.55	-130.55	OPh	*p*
4EWH	Ack1	T77	PPY	-130.82	-130.82	H	*p*
4CMB	PTR1	UEN	PPY	-130.85	-130.85	F	*p*
3BHM	CBR1	AB3	PP	-130.91	-130.91	OH	*m*
3VS3	Hck	VSE	PPY	-131.14	-131.14	OPh	*p*
3VRZ	Hck	VRZ	PPY	-131.65	-131.65	urea	*p*
2YM5	Chk1	YM5	PPY	-132.5	-132.5	MeOH	*m*
4JBV	CDPK1	V68	PP	-132.55	-132.55	napth	*m*
1WMA	Cbr1	AB3	PP	-132.64	-132.64	OH	*m*
5GTY	Egfr (T790M)	816	PP	-132.66	-132.66	Cl	*m*
3BHJ	CBR1	AB3	PP	-133.06	-133.06	OH	*m*
2BRN	Chk1	DF1	PPY	-133.19	-133.19	H	*p*
5UNP	CLK2	8FY	PPY	-136.4	-136.4	Isoquinoline	*m*
4CM1	PTR1	IQW	PPY	-137.94	-137.94	Me	*p*
4MX9	CDPK1	2E8	PP	-139.39	-139.39	napth	*m*
6BFA	CDPK1	UW5	PP	-143.27	-143.27	napth	*m*
3VS5	Hck	VSG	PPY	-143.66	-143.66	OPh	*p*
3VS2	Hck	VSB	PPY	-150.1	-150.1	OPh	*p*
4FEV	APH(3')-Ia	PP1	PP	-174.95	-174.95	Me	*p*
4FEW	APH(3')-Ia	PP2	PP	-179.78	-179.78	Cl	*p*

Scheme 1

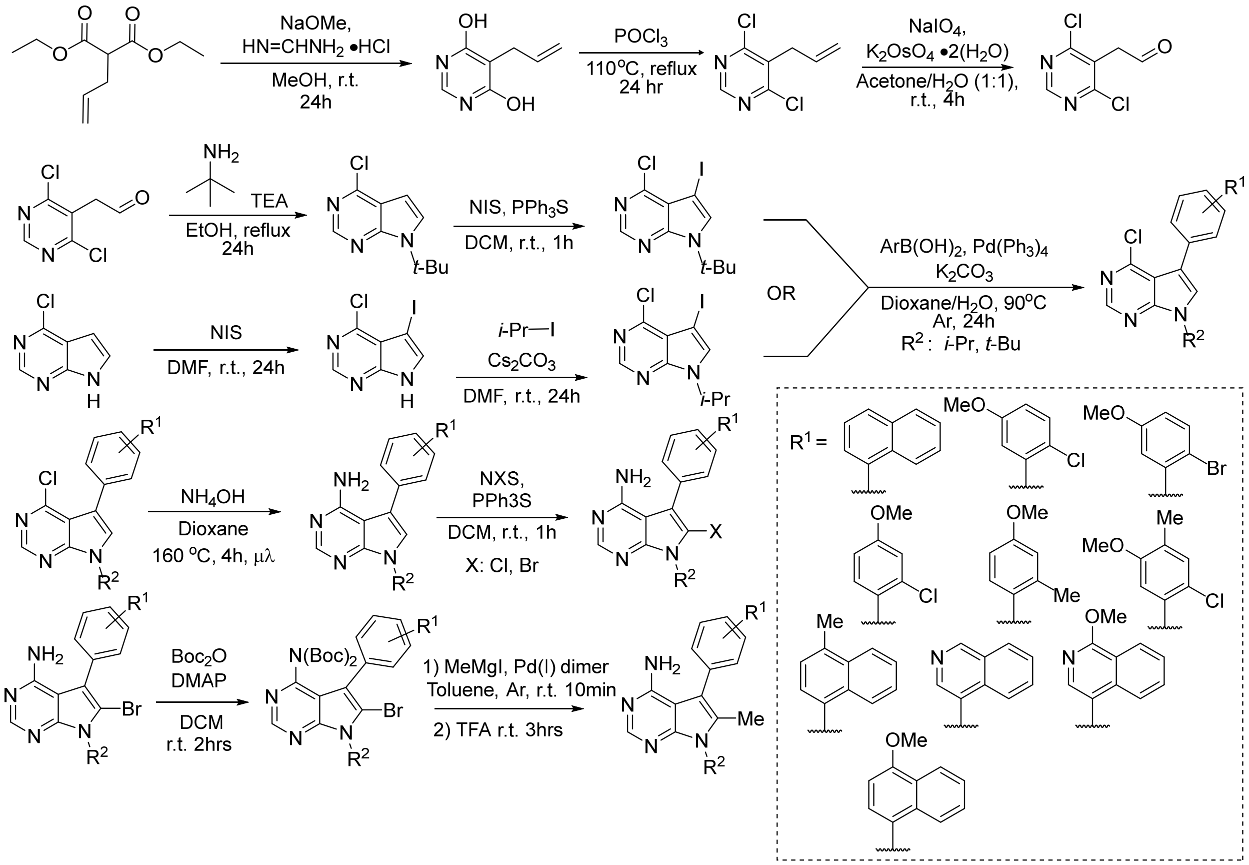
NaOMe,
HN=CHNH2 •HCl
MeOH, r.t.
24h
POCl3
110°C, reflux
24 hr
NaIO4,
K2OsO4 •2(H2O)
Acetone/H2O (1:1),
r.t., 4h
TEA
EtOH, reflux
24h
NIS, PPh3S
DCM, r.t., 1h
NIS
DMF, r.t., 24h
i-Pr—I
Cs2CO3
DMF, r.t., 24h
OR
ArB(OH)2, Pd(Ph3)4
K2CO3
Dioxane/H2O, 90°C
Ar, 24h
R2 : i-Pr, t-Bu
NH4OH
Dioxane
160 °C, 4h, μλ
NXS,
PPh3S
DCM, r.t., 1h
X: Cl, Br
Boc2O
DMAP
DCM
r.t. 2hrs
1) MeMgI, Pd(I) dimer
Toluene, Ar, r.t. 10min
2) TFA r.t. 3hrs
R1 =

Scheme 2

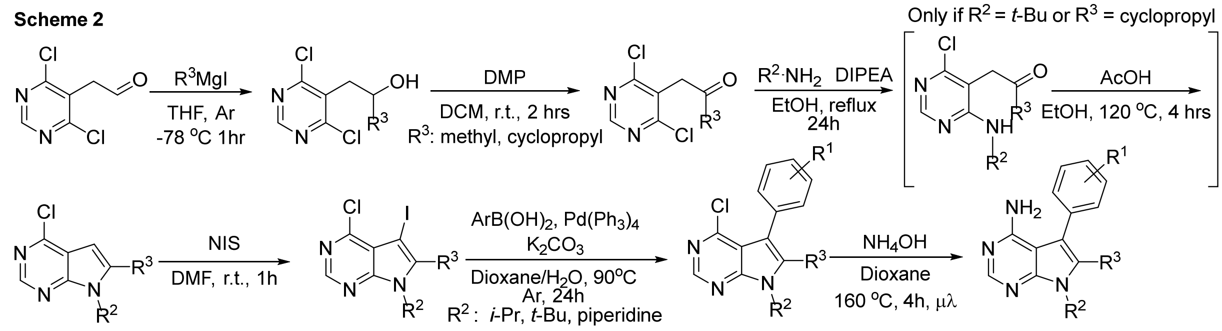
Only if R2 = t-Bu or R3 = cyclopropyl
R3MgI
THF, Ar
-78 °C 1hr
DMP
DCM, r.t., 2 hrs
R3: methyl, cyclopropyl
R2·NH2 DIPEA
EtOH, reflux
24h
AcOH
EtOH, 120 °C, 4 hrs
NIS
DMF, r.t., 1h
ArB(OH)2, Pd(Ph3)4
K2CO3
Dioxane/H2O, 90°C
Ar, 24h
R2 : i-Pr, t-Bu, piperidine
NH4OH
Dioxane
160 °C, 4h, μλ

Preparation of 7-(tert-butyl)-4-chloro-5-iodo-7H-pyrrolo[2,3-d]pyrimidine:

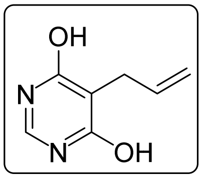

5-allylpyrimidine-4,6-diol:

Prepared following a modified literature procedure[6]. A solution of sodium methoxide (6 eq) in methanol (0.25M) was treated with formamidine hydrochloride (1.1 eq.) and stirred for 5 minutes open to air. Diethylallylmalonate (19.2 g, 95.9 mmol, 1 eq) was then added to the reaction mixture and stirred at room temperature for 2 days. The methanol was then evaporated *in vacuo.* The crude solid was dissolved in minimal DI water and brought to pH 5 using concentrated HCl. The solids were filtered, washed with DCM, and dried affording 10 g of 5-allylpyrimidine-4,6-diol (69% yield). The ^{1}H NMR matched those reported in literature[173].

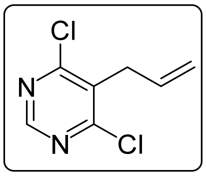

5-allyl-4,6-dichloropyrimidine:

Prepared following a modified literature procedure[3]. 5-allylpyrimidine-4,6-diol (10 g, 65.7 mmol, 1 eq.) was treated with $POCl_3$ (0.8 M). The mixture was refluxed (110ºC) for overnight and then cooled to room temperature. The reaction mixture was quenched by pouring the mixture slowly into a large beaker stirring ice and DI water. The mixture was extracted with dichloromethane. The organic layer was washed with saturated aqueous $NaHCO_3$ and brine, dried of sodium sulfate, filtered and concentrated to afford 11.15 g of 5-allyl-4,6-dichloropyrimidine as a light yellow oil (90% yield). The ^{1}H NMR matched those reported in literature[4].

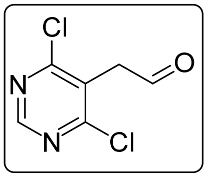

2-(4,6-dichloropyrimidin-5-yl)acetaldehyde:

Prepared following a modified literature procedure[3]. 5-allyl-4,6-dichloropyrimidine (11.15 g, 59.0 mmol, 1.0 eq.) was added to a 1:1 mixture of acetone and water (0.2 M) at room temperature. Potassium osmate dihydrate was added (0.02 eq.) followed by addition of sodium meta-periodate (3.5 eq.). The reaction mixture was stirred at room temperature overnight. The suspension was then filtered off and acetone was removed from the filtrate *in vacuo*. The desired product was extracted from the aqueous layer with dichloromethane. The organic layer was then washed with 10% sodium thiosulfate and brine, dried over sodium sulfate, filtered and concentrated to afford 10 g of 2-(4,6-dichloropyrimidin-5-yl)acetaldehyde as a light amber solid (89% yield). The ^{1}H NMR matched those reported in literature[4].

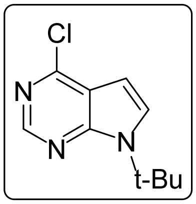

7-(*tert*-butyl)-4-chloro-7*H*-pyrrolo[2,3-*d*]pyrimidine:

Prepared following a modified literature procedure[3]. 2-(4,6-dichloropyrimidin-5-yl)acetaldehyde (10 g, 52.6 mmol, 1 eq.) was dissolved in ethanol (0.4 M). Triethylamine (2 eq.) was then added to the reaction mixture and stirred for ten minutes at room temperature. *Tert*-butylamine (1.5 eq.) was then added to the reaction mixture and refluxed (90 ºC) overnight. The reaction mixture was evaporated *in vacuo* and partitioned in brine and ethyl acetate. The organic layer was collected and concentrated. The organic extract was then purified by FCC (gradient of hexanes:ethyl acetate (97:3 to 90:10) to yield 7 g of 7-(*tert*-butyl)-4-chloro-7*H*-pyrrolo[2,3-*d*]pyrimidine as a yellow oil (63% yield). The ^{1}H NMR matched those reported in literature[5].

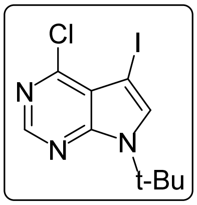

7-(*tert*-butyl)-4-chloro-5-iodo-7*H*-pyrrolo[2,3-*d*]pyrimidine:

Prepared following a modified literature procedure[3]. 7-(*tert*-butyl)-4-chloro-7*H*-pyrrolo[2,3-*d*]pyrimidine (7g, 33.1 mmol, 1 eq.) was dissolved in dichloromethane (0.1M) at r.t.. Triphenylphosphinesulfide (0.1 eq.) was then added and the reaction was stirred for five minutes followed by the addition of *N*-Iodosuccinimide (1.2 equiv.). The reaction mixture was then stirred at room temperature for one hour. The reaction mixture was then partitioned between 1:1 dichloromethane:sodium hydroxide and the organic layer was collected and concentrated. The organic extract was then purified using FCC gradient of hexanes:ethyl acetate (97:3 to 92:8) to yield 8.6 g of 7-(*tert*-butyl)-4-chloro-5-iodo-7*H*-pyrrolo[2,3-*d*]pyrimidine as a white solid (78% yield). The ^{1}H NMR matched those reported in literature[6].

Preparation of 7-(*alkyl*)-4-chloro-5-iodo-7*H*-pyrrolo[2,3-*d*]pyrimidine:

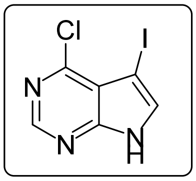

4-chloro-5-iodo-7*H*-pyrrolo[2,3-*d*]pyrimidine:

To 4-chloro-7H-pyrrolo[2,3-d]pyrimidine (1.00 g, 6.5 mmol, 1.0 eq) NIS (1.61 g, 7.15 mmol, 1.1 eq) was added and stirred for 30 minutes in DMF (2.6 M). The product was recrystallized from DMF by the addition of water to yield 1.27 g of 4-chloro-3-iodo-7Hpyrrolo[2,3-d]pyrimidine as a yellow solid (100% yield). ^{1}H NMR matched the literature[7].

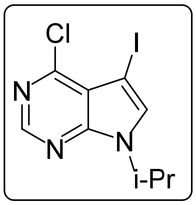

4-chloro-5-iodo-7-isopropyl-7*H*-pyrrolo[2,3-*d*]pyrimidine:

To 4-chloro-5-iodo-7H-pyrrolo[2,3-d]pyrimidine (5.59 g, 20.03 mmol, 1.0 eq) was Cs_2CO_3 (9.79 g, 30.05 mmol, 1.5 eq) added and dissolved into 55.9 mL DMF. After 3 minutes, 2-iodopropane (2.20 mL, 22.04 mmol, 1.1 eq) was added. The reaction was left to stir overnight. The product was recrystallized from DMF by the addition of water to yield 6.44 g of pure 4-chloro-5-iodo-7-isopropyl-7H-pyrrolo[2,3-d]pyrimidine as a yellow solid (100% yield). ^{1}H NMR matched the literature[7].

Preparation of 7-(*alkyl*)-4-chloro-5-iodo-6-methyl-7*H*-pyrrolo[2,3-*d*]pyrimidine

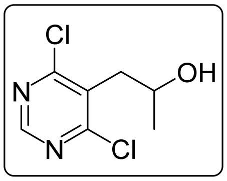

1-(4,6-dichloropyrimidin-5-yl)propan-2-ol:

2-(4,6-dichloropyrimidin-5-yl)acetaldehyde (1.26 g, 6.60 mmol, 1.0 eq) was dissolved into 33 mL THF under Argon atmosphere. The reaction flask was cooled down to -78ºC. Methylmagnesiumbromide (3M solution in diethyl ether) (5.5 mL, 16.50 mmol, 2.5 eq) was added dropwise and let stir for 1.5hr at -78ºC. Saturated aqueous ammonium chloride solution was added to quench the reaction and allowed to warm to room temperature. The reaction mixture was partitioned in ethyl acetate and brine. The organic layer was dried over sodium sulfate and concentrated. The crude extract was purified via FCC (8:2 Hex:EtAc gradient) to yield 533 mg of pure 1-(4,6-dichloropyrimidin-5-yl)propan-2-ol as a white solid (39% yield).

^{1}H NMR (400 MHz, $CDCl_3$) δ 8.58 (s, 1H), 4.24 – 4.17 (m, 1H), 3.10 (dd, J = 13.8, 8.4 Hz, 1H), 2.98 (dd, J = 13.7, 5.0 Hz, 1H), 2.11 (s, 1H), 1.31 (d, J = 6.2 Hz, 3H).

^{13}C NMR (101 MHz, $CDCl_3$) δ 162.43, 155.67, 130.71, 66.65, 39.30, 23.93.

MS (APCI) Calculated: $C_7H_9Cl_2N_2O$ $[M+H]^+$ 207.0 **Found:** 207.0 m/z

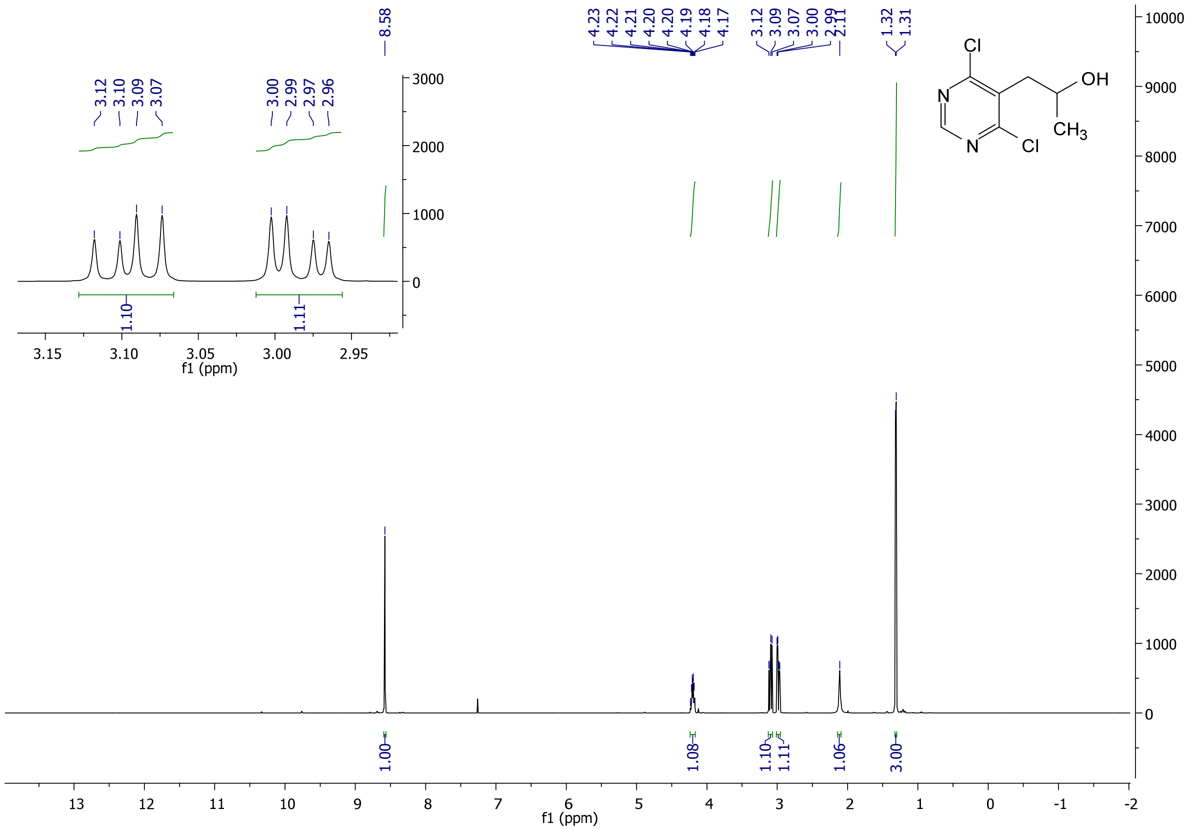

8.58
4.23 4.22 4.21 4.20 4.20 4.19 4.18 4.17
3.12 3.09 3.07 3.00 2.99 2.11
1.32 1.31
3.12 3.10 3.09 3.07
3.00 2.99 2.97 2.96
1.10
1.11
3.15 3.10 3.05 3.00 2.95
f1 (ppm)
3000 2000 1000 0
1.00
1.08
1.10
1.11
1.06
3.00
13 12 11 10 9 8 7 6 5 4 3 2 1 0 -1 -2
f1 (ppm)
10000 9000 8000 7000 6000 5000 4000 3000 2000 1000 0
Cl
N
N
Cl
OH
CH_3

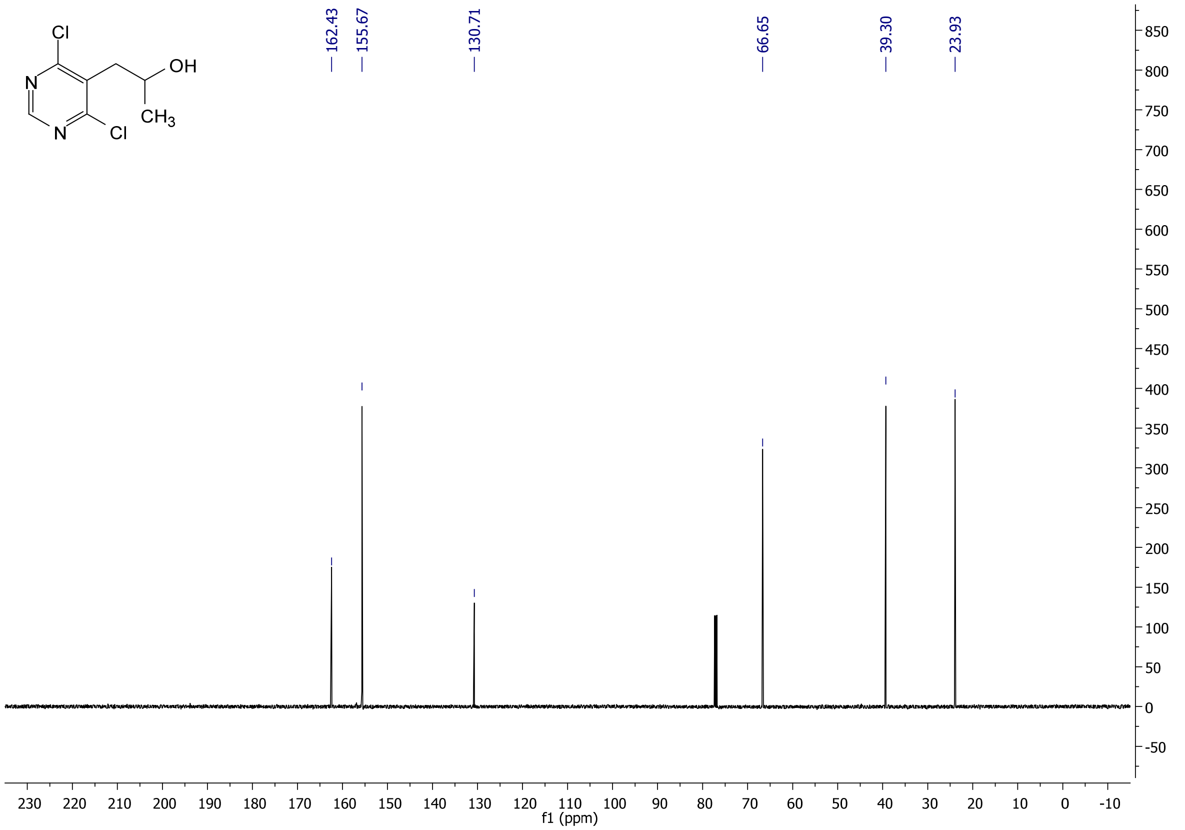

Cl
N
N
Cl
OH
CH_3
162.43
155.67
130.71
66.65
39.30
23.93
230 220 210 200 190 180 170 160 150 140 130 120 110 100 90 80 70 60 50 40 30 20 10 0 -10
f1 (ppm)
850 800 750 700 650 600 550 500 450 400 350 300 250 200 150 100 50 0 -50

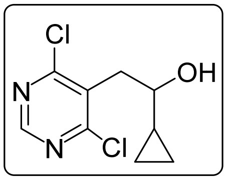

1-cyclopropyl-2-(4,6-dichloropyrimidin-5-yl)ethanol:

2-(4,6-dichloropyrimidin-5-yl)acetaldehyde (1 g, 5.23 mmol, 1.0 eq) was dissolved into 35 mL THF under Argon atmosphere. The reaction flask was cooled down to -78ºC. Cyclopropylmagnesiumbromide (1M solution in 2-MeTHF) (13.075 mL, 13.075 mmol, 2.5 eq) was added dropwise and let stir for 2.5hr at -78ºC. Saturated aqueous ammonium chloride solution was added to quench the reaction and allowed to warm to room temperature. The reaction mixture was partitioned in ethyl acetate and brine. The organic layer was dried over sodium sulfate and concentrated. The crude extract was purified via FCC (8:2 Hex:EtAc gradient) to yield 470 mg of pure 1-cyclopropyl-2-(4,6-dichloropyrimidin-5-yl)ethanol as a white solid (38% yield).

^{1}H NMR (400 MHz, $CDCl_3$) δ 8.57 (s, 1H), 3.26 – 3.16 (m, 3H), 2.27 (s, 1H), 1.04 (qt, J = 8.1, 4.9 Hz, 1H), 0.53 – 0.43 (m, 2H), 0.31 – 0.25 (m, 1H), 0.04 (m, 1H).

^{13}C NMR (101 MHz, $CDCl_3$) δ 162.32, 155.55, 130.64, 74.94, 37.55, 17.89, 3.00, 2.75.

MS (APCI) Calculated: $C_9H_{11}Cl_2N_2O$ $[M+H]^+$ 233.0 **Found:** 233.0

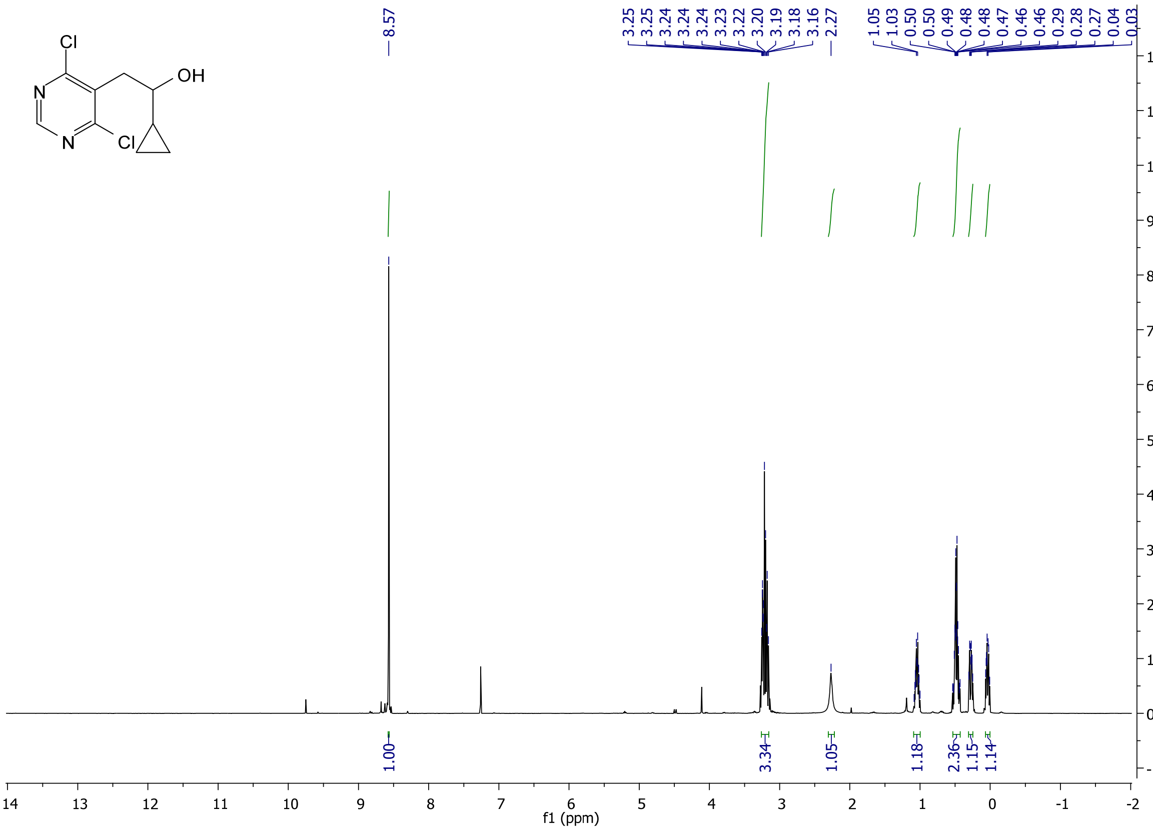
Cl
N
N
Cl
OH
8.57
3.25
3.25
3.24
3.24
3.24
3.23
3.22
3.20
3.19
3.18
3.16
2.27
1.05
1.03
0.50
0.50
0.49
0.48
0.48
0.47
0.46
0.46
0.29
0.28
0.27
0.04
0.03
1.00
3.34
1.05
1.18
2.36
1.15
1.14
1200
1100
1000
900
800
700
600
500
400
300
200
100
0
-100
14
13
12
11
10
9
8
7
6
5
4
3
2
1
0
-1
-2
f1 (ppm)

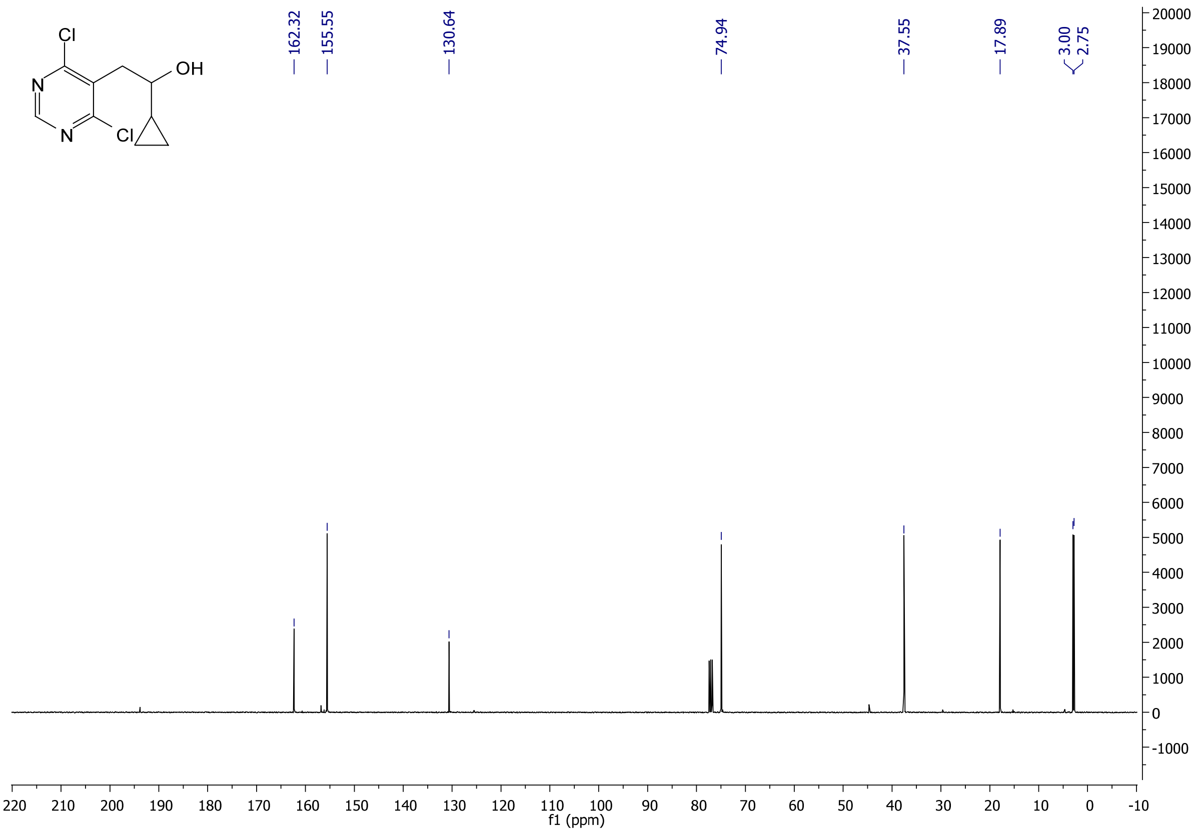
Cl
N
N
Cl
OH
162.32
155.55
130.64
74.94
37.55
17.89
3.00
2.75
20000
19000
18000
17000
16000
15000
14000
13000
12000
11000
10000
9000
8000
7000
6000
5000
4000
3000
2000
1000
0
-1000
220
210
200
190
180
170
160
150
140
130
120
110
100
90
80
70
60
50
40
30
20
10
0
-10
f1 (ppm)

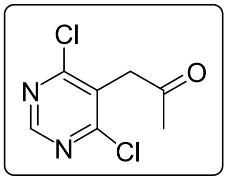

1-(4,6-dichloropyrimidin-5-yl)propan-2-one:

To 1-(4,6-dichloropyrimidin-5-yl)propan-2-ol (2.20 g, 10.6 mmol, 1.0 eq) was Dess-Martin reagent (9 g, 21.3 mmol, 2 eq) added and dissolved into 21 ml of DCM. The reaction was left to stir overnight. The reaction mixture was partitioned in DCM, sodium thiosulfate (aq.) and sodium bicarbonate (aq.) The organic layer was dried over sodium sulfate and concentrated. The crude extract was purified via FCC (8:2 Hex:EtAc) to yield 1.74 g of pure 1-(4,6-dichloropyrimidin-5-yl)propan-2-one as a white solid (80% yield).

^{1}H NMR (400 MHz, $CDCl_3$) δ 8.67 (s, 1H), 4.07 (s, 2H), 2.32 (s, 3H).

^{13}C NMR (101 MHz, $CDCl_3$) δ 200.72, 162.39, 156.50, 127.26, 44.55, 30.01.

MS (APCI) Calculated: $C_7H_7Cl_2N_2O$ $[M+H]^+$ 205.0 **Found:** 204.9 m/z

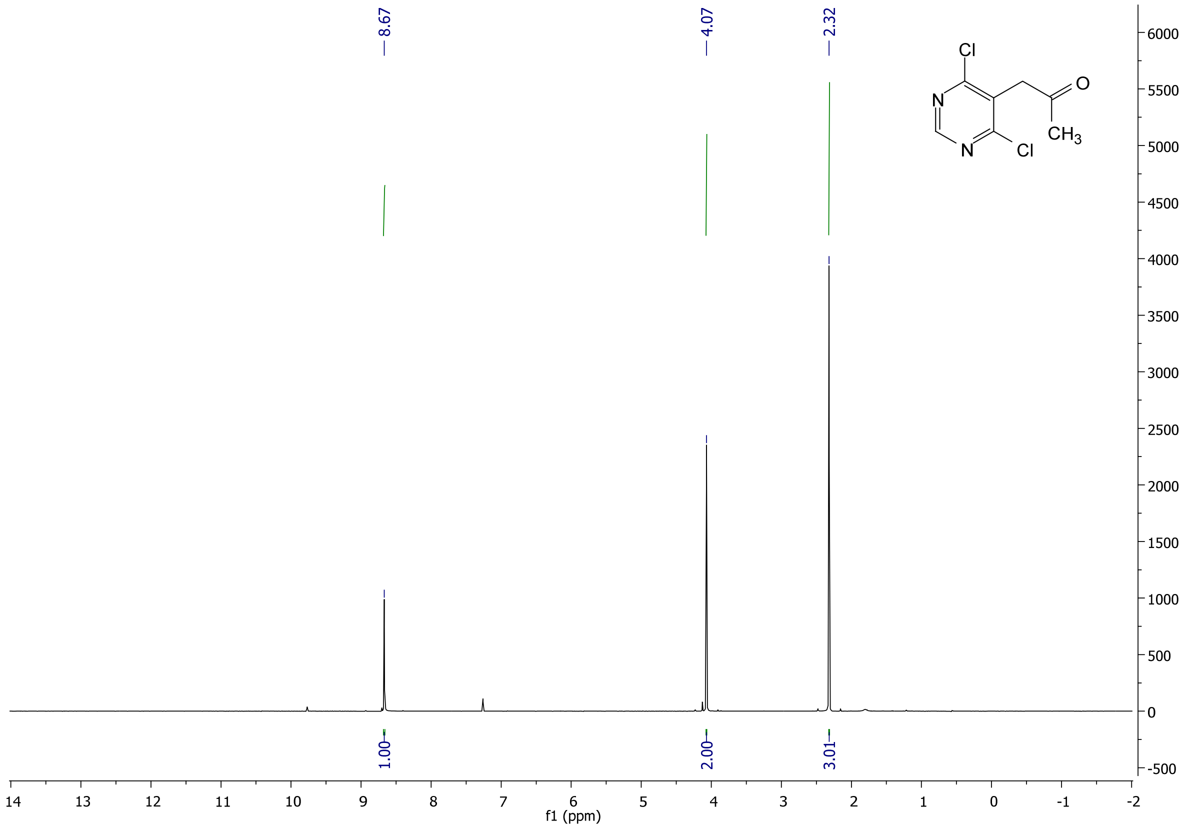
8.67
4.07
2.32
Cl
N
N
Cl
O
CH3
1.00
2.00
3.01
6000
5500
5000
4500
4000
3500
3000
2500
2000
1500
1000
500
0
-500
14 13 12 11 10 9 8 7 6 5 4 3 2 1 0 -1 -2
f1 (ppm)

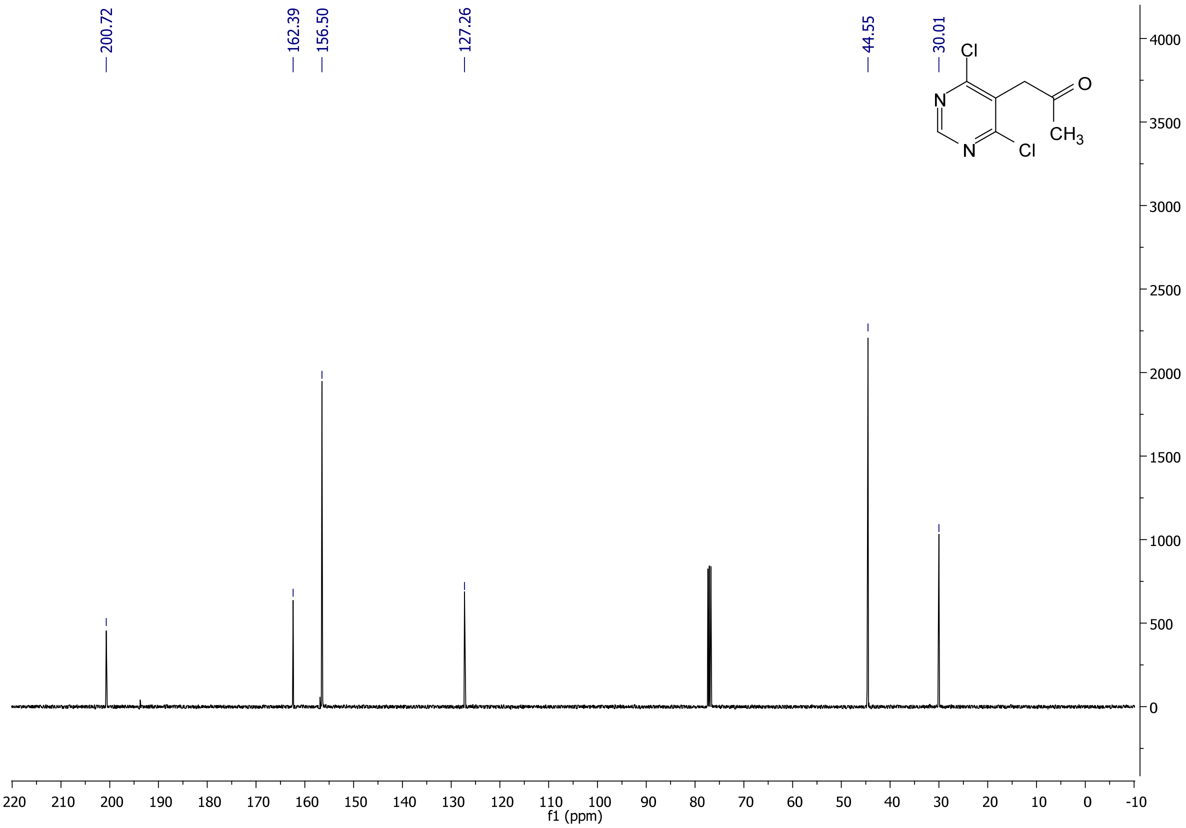
200.72
162.39
156.50
127.26
44.55
30.01
Cl
N
N
Cl
O
CH3
4000
3500
3000
2500
2000
1500
1000
500
0
220 210 200 190 180 170 160 150 140 130 120 110 100 90 80 70 60 50 40 30 20 10 0 -10
f1 (ppm)

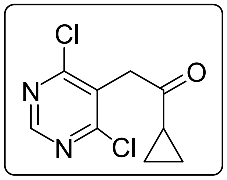

1-cyclopropyl-2-(4,6-dichloropyrimidin-5-yl)ethanone:

To 1-cyclopropyl-2-(4,6-dichloropyrimidin-5-yl)ethanol (400 mg, 1.7 mmol, 1.0 eq) was Dess-Martin reagent (1.08 g, 2.55 mmol, 1.5 eq) added and dissolved into 3.4 ml of DCM. The reaction was left to stir overnight. The reaction mixture was partitioned in DCM, sodium thiosulfate (aq.) and sodium bicarbonate (aq.) The organic layer was dried over sodium sulfate and concentrated. The crude extract was purified via FCC (8:2 Hex:EtAc) to yield 341 mg of pure 1-cyclopropyl-2-(4,6-dichloropyrimidin-5-yl)ethanone as a white solid (87% yield).

^{1}H NMR (400 MHz, $CDCl_3$) δ 8.68 (s, 1H), 4.22 (s, 2H), 2.06 (m, 1H), 1.17 – 1.13 (m, 2H), 1.01 (m, 2H).

^{13}C NMR (101 MHz, $CDCl_3$) δ 202.94, 162.45, 156.43, 127.41, 44.32, 20.87, 11.54.

MS (APCI) Calculated: $C_9H_9Cl_2N_2O$ $[M+H]^+$ 231.0 **Found:** 231.1

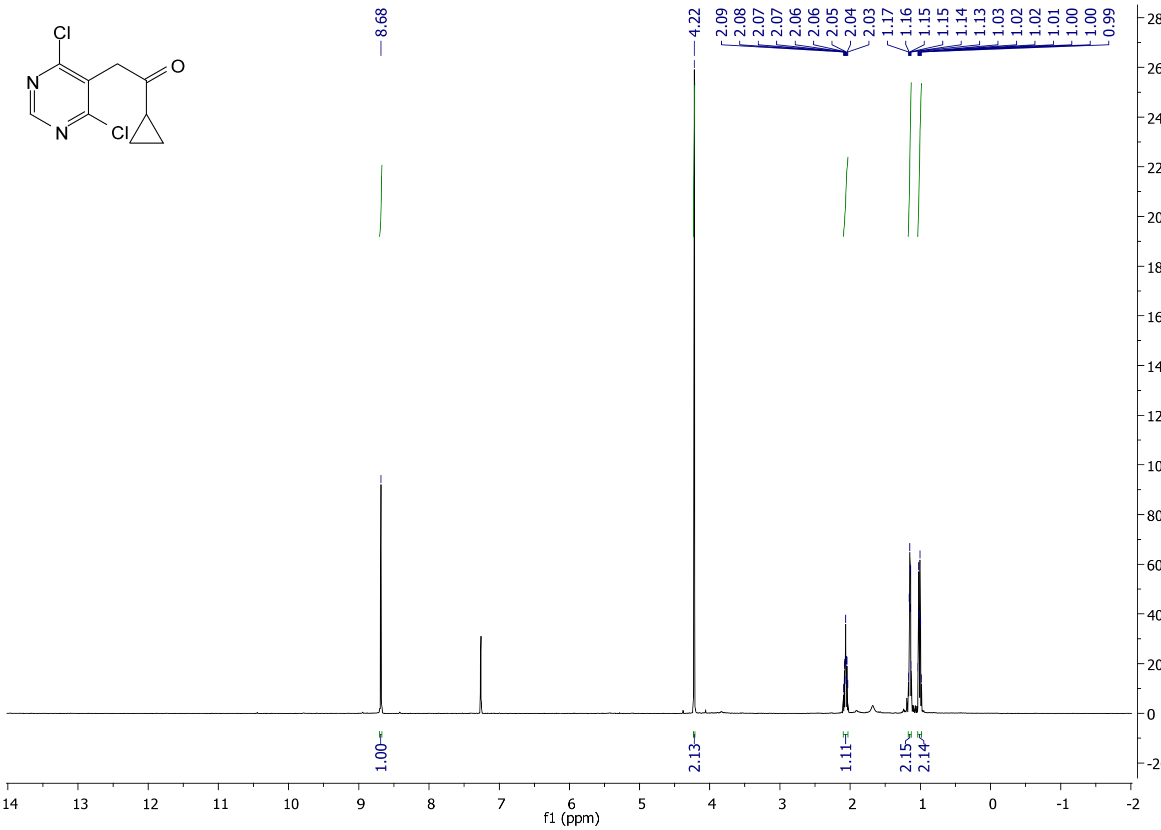
Cl
N
N
Cl
O
8.68
4.22
2.09
2.08
2.07
2.07
2.06
2.06
2.05
2.04
2.03
1.17
1.16
1.15
1.15
1.14
1.13
1.03
1.02
1.02
1.01
1.00
1.00
0.99
1.00
2.13
1.11
2.15
2.14
14
13
12
11
10
9
8
7
6
5
4
3
2
1
0
-1
-2
f1 (ppm)
2800
2600
2400
2200
2000
1800
1600
1400
1200
1000
800
600
400
200
0
-200

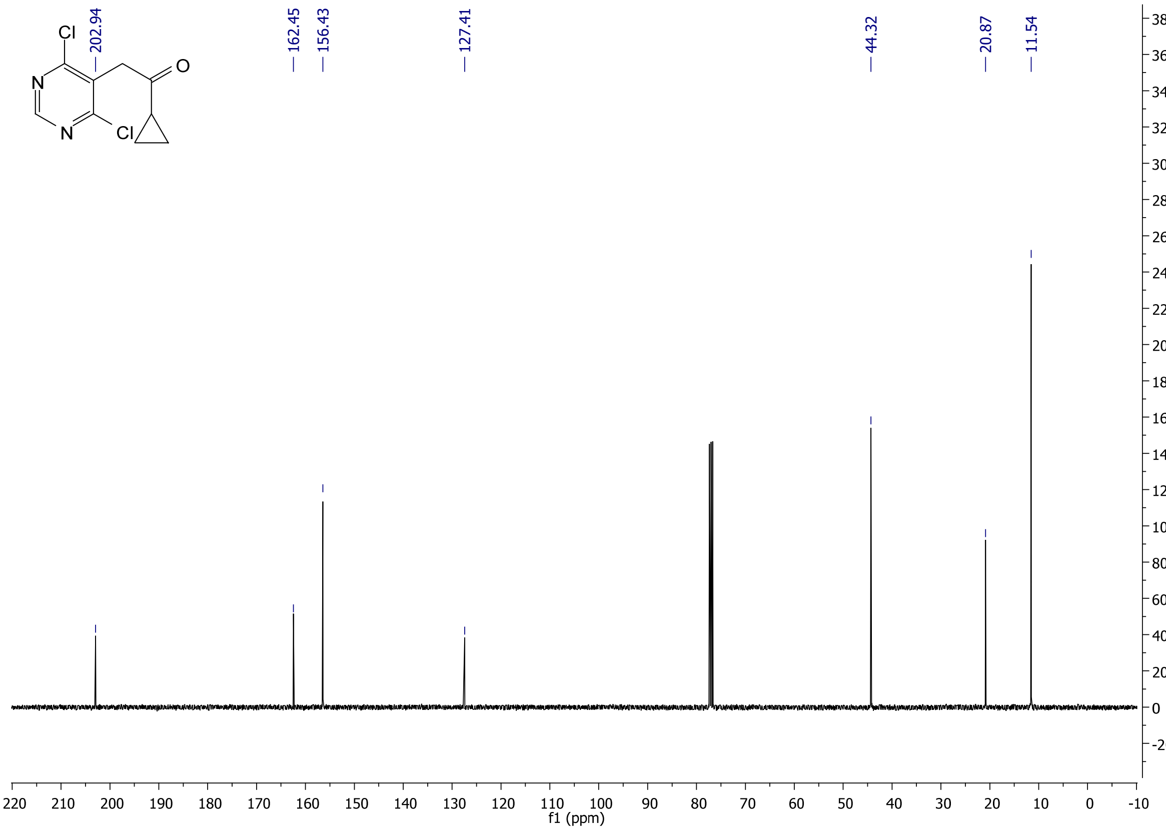
Cl
N
N
Cl
O
202.94
162.45
156.43
127.41
44.32
20.87
11.54
220
210
200
190
180
170
160
150
140
130
120
110
100
90
80
70
60
50
40
30
20
10
0
-10
f1 (ppm)
3800
3600
3400
3200
3000
2800
2600
2400
2200
2000
1800
1600
1400
1200
1000
800
600
400
200
0
-200

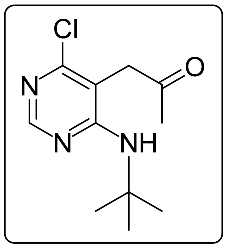

1-(4-(tert-butylamino)-6-chloropyrimidin-5-yl)propan-2-one:

To 1-(4,6-dichloropyrimidin-5-yl)propan-2-one (600 mg, 2.94 mmol, 1.0 eq) were tert-butylamine (355 ul, 3.38 mmol, 1.15 eq) and diisopropylethylamine (768 ul, 4.4 mmol, 1.5 eq) added and dissolved into 5.9 mL EtOH. The solution was stirred at 90ºC overnight. The reaction mixture was concentrated and the crude extract was purified by FCC (9:1 Hex: EtAc) to yield 270 mg of pure 1-(4-(tert-butylamino)-6-chloropyrimidin-5-yl)propan-2-one as a yellow solid (38% yield).

^{1}H NMR (400 MHz, $CDCl_3$) δ 8.26 (s, 1H), 5.67 (s, 1H), 3.65 (s, 2H), 2.26 (s, 3H), 1.45 (s, 9H).

^{13}C NMR (101 MHz, $CDCl_3$) δ 153.34, 149.80, 148.14, 140.70, 117.71, 100.80, 61.05, 30.81, 19.18.

MS (APCI) Calculated: $C_{11}H_{17}ClN_3O$ $[M+H]^+$ 242.1 **Found:** 242.1 m/z

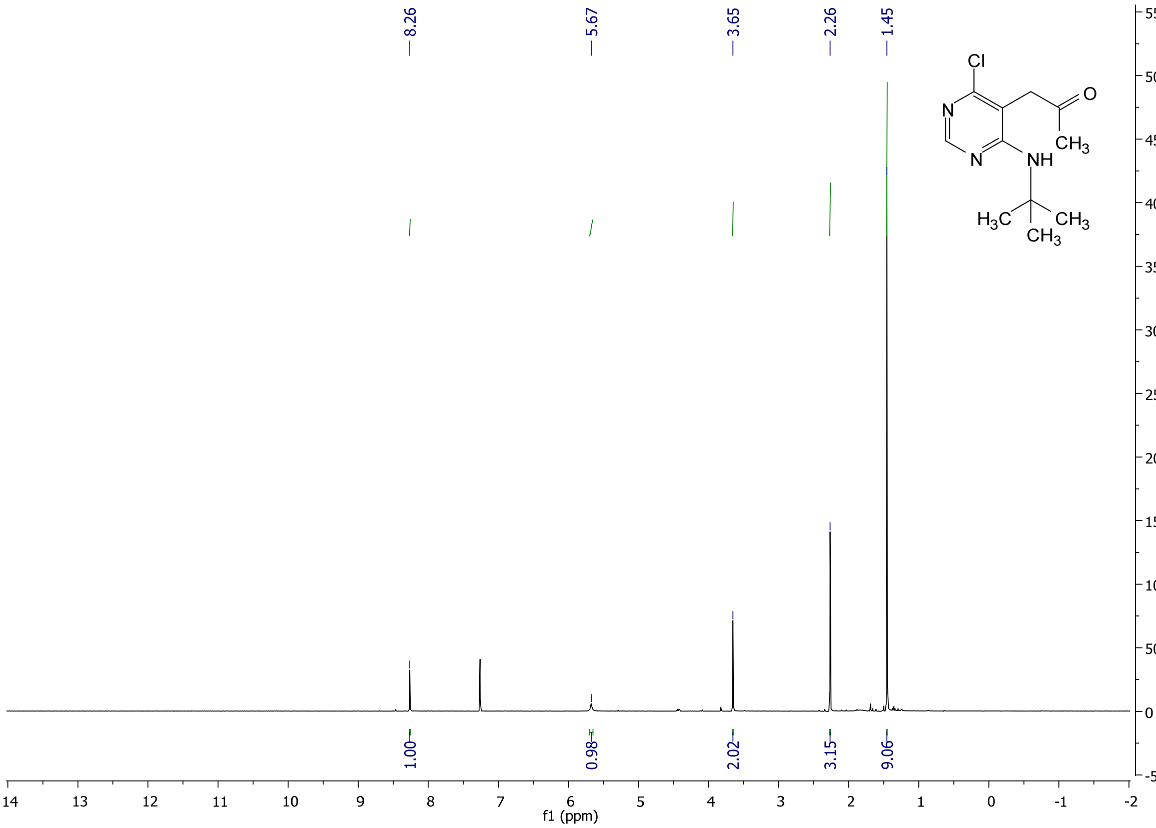
8.26
5.67
3.65
2.26
1.45
1.00
0.98
2.02
3.15
9.06
Cl
N
N
NH
O
CH3
H3C
CH3
CH3
5500
5000
4500
4000
3500
3000
2500
2000
1500
1000
500
0
-500
14
13
12
11
10
9
8
7
6
5
4
3
2
1
0
-1
-2
f1 (ppm)

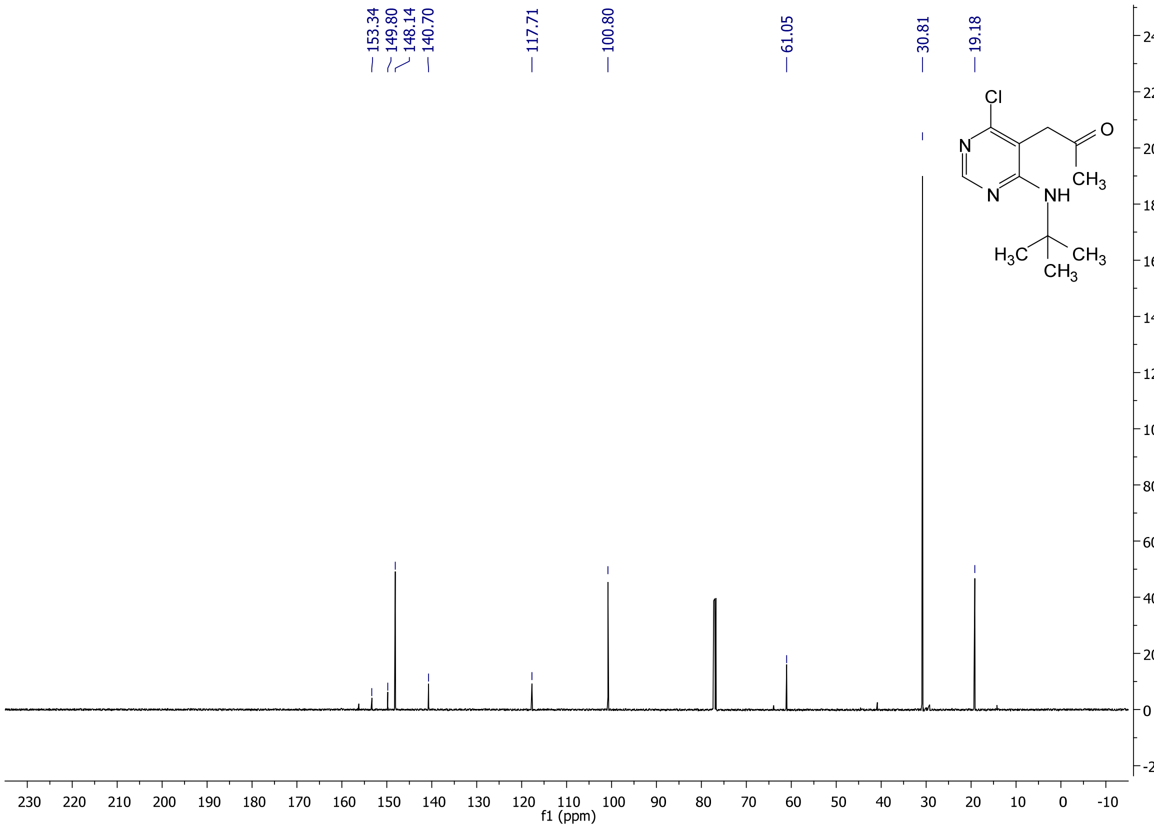
153.34
149.80
148.14
140.70
117.71
100.80
61.05
30.81
19.18
Cl
N
N
NH
O
CH3
H3C
CH3
CH3
2400
2200
2000
1800
1600
1400
1200
1000
800
600
400
200
0
-200
230
220
210
200
190
180
170
160
150
140
130
120
110
100
90
80
70
60
50
40
30
20
10
0
-10
f1 (ppm)

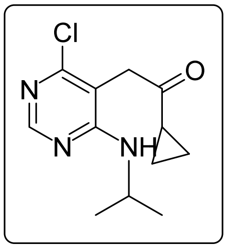

2-(4-chloro-6-(isopropylamino)pyrimidin-5-yl)-1-cyclopropylethanone:

To 1-(4,6-dichloropyrimidin-5-yl)propan-2-one (400 mg, 1.73 mmol, 1.0 eq) were isopropylamine (162 ul, 2 mmol, 1.15 eq) and diisopropylethylamine (452 ul, 2.6 mmol, 1.5 eq) added and dissolved into 3.5 mL EtOH. The solution was stirred at 90ºC overnight. The reaction mixture was concentrated and the crude extract was purified by FCC (9:1 Hex: EtAc) to yield 370 mg of pure 2-(4-chloro-6-(isopropylamino)pyrimidin-5-yl)-1-cyclopropylethanone as a yellow solid (84% yield).

^{1}H NMR (400 MHz, $CDCl_3$) δ 8.22 (s, 1H), 5.59 (d, J = 6.6 Hz, 1H), 4.21 (sept, J = 6.5 Hz, 1H), 3.75 (s, 2H), 2.07 (m, 1H), 1.16 (d, J = 6.5 Hz, 6H), 1.00 (m, 2H), 0.90 (m, 2H).

^{13}C NMR (101 MHz, $CDCl_3$) δ 207.85, 161.40, 157.94, 156.57, 107.49, 43.26, 42.90, 22.49, 20.51, 12.42.

MS (APCI) Calculated: $C_{12}H_{17}ClN_3O$ $[M+H]^+$ 254.1 **Found:** 254.1

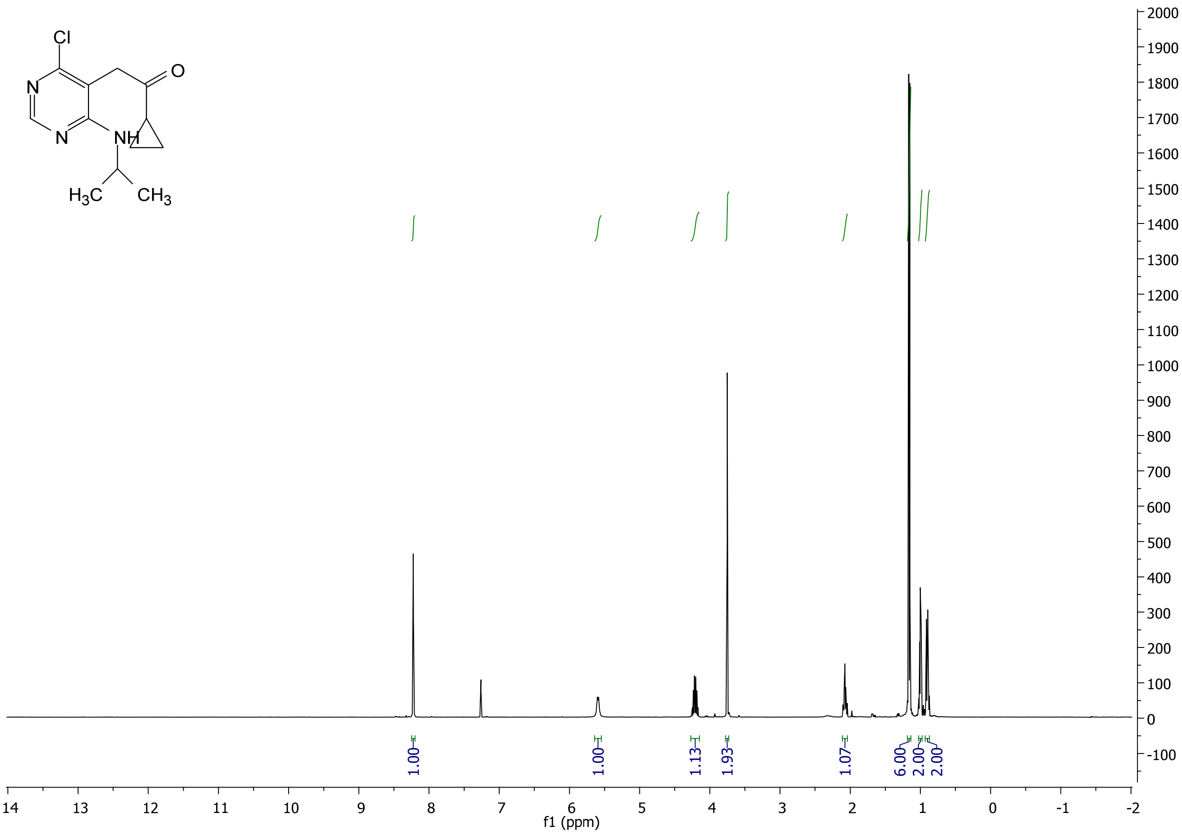
Cl
N
N
NH
O
H3C
CH3
1.00
1.00
1.13
1.93
1.07
6.00
2.00
2.00
f1 (ppm)
14
13
12
11
10
9
8
7
6
5
4
3
2
1
0
-1
-2
2000
1900
1800
1700
1600
1500
1400
1300
1200
1100
1000
900
800
700
600
500
400
300
200
100
0
-100

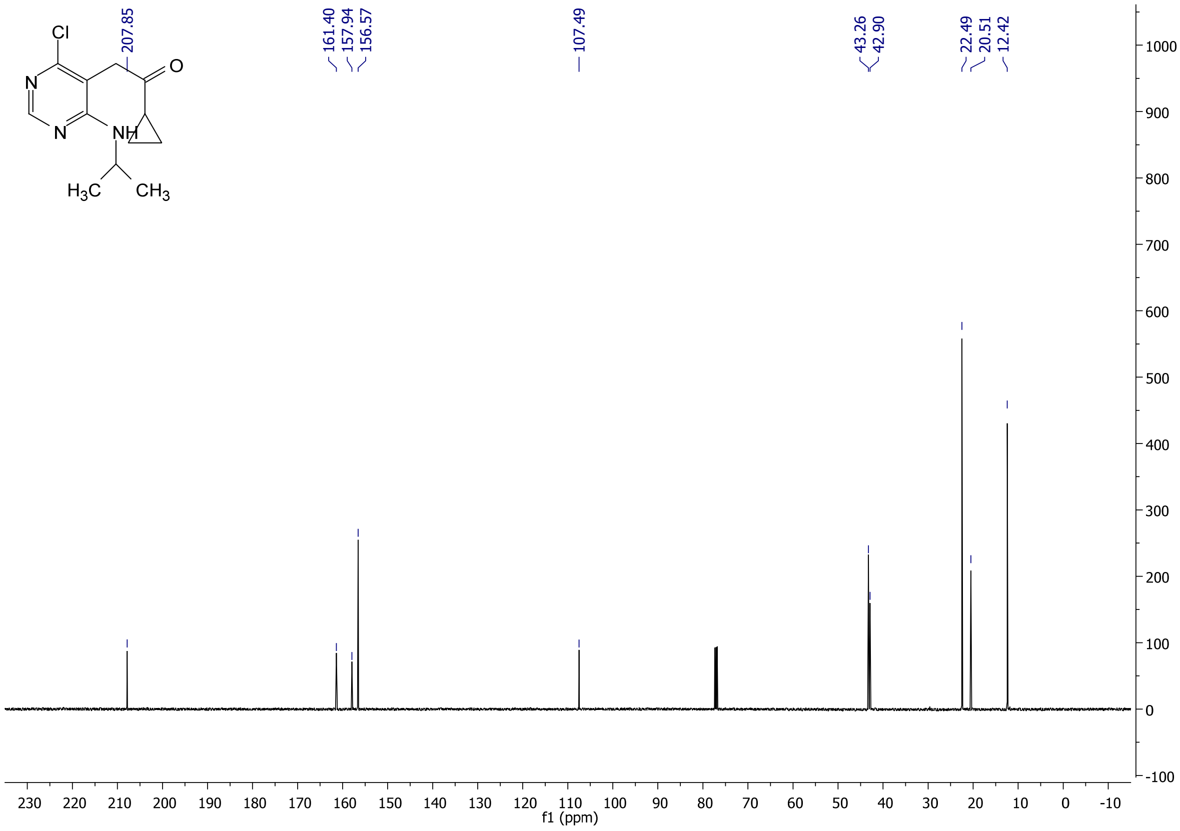
207.85
161.40
157.94
156.57
107.49
43.26
42.90
22.49
20.51
12.42
Cl
N
N
NH
O
H3C
CH3
f1 (ppm)
230
220
210
200
190
180
170
160
150
140
130
120
110
100
90
80
70
60
50
40
30
20
10
0
-10
1000
900
800
700
600
500
400
300
200
100
0
-100

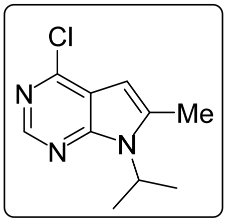

4-chloro-7-isopropyl-6-methyl-7*H*-pyrrolo[2,3-d]pyrimidine:

To 1-(4,6-dichloropyrimidin-5-yl)propan-2-one (600 mg, 2.94 mmol, 1.0 eq) were isopropylamine (290 ul, 3.38 mmol, 1.15 eq) and diisopropylethylamine (768 ul, 4.4 mmol, 1.5 eq) added and dissolved into 5.9 mL EtOH. The solution was stirred at 90ºC overnight. The reaction mixture was concentrated and the crude extract was purified by FCC (9:1 Hex: EtAc) to yield 415 mg of pure 4-chloro-7-isopropyl-6-methyl-7H-pyrrolo[2,3-d]pyrimidine as a yellow solid (67% yield).

^{1}H NMR (400 MHz, $CDCl_3$) δ 8.52 (s, 1H), 6.28 (d, J = 1.0 Hz, 1H), 4.87 – 4.76 (m, 1H), 2.49 (d, J = 0.9 Hz, 3H), 1.65 (d, J = 7.0 Hz, 6H).

^{13}C NMR (101 MHz, $CDCl_3$) δ 151.63, 149.94, 148.96, 138.89, 117.53, 97.83, 47.65, 21.35, 14.21.

MS (APCI) Calculated: $C_{10}H_{13}ClN_3$ $[M+H]^+$ 210.1 **Found:** 210.0 m/z

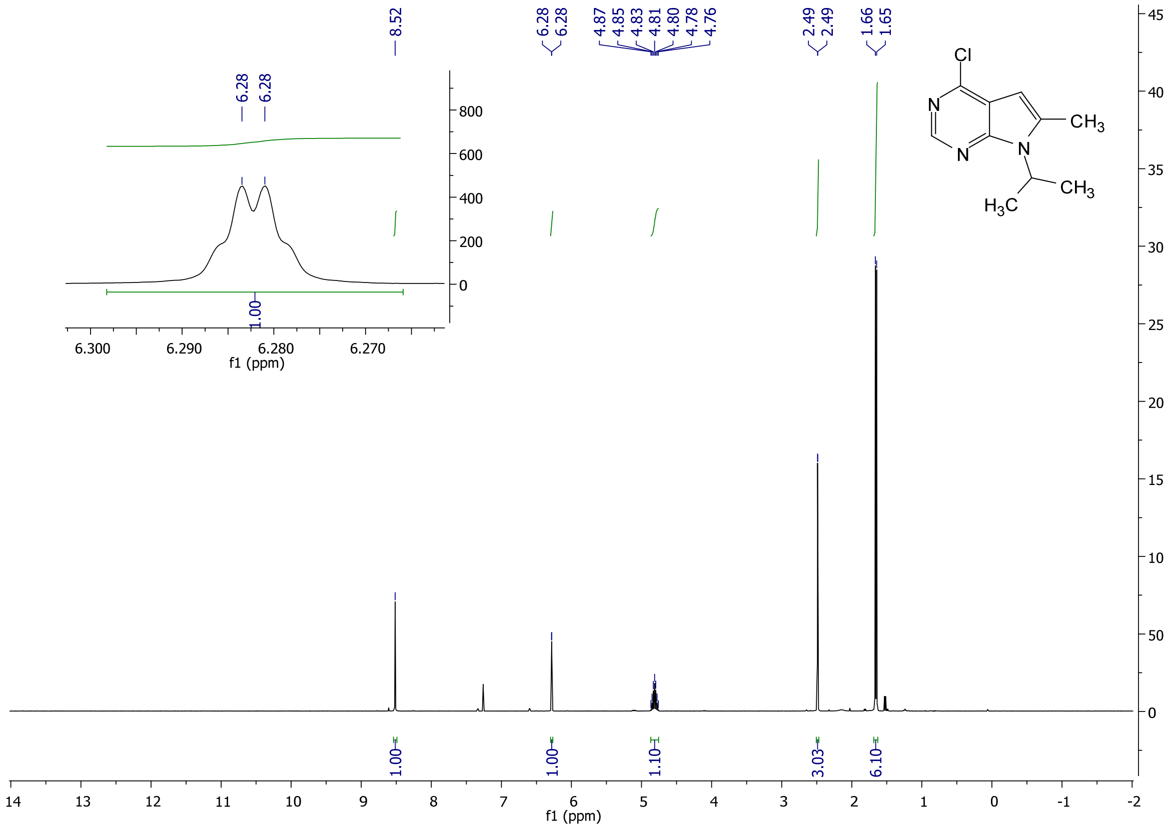
8.52
6.28
6.28
4.87
4.85
4.83
4.81
4.80
4.78
4.76
2.49
2.49
1.66
1.65
Cl
N
N
N
CH3
H3C
CH3
6.28
6.28
1.00
6.300
6.290
6.280
6.270
f1 (ppm)
1.00
1.00
1.10
3.03
6.10
14
13
12
11
10
9
8
7
6
5
4
3
2
1
0
-1
-2
f1 (ppm)
4500
4000
3500
3000
2500
2000
1500
1000
500
0

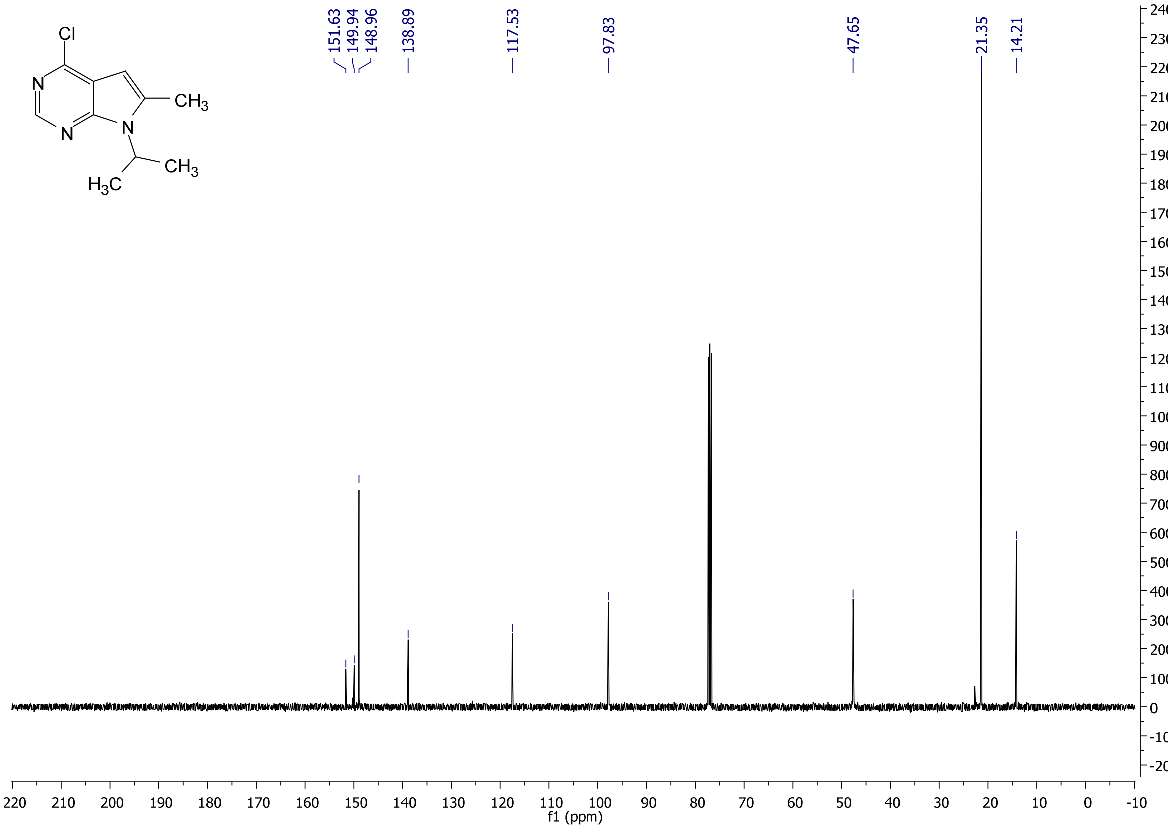
151.63
149.94
148.96
138.89
117.53
97.83
47.65
21.35
14.21
Cl
N
N
N
CH3
H3C
CH3
220
210
200
190
180
170
160
150
140
130
120
110
100
90
80
70
60
50
40
30
20
10
0
-10
f1 (ppm)
2400
2300
2200
2100
2000
1900
1800
1700
1600
1500
1400
1300
1200
1100
1000
900
800
700
600
500
400
300
200
100
0
-100
-200

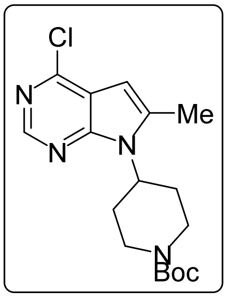

tert-butyl 4-(4-chloro-6-methyl-7H-pyrrolo[2,3-d]pyrimidin-7-yl)piperidine-1-carboxylate: To 1-(4,6-dichloropyrimidin-5-yl)propan-2-one (600 mg, 2.94 mmol, 1.0 eq) were 4-amino-1-boc-piperidine (677 mg, 3.38 mmol, 1.15 eq) and diisopropylethylamine (768 ul, 4.4 mmol, 1.5 eq) added and dissolved into 5.9 mL EtOH. The solution was stirred at 90°C overnight. The reaction mixture was concentrated and the crude extract was purified by FCC (9:1 Hex: EtAc) to yield 810 mg of pure tert-butyl 4-(4-chloro-6-methyl-7H-pyrrolo[2,3-d]pyrimidin-7-yl)piperidine-1-carboxylate as a yellow solid (68% yield).

^{1}H NMR (400 MHz, $CDCl_3$) δ 8.51 (s, 1H), 6.33 (d, J = 0.9 Hz, 1H), 4.47 (tt, J = 12.1, 3.8 Hz, 1H), 4.33 (s, 2H), 2.85 (s, 2H), 2.70 (qd, J = 12.5, 4.3 Hz, 2H), 2.51 (d, J = 0.9 Hz, 3H), 1.78 (d, J = 12.2 Hz, 2H), 1.50 (s, 9H).

^{13}C NMR (101 MHz, $CDCl_3$) δ 154.84, 151.99, 150.34, 149.26, 138.85, 117.60, 98.55, 80.11, 54.38, 43.86, 30.41, 28.59, 14.53.

MS (APCI) Calculated: $C_{17}H_{24}ClN_4O_2$ $[M+H]^+$ 351.2 **Found:** 351.1

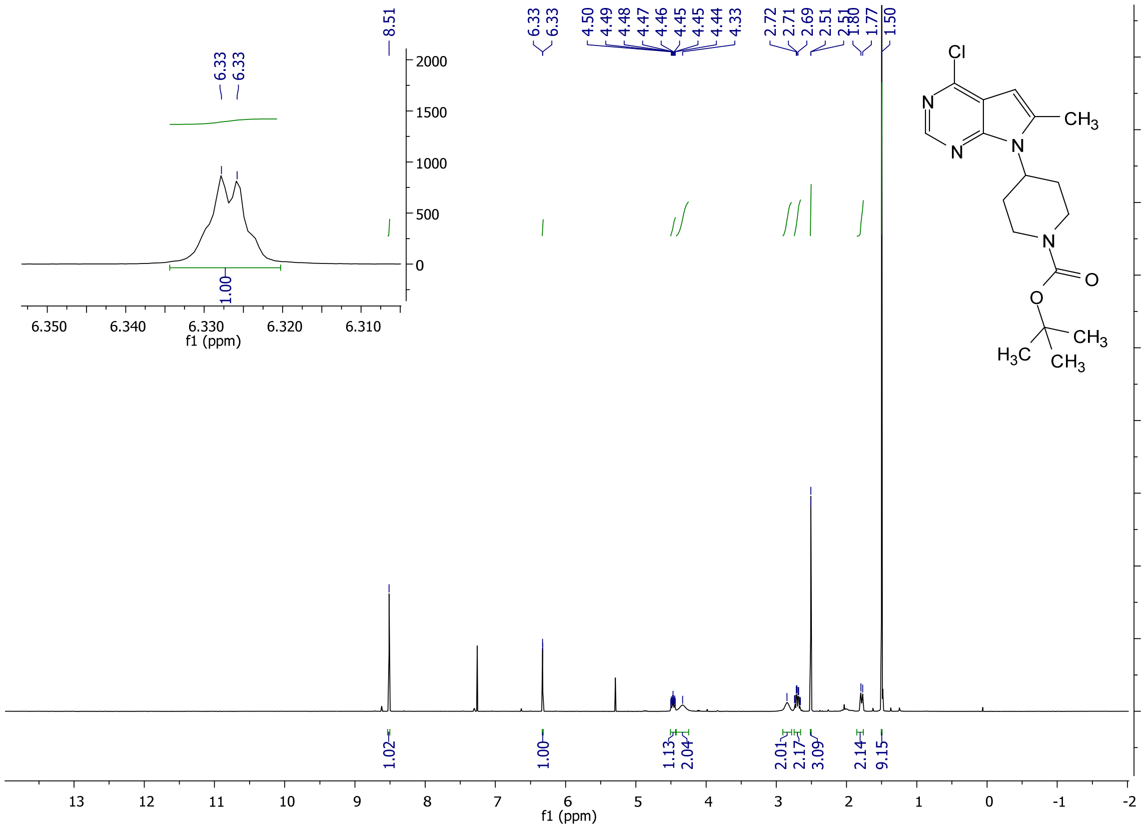
8.51
6.33
6.33
4.50
4.49
4.48
4.47
4.46
4.45
4.45
4.44
4.33
2.72
2.71
2.69
2.51
1.80
1.77
1.50
1.02
1.00
1.13
2.04
2.01
2.17
3.09
2.14
9.15
f1 (ppm)
Cl
N
N
N
CH3
N
O
O
CH3
H3C
CH3

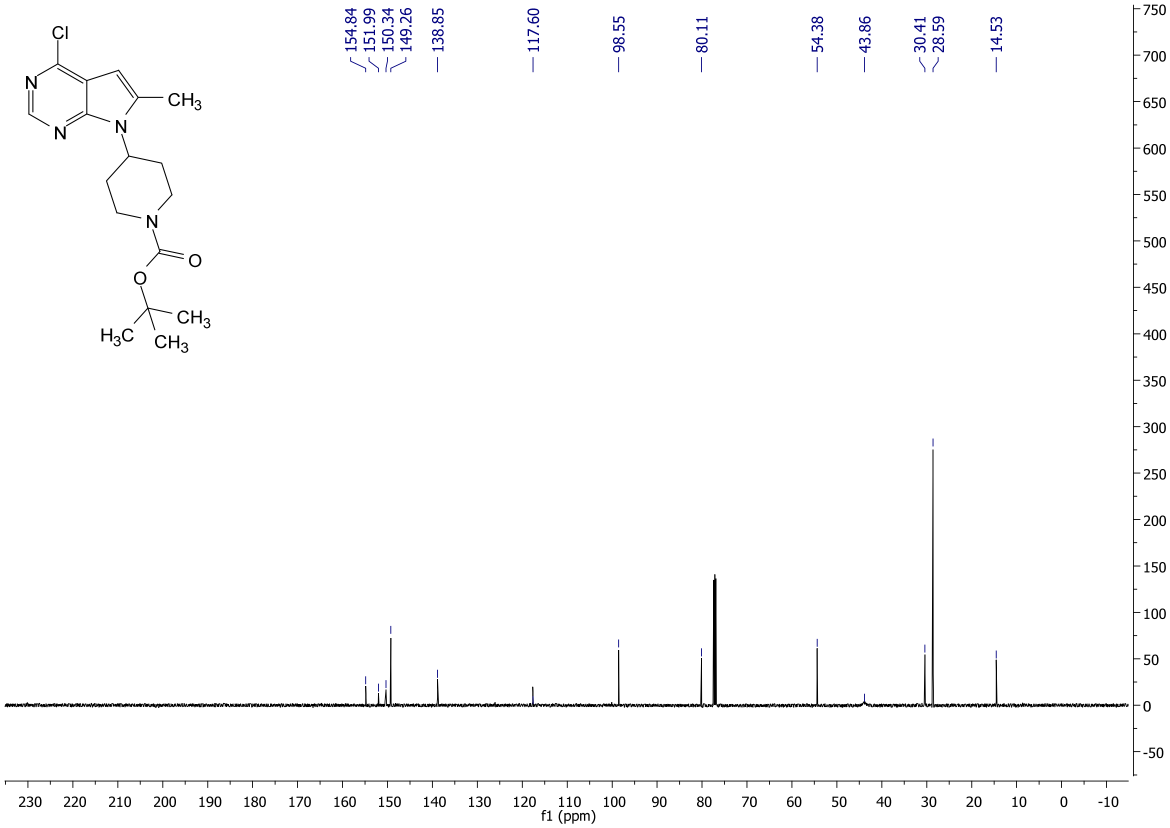
154.84
151.99
150.34
149.26
138.85
117.60
98.55
80.11
54.38
43.86
30.41
28.59
14.53
f1 (ppm)
Cl
N
N
N
CH3
N
O
O
CH3
H3C
CH3

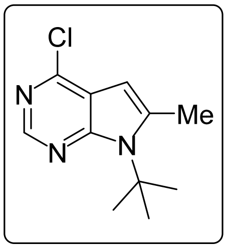

7-(tert-butyl)-4-chloro-6-methyl-7H-pyrrolo[2,3-d]pyrimidine:

To 1-(4-(tert-butylamino)-6-chloropyrimidin-5-yl)propan-2-one (204 mg, .844 mmol, 1.0 eq) was acetic acid (120 ul, 2.1 mmol, 2.5 eq) added and dissolved into 17 mL EtOH. The solution was reacted in a microwave reactor at 120ºC for 1 hour. The solvent was removed and the crude extract was purified by FCC (9:1 Hex:EtAc) to yield 117 mg of pure 7-(tert-butyl)-4-chloro-6-methyl-7H-pyrrolo[2,3-d]pyrimidine as a white solid (62% yield).

^{1}H NMR (400 MHz, $CDCl_3$) δ 8.52 (s, 1H), 6.28 (s, 1H), 2.65 (s, 3H), 1.89 (s, 9H).

^{13}C NMR (101 MHz, $CDCl_3$) δ 153.34, 149.80, 148.15, 140.69, 117.71, 100.81, 61.05, 30.82, 19.19.

MS (APCI) Calculated: $C_{11}H_{15}ClN_3$ $[M+H]^+$ 224.1 **Found:** 224.1 m/z

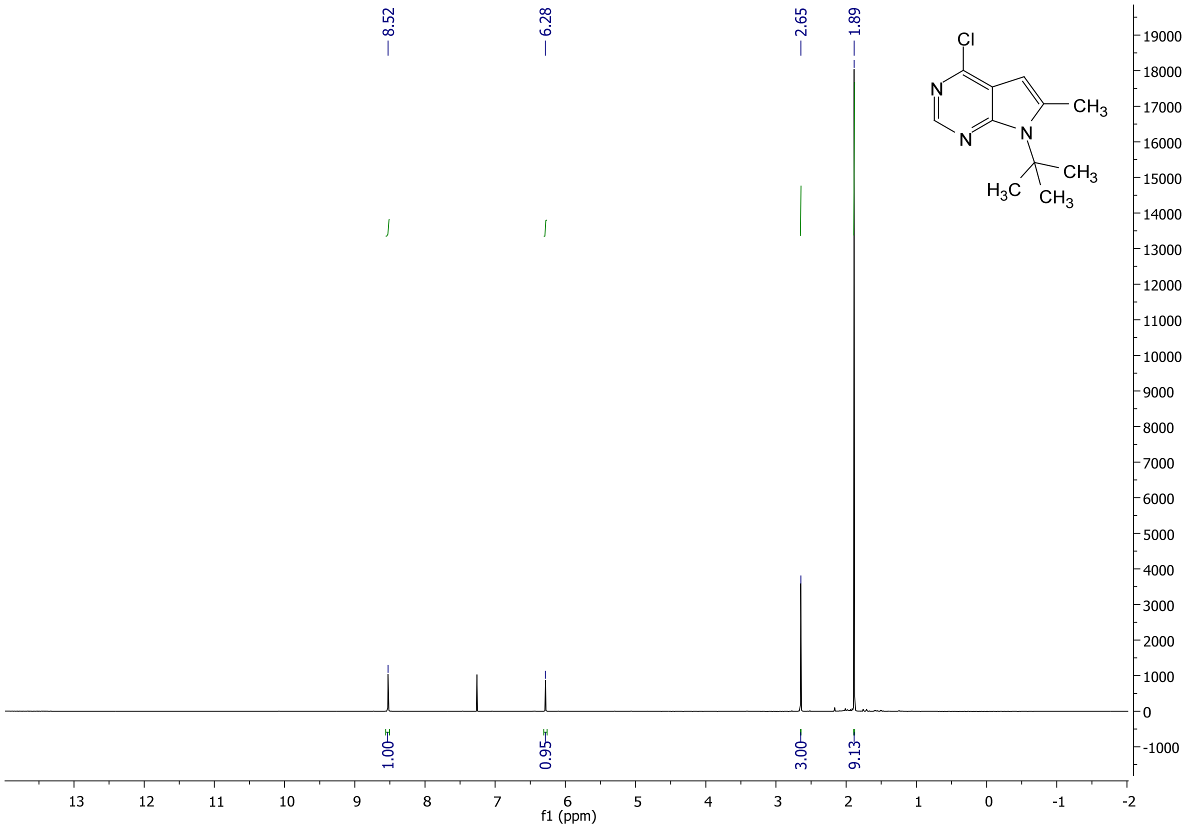
8.52
6.28
2.65
1.89
Cl
N
N
N
CH3
CH3
H3C
CH3
1.00
0.95
3.00
9.13
19000
18000
17000
16000
15000
14000
13000
12000
11000
10000
9000
8000
7000
6000
5000
4000
3000
2000
1000
0
-1000
13 12 11 10 9 8 7 6 5 4 3 2 1 0 -1 -2
f1 (ppm)

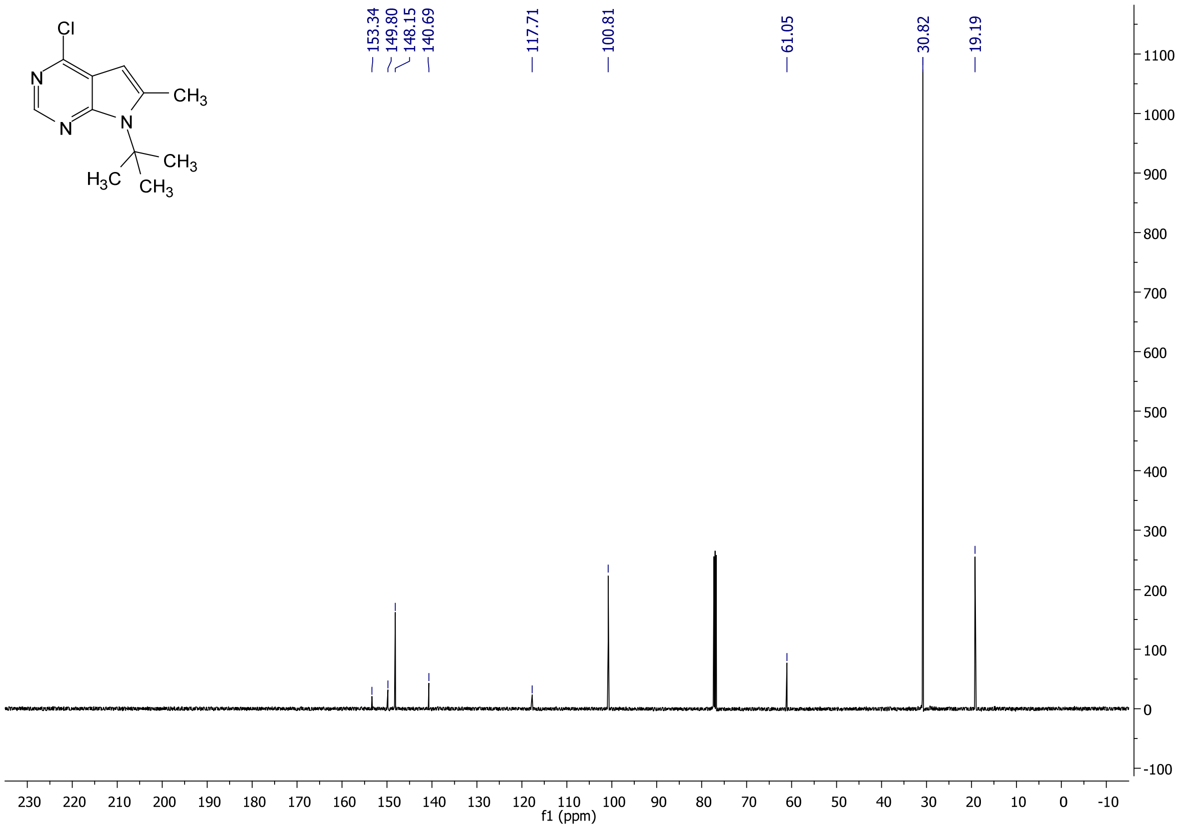
153.34
149.80
148.15
140.69
117.71
100.81
61.05
30.82
19.19
Cl
N
N
N
CH3
CH3
H3C
CH3
1100
1000
900
800
700
600
500
400
300
200
100
0
-100
230 220 210 200 190 180 170 160 150 140 130 120 110 100 90 80 70 60 50 40 30 20 10 0 -10
f1 (ppm)

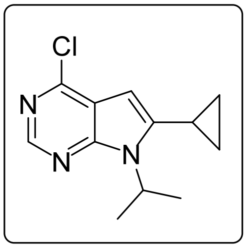

4-chloro-6-cyclopropyl-7-isopropyl-7*H*-pyrrolo[2,3-*d*]pyrimidine:

To 2-(4-chloro-6-(isopropylamino)pyrimidin-5-yl)-1-cyclopropylethanone (370 mg, 1.46 mmol, 1.0 eq) was acetic acid (208 ul, 3.64 mmol, 2.5 eq) added and dissolved into 15 mL EtOH. The solution was reacted in a microwave reactor at 120ºC for 1 hour. The solvent was removed and the crude extract was purified by FCC (9:1 Hex:EtAc) to yield 330 mg of pure 4-chloro-6-cyclopropyl-7-isopropyl-7H-pyrrolo[2,3-d]pyrimidine as a white solid (96% yield).

^{1}H NMR (400 MHz, $CDCl_3$) δ 8.52 (s, 1H), 6.16 (d, J = 1.0 Hz, 1H), 5.15 – 5.04 (m, 1H), 1.91 (m, 1H), 1.70 (d, J = 7.0 Hz, 6H), 1.09 – 1.04 (m, 2H), 0.84 – 0.79 (m, 2H).

^{13}C NMR (101 MHz, $CDCl_3$) δ 151.61, 150.38, 149.18, 145.12, 117.46, 95.35, 47.89, 21.36, 8.42, 7.10.

MS (APCI) Calculated: $C_{12}H_{15}ClN_3$ $[M+H]^+$ 236.1 **Found:** 236.1

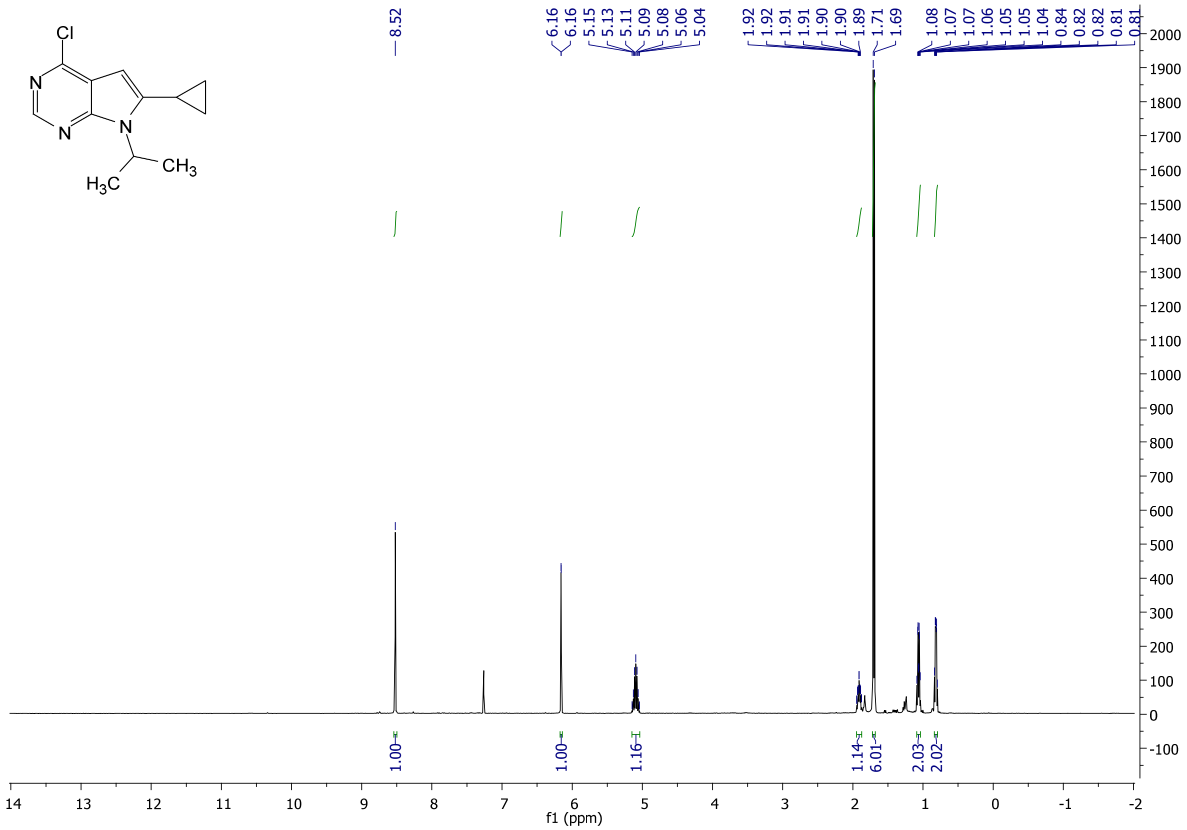
Cl
N
N
N
CH3
H3C
8.52
6.16
6.16
5.15
5.13
5.11
5.09
5.08
5.06
5.04
1.92
1.92
1.91
1.91
1.90
1.90
1.89
1.71
1.69
1.08
1.07
1.07
1.06
1.05
1.05
1.04
0.84
0.82
0.82
0.81
0.81
1.00
1.00
1.16
1.14
6.01
2.03
2.02
f1 (ppm)

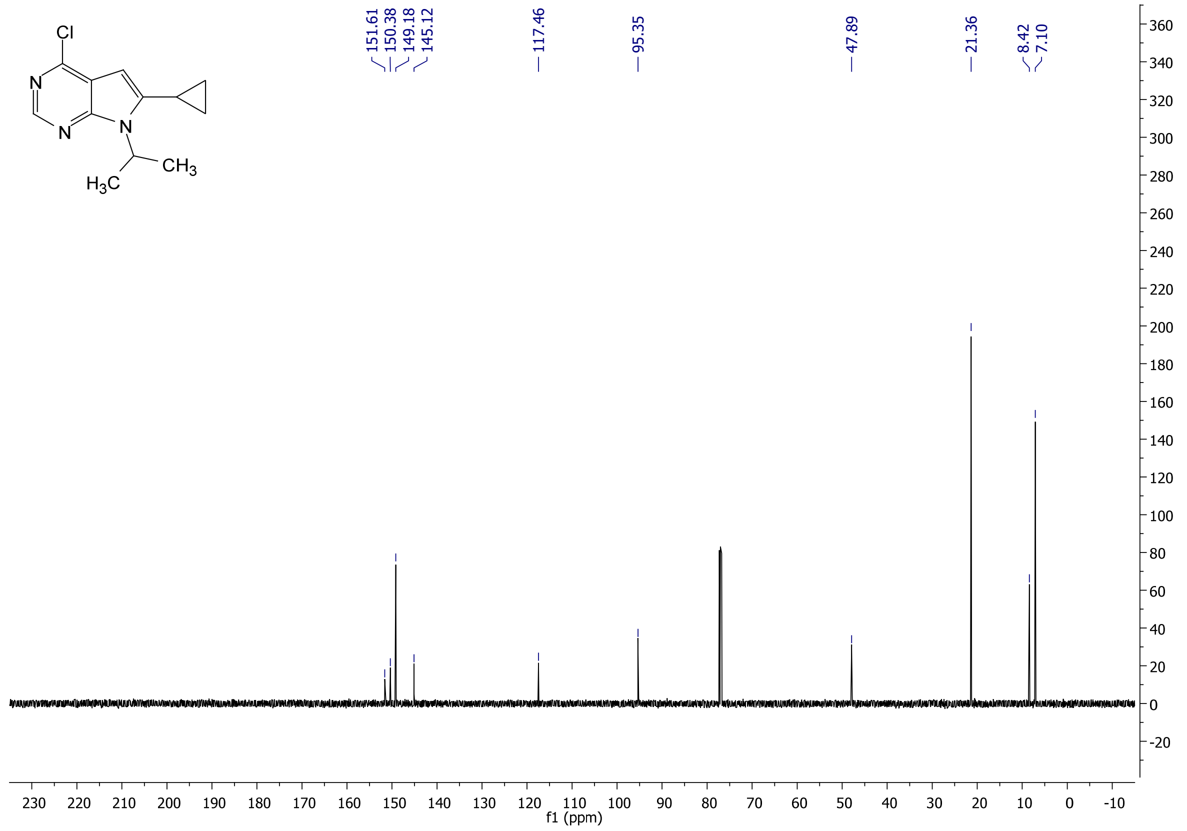
Cl
N
N
N
CH3
H3C
151.61
150.38
149.18
145.12
117.46
95.35
47.89
21.36
8.42
7.10
f1 (ppm)

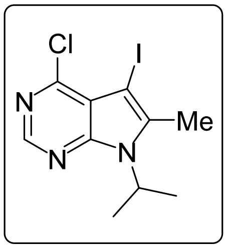

4-chloro-5-iodo-7-isopropyl-6-methyl-7H-pyrrolo[2,3-d]pyrimidine:

4-chloro-7-isopropyl-6-methyl-7H-pyrrolo[2,3-d]pyrimidine (390 mg, 1.86 mmol, 1 eq.) was added to N-Iodosuccinimide (502 mg, 2.23 mmol, 1.2 eq.) and dissolved in 12.4 mL of DMF at r.t.. The reaction mixture was then stirred at room temperature overnight. The reaction mixture was then partitioned between 10% sodium thiosulfate and EtAc, the organic layer was then washed with brine. Then the organic layer was collected, dried over sodium sulfate, and concentrated. The organic extract was then purified using FCC (Hex:EtAc (9.5: 0.5) to yield 497 mg of 7-(tert-butyl)-4-chloro-5-iodo-7H-pyrrolo[2,3-d]pyrimidine as a white solid (80% yield).

^{1}H NMR (400 MHz, $CDCl_3$) δ 8.52 (s, 1H), 5.00 – 4.89 (m, 1H), 2.57 (s, 3H), 1.65 (d, J = 7.0 Hz, 6H).

^{13}C NMR (101 MHz, $CDCl_3$) δ 151.49, 150.80, 148.97, 140.62, 117.10, 54.17, 49.23, 21.36, 15.22.

MS (APCI) Calculated: $C_{10}H_{12}ClIN_3$ $[M+H]^+$ 336.0 **Found:** 336.0 m/z

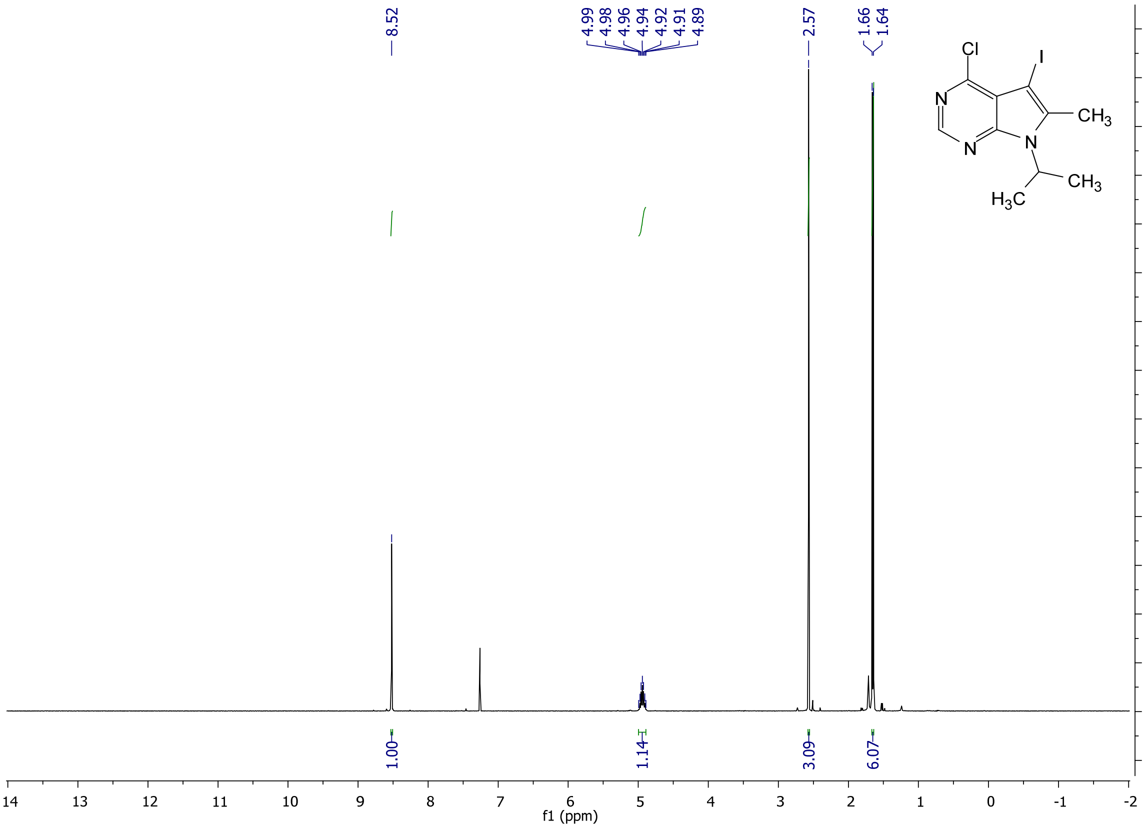
8.52
4.99
4.98
4.96
4.94
4.92
4.91
4.89
2.57
1.66
1.64
1.00
1.14
3.09
6.07
Cl
I
N
N
N
CH3
CH3
H3C
f1 (ppm)

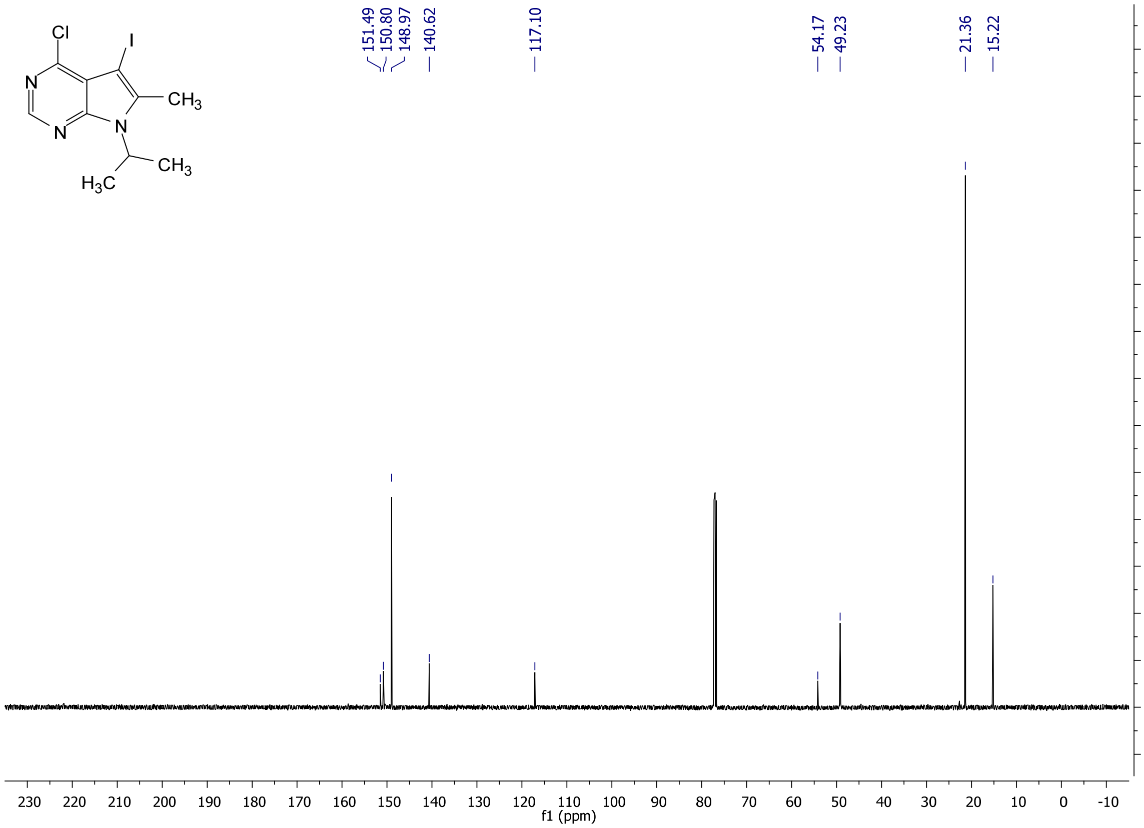
151.49
150.80
148.97
140.62
117.10
54.17
49.23
21.36
15.22
Cl
I
N
N
N
CH3
CH3
H3C
f1 (ppm)

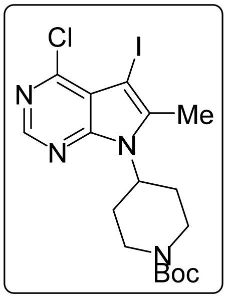

tert-butyl 4-(4-chloro-5-iodo-6-methyl-7H-pyrrolo[2,3-d]pyrimidin-7-yl)piperidine-1-carboxylate

tert-butyl 4-(4-chloro-6-methyl-7H-pyrrolo[2,3-d]pyrimidin-7-yl)piperidine-1-carboxylate (415 mg, 1.18 mmol, 1 eq.) was added to N-Iodosuccinimide (318.59 mg, 1.42 mmol, 1.2 eq.) and dissolved in 7.9 mL of DMF at r.t.. The reaction mixture was then stirred at room temperature overnight. The reaction mixture was then partitioned between 10% sodium thiosulfate and EtAc, the organic layer was then washed with brine. Then the organic layer was collected, dried over sodium sulfate, and concentrated. The organic extract was then purified using FCC (Hex:EtAc (9.5: 0.5) to yield 410 mg of 7-(tert-butyl)-4-chloro-5-iodo-7H-pyrrolo[2,3-d]pyrimidine as a white solid (84% yield). ^{1}**H NMR** (400 MHz, $CDCl_3$) δ 8.52 (s, 1H), 4.58 (t, J = 11.4 Hz, 1H), 4.34 (s, 2H), 2.84 (s, 2H), 2.70 (qd, J = 12.4, 3.9 Hz, 2H), 2.58 (s, 3H), 1.77 (d, J = 10.9 Hz, 2H), 1.50 (s, 9H).

^{13}**C NMR** (101 MHz, $CDCl_3$) δ 154.67, 151.65, 151.03, 149.06, 140.42, 117.11, 80.07, 55.76, 43.67, 30.22, 28.44, 15.40.

MS (APCI) Calculated: $C_{17}H_{23}ClIN_4O_2$ $[M+H]^+$ 477.1 **Found:** 477.1

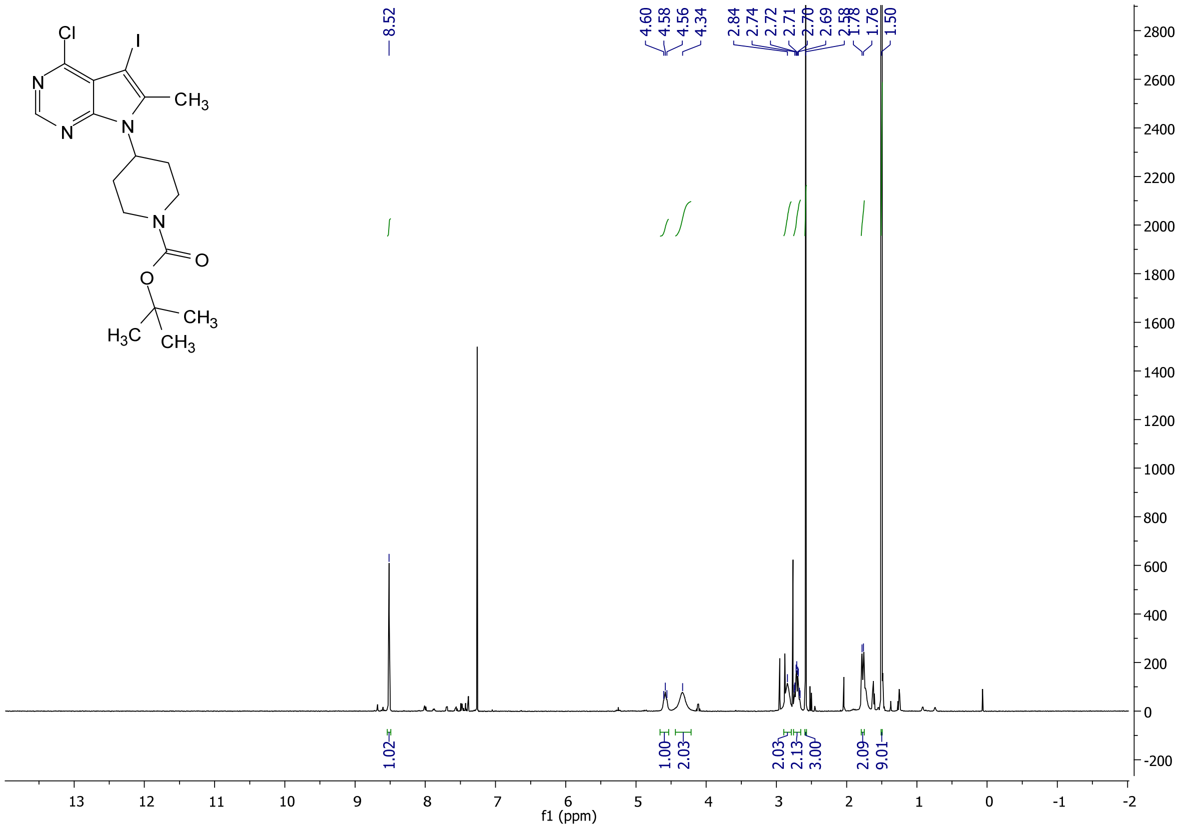
Cl
I
N
N
N
CH3
N
O
O
CH3
H3C
CH3
8.52
4.60
4.58
4.56
4.34
2.84
2.74
2.72
2.71
2.70
2.69
2.58
1.78
1.76
1.50
1.02
1.00
2.03
2.03
2.13
3.00
2.09
9.01
f1 (ppm)

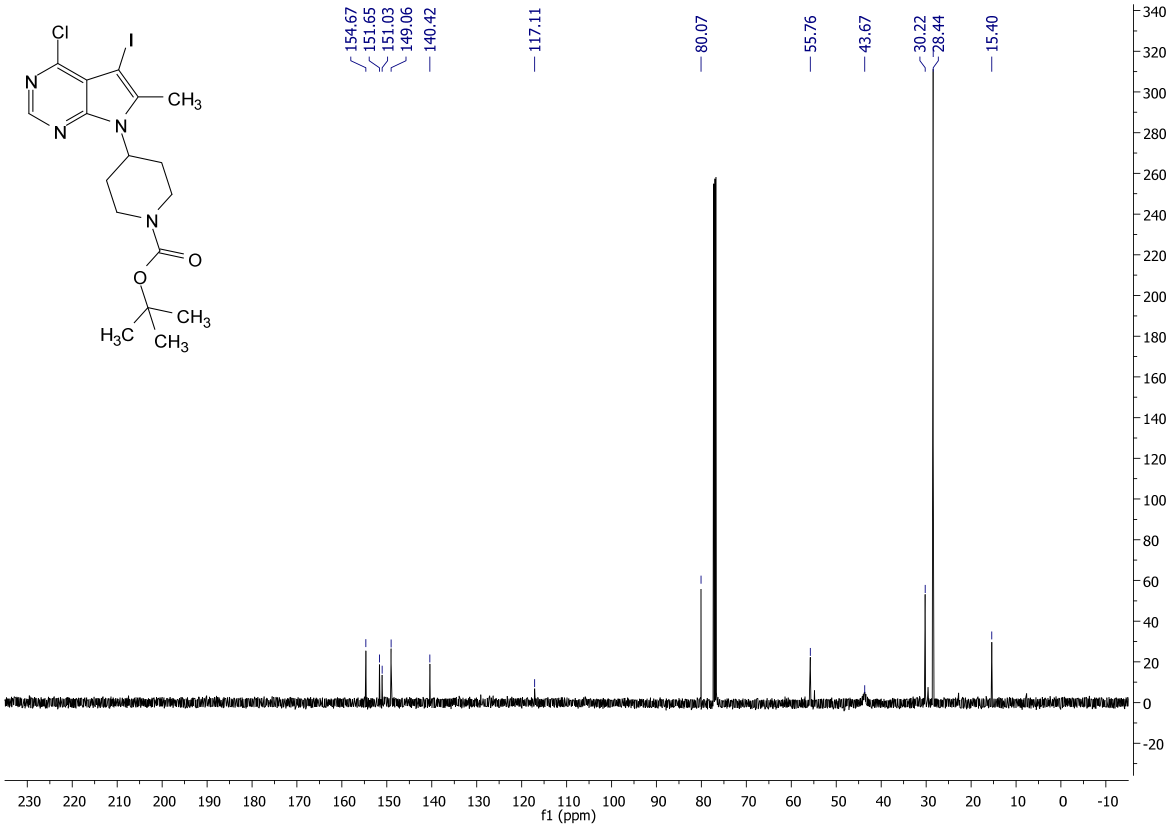
Cl
I
N
N
N
CH3
N
O
O
CH3
H3C
CH3
154.67
151.65
151.03
149.06
140.42
117.11
80.07
55.76
43.67
30.22
28.44
15.40
f1 (ppm)

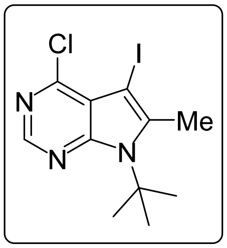

7-(tert-butyl)-4-chloro-5-iodo-6-methyl-7H-pyrrolo[2,3-d]pyrimidine

To 7-(tert-butyl)-4-chloro-6-methyl-7H-pyrrolo[2,3-d]pyrimidine (110 mg, .49 mmol, 1 eq.) was added to N-Iodosuccinimide (132 mg, .59 mmol, 1.2 eq.) and dissolved in 3.3 mL of DMF at r.t.. The reaction mixture was then stirred at room temperature overnight. The reaction mixture was then partitioned between 10% sodium thiosulfate and EtAc, the organic layer was then washed with brine. Then the organic layer was collected, dried over sodium sulfate, and concentrated. The organic extract was then purified using FCC (Hex:EtAc (9.5: 0.5) to yield 159 mg of 7-(tert-butyl)-4-chloro-5-iodo-6-methyl-7H-pyrrolo[2,3-d]pyrimidine as a white solid (93% yield).

^{1}H NMR (400 MHz, $CDCl_3$) δ 8.52 (s, 1H), 2.75 (s, 3H), 1.90 (s, 9H).

^{13}C NMR (101 MHz, $CDCl_3$) δ 153.15, 150.79, 147.93, 141.61, 117.50, 62.86, 58.67, 31.27, 19.97.

MS (APCI) Calculated: $C_{11}H_{14}ClIN_3$ $[M+H]^+$ 350.0 **Found:** 350.0 m/z

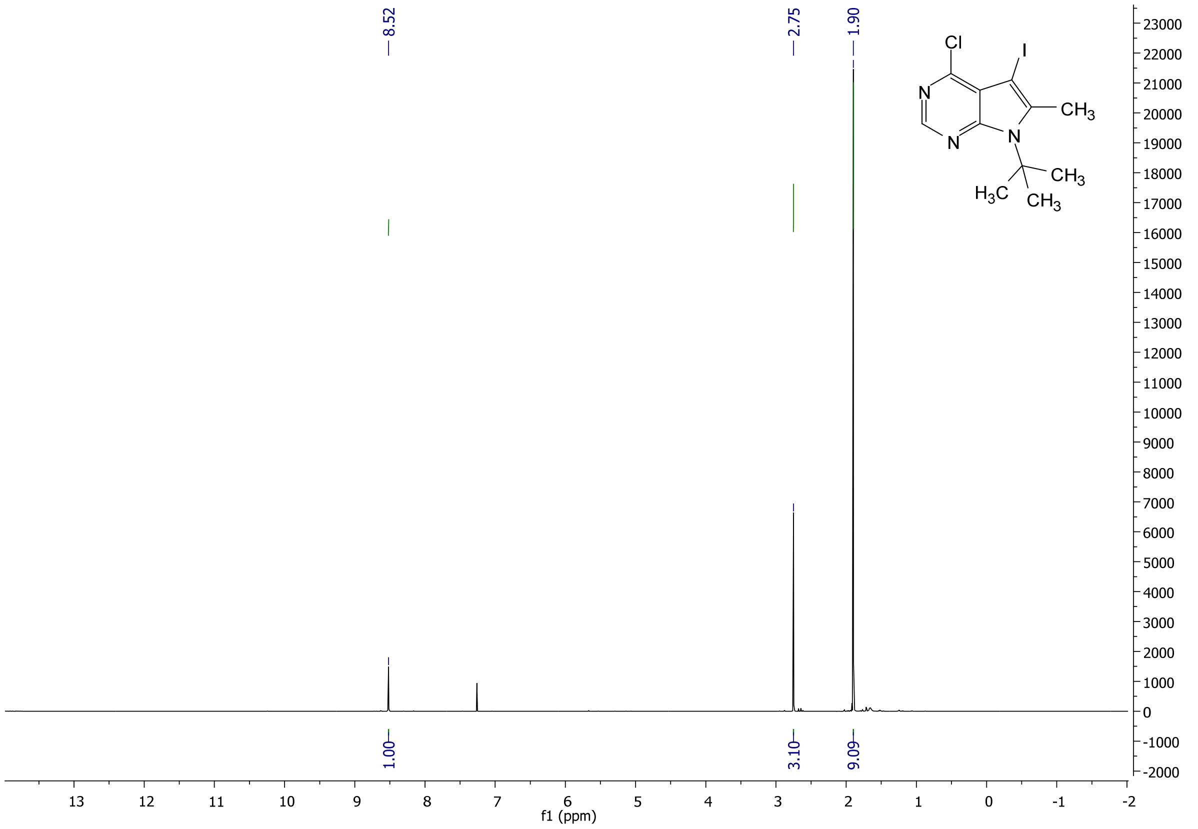
8.52
2.75
1.90
Cl
I
N
N
N
CH3
CH3
H3C
CH3
1.00
3.10
9.09
13 12 11 10 9 8 7 6 5 4 3 2 1 0 -1 -2
f1 (ppm)
23000 22000 21000 20000 19000 18000 17000 16000 15000 14000 13000 12000 11000 10000 9000 8000 7000 6000 5000 4000 3000 2000 1000 0 -1000 -2000

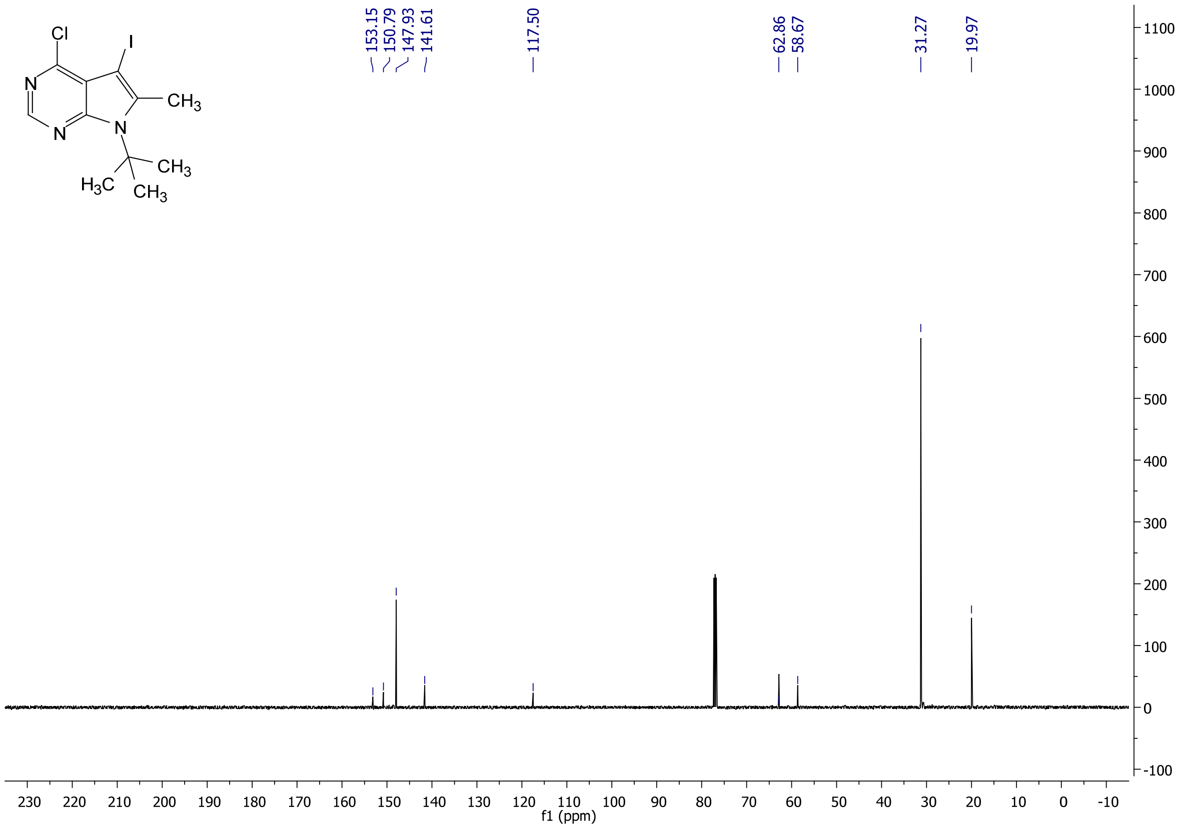
Cl
I
N
N
N
CH3
CH3
H3C
CH3
153.15
150.79
147.93
141.61
117.50
62.86
58.67
31.27
19.97
230 220 210 200 190 180 170 160 150 140 130 120 110 100 90 80 70 60 50 40 30 20 10 0 -10
f1 (ppm)
1100 1000 900 800 700 600 500 400 300 200 100 0 -100

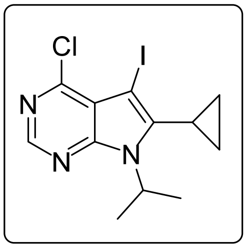

4-chloro-6-cyclopropyl-5-iodo-7-isopropyl-7H-pyrrolo[2,3-d]pyrimidine:

4-chloro-6-cyclopropyl-7-isopropyl-7H-pyrrolo[2,3-d]pyrimidine (330 mg, 1.4 mmol, 1 eq.) was added to N-Iodosuccinimide (378 mg, 1.68 mmol, 1.2 eq.) and dissolved in 9.3 mL of DMF at r.t.. The reaction mixture was then stirred at room temperature overnight. The reaction mixture was then partitioned between 10% sodium thiosulfate and EtAc, the organic layer was then washed with brine. Then the organic layer was collected, dried over sodium sulfate, and concentrated. The organic extract was then purified using FCC (Hex:EtAc (9.5: 0.5) to yield 420 mg of 4-chloro-6-cyclopropyl-5-iodo-7-isopropyl-7H-pyrrolo[2,3-d]pyrimidine as a white solid (83% yield).

^{1}H NMR (400 MHz, $CDCl_3$) δ 8.53 (s, 1H), 5.17 (hept, J = 6.9 Hz, 1H), 1.73 (m, 1H), 1.70 (d, J = 7.0 Hz, 6H), 1.27 – 1.22 (m, 2H), 0.95 – 0.91 (m, 2H).

^{13}C NMR (101 MHz, $CDCl_3$) δ 151.53, 151.30, 149.19, 142.92, 117.25, 54.52, 49.31, 21.04, 8.71, 8.52.

MS (APCI) Calculated: $C_{12}H_{14}ClIN_3$ $[M+H]^+$ 361.9 **Found:** 362.0

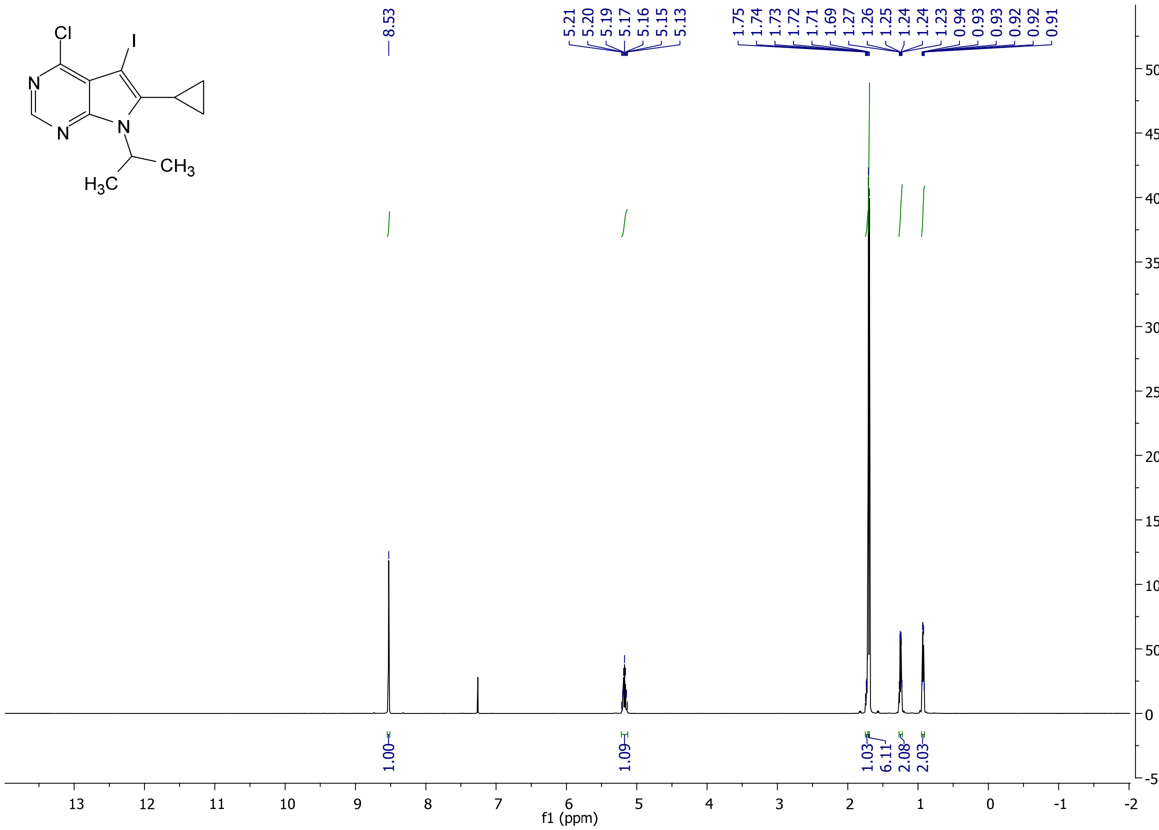
Cl
I
N
N
N
CH3
H3C
8.53
5.21
5.20
5.19
5.17
5.16
5.15
5.13
1.75
1.74
1.73
1.72
1.71
1.69
1.27
1.26
1.25
1.24
1.24
1.23
0.94
0.93
0.93
0.92
0.92
0.91
1.00
1.09
1.03
6.11
2.08
2.03
13 12 11 10 9 8 7 6 5 4 3 2 1 0 -1 -2
f1 (ppm)
5000
4500
4000
3500
3000
2500
2000
1500
1000
500
0
-500

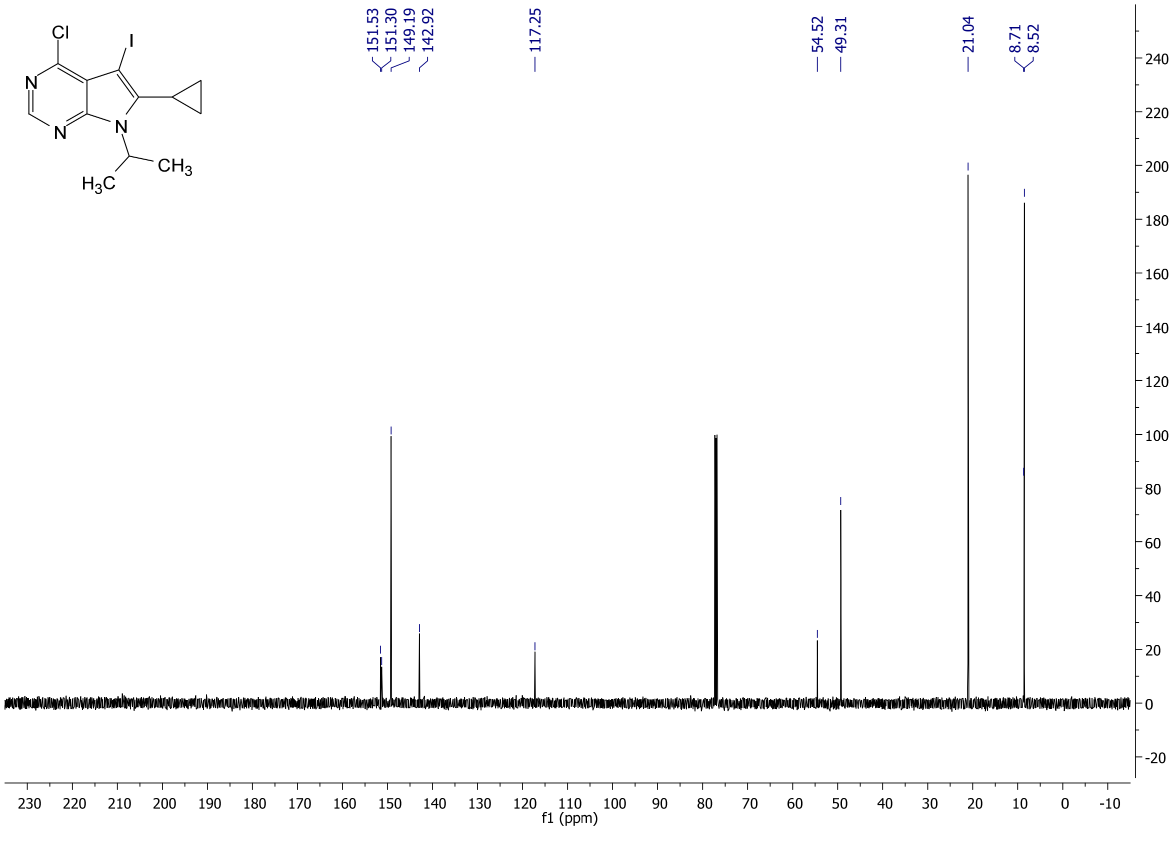
Cl
I
N
N
N
CH3
H3C
151.53
151.30
149.19
142.92
117.25
54.52
49.31
21.04
8.71
8.52
230 220 210 200 190 180 170 160 150 140 130 120 110 100 90 80 70 60 50 40 30 20 10 0 -10
f1 (ppm)
240
220
200
180
160
140
120
100
80
60
40
20
0
-20

General procedure for the cross coupling of aryl boronic acids to pyrrolopyrimidines (2.1a - 2.20a):

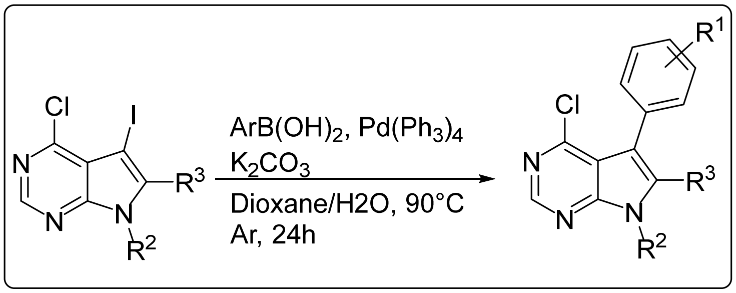

Iodinated pyrrolopyrimidine was combined with boronic acid (1.2 equiv), $Pd(Ph_3)_4$ (0.1 equiv.) and K_2CO_3 (2.5 equiv). Upon purging with argon gas, the mixture was dissolved in a 3:1 mixture of degassed dioxane/DI water (0.25M) and kept under inert argon atmosphere. The reaction mixture was heated at 90ºC for 18 hours. The reaction mixture was dissolved in 4:6 DI water: ethyl acetate and the organic layer was collected and concentrated. The organic extract was then purified using FCC (gradient of hexanes: ethyl acetate 95:5 to 90:10) to yield **2.1a** – **2.20a** (34-85% yields).

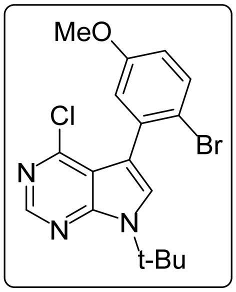

5-(2-bromo-5-methoxyphenyl)-7-(*tert*-butyl)-4-chloro-7*H*-pyrrolo[2,3-*d*]pyrimidine (2.1a): Following the general procedure A: 7-(*tert*-butyl)-4-chloro-5-iodo-7*H*-pyrrolo[2,3-*d*]pyrimidine (1.23 g, 3.67 mmol, 1.0 eq), was coupled with (2-bromo-5-methoxyphenyl)boronic acid. The mixture was thoroughly purged with vacuum then argon. Workup and purification was followed according to the general procedure to afford 1.01 g (70% yield) of **2.1a** as a yellow solid. The ^1H NMR matched those reported in literature.[1]

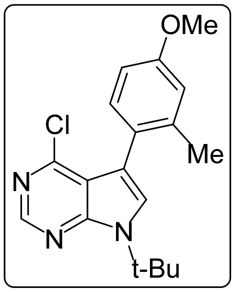

7-(*tert*-butyl)-4-chloro-5-(4-methoxy-2-methylphenyl)-7*H*-pyrrolo[2,3-*d*]pyrimidine (2.2a): Following the general procedure A: 7-(*tert*-butyl)-4-chloro-5-iodo-7*H*-pyrrolo[2,3-*d*]pyrimidine (800 mg, 2.384 mmol, 1.0 eq), was coupled with (4-methoxy-2-methylphenyl)boronic acid. The mixture was thoroughly purged with vacuum then argon. Workup and purification was followed according to the general procedure to afford 591mg (75% yield) of **2.2a** as a yellow solid.

^{1}H NMR (400 MHz, $CDCl_3$) δ 8.62 (s, 1H), 7.24 (s, 1H), 7.16 (d, J = 8.3 Hz, 1H), 6.84 (d, J = 2.7 Hz, 1H), 6.77 (dd, J = 8.3, 2.7 Hz, 1H), 3.85 (s, 3H), 2.15 (s, 3H), 1.83 (s, 9H)

^{13}C NMR (101 MHz, $CDCl_3$) δ 159.48, 152.13, 151.12, 149.26, 139.79, 132.53, 125.87, 125.38, 117.40, 115.34, 113.96, 110.58, 57.95, 55.37, 29.44, 21.01

MS (APCI) Calculated: $C_{18}H_{21}ClN_3O$ $[M+H]^+$ 330.1 **Found:** 330.0

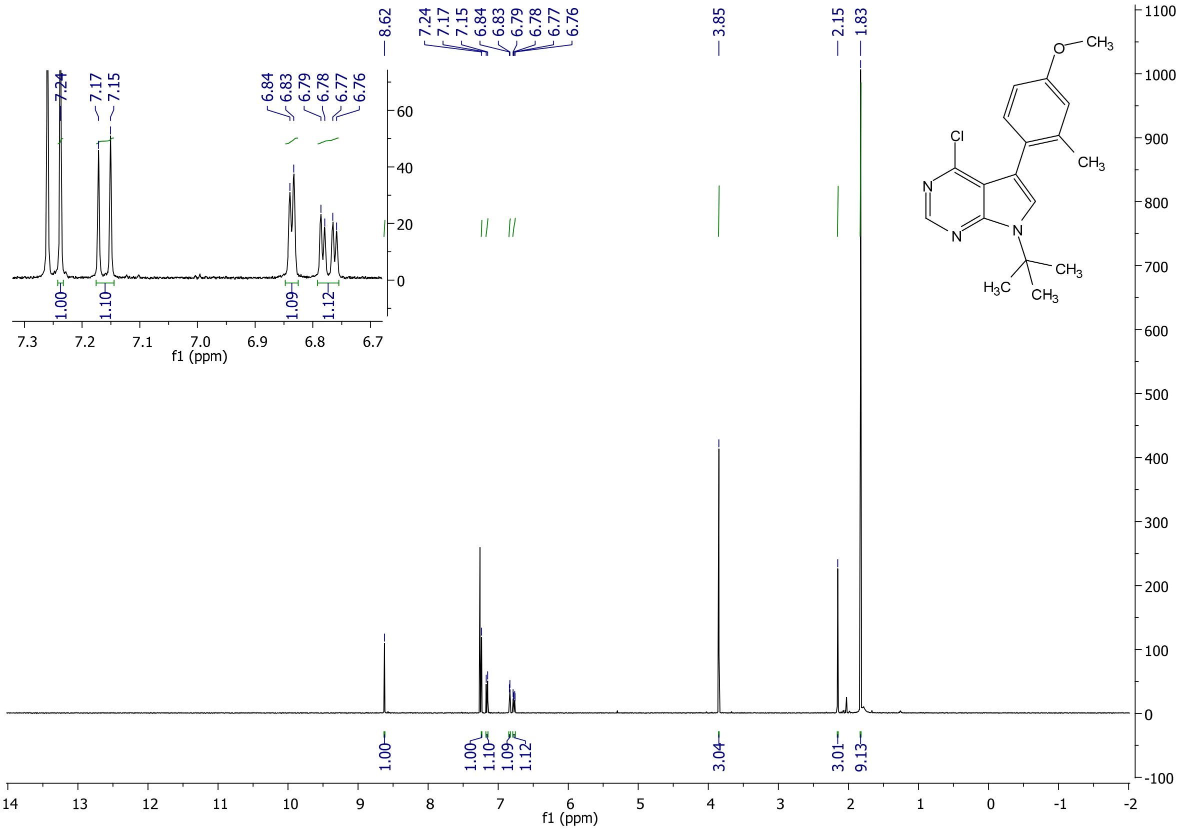

8.62
7.24
7.17
7.15
6.84
6.83
6.79
6.78
6.77
6.76
3.85
2.15
1.83
1.00
1.10
1.09
1.12
3.04
3.01
9.13
f1 (ppm)
Cl
N
N
N
O
CH3
CH3
H3C
CH3
CH3

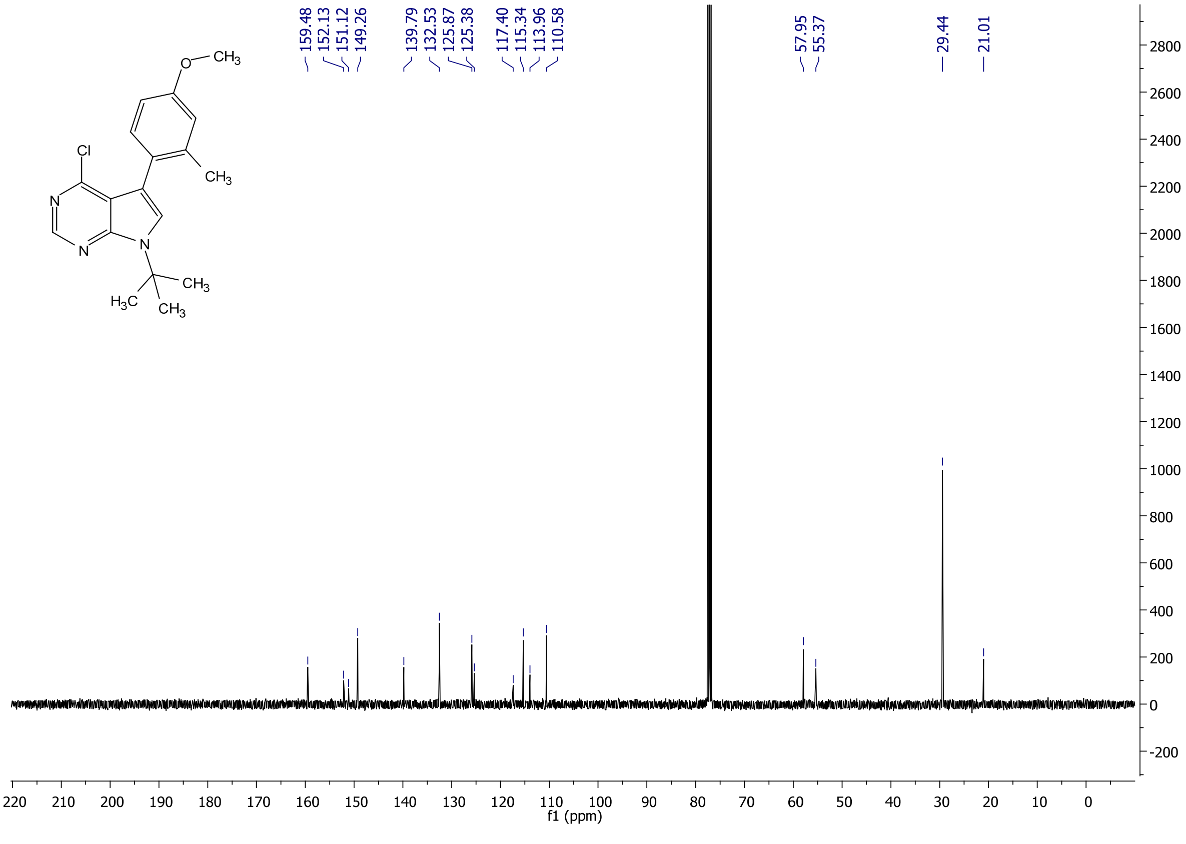

159.48
152.13
151.12
149.26
139.79
132.53
125.87
125.38
117.40
115.34
113.96
110.58
57.95
55.37
29.44
21.01
f1 (ppm)
Cl
N
N
N
O
CH3
CH3
H3C
CH3
CH3

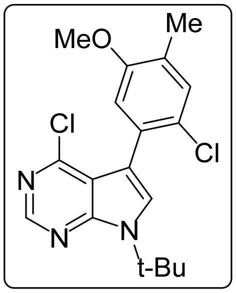

7-(*tert*-butyl)-4-chloro-5-(2-chloro-5-methoxy-4-methylphenyl)-7*H*-pyrrolo[2,3-*d*]pyrimidine (2.3a):

Following the general procedure A: 7-(*tert*-butyl)-4-chloro-5-iodo-7*H*-pyrrolo[2,3-*d*]pyrimidine (376 mg, 1.12 mmol, 1.0 eq), was coupled with (2-chloro-5-methoxy-4-methylphenyl)boronic acid. The mixture was thoroughly purged with vacuum then argon. Workup and purification was followed according to the general procedure to afford 220mg (54% yield) of **2.3a** as a yellowish-orange solid.

^{1}H NMR (500 MHz, $CDCl_3$) δ 8.64 (s, 1H), 7.39 (s, 1H), 7.23 (s, 1H), 6.83 (s, 1H), 3.82 (s, 3H), 2.25 (s, 3H), 1.84 (s, 9H)

^{13}C NMR (101 MHz, $CDCl_3$) δ 155.88, 152.07, 151.10, 149.32, 130.96, 130.04, 128.15, 126.80, 125.85, 117.04, 114.76, 112.11, 58.18, 55.77, 29.40, 16.03

MS (APCI) Calculated: $C_{18}H_{20}Cl_2N_3O$ $[M+H]^+$ 364.1 **Found**: 364.2

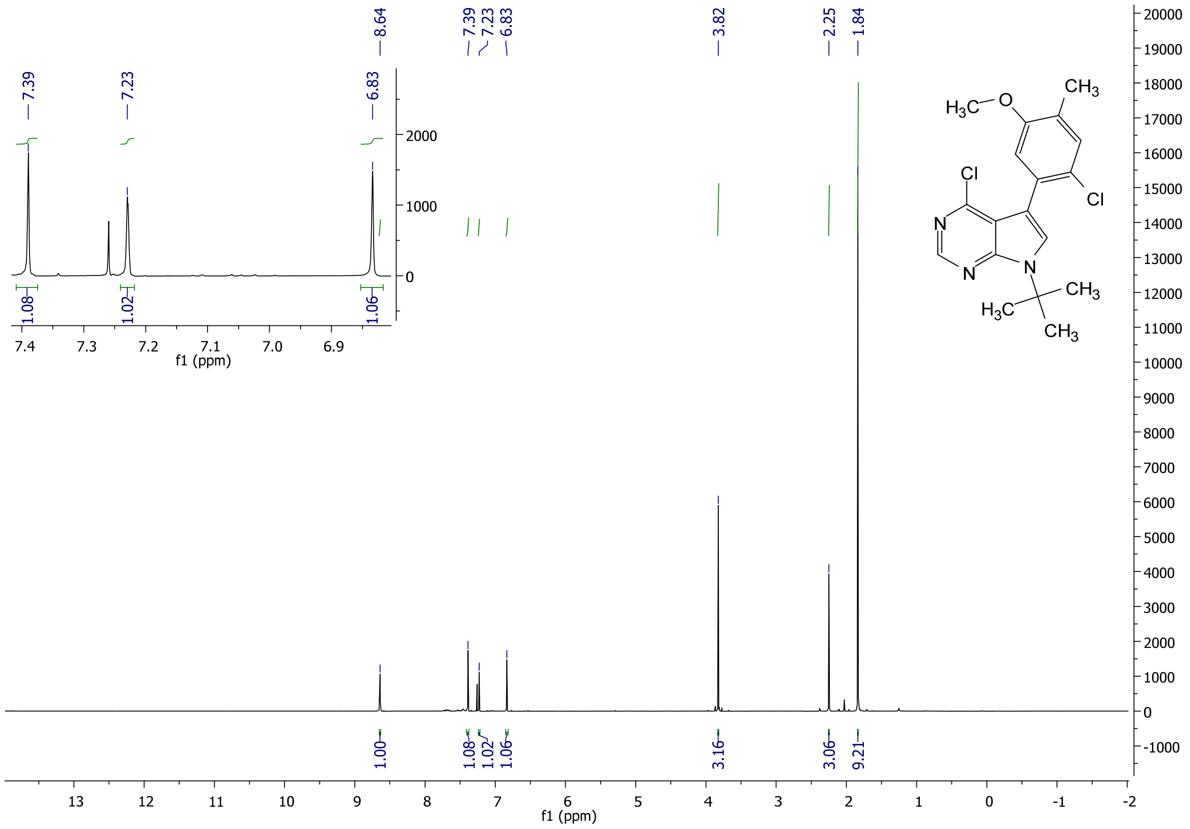
8.64
7.39
7.23
6.83
3.82
2.25
1.84
1.00
1.08
1.02
1.06
3.16
3.06
9.21
f1 (ppm)
H3C
O
CH3
Cl
Cl
N
N
N
CH3
H3C
CH3

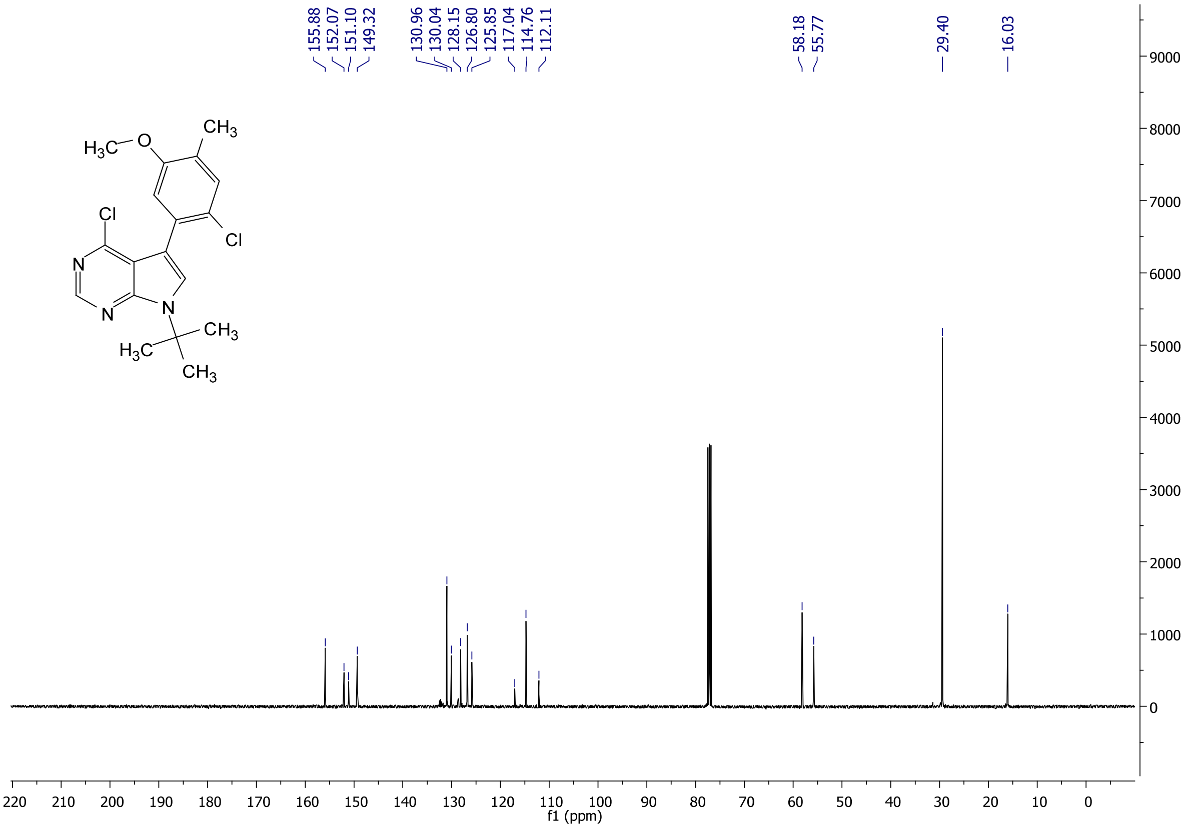
155.88
152.07
151.10
149.32
130.96
130.04
128.15
126.80
125.85
117.04
114.76
112.11
58.18
55.77
29.40
16.03
f1 (ppm)
H3C
O
CH3
Cl
Cl
N
N
N
CH3
H3C
CH3

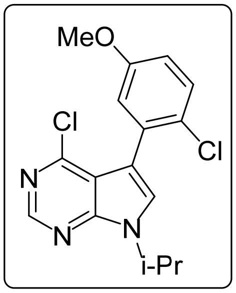

4-chloro-5-(2-chloro-5-methoxyphenyl)-7-isopropyl-7*H*-pyrrolo[2,3-*d*]pyrimidine (2.4a):

Following the general procedure: 4-chloro-5-iodo-7-isopropyl-7*H*-pyrrolo[2,3-*d*]pyrimidine (1.5 g, 4.66 mmol, 1.0 eq), was coupled with (2-chloro-5-methoxyphenyl)boronic acid. The mixture was thoroughly purged with vacuum then argon. Workup and purification were followed according to the general procedure to afford 900mg (57% yield) of **2.4a** as a yellowish-orange solid.

^{1}H NMR (500 MHz, $CDCl_3$) δ 8.66 (s, 1H), 7.38 (d, J = 8.8 Hz, 1H), 7.37 (s, 1H), 6.95 (d, J = 3.0 Hz, 1H), 6.89 (dd, J = 8.8, 3.0 Hz, 1H), 5.21 (hept, J = 6.8 Hz, 1H), 3.83 (s, 3H), 1.59 (d, J = 6.8 Hz, 6H)

^{13}C NMR (101 MHz, $CDCl_3$) δ 157.85, 152.03, 150.53, 150.27, 132.85, 130.08, 126.61, 125.56, 118.48, 115.96, 115.10, 113.49, 55.75, 47.05, 22.85

MS (APCI) Calculated: $C_{16}H_{16}Cl_2N_3O$ $[M+H]^+$ 336.1 **Found:** 336.0 m/z

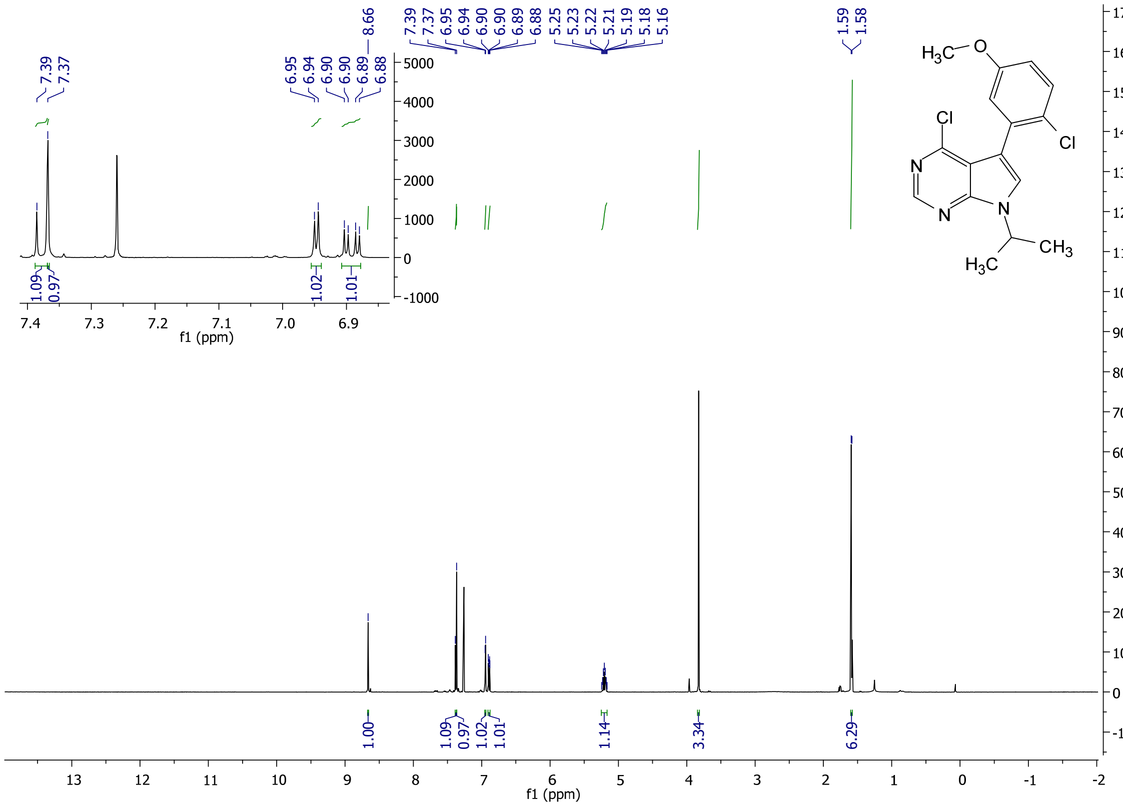
8.66
7.39
7.37
6.95
6.94
6.90
6.90
6.89
6.88
5.25
5.23
5.22
5.21
5.19
5.18
5.16
1.59
1.58
1.00
1.09
0.97
1.02
1.01
1.14
3.34
6.29
f1 (ppm)
H3C
O
Cl
Cl
N
N
N
CH3
H3C

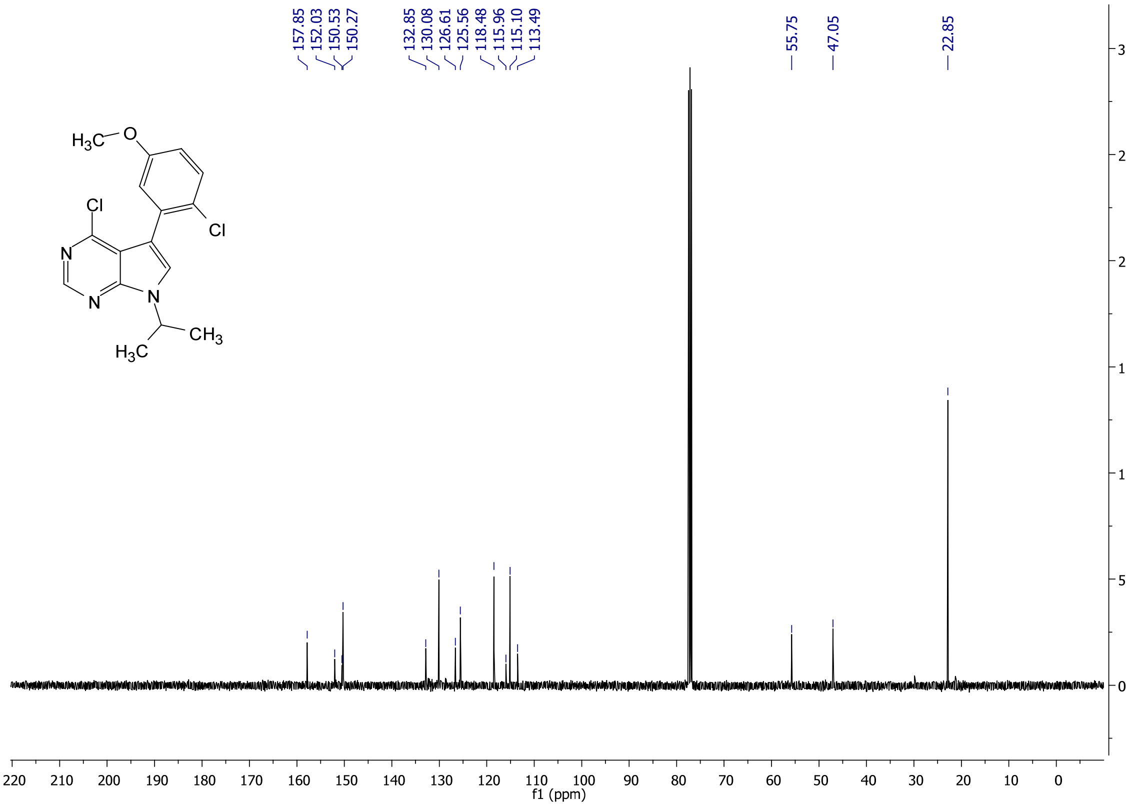
157.85
152.03
150.53
150.27
132.85
130.08
126.61
125.56
118.48
115.96
115.10
113.49
55.75
47.05
22.85
f1 (ppm)
H3C
O
Cl
Cl
N
N
N
CH3
H3C

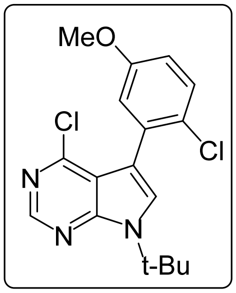

7-(*tert*-butyl)-4-chloro-5-(2-chloro-5-methoxyphenyl)-7*H*-pyrrolo[2,3-d]pyrimidine (2.6a): Following the general procedure A: 7-(*tert*-butyl)-4-chloro-5-iodo-7*H*-pyrrolo[2,3-*d*]pyrimidine (1.35 g, 4.02 mmol, 1.0 eq), was coupled with (2-chloro-5-methoxyphenyl)boronic acid. The mixture was thoroughly purged with vacuum then argon. Workup and purification was followed according to the general procedure to afford 1.24g (89% yield) of **2.6a** as a yellowish-orange solid.

^{1}H NMR (400 MHz, $CDCl_3$) δ 8.65 (s, 1H), 7.39 (s, 1H), 7.37 (d, J = 8.8 Hz, 1H), 6.94 (d, J = 3.0 Hz, 1H), 6.88 (dd, J = 8.8, 3.1 Hz, 1H), 3.82 (s, 3H), 1.84 (s, 9H)

^{13}C NMR (101 MHz, $CDCl_3$) δ 157.67, 151.94, 150.97, 149.21, 133.05, 129.85, 126.62, 118.32, 116.87, 114.84, 111.86, 58.11, 55.59, 29.26

MS (APCI) Calculated: $C_{17}H_{18}Cl_2N_3O$ $[M+H]^+$ 350.1 **Found**: 350.0

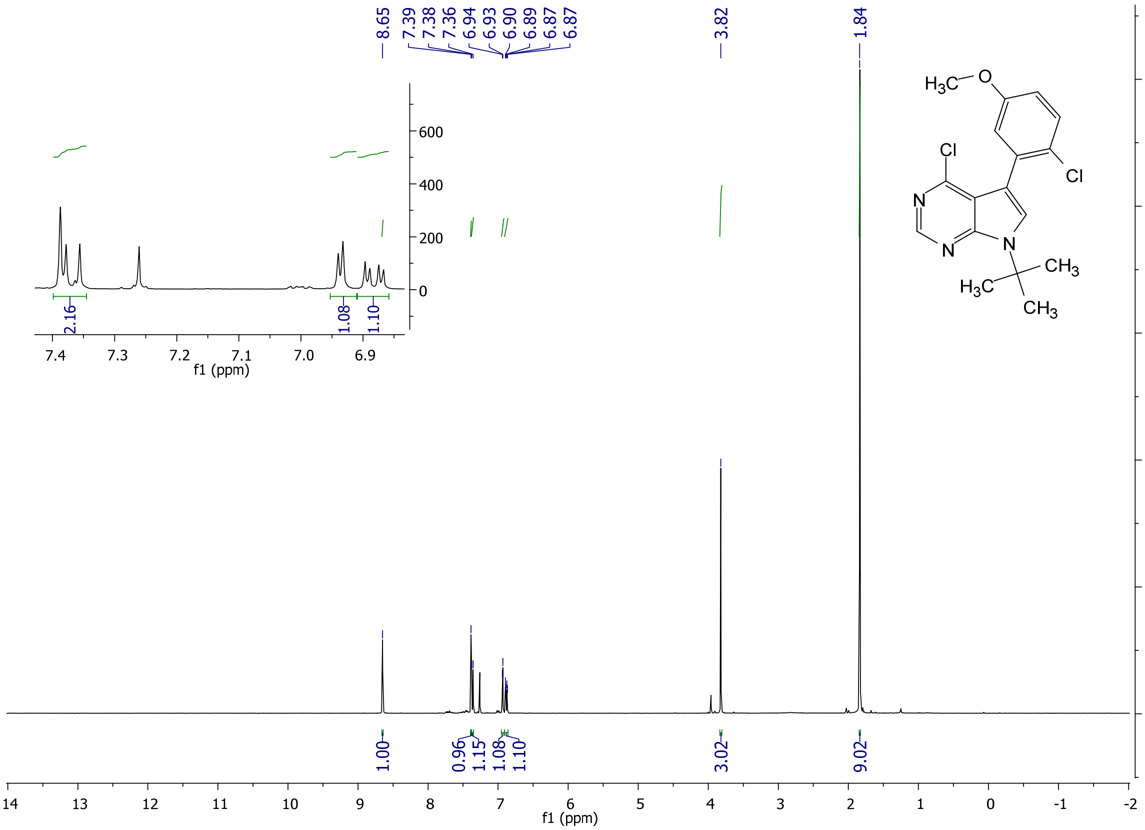
8.65
7.39
7.38
7.36
6.94
6.93
6.90
6.89
6.87
6.87
3.82
1.84
2.16
1.08
1.10
7.4
7.3
7.2
7.1
7.0
6.9
f1 (ppm)
600
400
200
0
1.00
0.96
1.15
1.08
1.10
3.02
9.02
2500
2000
1500
1000
500
0
14
13
12
11
10
9
8
7
6
5
4
3
2
1
0
-1
-2
f1 (ppm)
H_3C O
Cl
Cl
N
N
N
CH_3
H_3C
CH_3

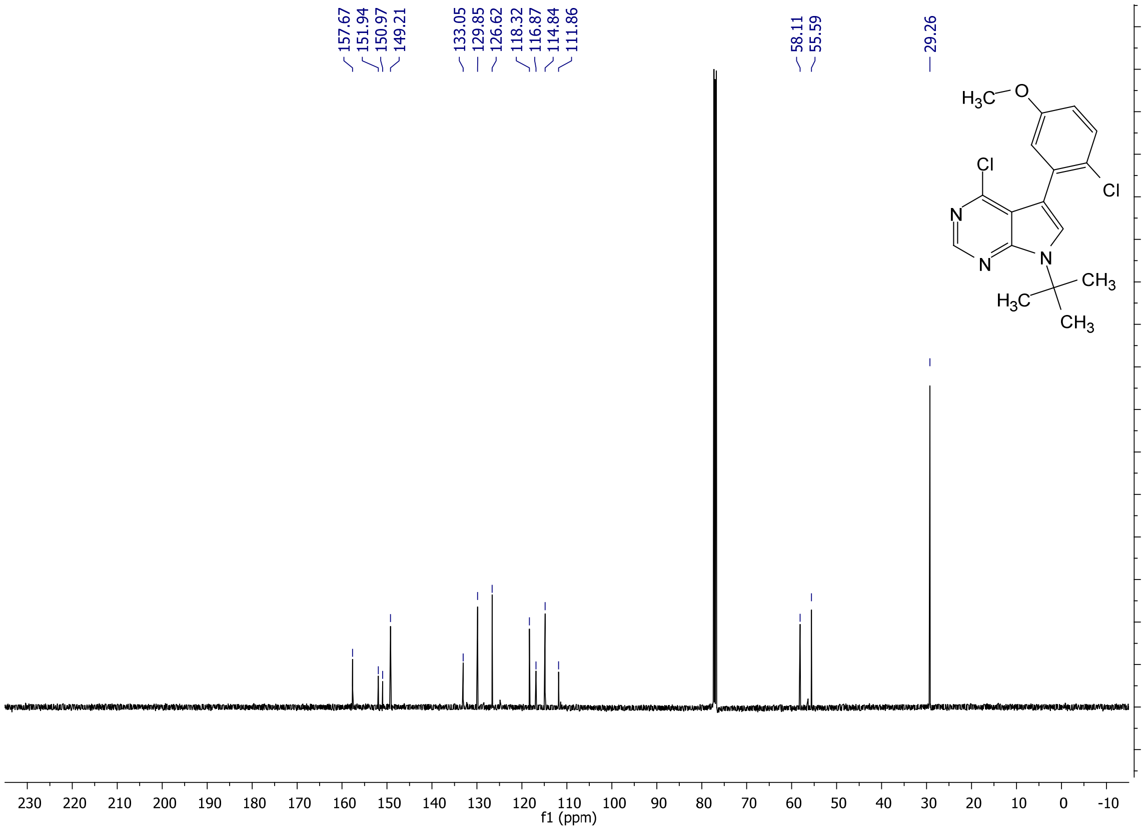
157.67
151.94
150.97
149.21
133.05
129.85
126.62
118.32
116.87
114.84
111.86
58.11
55.59
29.26
800
750
700
650
600
550
500
450
400
350
300
250
200
150
100
50
0
-50
230
220
210
200
190
180
170
160
150
140
130
120
110
100
90
80
70
60
50
40
30
20
10
0
-10
f1 (ppm)
H_3C O
Cl
Cl
N
N
N
CH_3
H_3C
CH_3

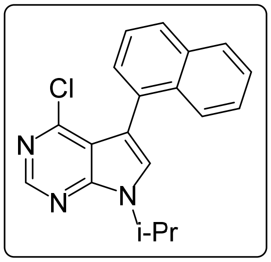

4-chloro-7-isopropyl-5-(naphthalen-1-yl)-7*H*-pyrrolo[2,3-d]pyrimidine (2.9a):

Following the general procedure: 4-chloro-5-iodo-7-isopropyl-7*H*-pyrrolo[2,3-*d*]pyrimidine (954 mg, 2.97 mmol, 1.0 eq), was coupled with napthalen-1-ylboronic acid. The mixture was thoroughly purged with vacuum then argon. Workup and purification was followed according to the general procedure to afford 754 mg (79% yield) of **2.9a** as a light yellow solid. The ^{1}H NMR matched those reported in literature.[8]

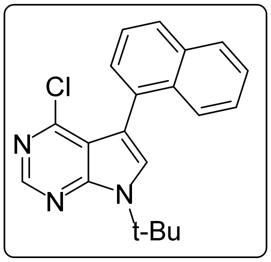

7-(*tert*-butyl)-4-chloro-5-(naphthalen-1-yl)-7*H*-pyrrolo[2,3-d]pyrimidine (2.10a):

Following the general procedure A: 7-(*tert*-butyl)-4-chloro-5-iodo-7*H*-pyrrolo[2,3-*d*]pyrimidine (1.69 g, 5.03 mmol, 1.0 eq), was coupled with naphthalene-1-boronic acid. The mixture was thoroughly purged with vacuum then argon. Workup and purification was followed according to the general procedure to afford 936mg (55% yield) of **2.10a** as a yellowish-orange solid.

^{1}H NMR (400 MHz, $CDCl_3$) δ 8.68 (s, 1H), 7.91 (d, J = 8.0 Hz, 2H), 7.67 (d, J = 8.4 Hz, 1H), 7.55 – 7.47 (m, 3H), 7.44 (s, 1H), 7.41 (ddd, J = 8.2, 6.8, 1.3 Hz, 1H), 1.88 (s, 9H)

^{13}C NMR (101 MHz, $CDCl_3$) δ 152.40, 151.25, 149.50, 133.93, 133.52, 131.21, 129.17, 128.36, 128.28, 126.87, 126.33, 126.20, 125.95, 125.15, 117.91, 112.84, 58.17, 29.46

MS (APCI) Calculated: $C_{20}H_{19}ClN_3$ $[M+H]^+$ 336.1 **Found:** 336.2

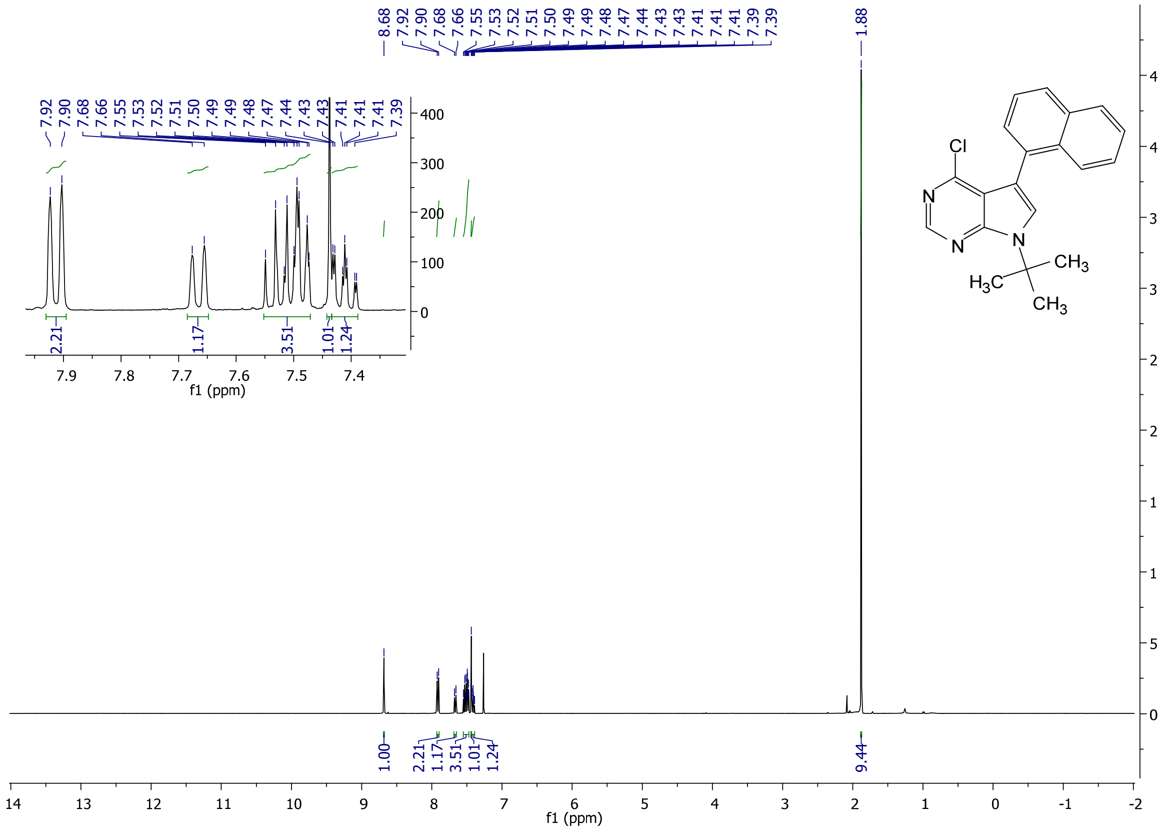
8.68
7.92
7.90
7.68
7.66
7.55
7.53
7.52
7.51
7.50
7.49
7.49
7.48
7.47
7.44
7.43
7.43
7.41
7.41
7.41
7.39
1.88
2.21
1.17
3.51
1.01
1.24
1.00
9.44
f1 (ppm)
Cl
N
N
N
CH3
H3C
CH3

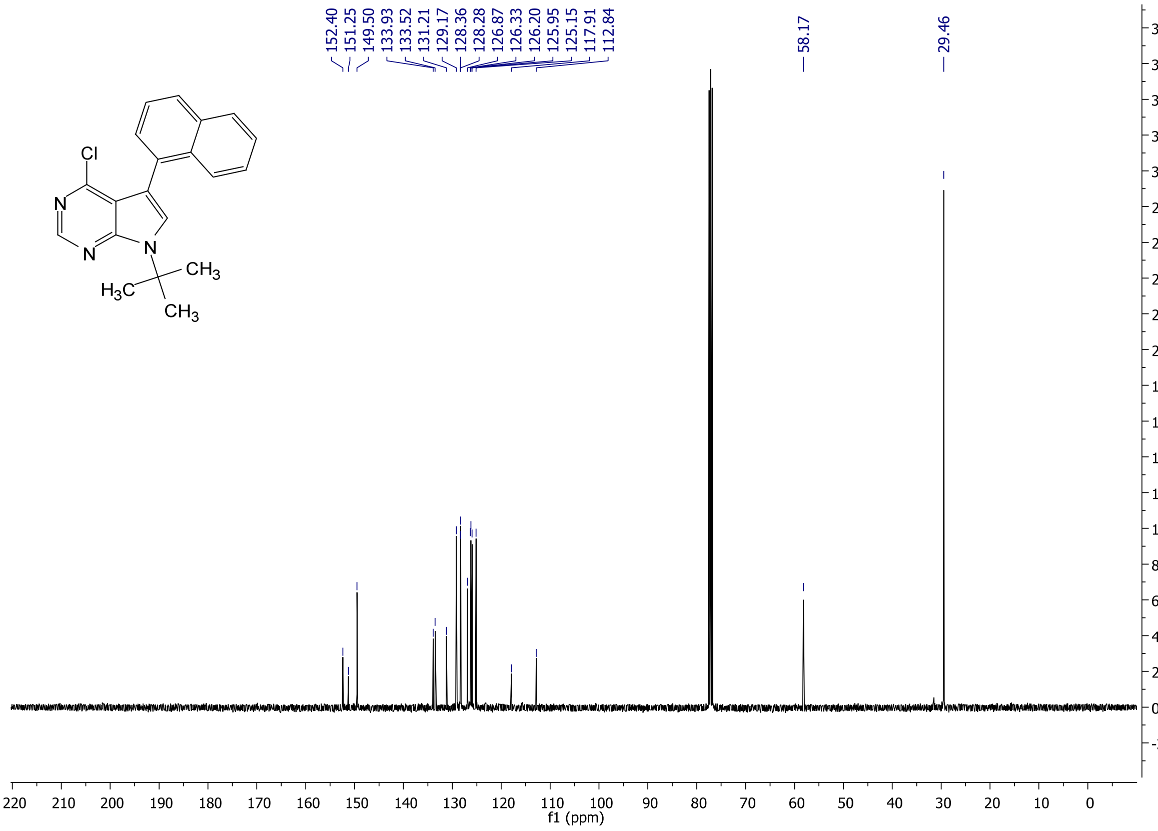
152.40
151.25
149.50
133.93
133.52
131.21
129.17
128.36
128.28
126.87
126.33
126.20
125.95
125.15
117.91
112.84
58.17
29.46
f1 (ppm)
Cl
N
N
N
CH3
H3C
CH3

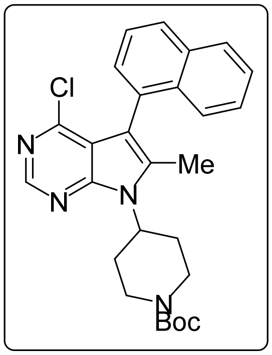

tert-butyl 4-(4-chloro-6-methyl-5-(naphthalen-1-yl)-7_H_-pyrrolo[2,3-_d_]pyrimidin-7-yl)piperidine-1-carboxylate (2.11a):

Following the general procedure A: _tert_-butyl 4-(4-chloro-5-iodo-6-methyl-7_H_-pyrrolo[2,3-_d_]pyrimidin-7-yl)piperidine-1-carboxylate (80 mg, .168 mmol, 1.0 eq), was coupled with naphthalene-1-boronic acid. The mixture was thoroughly purged with vacuum then argon. Workup and purification was followed according to the general procedure to afford 58 mg (72% yield) of **2.11a** as a white solid.

^{1}H NMR (500 MHz, $CDCl_3$) δ 8.55 (s, 1H), 7.89 (d, J = 8.1 Hz, 2H), 7.54 – 7.49 (m, 1H), 7.47 – 7.39 (m, 3H), 7.37 – 7.33 (m, 1H), 4.60 (s, 1H), 4.36 (s, 2H), 2.91 – 2.77 (m, 4H), 2.24 (s, 3H), 1.91 (t, J = 9.6 Hz, 2H), 1.51 (s, 9H).

^{13}C NMR (101 MHz, $CDCl_3$) δ 154.74, 151.39, 150.75, 149.20, 136.84, 133.85, 133.48, 130.70, 129.68, 128.29, 126.14, 125.90, 125.79, 125.11, 116.95, 111.05, 98.34, 79.97, 54.65, 43.79, 30.33, 28.48, 12.09.

MS (APCI) Calculated: $C_{27}H_{30}ClN_4O_2$ $[M+H]^+$ 477.2 **Found:** 477.2

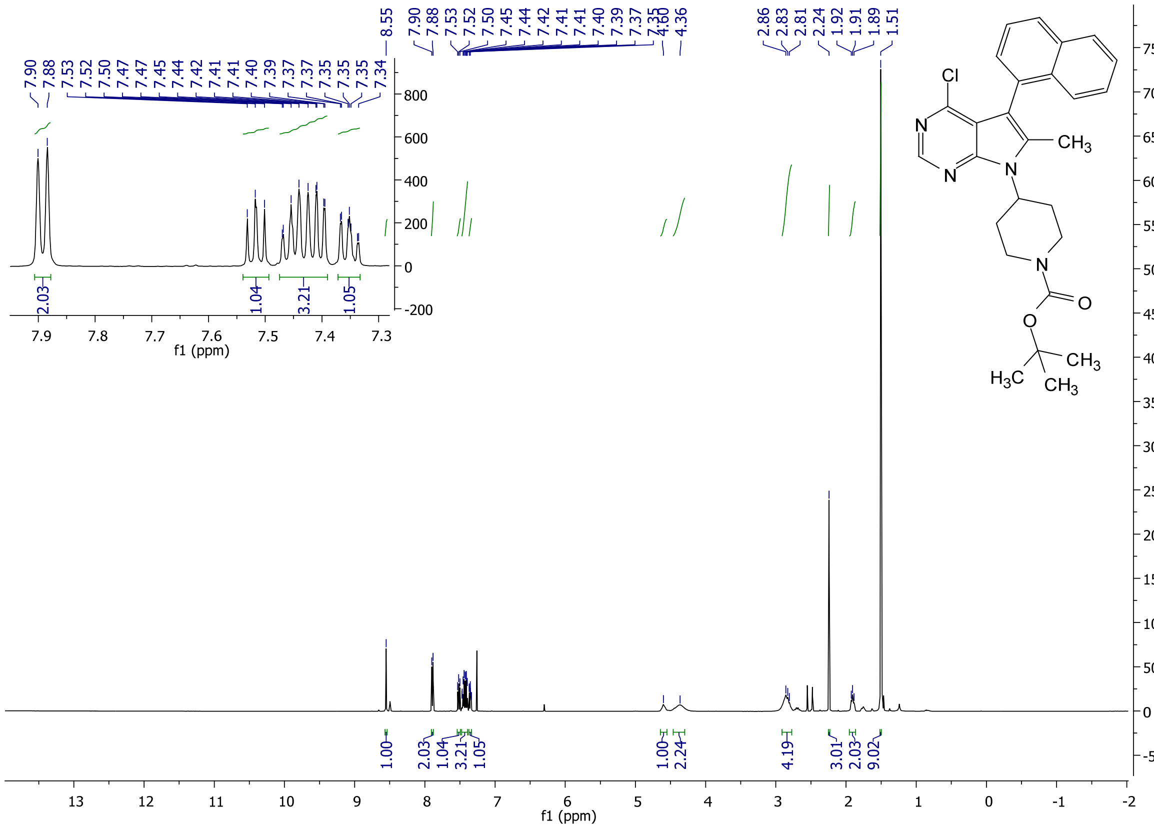

7.90
7.88
7.53
7.52
7.50
7.47
7.47
7.45
7.44
7.42
7.41
7.41
7.40
7.39
7.37
7.37
7.35
7.35
7.35
7.34
2.03
1.04
3.21
1.05
f1 (ppm)
8.55
7.90
7.88
7.53
7.52
7.50
7.45
7.44
7.42
7.41
7.41
7.40
7.39
7.37
7.35
4.60
4.36
2.86
2.83
2.81
2.24
1.92
1.91
1.89
1.51
1.00
2.03
1.04
3.21
1.05
1.00
2.24
4.19
3.01
2.03
9.02
f1 (ppm)
Cl
N
N
N
CH3
N
O
O
CH3
H3C
CH3

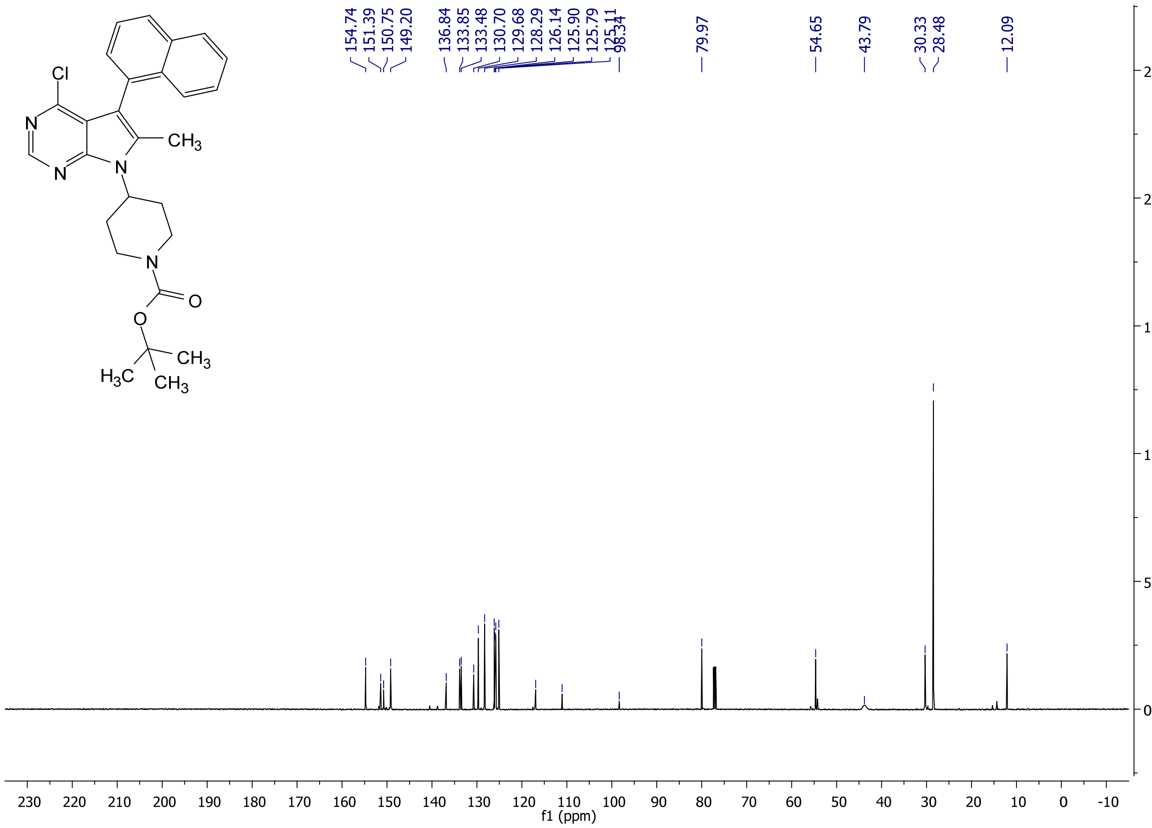

154.74
151.39
150.75
149.20
136.84
133.85
133.48
130.70
129.68
128.29
126.14
125.90
125.79
125.11
98.34
79.97
54.65
43.79
30.33
28.48
12.09
f1 (ppm)
Cl
N
N
N
CH3
N
O
O
CH3
H3C
CH3

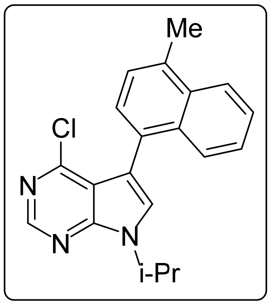

4-chloro-7-isopropyl-5-(4-methylnaphthalen-1-yl)-7*H*-pyrrolo[2,3-*d*]pyrimidine (2.12a):

Following the general procedure A: 4-chloro-5-iodo-7-isopropyl-7*H*-pyrrolo[2,3-*d*]pyrimidine (1.5 g, 4.66 mmol, 1.0 eq), was coupled with naphthalene-1-boronic acid. The mixture was thoroughly purged with vacuum then argon. Workup and purification was followed according to the general procedure to afford 1.23g (79% yield) of **2.12a** as a white solid.

^{1}H NMR (400 MHz, $CDCl_3$) δ 8.69 (s, 1H), 8.07 (d, J = 8.0 Hz, 1H), 7.69 (d, J = 8.4 Hz, 1H), 7.54 (ddd, J = 8.3, 6.8, 1.3 Hz, 1H), 7.44 – 7.39 (m, J = 6.8, 4.9, 1.3 Hz, 1H), 7.38 (t, J = 4.2 Hz, 3H), 5.31 – 5.21 (m, 1H), 2.77 (s, 3H), 1.65 – 1.59 (m, 6H).

^{13}C NMR (101 MHz, $CDCl_3$) δ 152.40, 150.63, 150.41, 134.76, 133.81, 132.62, 129.13, 128.85, 126.83, 125.95, 125.83, 125.77, 125.45, 124.43, 116.91, 114.59, 46.87, 22.86, 19.67.

MS (APCI) Calculated: $C_{20}H_{19}ClN_3$ $[M+H]^+$ 336.1 **Found:** 336.1

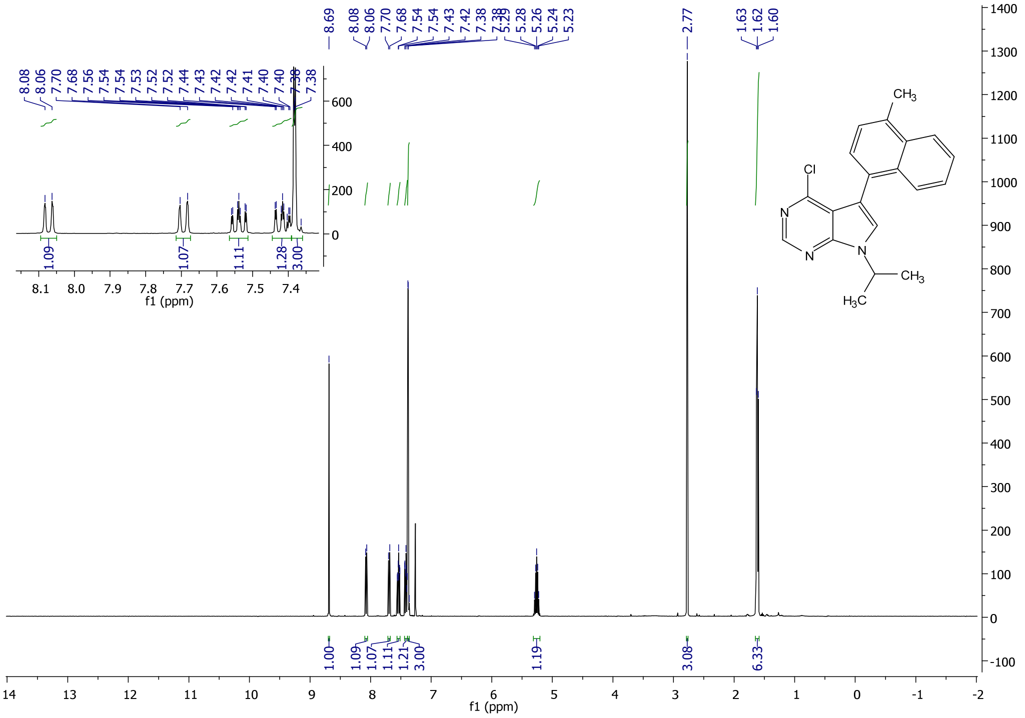
8.69
8.08
8.06
7.70
7.68
7.54
7.54
7.43
7.42
7.38
7.38
5.29
5.28
5.26
5.24
5.23
2.77
1.63
1.62
1.60
8.08
8.06
7.70
7.68
7.56
7.54
7.54
7.53
7.52
7.44
7.43
7.42
7.42
7.41
7.40
7.38
7.38
1.09
1.07
1.11
1.28
3.00
f1 (ppm)
1.00
1.09
1.07
1.11
1.21
3.00
1.19
3.08
6.33
f1 (ppm)
CH3
Cl
N
N
N
CH3
H3C

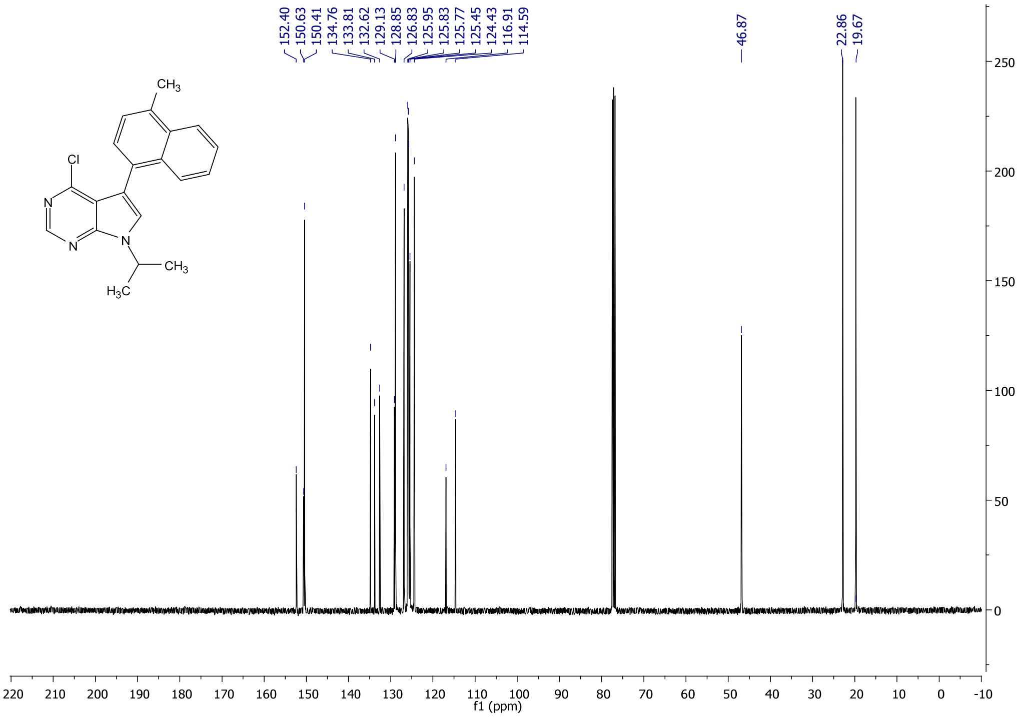
152.40
150.63
150.41
134.76
133.81
132.62
129.13
128.85
126.83
125.95
125.83
125.77
125.45
124.43
116.91
114.59
46.87
22.86
19.67
CH3
Cl
N
N
N
CH3
H3C
f1 (ppm)

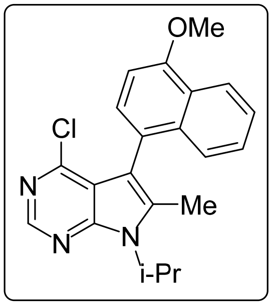

4-chloro-7-isopropyl-5-(4-methoxynaphthalen-1-yl)-6-methyl-7H-pyrrolo[2,3-d]pyrimidine (2.13a):

Following the general procedure A: 4-chloro-5-iodo-7-isopropyl-6-methyl-7*H*-pyrrolo[2,3-*d*]pyrimidine (125 mg, .372 mmol, 1.0 eq), was coupled with (4-methoxynaphthalen-1-yl)boronic acid. The mixture was thoroughly purged with vacuum then argon. Workup and purification was followed according to the general procedure to afford 96 mg (70% yield) of **2.13a** as a white solid.

^{1}H NMR (500 MHz, $CDCl_3$) δ 8.58 (s, 1H), 8.35 (d, J = 8.4 Hz, 1H), 7.48 (td, J = 8.6, 4.4 Hz, 1H), 7.39 (d, J = 3.7 Hz, 2H), 7.33 (d, J = 7.8 Hz, 1H), 6.89 (d, J = 7.8 Hz, 1H), 5.04 – 4.94 (m, 1H), 4.07 (s, 3H), 2.25 (s, 3H), 1.77 (t, J = 7.2 Hz, 6H).

^{13}C NMR (101 MHz, $CDCl_3$) δ 155.41, 151.17, 150.50, 148.96, 137.24, 134.78, 129.64, 126.56, 125.79, 125.51, 125.03, 122.83, 122.17, 117.10, 110.71, 103.17, 55.53, 48.05, 21.48, 11.93.

MS (APCI) Calculated: $C_{21}H_{21}ClN_3O$ $[M+H]^+$ 366.1 **Found:** 366.1

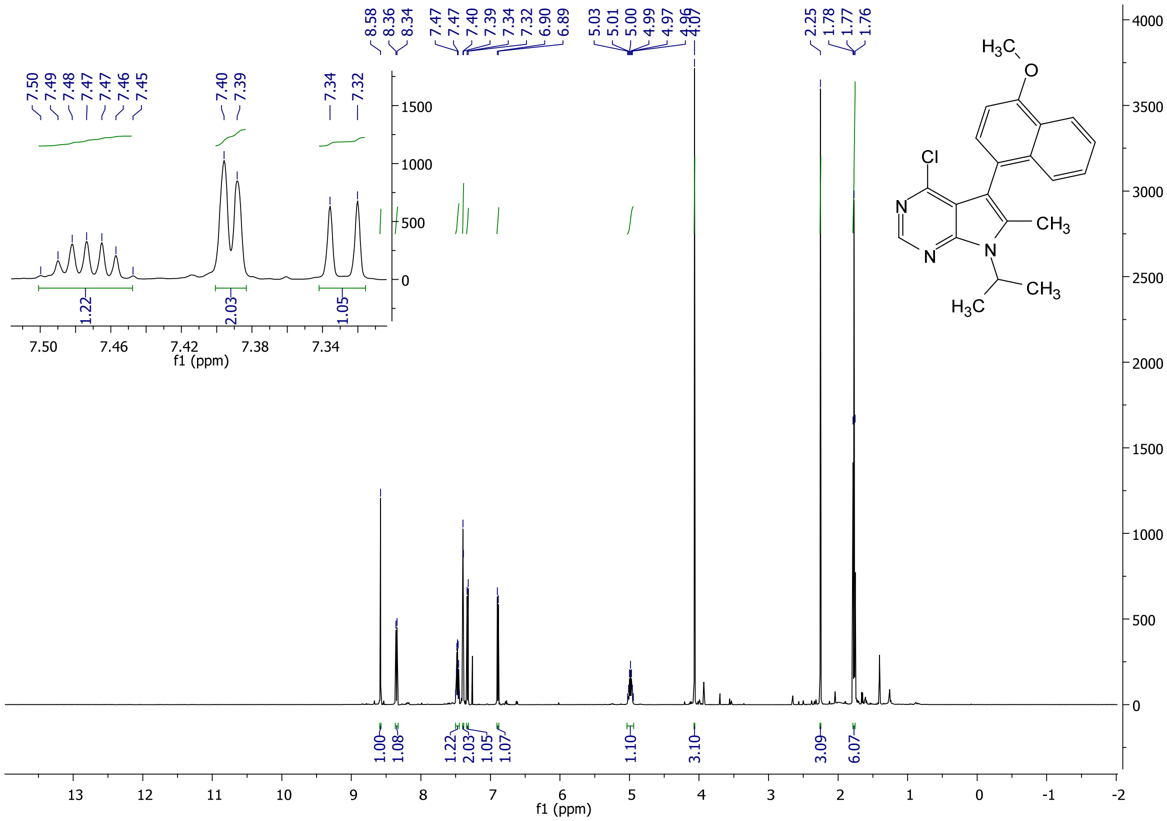

8.58
8.36
8.34
7.47
7.47
7.40
7.39
7.34
7.32
6.90
6.89
5.03
5.01
5.00
4.99
4.97
4.96
4.07
2.25
1.78
1.77
1.76
7.50
7.49
7.48
7.47
7.47
7.46
7.45
7.40
7.39
7.34
7.32
1.22
2.03
1.05
1.00
1.08
1.22
2.03
1.05
1.07
1.10
3.10
3.09
6.07
f1 (ppm)
Cl
N
N
N
CH3
H3C
CH3
H3C
O

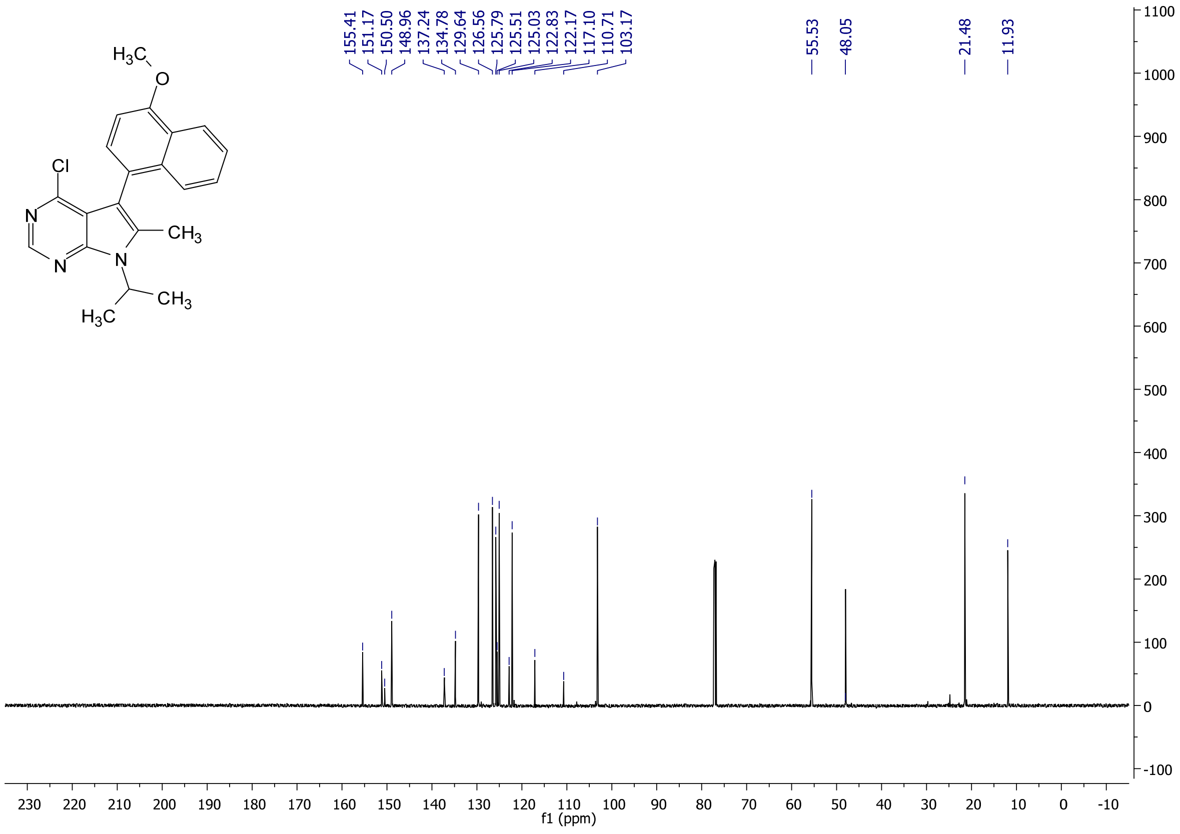

155.41
151.17
150.50
148.96
137.24
134.78
129.64
126.56
125.79
125.51
125.03
122.83
122.17
117.10
110.71
103.17
55.53
48.05
21.48
11.93
f1 (ppm)
H3C
O
Cl
N
N
N
CH3
H3C
CH3

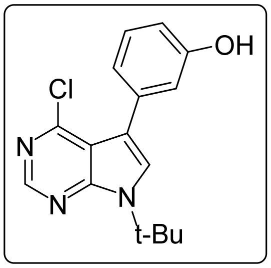

3-(7-(*tert*-butyl)-4-chloro-7*H*-pyrrolo[2,3-d]pyrimidin-5-yl)phenol (2.15a):

Following the general procedure: 7-(*tert*-butyl)-4-chloro-5-iodo-7*H*-pyrrolo[2,3-*d*]pyrimidine (450 mg, 1.34 mmol, 1.0 eq), was coupled with (3-hydroxyphenyl)boronic acid. The mixture was thoroughly purged with vacuum then argon. Workup and purification was followed according to the general procedure to afford 313 mg (77% yield) of **2.15a** as a white solid.

^{1}H NMR (500 MHz, $CDCl_3$) δ 8.64 (s, 1H), 7.39 (s, 1H), 7.29 - 7.26 (m, 1H), 7.04 - 7.02 (m, 2H), 6.92 – 6.88 (m, 1H), 1.82 (s, 9H)

^{13}C NMR (101 MHz, $CDCl_3$) δ 155.78, 151.67, 151.44, 148.84, 134.54, 129.28, 126.59, 122.48, 117.75, 116.11, 115.59, 114.66, 58.30, 29.38

MS (APCI) Calculated: $C_{16}H_{17}ClN_3O$ $[M+H]^+$ 302.1 **Found:** 302.0 m/z

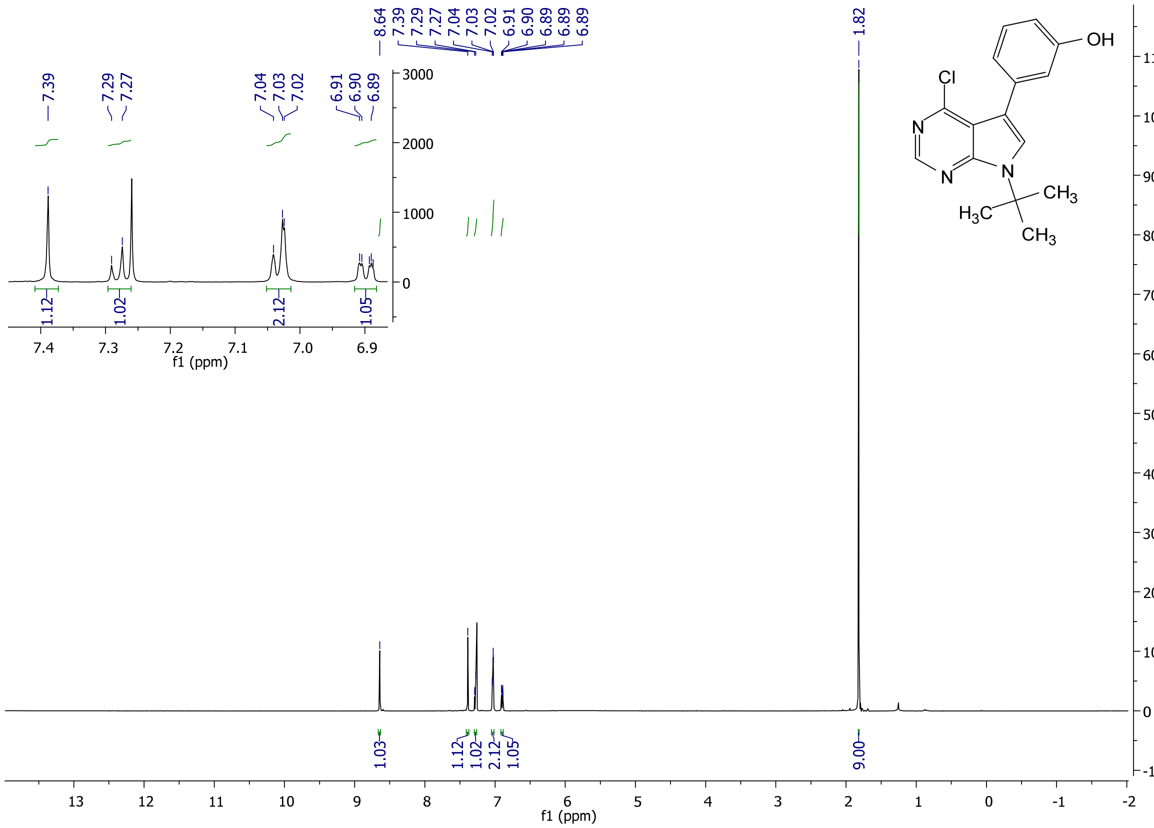
8.64
7.39
7.29
7.27
7.04
7.03
7.02
6.91
6.90
6.89
6.89
6.89
1.82
1.03
1.12
1.02
2.12
1.05
9.00
f1 (ppm)
Cl
OH
N
N
N
H_3C
CH_3
CH_3

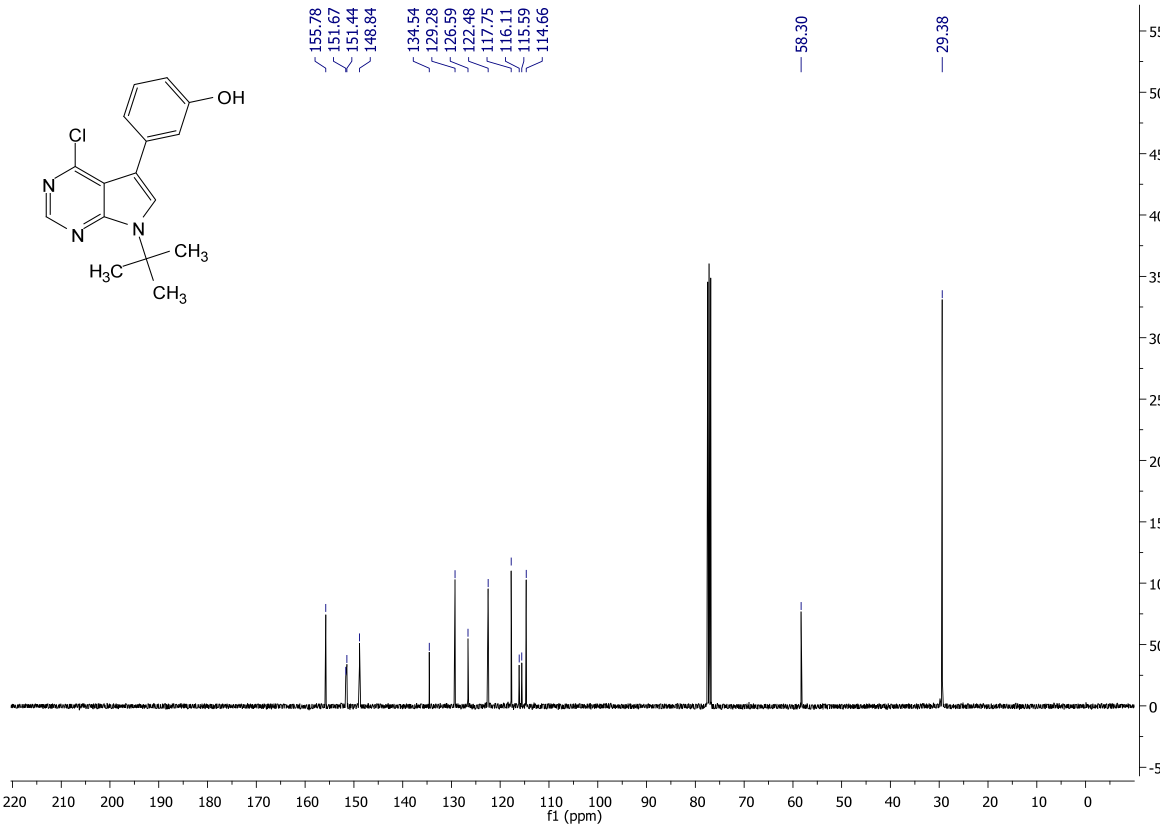
155.78
151.67
151.44
148.84
134.54
129.28
126.59
122.48
117.75
116.11
115.59
114.66
58.30
29.38
f1 (ppm)
Cl
OH
N
N
N
H_3C
CH_3
CH_3

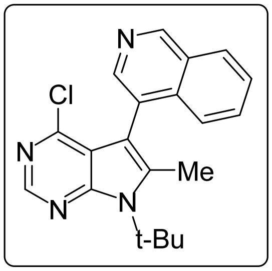

4-(7-(tert-butyl)-4-chloro-6-methyl-7H-pyrrolo[2,3-d]pyrimidin-5-yl)isoquinoline (2.16a): Following the general procedure: 7-(tert-butyl)-4-chloro-5-iodo-6-methyl-7H-pyrrolo[2,3-d]pyrimidine (120 mg, .343 mmol, 1.0 eq), was coupled with isoquinolin-4-ylboronic acid. The mixture was thoroughly purged with vacuum then argon. Workup and purification were followed according to the general procedure to afford 41 mg (34% yield) of **2.16a** as a white solid.

^{1}H NMR (400 MHz, $CDCl_3$) δ δ 9.31 (s, 1H), 8.59 (s, 1H), 8.45 (s, 1H), 8.08 – 8.02 (m, 1H), 7.64 – 7.60 (m, 2H), 7.46 – 7.41 (m, 1H), 2.39 (s, 3H), 2.00 (s, 9H).

^{13}C NMR (101 MHz, $CDCl_3$) δ 152.89, 152.41, 150.48, 148.52, 145.44, 139.26, 136.70, 130.67, 128.12, 127.86, 127.27, 125.36, 124.98, 117.24, 108.67, 61.82, 31.09, 16.23.

MS (APCI) Calculated: $C_{20}H_{20}ClN_4$ $[M+H]^+$ 351.1 **Found:** 351.1 m/z

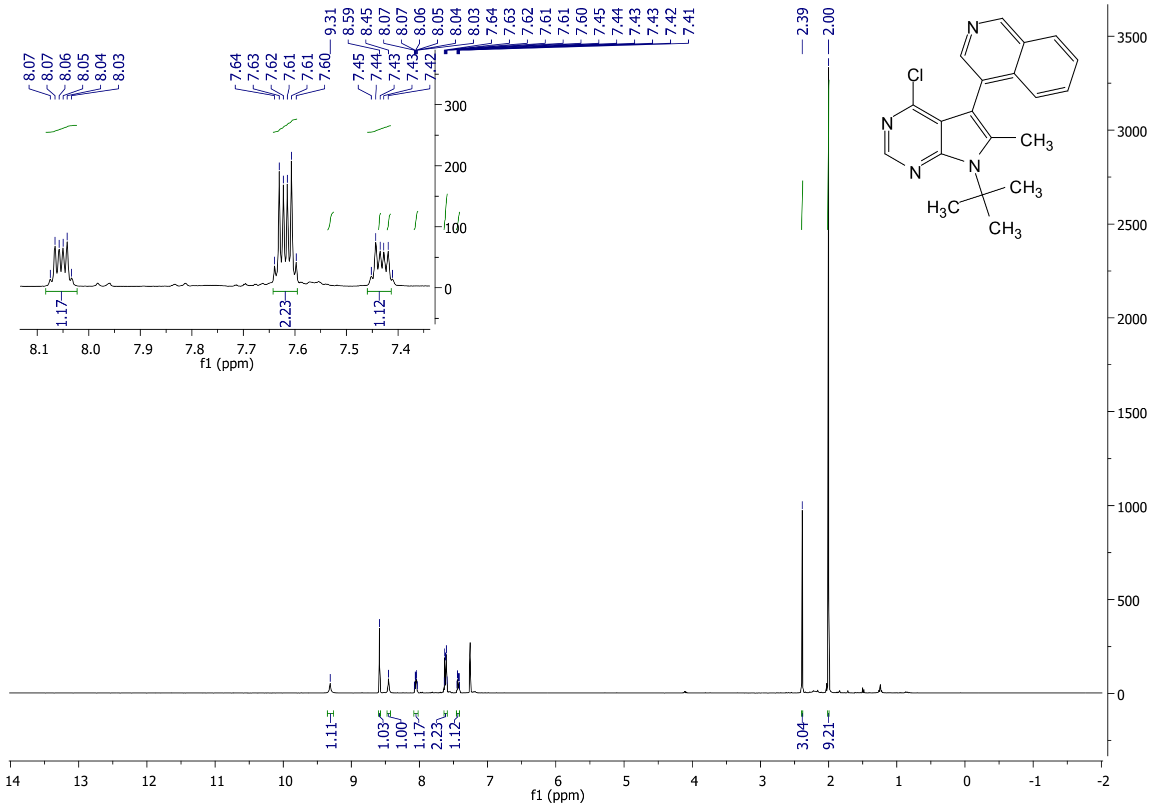
8.07
8.07
8.06
8.05
8.04
8.03
7.64
7.63
7.62
7.61
7.61
7.60
7.45
7.44
7.43
7.43
7.42
1.17
2.23
1.12
8.1
8.0
7.9
7.8
7.7
7.6
7.5
7.4
f1 (ppm)
300
200
100
0
9.31
8.59
8.45
8.07
8.07
8.06
8.05
8.04
8.03
7.64
7.63
7.62
7.61
7.61
7.60
7.45
7.44
7.43
7.43
7.42
7.41
2.39
2.00
N
Cl
N
N
N
CH3
H3C
CH3
CH3
1.11
1.03
1.00
1.17
2.23
1.12
3.04
9.21
3500
3000
2500
2000
1500
1000
500
0
14
13
12
11
10
9
8
7
6
5
4
3
2
1
0
-1
-2
f1 (ppm)

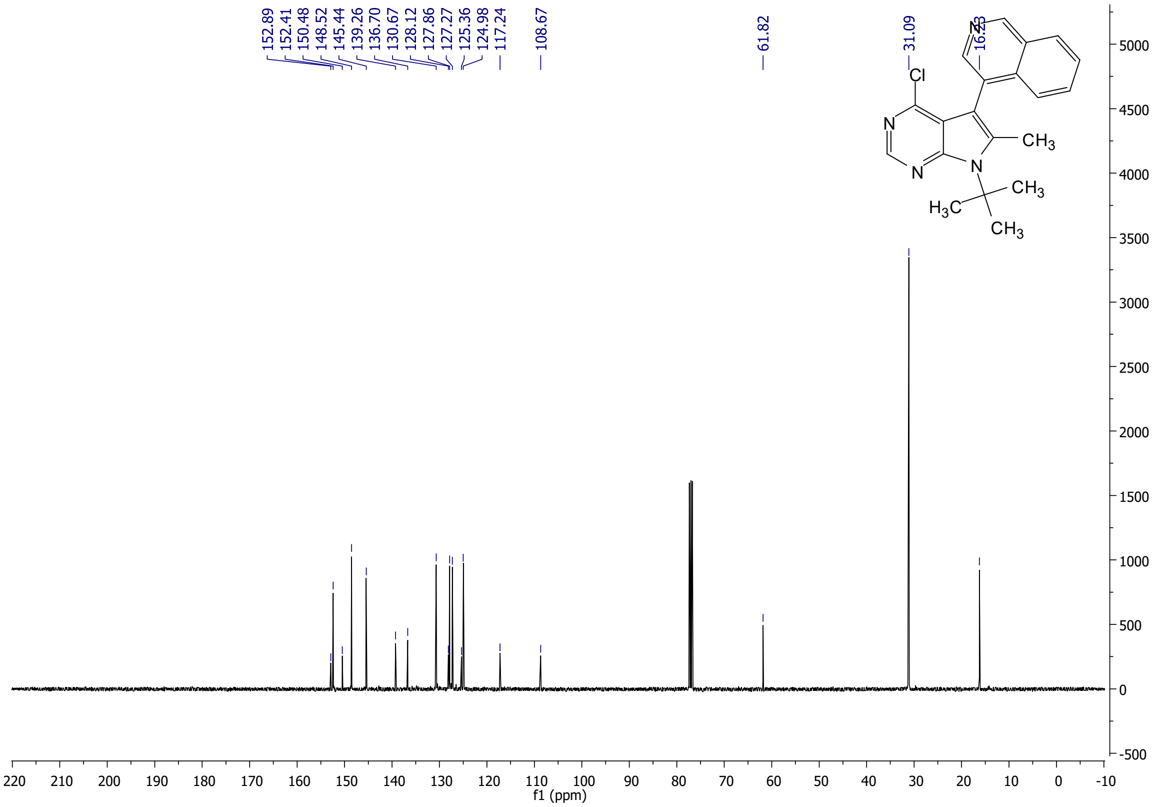
152.89
152.41
150.48
148.52
145.44
139.26
136.70
130.67
128.12
127.86
127.27
125.36
124.98
117.24
108.67
61.82
31.09
16.23
N
Cl
N
N
N
CH3
H3C
CH3
CH3
5000
4500
4000
3500
3000
2500
2000
1500
1000
500
0
-500
220
210
200
190
180
170
160
150
140
130
120
110
100
90
80
70
60
50
40
30
20
10
0
-10
f1 (ppm)

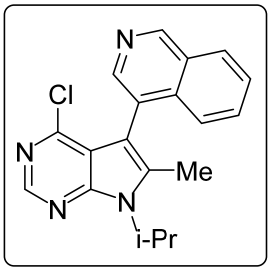

4-(4-chloro-7-isopropyl-6-methyl-7*H*-pyrrolo[2,3-*d*]pyrimidin-5-yl)isoquinoline (2.17a): Following the general procedure: 4-chloro-5-iodo-7-isopropyl-6-methyl-7*H*-pyrrolo[2,3-*d*]pyrimidine (100 mg, .298 mmol, 1.0 eq), was coupled with isoquinolin-4-ylboronic acid. The mixture was thoroughly purged with vacuum then argon. Workup and purification were followed according to the general procedure to afford 64 mg (49% yield) of **2.17a** as a yellow-white solid.

^{1}H NMR (500 MHz, $CDCl_3$) δ 9.32 (s, 1H), 8.59 (s, 1H), 8.47 (s, 1H), 8.08 – 8.04 (m, 1H), 7.65 – 7.61 (m, 2H), 7.52 – 7.47 (m, 1H), 4.99 (dq, J = 13.8, 7.0 Hz, 1H), 2.29 (s, 3H), 1.79 – 1.76 (m, 6H).

^{13}C NMR (101 MHz, $CDCl_3$) δ 152.31, 151.53, 150.65, 149.54, 145.05, 137.85, 136.82, 130.92, 128.05, 127.51, 125.19, 117.12, 106.84, 48.39, 21.55, 12.07.

MS (APCI) Calculated: $C_{19}H_{18}ClN_4$ $[M+H]^+$ 337.1 **Found:** 337.2 m/z

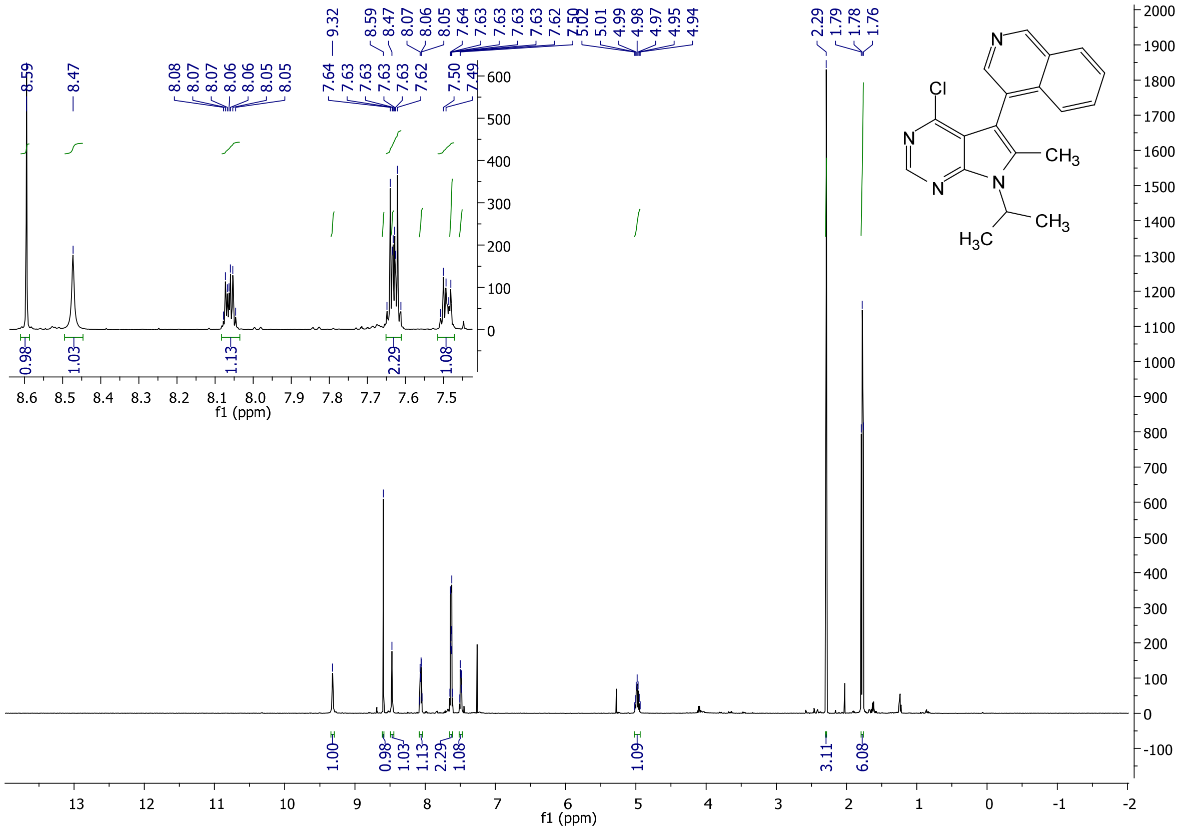

9.32
8.59
8.47
8.07
8.06
8.05
7.64
7.63
7.63
7.63
7.63
7.62
7.50
5.02
5.01
4.99
4.98
4.97
4.95
4.94
2.29
1.79
1.78
1.76
8.59
8.47
8.08
8.07
8.07
8.06
8.06
8.05
8.05
7.64
7.63
7.63
7.63
7.63
7.62
7.50
7.49
0.98
1.03
1.13
2.29
1.08
f1 (ppm)
1.00
0.98
1.03
1.13
2.29
1.08
1.09
3.11
6.08
f1 (ppm)
N
Cl
N
N
N
CH3
CH3
H3C

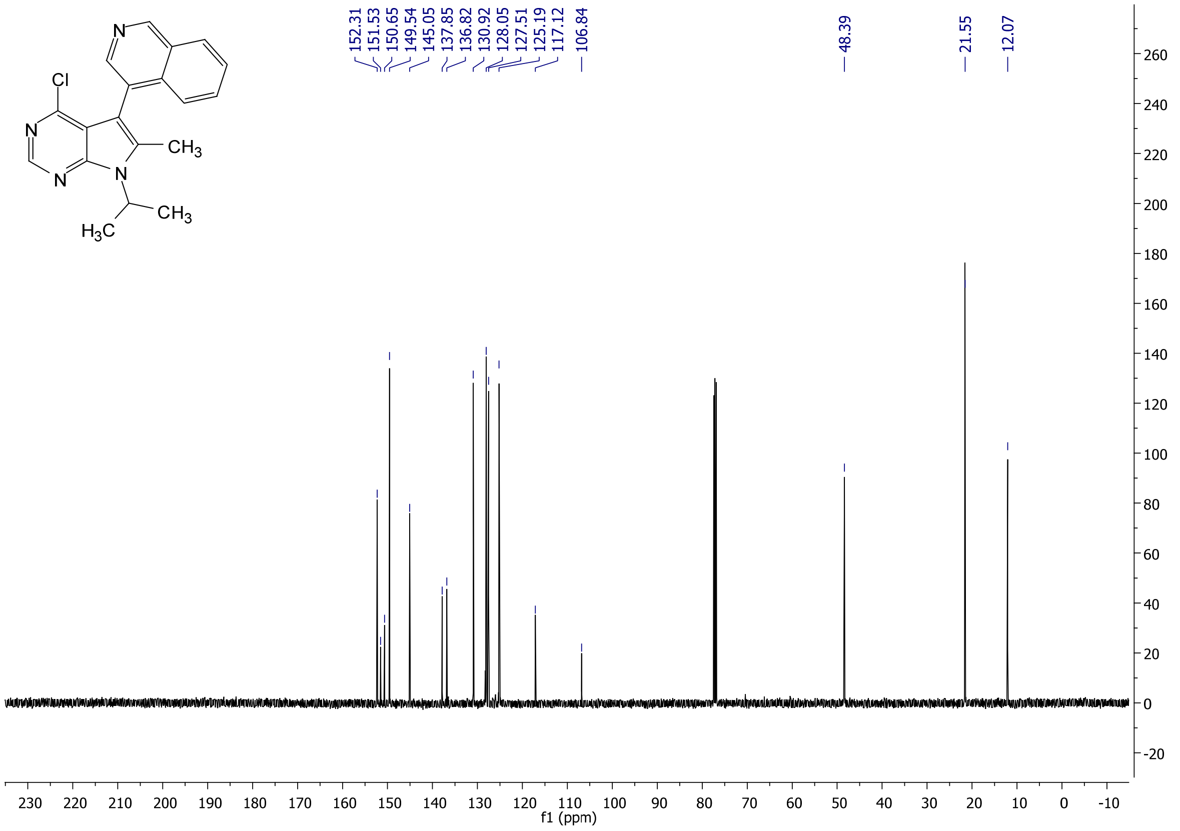

152.31
151.53
150.65
149.54
145.05
137.85
136.82
130.92
128.05
127.51
125.19
117.12
106.84
48.39
21.55
12.07
f1 (ppm)
N
Cl
N
N
N
CH3
CH3
H3C

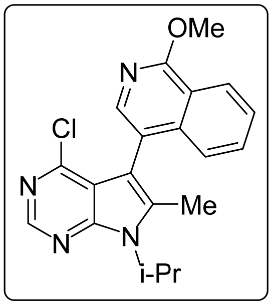

4-(4-chloro-7-isopropyl-6-methyl-7H-pyrrolo[2,3-d]pyrimidin-5-yl)-1-methoxyisoquinoline (2.18a):

Following the general procedure A: 4-chloro-5-iodo-7-isopropyl-6-methyl-7*H*-pyrrolo[2,3-*d*]pyrimidine (120 mg, .358 mmol, 1.0 eq), was coupled with (1-methoxyisoquinolin-4-yl)boronic acid. The mixture was thoroughly purged with vacuum then argon. Workup and purification was followed according to the general procedure to afford 82 mg (63% yield) of **2.18a** as a yellow-white solid.

^{1}**H NMR** (500 MHz, $CDCl_3$) δ 8.57 (s, 1H), 8.33 – 8.30 (m, 1H), 7.93 (s, 1H), 7.59 – 7.51 (m, 2H), 7.33 (dd, J = 7.4, 1.3 Hz, 1H), 4.97 (m, 1H), 4.19 (s, 3H), 2.29 (s, 3H), 1.76 (dd, J = 6.9, 5.2 Hz, 6H.

^{13}**C NMR** (101 MHz, $CDCl_3$) δ 160.93, 151.36, 150.55, 149.23, 141.77, 138.58, 137.82, 130.58, 126.55, 124.87, 124.30, 119.21, 118.71, 117.20, 107.18, 53.80, 48.15, 21.45, 11.85.

MS (APCI) Calculated: $C_{20}H_{20}ClN_4O$ $[M+H]^+$ 367.1 **Found:** 367.1

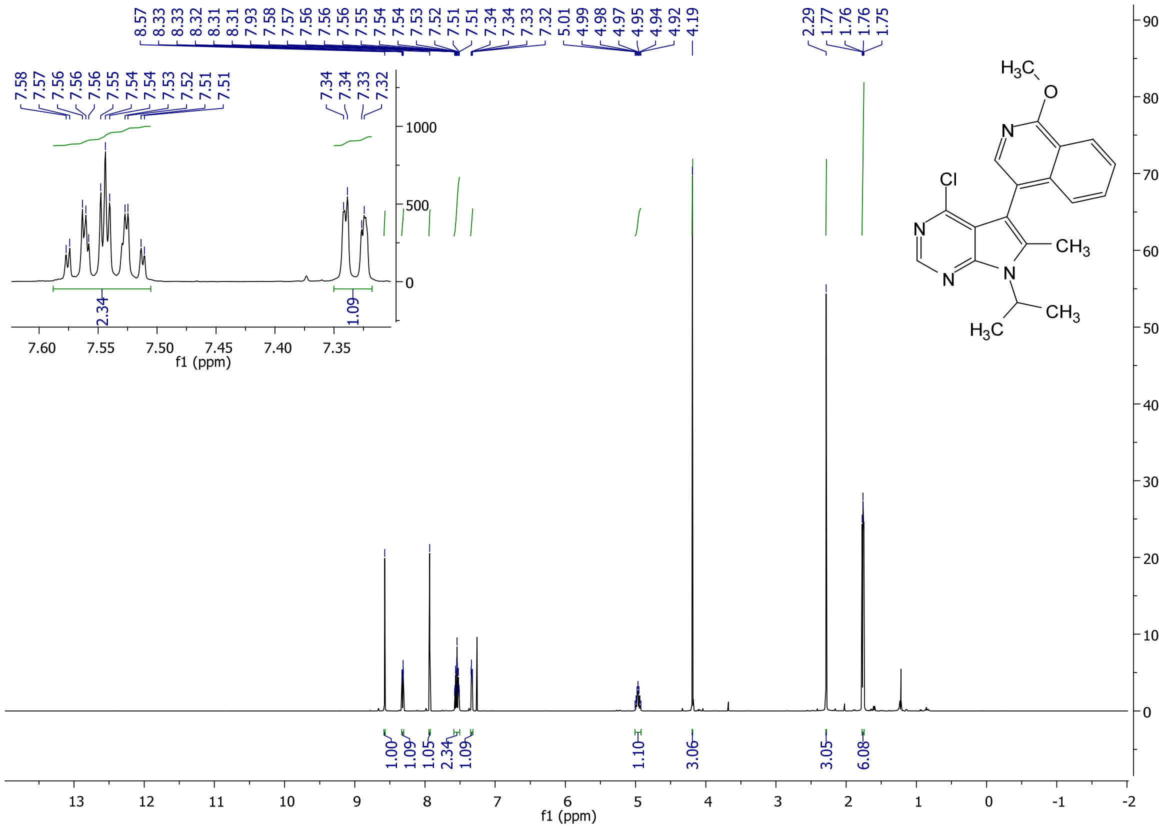

8.57
8.33
8.33
8.32
8.31
8.31
7.93
7.58
7.57
7.56
7.56
7.56
7.55
7.54
7.54
7.53
7.52
7.51
7.51
7.34
7.34
7.33
7.32
5.01
4.99
4.98
4.97
4.95
4.94
4.92
4.19
2.29
1.77
1.76
1.76
1.75
1.00
1.09
1.05
2.34
1.09
1.10
3.06
3.05
6.08
f1 (ppm)
H3C
O
N
Cl
N
N
N
CH3
CH3
H3C

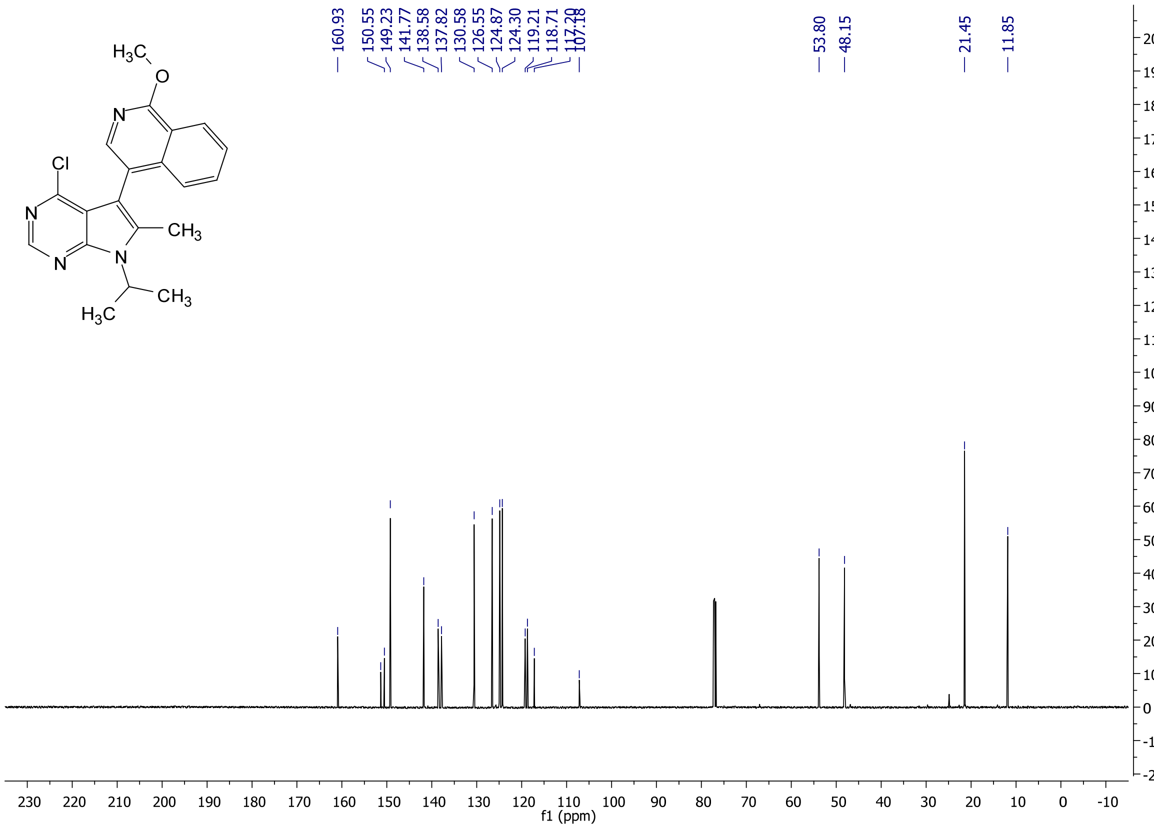

160.93
150.55
149.23
141.77
138.58
137.82
130.58
126.55
124.87
124.30
119.21
118.71
117.20
107.18
53.80
48.15
21.45
11.85
f1 (ppm)
H3C
O
N
Cl
N
N
N
CH3
CH3
H3C

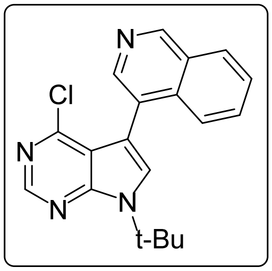

4-(7-(*tert*-butyl)-4-chloro-7*H*-pyrrolo[2,3-*d*]pyrimidin-5-yl)isoquinoline (2.20a):

Following the general procedure: 7-(*tert*-butyl)-4-chloro-5-iodo-7*H*-pyrrolo[2,3-*d*]pyrimidine (970 mg, 2.88 mmol, 1.0 eq), was coupled with isoquinolin-4-ylboronic acid. The mixture was thoroughly purged with vacuum then argon. Workup and purification were followed according to the general procedure to afford 471 mg (49% yield) of **2.20a** as an orange solid.

^{1}H NMR (400 MHz, $CDCl_3$) δ 9.32 (s, 1H), 8.69 (s, 1H), 8.52 (s, 1H), 8.10 – 8.06 (m, 1H), 7.71 – 7.64 (m, 3H), 7.49 (s, 1H), 1.88 (s, 9H)

^{13}C NMR (101 MHz, $CDCl_3$) δ 152.38, 151.77, 151.53, 149.91, 143.13, 136.86, 131.27, 128.10, 128.06, 127.81, 127.37, 125.81, 125.52, 117.91, 108.64, 58.48, 29.41

MS (APCI) Calculated: $C_{19}H_{18}ClN_4$ $[M+H]^+$ 337.1 **Found:** 337.2 m/z

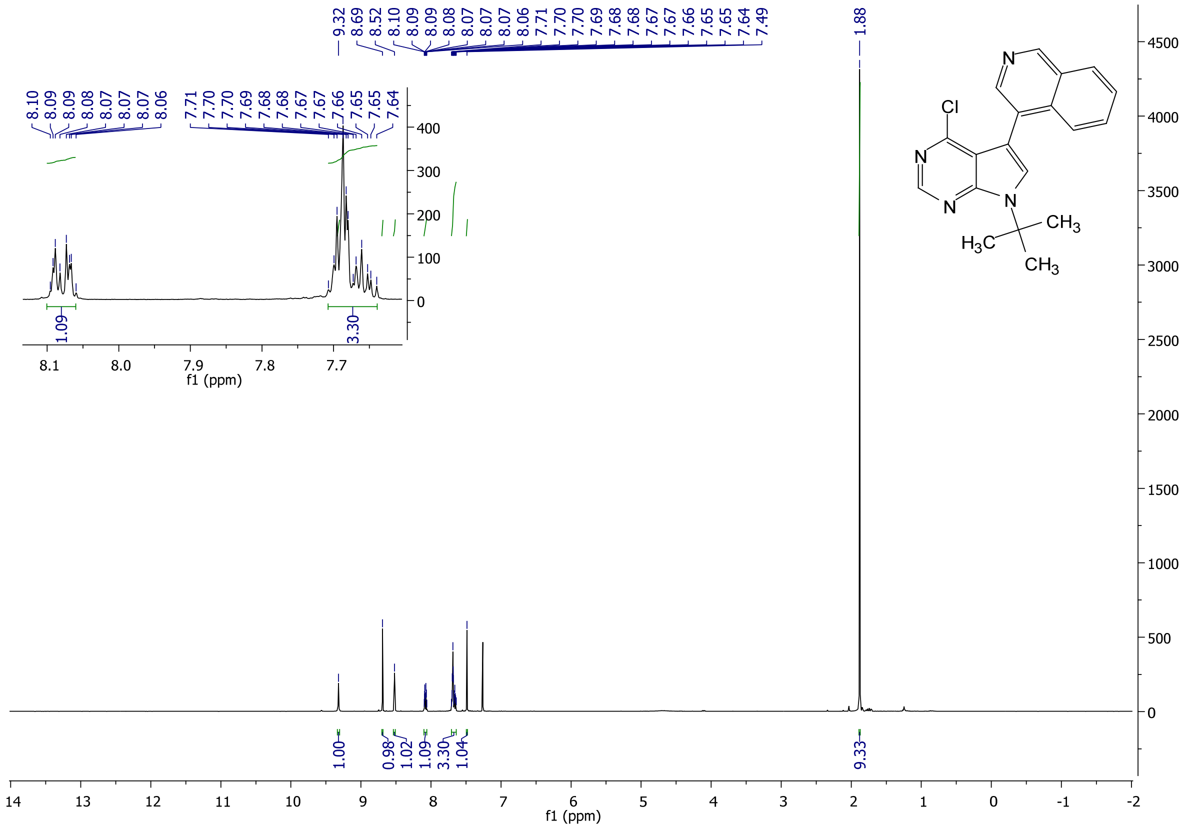

9.32
8.69
8.52
8.10
8.09
8.09
8.08
8.07
8.07
8.07
8.06
7.71
7.70
7.70
7.69
7.68
7.68
7.67
7.66
7.65
7.65
7.64
7.49
1.88
8.10
8.09
8.09
8.08
8.07
8.07
8.07
8.06
7.71
7.70
7.70
7.69
7.68
7.68
7.67
7.67
7.66
7.65
7.65
7.64
400
300
200
100
0
1.09
3.30
8.1
8.0
7.9
7.8
7.7
f1 (ppm)
Cl
N
N
N
N
H3C
CH3
CH3
4500
4000
3500
3000
2500
2000
1500
1000
500
0
1.00
0.98
1.02
1.09
3.30
1.04
9.33
14
13
12
11
10
9
8
7
6
5
4
3
2
1
0
-1
-2
f1 (ppm)

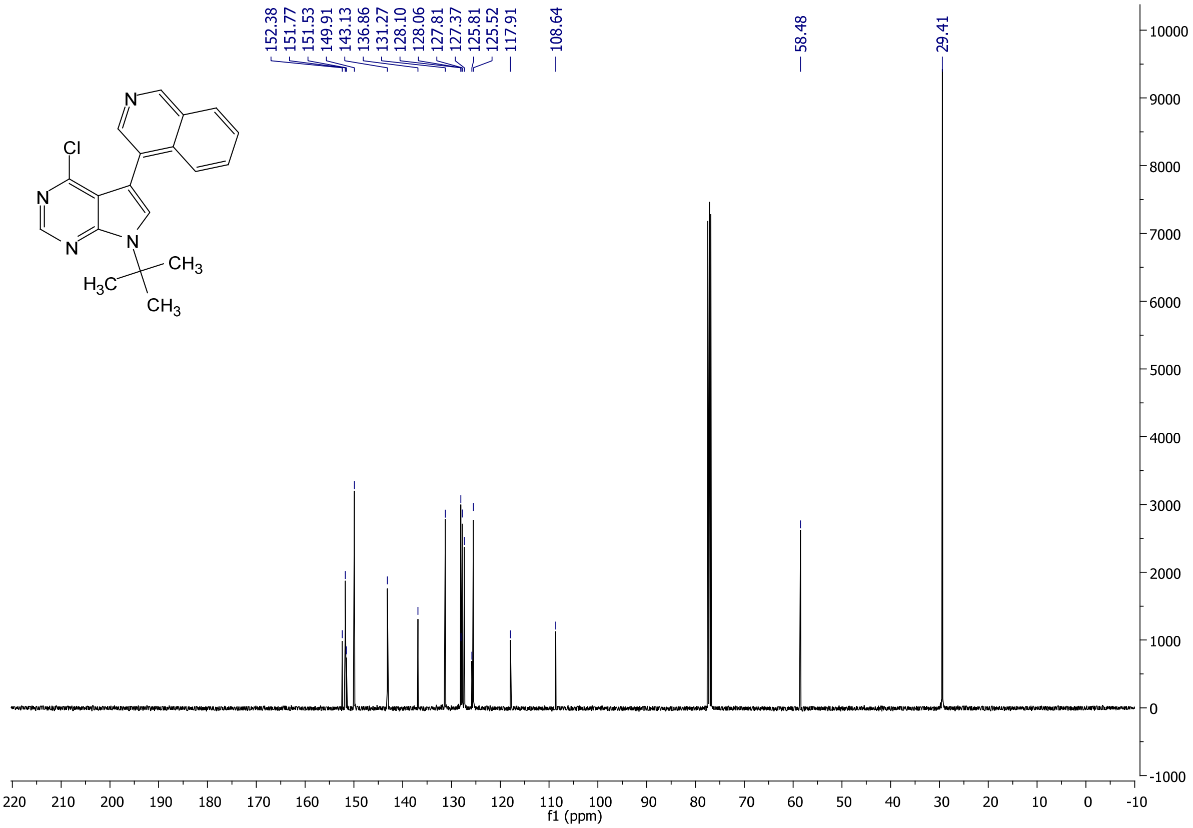

152.38
151.77
151.53
149.91
143.13
136.86
131.27
128.10
128.06
127.81
127.37
125.81
125.52
117.91
108.64
58.48
29.41
Cl
N
N
N
N
H3C
CH3
CH3
10000
9000
8000
7000
6000
5000
4000
3000
2000
1000
0
-1000
220
210
200
190
180
170
160
150
140
130
120
110
100
90
80
70
60
50
40
30
20
10
0
-10
f1 (ppm)

General procedure of the amination of pyrrolopyrimidines (2.1b – 2.20b):

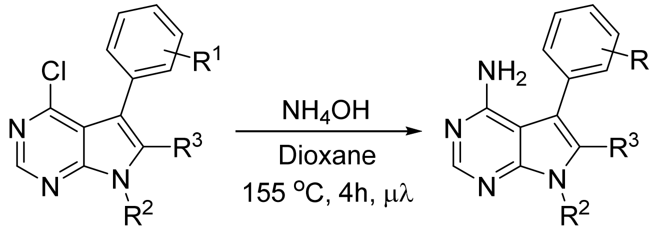

2.1a – 2.20a was dissolved in a 2:1 mixture of dioxane and 28% ammonium hydroxide (35 eq.) and placed in a microwave reaction vessel equipped with a stir bar. The vessel was placed in Monowave 400 by Anton Paar and heated to 155ºC over 20min, and then held at 155ºC for 3 hours and 30 minutes. Upon cooling to room temperature the precipitate was filtered and washed with DI water and a mixture of 9:1 hexanes:ethyl acetate. The solids were dried, yielding **2.1b – 2.20b** in 42-88% yield.

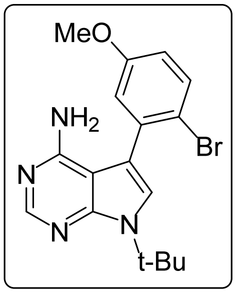

5-(2-bromo-5-methoxyphenyl)-7-(*tert*-butyl)-7*H*-pyrrolo[2,3-*d*]pyrimidin-4-amine (2.1b):

Following the general procedure: **2.1a** (350 mg, .887 mmol, 1 eq.) was dissolved in a 2:1 mixture of dioxane and 28% ammonium hydroxide (35 eq.). The reaction proceeded according to the general procedure. Workup and purification was followed according to the general procedure to afford 243 mg of **2.1b** (73% yield) as a white crystalline solid.

^{1}H NMR (400 MHz, $CDCl_3$) δ 8.30 (s, 1H), 7.57 (d, J = 8.8 Hz, 1H), 7.13 (s, 1H), 6.95 (d, J = 3.1 Hz, 1H), 6.80 (dd, J = 8.8, 3.1 Hz, 1H), 5.00 (s, 2H), 3.81 (s, 3H), 1.80 (s, 9H).

^{13}C NMR (101 MHz, $CDCl_3$) δ 158.82, 156.55, 150.15, 150.07, 136.45, 133.84, 122.04, 117.49, 115.32, 115.04, 112.58, 103.36, 57.16, 55.56, 29.38.

MS (APCI) Calculated: $C_{17}H_{20}BrN_4O$ $[M+H]^+$ 375.1 **Found**: 375.1

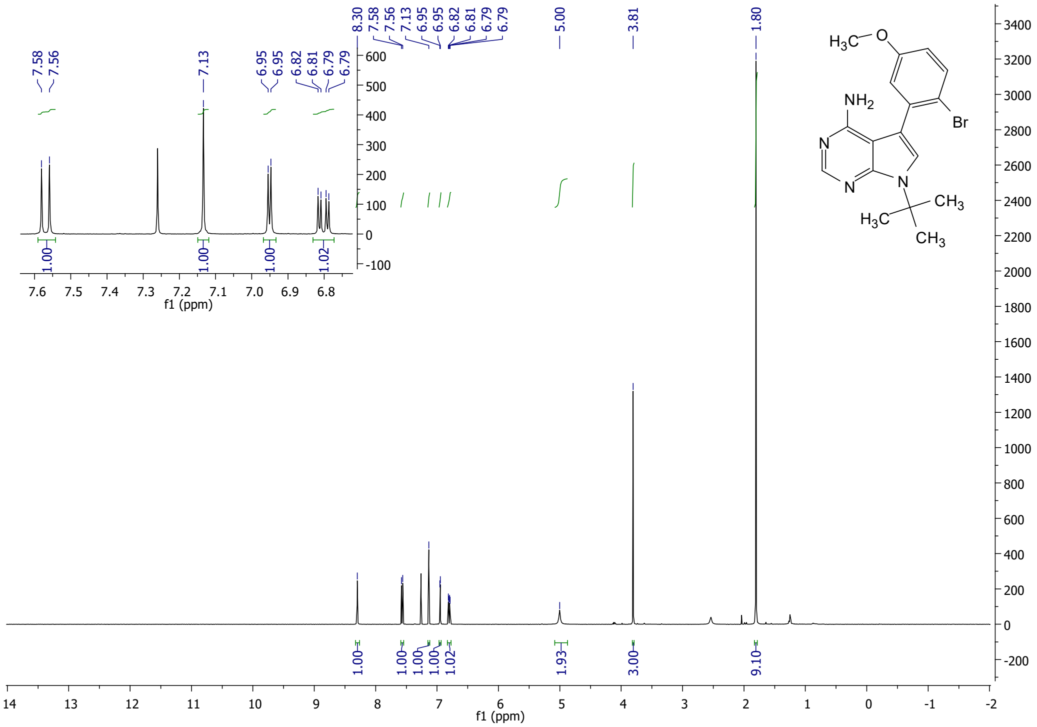

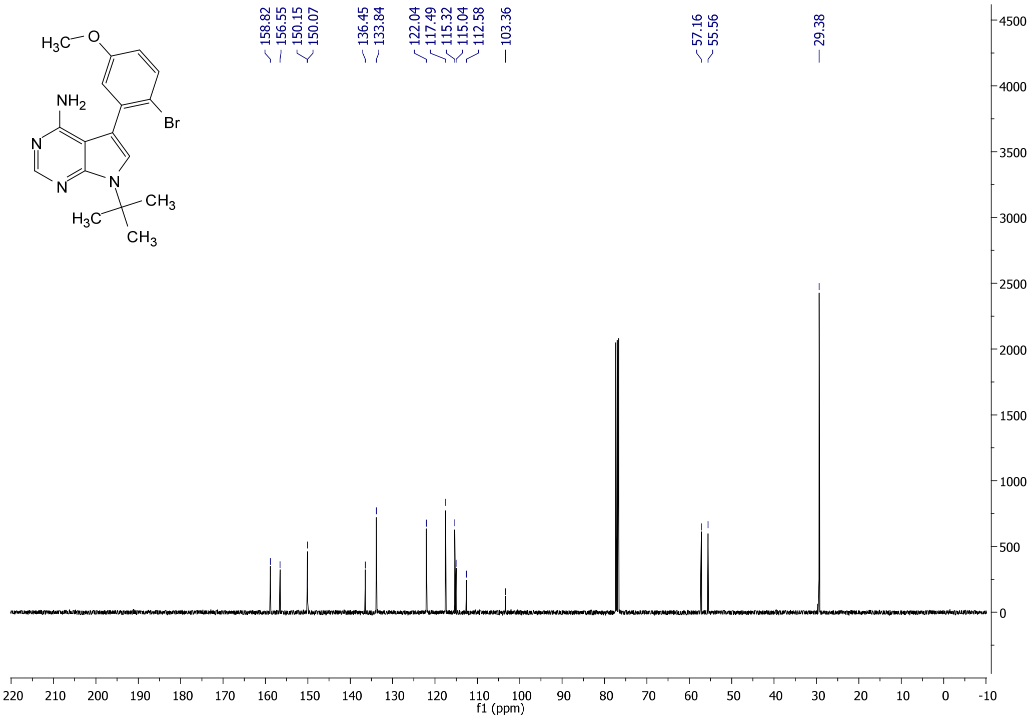

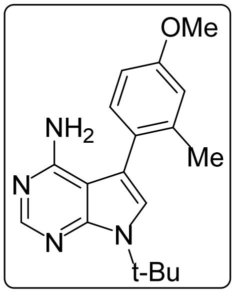

7-(*tert*-butyl)-5-(4-methoxy-2-methylphenyl)-7*H*-pyrrolo[2,3-*d*]pyrimidin-4-amine: Insertcompound (2.2b):

2.2a (695 mg, 2.11 mmol, 1.0 eq.) was dissolved in a 2:1 mixture of dioxane and 28% ammonium hydroxide (35 eq.). The reaction proceeded according to the general procedure. Workup and purification was followed according to the general procedure to afford 512 mg of **2.2b** (78% yield) as a white crystalline solid.

^{1}H NMR (500 MHz, $CDCl_3$) δ 8.27 (s, 1H), 7.22 (d, J = 8.3 Hz, 1H), 6.95 (s, 1H), 6.86 (d, J = 2.7 Hz, 1H), 6.79 (dd, J = 8.3, 2.7 Hz, 1H), 4.96 (s, 2H), 3.84 (s, 3H), 2.21 (s, 3H), 1.80 (s, 9H)

^{13}C NMR (101 MHz, $CDCl_3$) δ 159.48, 156.74, 150.08, 149.59, 139.26, 132.17, 126.33, 120.94, 116.02, 112.89, 111.35, 104.03, 57.12, 55.43, 29.60, 20.80.

MS (APCI) Calculated: $C_{18}H_{23}N_4O$ $[M+H]^+$ 311.2 **Found**: 311.2

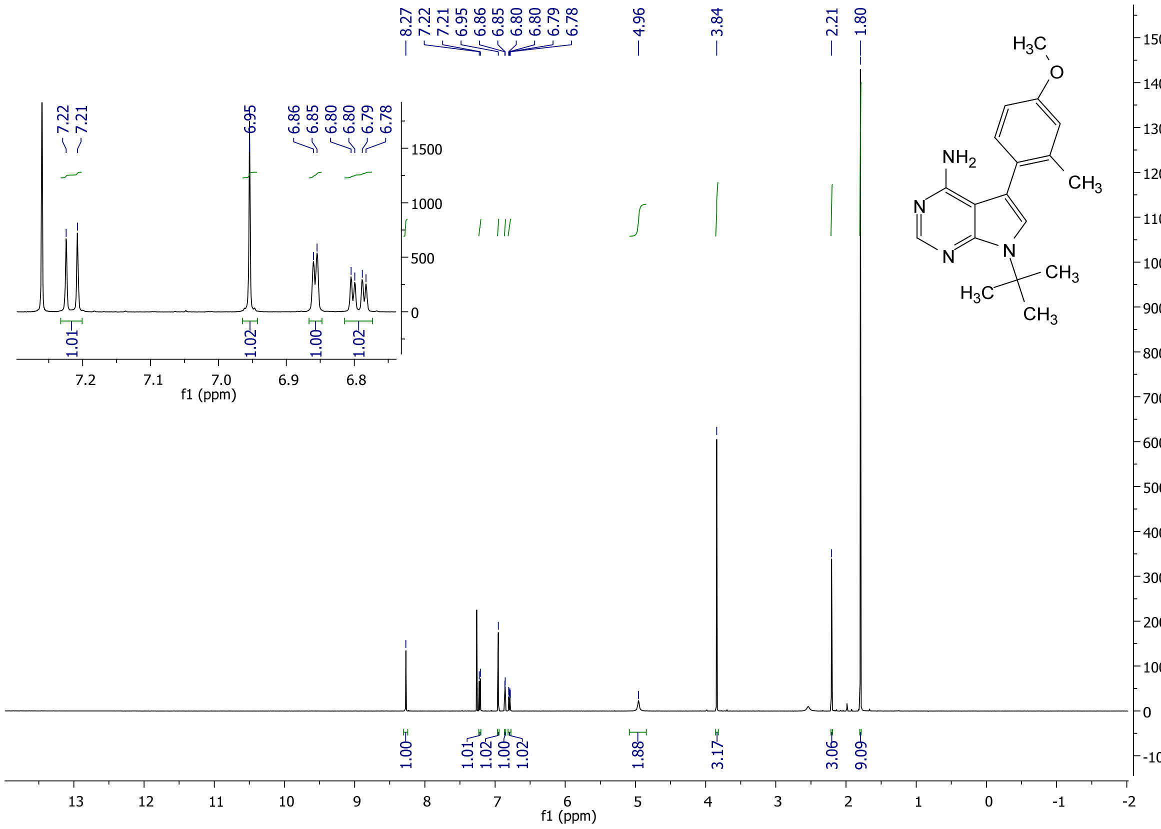

8.27
7.22
7.21
6.95
6.86
6.85
6.80
6.80
6.79
6.78
4.96
3.84
2.21
1.80
1.00
1.01
1.02
1.00
1.02
1.88
3.17
3.06
9.09
f1 (ppm)
NH$_2$
N
N
N
H$_3$C
O
CH$_3$
H$_3$C
CH$_3$
CH$_3$

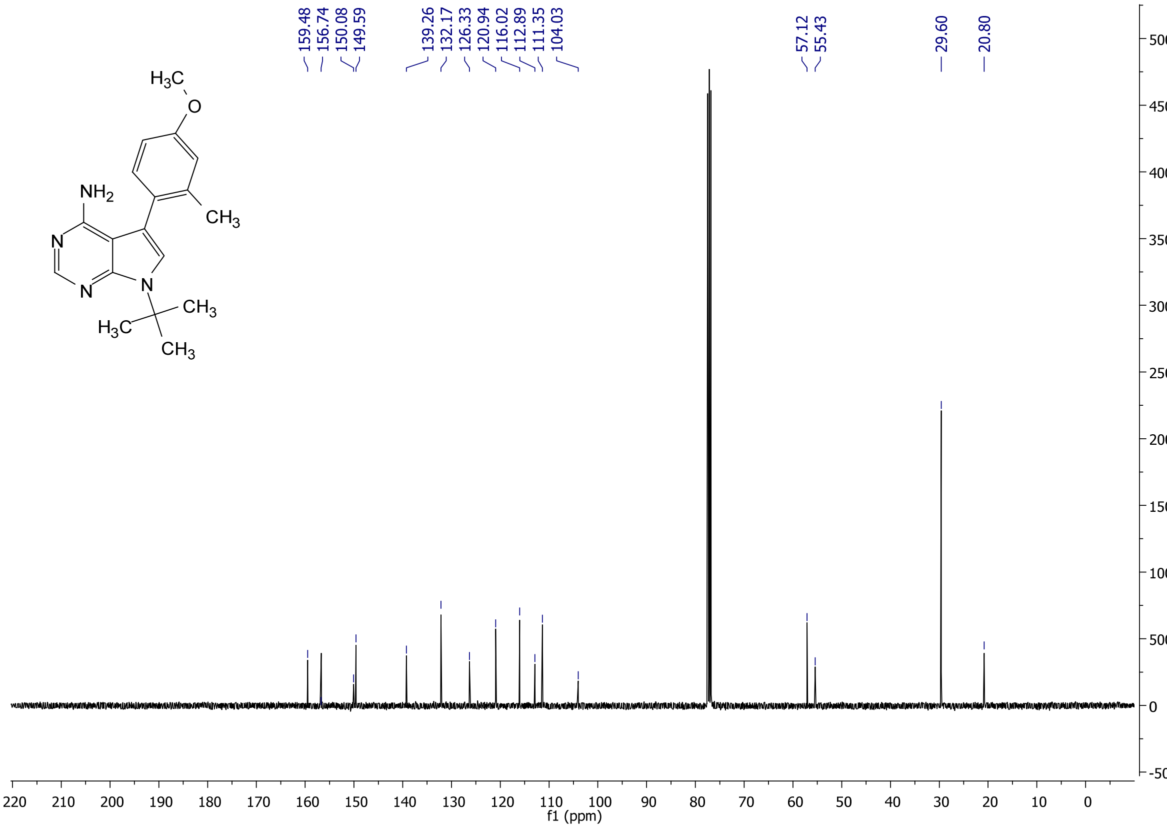

159.48
156.74
150.08
149.59
139.26
132.17
126.33
120.94
116.02
112.89
111.35
104.03
57.12
55.43
29.60
20.80
f1 (ppm)
NH$_2$
N
N
N
H$_3$C
O
CH$_3$
H$_3$C
CH$_3$
CH$_3$

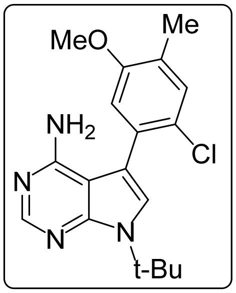

7-(*tert*-butyl)-5-(2-chloro-5-methoxy-4-methylphenyl)-7*H*-pyrrolo[2,3-d]pyrimidin-4-amine (2.3b): Following the general procedure: **2.3a** (364 mg, .563 mmol, 1.0 eq.) was dissolved in a 2:1 mixture of dioxane and 28% ammonium hydroxide (35 eq.). The reaction proceeded according to the general procedure. Workup and purification was followed according to the general procedure to afford 150 mg of **2.3b** (77% yield) as a yellow-white crystalline solid.

^{1}H NMR (400 MHz, $CDCl_3$) δ 8.30 (s, 1H), 7.25 (s, 1H), 7.14 (s, 1H), 6.83 (s, 1H), 5.05 (s, 2H), 3.82 (s, 3H), 2.23 (s, 3H), 1.80 (s, 9H)

^{13}C NMR (101 MHz, $CDCl_3$) δ 156.79, 156.48, 150.34, 150.19, 131.72, 131.35, 128.12, 124.74, 122.18, 113.72, 111.09, 103.68, 57.27, 55.80, 29.52, 15.97.

MS (APCI) Calculated: $C_{18}H_{22}ClN_4O$ $[M+H]^+$ 345.2 **Found**: 345.1

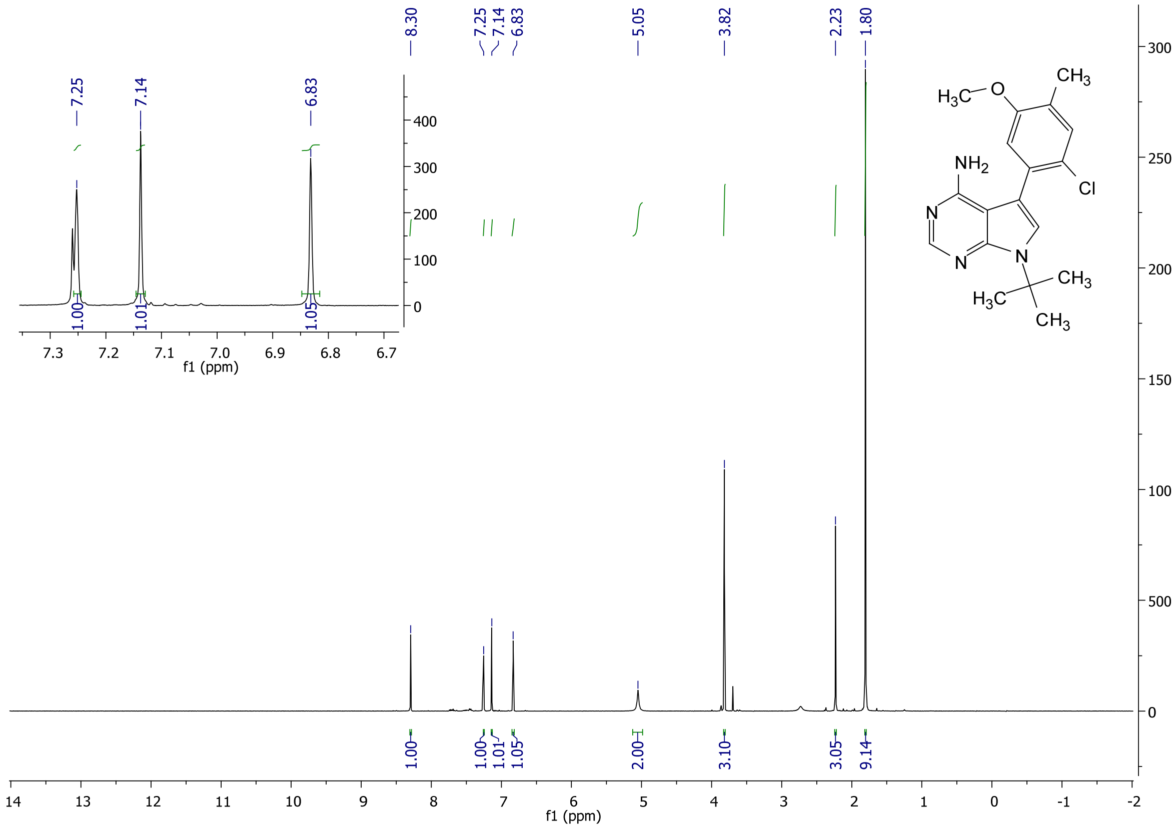
8.30
7.25
7.14
6.83
5.05
3.82
2.23
1.80
1.00
1.00
1.01
1.05
2.00
3.10
3.05
9.14
f1 (ppm)
H_3C
O
CH_3
NH_2
Cl
N
N
N
CH_3
H_3C
CH_3

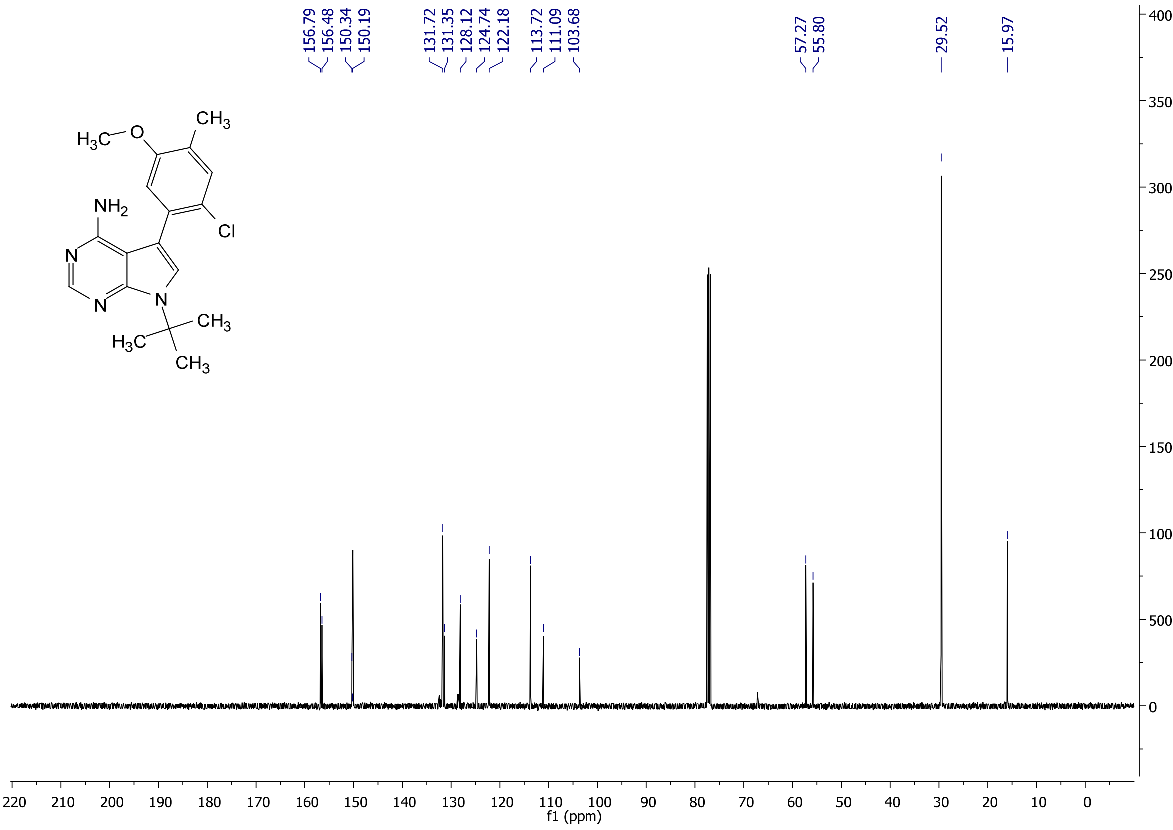
156.79
156.48
150.34
150.19
131.72
131.35
128.12
124.74
122.18
113.72
111.09
103.68
57.27
55.80
29.52
15.97
f1 (ppm)
H_3C
O
CH_3
NH_2
Cl
N
N
N
CH_3
H_3C
CH_3

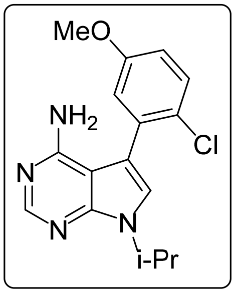

5-(2-chloro-5-methoxyphenyl)-7-isopropyl-7*H*-pyrrolo[2,3-d]pyrimidin-4-amine (2.4b): Following the general procedure: **2.4a** (702mg, 2.09 mmol, 1 eq.) was dissolved in a 2:1 mixture of dioxane and 28% ammonium hydroxide (35 eq.). The reaction proceeded according to the general procedure. Workup and purification were followed according to the general procedure to afford 512 mg of **2.4b** (77% yield) as a white crystalline solid.

^{1}H NMR (400 MHz, $CDCl_3$) δ 8.31 (s, 1H), 7.40 (d, J = 8.8 Hz, 1H), 7.12 (s, 1H), 6.94 (d, J = 3.1 Hz, 1H), 6.86 (dd, J = 8.8, 3.1 Hz, 1H), 5.13 (s, 2H), 5.10 (p, 6.8 Hz, 1H), 3.81 (s, 3H), 1.53 (d, J = 6.8 Hz, 6H).

^{13}C NMR (126 MHz, $CDCl_3$) δ 158.41, 156.78, 151.37, 149.71, 134.32, 130.97, 125.39, 120.91, 117.38, 114.98, 112.36, 102.21, 55.75, 46.05, 23.00.

MS (APCI) Calculated: $C_{16}H_{18}ClN_4O$ $[M+H]^+$ 317.1 **Found**: 317.1 m/z

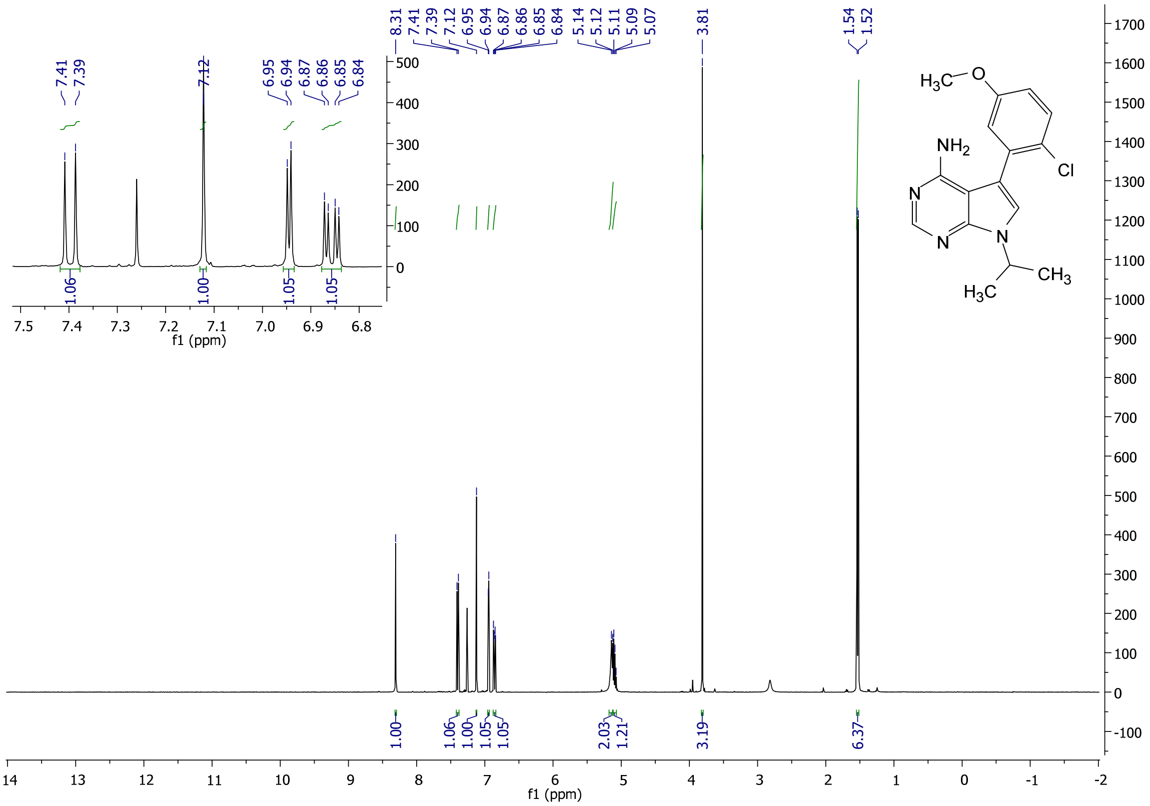
8.31
7.41
7.39
7.12
6.95
6.94
6.87
6.86
6.85
6.84
5.14
5.12
5.11
5.09
5.07
3.81
1.54
1.52
7.41
7.39
7.12
6.95
6.94
6.87
6.86
6.85
6.84
1.06
1.00
1.05
1.05
7.5 7.4 7.3 7.2 7.1 7.0 6.9 6.8
f1 (ppm)
500 400 300 200 100 0
1.00
1.06
1.00
1.05
1.05
2.03
1.21
3.19
6.37
14 13 12 11 10 9 8 7 6 5 4 3 2 1 0 -1 -2
f1 (ppm)
1700 1600 1500 1400 1300 1200 1100 1000 900 800 700 600 500 400 300 200 100 0 -100
H_3C O
NH_2
Cl
N
N
N
CH_3
H_3C

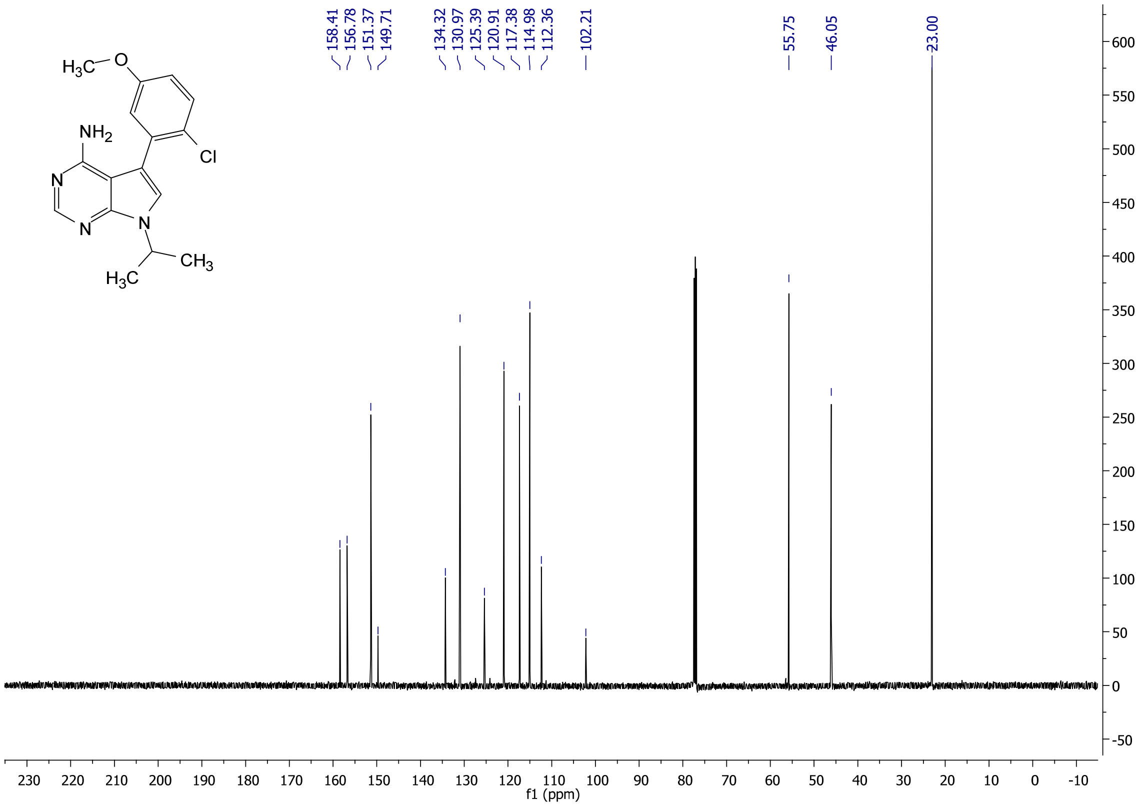
158.41
156.78
151.37
149.71
134.32
130.97
125.39
120.91
117.38
114.98
112.36
102.21
55.75
46.05
23.00
H_3C O
NH_2
Cl
N
N
N
CH_3
H_3C
230 220 210 200 190 180 170 160 150 140 130 120 110 100 90 80 70 60 50 40 30 20 10 0 -10
f1 (ppm)
600 550 500 450 400 350 300 250 200 150 100 50 0 -50

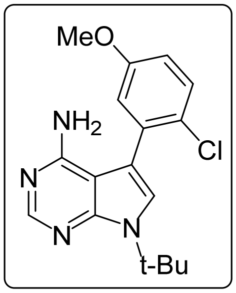

7-(*tert*-butyl)-5-(2-chloro-5-methoxyphenyl)-7*H*-pyrrolo[2,3-*d*]pyrimidin-4-amine (2.6b): Following the general procedure: **2.6a** (300 mg, 0.856 mmol, 1.0 eq) was dissolved in a 2:1 mixture of dioxane and 28% ammonium hydroxide (35 equiv). The reaction proceeded according to the general procedure. Workup and purification were followed according to the general procedure to afford 213mg of **2.6b** (64% yield) as a white crystalline solid.

^{1}H NMR (400 MHz, $CDCl_3$) δ 8.29 (s, 1H), 7.40 (d, J = 8.8 Hz, 1H), 7.17 (s, 1H), 6.93 (d, J = 3.0 Hz, 1H), 6.87 (dd, J = 8.8, 3.1 Hz, 1H), 5.32 (s, 2H), 3.81 (s, 3H), 1.81 (s, 9H)

^{13}C NMR (101 MHz, $CDCl_3$) δ 158.30, 155.95, 149.90, 148.55, 133.99, 130.85, 125.29, 122.57, 117.30, 114.98, 111.12, 103.24, 57.46, 55.62, 29.39

MS (APCI) Calculated: $C_{17}H_{20}ClN_4O$ $[M+H]^+$ 331.1 **Found**: 331.1

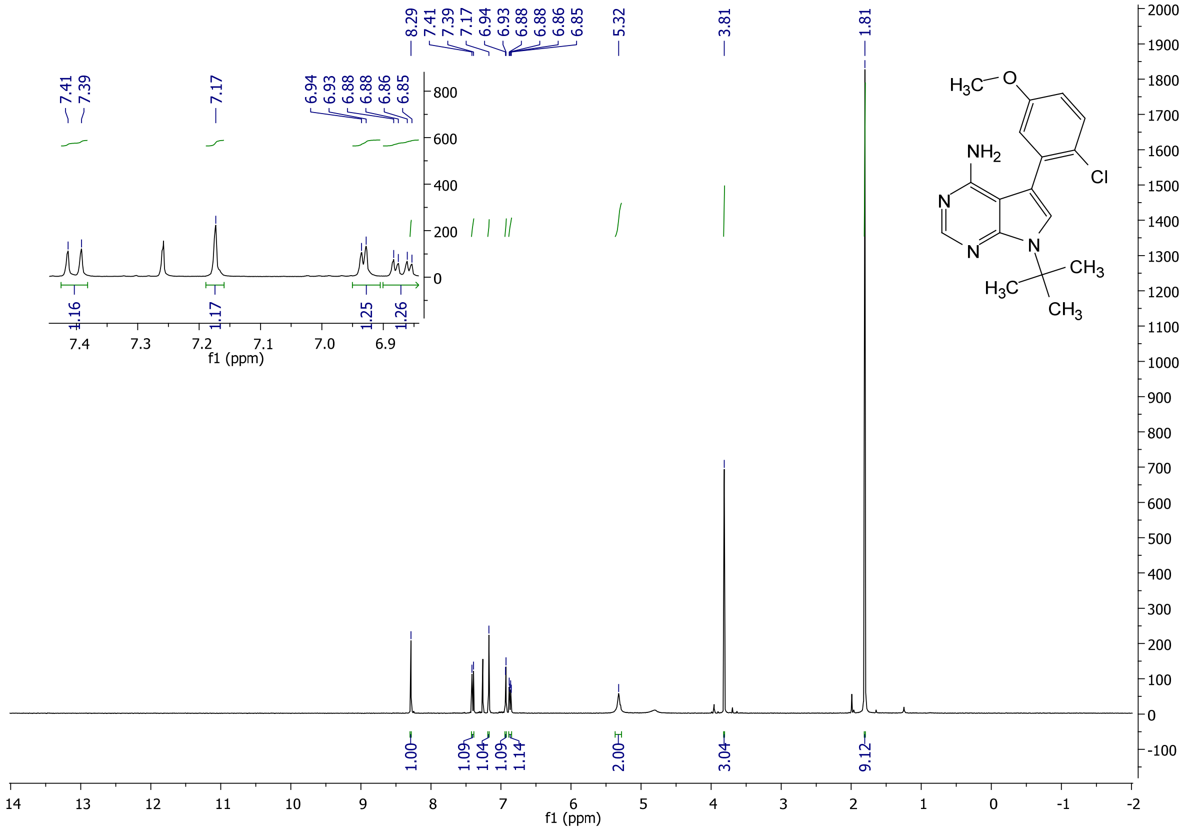
8.29
7.41
7.39
7.17
6.94
6.93
6.88
6.88
6.86
6.85
5.32
3.81
1.81
1.00
1.09
1.04
1.09
1.14
2.00
3.04
9.12
1.16
1.17
1.25
1.26
f1 (ppm)
H_3C—O
NH_2
Cl
N
N
N
CH_3
H_3C
CH_3

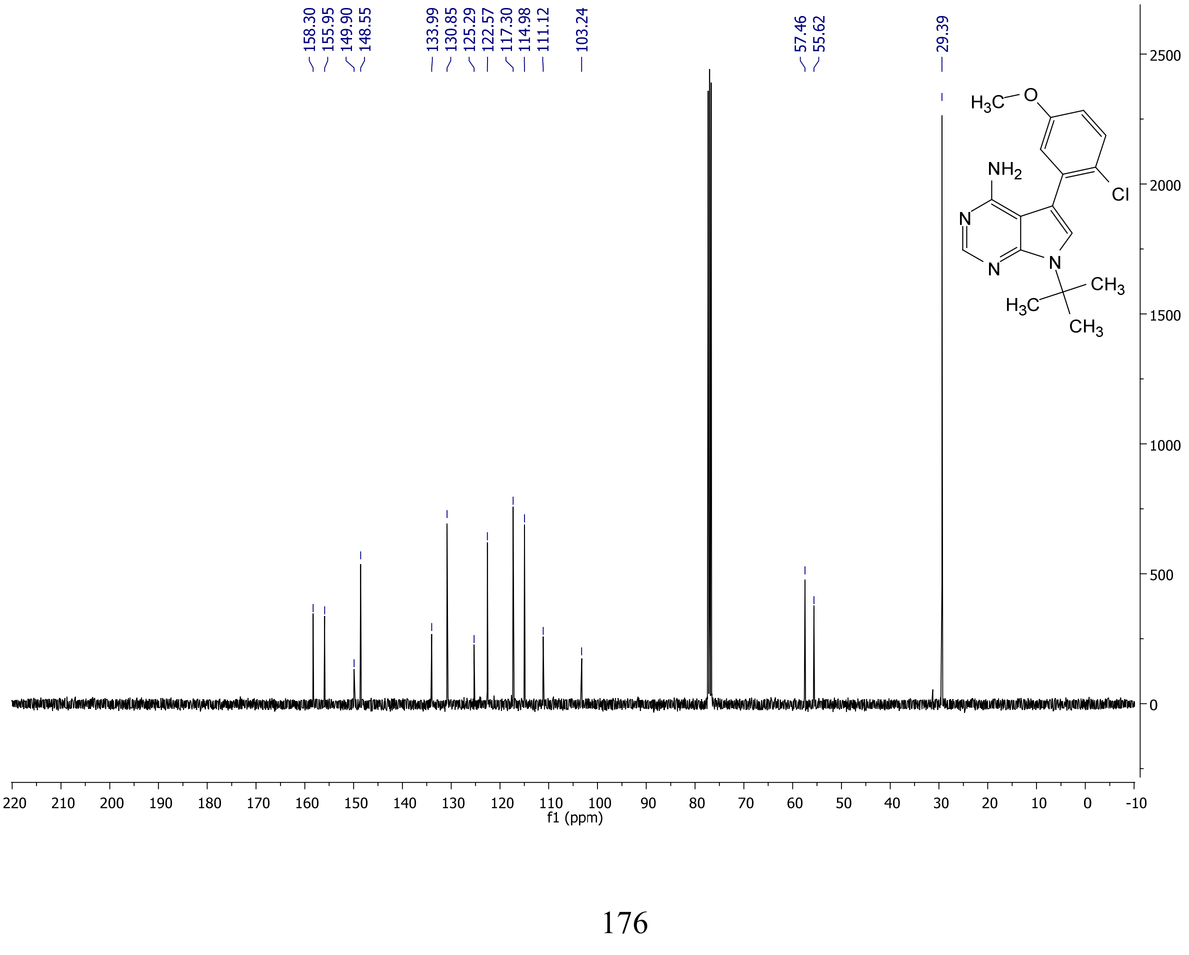
158.30
155.95
149.90
148.55
133.99
130.85
125.29
122.57
117.30
114.98
111.12
103.24
57.46
55.62
29.39
f1 (ppm)
H_3C—O
NH_2
Cl
N
N
N
CH_3
H_3C
CH_3

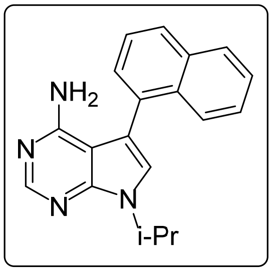

7-isopropyl-5-(napthalen-1-yl)-7*H*-pyrrolo[2,3-*d*]pyrimidin-4-amine (2.9b):

Following the general procedure: **2.9a** (950 mg, 2.95 mmol, 1.0 eq.) was dissolved in a 2:1 mixture of dioxane and 28% ammonium hydroxide (35 eq.). The reaction proceeded according to the general procedure. Workup and purification were followed according to the general procedure to afford 784 mg of **2.9b** (88% yield) as a white crystalline solid.

^{1}H NMR (400 MHz, $CDCl_3$) δ 8.32 (s, 1H), 7.95 - 7.85 (m, 3H), 7.56 – 7.49 (m, 3H), 7.46 (t, J = 7.5 Hz, 1H), 7.12 (s, 1H), 5.17 (hept, J = 6.6 Hz, 1H), 4.88 (s, 2H), 1.57 (t, J = 6.9 Hz, 6H).

^{13}C NMR (101 MHz, $CDCl_3$) δ 156.87, 151.34, 149.78, 133.98, 132.67, 132.21, 128.53, 128.45, 128.29, 126.76, 126.39, 126.11, 125.60, 120.53, 113.48, 103.02, 46.01, 23.04

MS (APCI) Calculated: $C_{19}H_{19}N_4$ $[M+H]^+$ 303.2 **Found**: 303.0 m/z

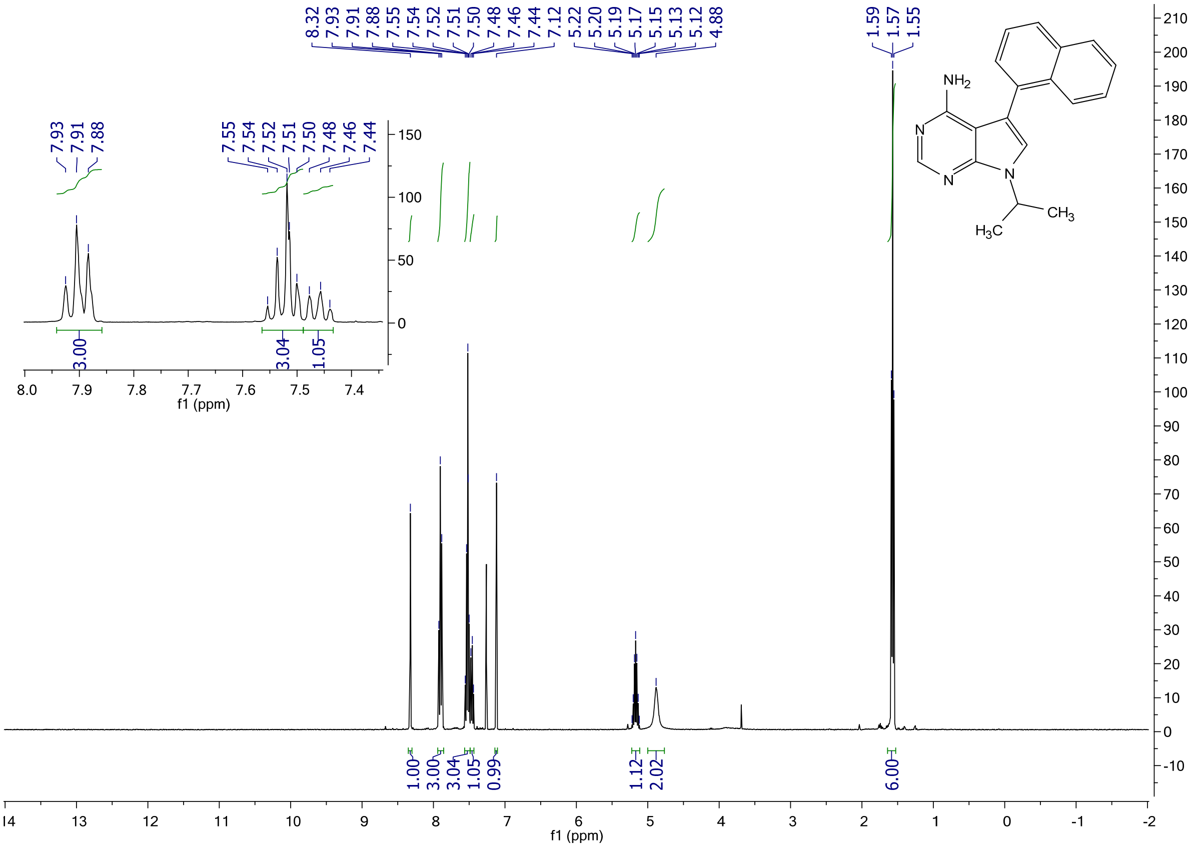
8.32
7.93
7.91
7.88
7.55
7.54
7.52
7.51
7.50
7.48
7.46
7.44
7.12
5.22
5.20
5.19
5.17
5.15
5.13
5.12
4.88
1.59
1.57
1.55
NH$_2$
N
N
N
CH$_3$
H$_3$C
1.00
3.00
3.04
1.05
0.99
1.12
2.02
6.00
f1 (ppm)
14 13 12 11 10 9 8 7 6 5 4 3 2 1 0 -1 -2
210 200 190 180 170 160 150 140 130 120 110 100 90 80 70 60 50 40 30 20 10 0 -10
8.0 7.9 7.8 7.7 7.6 7.5 7.4
150 100 50 0

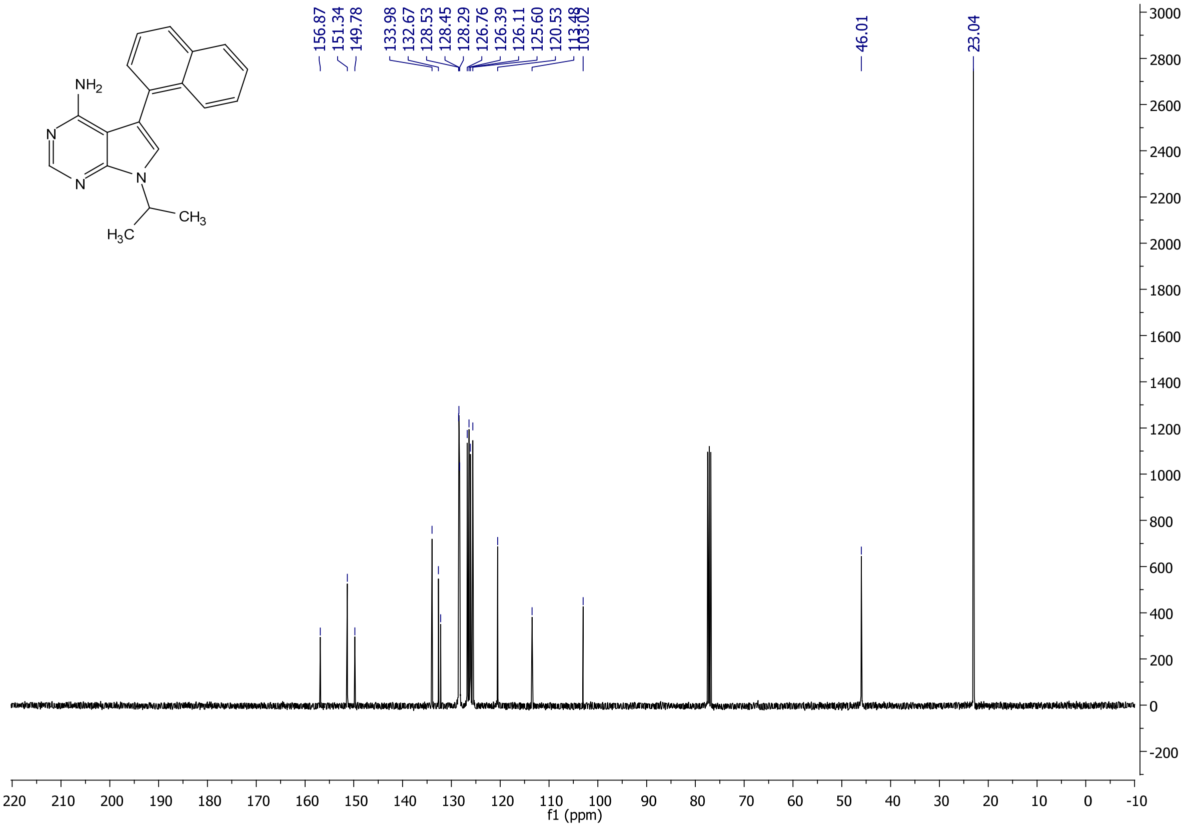
156.87
151.34
149.78
133.98
132.67
128.53
128.45
128.29
126.76
126.39
126.11
125.60
120.53
113.48
103.02
46.01
23.04
NH$_2$
N
N
N
CH$_3$
H$_3$C
f1 (ppm)
220 210 200 190 180 170 160 150 140 130 120 110 100 90 80 70 60 50 40 30 20 10 0 -10
3000 2800 2600 2400 2200 2000 1800 1600 1400 1200 1000 800 600 400 200 0 -200

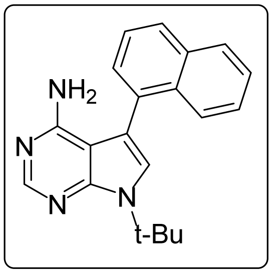

7-(*tert*-butyl)-5-(naphthalen-1-yl)-7*H*-pyrrolo[2,3-*d*]pyrimidin-4-amine (2.10b):

Following the general procedure: **2.10a** (1.26g, 3.77 mmol, 1.0 eq.) was dissolved in a 2:1 mixture of dioxane and 28% ammonium hydroxide (35 eq.). The reaction proceeded according to the general procedure. Workup and purification was followed according to the general procedure to afford 1.17 g of **2.10b** (98% yield) as a white crystalline solid.

^{1}H NMR (400 MHz, $CDCl_3$) δ 8.32 (s, 1H), 7.92 - 7.87 (m, 3H), 7.56 – 7.43 (m, 4H), 7.16 (s, 1H), 4.84 (s, 2H), 1.84 (s, 9H).

^{13}C NMR (101 MHz, $CDCl_3$) δ 156.98, 150.55, 150.48, 133.48, 133.94, 128.55, 128.40, 128.17, 126.68, 126.34, 126.23, 125.58, 111.98, 104.43, 57.16, 29.54

MS (APCI) Calculated: $C_{20}H_{21}N_4$ $[M+H]^+$ 317.2 **Found**: 317.3

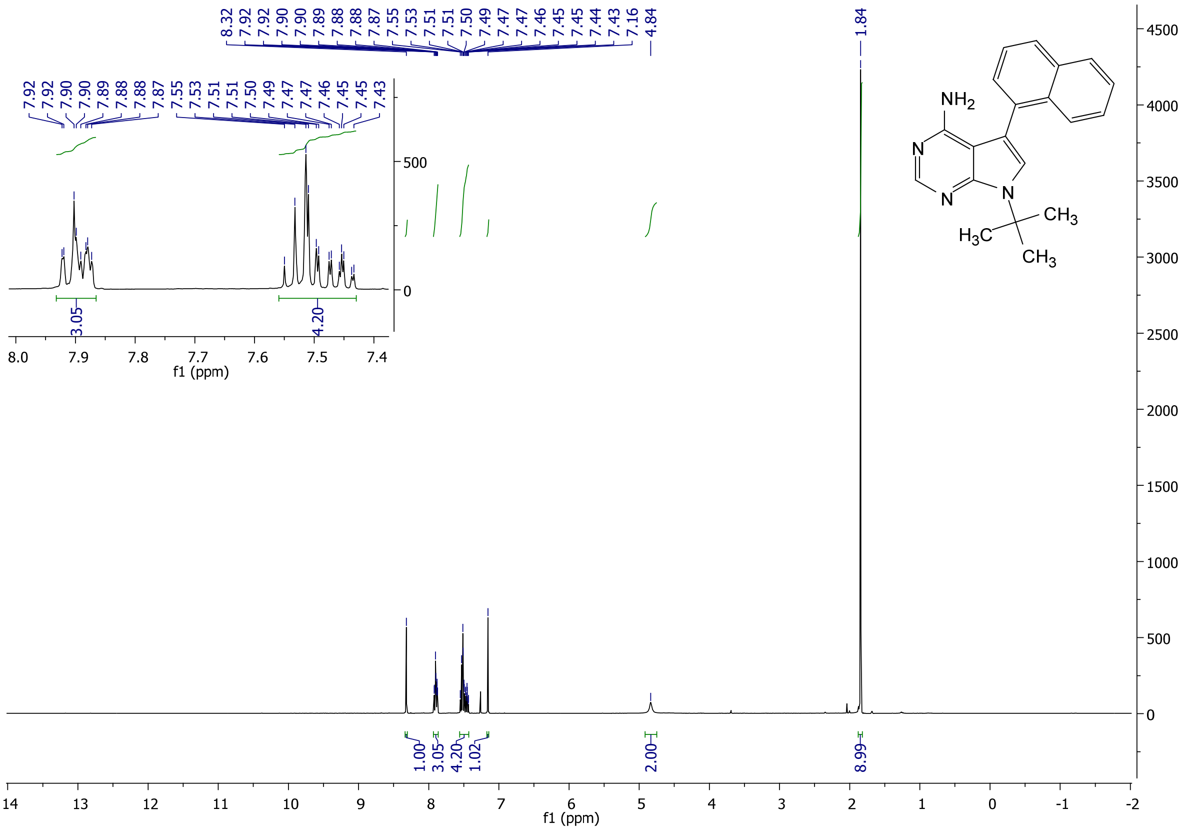
8.32
7.92
7.92
7.90
7.90
7.89
7.88
7.88
7.87
7.55
7.53
7.51
7.51
7.50
7.49
7.47
7.47
7.46
7.45
7.45
7.44
7.43
7.16
4.84
1.84
NH_2
N
N
N
CH_3
H_3C
CH_3
500
0
3.05
4.20
8.0
7.9
7.8
7.7
7.6
7.5
7.4
f1 (ppm)
1.00
3.05
4.20
1.02
2.00
8.99
4500
4000
3500
3000
2500
2000
1500
1000
500
0
14
13
12
11
10
9
8
7
6
5
4
3
2
1
0
-1
-2
f1 (ppm)

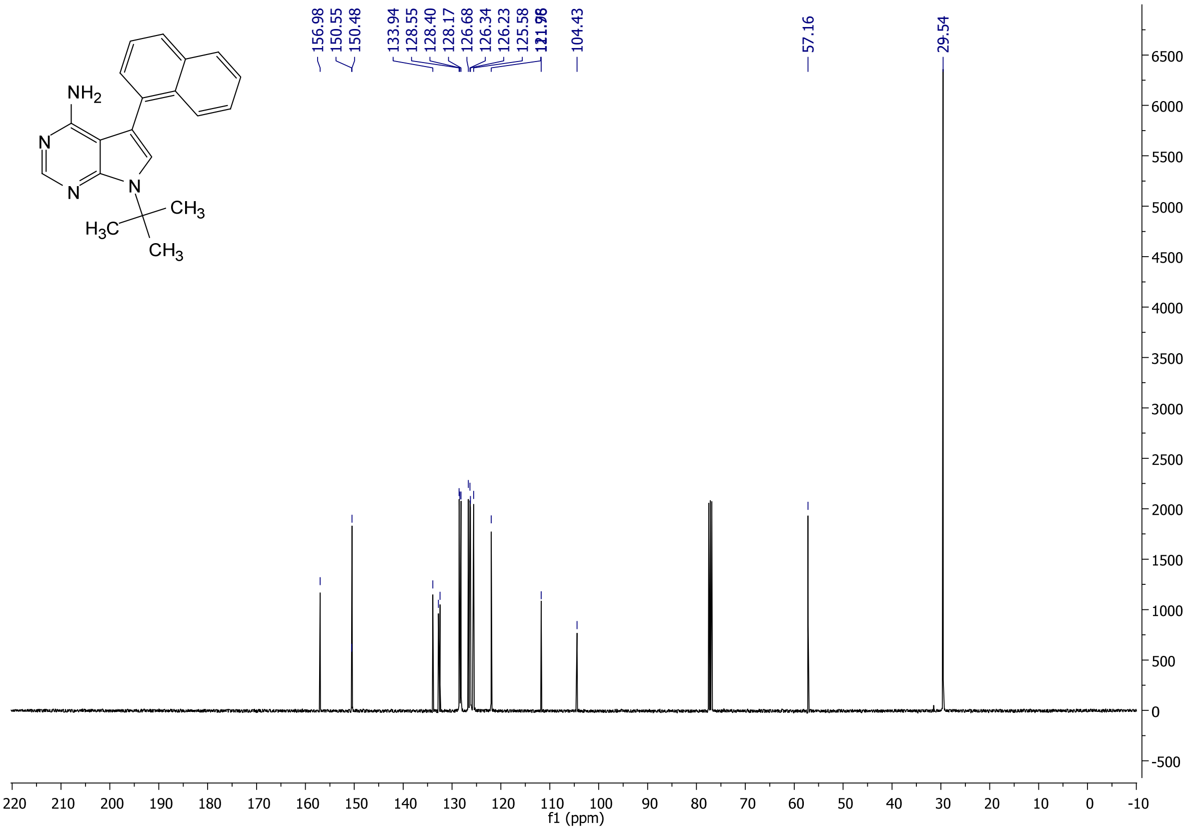
156.98
150.55
150.48
133.94
128.55
128.40
128.17
126.68
126.34
126.23
125.58
121.98
111.96
104.43
57.16
29.54
NH_2
N
N
N
CH_3
H_3C
CH_3
6500
6000
5500
5000
4500
4000
3500
3000
2500
2000
1500
1000
500
0
-500
220
210
200
190
180
170
160
150
140
130
120
110
100
90
80
70
60
50
40
30
20
10
0
-10
f1 (ppm)

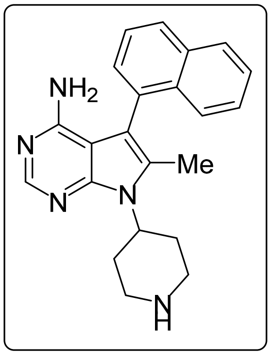

6-methyl-5-(naphthalen-1-yl)-7-(piperidin-4-yl)-7H-pyrrolo[2,3-d]pyrimidin-4-amine (2.11):

Following the general procedure: **2.11a** (71 mg, .179 mmol, 1 eq.) was dissolved in a 2:1 mixture of dioxane and 28% ammonium hydroxide (35 eq.). The reaction and workup were followed according to the general procedure. The crude material was added to 1:1 mixture of TFA and DCM and stirred at room temperature overnight. Purification was followed according to the general procedure to afford 21 mg of **2.11** as a yellow solid (40% yield over two steps).

MS (APCI) Calculated: $C_{22}H_{23}N_5$ $[M+H]^+$ 357.2 **Found**: 357.2

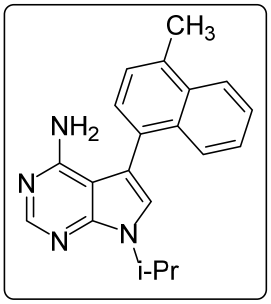

7-isopropyl-5-(4-methylnaphthalen-1-yl)-7*H*-pyrrolo[2,3-*d*]pyrimidin-4-amine (2.12b): Following the general procedure: **2.12a** (900 mg, 2.69 mmol, 1.0 eq.) was dissolved in a 2:1 mixture of dioxane and 28% ammonium hydroxide (35 eq.). The reaction proceeded according to the general procedure. Workup and purification was followed according to the general procedure to afford 620 mg of **2.12b** (73% yield) as a white crystalline solid.

^{1}H NMR (400 MHz, $CDCl_3$) δ 8.32 (s, 1H), 8.07 (d, J = 8.5 Hz, 1H), 7.91 (d, J = 7.8 Hz, 1H), 7.56 (ddd, J = 8.3, 6.8, 1.3 Hz, 1H), 7.46 (ddd, J = 8.2, 6.8, 1.3 Hz, 1H), 7.43 - 7.36 (m, 2H), 7.09 (s, 1H), 5.22 – 5.10 (m, 1H), 4.83 (s, 2H), 2.75 (s, 3H), 1.57 (t, J = 7.0 Hz, 6H)

^{13}C NMR (101 MHz, $CDCl_3$) δ 156.97, 151.60, 149.78, 134.65, 133.06, 132.77, 130.48, 128.29, 126.77, 126.41, 126.36, 126.21, 124.60, 120.35, 113.62, 103.20, 45.93, 23.07, 19.69

MS (APCI) Calculated: $C_{20}H_{21}N_4$ $[M+H]^+$ 317.2 **Found**: 317.1

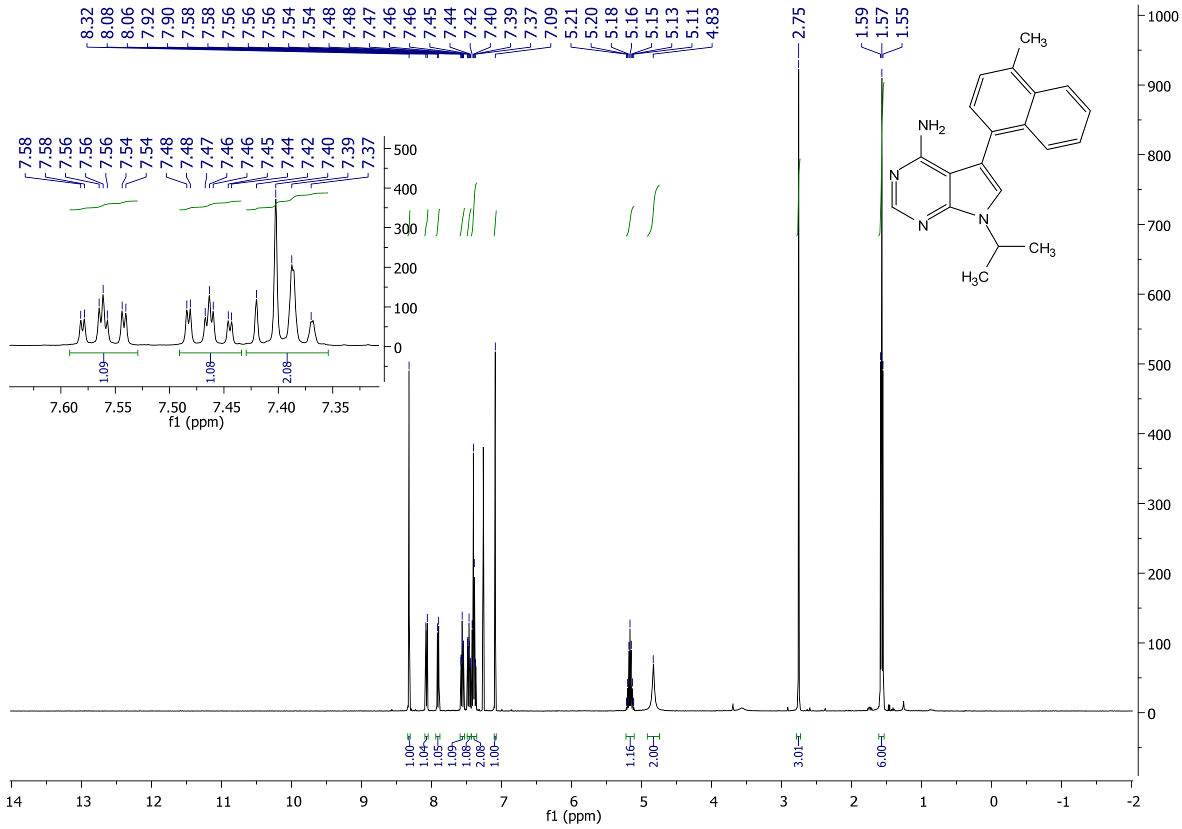
8.32 8.08 8.06 7.92 7.90 7.58 7.58 7.56 7.56 7.56 7.54 7.54 7.48 7.48 7.47 7.46 7.46 7.45 7.44 7.42 7.40 7.39 7.37 7.09 5.21 5.20 5.18 5.16 5.15 5.13 5.11 4.83
2.75
1.59 1.57 1.55
7.58 7.58 7.56 7.56 7.56 7.54 7.54 7.48 7.48 7.47 7.46 7.46 7.45 7.44 7.42 7.40 7.39 7.37
1.09 1.08 2.08
7.60 7.55 7.50 7.45 7.40 7.35
f1 (ppm)
0 100 200 300 400 500
1.00 1.04 1.05 1.09 1.08 2.08 1.00 1.16 2.00 3.01 6.00
14 13 12 11 10 9 8 7 6 5 4 3 2 1 0 -1 -2
f1 (ppm)
0 100 200 300 400 500 600 700 800 900 1000
CH3
NH2
N
N
N
CH3
H3C

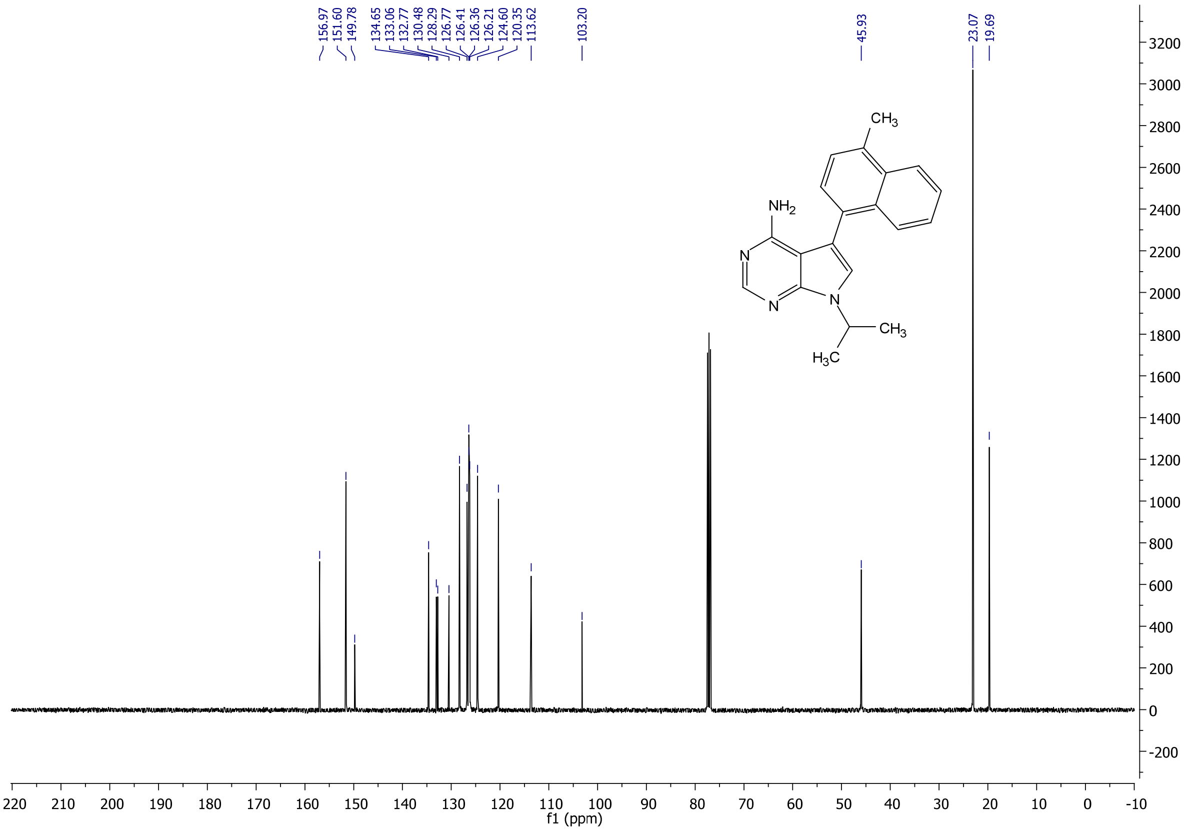
156.97 151.60 149.78
134.65 133.06 132.77 130.48 128.29 126.77 126.41 126.36 126.21 124.60 120.35 113.62
103.20
45.93
23.07 19.69
CH3
NH2
N
N
N
CH3
H3C
-200 0 200 400 600 800 1000 1200 1400 1600 1800 2000 2200 2400 2600 2800 3000 3200
220 210 200 190 180 170 160 150 140 130 120 110 100 90 80 70 60 50 40 30 20 10 0 -10
f1 (ppm)

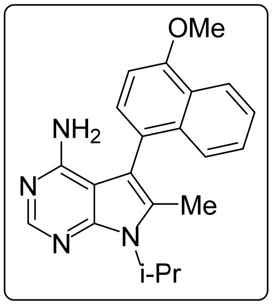

7-isopropyl-5-(4-methoxynaphthalen-1-yl)-6-methyl-7H-pyrrolo[2,3-d]pyrimidin-4-amine (2.13):

Following the general procedure: **2.13a** (82 mg, .224 mmol, 1 eq.) was dissolved in a 2:1 mixture of dioxane and 28% ammonium hydroxide (35 eq.). The reaction, workup and purification were followed according to the general procedure to afford 69 mg of **2.13** as a yellow solid (87%).

^{1}H NMR (400 MHz, $CDCl_3$) δ 8.35 (dd, J = 8.3, 0.7 Hz, 1H), 8.25 (s, 1H), 7.57 (d, J = 8.8 Hz, 1H), 7.50 (ddd, J = 8.3, 6.8, 1.3 Hz, 1H), 7.44 (ddd, J = 8.2, 6.8, 1.4 Hz, 1H), 7.38 (d, J = 7.8 Hz, 1H), 6.90 (d, J = 7.8 Hz, 1H), 5.03 – 4.94 (m, 1H), 4.58 (s, 2H), 4.06 (s, 3H), 2.20 (s, 3H), 1.73 (dd, J = 7.0, 4.5 Hz, 6H).

^{13}C NMR (101 MHz, $CDCl_3$) δ 155.72, 155.39, 149.89, 133.96, 131.55, 129.14, 127.04, 125.99, 125.80, 125.52, 123.99, 122.29, 109.78, 106.58, 103.45, 103.31, 55.59, 47.07, 21.72, 11.73.

MS (APCI) Calculated: $C_{20}H_{21}N_5O$ $[M+H]^+$ 346.2 **Found**: 346.2

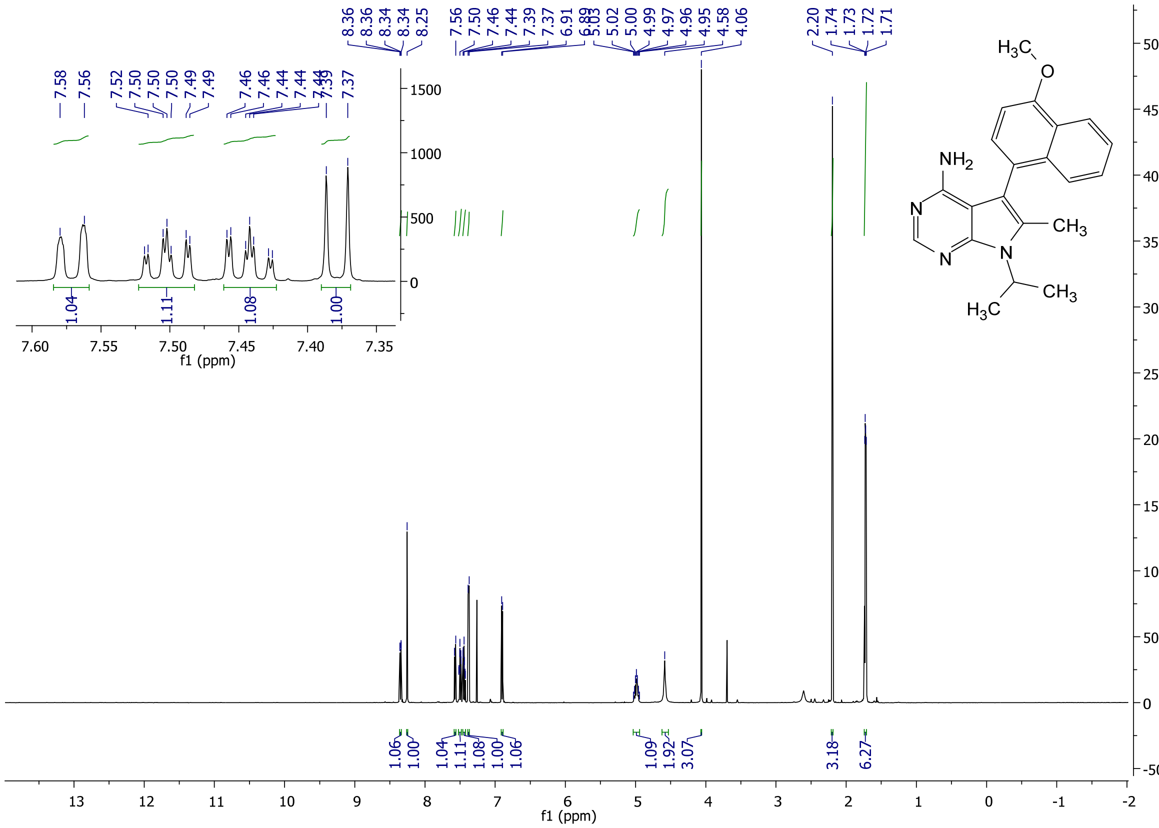
8.36
8.36
8.34
8.34
8.25
7.56
7.50
7.46
7.44
7.39
7.37
6.91
6.89
5.03
5.02
5.00
4.99
4.97
4.96
4.95
4.58
4.06
2.20
1.74
1.73
1.72
1.71
7.58
7.56
7.52
7.50
7.50
7.50
7.49
7.49
7.46
7.46
7.44
7.44
7.39
7.37
1.04
1.11
1.08
1.00
7.60 7.55 7.50 7.45 7.40 7.35
f1 (ppm)
1500
1000
500
0
H_3C
O
NH_2
N
N
N
CH_3
H_3C
CH_3
5000
4500
4000
3500
3000
2500
2000
1500
1000
500
0
-500
1.06
1.00
1.04
1.11
1.08
1.00
1.06
1.09
1.92
3.07
3.18
6.27
13 12 11 10 9 8 7 6 5 4 3 2 1 0 -1 -2
f1 (ppm)

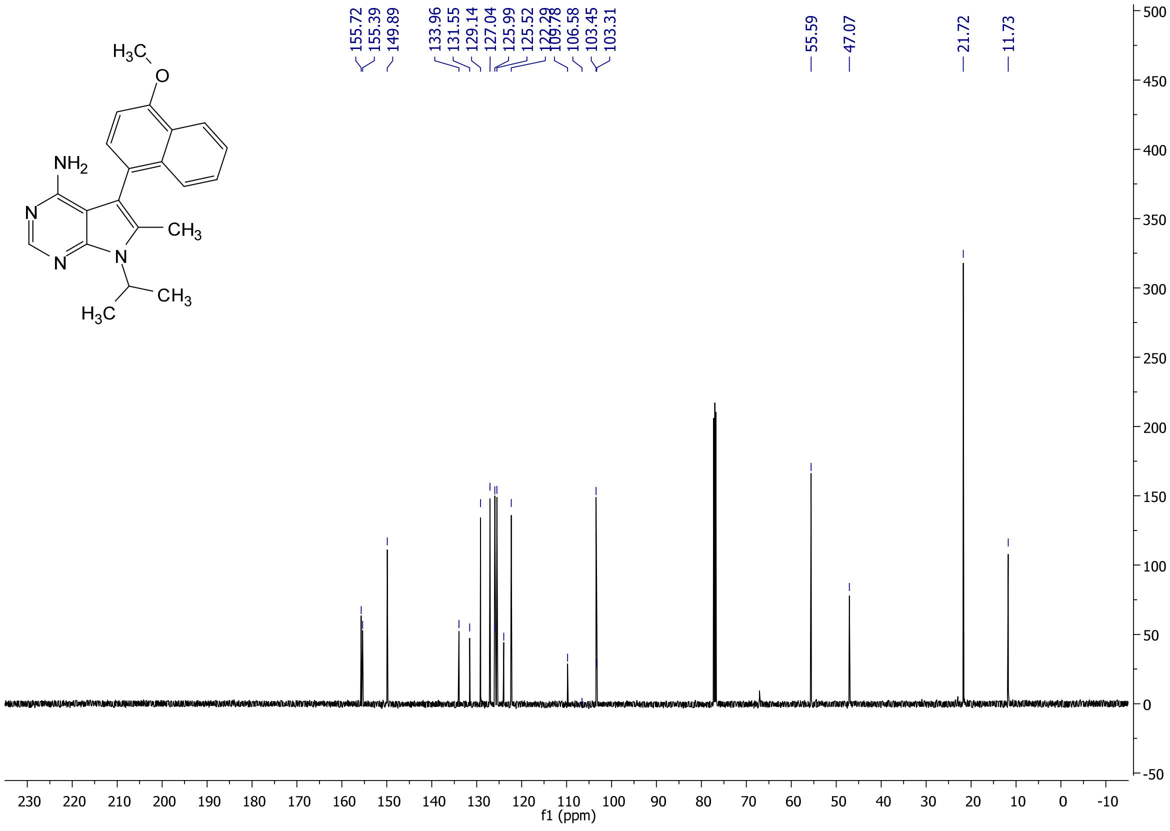
155.72
155.39
149.89
133.96
131.55
129.14
127.04
125.99
125.52
122.29
109.78
106.58
103.45
103.31
55.59
47.07
21.72
11.73
H_3C
O
NH_2
N
N
N
CH_3
H_3C
CH_3
500
450
400
350
300
250
200
150
100
50
0
-50
230 220 210 200 190 180 170 160 150 140 130 120 110 100 90 80 70 60 50 40 30 20 10 0 -10
f1 (ppm)

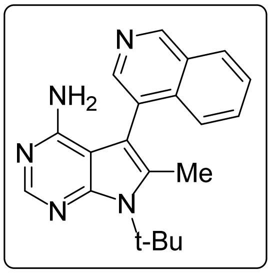

7-(tert-butyl)-5-(isoquinolin-4-yl)-6-methyl-7H-pyrrolo[2,3-d]pyrimidin-4-amine (2.16): Following the general procedure: **2.16a** (40 mg, .114 mmol, 1 eq.) was dissolved in a 2:1 mixture of dioxane and 28% ammonium hydroxide (35 eq.). The reaction proceeded according to the general procedure. Workup and purification were followed according to the general procedure to afford 32 mg of **2.16** as a white crystalline solid (85% yield).

^{1}H NMR (400 MHz, $CDCl_3$) δ 9.31 (s, 1H), 8.52 (s, 1H), 8.26 (s, 1H), 8.06 (d, J = 7.0 Hz, 1H), 7.71 – 7.59 (m, 3H), 4.41 (s, 2H), 2.30 (s, 3H), 1.97 (s, 9H).

^{13}C NMR (101 MHz, $CDCl_3$) δ 155.67, 152.55, 152.02, 149.57, 145.17, 135.90, 133.63, 131.10, 128.31, 127.90, 127.74, 126.53, 125.27, 107.49, 103.78, 60.76, 31.17, 15.92.

MS (APCI) Calculated: $C_{20}H_{22}N_5$ $[M+H]^+$ 332.2 **Found**: 332.2 m/z

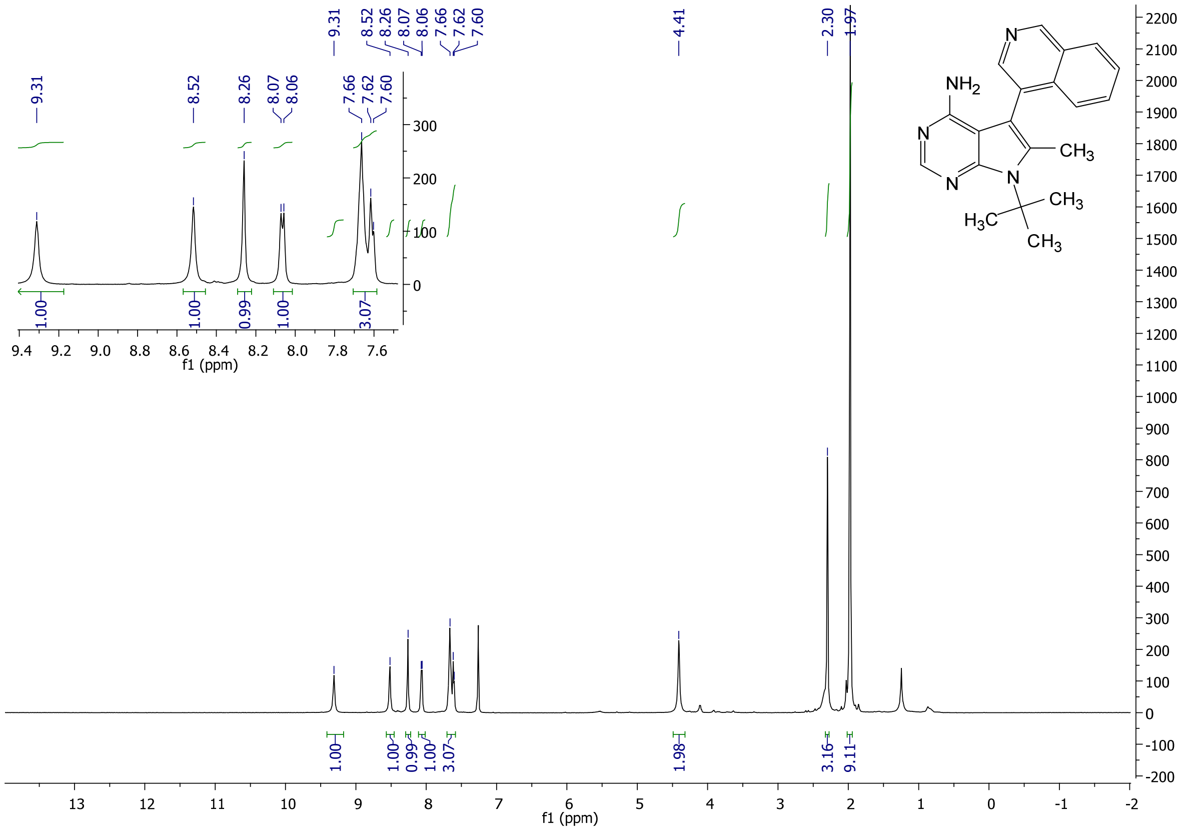
9.31
8.52
8.26
8.07
8.06
7.66
7.62
7.60
4.41
2.30
1.97
1.00
1.00
0.99
1.00
3.07
1.98
3.16
9.11
f1 (ppm)
NH$_2$
N
N
N
N
CH$_3$
CH$_3$
H$_3$C
CH$_3$

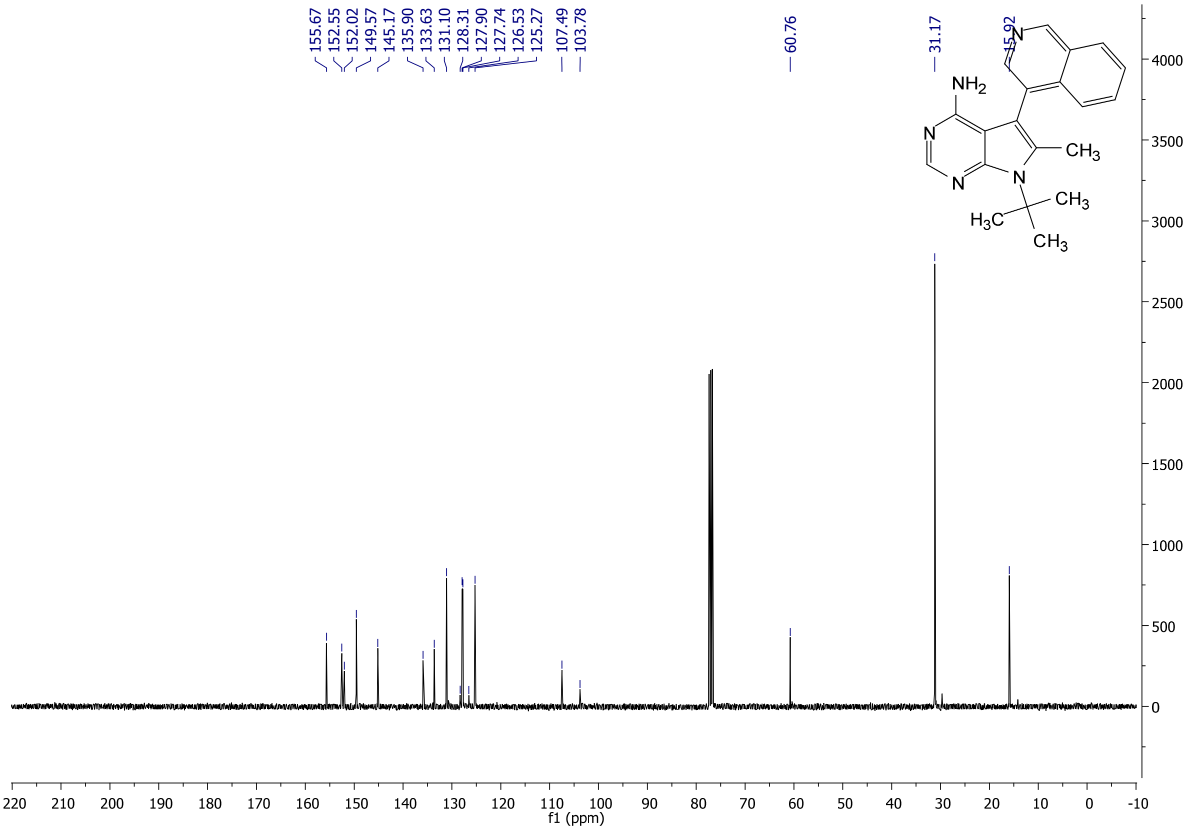
155.67
152.55
152.02
149.57
145.17
135.90
133.63
131.10
128.31
127.90
127.74
126.53
125.27
107.49
103.78
60.76
31.17
15.92
f1 (ppm)
NH$_2$
N
N
N
N
CH$_3$
CH$_3$
H$_3$C
CH$_3$

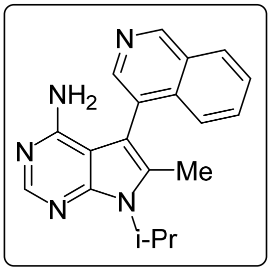

7-isopropyl-5-(isoquinolin-4-yl)-6-methyl-7H-pyrrolo[2,3-d]pyrimidin-4-amine (2.17): Following the general procedure: **2.17a** (60 mg, .179 mmol, 1 eq.) was dissolved in a 2:1 mixture of dioxane and 28% ammonium hydroxide (35 eq.). The reaction proceeded according to the general procedure. Workup and purification were followed according to the general procedure to afford 34 mg of **2.17** as a white crystalline solid (60% yield).

^{1}H NMR (400 MHz, $CDCl_3$) δ 9.30 (s, 1H), 8.52 (s, 1H), 8.26 (s, 1H), 8.09 – 8.04 (m, 1H), 7.68 – 7.64 (m, 3H), 5.03 – 4.94 (m, 1H), 4.65 (s, 2H), 2.22 (s, 3H), 1.73 (dd, J = 6.9, 5.6 Hz, 6H).

^{13}C NMR (101 MHz, $CDCl_3$) δ 155.63, 152.46, 150.39, 150.18, 144.95, 135.71, 132.36, 132.03, 131.13, 128.46, 127.97, 127.76, 125.18, 105.95, 103.16, 47.36, 21.63, 11.75.

MS (APCI) Calculated: $C_{20}H_{20}N_4$ $[M+H]^+$ 316.2 **Found**: 316.2 m/z

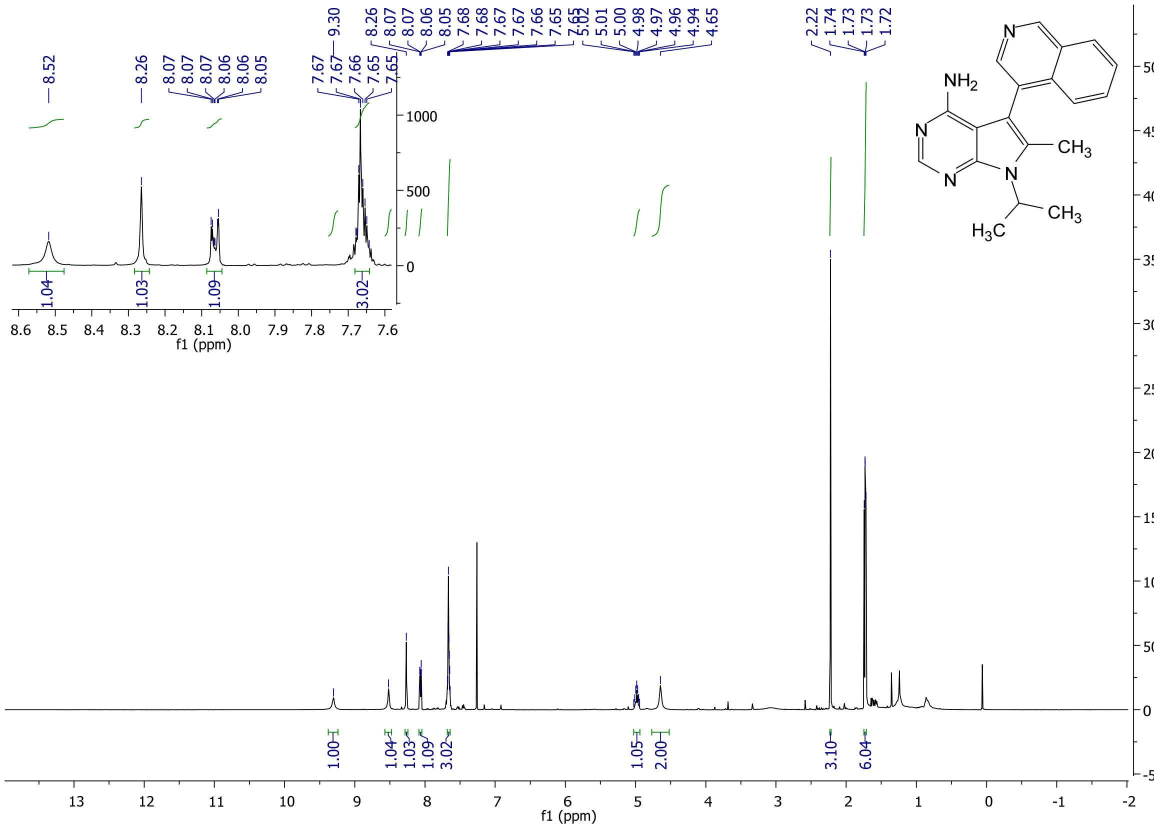

9.30
8.52
8.26
8.07
8.07
8.07
8.06
8.06
8.05
7.68
7.68
7.67
7.67
7.67
7.66
7.65
7.65
7.65
5.02
5.01
5.00
4.98
4.97
4.96
4.94
4.65
2.22
1.74
1.73
1.73
1.72
1.04
1.03
1.09
3.02
1.00
1.05
2.00
3.10
6.04
NH2
N
N
N
N
CH3
CH3
H3C
f1 (ppm)

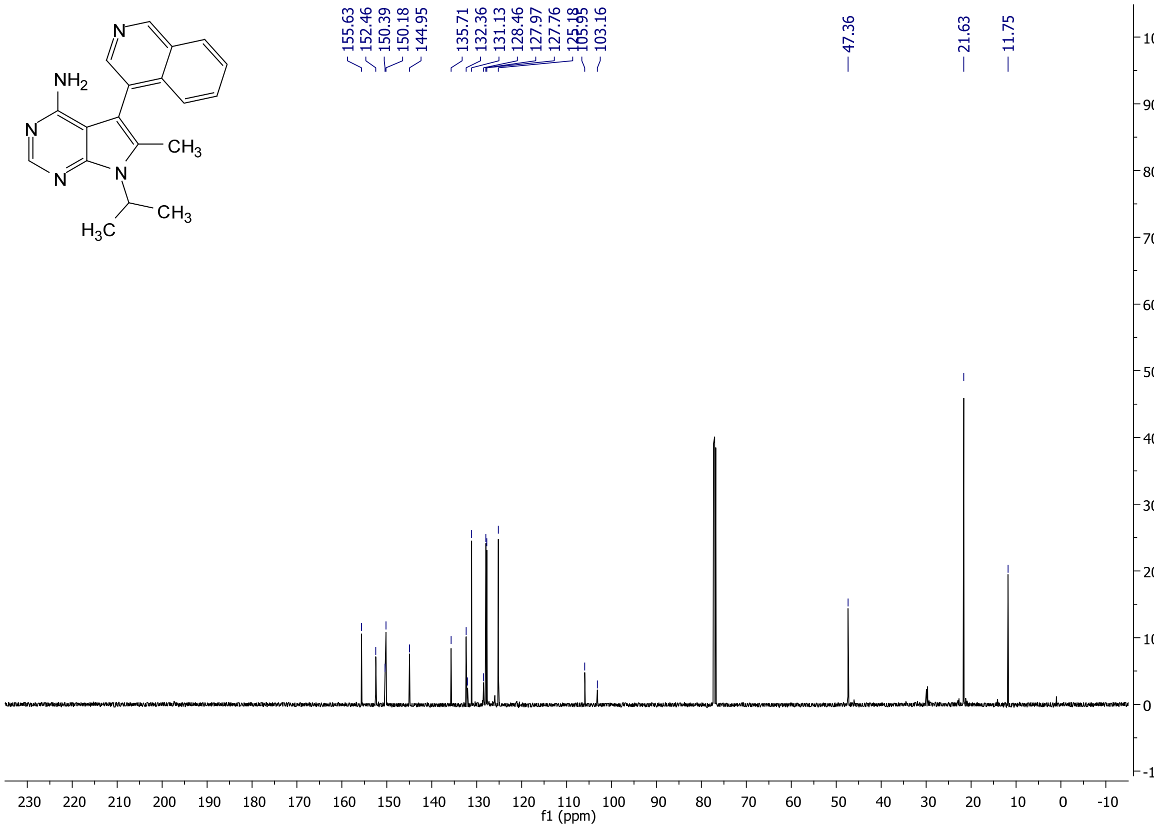

155.63
152.46
150.39
150.18
144.95
135.71
132.36
131.13
128.46
127.97
127.76
125.18
105.95
103.16
47.36
21.63
11.75
NH2
N
N
N
N
CH3
CH3
H3C
f1 (ppm)

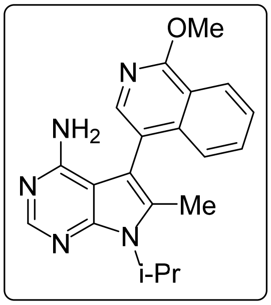

7-isopropyl-5-(1-methoxyisoquinolin-4-yl)-6-methyl-7H-pyrrolo[2,3-d]pyrimidin-4-amine (2.18):

Following the general procedure: **2.18a** (60 mg, .164 mmol, 1 eq.) was dissolved in a 2:1 mixture of dioxane and 28% ammonium hydroxide (35 eq.). The reaction, workup and purification were followed according to the general procedure to afford 24 mg of **2.18** as a yellow solid (42%).

^{1}H NMR (400 MHz, $CDCl_3$) δ 8.36 – 8.33 (m, 1H), 8.25 (s, 1H), 7.99 (s, 1H), 7.67 – 7.57 (m, 2H), 7.49 (d, J = 7.6 Hz, 1H), 4.98 (, 1H), 4.93 (s, , 2H), 4.19 (s, 3H), 2.23 (s, 3H), 1.74 (dd, J = 7.0, 3.1 Hz, 6H).

^{13}C NMR (101 MHz, $CDCl_3$) δ δ 161.03, 154.89, 149.79, 148.42, 141.60, 137.54, 132.87, 131.19, 127.14, 124.83, 124.53, 119.45, 119.24, 106.60, 103.13, 53.88, 47.50, 21.65, 11.62.

MS (APCI) Calculated: $C_{20}H_{21}N_5O$ $[M+H]^+$ 347.2 **Found**: 347.2

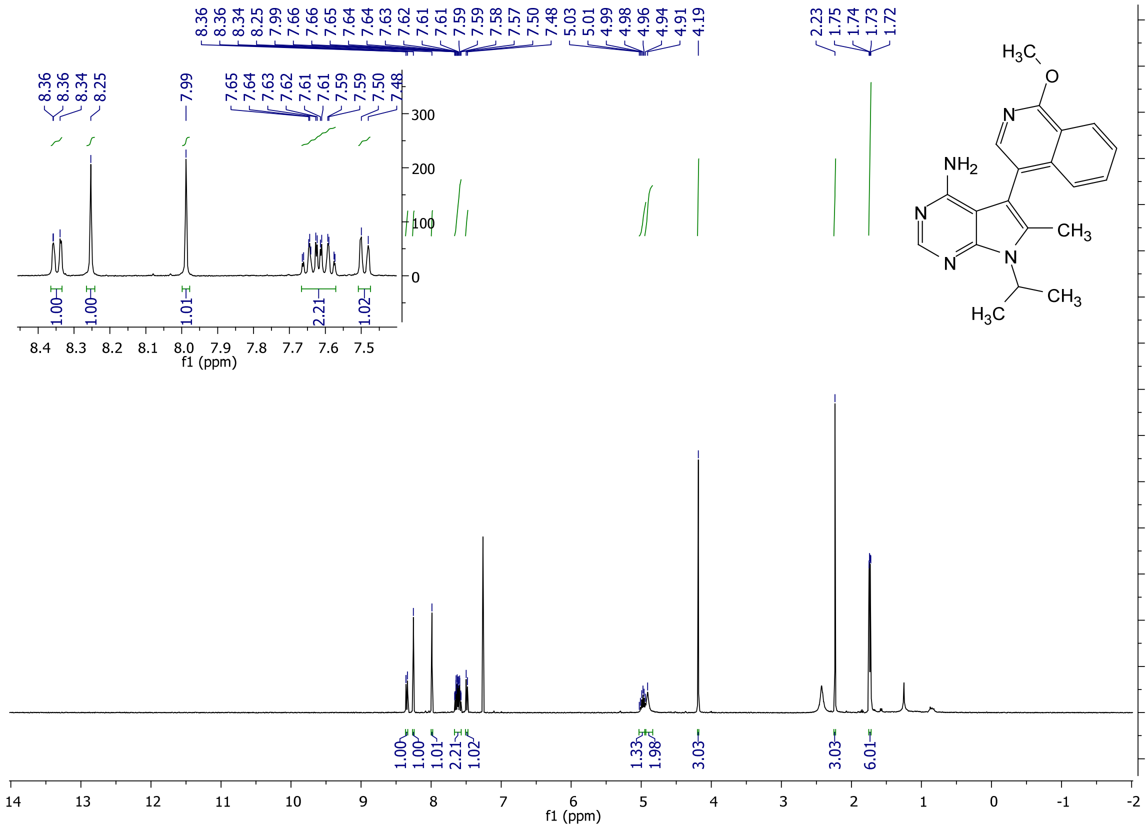
8.36 8.36 8.34 8.25 7.99 7.66 7.66 7.65 7.64 7.64 7.63 7.62 7.61 7.61 7.59 7.59 7.58 7.57 7.50 7.48 5.03 5.01 4.99 4.98 4.96 4.94 4.91 4.19 2.23 1.75 1.74 1.73 1.72
8.36 8.36 8.34 8.25 7.99 7.65 7.64 7.63 7.62 7.61 7.61 7.59 7.59 7.50 7.48
1.00 1.00 1.01 2.21 1.02
8.4 8.3 8.2 8.1 8.0 7.9 7.8 7.7 7.6 7.5
f1 (ppm)
1.00 1.00 1.01 2.21 1.02 1.33 1.98 3.03 3.03 6.01
14 13 12 11 10 9 8 7 6 5 4 3 2 1 0 -1 -2
f1 (ppm)
1500 1400 1300 1200 1100 1000 900 800 700 600 500 400 300 200 100 0 -100
H3C
O
N
NH2
N
N
N
CH3
H3C
CH3

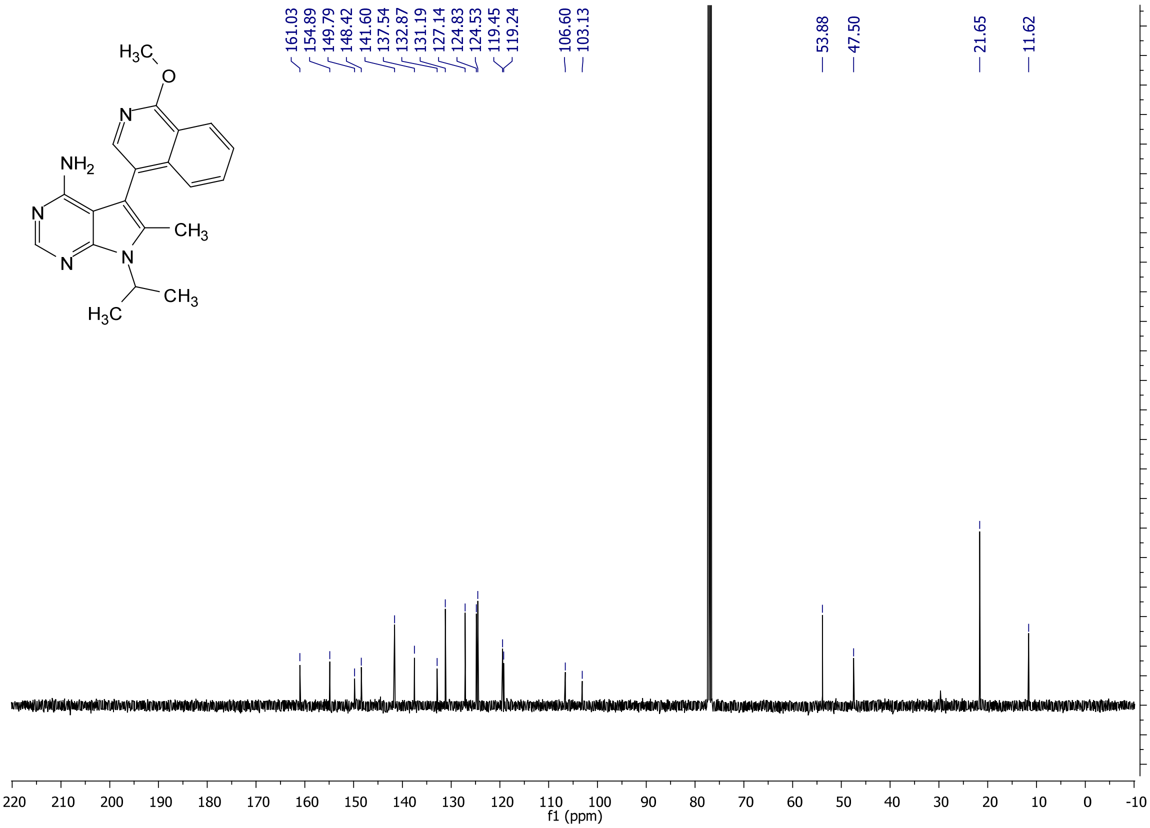
161.03 154.89 149.79 148.42 141.60 137.54 132.87 131.19 127.14 124.83 124.53 119.45 119.24 106.60 103.13 53.88 47.50 21.65 11.62
220 210 200 190 180 170 160 150 140 130 120 110 100 90 80 70 60 50 40 30 20 10 0 -10
f1 (ppm)
2300 2200 2100 2000 1900 1800 1700 1600 1500 1400 1300 1200 1100 1000 900 800 700 600 500 400 300 200 100 0 -100 -200
H3C
O
N
NH2
N
N
N
CH3
H3C
CH3

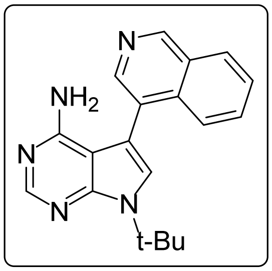

7-(*tert*-butyl)-5-(isoquinolin-4-yl)-7*H*-pyrrolo[2,3-*d*]pyrimidin-4-amine (2.20):

Following the general procedure: **2.20a** (337 mg, 1 mmol, 1 eq.) was dissolved in a 2:1 mixture of dioxane and 28% ammonium hydroxide (35 eq.). The reaction proceeded according to the general procedure. Workup and purification were followed according to the general procedure to afford 213 mg of **2.20** as a white crystalline solid (67% yield).

^{1}H NMR (400 MHz, $CDCl_3$) δ 9.28 (s, 1H), 8.55 (s, 1H), 8.33 (s, 1H), 8.07 (dd, J = 7.6, 1.7 Hz, 1H), 7.85 (d, J = 8.5 Hz, 1H), 7.72 -7.7.67 (m, 2H), 7.22 (s, 1H), 4.94 (s, 2H), 1.85 (s, 9H)

^{13}C NMR (101 MHz, $CDCl_3$) δ 156.29, 152.63, 150.72, 149.50, 144.18, 135.27, 131.36, 128.49, 128.11, 127.94, 125.87, 125.11, 123.03, 108.32, 104.32, 57.73, 29.57

MS (APCI) Calculated: $C_{19}H_{20}N_5$ $[M+H]^+$ 318.2 **Found**: 318.1 m/z

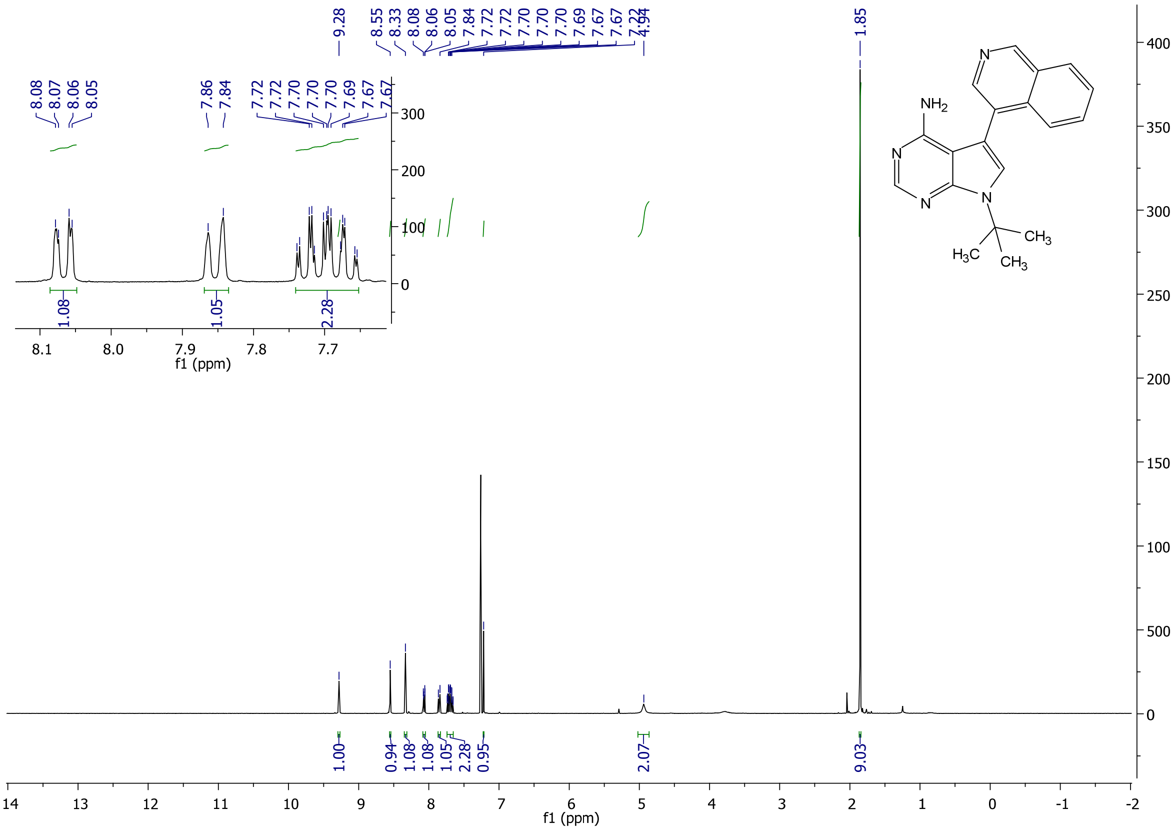
9.28
8.55
8.33
8.08
8.06
8.05
7.84
7.72
7.72
7.70
7.70
7.70
7.69
7.67
7.67
7.22
4.94
1.85
8.08
8.07
8.06
8.05
7.86
7.84
7.72
7.72
7.70
7.70
7.70
7.69
7.67
7.67
300
200
100
0
1.08
1.05
2.28
8.1
8.0
7.9
7.8
7.7
f1 (ppm)
NH2
N
N
N
N
CH3
H3C
CH3
4000
3500
3000
2500
2000
1500
1000
500
0
1.00
0.94
1.08
1.08
1.05
2.28
0.95
2.07
9.03
14
13
12
11
10
9
8
7
6
5
4
3
2
1
0
-1
-2
f1 (ppm)

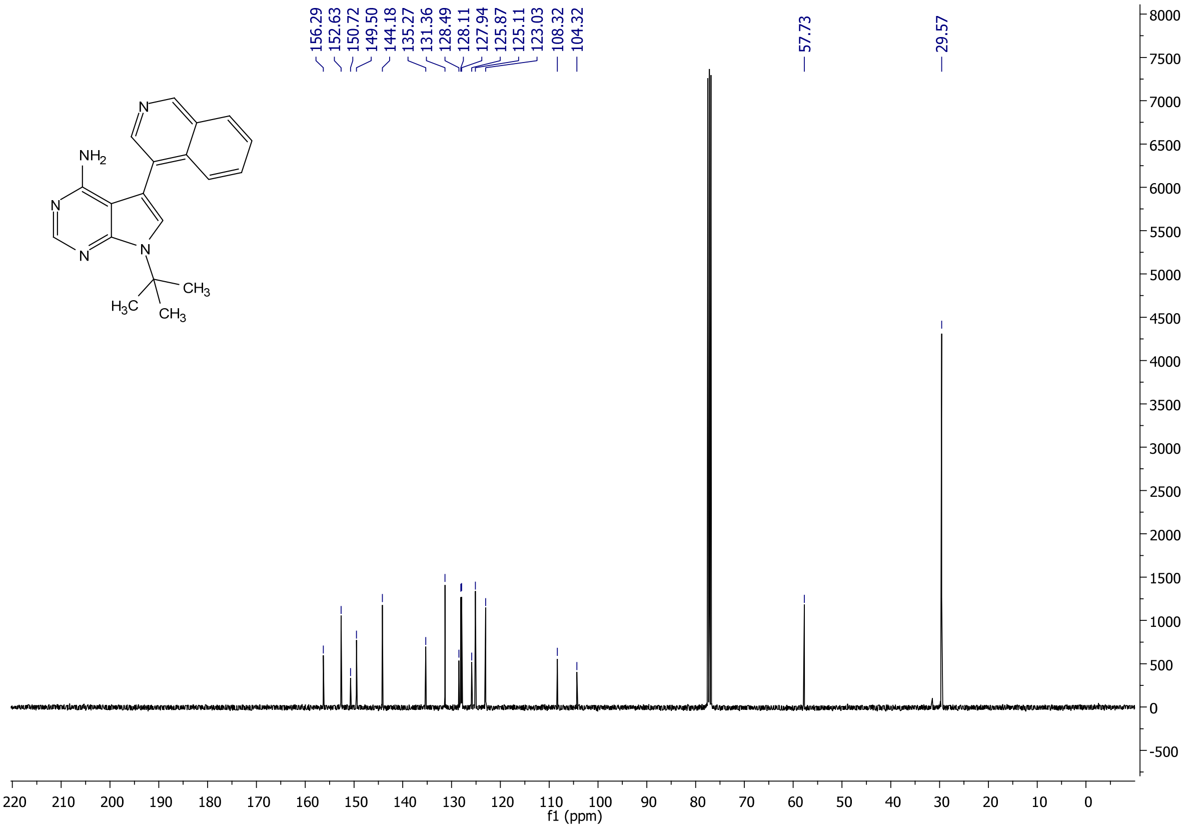
156.29
152.63
150.72
149.50
144.18
135.27
131.36
128.49
128.11
127.94
125.87
125.11
123.03
108.32
104.32
57.73
29.57
NH2
N
N
N
N
CH3
H3C
CH3
8000
7500
7000
6500
6000
5500
5000
4500
4000
3500
3000
2500
2000
1500
1000
500
0
-500
220
210
200
190
180
170
160
150
140
130
120
110
100
90
80
70
60
50
40
30
20
10
0
f1 (ppm)

General procedure for the halogenation of aminated pyrrolopyrimidines (2.1c – 2.20c):

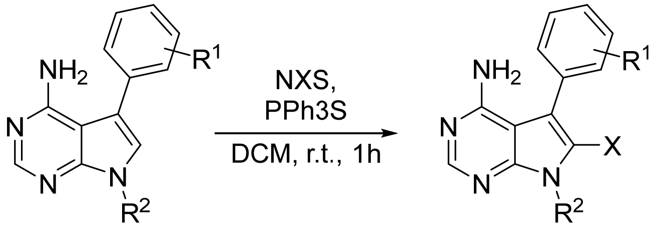

2.1b – **2.20b** was dissolved in dichloromethane (0.1M) at room temperature. Triphenylphosphinesulfide (0.1M) was then added and the reaction mixture was stirred for five minutes followed by the addition of *N*-chlorosuccinimide (NCS) or *N*-bromosuccinimide (NBS) (1.2 equiv). The reaction mixture was then stirred for 8 hours. Upon completion (monitored by TLC), the reaction was partitioned between dichloromethane and sodium hydroxide. The aqueous layer was backwashed 2x with dichloromethane, after which the organic layers were combined and dried with sodium sulfate. The combined organic layers were evaporated and purified by FCC (gradient of hexanes: ethyl acetate 80:20 to 60:40) affording **2.1c – 2.20c** in 49-59% yields.

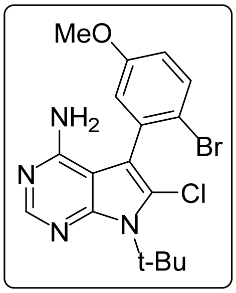

5-(2-bromo-5-methoxyphenyl)-7-(*tert*-butyl)-6-chloro-7*H*-pyrrolo[2,3-*d*]pyrimidin-4-amine (2.1c):

Following the general procedure D: **2.1b** (134.8 mg, .359 mmol, 1.0 eq) was reacted with NCS. Workup and purification was followed according to the general procedure to afford 124mg (84% yield) of **2.1c** as a white solid.

^{1}H NMR (500 MHz, $CDCl_3$) δ 8.23 (s, 1H), 7.61 (d, J = 8.8 Hz, 1H), 6.93 (d, J = 3.0 Hz, 1H), 6.89 (dd, J = 8.8, 3.1 Hz, 1H), 5.17 (s, 2H), 3.82 (s, 3H), 2.00 (s, 9H).

^{13}C NMR (101 MHz, $CDCl_3$) δ 159.13, 154.35, 149.97, 147.44, 134.28, 134.02, 123.18, 117.92, 116.73, 115.93, 113.75, 102.18, 63.23, 55.78, 31.44

MS (APCI) Calculated: $C_{17}H_{19}BrClN_4$**O** $[M+H]^+$ 409.0 **Found:** 408.9

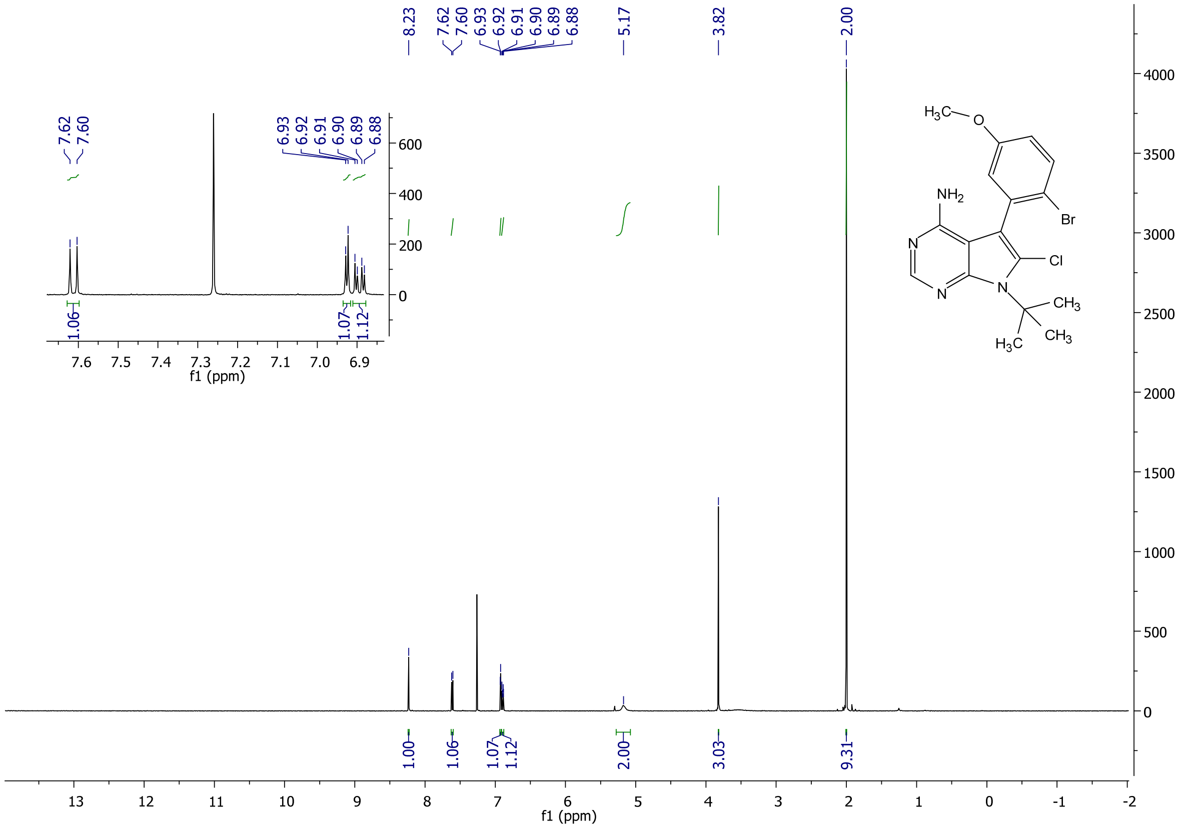

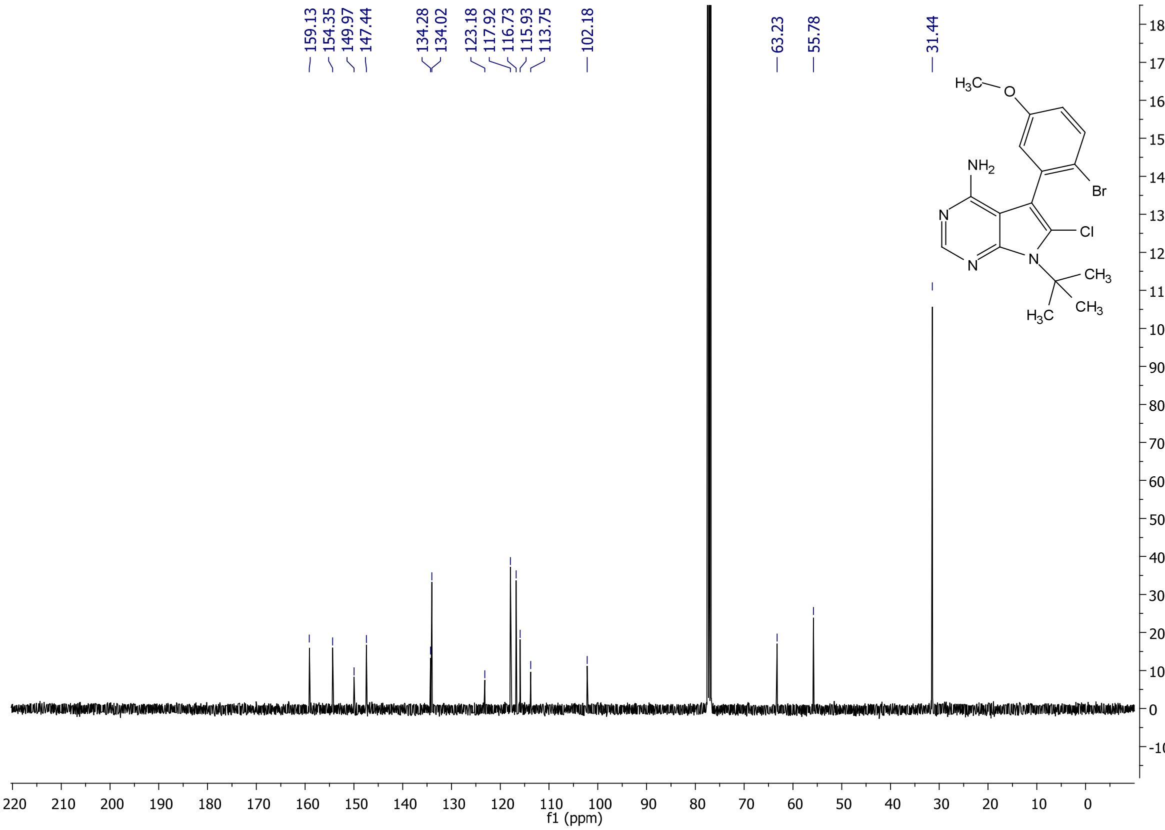
159.13
154.35
149.97
147.44
134.28
134.02
123.18
117.92
116.73
115.93
113.75
102.18
63.23
55.78
31.44
H_3C
O
NH_2
Br
N
Cl
N
N
CH_3
CH_3
H_3C
1800
1700
1600
1500
1400
1300
1200
1100
1000
900
800
700
600
500
400
300
200
100
0
-100
220
210
200
190
180
170
160
150
140
130
120
110
100
90
80
70
60
50
40
30
20
10
0
f1 (ppm)

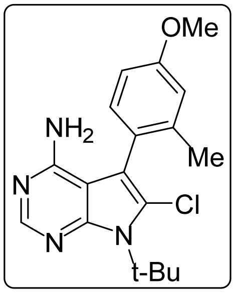

7-(*tert*-butyl)-6-chloro-5-(5-methoxy-2-methylphenyl)-7*H*-pyrrolo[2,3-d]pyrimidin-4-amine (2.2): Following the general procedure D: **2.2b** (108 mg, .351 mmol, 1.0 eq) was reacted with NCS. Workup and purification was followed according to the general procedure to afford 82 mg (68% yield) of **2.2** as a white solid.

^{1}H NMR (400 MHz, $CDCl_3$) δ 8.21 (s, 1H), 7.18 (d, J = 8.3 Hz, 1H), 6.88 (d, J = 2.7 Hz, 1H), 6.82 (dd, J = 8.3, 2.7 Hz, 1H), 4.86 (s, 2H), 3.84 (s, 3H), 2.13 (s, 3H), 1.98 (s, 9H)

^{13}C NMR (101 MHz, $CDCl_3$) δ 159.87, 155.71, 150.58, 149.82, 140.01, 132.20, 124.25, 121.73, 115.91, 112.89, 111.59, 102.81, 62.29, 55.33, 31.44, 20.34

MS (APCI) Calculated: $C_{18}H_{22}ClN_4O$ $[M+H]^+$ 345.2 **Found:** 345.1

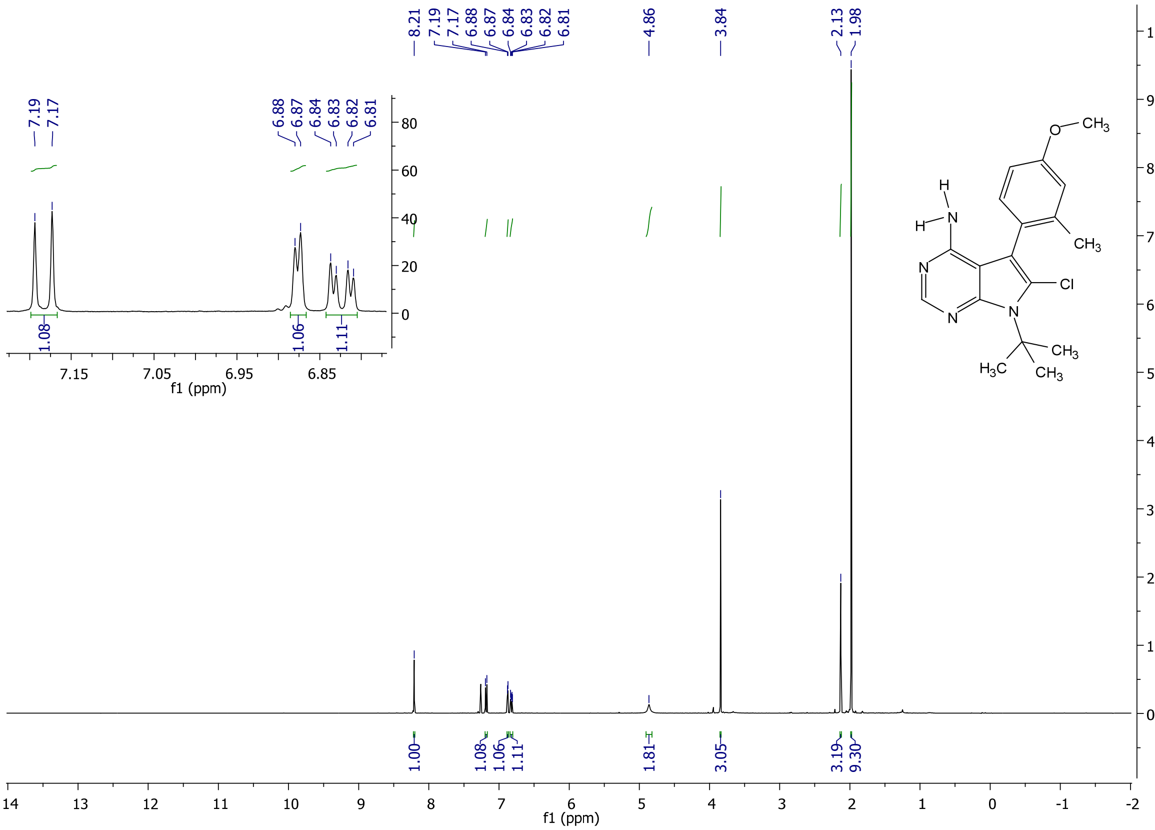
8.21
7.19
7.17
6.88
6.87
6.84
6.83
6.82
6.81
4.86
3.84
2.13
1.98
1.00
1.08
1.06
1.11
1.81
3.05
3.19
9.30
f1 (ppm)
H
H
N
N
N
N
O
CH3
CH3
Cl
CH3
H3C
CH3

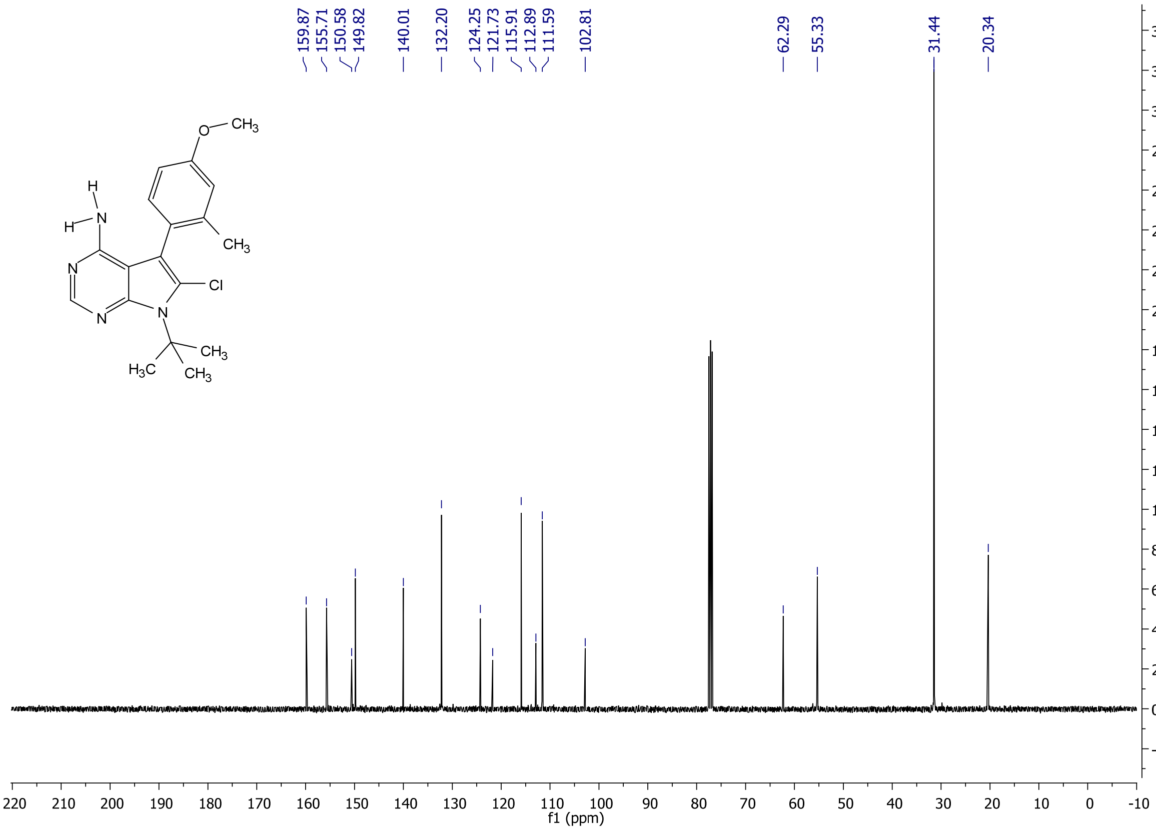
159.87
155.71
150.58
149.82
140.01
132.20
124.25
121.73
115.91
112.89
111.59
102.81
62.29
55.33
31.44
20.34
f1 (ppm)
H
H
N
N
N
N
O
CH3
CH3
Cl
CH3
H3C
CH3

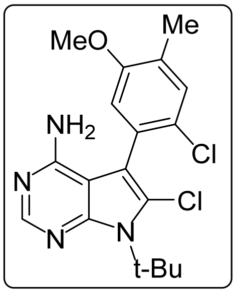

7-(*tert*-butyl)-6-chloro-5-(2-chloro-5-methoxy-4-methylphenyl)-7*H*-pyrrolo[2,3-d]pyrimidin-4-amine (2.3):

Following the general procedure: **2.3b** (80 mg, .232 mmol, 1.0 eq) was reacted with NCS. Workup and purification was followed according to the general procedure to afford 40 mg (45% yield) of **2.3** as a yellowish-orange solid.

^{1}H NMR (400 MHz, $CDCl_3$) δ 8.23 (s, 1H), 7.60 (d, J = 8.8 Hz, 1H), 6.92 (d, J = 3.0 Hz, 1H), 6.89 (dd, J = 8.8, 3.1 Hz, 1H), 4.80 (s, 2H), 3.82 (s, 3H), 2.03 (s, 9H)

^{13}C NMR (101 MHz, $CDCl_3$) δ 159.04, 155.28, 151.73, 149.86, 136.09, 133.85, 118.01, 117.14, 116.56, 116.11, 109.31, 103.32, 62.96, 55.76, 31.79

MS (APCI) Calculated: $C_{18}H_{21}Cl_2N_4O$ $[M+H]^+$ 379.1 **Found:** 379.1

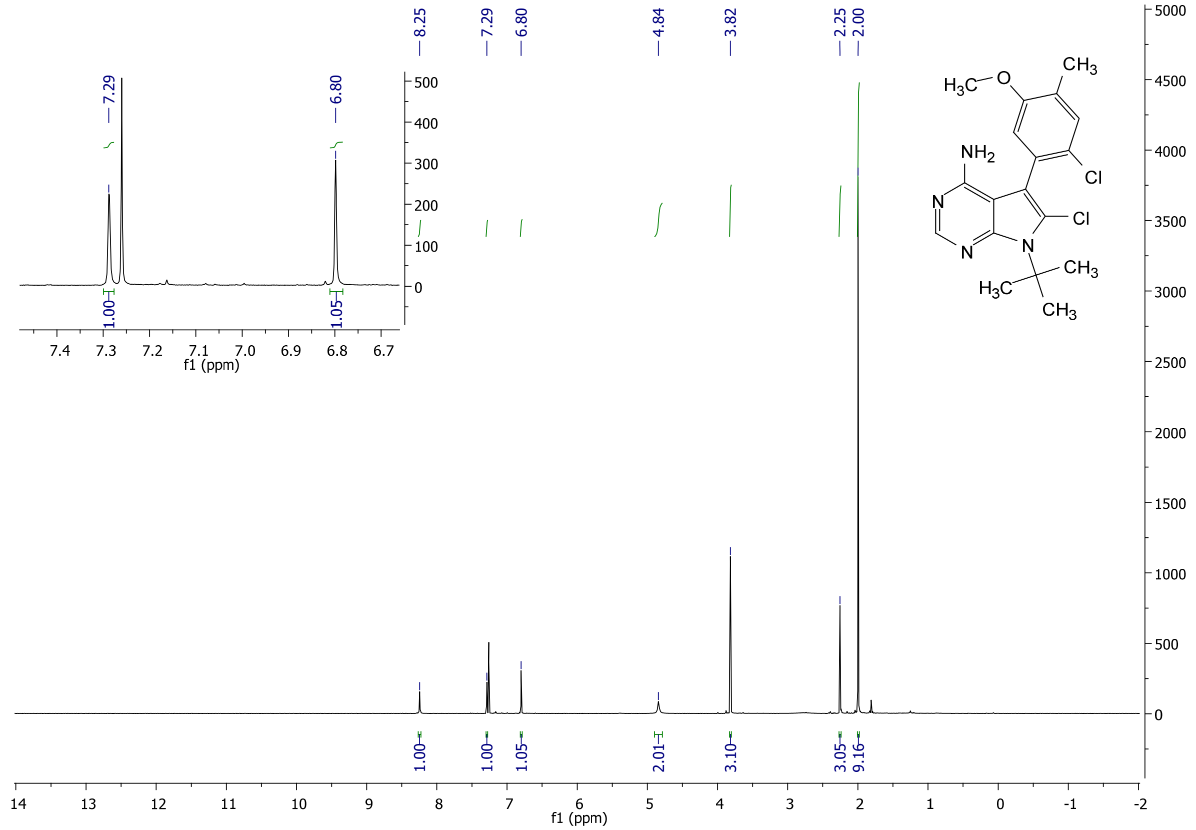

8.25
7.29
6.80
4.84
3.82
2.25
2.00
7.29
6.80
1.00
1.05
7.4 7.3 7.2 7.1 7.0 6.9 6.8 6.7
f1 (ppm)
500 400 300 200 100 0
H3C O CH3
NH2
N
Cl
Cl
N N
H3C CH3
CH3
5000 4500 4000 3500 3000 2500 2000 1500 1000 500 0
1.00 1.00 1.05 2.01 3.10 3.05 9.16
14 13 12 11 10 9 8 7 6 5 4 3 2 1 0 -1 -2
f1 (ppm)

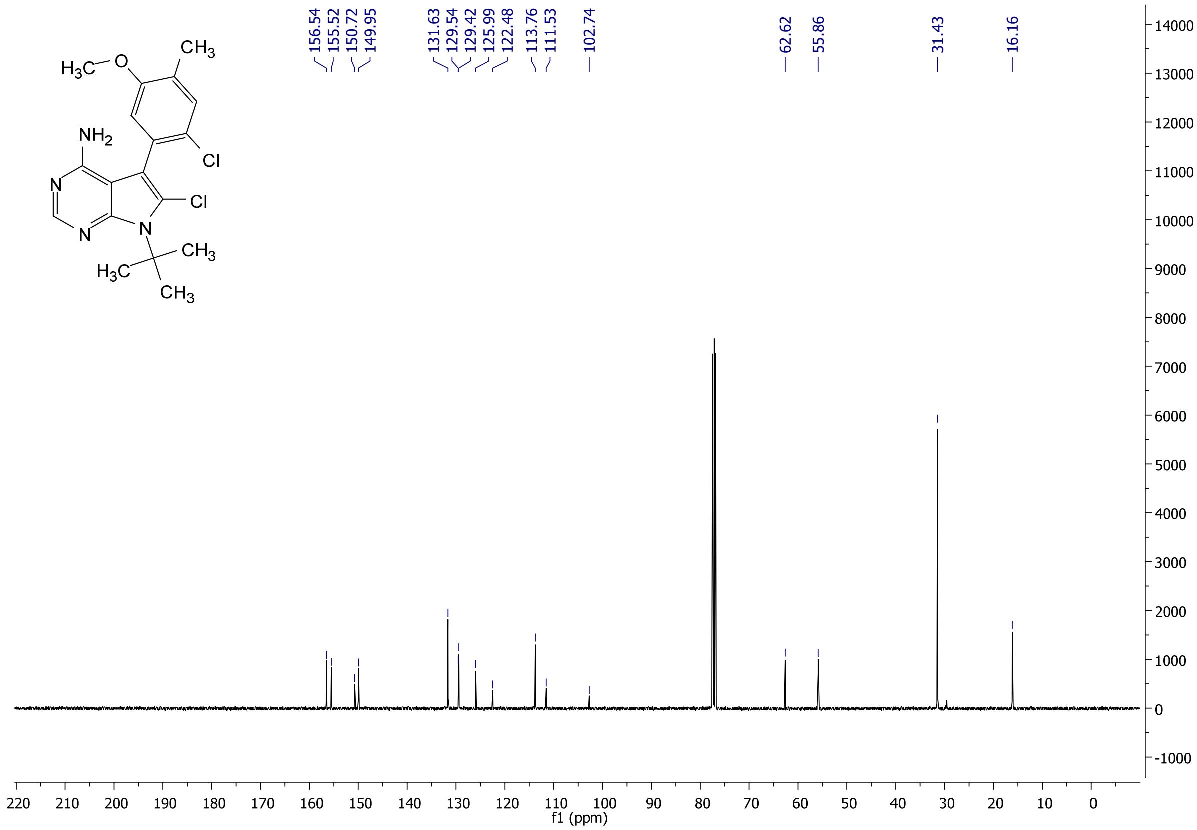

156.54
155.52
150.72
149.95
131.63
129.54
129.42
125.99
122.48
113.76
111.53
102.74
62.62
55.86
31.43
16.16
H3C O CH3
NH2
N
Cl
Cl
N N
H3C CH3
CH3
14000 13000 12000 11000 10000 9000 8000 7000 6000 5000 4000 3000 2000 1000 0 -1000
220 210 200 190 180 170 160 150 140 130 120 110 100 90 80 70 60 50 40 30 20 10 0
f1 (ppm)

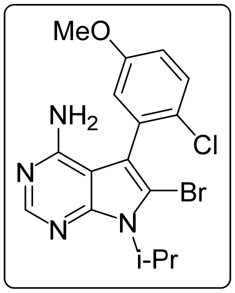

6-bromo-5-(2-chloro-5-methoxyphenyl)-7-isopropyl-7*H*-pyrrolo[2,3-d]pyrimidin-4-amine (2.4c): Following the general procedure: **2.4b** (200 mg, .633 mmol, 1.0 eq) was reacted with NBS. Workup and purification were followed according to the general procedure to afford 123 mg (49% yield) of **2.4c** as a maroon solid.

^{1}H NMR (400 MHz, $CDCl_3$) δ 8.26 (s, 1H), 7.43 (d, J = 8.7 Hz, 1H), 6.94 (m, 2H), 5.11 (dt, J = 14.5, 7.3 Hz, 1H), 4.99 (s, 2H), 3.82 (s, 3H), 1.73 (dd, J = 7.0, 4.7 Hz, 6H).

^{13}C NMR (101 MHz, $CDCl_3$) 158.39, 155.34, 150.54, 150.00, 133.16, 130.89, 126.43, 117.80, 116.19, 112.80, 110.52, 103.26, 55.80, 49.93, 21.38.

MS (APCI) Calculated: $C_{16}H_{17}BrClN_4O$ $[M+H]^+$ 395.0 **Found:** 395.0 m/z

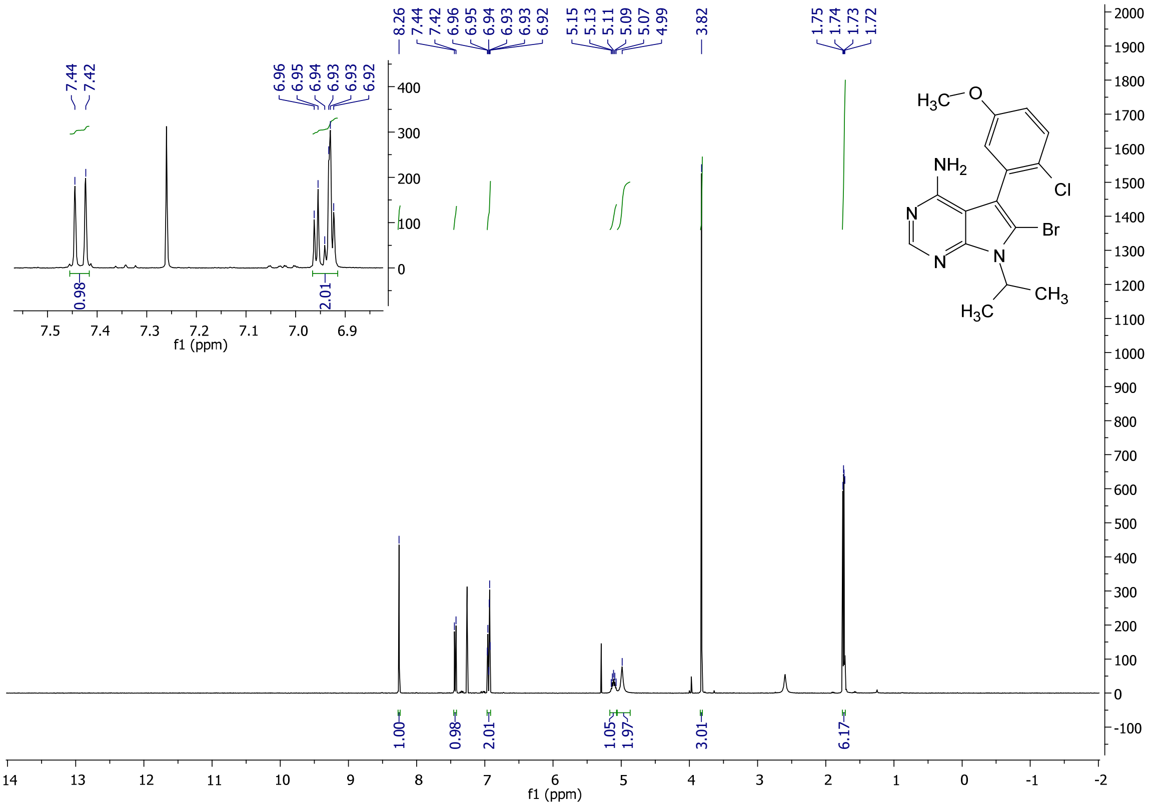
8.26
7.44
7.42
6.96
6.95
6.94
6.93
6.93
6.92
5.15
5.13
5.11
5.09
5.07
4.99
3.82
1.75
1.74
1.73
1.72
1.00
0.98
2.01
1.05
1.97
3.01
6.17
f1 (ppm)
0.98
2.01
f1 (ppm)
H3C
O
NH2
Cl
N
Br
N
N
CH3
H3C

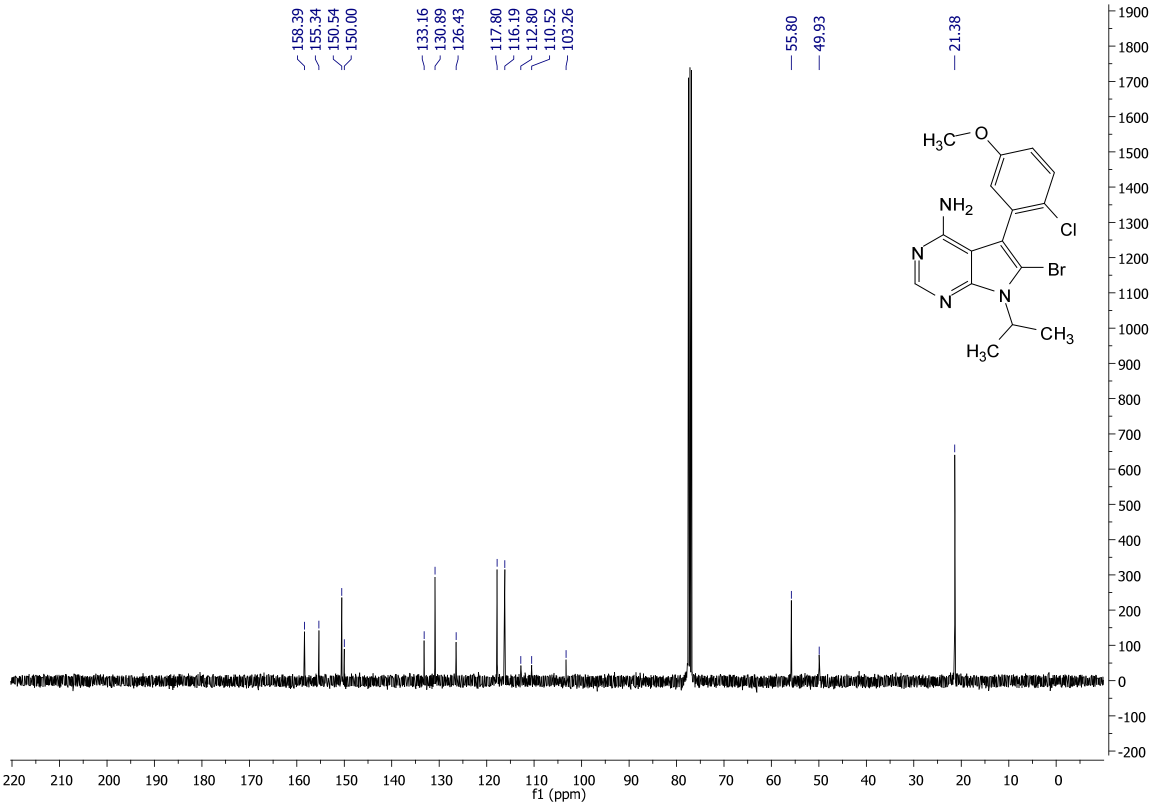
158.39
155.34
150.54
150.00
133.16
130.89
126.43
117.80
116.19
112.80
110.52
103.26
55.80
49.93
21.38
f1 (ppm)
H3C
O
NH2
Cl
N
Br
N
N
CH3
H3C

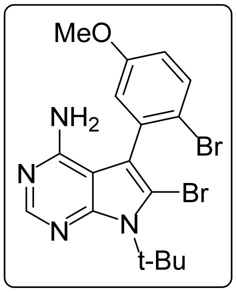

6-bromo-5-(2-bromo-5-methoxyphenyl)-7-(*tert*-butyl)-7*H*-pyrrolo[2,3-d]pyrimidin-4-amine (2.5c): Following the general procedure D: **2.1b** (402 mg, 1.07 mmol, 1.0 eq) was reacted with NBS. Workup and purification was followed according to the general procedure to afford 145 mg (30% yield) of **2.5c** as a yellowish-orange solid.

^{1}H NMR (400 MHz, $CDCl_3$) δ 8.23 (s, 1H), 7.60 (d, J = 8.8 Hz, 1H), 6.92 (d, J = 3.0 Hz, 1H), 6.89 (dd, J = 8.8, 3.1 Hz, 1H), 4.80 (s, 2H), 3.82 (s, 3H), 2.03 (s, 9H)

^{13}C NMR (101 MHz, $CDCl_3$) δ 159.04, 155.28, 151.73, 149.86, 136.09, 133.85, 118.01, 117.14, 116.56, 116.11, 109.31, 103.32, 62.96, 55.76, 31.79

MS (APCI) Calculated: $C_{17}H_{18}Br_2N_4O$ $[M+H]^+$ 452.0 **Found:** 451.9

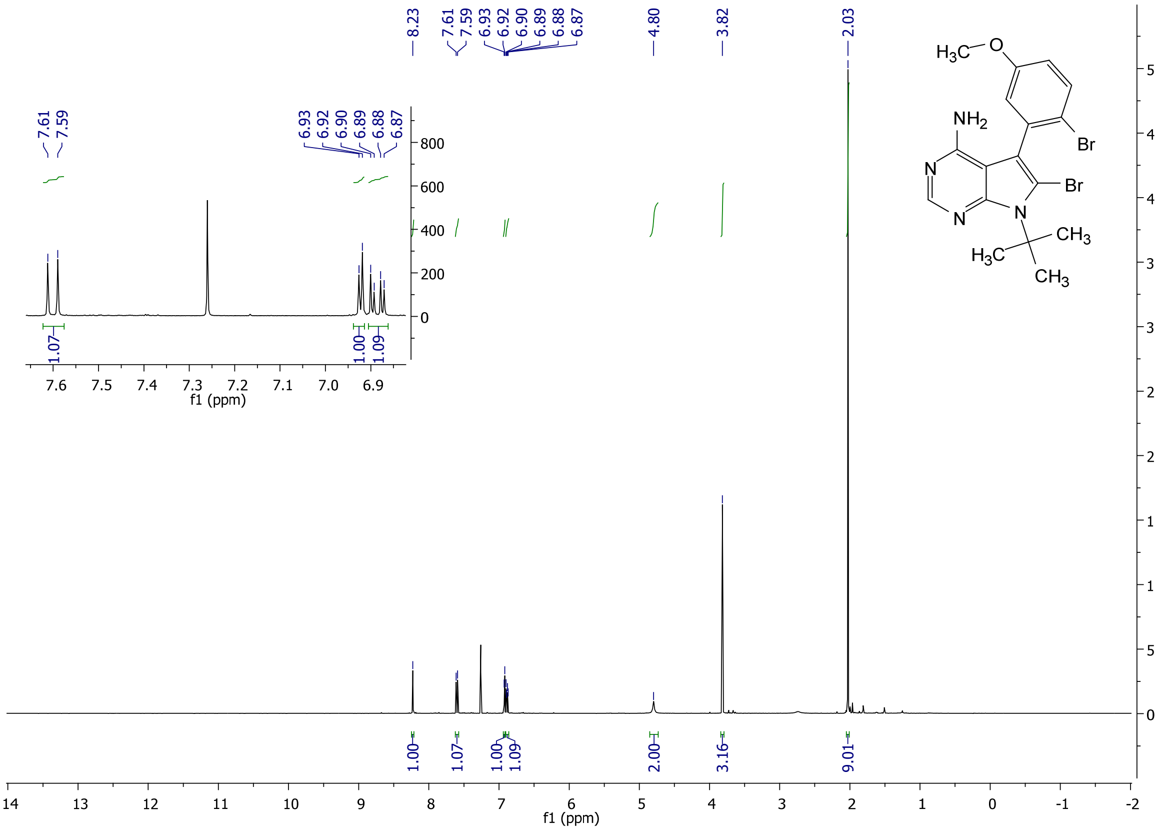
8.23
7.61
7.59
6.93
6.92
6.90
6.89
6.88
6.87
4.80
3.82
2.03
1.00
1.07
1.00
1.09
2.00
3.16
9.01
H3C
O
NH2
Br
N
Br
N
N
CH3
H3C
CH3
f1 (ppm)
14
13
12
11
10
9
8
7
6
5
4
3
2
1
0
-1
-2
5000
4500
4000
3500
3000
2500
2000
1500
1000
500
0
7.6
7.5
7.4
7.3
7.2
7.1
7.0
6.9
800
600
400
200
0

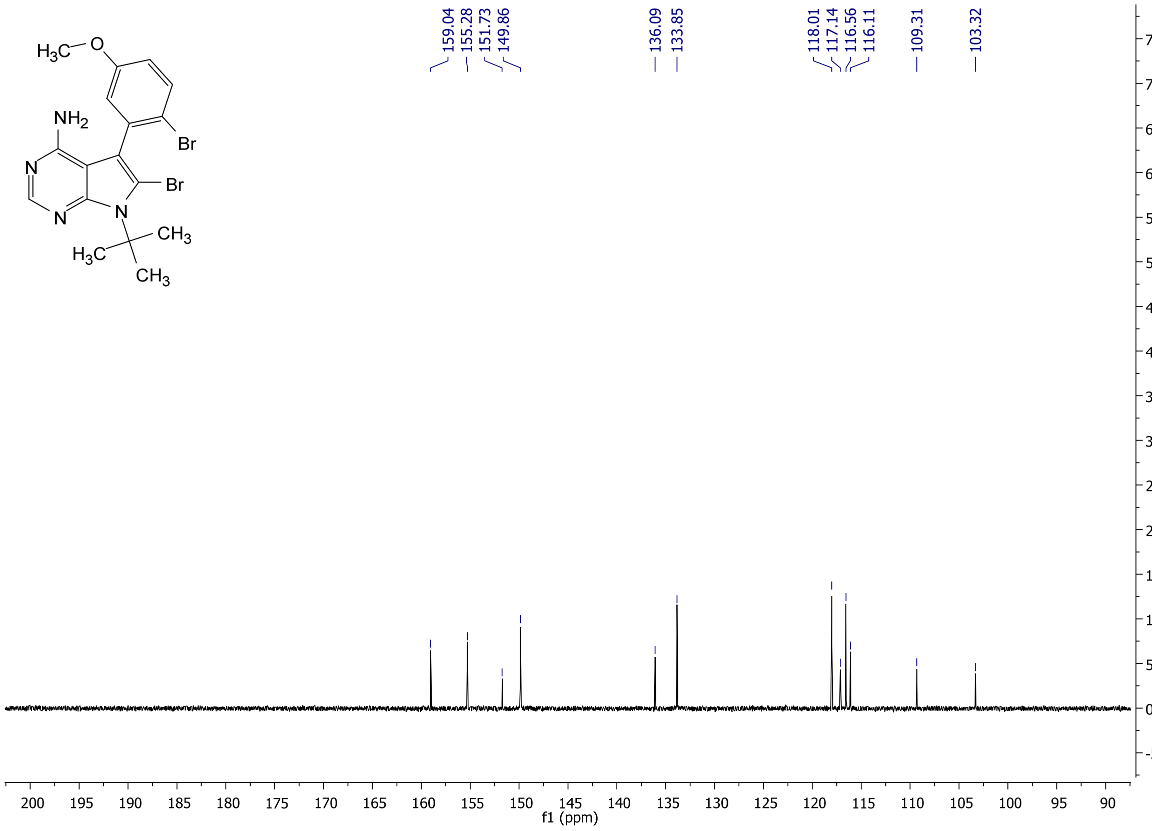
159.04
155.28
151.73
149.86
136.09
133.85
118.01
117.14
116.56
116.11
109.31
103.32
H3C
O
NH2
Br
N
Br
N
N
CH3
H3C
CH3
f1 (ppm)
200
195
190
185
180
175
170
165
160
155
150
145
140
135
130
125
120
115
110
105
100
95
90
7500
7000
6500
6000
5500
5000
4500
4000
3500
3000
2500
2000
1500
1000
500
0
-500

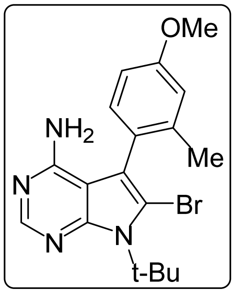

6-bromo-7-(*tert*-butyl)-5-(4-methoxy-2-methylphenyl)-7*H*-pyrrolo[2,3-*d*]pyrimidin-4-amine (2.7c): Following the general procedure D: **2.2b** (52 mg, 0.168 mmol, 1.0 eq) was reacted with NBS. Workup and purification were followed according to the general procedure to afford 20mg (31% yield) of **2.7c** as a brown solid.

^{1}H NMR (500 MHz, $CDCl_3$) δ 8.20 (s, 1H), 7.17 (d, J = 8.3 Hz, 1H), 6.88 (d, J = 2.6 Hz, 1H), 6.83 (dd, J = 8.3, 2.7 Hz, 1H), 4.81 (s, 2H), 3.85 (s, 3H), 2.11 (s, 3H), 2.02 (s, 9H).

^{13}C NMR (101 MHz, $CDCl_3$) δ 159.91, 155.51, 151.67, 149.66, 139.93, 132.24, 125.48, 116.94, 115.90, 111.62, 109.00, 103.59, 62.64, 55.34, 31.81, 20.41

MS (APCI) Calculated: $C_{18}H_{22}BrN_4O$ $[M+H]^+$ 389.1 **Found:** 389.0

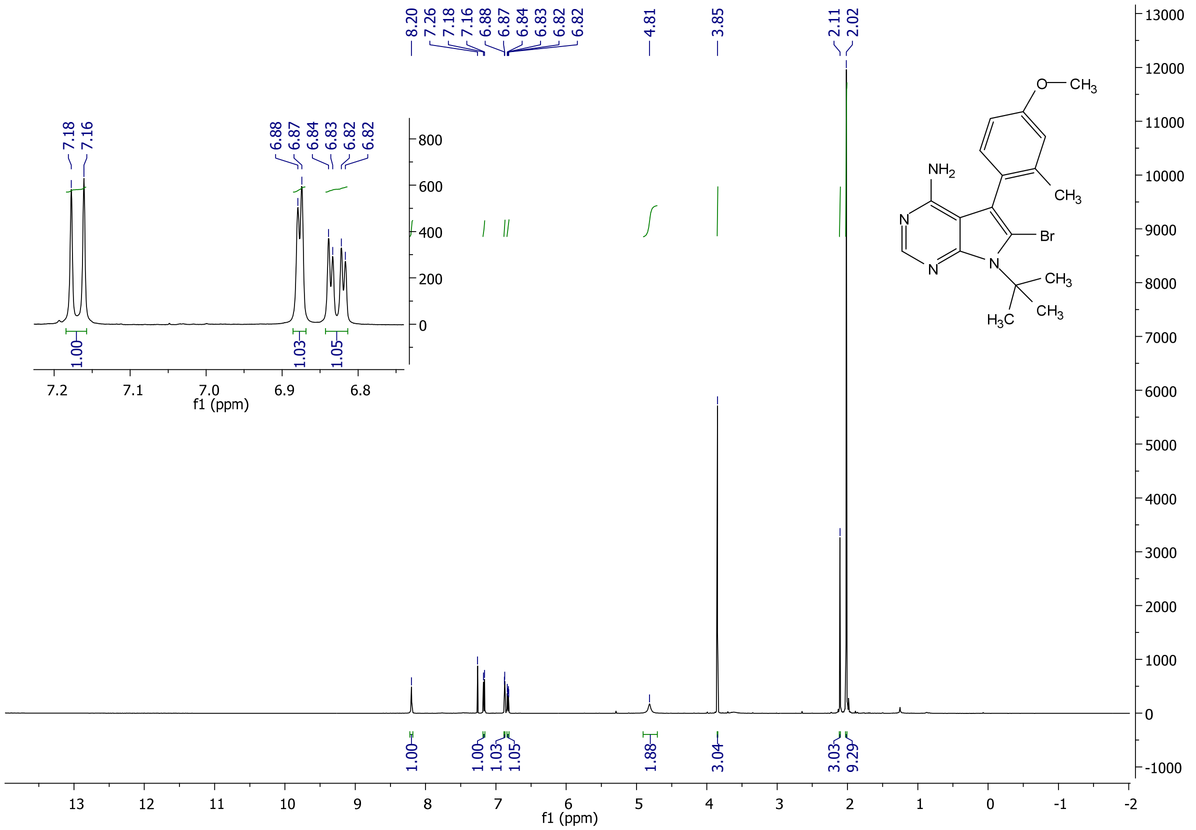
8.20
7.26
7.18
7.16
6.88
6.87
6.84
6.83
6.82
6.82
4.81
3.85
2.11
2.02
1.00
1.00
1.03
1.05
1.88
3.04
3.03
9.29
7.18
7.16
6.88
6.87
6.84
6.83
6.82
6.82
1.00
1.03
1.05
7.2
7.1
7.0
6.9
6.8
f1 (ppm)
800
600
400
200
0
NH$_2$
N
N
N
Br
CH$_3$
O
CH$_3$
CH$_3$
CH$_3$
H$_3$C
13000
12000
11000
10000
9000
8000
7000
6000
5000
4000
3000
2000
1000
0
-1000
13
12
11
10
9
8
7
6
5
4
3
2
1
0
-1
-2
f1 (ppm)

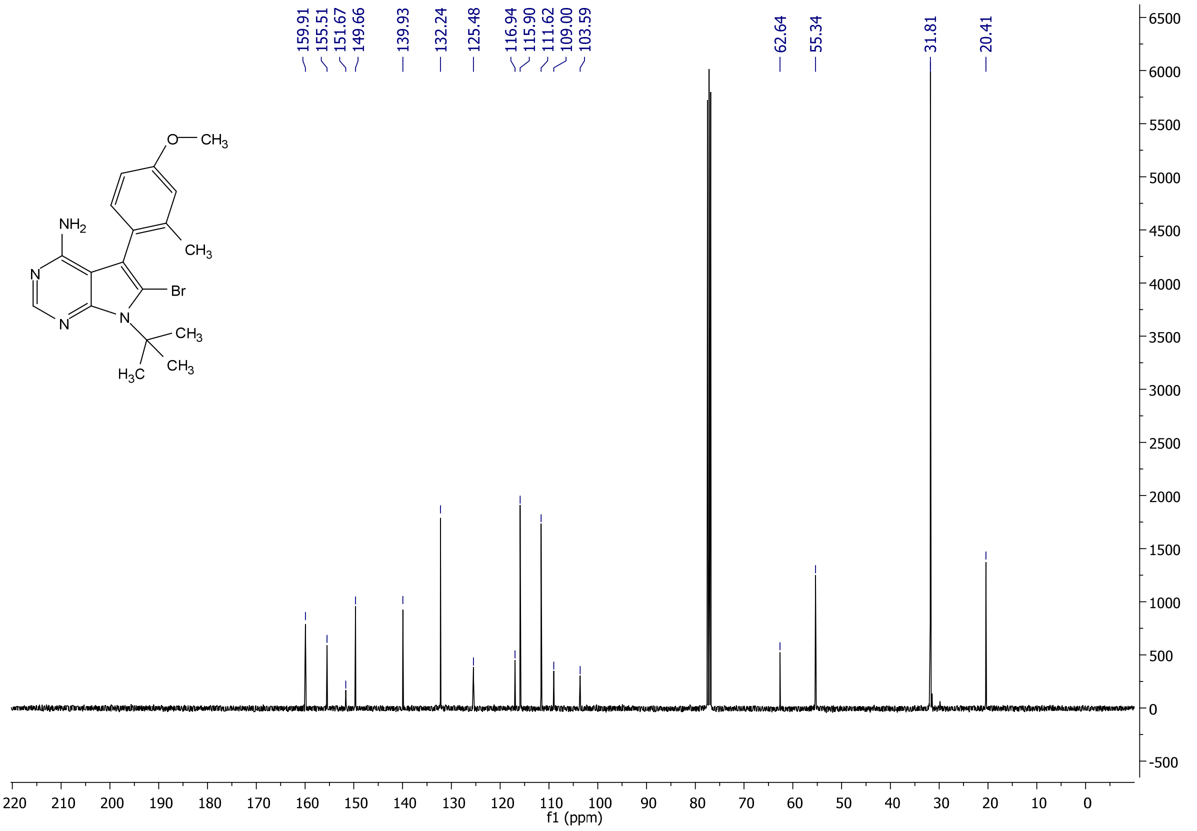
159.91
155.51
151.67
149.66
139.93
132.24
125.48
116.94
115.90
111.62
109.00
103.59
62.64
55.34
31.81
20.41
NH$_2$
N
N
N
Br
CH$_3$
O
CH$_3$
CH$_3$
CH$_3$
H$_3$C
6500
6000
5500
5000
4500
4000
3500
3000
2500
2000
1500
1000
500
0
-500
220
210
200
190
180
170
160
150
140
130
120
110
100
90
80
70
60
50
40
30
20
10
0
f1 (ppm)

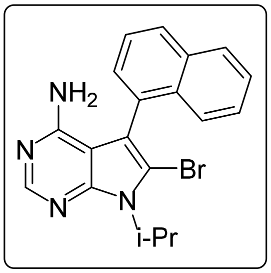

6-bromo-7-isopropyl-5-(naphthalen-1-yl)-7*H*-pyrrolo[2,3-d]pyrimidin-4-amine (2.9c):

Following the general procedure: **2.9b** (900 mg, 2.97 mmol, 1.0 eq) was reacted with NBS. Workup and purification were followed according to the general procedure to afford 670 mg (59% yield) of **2.9c** as a light amber solid.

^{1}H NMR (400 MHz, $CDCl_3$) δ 8.27 (s, 1H), 7.96 (t, J = 9.2 Hz, 2H), 7.61 (t, J = 7.2 Hz, 2H), 7.55-7.50 (m, 2H), 7.50 – 7.45 (m, 1H), 5.23 – 5.14 (m, 1H), 5.07 (s, 2H), 1.79 (t, J = 6.9 Hz, 6H).

^{13}C NMR (101 MHz, $CDCl_3$) δ 155.20, 150.25, 149.99, 133.81, 132.27, 130.60, 129.31, 129.08, 128.48, 126.88, 126.46, 125.83, 125.47, 113.29, 109.99, 103.84, 49.84, 21.33.

MS (APCI) Calculated: $C_{19}H_{18}BrN_4$ $[M+H]^+$ 381.1 **Found:** 381.1 m/z

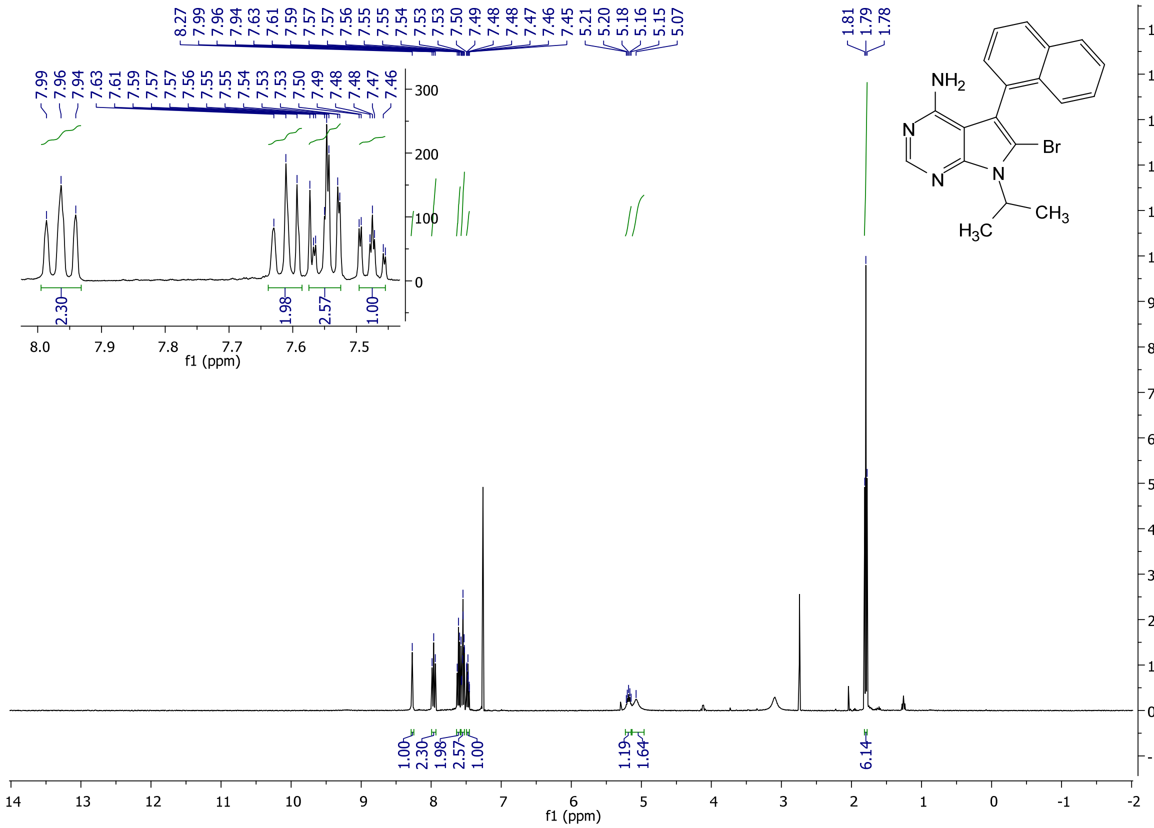
8.27
7.99
7.96
7.94
7.63
7.61
7.59
7.57
7.57
7.56
7.55
7.55
7.54
7.53
7.53
7.50
7.49
7.48
7.48
7.47
7.46
7.45
5.21
5.20
5.18
5.16
5.15
5.07
1.81
1.79
1.78
NH2
N
N
N
Br
CH3
H3C
2.30
1.98
2.57
1.00
8.0
7.9
7.8
7.7
7.6
7.5
f1 (ppm)
300
200
100
0
1.00
2.30
1.98
2.57
1.00
1.19
1.64
6.14
1500
1400
1300
1200
1100
1000
900
800
700
600
500
400
300
200
100
0
-100
14
13
12
11
10
9
8
7
6
5
4
3
2
1
0
-1
-2
f1 (ppm)

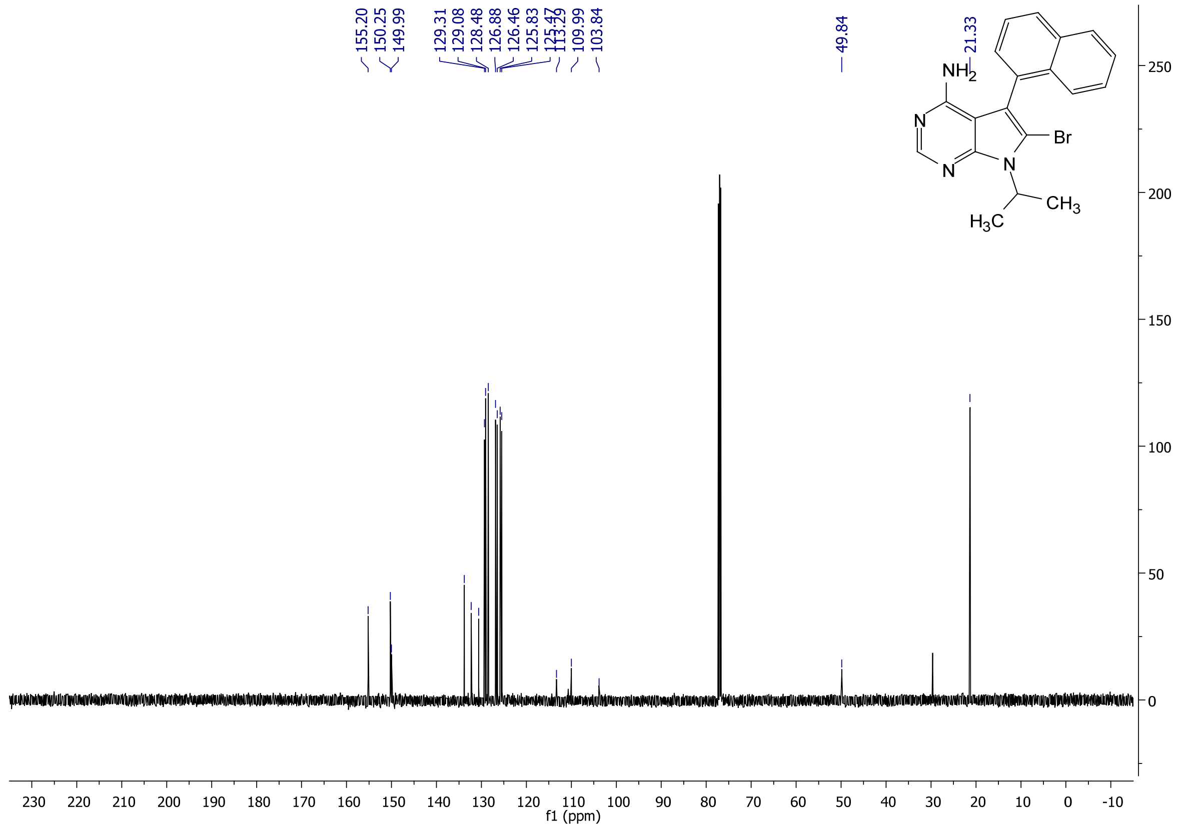
155.20
150.25
149.99
129.31
129.08
128.48
126.88
126.46
125.83
125.47
113.29
109.99
103.84
49.84
21.33
NH2
N
N
N
Br
CH3
H3C
250
200
150
100
50
0
230
220
210
200
190
180
170
160
150
140
130
120
110
100
90
80
70
60
50
40
30
20
10
0
-10
f1 (ppm)

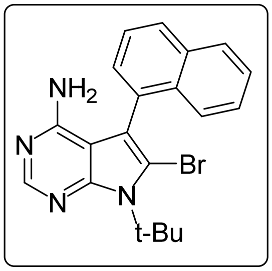

6-bromo-7-(tert-butyl)-5-(naphthalen-1-yl)-7*H*-pyrrolo[2,3-*d*]pyrimidin-4-amine (2.10c):

Following the general procedure: **2.10b** (1.07 g, 3.38 mmol, 1.0 eq) was reacted with NBS. Workup and purification was followed according to the general procedure to afford 358 mg (27% yield) of **2.10c** as a brown-red solid.

^{1}H NMR (400 MHz, $CDCl_3$) δ 8.24 (s, 1H), 7.98 – 7.91 (m, 2H), 7.61 – 7.50 (m, 4H), 7.45 (ddd, J = 8.1, 6.9, 1.2 Hz, 1H), 4.55 (s, 2H), 2.08 (s, 9H)

^{13}C NMR (101 MHz, $CDCl_3$) δ 155.65, 152.07, 150.40, 133.84, 132.58, 131.70, 129.46, 129.10, 128.52, 126.92, 126.52, 126.05, 125.57, 115.62, 109.62, 104.29, 62.82, 31.86

MS (APCI) Calculated: $C_{20}H_{20}BrN_4$ $[M+H]^+$ 395.1 **Found:** 395.0

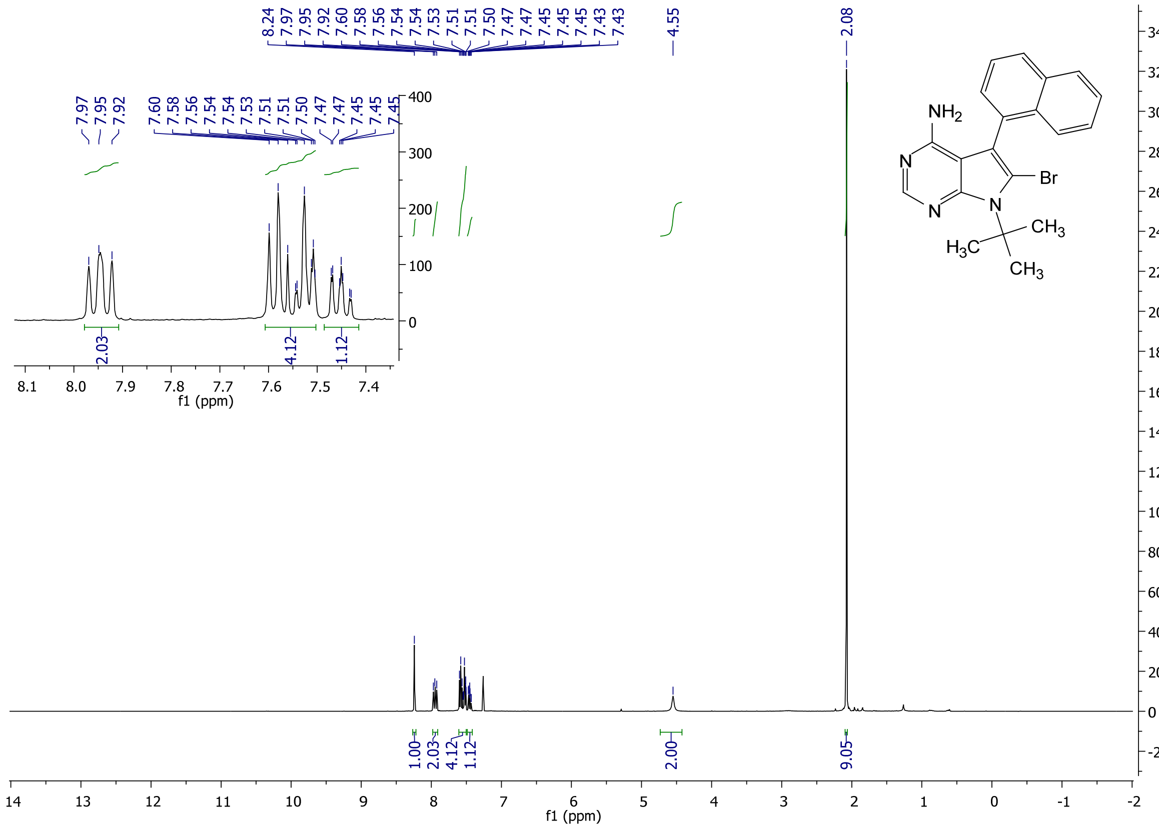
8.24
7.97
7.95
7.92
7.60
7.58
7.56
7.54
7.54
7.53
7.51
7.51
7.50
7.47
7.47
7.45
7.45
7.45
7.43
7.43
4.55
2.08
1.00
2.03
4.12
1.12
2.00
9.05
f1 (ppm)
NH2
N
N
N
Br
CH3
H3C
CH3

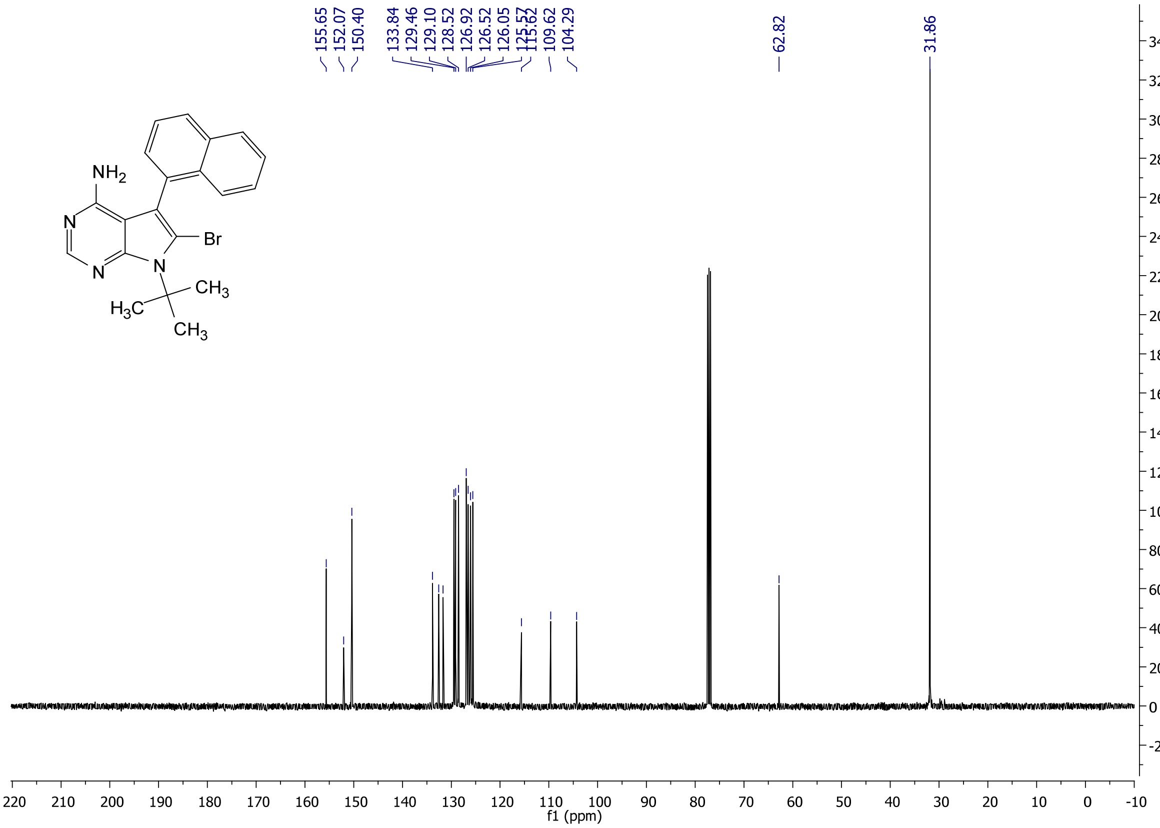
155.65
152.07
150.40
133.84
129.46
129.10
128.52
126.92
126.52
126.05
125.57
115.62
109.62
104.29
62.82
31.86
f1 (ppm)
NH2
N
N
N
Br
CH3
H3C
CH3

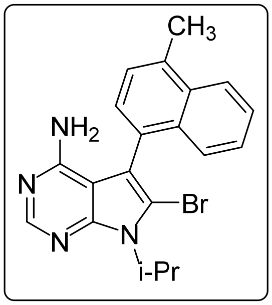

6-bromo-7-isopropyl-5-(4-methylnaphthalen-1-yl)-7*H*-pyrrolo[2,3-*d*]pyrimidin-4-amine (2.14c): Following the general procedure: **2.14b** (600 mg, 1.816 mmol, 1.0 eq) was reacted with NBS. Workup and purification were followed according to the general procedure to afford 451 mg (63% yield) of **2.14c** as a yellowish-orange solid.

^{1}H NMR (400 MHz, $CDCl_3$) δ 8.26 (s, 1H), 8.10 (d, J = 7.7 Hz, 1H), 7.65 – 7.55 (m, 2H), 7.47 (t, J = 8.4 Hz, 1H), 7.43 (s, 2H), 5.21 – 5.13 (m, 1H), 5.02 (s, 2H), 2.78 (s, 3H), 1.79 (t, J = 7.9 Hz, 6H).

^{13}C NMR (101 MHz, $CDCl_3$) δ 154.76, 149.73, 149.01, 135.96, 133.10, 132.29, 129.16, 128.51, 126.72, 126.49, 126.38, 124.86, 113.98, 103.91, 50.20, 21.49, 21.46, 19.82.

MS (APCI) Calculated: $C_{20}H_{20}BrN_4$ $[M+H]^+$ 395.1 **Found:** 395.0

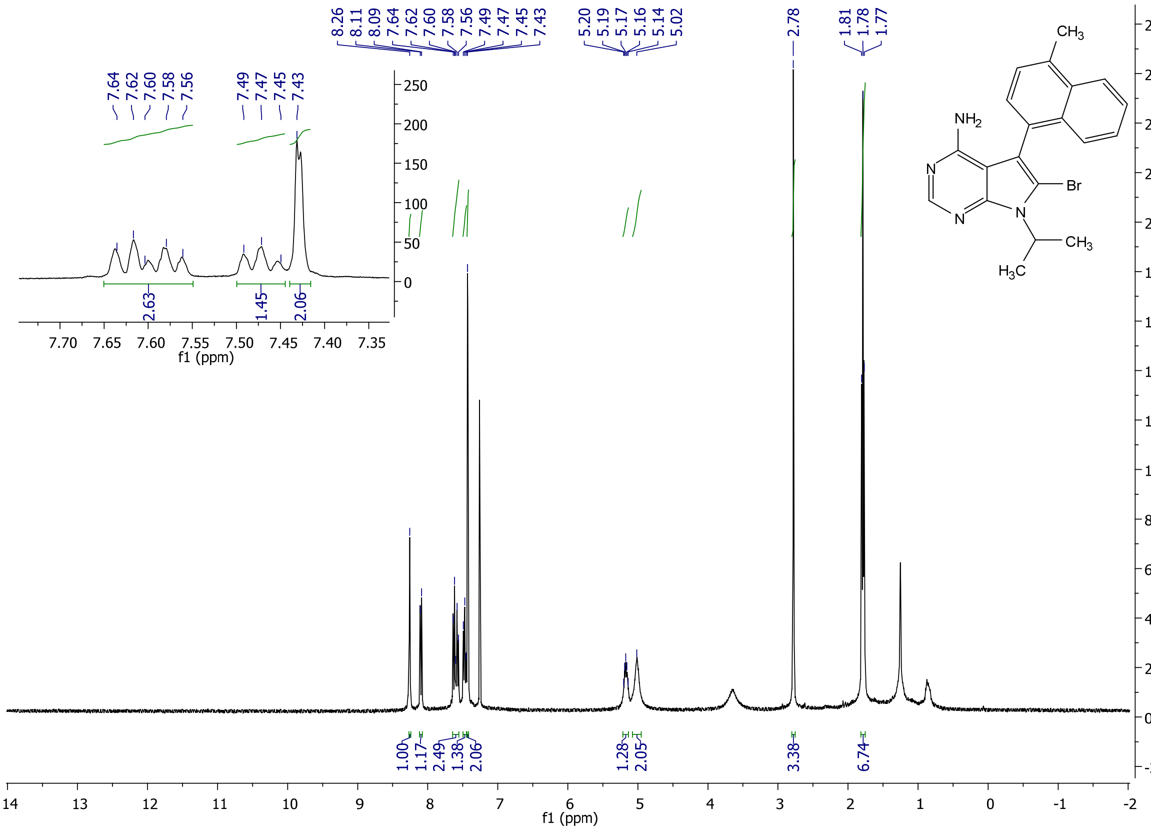
8.26
8.11
8.09
7.64
7.62
7.60
7.58
7.56
7.49
7.47
7.45
7.43
5.20
5.19
5.17
5.16
5.14
5.02
2.78
1.81
1.78
1.77
7.64
7.62
7.60
7.58
7.56
7.49
7.47
7.45
7.43
2.63
1.45
2.06
7.70 7.65 7.60 7.55 7.50 7.45 7.40 7.35
f1 (ppm)
250
200
150
100
50
0
CH3
NH2
N
N
N
Br
CH3
H3C
1.00
1.17
2.49
1.38
2.06
1.28
2.05
3.38
6.74
14 13 12 11 10 9 8 7 6 5 4 3 2 1 0 -1 -2
f1 (ppm)
280
260
240
220
200
180
160
140
120
100
80
60
40
20
0
-20

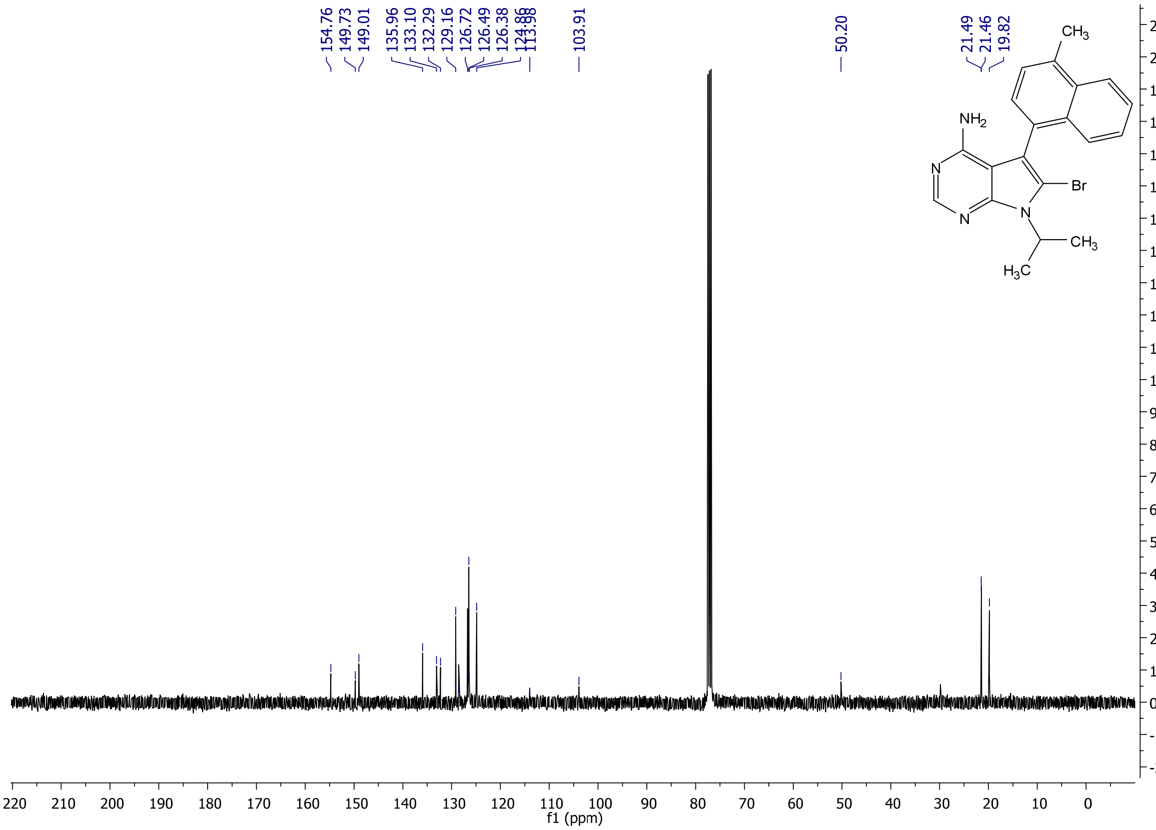
154.76
149.73
149.01
135.96
133.10
132.29
129.16
126.72
126.49
126.38
124.86
113.98
103.91
50.20
21.49
21.46
19.82
CH3
NH2
N
N
N
Br
CH3
H3C
220 210 200 190 180 170 160 150 140 130 120 110 100 90 80 70 60 50 40 30 20 10 0
f1 (ppm)
2100
2000
1900
1800
1700
1600
1500
1400
1300
1200
1100
1000
900
800
700
600
500
400
300
200
100
0
-100
-200

General procedure for the 6-cyano pyrrolopyrimidines (2.8e):

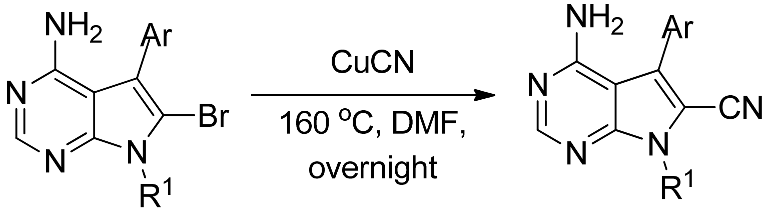

A microwave reaction vessel equipped with **2.7c** (1 equiv.), CuCN (3 equiv.), and a stir bar was placed in a round bottom and evacuated and backfilled with argon. The solids were dissolved with degassed DMF (0.08M) and heated in the microwave at 180ºC for 1 hour. The reaction mixture was cooled to room temperature and partitioned in a 1:1 mixture of aqueous LiCl (5%) and ethyl acetate. The aqueous layer was backwashed two more times with ethyl acetate, and the combined organic layers were dried with sodium sulfate and concentrated. The resulting crude mixture was purified by FCC (Hexanes:Ethyl Acetate 80:20 to 60:40), affording **2.8d** in 70-90% yields.

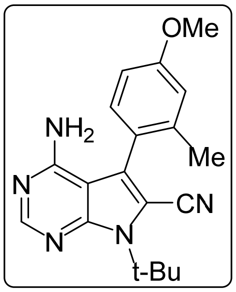

4-amino-7-(*tert*-butyl)-5-(4-methoxy-2-methylphenyl)-7*H*-pyrrolo[2,3-d]pyrimidine-6-carbonitrile (2.8d):

Following the general procedure: **2.7c** (100 mg, .258 mmol, 1 equiv.), CuCN (3 equiv.), and a stir bar was evacuated and backfilled with argon. The solids were dissolved with degassed DMF (0.08M) and the reaction proceeded according to the general procedure. Workup and purification were followed according to the general procedure to afford 80 mg (92% yield) of **2.8d** as a brown solid.

^{1}H NMR (400 MHz, $CDCl_3$) δ 8.30 (s, 1H), 7.23 (d, J = 8.4 Hz, 1H), 6.89 (d, J = 2.6 Hz, 1H), 6.84 (dd, J = 8.4, 2.6 Hz, 1H), 5.39 (s, 2H), 3.84 (s, 3H), 2.18 (s, 3H), 1.97 (s, 9H)

^{13}C NMR (101 MHz, $CDCl_3$) δ 160.42, 158.08, 153.87, 151.51, 139.14, 131.61, 129.19, 122.54, 116.39, 114.94, 111.98, 104.61, 102.98, 61.54, 55.35, 30.50, 20.28

MS (APCI) Calculated: $C_{19}H_{22}N_5O$ $[M+H]^+$ 336.2 **Found:** 336.1

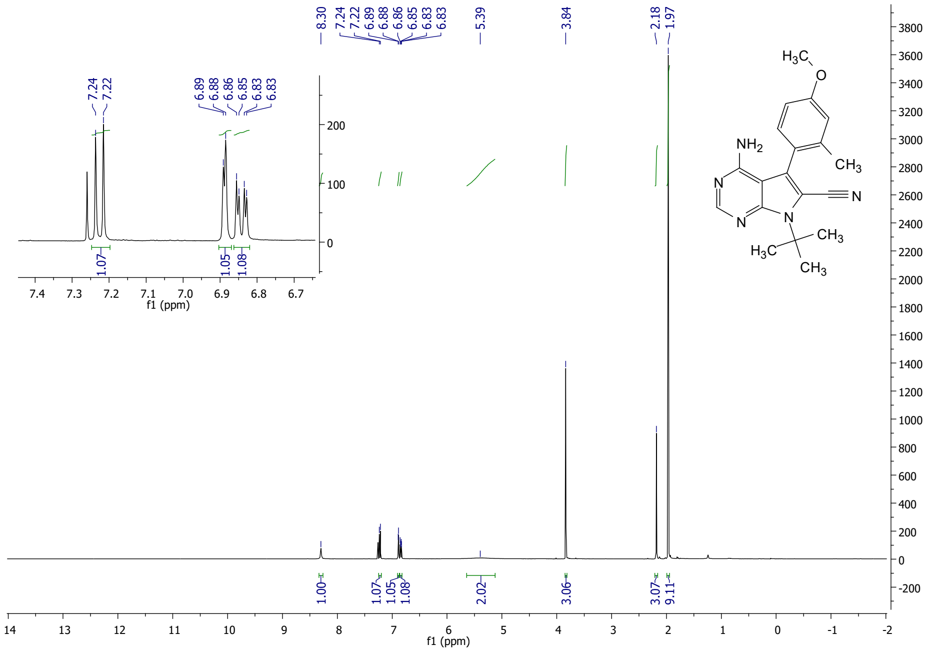

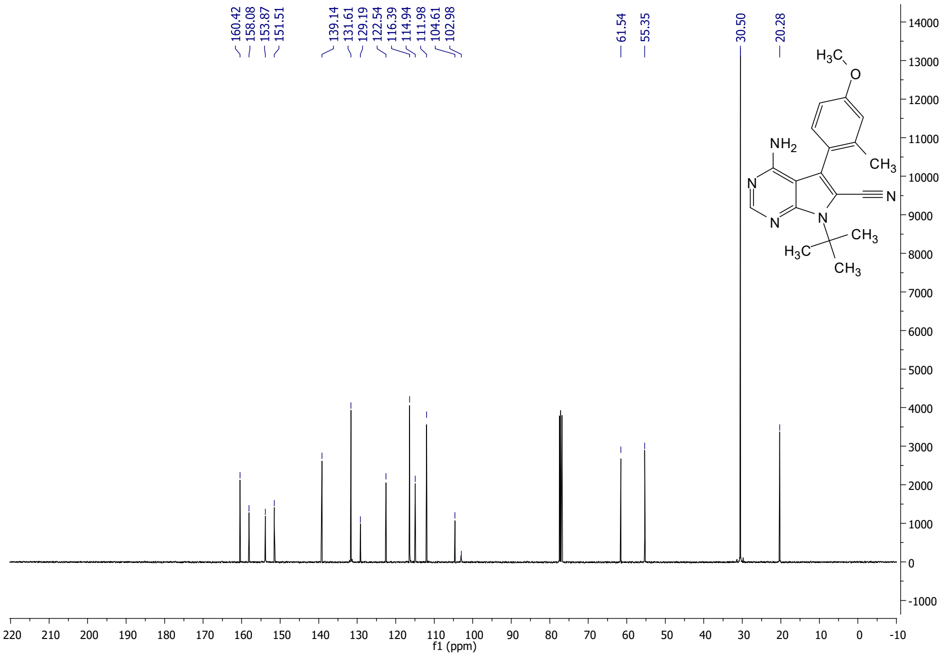

General procedure for the 6-aminomethylated pyrrolopyrimidines (2.8):

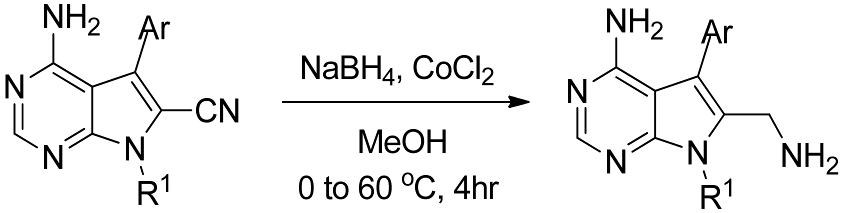

2.8d and cobalt (II) chloride (2 equiv.) were stirred in a solution of Methanol (0.1M) and cooled to 0ºC. Sodium borohydride was added in portions to the reaction mixture over 5min. The reaction mixture was then heated to 60 minutes and stirred for 4 hours. The methanol was then evaporated, and the resulting residue was partitioned between ethyl acetate and brine (1:1).

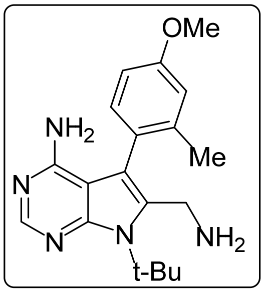

6-(aminomethyl)-7-(*tert*-butyl)-5-(4-methoxy-2-methylphenyl)-7*H*-pyrrolo[2,3-d]pyrimidin-4-amine (2.8): Following the general procedure: **2.8d** (80 mg, .237 mmol, 1 equiv.), $CoCl_2$ (2 equiv.), and a stir bar was evacuated and backfilled with argon. The solids were dissolved with dry MeOH (0.1M) and after cooling to 0ºC, $NaBH_4$ (5 equiv.) was added. Workup and purification were followed according to the general procedure to afford 7 mg (9% yield) of **2.8** as a brown solid.

MS (APCI) Calculated: $C_{22}H_{23}N_5$ $[M+H]^+$ 339.4 **Found**: 339.4

General procedure for the boc-protected pyrrolopyrimidines (2.1d – 2.20d):

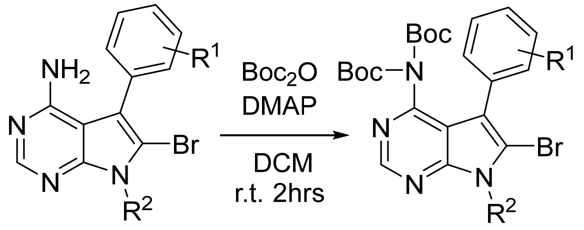

2.1c – **2.20c** (1 equiv.) and DMAP (0.1 equiv) were dissolved in DCM in a vial equipped with a stir bar. Boc_2O (3 equiv.) was then added slowly to the stirring reaction mixture and stirred for 2 hours at room temperature. Upon completion the solvent was removed and the crude mixture was purified using FCC (gradient of hexanes: ethyl acetate 95:5 to 90:10) to yield **2.1d** – **2.20d** (62-79%).

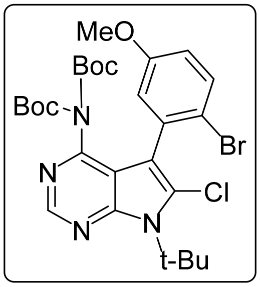

Boc-protected 5-(2-bromo-5-methoxyphenyl)-7-(*tert*-butyl)-6-chloro-7*H*-pyrrolo[2,3-*d*]pyrimidin-4-amine (2.1d):

Following the general procedure: **2.1c** (145 mg, .354 mmol, 1.0 eq) was reacted with DMAP and Boc_2O in DCM. Workup and purification was followed according to the general procedure to afford 200 mg (93% yield) of **2.1d** as a white solid.

^{1}H NMR (400 MHz, $CDCl_3$) δ 8.77 (s, 1H), 7.53 (d, J = 8.8 Hz, 1H), 6.91 (d, J = 3.0 Hz, 1H), 6.83 (dd, J = 8.8, 3.1 Hz, 1H), 3.77 (s, 3H), 2.02 (s, 9H), 1.41 (s, 9H), 1.31 (s, 9H)

^{13}C NMR (101 MHz, $CDCl_3$) δ 158.68, 153.54, 151.26, 150.56, 149.85, 133.84, 133.41, 133.36, 129.05, 118.77, 116.44, 115.34, 114.74, 112.94, 83.53, 83.42, 63.30, 55.59, 31.41, 28.05, 27.94

MS (APCI) Calculated: $C_{27}H_{35}BrClN_4O_5$ $[M+H]^+$ 609.2 **Found:** 609.1

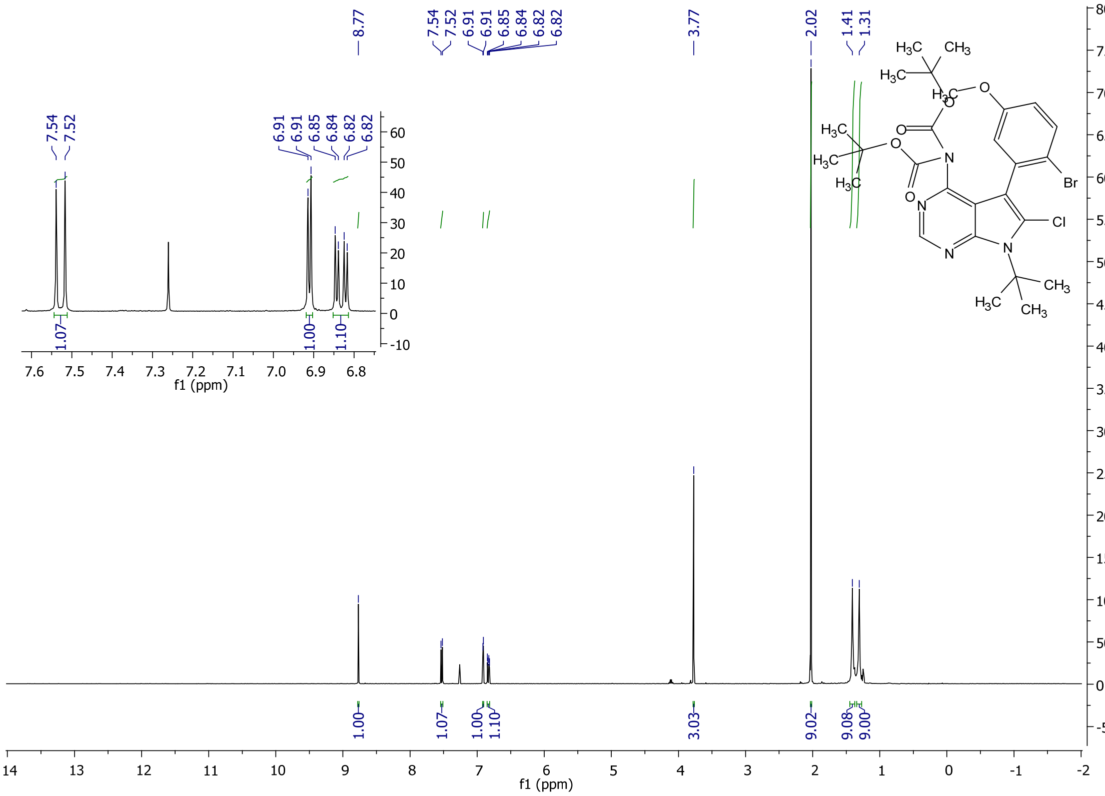

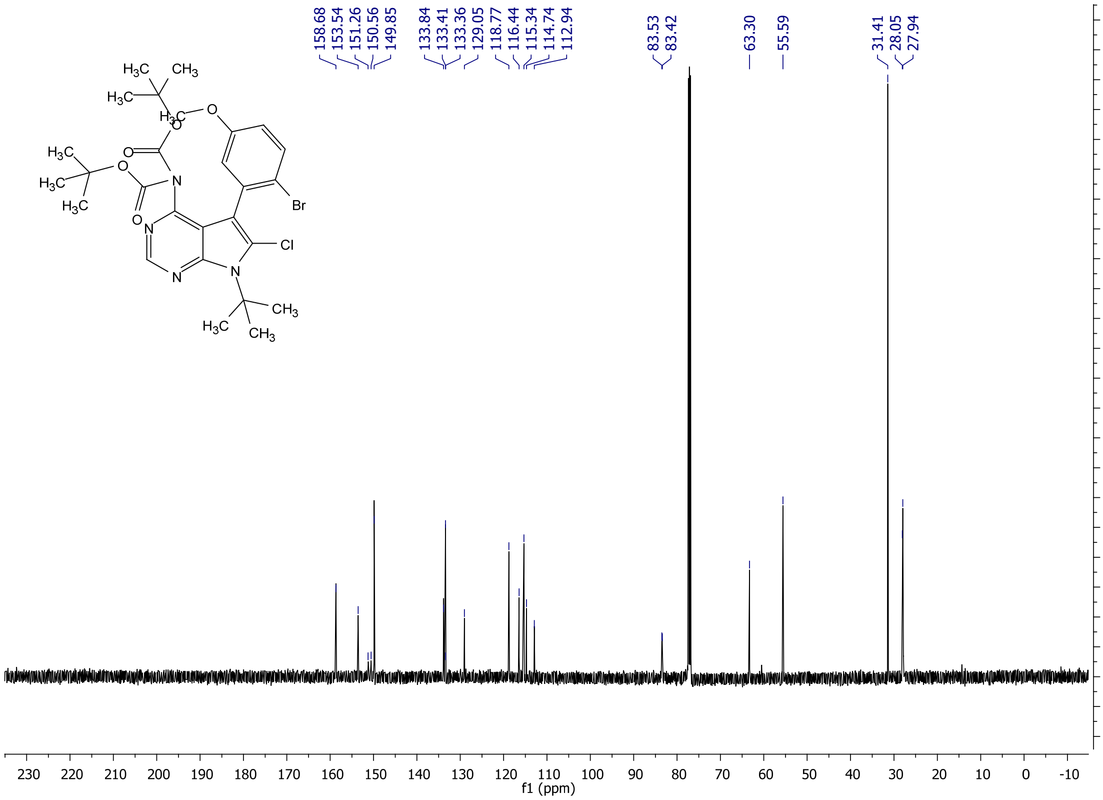

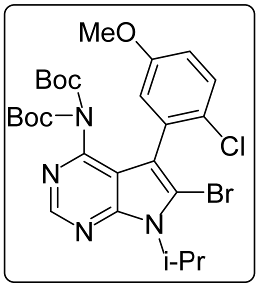

Boc-protected 6-bromo-5-(2-chloro-5-methoxyphenyl)-7-isopropyl-7*H*-pyrrolo[2,3-*d*]pyrimidin-4-amine (2.4d):

Following the general procedure: **2.4c** (80 mg, .202 mmol, 1.0 eq) was reacted with DMAP and Boc_2O in DCM. Workup and purification was followed according to the general procedure to afford 75 mg (62% yield) of **2.4d** as a white solid.

^{1}H NMR (500 MHz, $CDCl_3$) δ 8.78 (s, 1H), 7.35 (d, J = 9.6 Hz, 1H), 6.90 (m, 2H), 5.16 (dt, J = 13.6, 6.8 Hz, 1H), 3.77 (s, 3H), 1.76 (dd, J = 8.5, 7.0 Hz, 6H), 1.34 (d, J = 24.4 Hz, 18H).

^{13}C NMR (126 MHz, $CDCl_3$) δ 158.02, 152.76, 151.09, 150.51, 149.96, 132.25, 130.33, 126.62, 118.54, 117.98, 115.43, 115.18, 112.51, 83.50, 55.62, 50.60, 27.93, 21.21, 21.17.

MS (APCI) Calculated: $C_{26}H_{33}BrClN_4O_5$ $[M+H]^+$ 595.1 **Found:** 595.2

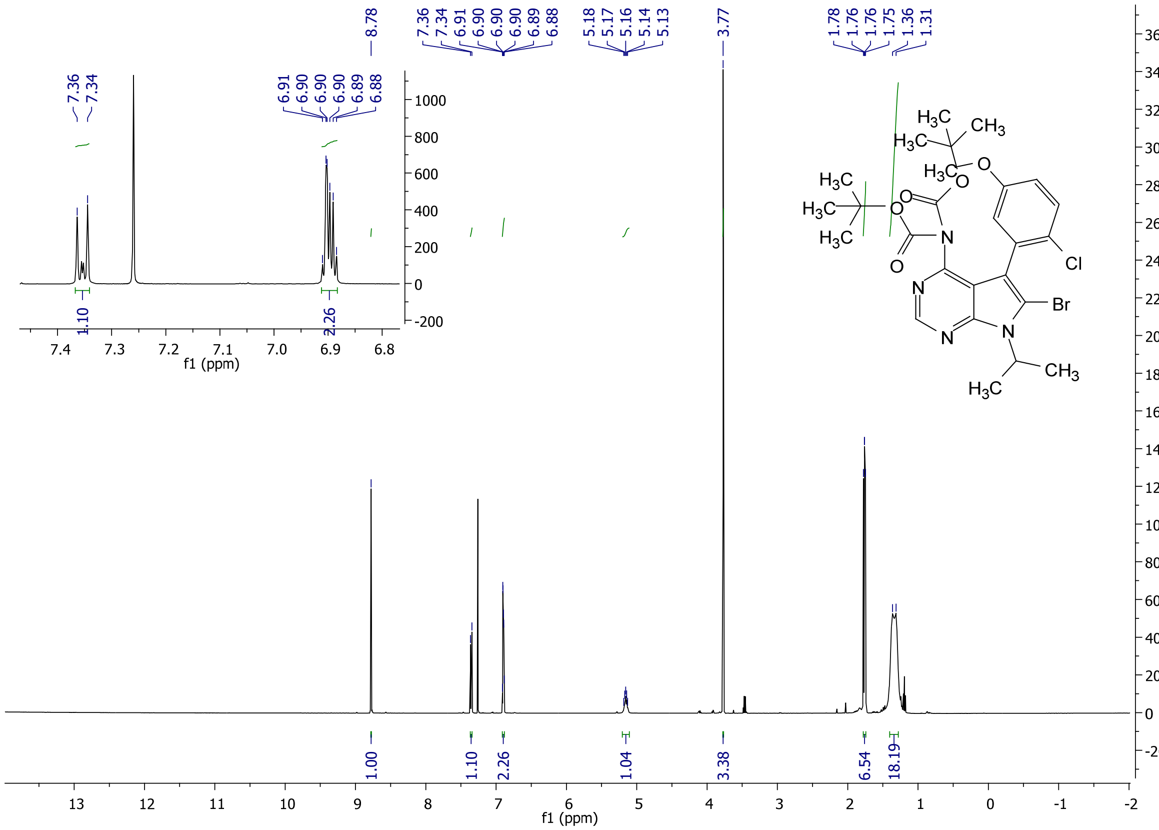

8.78
7.36
7.34
6.91
6.90
6.90
6.90
6.89
6.88
5.18
5.17
5.16
5.14
5.13
3.77
1.78
1.76
1.76
1.75
1.36
1.31
1.00
1.10
2.26
1.04
3.38
6.54
18.19
f1 (ppm)
H3C
CH3
O
N
Cl
Br

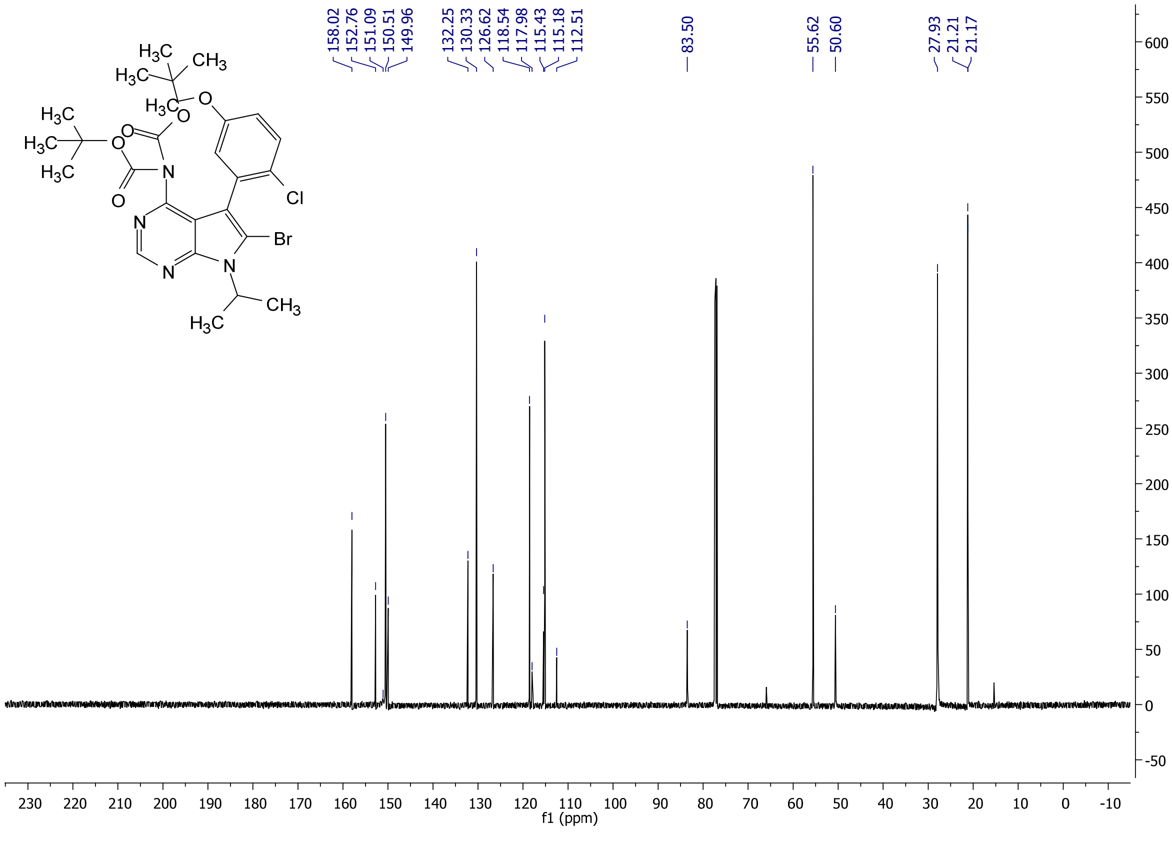

158.02
152.76
151.09
150.51
149.96
132.25
130.33
126.62
118.54
117.98
115.43
115.18
112.51
83.50
55.62
50.60
27.93
21.21
21.17
f1 (ppm)
H3C
CH3
O
N
Cl
Br

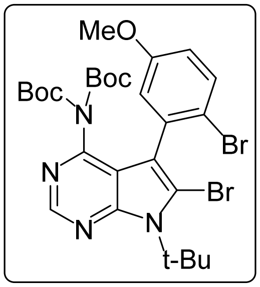

Boc protected 6-bromo-5-(2-bromo-5-methoxyphenyl)-7-(tert-butyl)-7*H*-pyrrolo[2,3-*d*]pyrimidin-4-amine (2.5d):

Following the general procedure: **2.5c** (95 mg, .21 mmol, 1.0 eq) was reacted with DMAP and Boc_2O in DCM. Workup and purification was followed according to the general procedure to afford 111mg (81% yield) of **2.5d** as a white solid.

^{1}H NMR (400 MHz, $CDCl_3$) δ 8.76 (s, 1H), 7.53 (d, J = 8.8 Hz, 1H), 6.89 (d, J = 3.0 Hz, 1H), 6.84 (dd, J = 8.8, 3.1 Hz, 1H), 3.78 (s, 3H), 2.06 (s, 9H), 1.40 (s, 9H), 1.33 (s, 9H).

^{13}C NMR (101 MHz, $CDCl_3$) δ 158.70, 154.56, 151.21, 150.57, 149.78, 149.74, 135.10, 133.43, 118.79, 117.23, 116.85, 116.51, 115.51, 115.27, 83.60, 83.53, 63.66, 55.59, 31.80, 28.08, 28.01

MS (APCI) Calculated: $C_{27}H_{35}Br_2N_4O_5$ $[M+H]^+$ 653.1 **Found:** 653.1

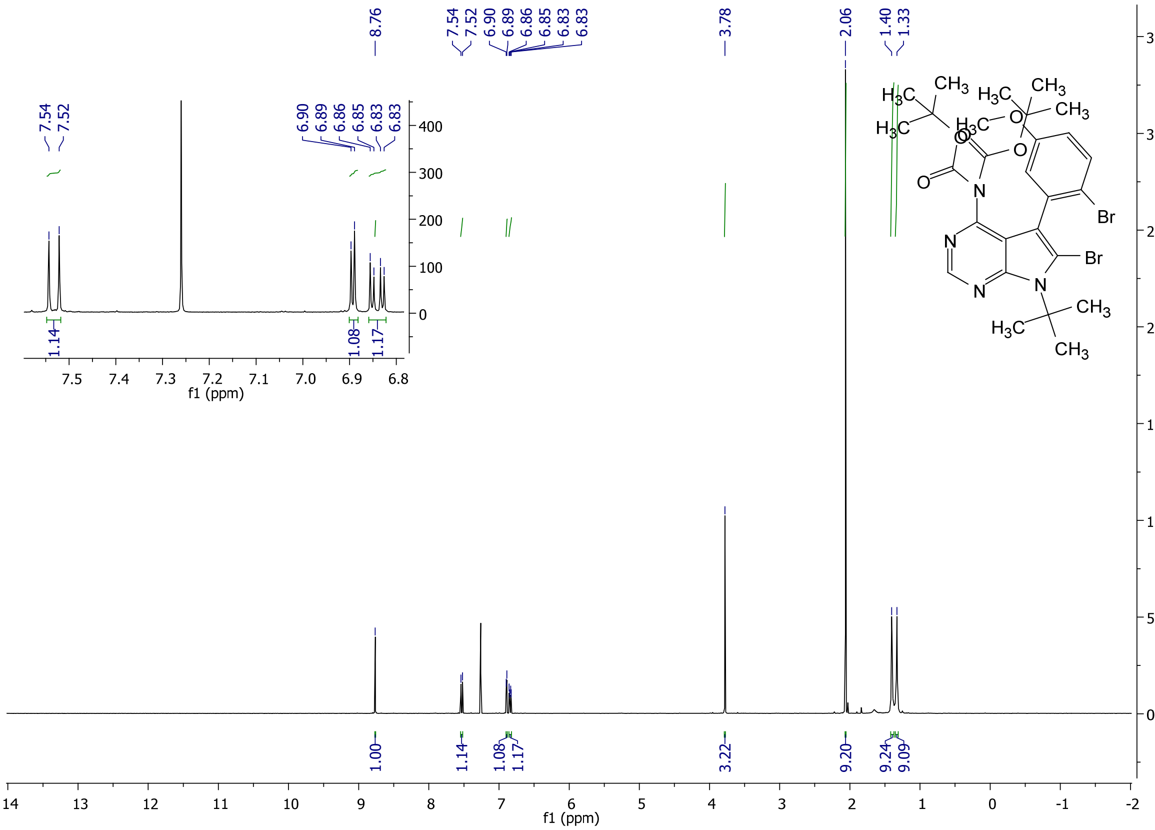
8.76
7.54
7.52
6.90
6.89
6.86
6.85
6.83
6.83
3.78
2.06
1.40
1.33
1.00
1.14
1.08
1.17
3.22
9.20
9.24
9.09
f1 (ppm)
Br
Br
N
N
N
N
O
O
O
O
H_3C
CH_3
f1 (ppm)

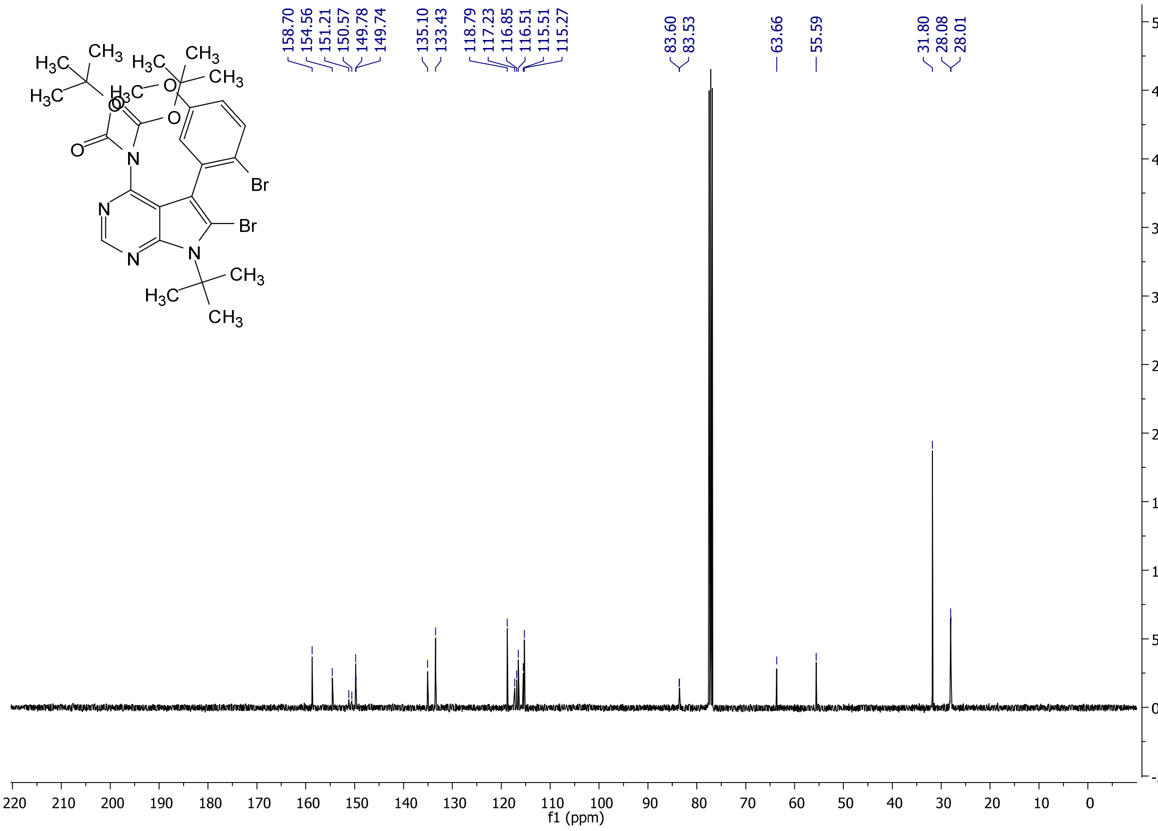
158.70
154.56
151.21
150.57
149.78
149.74
135.10
133.43
118.79
117.23
116.85
116.51
115.51
115.27
83.60
83.53
63.66
55.59
31.80
28.08
28.01
Br
Br
N
N
N
N
O
O
O
O
H_3C
CH_3
f1 (ppm)

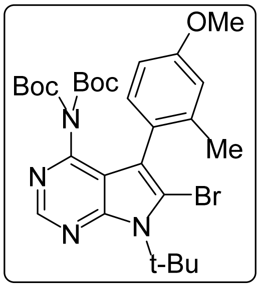

Boc-protected 6-bromo-7-(*tert*-butyl)-5-(4-methoxy-2-methylphenyl)-7*H*-pyrrolo[2,3-*d*]pyrimidin-4-amine (2.7d):

Following the general procedure: **2.7c** (72 mg, .185 mmol, 1.0 eq) was reacted with DMAP and Boc_2O in DCM. Workup and purification was followed according to the general procedure to afford 80 mg (73% yield) of **2.7d** as a white solid.

^{1}H NMR (400 MHz, $CDCl_3$) δ 8.76 (s, 1H), 7.10 (d, J = 8.4 Hz, 1H), 6.80 (d, J = 2.5 Hz, 1H), 6.74 (dd, J = 8.4, 2.7 Hz, 1H), 3.84 (s, 3H), 2.08 (s, 3H), 2.05 (s, 9H), 1.42 (s, 9H), 1.30 (s, 9H)

^{13}C NMR (101 MHz, $CDCl_3$) δ 159.39, 154.67, 151.09, 150.78, 149.96, 149.75, 139.64, 131.86, 124.89, 116.87, 116.55, 115.88, 115.74, 111.10, 83.25, 63.25, 55.22, 31.76, 28.13, 27.89, 20.37.

MS (APCI) Calculated: $C_{28}H_{38}BrN_4O_5$ $[M+H]^+$ 589.2 **Found:** 589.2

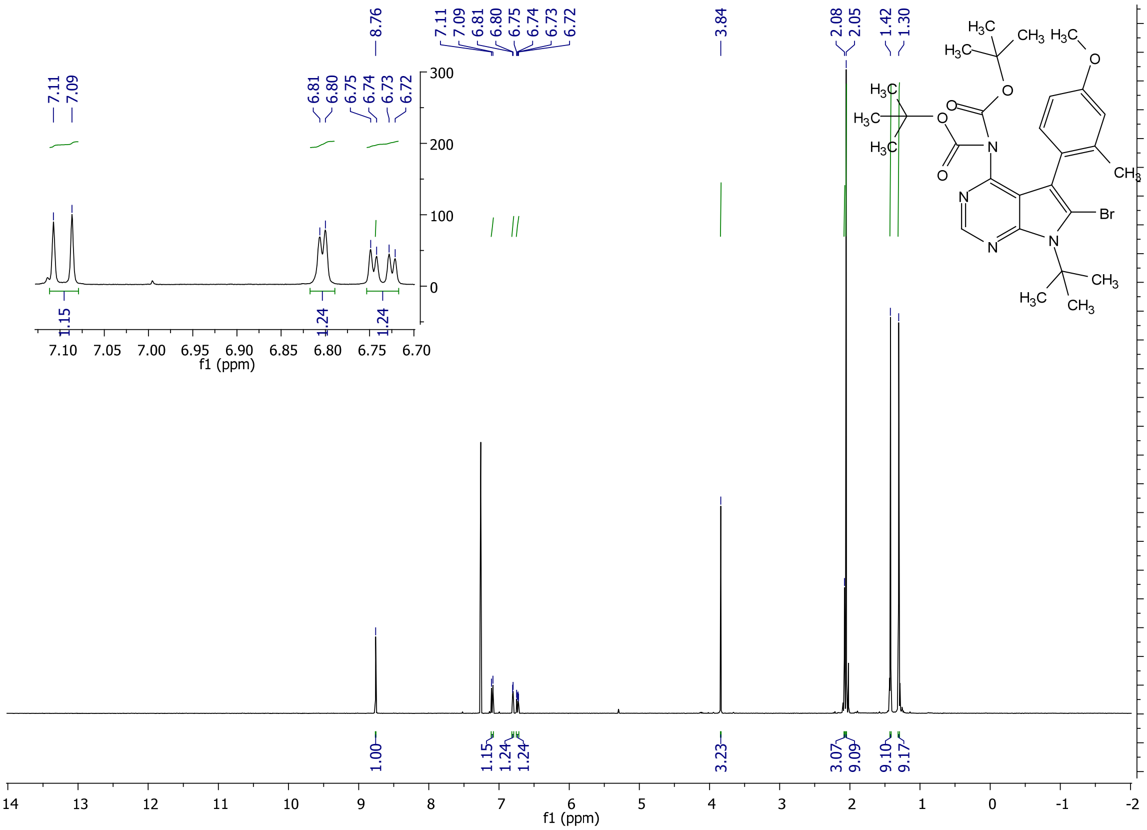
8.76
7.11
7.09
6.81
6.80
6.75
6.74
6.73
6.72
3.84
2.08
2.05
1.42
1.30
1.00
1.15
1.24
1.24
3.23
3.07
9.09
9.10
9.17
f1 (ppm)
Br
N
O
H_3C
CH_3

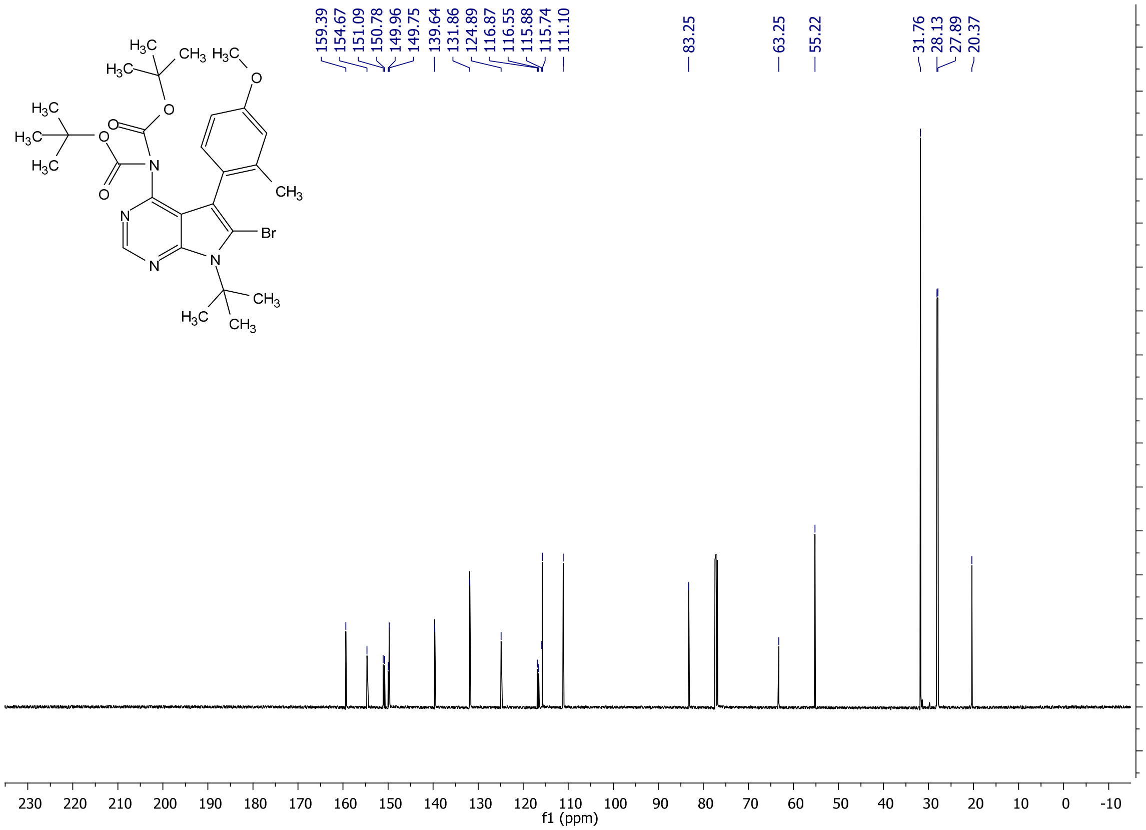
159.39
154.67
151.09
150.78
149.96
149.75
139.64
131.86
124.89
116.87
116.55
115.88
115.74
111.10
83.25
63.25
55.22
31.76
28.13
27.89
20.37
f1 (ppm)
Br
N
O
H_3C
CH_3

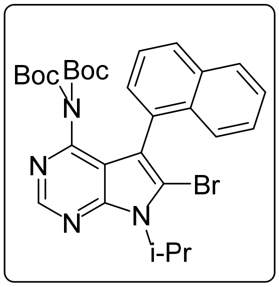

Boc-protected 6-bromo-7-isopropyl-5-(naphthalen-1-yl)-7H-pyrrolo[2,3-d]pyrimidin-4-amine (2.9d):

Following the general procedure: **2.9c** (500 mg, 1.31 mmol, 1.0 eq) was reacted with DMAP and Boc_2O in DCM. Workup and purification were followed according to the general procedure to afford 600mg (79% yield) of **2.9d** as a yellow-white solid.

^{1}H NMR (500 MHz, $CDCl_3$) δ 8.83 (s, 1H), 7.93 – 7.87 (m, 2H), 7.58 (d, J = 8.4 Hz, 1H), 7.53 – 7.43 (m, 3H), 7.39 (ddd, J = 8.2, 6.8, 1.3 Hz, 1H), 5.22 (sept, J = 6.6 Hz, 1H), 1.82 (dd, J = 10.0, 7.0 Hz, 6H), 1.41 (s, 9H), 0.81 (s, 9H).

^{13}C NMR (101 MHz, $CDCl_3$) δ 152.94, 150.74, 150.55, 150.25, 150.13, 133.81, 132.18, 129.87, 128.89, 128.54, 128.22, 126.50, 126.23, 125.86, 125.23, 117.88, 116.28, 113.05, 83.26, 83.04, 50.50, 27.99, 27.17, 21.20, 21.14.

MS (APCI) Calculated: $C_{30}H_{36}BrN_4O_4$ $[M+H]^+$ 580.2 **Found:** 580.1 m/z

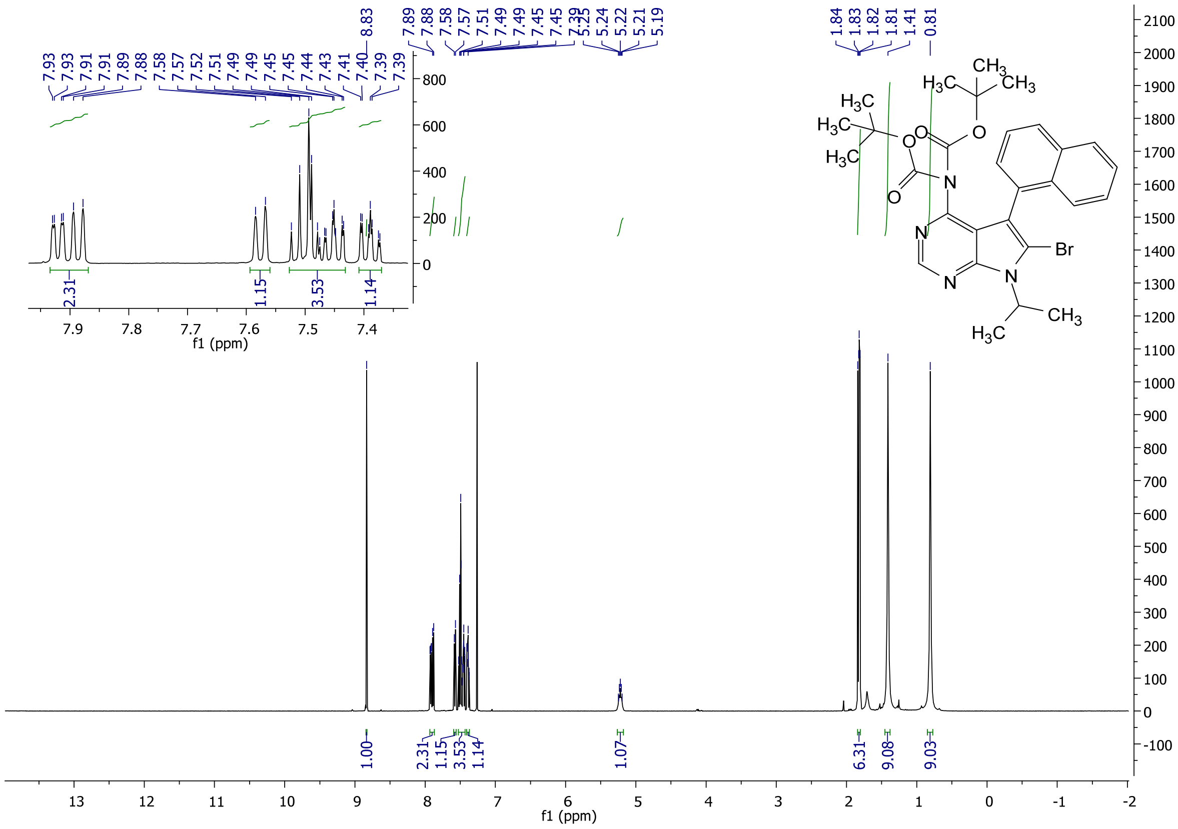
7.93
7.93
7.91
7.91
7.89
7.88
7.58
7.57
7.52
7.51
7.51
7.49
7.49
7.45
7.45
7.44
7.43
7.41
7.40
7.39
7.39
8.83
7.89
7.88
7.58
7.57
7.51
7.49
7.49
7.45
7.45
7.39
5.25
5.24
5.22
5.21
5.19
1.84
1.83
1.82
1.81
1.41
0.81
2.31
1.15
3.53
1.14
1.00
2.31
1.15
3.53
1.14
1.07
6.31
9.08
9.03
f1 (ppm)
f1 (ppm)
CH3
H3C
CH3
H3C
H3C
H3C
O
O
O
O
N
N
N
N
Br
CH3
H3C

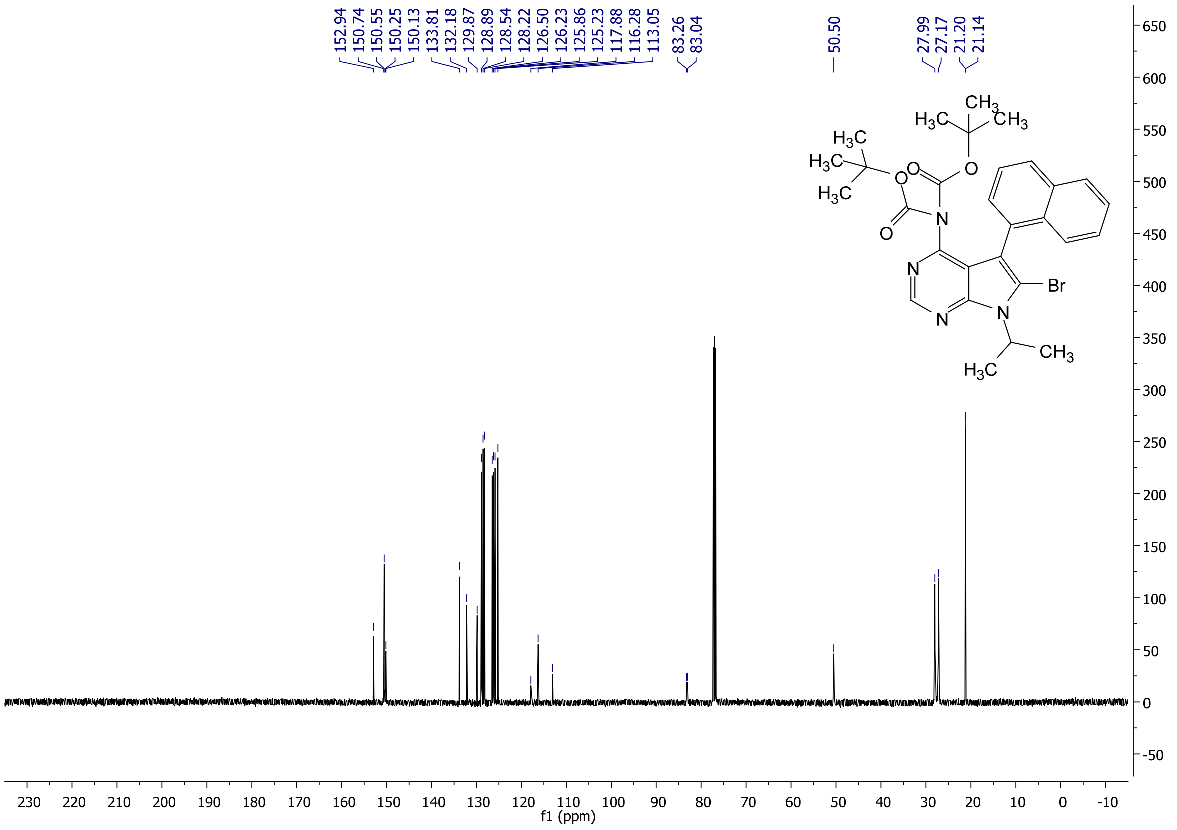
152.94
150.74
150.55
150.25
150.13
133.81
132.18
129.87
128.89
128.54
128.22
126.50
126.23
125.86
125.23
117.88
116.28
113.05
83.26
83.04
50.50
27.99
27.17
21.20
21.14
f1 (ppm)
CH3
H3C
CH3
H3C
H3C
H3C
O
O
O
O
N
N
N
N
Br
CH3
H3C

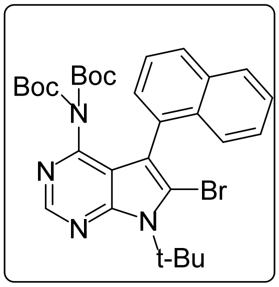

Boc-protected 6-bromo-7-(*tert*-butyl)-5-(naphthalen-1-yl)-7*H*-pyrrolo[2,3-*d*]pyrimidin-4-amine (2.10d):

Following the general procedure: **2.10c** (300 mg, .754 mmol, 1.0 eq) was reacted with DMAP and Boc_2O in DCM. Workup and purification was followed according to the general procedure to afford 309 mg (69% yield) of **2.10d** as a white solid.

^{1}H NMR (400 MHz, $CDCl_3$) δ 8.81 (s, 1H), 7.92 (d, J = 8.0 Hz, 1H), 7.88 (d, J = 7.6 Hz, 1H), 7.54 – 7.36 (m, 6H), 2.11 (s, 9H), 1.42 (s, 9H), 0.79 (s, 9H)

^{13}C NMR (101 MHz, $CDCl_3$) δ 154.88, 150.83, 150.38, 150.10, 149.95, 133.88, 132.42, 130.73, 128.85, 128.60, 128.34, 126.63, 126.36, 125.96, 125.43, 117.22, 116.48, 115.69, 83.34, 83.09, 63.62, 31.86, 28.16, 27.28

MS (APCI) Calculated: $C_{30}H_{36}BrN_4O_4$ $[M+H]^+$ 595.2 **Found:** 595.2

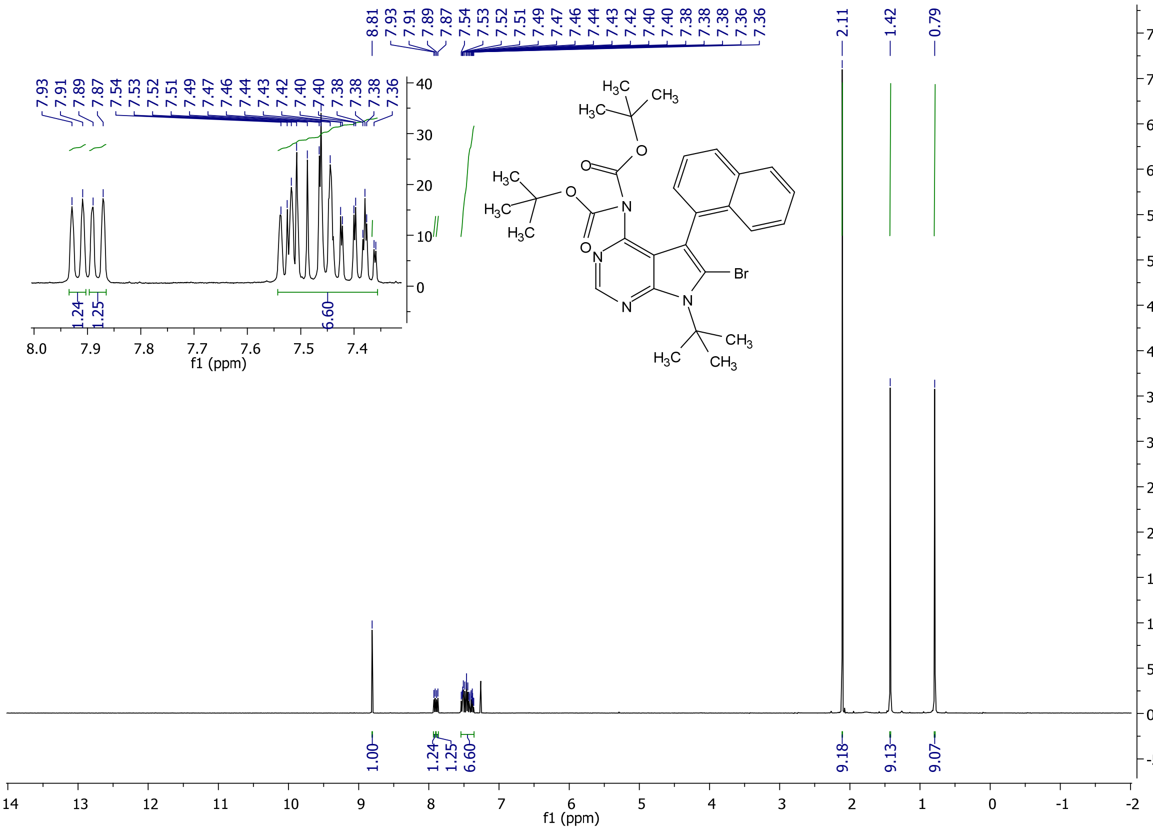
8.81
7.93
7.91
7.89
7.87
7.54
7.53
7.52
7.51
7.49
7.47
7.46
7.44
7.43
7.42
7.40
7.40
7.38
7.38
7.38
7.36
7.36
2.11
1.42
0.79
1.00
1.24
1.25
6.60
9.18
9.13
9.07
f1 (ppm)
Br
N
O
CH3
H3C

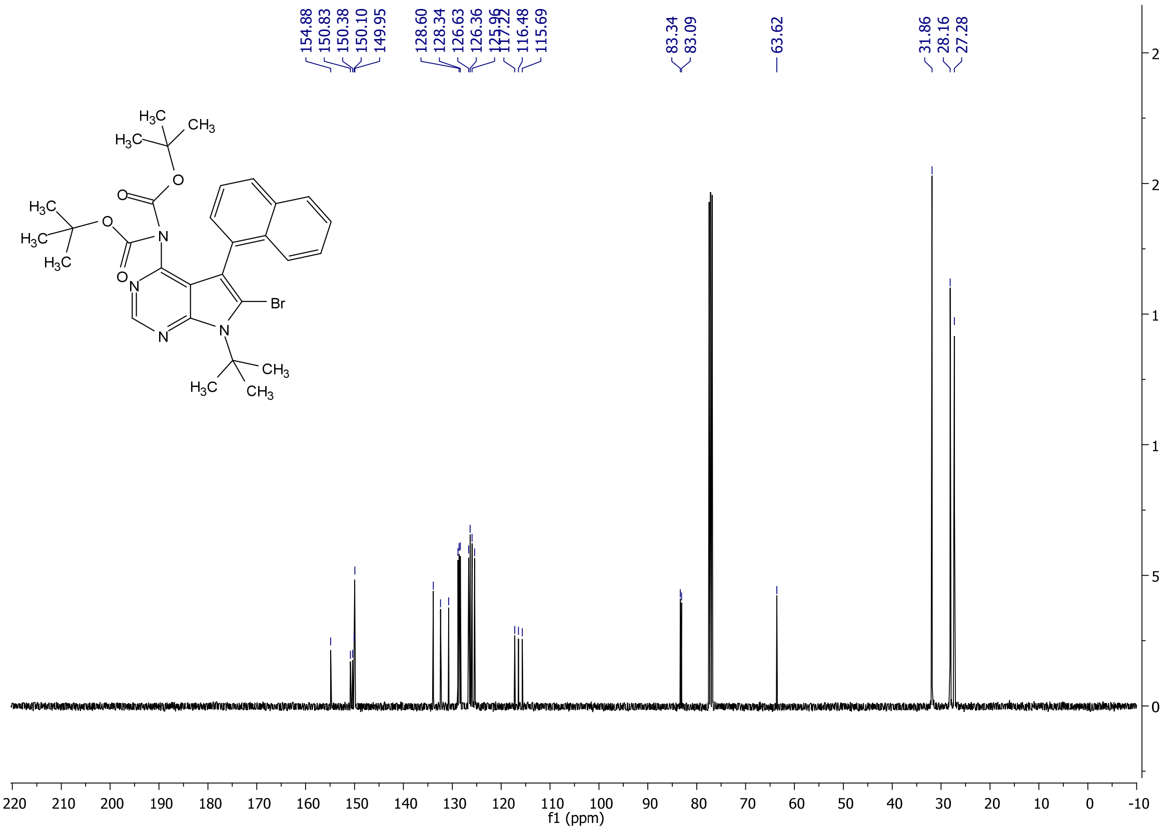
154.88
150.83
150.38
150.10
149.95
128.60
128.34
126.63
126.36
125.96
117.22
116.48
115.69
83.34
83.09
63.62
31.86
28.16
27.28
f1 (ppm)
Br
N
O
CH3
H3C

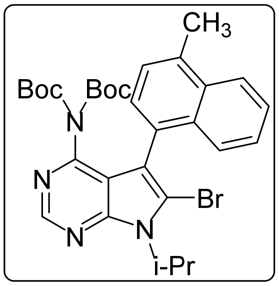

Boc-protected 6-bromo-7-isopropyl-5-(4-methylnaphthalen-1-yl)-7*H*-pyrrolo[2,3-*d*]pyrimidin-4-amine (2.12d):

Following the general procedure: **2.12c** (150 mg, .379 mmol, 1.0 eq) was reacted with DMAP and Boc_2O in DCM. Workup and purification were followed according to the general procedure to afford 215mg (95% yield) of **2.12d** as a white solid.

^{1}H NMR (400 MHz, $CDCl_3$) δ 8.83 (s, 1H), 8.04 (d, J = 8.4 Hz, 1H), 7.59 (d, J = 8.4 Hz, 1H), 7.49 (ddd, J = 8.3, 6.8, 1.3 Hz, 1H), 7.42 – 7.33 (m, 3H), 5.21 (dt, J = 13.8, 6.9 Hz, 1H), 2.76 (s, 3H), 1.85 – 1.77 (m, 6H), 1.40 (s, 9H), 0.81 (s, 9H).

^{13}C NMR (101 MHz, $CDCl_3$) δ 152.91, 150.75, 150.46, 150.30, 150.00, 134.72, 132.87, 132.15, 128.65, 128.06, 127.07, 126.12, 125.86, 125.70, 124.37, 117.95, 116.33, 113.28, 83.13, 82.89, 50.47, 27.96, 27.15, 21.19, 21.13, 19.66.

MS (APCI) Calculated: $C_{30}H_{36}BrN_4O_4$ $[M+H]^+$ 595.2 **Found:** 595.0

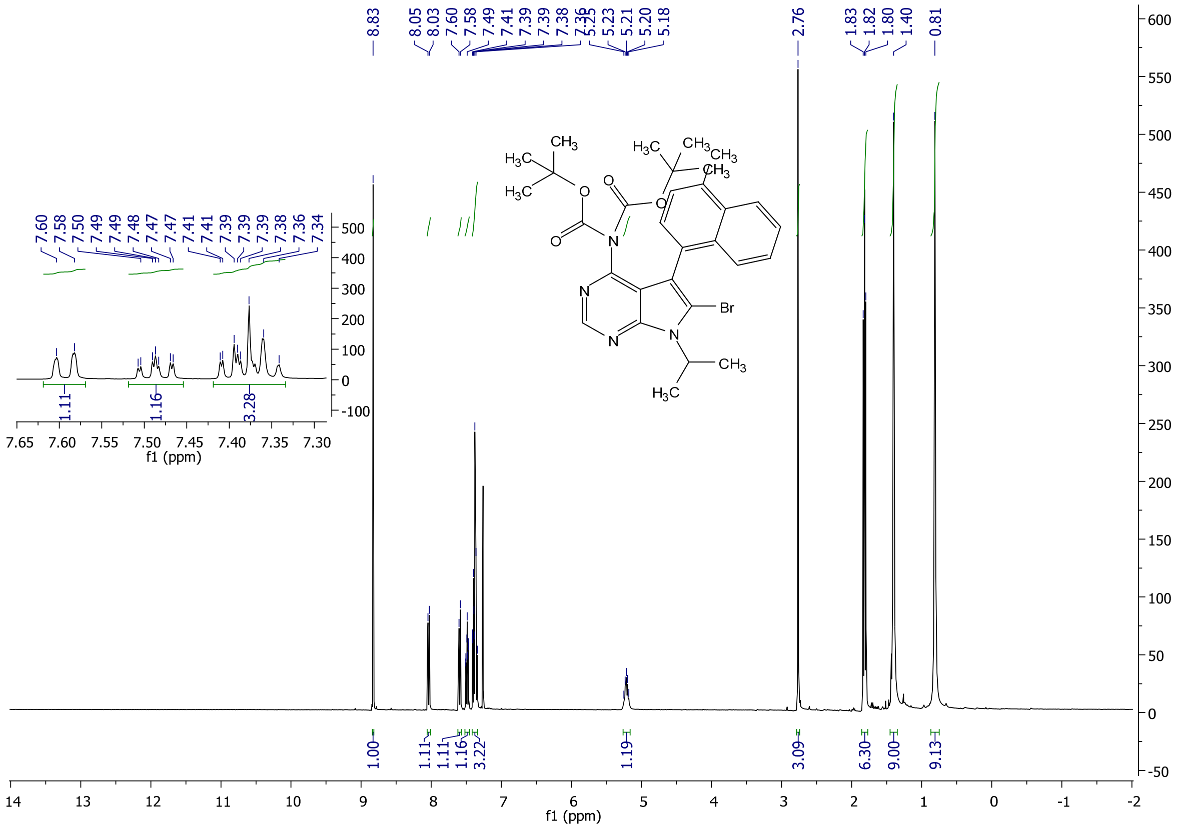
8.83
8.05
8.03
7.60
7.58
7.49
7.41
7.39
7.39
7.38
7.36
7.35
5.23
5.21
5.20
5.18
2.76
1.83
1.82
1.80
1.40
0.81
1.00
1.11
1.11
1.16
3.22
1.19
3.09
6.30
9.00
9.13
7.60
7.58
7.50
7.49
7.49
7.48
7.47
7.47
7.41
7.41
7.39
7.39
7.39
7.38
7.36
7.34
1.11
1.16
3.28
f1 (ppm)
CH3
H3C
H3C
O
O
O
N
N
N
N
Br
CH3
H3C

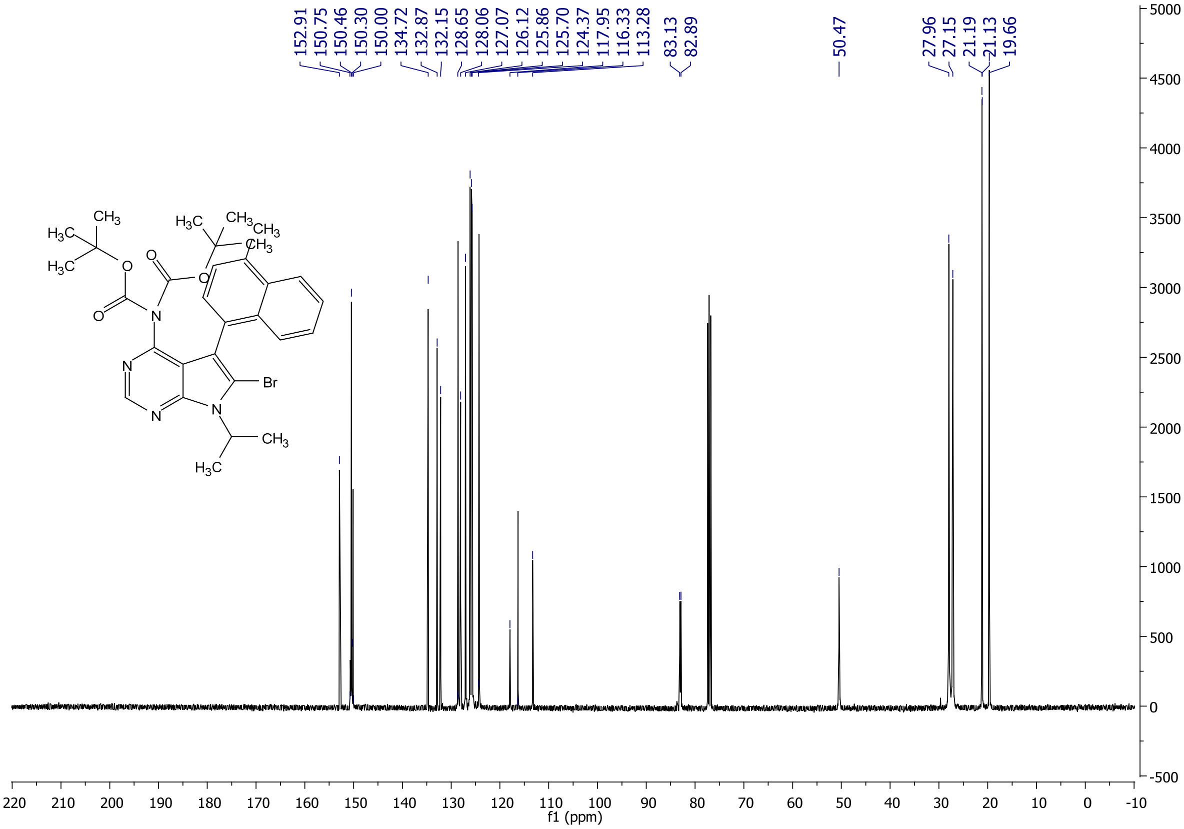
152.91
150.75
150.46
150.30
150.00
134.72
132.87
132.15
128.65
128.06
127.07
126.12
125.86
125.70
124.37
117.95
116.33
113.28
83.13
82.89
50.47
27.96
27.15
21.19
21.13
19.66
f1 (ppm)
CH3
H3C
H3C
O
O
O
N
N
N
N
Br
CH3
H3C

General procedure for the 6-methylated pyrrolopyrimidines (2.1 – 2.20):

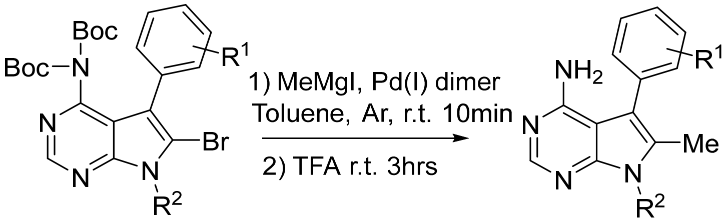

A vial with **2.1d – 2.20d** (1 equiv.), Pd(I) dimer (0.075 equiv) and stir bar was evacuated and charged with argon. Dry, degassed toluene (0.08M) was then added under argon. MeMgI (4 equiv.) was added dropwise to the stirred solution over 3 minutes. Product conversion was monitored by mass spectrometry and TLC. If starting material still persists after 30 minutes, Pd(I) dimer (0.075 equiv) and MeMgI (4 equiv) were added under argon. Upon consumption of starting material, the reaction mixture was diluted slightly with DCM and TFA (4 equiv.) was added. The reaction mixture was stirred for 3 more hours then partitioned in DCM : Brine mixture in a separatory funnel. After extraction and evaporation of the organic layer, flash column chromatography (60:40 Hexanes : EtOAc) was used to purify the product yielding **2.1** – **2.20m** (43-62% yield).

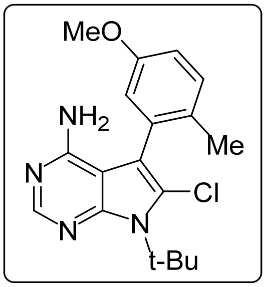

7-(*tert*-butyl)-6-chloro-5-(5-methoxy-2-methylphenyl)-7*H*-pyrrolo[2,3-*d*]pyrimidin-4-amine (2.1):

Following the general procedure: **2.1d** (60 mg, .098 mmol, 1.0 eq), was coupled with MeMgI. The mixture was thoroughly purged with vacuum then argon. Workup and purification was followed according to the general procedure to afford 15 mg (44% yield) of **2.1** as a white solid.

^{1}H NMR (400 MHz, $CDCl_3$) δ 8.23 (s, 1H), 7.24 (d, J = 8.5 Hz, 1H), 6.90 (dd, J = 8.4, 2.8 Hz, 1H), 6.82 (d, J = 2.8 Hz, 1H), 4.88 (s, 2H), 3.80 (s, 3H), 2.08 (s, 3H), 1.99 (s, 9H)

^{13}C NMR (101 MHz, $CDCl_3$) δ 157.79, 155.52, 150.62, 149.75, 133.09, 131.44, 130.32, 121.48, 116.15, 114.76, 113.34, 102.49, 62.45, 55.49, 31.46, 19.02

MS (APCI) Calculated: $C_{18}H_{22}ClN_4O$ $[M+H]^+$ 345.2 **Found:** 345.1

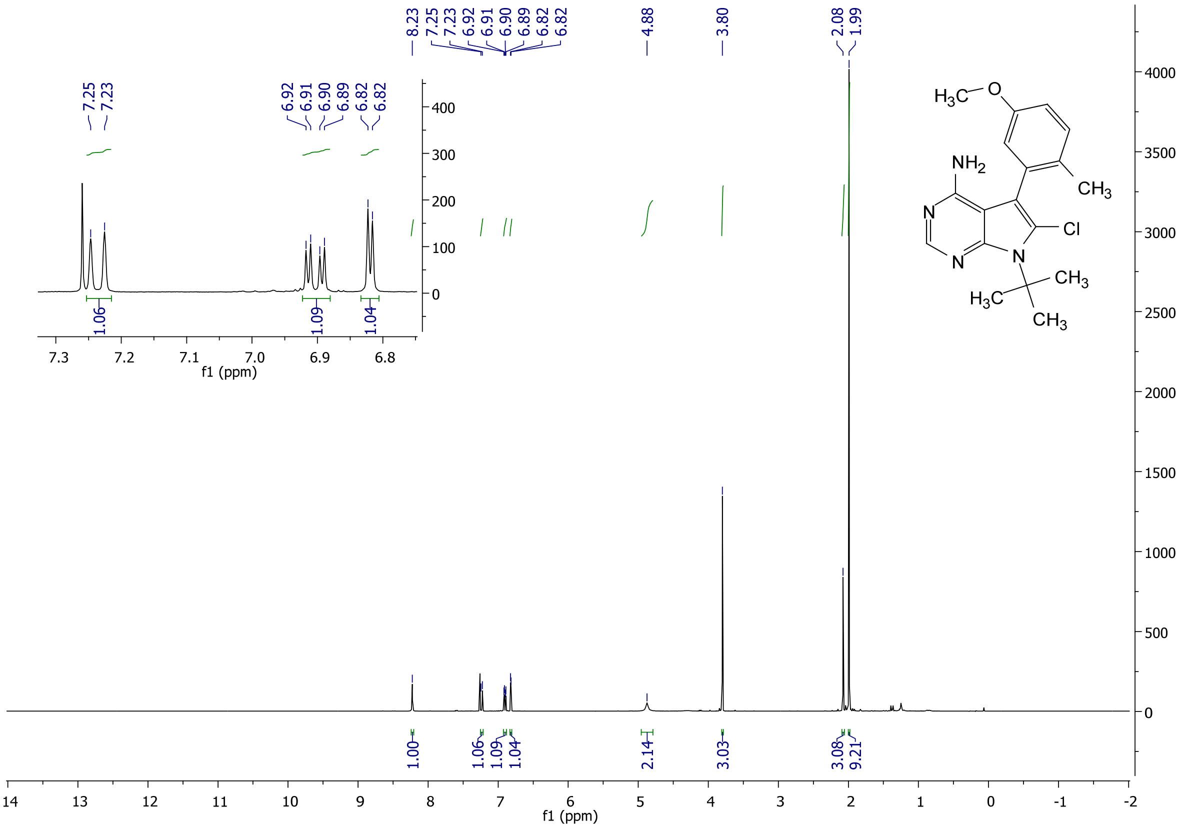
8.23
7.25
7.23
6.92
6.91
6.90
6.89
6.82
6.82
4.88
3.80
2.08
1.99
1.00
1.06
1.09
1.04
2.14
3.03
3.08
9.21
f1 (ppm)
H_3C–O
NH_2
CH_3
N
Cl
N
N
CH_3
H_3C
CH_3

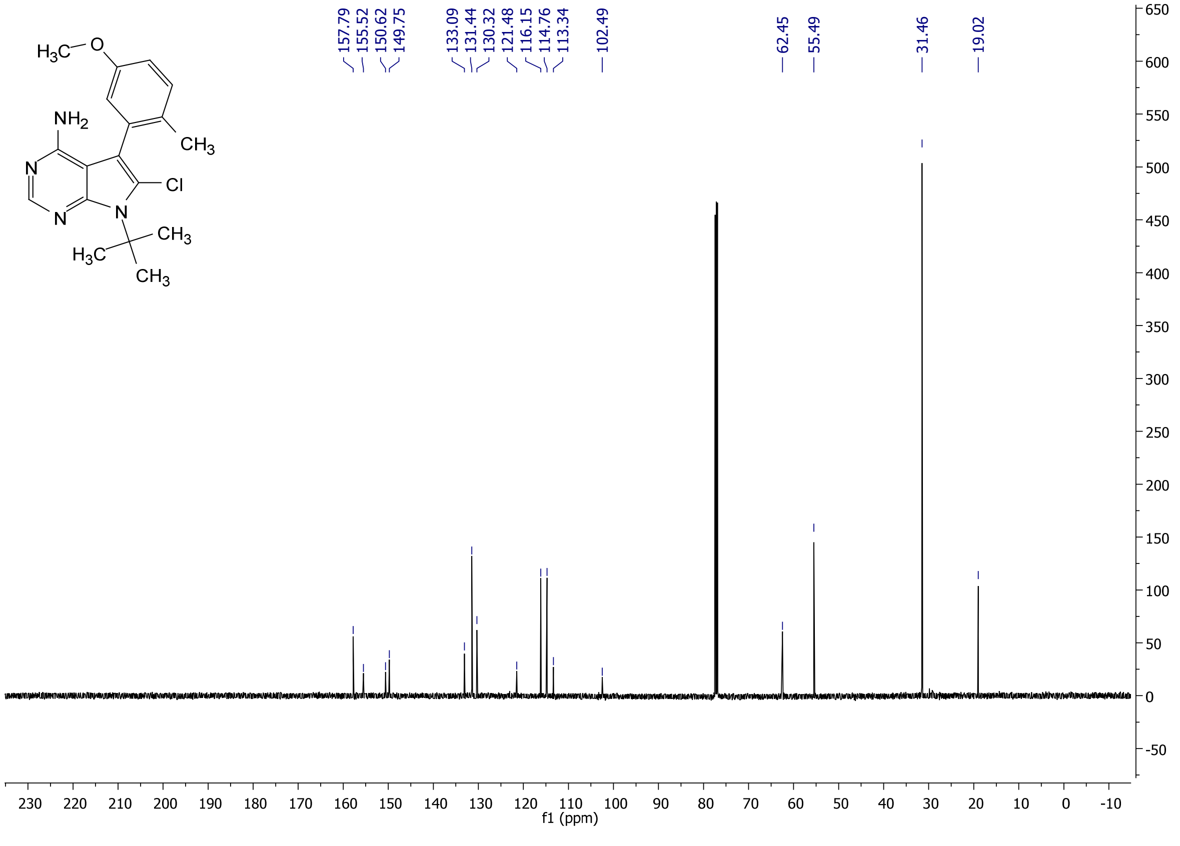
157.79
155.52
150.62
149.75
133.09
131.44
130.32
121.48
116.15
114.76
113.34
102.49
62.45
55.49
31.46
19.02
f1 (ppm)
H_3C–O
NH_2
CH_3
N
Cl
N
N
CH_3
H_3C
CH_3

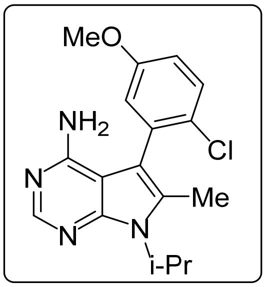

5-(2-chloro-5-methoxyphenyl)-7-isopropyl-6-methyl-7*H*-pyrrolo[2,3-*d*]pyrimidin-4-amine (2.4):

Following the general procedure: **2.4d** (220 mg, 0.37 mmol, 1.0 eq), was coupled with MeMgI. The mixture was thoroughly purged with vacuum then argon. Workup and purification was followed according to the general procedure to afford 53 mg (43% yield) of **2.4** as a white solid.

^{1}H NMR (400 MHz, $CDCl_3$) δ 8.24 (s, 1H), 7.40 (dd, J = 8.3, 0.7 Hz, 1H), 6.90 – 6.87 (m, 2H), 4.96 – 4.88 (m, 1H), 4.81 (s, 2H), 3.79 (s, 3H), 2.25 (s, 3H), 1.67 (dd, J = 7.0, 1.0 Hz, 6H).

^{13}C NMR (101 MHz, $CDCl_3$) δ 158.22, 155.90, 150.43, 150.18, 134.69, 131.36, 130.71, 126.81, 117.81, 115.26, 109.37, 102.33, 55.68, 47.19, 21.70, 11.99.

MS (APCI) Calculated: $[M+H]^+$ 331.1 **Found:** 331.1 m/z

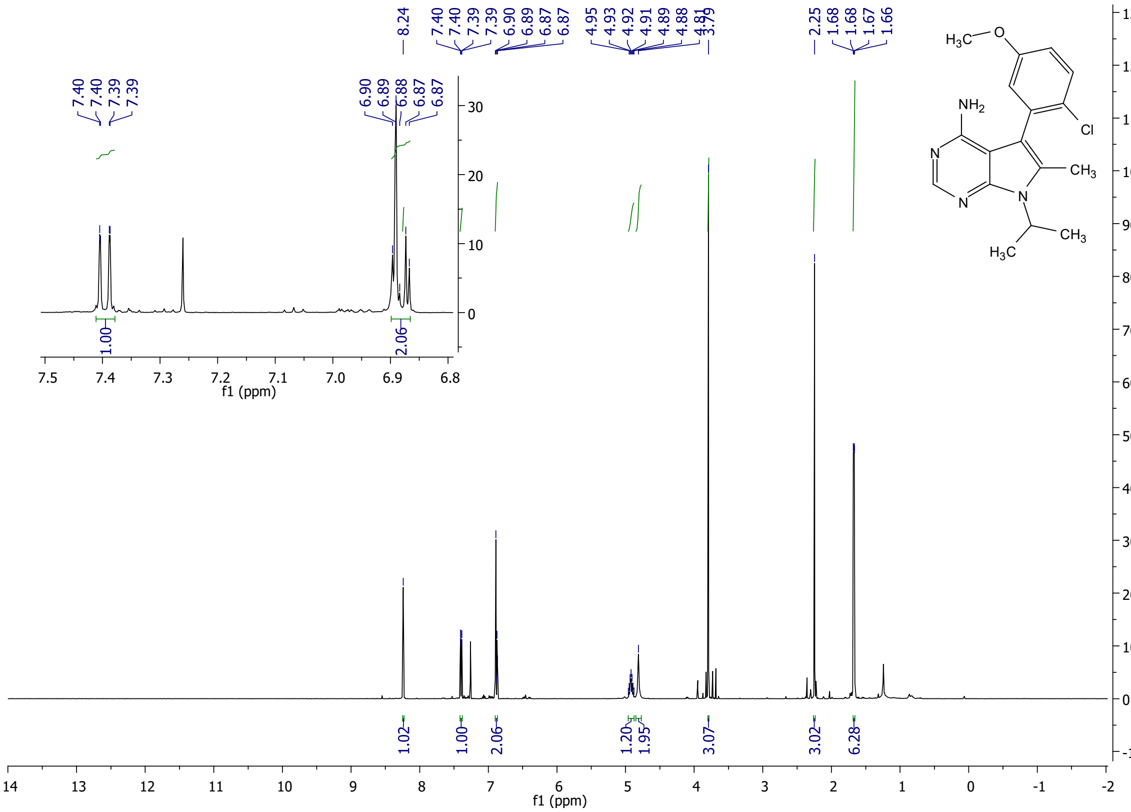
8.24
7.40
7.40
7.39
7.39
6.90
6.89
6.87
6.87
4.95
4.93
4.92
4.91
4.89
4.88
3.81
3.79
2.25
1.68
1.68
1.67
1.66
1.02
1.00
2.06
1.20
1.95
3.07
3.02
6.28
f1 (ppm)
H3C
O
NH2
Cl
N
N
N
CH3
CH3
H3C

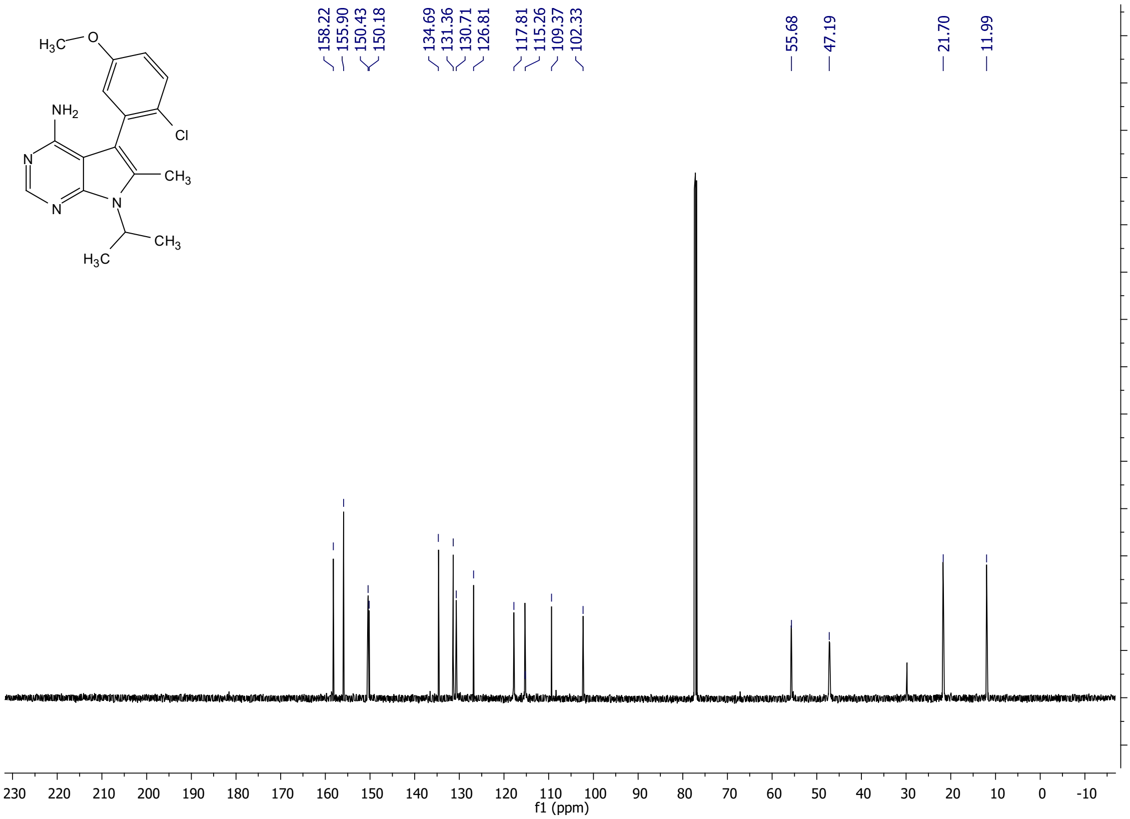
158.22
155.90
150.43
150.18
134.69
131.36
130.71
126.81
117.81
115.26
109.37
102.33
55.68
47.19
21.70
11.99
f1 (ppm)
H3C
O
NH2
Cl
N
N
N
CH3
CH3
H3C

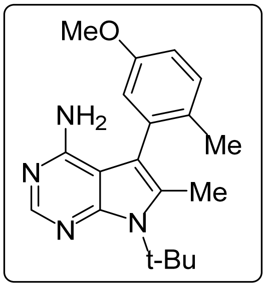

7-(*tert*-butyl)-5-(5-methoxy-2-methylphenyl)-6-methyl-7*H*-pyrrolo[2,3-*d*]pyrimidin-4-amine (2.5):

Following the general procedure: **2.5d** (120 mg, .183 mmol, 1.0 eq), was coupled with MeMgI. The mixture was thoroughly purged with vacuum then argon. Workup and purification were followed according to the general procedure to afford 41 mg (69% yield) of **2.5** as a white solid.

^{1}H NMR (400 MHz, $CDCl_3$) δ 8.22 (s, 1H), 7.21 (d, J = 8.4 Hz, 1H), 6.86 (dd, J = 8.2, 2.1 Hz, 1H), 6.79 (d, J = 2.2 Hz, 1H), 4.62 (s, 2H), 3.79 (s, 3H), 2.31 (s, 3H), 2.02 (s, 3H), 1.92 (s, 9H).

^{13}C NMR (101 MHz, $CDCl_3$) δ 157.53, 155.65, 151.46, 149.04, 135.58, 131.38, 131.06, 130.43, 116.44, 113.86, 113.12, 102.77, 60.29, 55.32, 31.16, 19.06, 15.61.

MS (APCI) Calculated: $C_{19}H_{25}N_4O$ $[M+H]^+$ 325.0 **Found:** 325.0

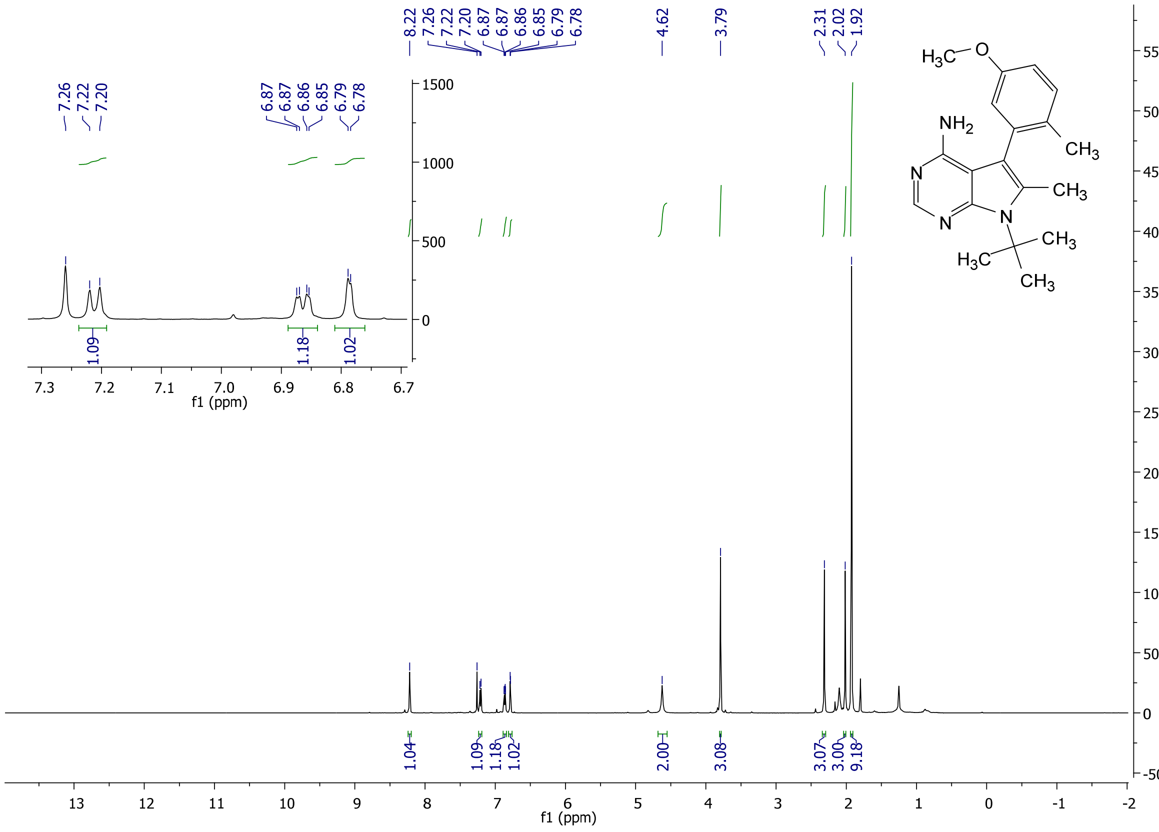
8.22
7.26
7.22
7.20
6.87
6.87
6.86
6.85
6.79
6.78
4.62
3.79
2.31
2.02
1.92
1.04
1.09
1.18
1.02
2.00
3.08
3.07
3.00
9.18
1.09
1.18
1.02
f1 (ppm)
H3C
O
NH2
N
N
N
CH3
CH3
H3C
CH3
CH3

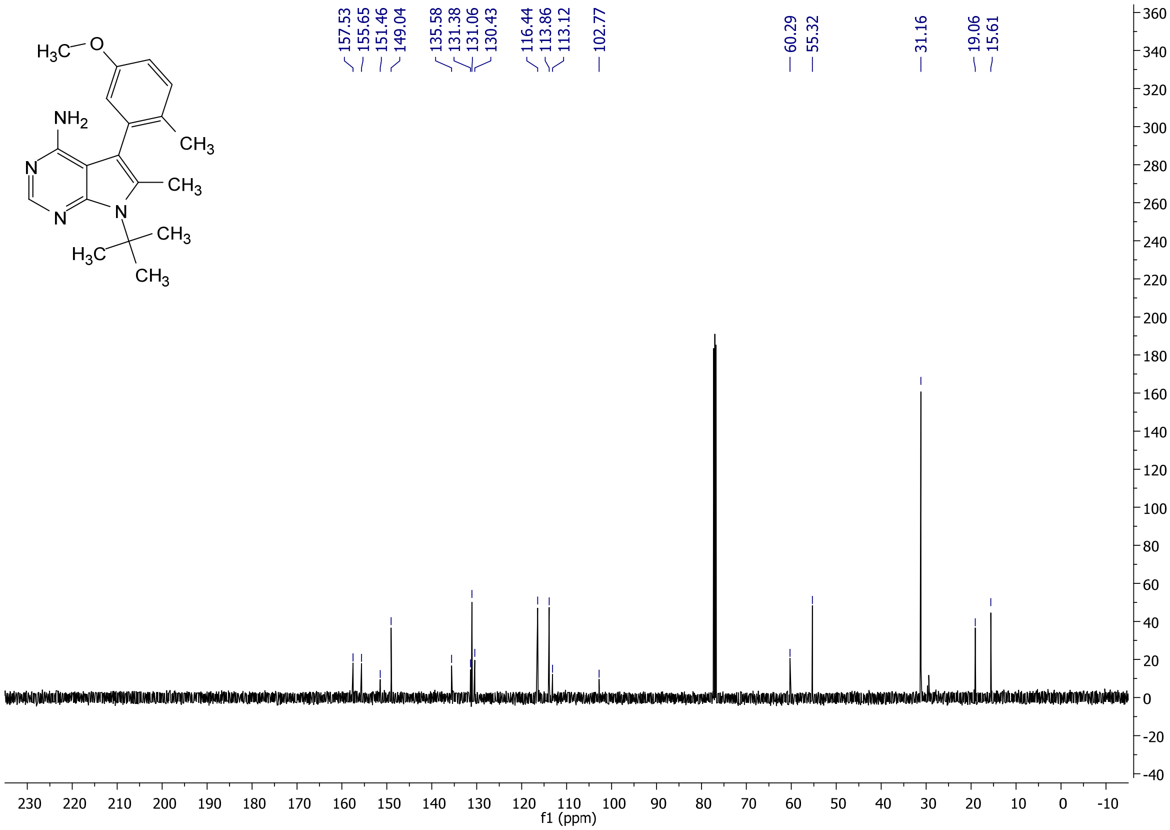
157.53
155.65
151.46
149.04
135.58
131.38
131.06
130.43
116.44
113.86
113.12
102.77
60.29
55.32
31.16
19.06
15.61
f1 (ppm)
H3C
O
NH2
N
N
N
CH3
CH3
H3C
CH3
CH3

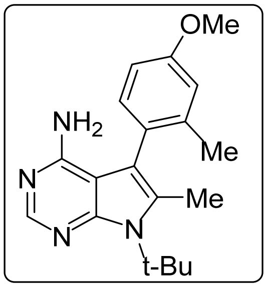

7-(*tert*-butyl)-5-(4-methoxy-2-methylphenyl)-6-methyl-7*H*-pyrrolo[2,3-*d*]pyrimidin-4-amine (2.7):

Following the general procedure: **2.7d** (80 mg, .136 mmol, 1.0 eq), was coupled with MeMgI. The mixture was thoroughly purged with vacuum then argon. Workup and purification were followed according to the general procedure to afford 22 mg (50% yield) of **2.7** as a white solid.

^{1}H NMR (400 MHz, $CDCl_3$) δ 8.20 (s, 1H), 7.14 (d, J = 8.3 Hz, 1H), 6.86 (d, J = 2.7 Hz, 1H), 6.79 (dd, J = 8.3, 2.7 Hz, 1H), 4.68 (s, 2H), 3.84 (s, 3H), 2.29 (s, 3H), 2.06 (s, 3H), 1.91 (s, 9H)

^{13}C NMR (101 MHz, $CDCl_3$) δ 159.29, 155.67, 151.34, 148.71, 139.97, 132.42, 131.79, 126.57, 115.60, 112.66, 111.26, 103.11, 60.24, 55.21, 31.17, 20.40, 15.53

MS (APCI) Calculated: $C_{19}H_{25}N_4O$ $[M+H]^+$ 325.2 **Found:** 325.2

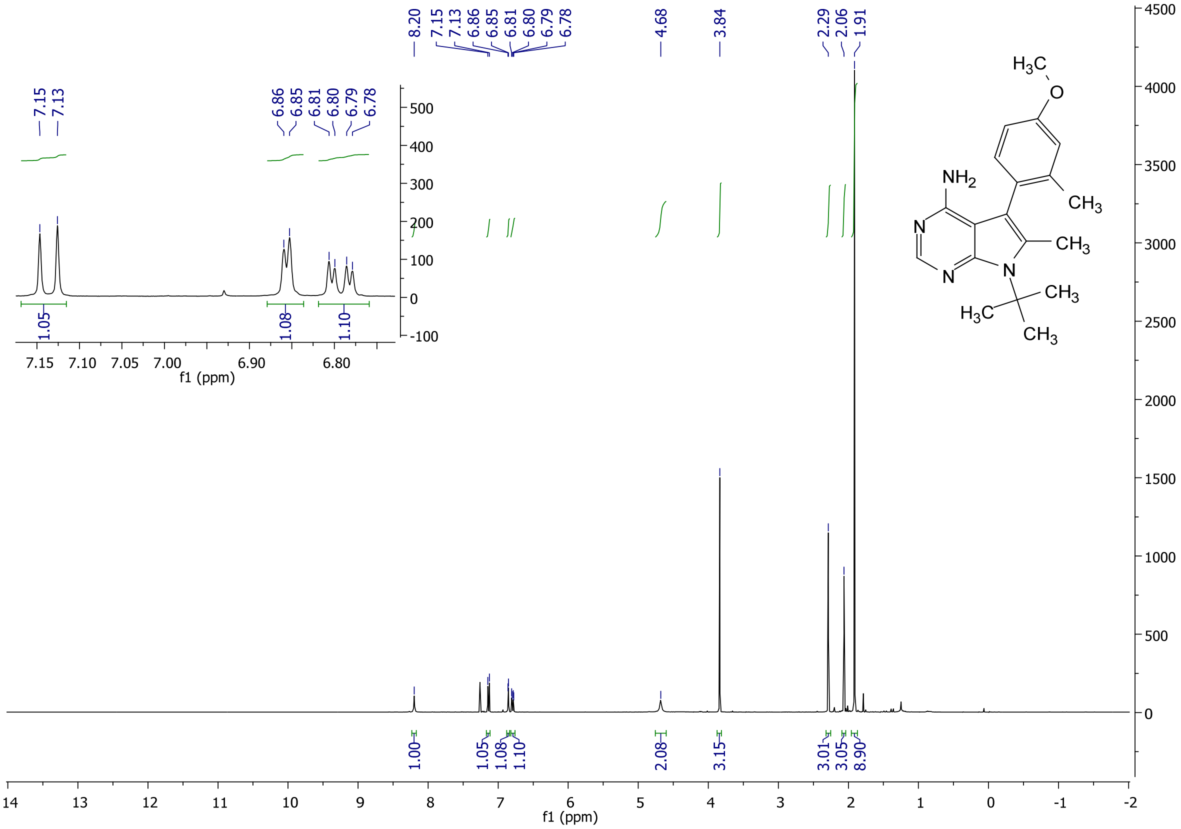
8.20
7.15
7.13
6.86
6.85
6.81
6.80
6.79
6.78
4.68
3.84
2.29
2.06
1.91
1.00
1.05
1.08
1.10
2.08
3.15
3.01
3.05
8.90
f1 (ppm)
NH_2
N
N
N
H_3C
O
CH_3
CH_3
CH_3
H_3C
CH_3

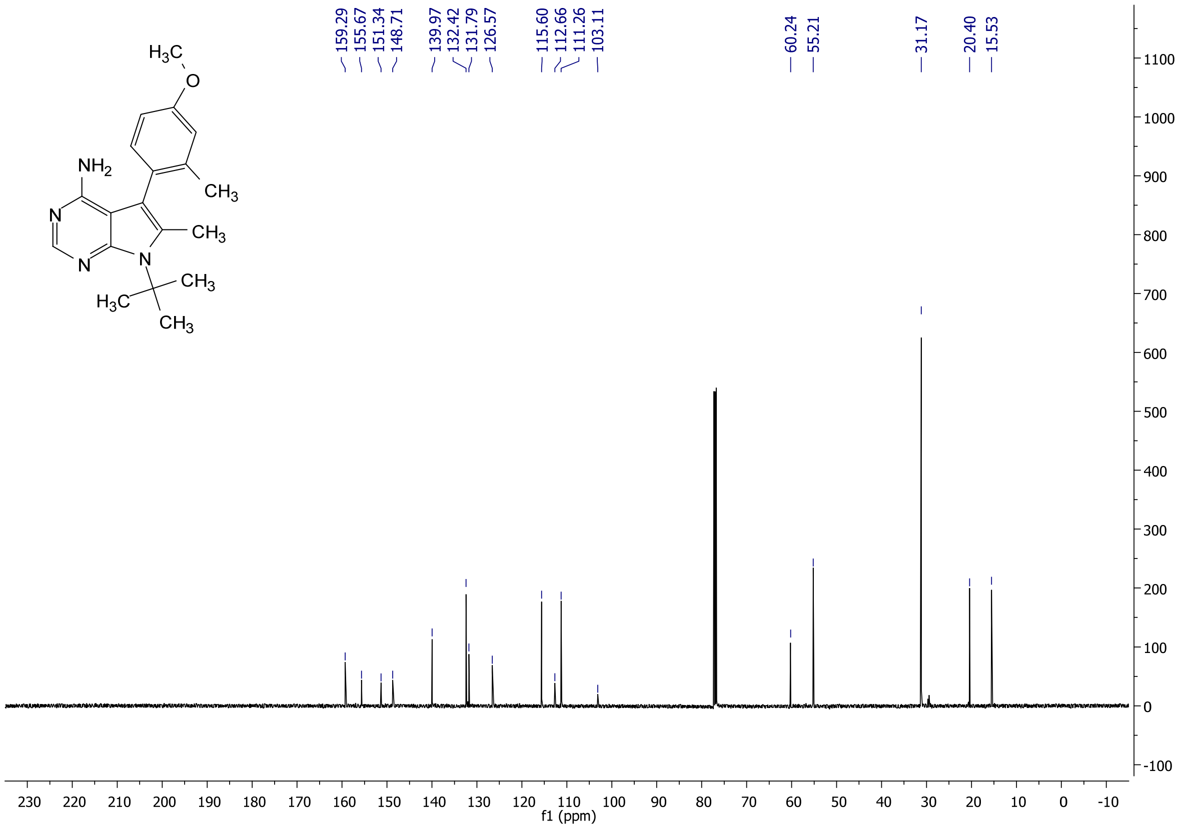
159.29
155.67
151.34
148.71
139.97
132.42
131.79
126.57
115.60
112.66
111.26
103.11
60.24
55.21
31.17
20.40
15.53
f1 (ppm)
NH_2
N
N
N
H_3C
O
CH_3
CH_3
CH_3
H_3C
CH_3

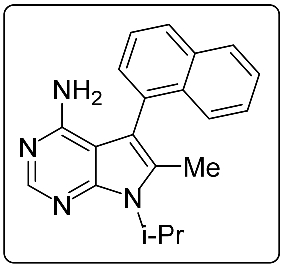

7-isopropyl-6-methyl-5-(naphthalen-1-yl)-7*H*-pyrrolo[2,3-*d*]pyrimidin-4-amine (2.9): Following the general procedure: **2.9d** (74 mg, .127 mmol, 1.0 eq), was coupled with MeMgI. The mixture was thoroughly purged with vacuum then argon. Workup and purification was followed according to the general procedure to afford 25 mg (62% yield) of **2.9** as a white solid. The ^{1}H NMR matched those reported in literature.[8]

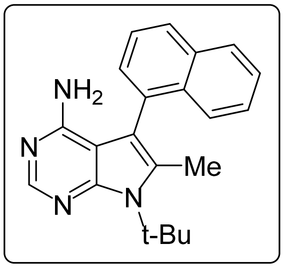

7-(*tert*-butyl)-6-methyl-5-(naphthalen-1-yl)-7*H*-pyrrolo[2,3-*d*]pyrimidin-4-amine (2.10): Following the general procedure: **2.10d** (300 mg, .503 mmol, 1.0 eq), was coupled with MeMgI. The mixture was thoroughly purged with vacuum then argon. Workup and purification was followed according to the general procedure to afford 74 mg (44% yield) of **2.10** as a yellowish-orange solid.

^{1}H NMR (500 MHz, $CDCl_3$) δ 8.23 (s, 1H), 7.93 (d, J = 8.3 Hz, 2H), 7.58 – 7.51 (m, 3H), 7.48 – 7.43 (m, 2H), 4.89 (s, 2H), 2.30 (s, 3H), 1.98 (s, 9H).

^{13}C NMR (101 MHz, $CDCl_3$) δ 154.56, 151.08, 146.53, 133.92, 133.87, 133.20, 132.14, 129.45, 128.76, 128.57, 126.94, 126.54, 126.16, 125.59, 112.28, 103.46, 61.19, 31.40, 16.11.

MS (APCI) Calculated: $C_{21}H_{23}N_4$ $[M+H]^+$ 331.2 **Found:** 331.1

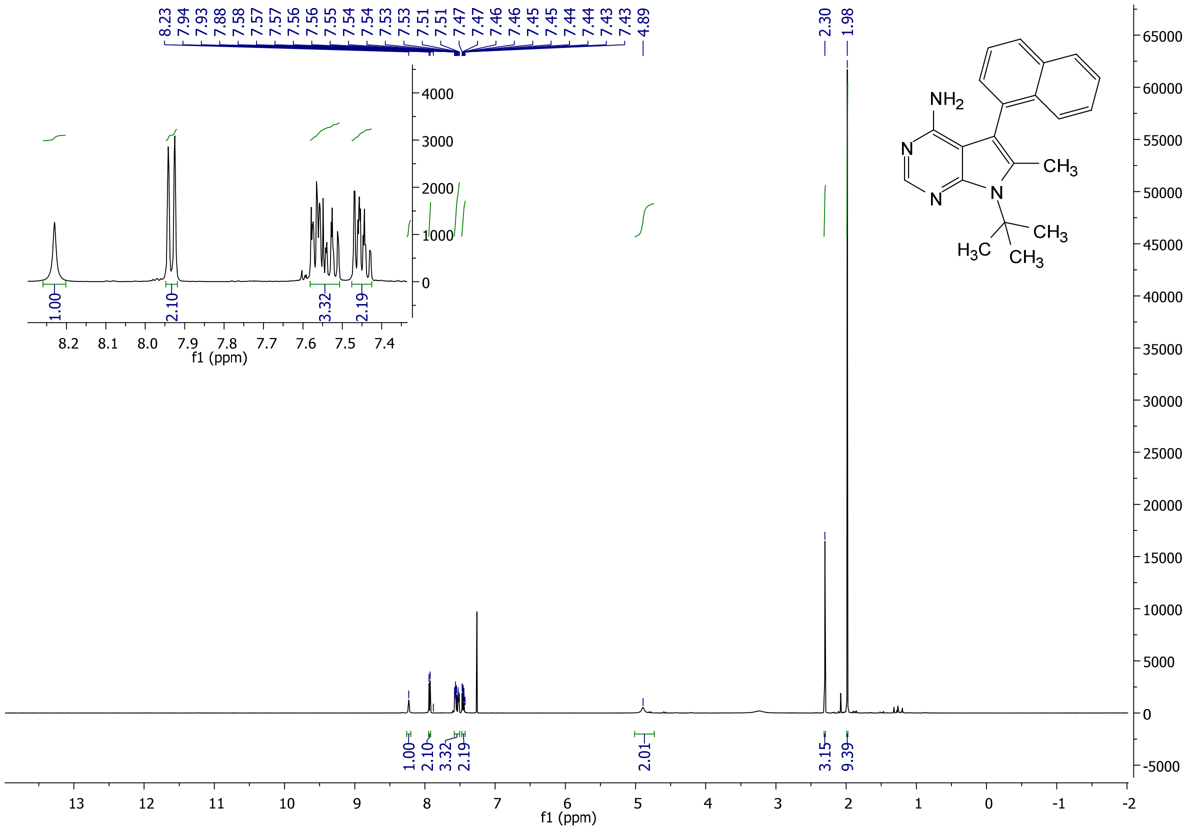
8.23
7.94
7.93
7.88
7.58
7.57
7.56
7.55
7.54
7.54
7.53
7.53
7.51
7.51
7.47
7.47
7.46
7.45
7.45
7.44
7.44
7.43
7.43
4.89
2.30
1.98
NH2
N
N
N
CH3
CH3
H3C
CH3
1.00
2.10
3.32
2.19
8.2
8.1
8.0
7.9
7.8
7.7
7.6
7.5
7.4
f1 (ppm)
4000
3000
2000
1000
0
1.00
2.10
3.32
2.19
2.01
3.15
9.39
13
12
11
10
9
8
7
6
5
4
3
2
1
0
-1
-2
f1 (ppm)
65000
60000
55000
50000
45000
40000
35000
30000
25000
20000
15000
10000
5000
0
-5000

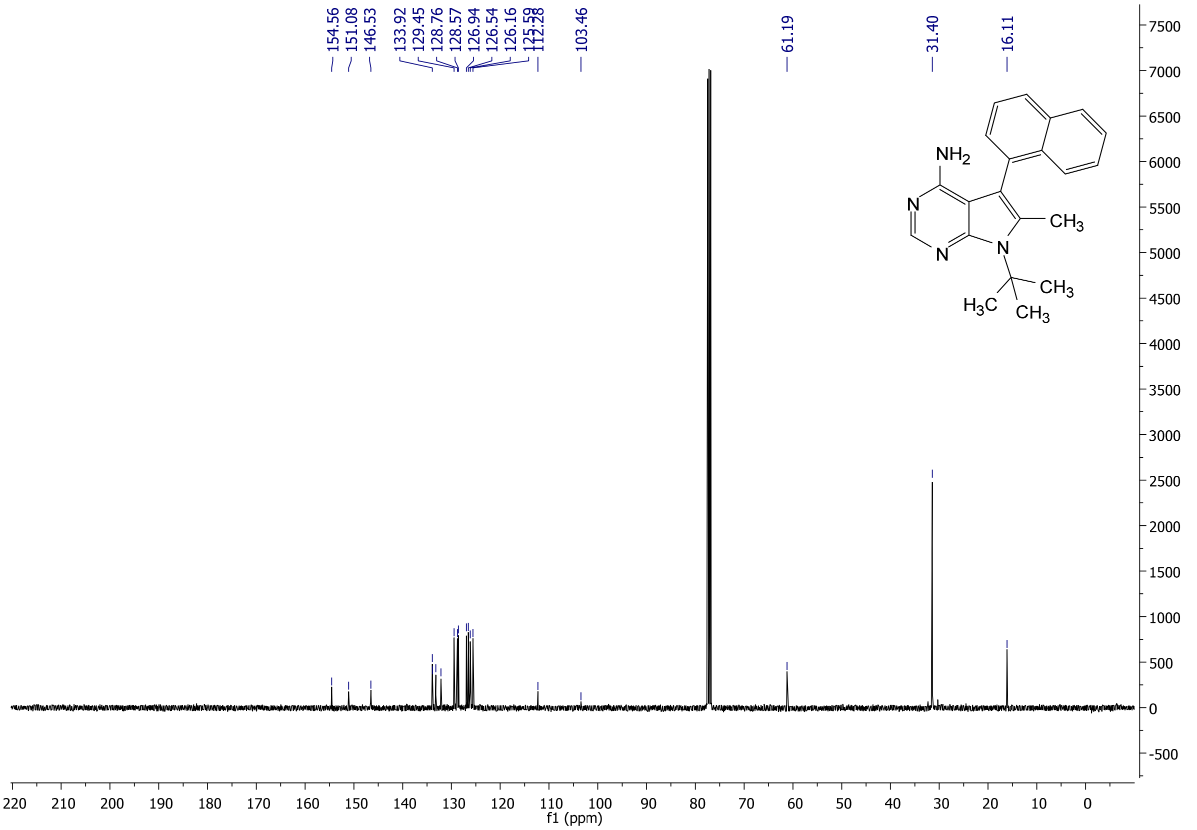
154.56
151.08
146.53
133.92
129.45
128.76
128.57
126.94
126.54
126.16
125.59
112.28
103.46
61.19
31.40
16.11
NH2
N
N
N
CH3
CH3
H3C
CH3
220
210
200
190
180
170
160
150
140
130
120
110
100
90
80
70
60
50
40
30
20
10
0
f1 (ppm)
7500
7000
6500
6000
5500
5000
4500
4000
3500
3000
2500
2000
1500
1000
500
0
-500

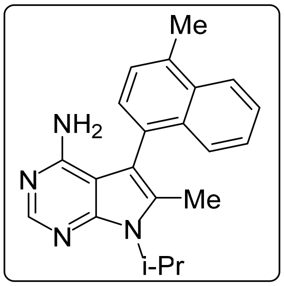

7-isopropyl-6-methyl-5-(4-methylnaphthalen-1-yl)-7*H*-pyrrolo[2,3-*d*]pyrimidin-4-amine (2.12):

Following the general procedure: **2.12d** (80 mg, 0.135 mmol, 1.0 eq) was coupled with MeMgI. The mixture was thoroughly purged with vacuum then argon. Workup and purification was followed according to the general procedure to afford 35 mg (78% yield) of **2.12** as a white-yellow solid.

^{1}H NMR (400 MHz, $CDCl_3$) δ 8.24 (s, 1H), 8.08 (d, J = 8.1 Hz, 1H), 7.65 (d, J = 7.8 Hz, 1H), 7.56 (ddd, J = 8.3, 6.8, 1.3 Hz, 1H), 7.45 (ddd, J = 8.2, 6.8, 1.2 Hz, 1H), 7.42 - 7.35 (m, 2H), 4.98 (dt, J = 14.1, 7.1 Hz, 1H), 4.82 (s, 2H), 2.77 (s, 3H), 2.21 (s, 3H), 1.74 (dd, J = 7.0, 4.5 Hz, 6H)

^{13}C NMR (101 MHz, $CDCl_3$) δ 155.01, 149.62, 148.46, 134.79, 132.99, 132.95, 131.85, 129.95, 128.85, 126.66, 126.28, 126.11, 124.56, 110.39, 102.98, 47.31, 21.70, 19.57, 11.74

MS (APCI) Calculated: $C_{21}H_{23}N_4$ $[M+H]^+$ 331.2 **Found:** 331.1

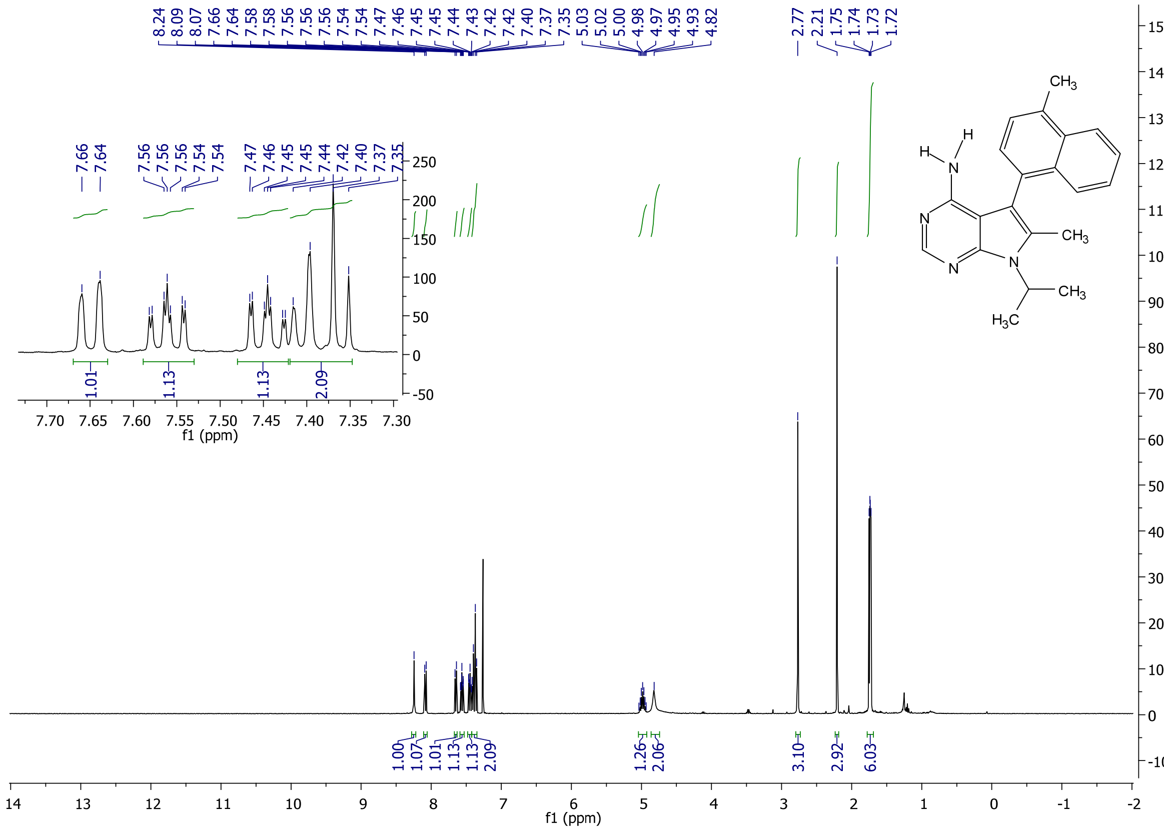
8.24
8.09
8.07
7.66
7.64
7.58
7.58
7.56
7.56
7.56
7.54
7.54
7.47
7.46
7.45
7.45
7.44
7.43
7.42
7.42
7.40
7.37
7.35
5.03
5.02
5.00
4.98
4.97
4.95
4.93
4.82
2.77
2.21
1.75
1.74
1.73
1.72
CH3
H
H
N
N
N
N
CH3
CH3
H3C
1.01
1.13
1.13
2.09
7.70 7.65 7.60 7.55 7.50 7.45 7.40 7.35 7.30
f1 (ppm)
250 200 150 100 50 0 -50
1.00
1.07
1.01
1.13
1.13
2.09
1.26
2.06
3.10
2.92
6.03
14 13 12 11 10 9 8 7 6 5 4 3 2 1 0 -1 -2
f1 (ppm)
1500 1400 1300 1200 1100 1000 900 800 700 600 500 400 300 200 100 0 -100

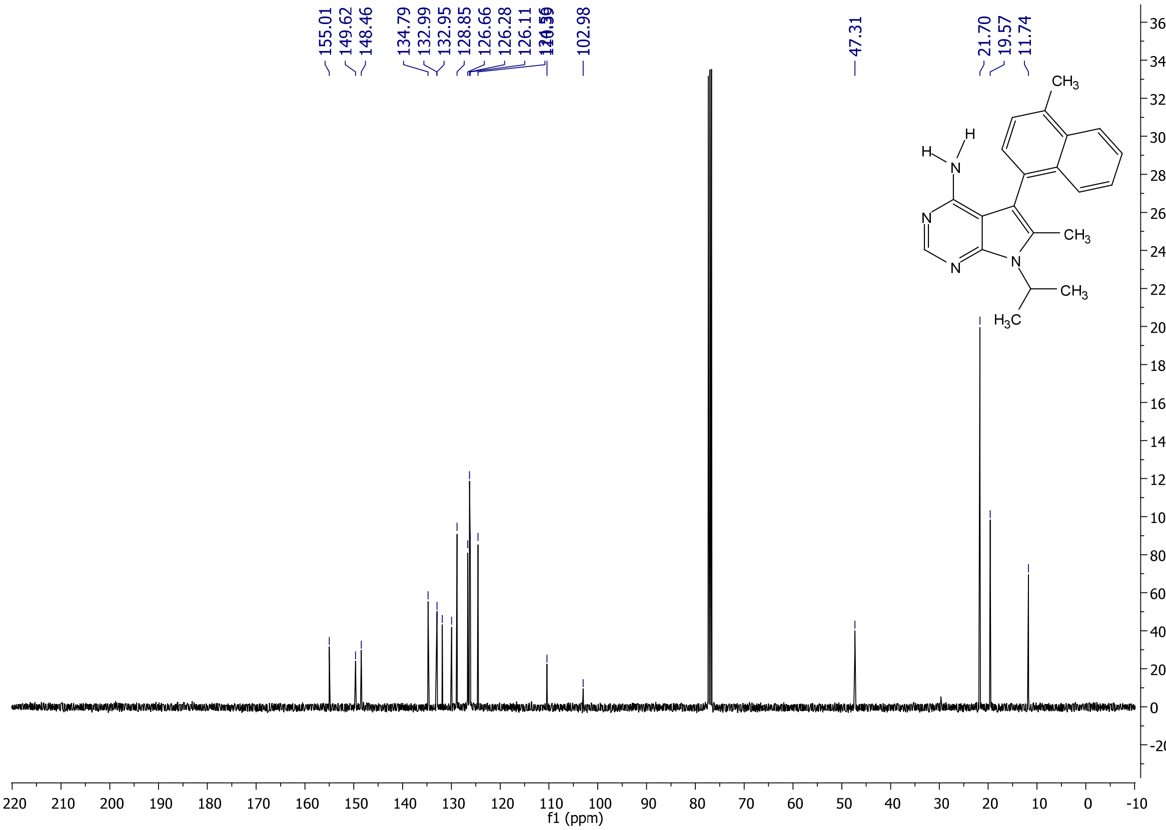
155.01
149.62
148.46
134.79
132.99
132.95
128.85
126.66
126.28
126.11
124.56
110.39
102.98
47.31
21.70
19.57
11.74
CH3
H
H
N
N
N
N
CH3
CH3
H3C
220 210 200 190 180 170 160 150 140 130 120 110 100 90 80 70 60 50 40 30 20 10 0 -10
f1 (ppm)
3600 3400 3200 3000 2800 2600 2400 2200 2000 1800 1600 1400 1200 1000 800 600 400 200 0 -200

Procedure for the tetrahydronaphthalenyl pyrrolopyrimidines:

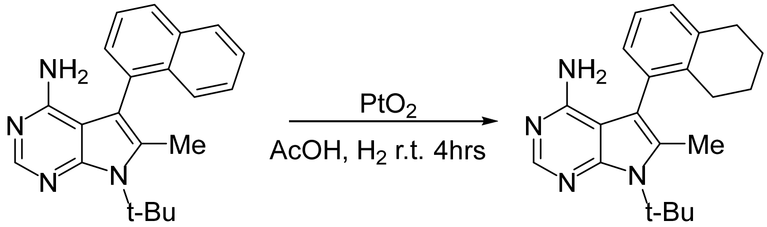

7-(*tert*-butyl)-6-methyl-5-(5,6,7,8-tetrahydronaphthalen-1-yl)-7*H*-pyrrolo[2,3-*d*]pyrimidin-4-amine (2.14):

A vial with **2.10** (50 mg, .15 mmol, 1 equiv.), PtO_2 (0.2 equiv) and stir bar was evacuated and charged with argon. Acetic acid (0.1M) was then added under argon. The mixture was quickly (~3 seconds) subjected to vacuum to remove argon and backfilled with hydrogen gas. The reaction was stirred for 2 hours with a hydrogen balloon connected to vial and product conversion was monitored by mass spectrometry and TLC. If starting material still persists after 2 hours, PtO_2 (0.2 equiv) was added after removal of hydrogen gas. Again, the reaction mixture was quickly vacuumed and backfilled with a hydrogen balloon and stirred for 2 more hours. Upon consumption of starting material, the reaction mixture was evaporated, redissolved in EtOAc, then sent on through a celite plug. The dissolved mixture was partitioned in EtOAc : $NaHCO_3$ mixture in a separatory funnel. After extraction and evaporation of the organic layer, flash column chromatography (70:30 Hexanes : EtOAc) was used to purify 29 mg of **2.14** as a light yellow solid (58% yield).

^{1}H NMR (500 MHz, $CDCl_3$) δ 8.18 (s, 1H), 7.18 - 7.12 (m, 2H), 7.03 (dd, J = 6.9, 1.7 Hz, 1H), 5.07 (s, 2H), 2.84 (t, J = 6.3 Hz, 2H), 2.41 -2.35 (m, 1H), 2.31 (s, 3H), 2.30 – 2.24 (m, 1H), 1.92 (s, 9H), 1.80 – 1.75 (m, 2H), 1.72 - 1.68 (m, 2H)

^{13}C NMR (101 MHz, $CDCl_3$) δ 153.91, 150.41, 144.62, 138.46, 137.63, 133.54, 132.83, 129.75, 128.75, 125.77, 114.22, 102.36, 61.17, 31.37, 30.05, 27.73, 23.29, 23.04, 15.80

MS (APCI) Calculated: $C_{21}H_{27}N_4$ $[M+H]^+$ 355.2 **Found:** 355.0

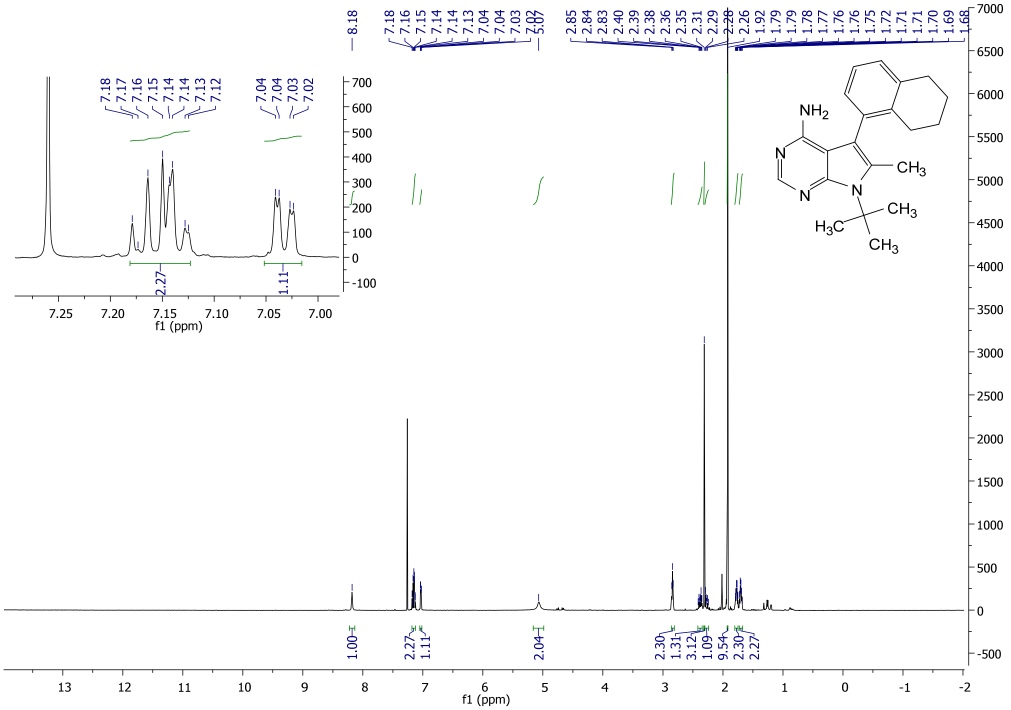

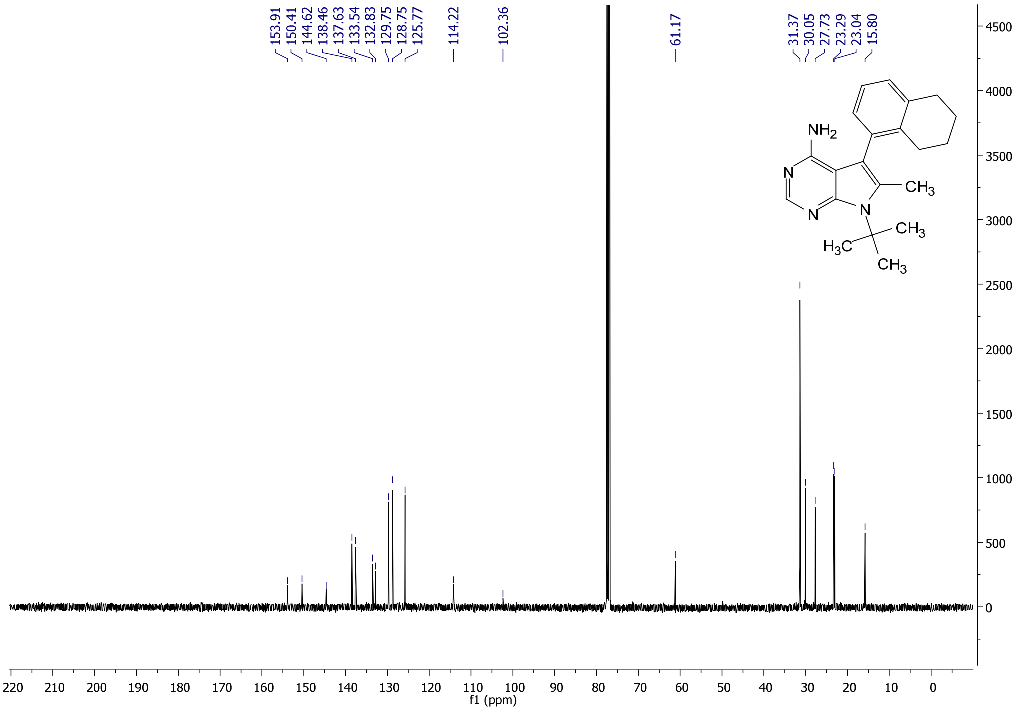

Procedure for the sulfofluoro pyrrolopyrimidines:

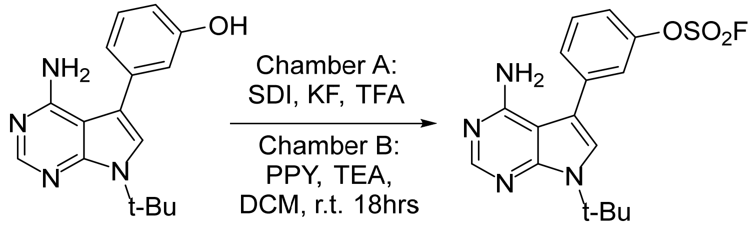

3-(4-amino-7-(*tert*-butyl)-7*H*-pyrrolo[2,3-*d*]pyrimidin-5-yl)phenyl sulfofluoridate (2.15):

A 25ml round bottom flask with **2.15a** (100 mg, .354 mmol, 1 equiv.), TEA (148 ul, 1.062 mmol, 3 equiv.), DCM (1.42 ml, .25M) and a stir bar was evacuated of air. In a separate 100 ml pressure vessel, SDI (1.189 g, 6 mmol, 1 equiv.), KF (.906 g, 15.6 mmol, 2.6 equiv.) and TFA (4 ml, 1.5M) and a stir bar were added and capped. After generation of gas in pressure vessel (~10min), gas was transferred via cannula to the round bottom flask. After reaction mixture was stirred at r.t. for 18 hours, solvent was then evaporated and crude oil was purified by flash column chromatography (70:30 Hexanes : EtOAc) yielding 23 mg of **2.15** as a white solid (18% yield).

^{1}H NMR (500 MHz, $CDCl_3$) δ 8.33 (s, 1H), 7.59 – 7.53 (m, 2H), 7.47 (s, 1H), 7.34 – 7.30 (m, 1H), 7.16 (s, 1H), 5.34 (s, 2H), 1.81 (s, 9H)

^{13}C NMR (101 MHz, $CDCl_3$) δ 156.58, 151.21, 150.46, 150.12, 138.17, 131.04, 128.97, 122.07, 121.22, 119.17, 112.92, 102.16, 57.67, 29.49

^{19}F NMR (470 MHz, $CDCl_3$) δ 39.36

MS (APCI) Calculated: $C_{16}H_{18}FN_4O_3S$ $[M+H]^+$ 365.1 **Found:** 365.0 m/z

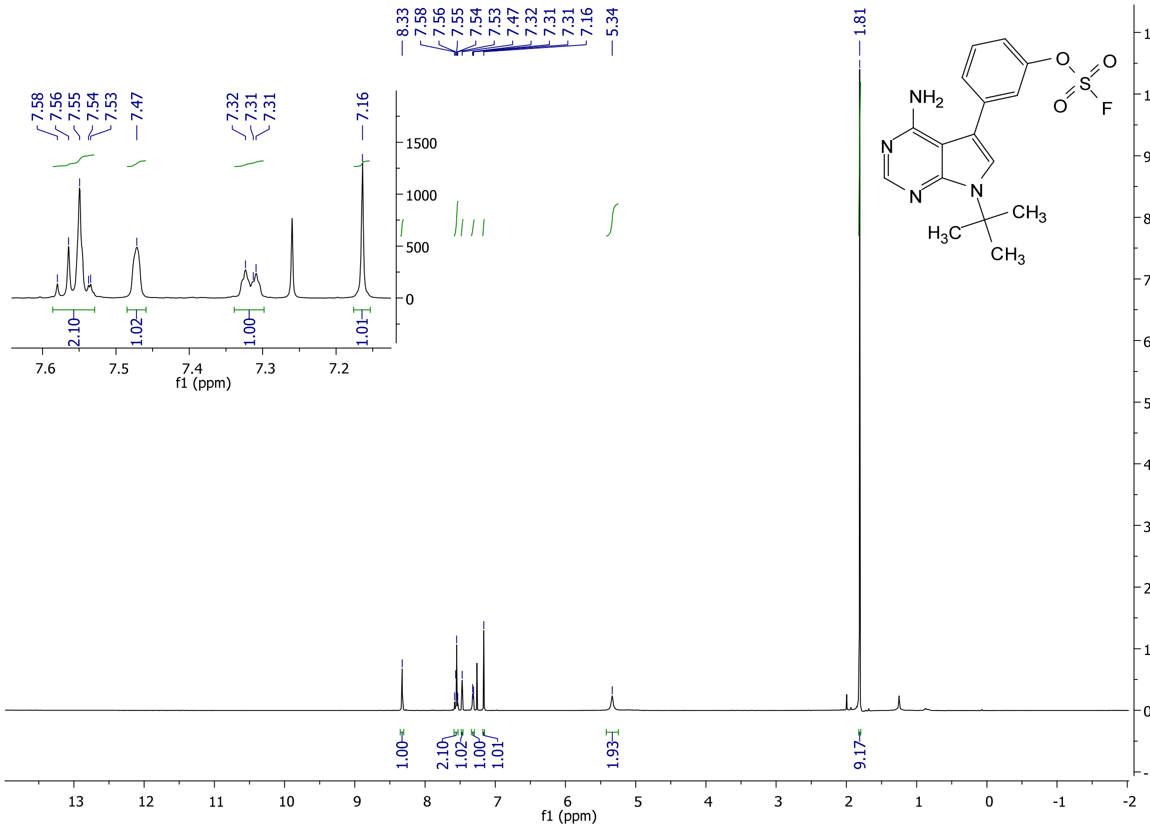
8.33
7.58
7.56
7.55
7.54
7.53
7.47
7.32
7.31
7.31
7.16
5.34
1.81
1.00
2.10
1.02
1.00
1.01
1.93
9.17
7.6
7.5
7.4
7.3
7.2
f1 (ppm)
1500
1000
500
0
NH2
N
N
N
O
S
O
O
F
CH3
H3C
CH3
11000
10000
9000
8000
7000
6000
5000
4000
3000
2000
1000
0
-1000
13
12
11
10
9
8
7
6
5
4
3
2
1
0
-1
-2
f1 (ppm)

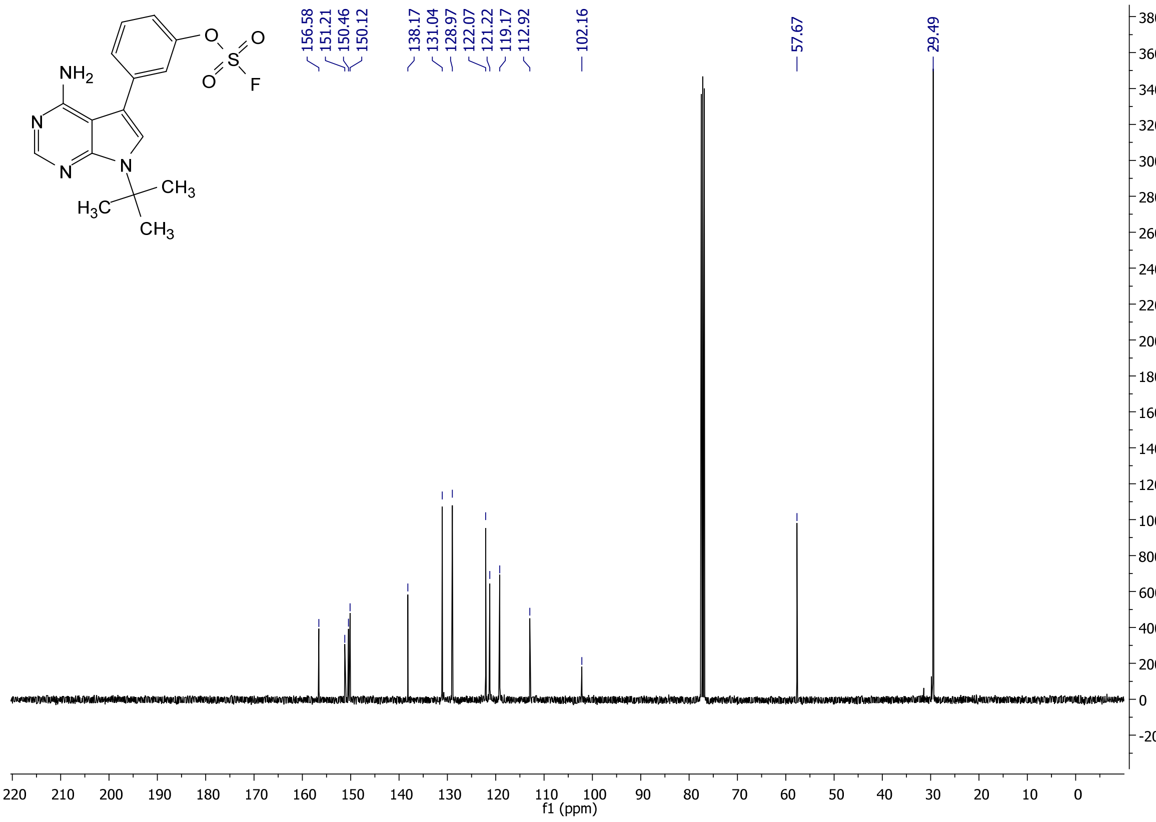
NH2
N
N
N
O
S
O
O
F
CH3
H3C
CH3
156.58
151.21
150.46
150.12
138.17
131.04
128.97
122.07
121.22
119.17
112.92
102.16
57.67
29.49
3800
3600
3400
3200
3000
2800
2600
2400
2200
2000
1800
1600
1400
1200
1000
800
600
400
200
0
-200
220
210
200
190
180
170
160
150
140
130
120
110
100
90
80
70
60
50
40
30
20
10
0
f1 (ppm)

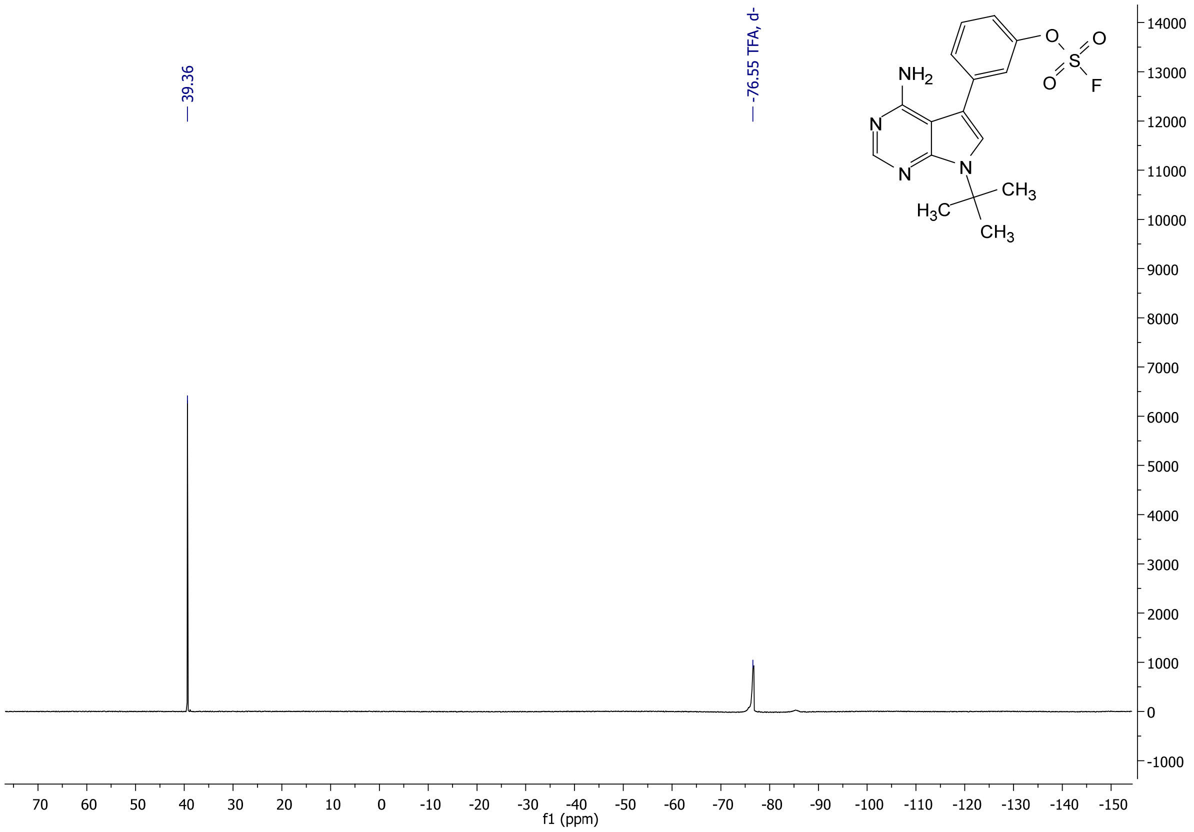
39.36
-76.55 TFA, d-
NH2
N
N
N
O
S
O
O
F
H3C
CH3
CH3
14000
13000
12000
11000
10000
9000
8000
7000
6000
5000
4000
3000
2000
1000
0
-1000
70
60
50
40
30
20
10
0
-10
-20
-30
-40
-50
-60
-70
-80
-90
-100
-110
-120
-130
-140
-150
f1 (ppm)

Chiral HPLC Data

Chiral HPLC Trace of **2.1**

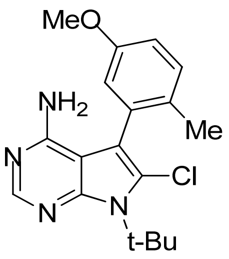

2.1 was measured with HPLC analysis using Chiralpak IA Hexanes/EtOH (80:20), flow rate = 1.0 mL/min, injection volume = 5 ul.

Racemic Standard of 2.1

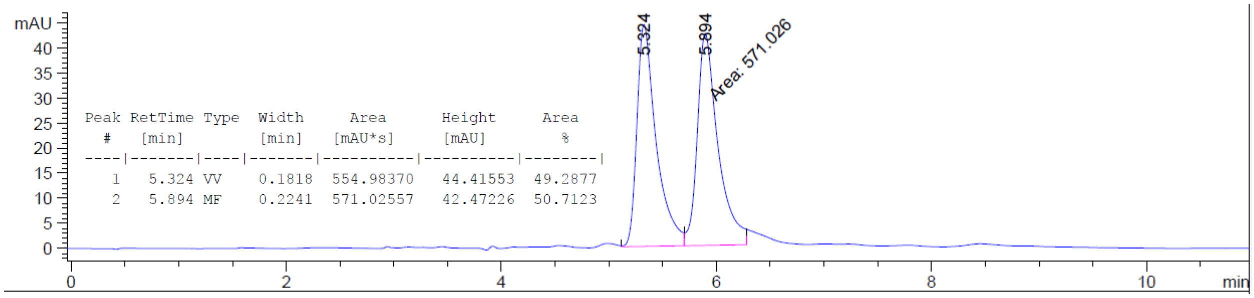

```
Peak RetTime Type  Width     Area      Height     Area
  #   [min]        [min]   [mAU*s]     [mAU]       %
----|-------|----|-------|----------|----------|--------|
   1   5.324 VV    0.1818  554.98370   44.41553  49.2877
   2   5.894 MF    0.2241  571.02557   42.47226  50.7123
```

(*R*a)-2.1

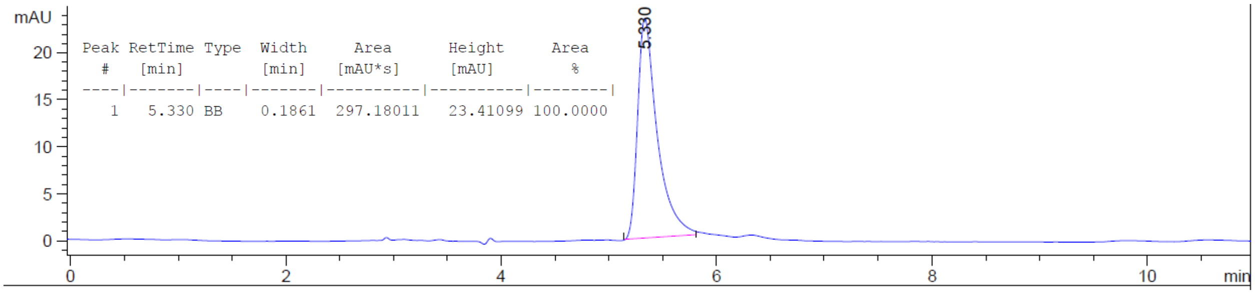

```
Peak RetTime Type  Width     Area      Height     Area
  #   [min]        [min]   [mAU*s]     [mAU]       %
----|-------|----|-------|----------|----------|--------|
   1   5.330 BB    0.1861  297.18011   23.41099 100.0000
```

(*S*a)-2.1

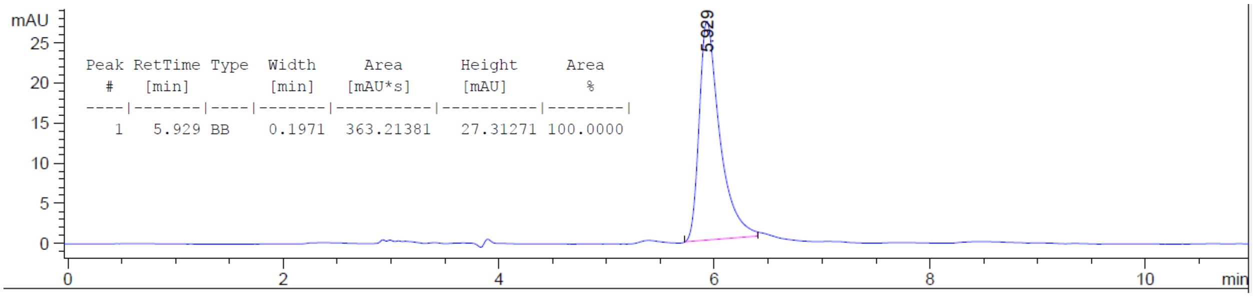

```
Peak RetTime Type  Width     Area      Height     Area
  #   [min]        [min]   [mAU*s]     [mAU]       %
----|-------|----|-------|----------|----------|--------|
   1   5.929 BB    0.1971  363.21381   27.31271 100.0000
```

Chiral HPLC Trace of **2.2**

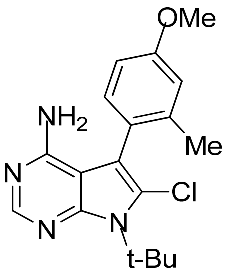

2.2 was measured with HPLC analysis using Chiralpak IA Hexanes/EtOH (80:20), flow rate = 1.0 mL/min, injection volume = 5 ul.

Racemic Standard of 2.2

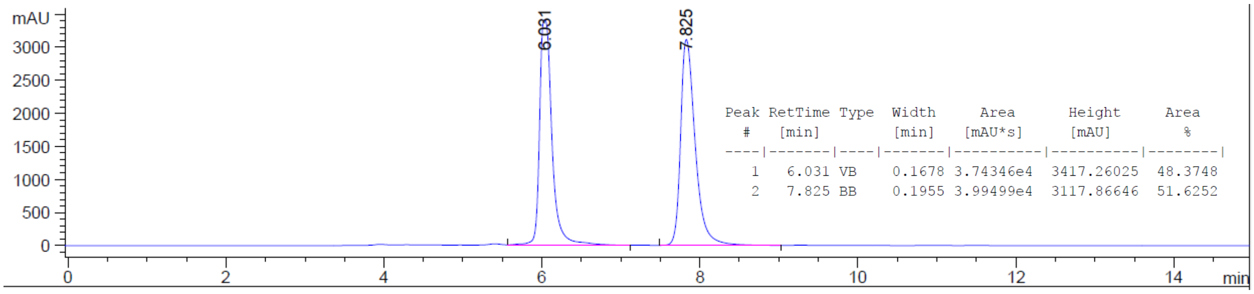

```
Peak RetTime Type  Width     Area      Height     Area
  #   [min]        [min]   [mAU*s]     [mAU]        %
----|-------|----|-------|----------|----------|--------|
  1   6.031 VB    0.1678 3.74346e4  3417.26025  48.3748
  2   7.825 BB    0.1955 3.99499e4  3117.86646  51.6252
```

(*R*a)-2.2

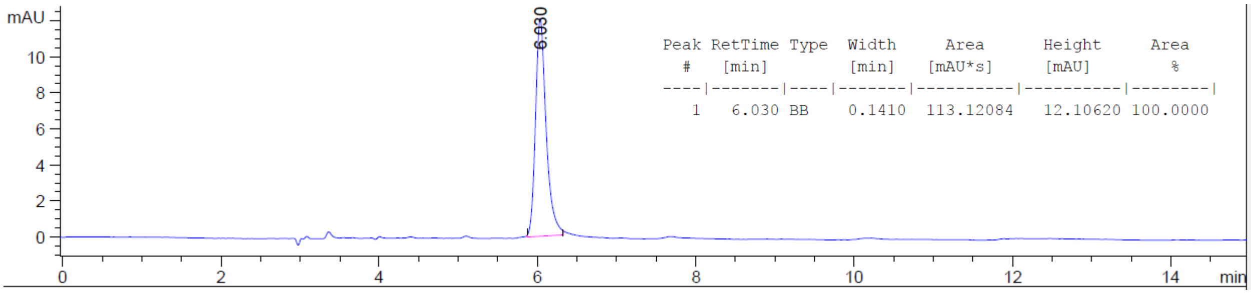

```
Peak RetTime Type  Width     Area      Height     Area
  #   [min]        [min]   [mAU*s]     [mAU]        %
----|-------|----|-------|----------|----------|--------|
  1   6.030 BB    0.1410  113.12084   12.10620 100.0000
```

(*S*a)-2.2

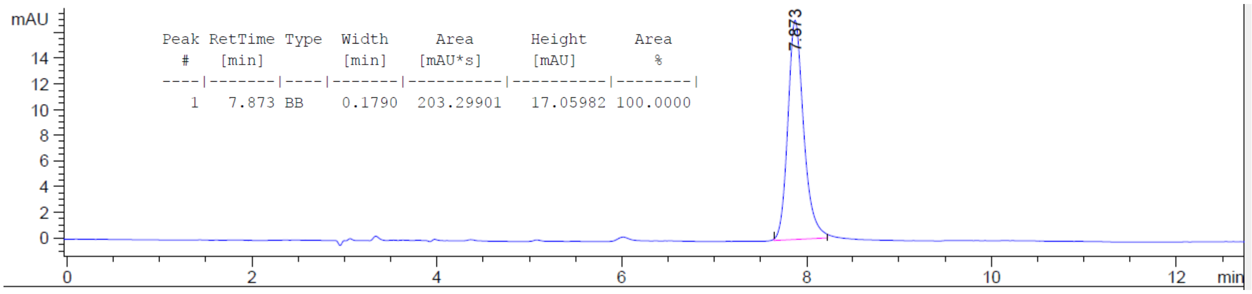

```
Peak RetTime Type  Width     Area      Height     Area
  #   [min]        [min]   [mAU*s]     [mAU]        %
----|-------|----|-------|----------|----------|--------|
  1   7.873 BB    0.1790  203.29901   17.05982 100.0000
```

Chiral HPLC Trace of **2.3**

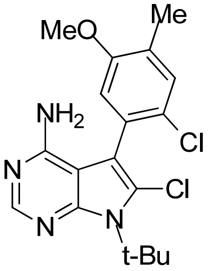

2.3 was measured with HPLC analysis using Chiralpak IA Hexanes/EtOH (80:20), flow rate = 1.0 mL/min, injection volume = 5 ul.

Racemic Standard of 2.3

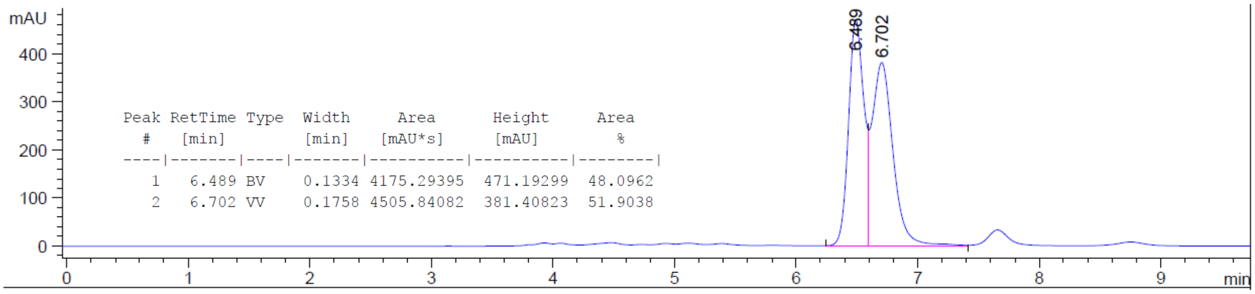

```
Peak RetTime Type  Width     Area      Height     Area
  #   [min]        [min]   [mAU*s]     [mAU]       %
----|-------|----|-------|----------|----------|--------|
  1   6.489 BV    0.1334 4175.29395  471.19299  48.0962
  2   6.702 VV    0.1758 4505.84082  381.40823  51.9038
```

(R_a)-2.3

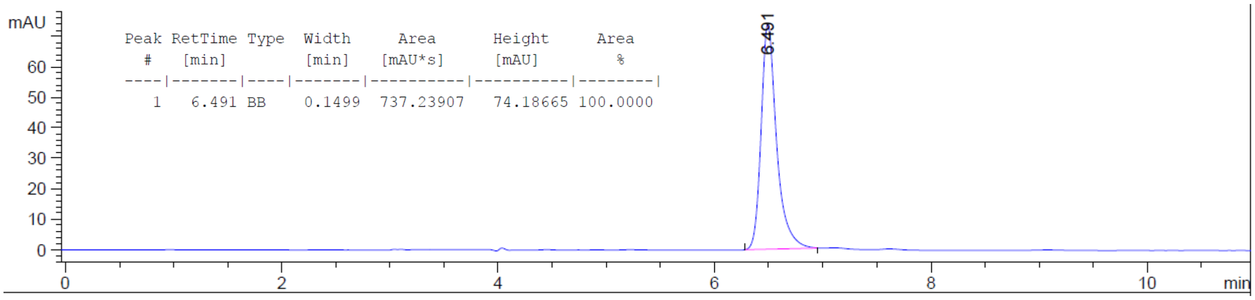

```
Peak RetTime Type  Width     Area      Height     Area
  #   [min]        [min]   [mAU*s]     [mAU]       %
----|-------|----|-------|----------|----------|--------|
  1   6.491 BB    0.1499  737.23907   74.18665 100.0000
```

(S_a)-2.3

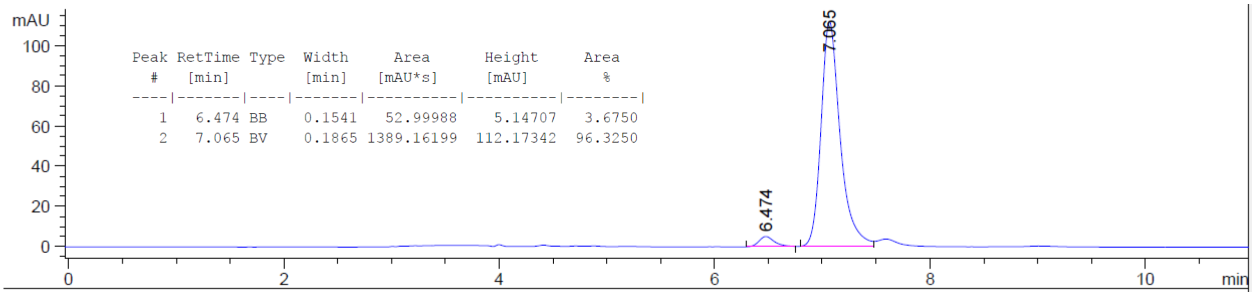

```
Peak RetTime Type  Width     Area      Height     Area
  #   [min]        [min]   [mAU*s]     [mAU]       %
----|-------|----|-------|----------|----------|--------|
  1   6.474 BB    0.1541   52.99988    5.14707   3.6750
  2   7.065 BV    0.1865 1389.16199  112.17342  96.3250
```

Chiral HPLC Trace of **2.4**

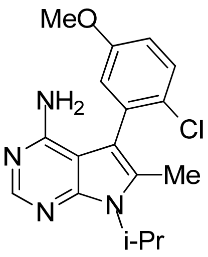

2.4 was measured with HPLC analysis using Chiralpak IA Hexanes/EtOH (80:20), flow rate = 1.0 mL/min, injection volume = 5 ul.

Racemic Standard of 2.4

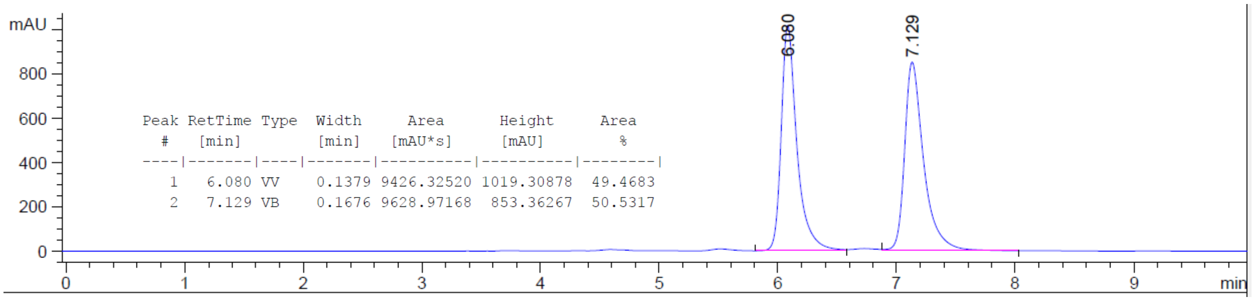

```
Peak RetTime Type  Width     Area       Height     Area
  #    [min]        [min]   [mAU*s]     [mAU]       %
----|-------|----|-------|----------|----------|--------|
   1   6.080 VV    0.1379 9426.32520 1019.30878  49.4683
   2   7.129 VB    0.1676 9628.97168  853.36267  50.5317
```

(R_a)-2.4

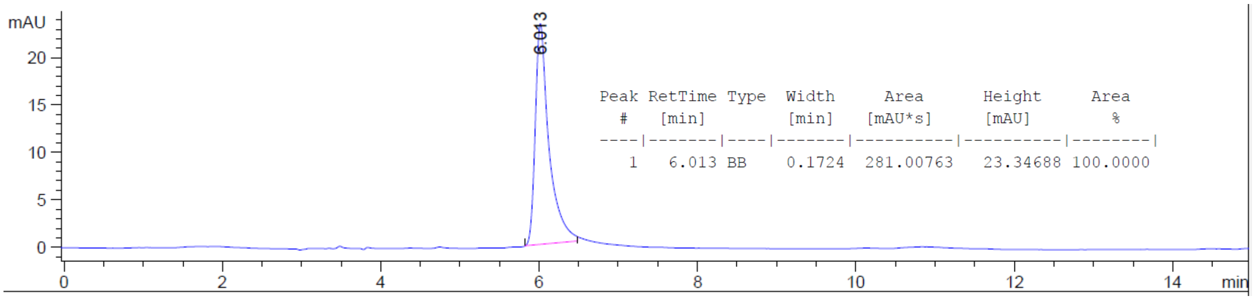

```
Peak RetTime Type  Width     Area       Height     Area
  #    [min]        [min]   [mAU*s]     [mAU]       %
----|-------|----|-------|----------|----------|--------|
   1   6.013 BB    0.1724  281.00763   23.34688 100.0000
```

(S_a)-2.4

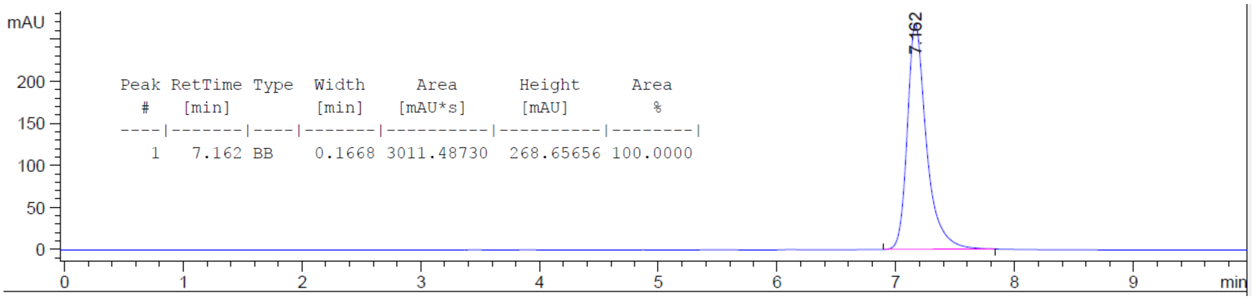

```
Peak RetTime Type  Width     Area       Height     Area
  #    [min]        [min]   [mAU*s]     [mAU]       %
----|-------|----|-------|----------|----------|--------|
   1   7.162 BB    0.1668 3011.48730  268.65656 100.0000
```

Chiral HPLC Trace of **2.5**

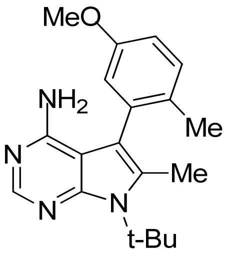

2.5 was measured with HPLC analysis using Chiralpak IA Hexanes/EtOH (90:10), flow rate = 1.0 mL/min, injection volume = 5 ul.

Racemic Standard of 2.5

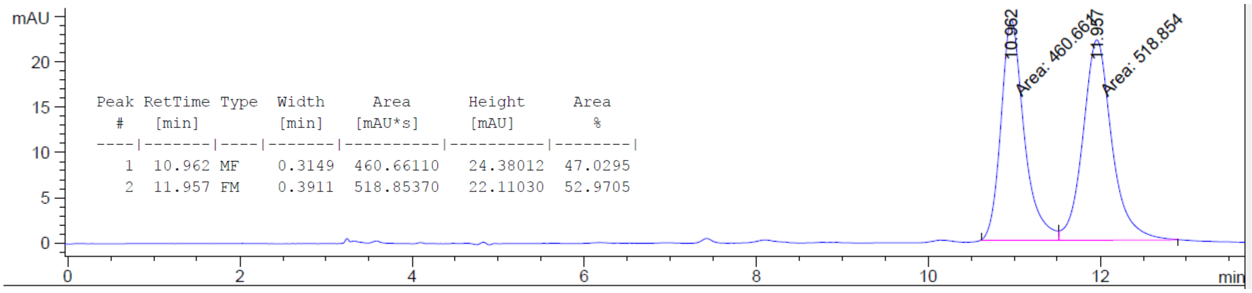

```
Peak RetTime Type  Width     Area      Height     Area
  #   [min]         [min]   [mAU*s]     [mAU]       %
----|-------|----|-------|----------|----------|--------|
   1  10.962 MF    0.3149  460.66110   24.38012  47.0295
   2  11.957 FM    0.3911  518.85370   22.11030  52.9705
```

(R_a)-2.5

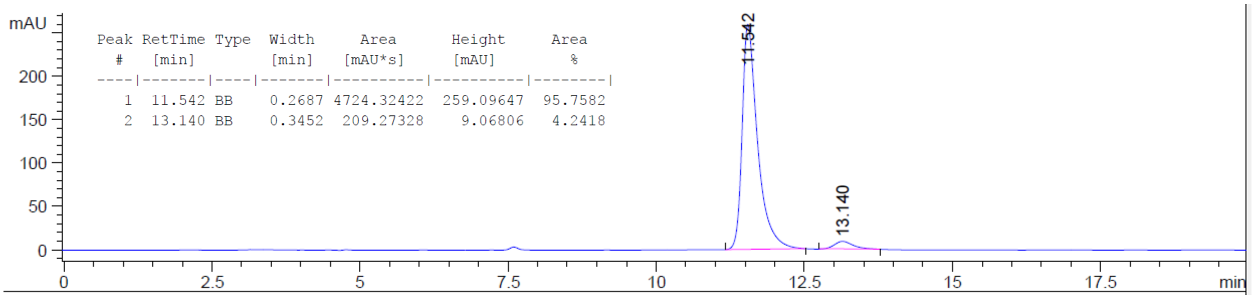

```
Peak RetTime Type  Width     Area      Height     Area
  #   [min]         [min]   [mAU*s]     [mAU]       %
----|-------|----|-------|----------|----------|--------|
   1  11.542 BB    0.2687 4724.32422  259.09647  95.7582
   2  13.140 BB    0.3452  209.27328    9.06806   4.2418
```

(S_a)-2.5

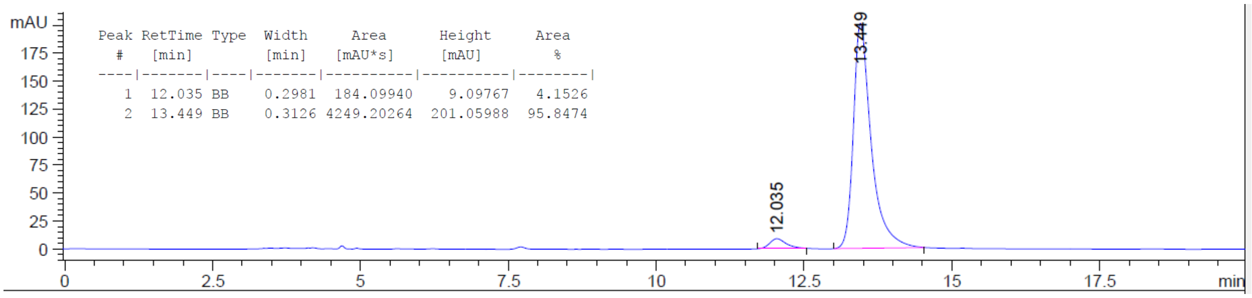

```
Peak RetTime Type  Width     Area      Height     Area
  #   [min]         [min]   [mAU*s]     [mAU]       %
----|-------|----|-------|----------|----------|--------|
   1  12.035 BB    0.2981  184.09940    9.09767   4.1526
   2  13.449 BB    0.3126 4249.20264  201.05988  95.8474
```

Chiral HPLC Trace of **2.6**

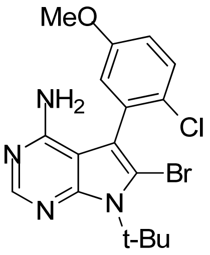

2.6 was measured with HPLC analysis using Chiralpak IA Hexanes/EtOH (80:20), flow rate = 1.0 mL/min, injection volume = 5 ul.

Racemic Standard of 2.6

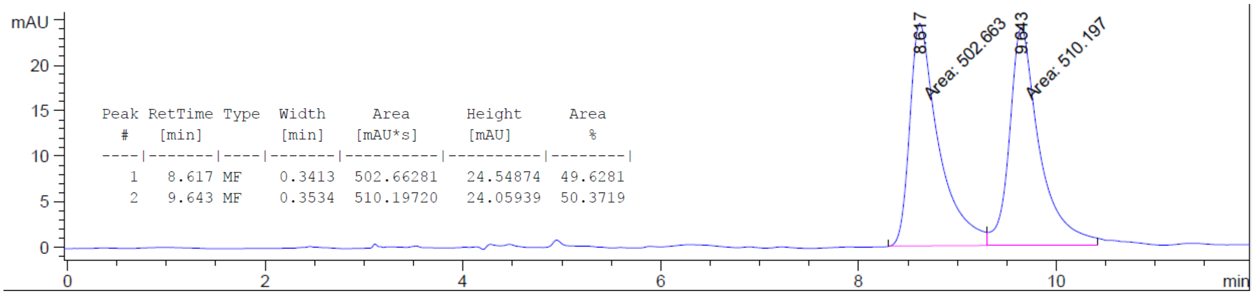
```
Peak RetTime Type  Width     Area       Height     Area
  #   [min]        [min]   [mAU*s]      [mAU]       %
----|-------|----|-------|----------|----------|--------|
   1   8.617 MF     0.3413  502.66281   24.54874  49.6281
   2   9.643 MF     0.3534  510.19720   24.05939  50.3719
```

(*R*a)-2.6

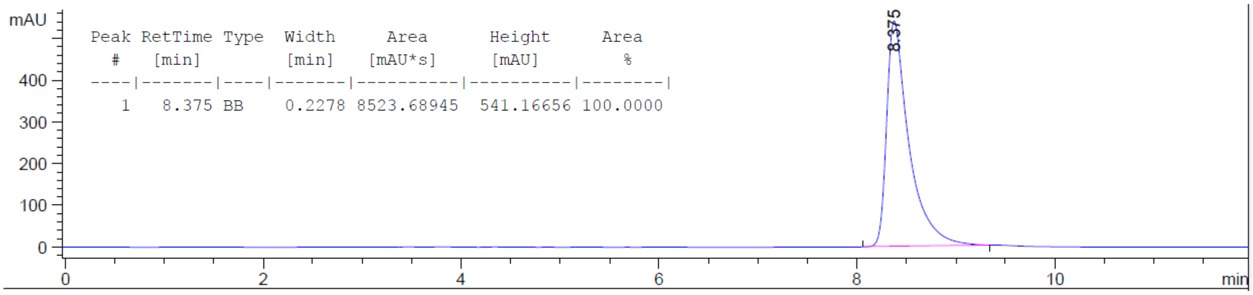
```
Peak RetTime Type  Width     Area       Height     Area
  #   [min]        [min]   [mAU*s]      [mAU]       %
----|-------|----|-------|----------|----------|--------|
   1   8.375 BB     0.2278 8523.68945  541.16656 100.0000
```

(*S*a)-2.6

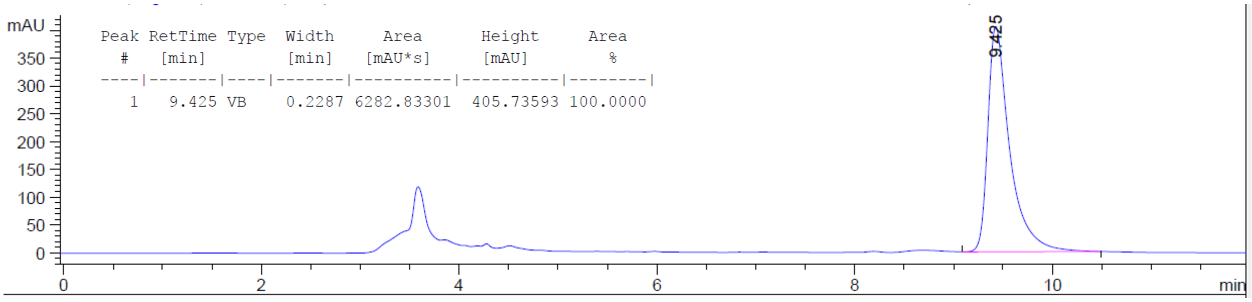
```
Peak RetTime Type  Width     Area       Height     Area
  #   [min]        [min]   [mAU*s]      [mAU]       %
----|-------|----|-------|----------|----------|--------|
   1   9.425 VB     0.2287 6282.83301  405.73593 100.0000
```

Chiral HPLC Trace of **2.7**

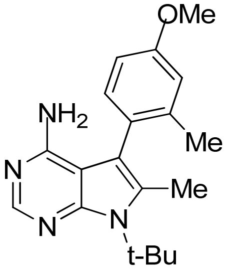

2.7 was measured with HPLC analysis using Chiralpak IA Hexanes/EtOH (80:20), flow rate = 1.0 mL/min, injection volume = 5 ul.

Racemic Standard of 2.7

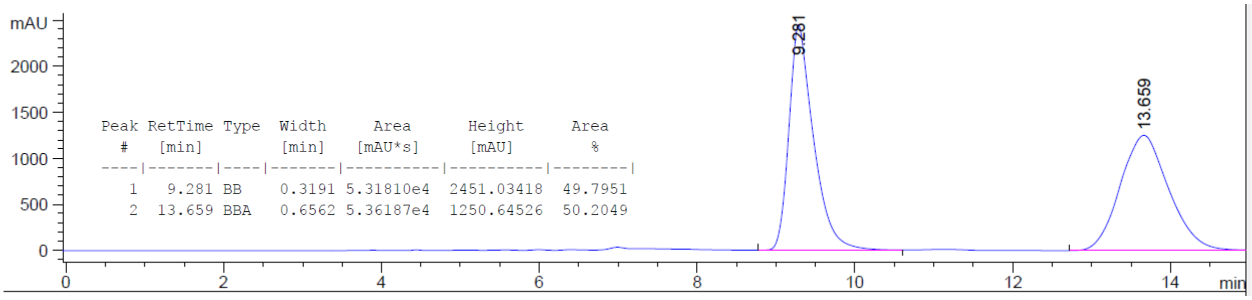

```
Peak RetTime Type  Width     Area      Height     Area
  #   [min]        [min]   [mAU*s]     [mAU]        %
----|-------|----|-------|----------|----------|--------|
   1   9.281 BB    0.3191 5.31810e4  2451.03418  49.7951
   2  13.659 BBA   0.6562 5.36187e4  1250.64526  50.2049
```

(R_a)-2.7

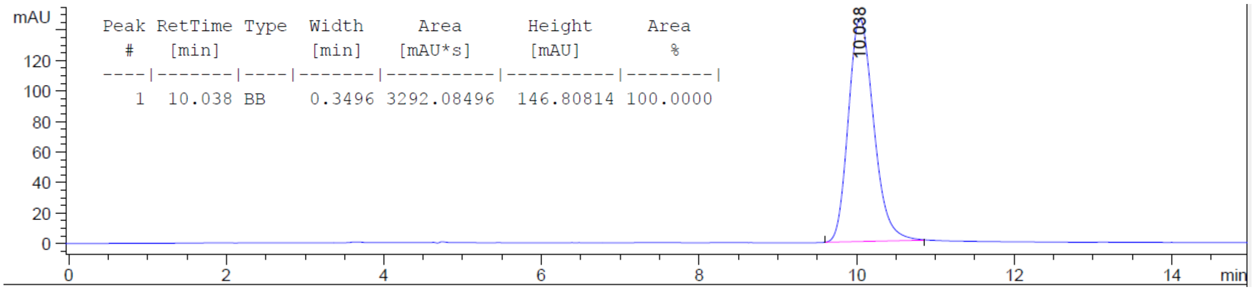

```
Peak RetTime Type  Width     Area      Height     Area
  #   [min]        [min]   [mAU*s]     [mAU]        %
----|-------|----|-------|----------|----------|--------|
   1  10.038 BB    0.3496 3292.08496  146.80814 100.0000
```

(S_a)-2.7

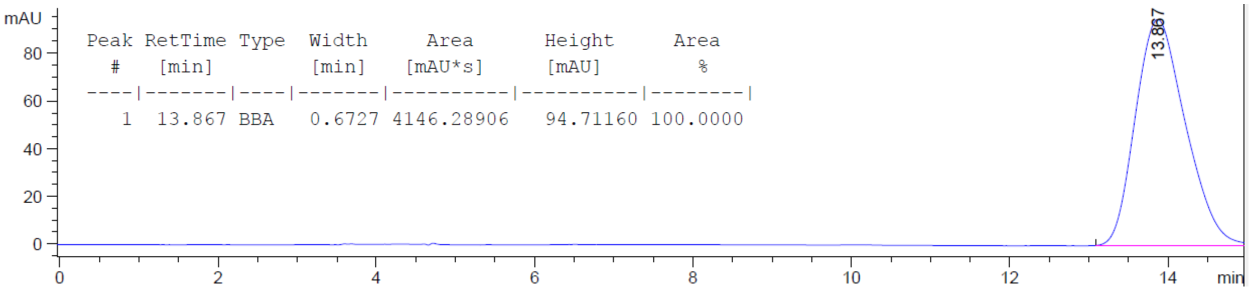

```
Peak RetTime Type  Width     Area      Height     Area
  #   [min]        [min]   [mAU*s]     [mAU]        %
----|-------|----|-------|----------|----------|--------|
   1  13.867 BBA   0.6727 4146.28906   94.71160 100.0000
```

Chiral HPLC Trace of **2.8**

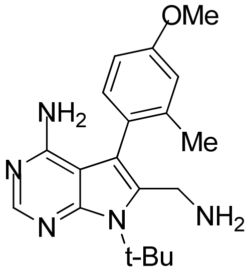

2.8 was measured with HPLC analysis using Chiralpak IA Hexanes/EtOH (85:15), flow rate = 1.0 mL/min, injection volume = 5 ul.

Racemic Standard of 2.8

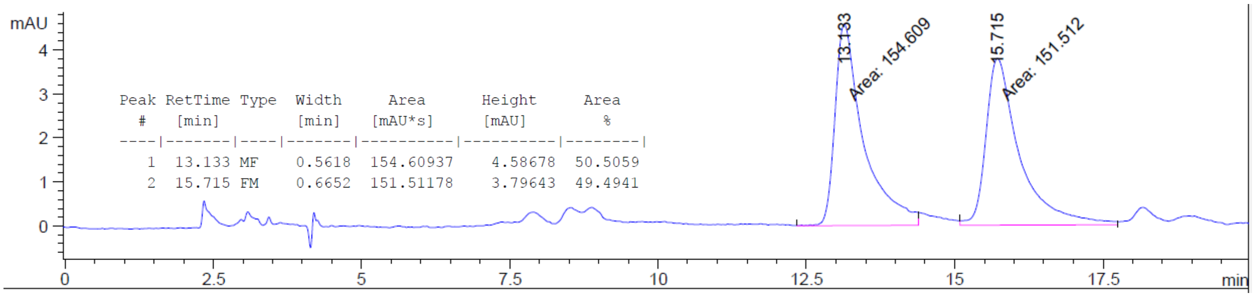

```
Peak RetTime Type  Width     Area       Height      Area
  #   [min]        [min]   [mAU*s]      [mAU]        %
----|-------|----|-------|----------|----------|--------|
  1  13.133 MF    0.5618  154.60937    4.58678  50.5059
  2  15.715 FM    0.6652  151.51178    3.79643  49.4941
```

(*R*a)-2.8

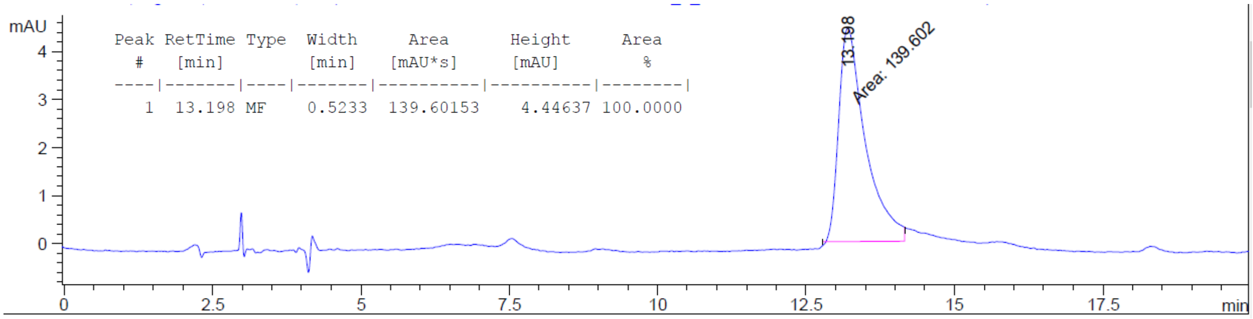

```
Peak RetTime Type  Width     Area      Height      Area
  #   [min]        [min]   [mAU*s]     [mAU]        %
----|-------|----|-------|----------|----------|--------|
  1  13.198 MF    0.5233  139.60153    4.44637 100.0000
```

(*S*a)-2.8

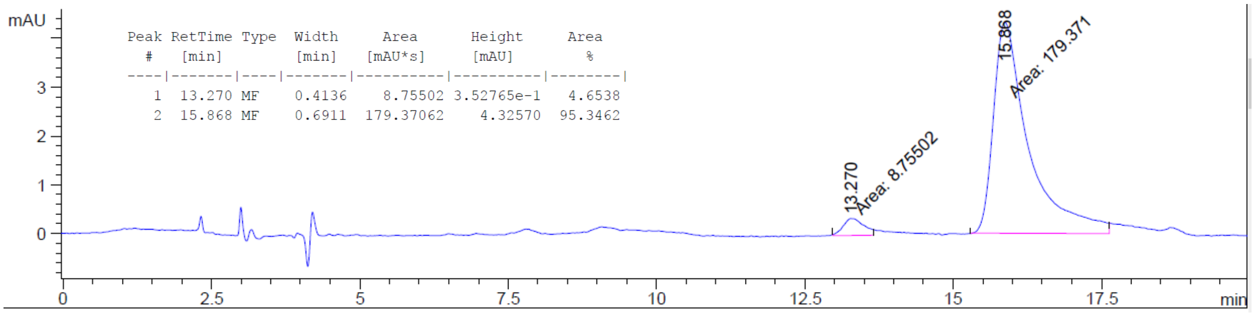

```
Peak RetTime Type  Width     Area      Height      Area
  #   [min]        [min]   [mAU*s]     [mAU]        %
----|-------|----|-------|----------|----------|--------|
  1  13.270 MF    0.4136    8.75502 3.52765e-1   4.6538
  2  15.868 MF    0.6911  179.37062    4.32570  95.3462
```

Chiral HPLC Trace of **2.9**

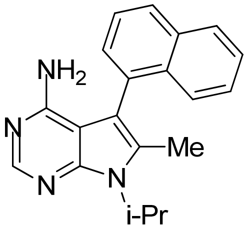

2.9 was measured with HPLC analysis using Chiralpak IA Hexanes/EtOH (80:20), flow rate = 1.0 mL/min, injection volume = 5 ul.

Racemic Standard of 2.9

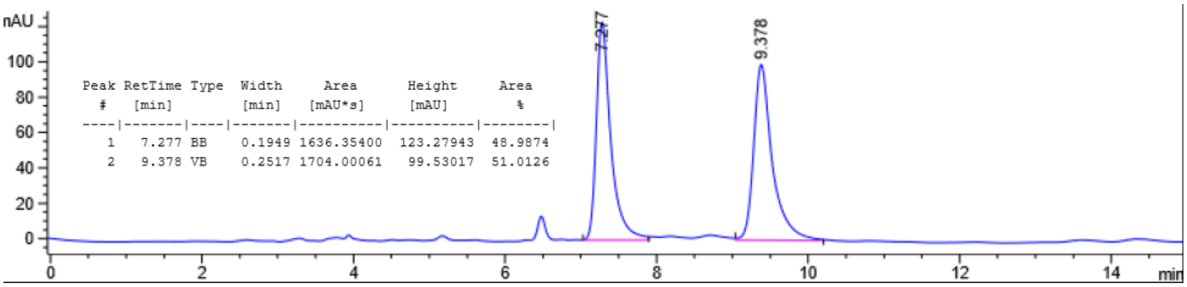

```
Peak RetTime Type  Width     Area      Height     Area
  #   [min]        [min]   [mAU*s]     [mAU]       %
----|-------|----|-------|----------|----------|--------|
   1   7.277 BB    0.1949 1636.35400  123.27943  48.9874
   2   9.378 VB    0.2517 1704.00061   99.53017  51.0126
```

(*R*a)-2.9

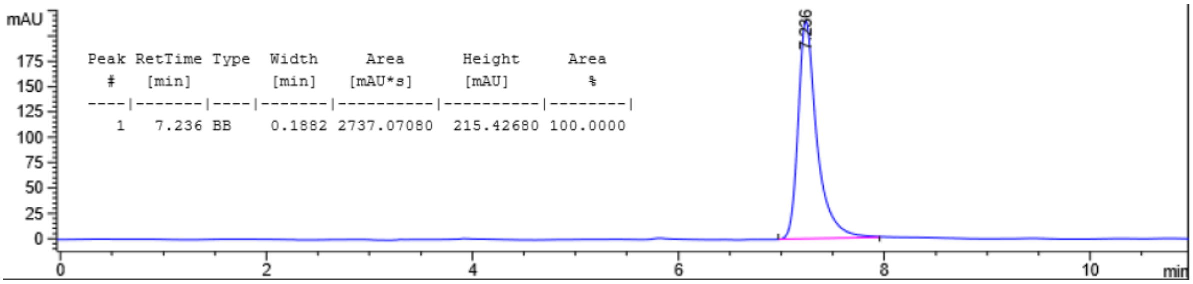

```
Peak RetTime Type  Width     Area      Height     Area
  #   [min]        [min]   [mAU*s]     [mAU]       %
----|-------|----|-------|----------|----------|--------|
   1   7.236 BB    0.1882 2737.07080  215.42680 100.0000
```

(*S*a)-2.9

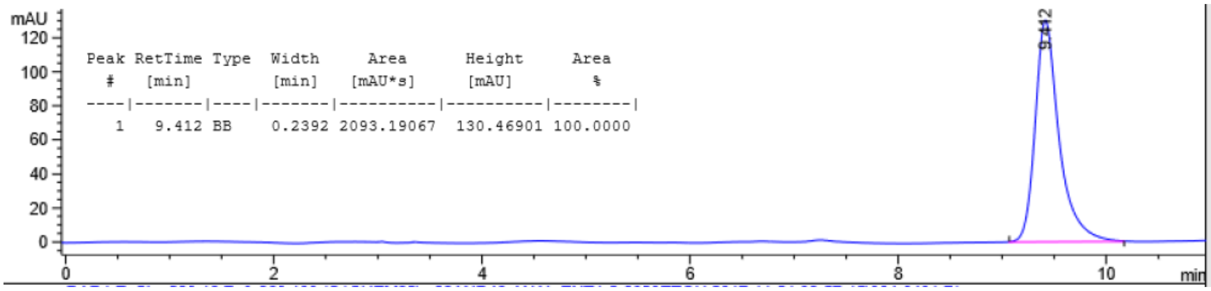

```
Peak RetTime Type  Width     Area      Height     Area
  #   [min]        [min]   [mAU*s]     [mAU]       %
----|-------|----|-------|----------|----------|--------|
   1   9.412 BB    0.2392 2093.19067  130.46901 100.0000
```

Chiral HPLC Trace of **2.10**

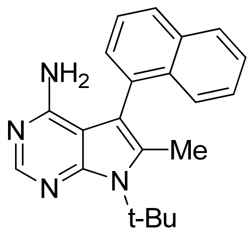

2.10 was measured with HPLC analysis using Chiralpak IA Hexanes/EtOH (80:20), flow rate = 1.0 mL/min, injection volume = 5 ul.

Racemic Standard of 2.10

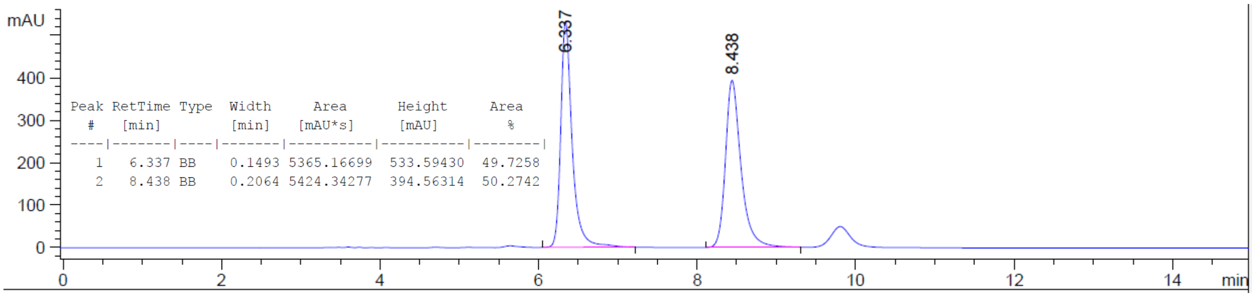

```
Peak RetTime Type  Width     Area      Height     Area
  #   [min]        [min]   [mAU*s]     [mAU]       %
----|-------|----|-------|----------|----------|--------|
  1   6.337 BB    0.1493 5365.16699  533.59430  49.7258
  2   8.438 BB    0.2064 5424.34277  394.56314  50.2742
```

(*R*a)-2.10

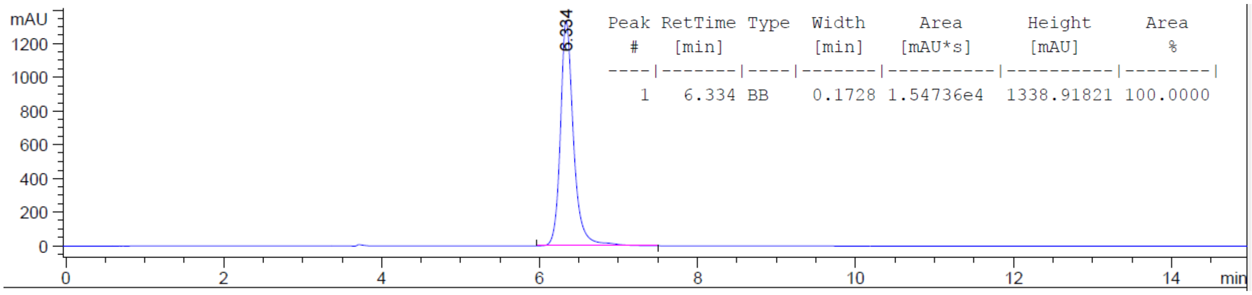

```
Peak RetTime Type  Width     Area      Height     Area
  #   [min]        [min]   [mAU*s]     [mAU]       %
----|-------|----|-------|----------|----------|--------|
  1   6.334 BB    0.1728 1.54736e4 1338.91821 100.0000
```

(*S*a)-2.10

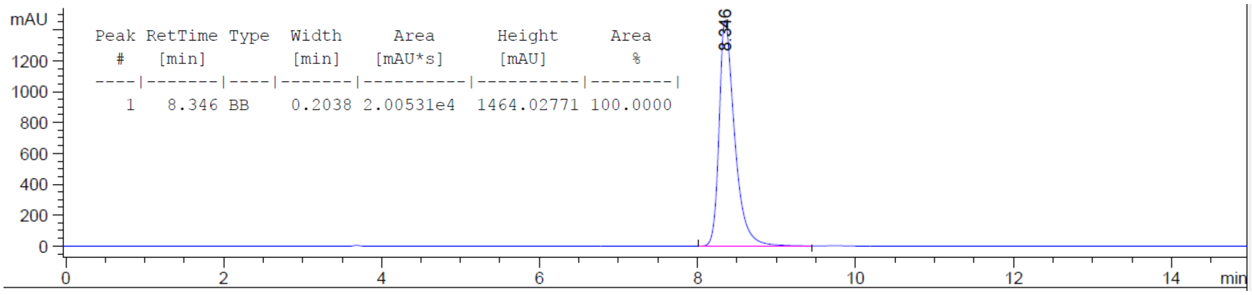

```
Peak RetTime Type  Width     Area      Height     Area
  #   [min]        [min]   [mAU*s]     [mAU]       %
----|-------|----|-------|----------|----------|--------|
  1   8.346 BB    0.2038 2.00531e4 1464.02771 100.0000
```

Chiral HPLC Trace of **2.11**

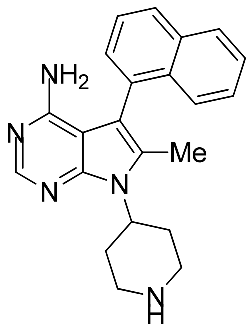

2.11 was measured with HPLC analysis using Chiralpak IA Hexanes/EtOH (80:20), flow rate = 1.0 mL/min, injection volume = 5 ul. ***2.11** atropisomers were separated with Boc protecting group on piperidine.

Racemic Standard of 2.11

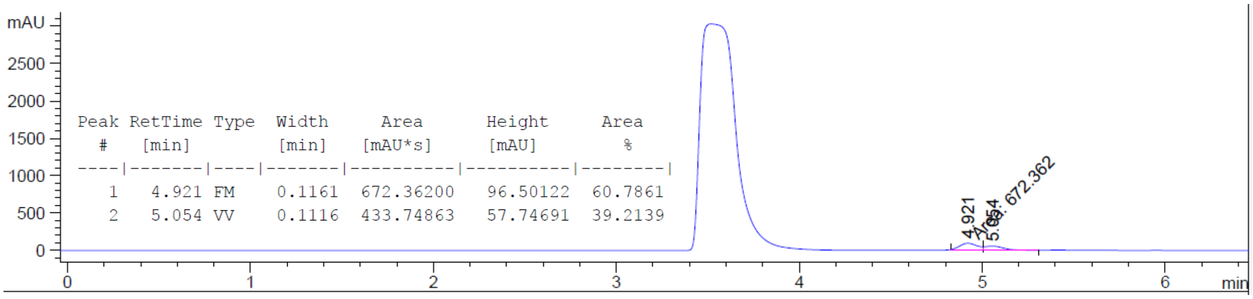

```
Peak RetTime Type  Width     Area      Height     Area
  #   [min]        [min]   [mAU*s]     [mAU]        %
----|-------|----|-------|----------|----------|--------|
  1    4.921 FM    0.1161  672.36200   96.50122  60.7861
  2    5.054 VV    0.1116  433.74863   57.74691  39.2139
```

(R_a)-2.11

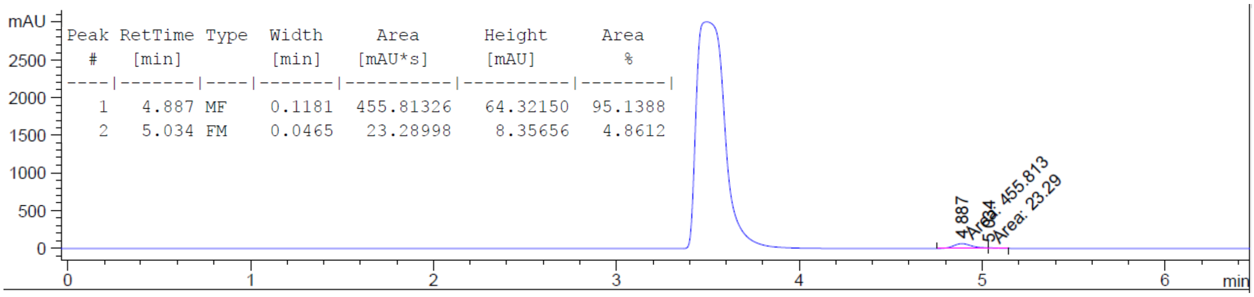

```
Peak RetTime Type  Width     Area      Height     Area
  #   [min]        [min]   [mAU*s]     [mAU]        %
----|-------|----|-------|----------|----------|--------|
  1    4.887 MF    0.1181  455.81326   64.32150  95.1388
  2    5.034 FM    0.0465   23.28998    8.35656   4.8612
```

(S_a)-2.11

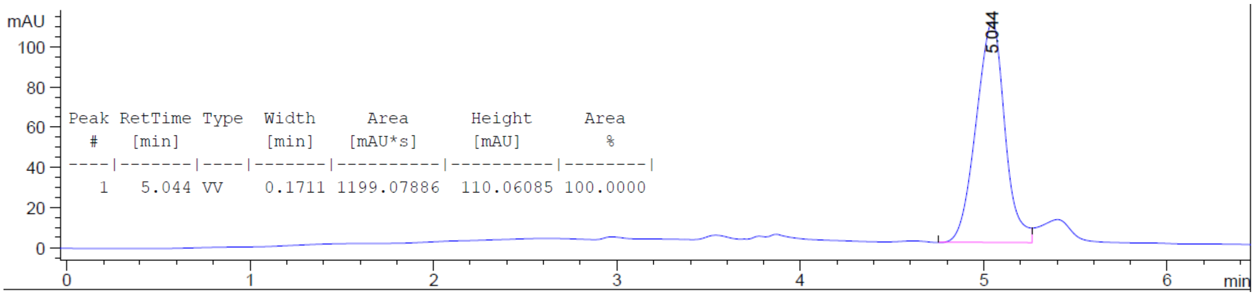

```
Peak RetTime Type  Width     Area      Height     Area
  #   [min]        [min]   [mAU*s]     [mAU]        %
----|-------|----|-------|----------|----------|--------|
  1    5.044 VV    0.1711 1199.07886  110.06085 100.0000
```

Chiral HPLC Trace of **2.12**

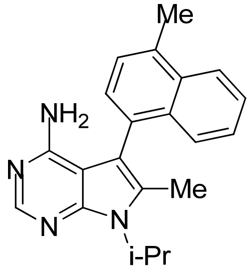

2.12 was measured with HPLC analysis using Chiralpak IA Hexanes/EtOH (80:20), flow rate = 1.0 mL/min, injection volume = 5 ul.

Racemic Standard of 2.12

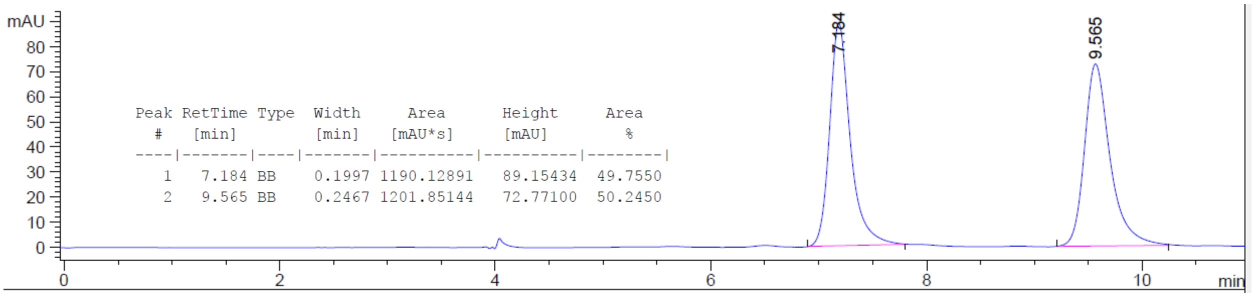
```
Peak RetTime Type  Width     Area      Height     Area
 #    [min]        [min]   [mAU*s]     [mAU]       %
----|-------|----|-------|----------|----------|--------|
  1   7.184 BB    0.1997 1190.12891   89.15434  49.7550
  2   9.565 BB    0.2467 1201.85144   72.77100  50.2450
```

(*R*$_{a}$)-2.12

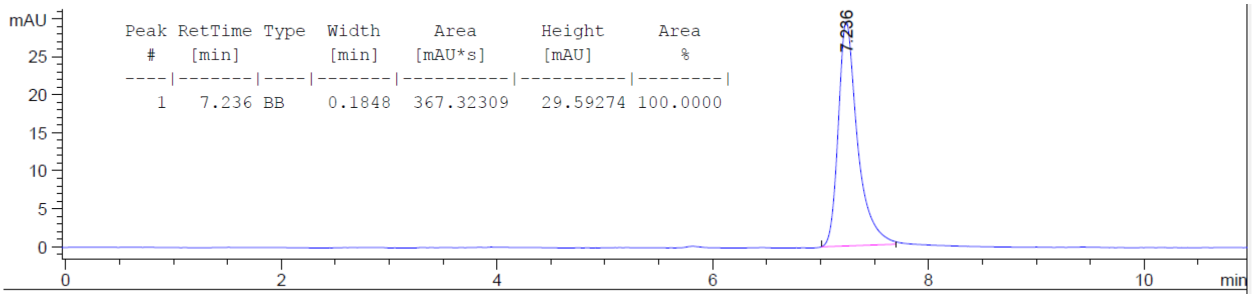
```
Peak RetTime Type  Width     Area      Height     Area
 #    [min]        [min]   [mAU*s]     [mAU]       %
----|-------|----|-------|----------|----------|--------|
  1   7.236 BB    0.1848  367.32309   29.59274 100.0000
```

(*S*$_{a}$)-2.12

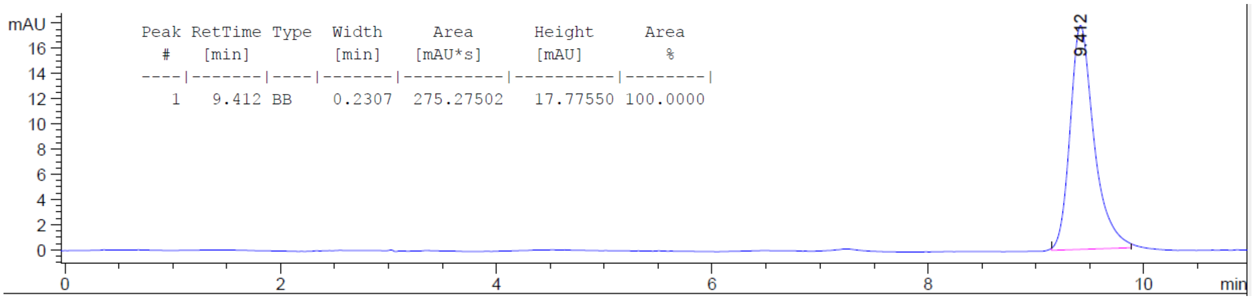
```
Peak RetTime Type  Width     Area      Height     Area
 #    [min]        [min]   [mAU*s]     [mAU]       %
----|-------|----|-------|----------|----------|--------|
  1   9.412 BB    0.2307  275.27502   17.77550 100.0000
```

Chiral HPLC Trace of **2.13**

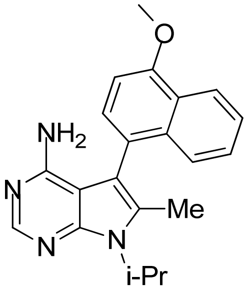

2.13 was measured with HPLC analysis using Chiralpak IA Hexanes/EtOH (70:30), flow rate = 1.0 mL/min, injection volume = 5 ul.

Racemic Standard of 2.13

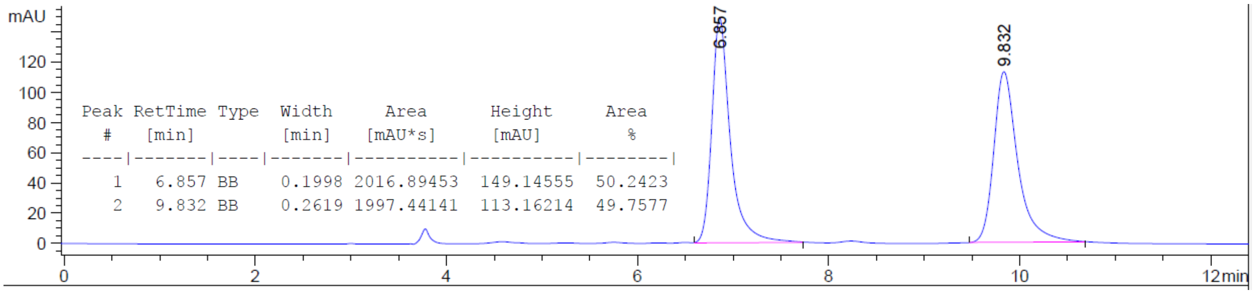

```
Peak RetTime Type  Width     Area      Height     Area
  #   [min]        [min]   [mAU*s]     [mAU]       %
----|-------|----|-------|----------|----------|--------|
  1   6.857 BB    0.1998 2016.89453  149.14555  50.2423
  2   9.832 BB    0.2619 1997.44141  113.16214  49.7577
```

(*R*a)-2.13

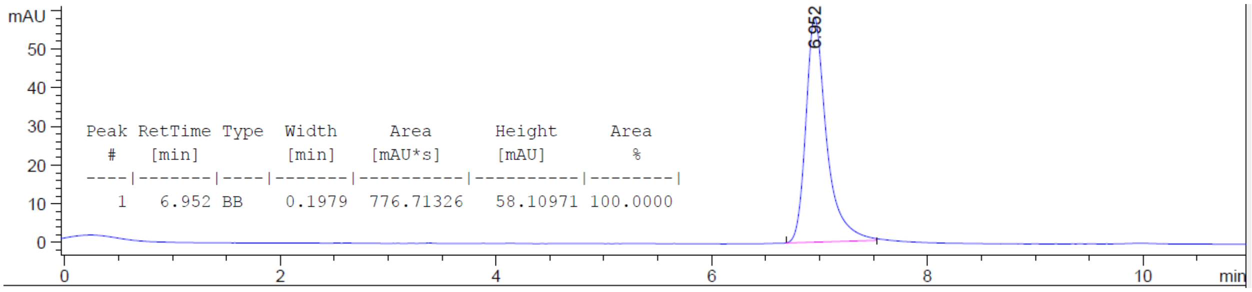

```
Peak RetTime Type  Width     Area      Height     Area
  #   [min]        [min]   [mAU*s]     [mAU]       %
----|-------|----|-------|----------|----------|--------|
  1   6.952 BB    0.1979  776.71326   58.10971 100.0000
```

(*S*a)-2.13

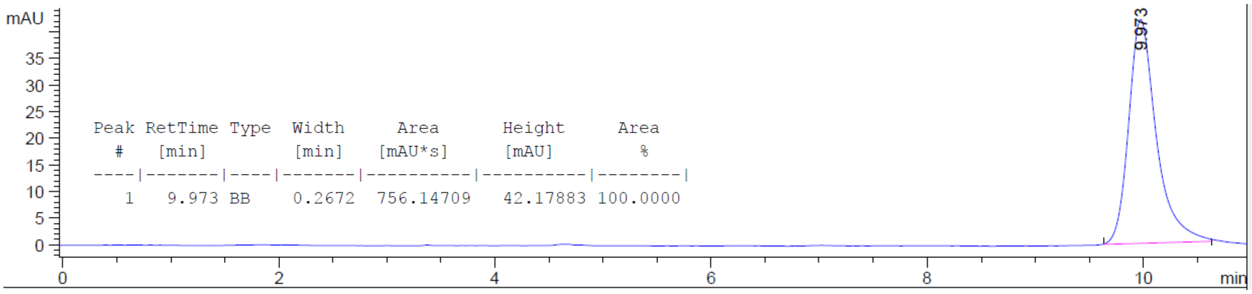

```
Peak RetTime Type  Width     Area      Height     Area
  #   [min]        [min]   [mAU*s]     [mAU]       %
----|-------|----|-------|----------|----------|--------|
  1   9.973 BB    0.2672  756.14709   42.17883 100.0000
```

Chiral HPLC Trace of **2.14**

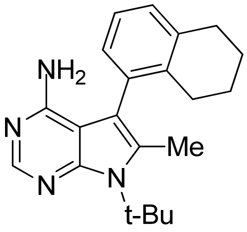

2.14 was measured with HPLC analysis using Chiralpak IA Hexanes/EtOH (80:20), flow rate = 1.0 mL/min, injection volume = 5 ul.

Racemic Standard of 2.14

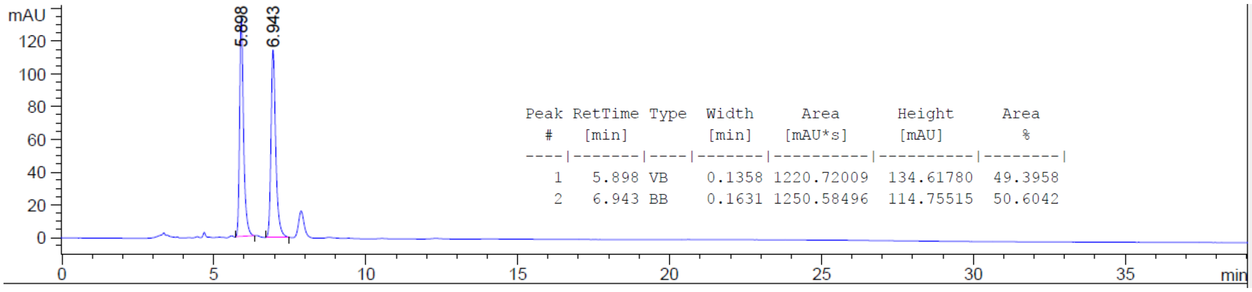

```
Peak RetTime Type  Width      Area       Height      Area
  #   [min]        [min]    [mAU*s]      [mAU]        %
----|-------|----|-------|----------|----------|--------|
  1   5.898 VB    0.1358 1220.72009  134.61780  49.3958
  2   6.943 BB    0.1631 1250.58496  114.75515  50.6042
```

(*R*a)-2.14

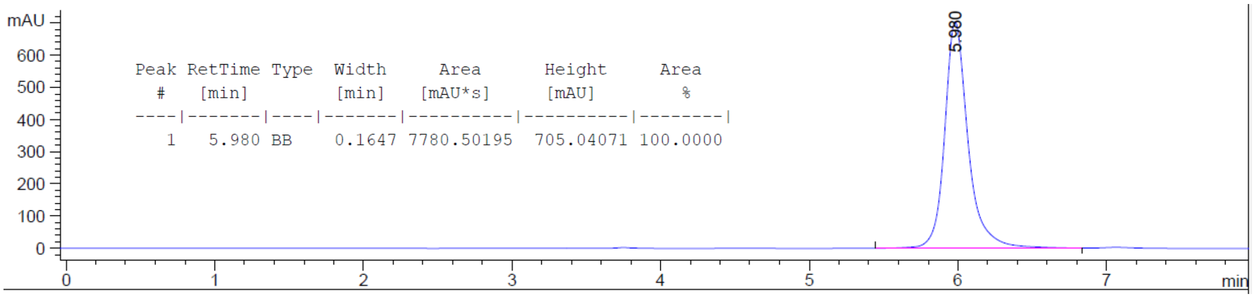

```
Peak RetTime Type  Width      Area      Height      Area
  #   [min]        [min]    [mAU*s]     [mAU]        %
----|-------|----|-------|----------|----------|--------|
  1   5.980 BB    0.1647 7780.50195  705.04071 100.0000
```

(*S*a)-2.14

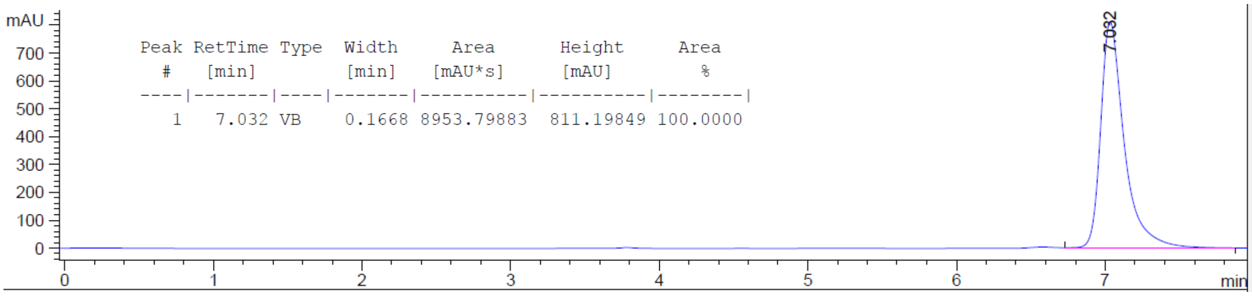

```
Peak RetTime Type  Width      Area      Height      Area
  #   [min]        [min]    [mAU*s]     [mAU]        %
----|-------|----|-------|----------|----------|--------|
  1   7.032 VB    0.1668 8953.79883  811.19849 100.0000
```

Chiral HPLC Trace of **2.16**

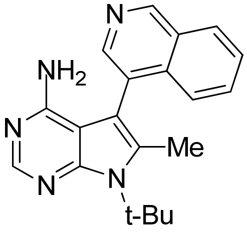

2.16 was measured with HPLC analysis using Chiralpak IA Hexanes/EtOH (50:50), flow rate = 1.0 mL/min, injection volume = 5 ul.

Racemic Standard of 2.16

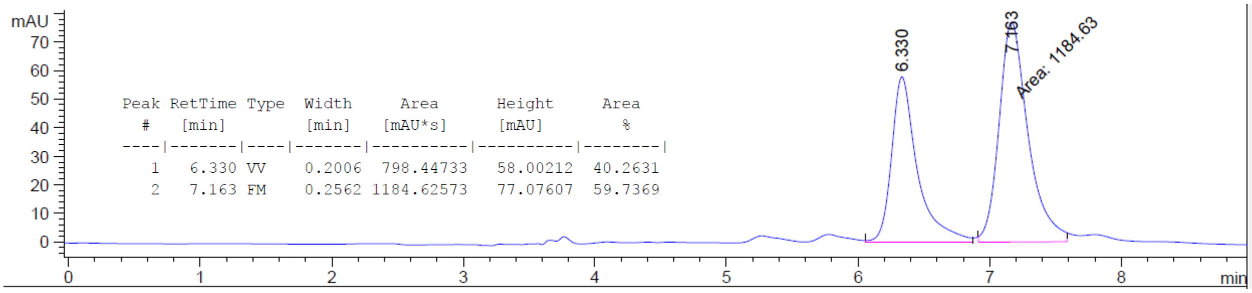

```
Peak RetTime Type  Width     Area      Height     Area
  #   [min]         [min]   [mAU*s]     [mAU]      %
----|-------|----|-------|----------|----------|--------|
  1    6.330 VV    0.2006  798.44733   58.00212  40.2631
  2    7.163 FM    0.2562 1184.62573   77.07607  59.7369
```

(*R*a)-2.16

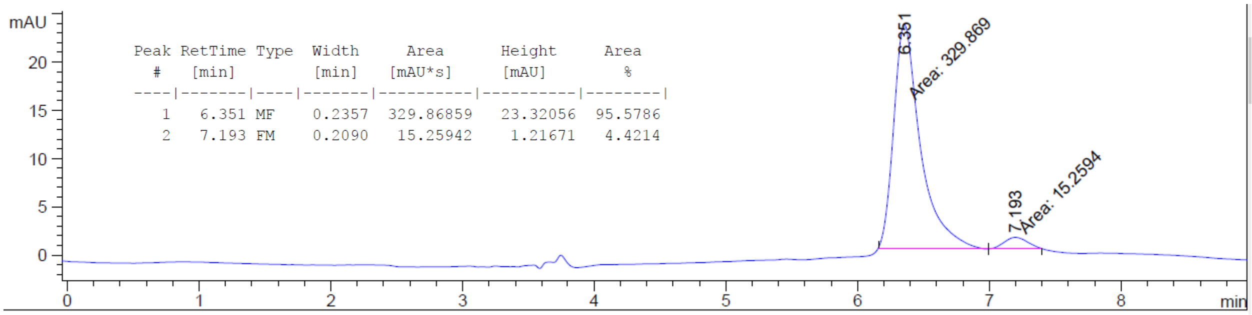

```
Peak RetTime Type  Width     Area      Height     Area
  #   [min]         [min]   [mAU*s]     [mAU]      %
----|-------|----|-------|----------|----------|--------|
  1    6.351 MF    0.2357  329.86859   23.32056  95.5786
  2    7.193 FM    0.2090   15.25942    1.21671   4.4214
```

(*S*a)-2.16

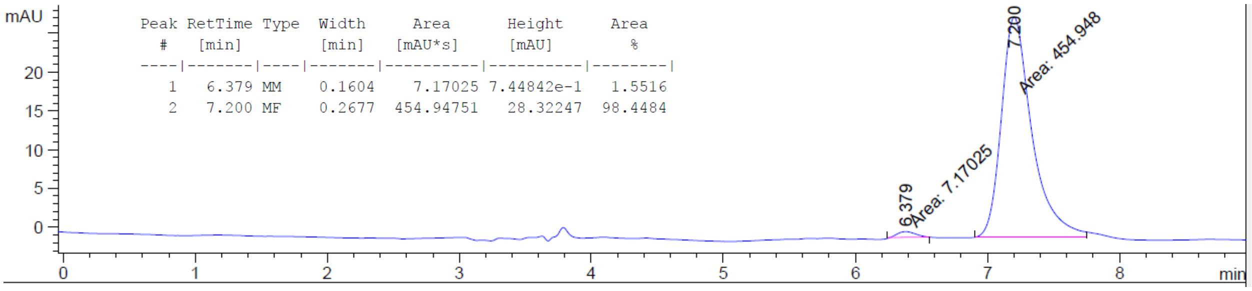

```
Peak RetTime Type  Width     Area      Height     Area
  #   [min]         [min]   [mAU*s]     [mAU]      %
----|-------|----|-------|----------|----------|--------|
  1    6.379 MM    0.1604    7.17025 7.44842e-1   1.5516
  2    7.200 MF    0.2677  454.94751   28.32247  98.4484
```

Chiral HPLC Trace of **2.17**

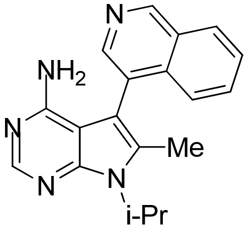

2.17 was measured with HPLC analysis using Chiralpak IA Hexanes/EtOH (50:50), flow rate = 1.0 mL/min, injection volume = 5 ul.

Racemic Standard of 2.17

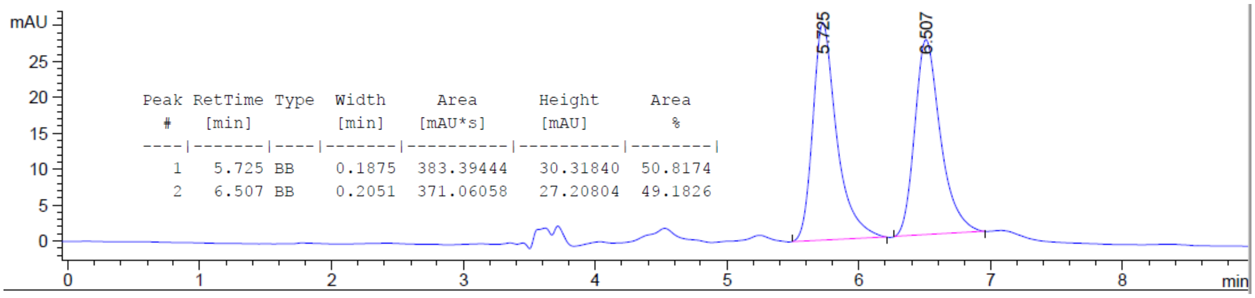

```
Peak RetTime Type  Width     Area      Height     Area
  #   [min]        [min]   [mAU*s]     [mAU]        %
----|-------|----|-------|----------|----------|--------|
   1   5.725 BB    0.1875  383.39444   30.31840  50.8174
   2   6.507 BB    0.2051  371.06058   27.20804  49.1826
```

(*R*$_a$)-2.17

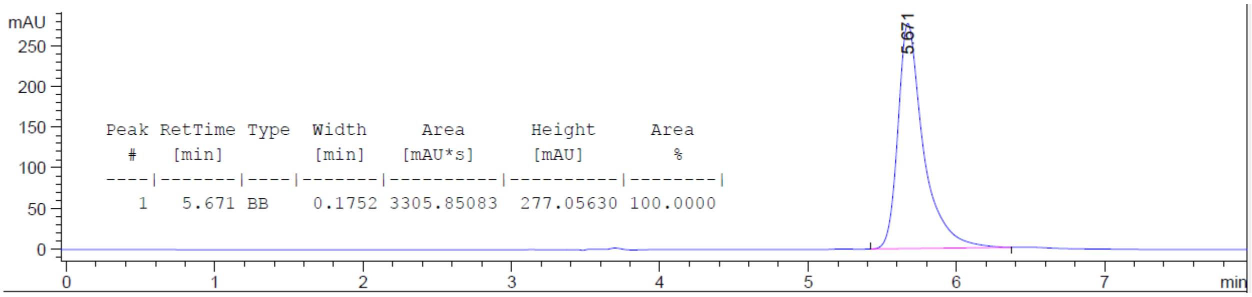

```
Peak RetTime Type  Width     Area      Height     Area
  #   [min]        [min]   [mAU*s]     [mAU]        %
----|-------|----|-------|----------|----------|--------|
   1   5.671 BB    0.1752 3305.85083  277.05630 100.0000
```

(*S*$_a$)-2.17

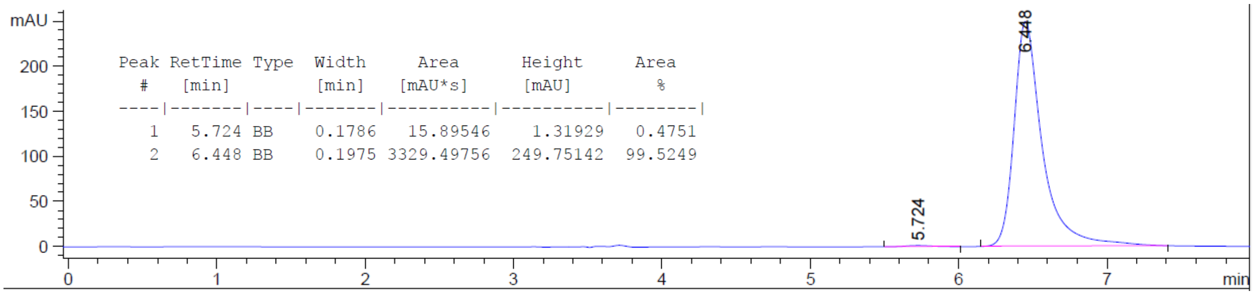

```
Peak RetTime Type  Width     Area      Height     Area
  #   [min]        [min]   [mAU*s]     [mAU]        %
----|-------|----|-------|----------|----------|--------|
   1   5.724 BB    0.1786   15.89546    1.31929   0.4751
   2   6.448 BB    0.1975 3329.49756  249.75142  99.5249
```

Chiral HPLC Trace of **2.18**

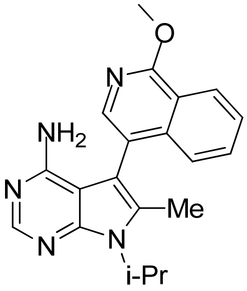

2.18 was measured with HPLC analysis using Chiralpak IA Hexanes/IprOH (50:50), flow rate = 1.0 mL/min, injection volume = 5 ul.

Racemic Standard of 2.18

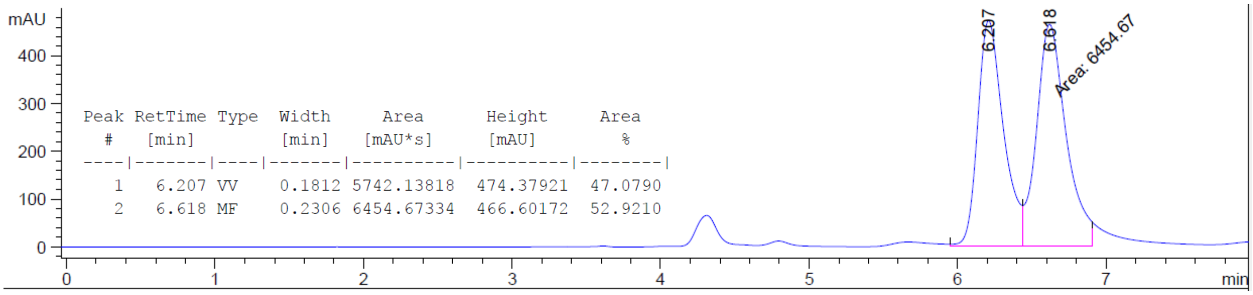

```
Peak RetTime Type  Width     Area      Height     Area
  #   [min]        [min]   [mAU*s]     [mAU]        %
----|-------|----|-------|----------|----------|--------|
  1   6.207 VV    0.1812 5742.13818  474.37921  47.0790
  2   6.618 MF    0.2306 6454.67334  466.60172  52.9210
```

(*R*$_a$)-2.18

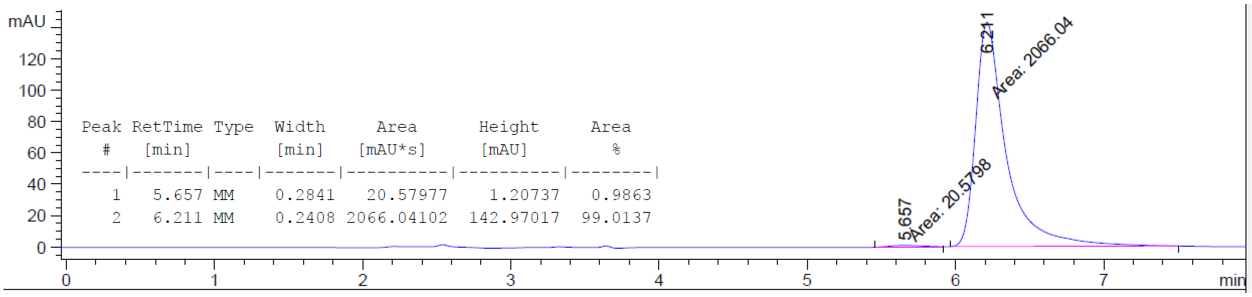

```
Peak RetTime Type  Width     Area      Height     Area
  #   [min]        [min]   [mAU*s]     [mAU]        %
----|-------|----|-------|----------|----------|--------|
  1   5.657 MM    0.2841   20.57977    1.20737   0.9863
  2   6.211 MM    0.2408 2066.04102  142.97017  99.0137
```

(*S*$_a$)-2.18

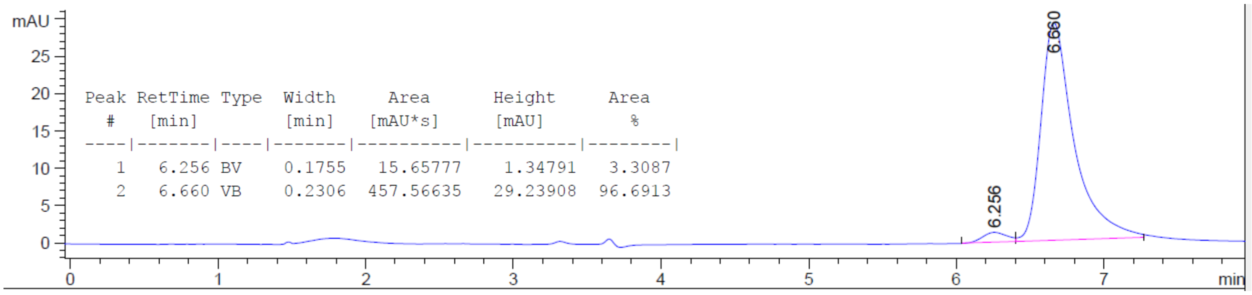

```
Peak RetTime Type  Width     Area      Height     Area
  #   [min]        [min]   [mAU*s]     [mAU]        %
----|-------|----|-------|----------|----------|--------|
  1   6.256 BV    0.1755   15.65777    1.34791   3.3087
  2   6.660 VB    0.2306  457.56635   29.23908  96.6913
```

Predictive Calculated and Experimental Circular Dichroism

All geometry optimizations and frequency calculations were performed in Gaussian 09[2] using density functional theory, DFT B3LYP/6-31g(d) in gas phase. Calculated CD spectra were calculated from the minimized conformations using TD-DFT B3LYP/6-31g(d) CPCM (EtOH) n=30. Experimental circular dichroism spectra were collected at 25 °C on an Aviv model 420 CD spectrophotometer using a 1 mm cuvette. Study compounds were dissolved in 50:50 mixture of Hexanes:Ethanol (100uM) and spectra collected in duplicate from 340 to 200 nm at 1 nm intervals using a 1 nm bandwidth and 1 s averaging time.

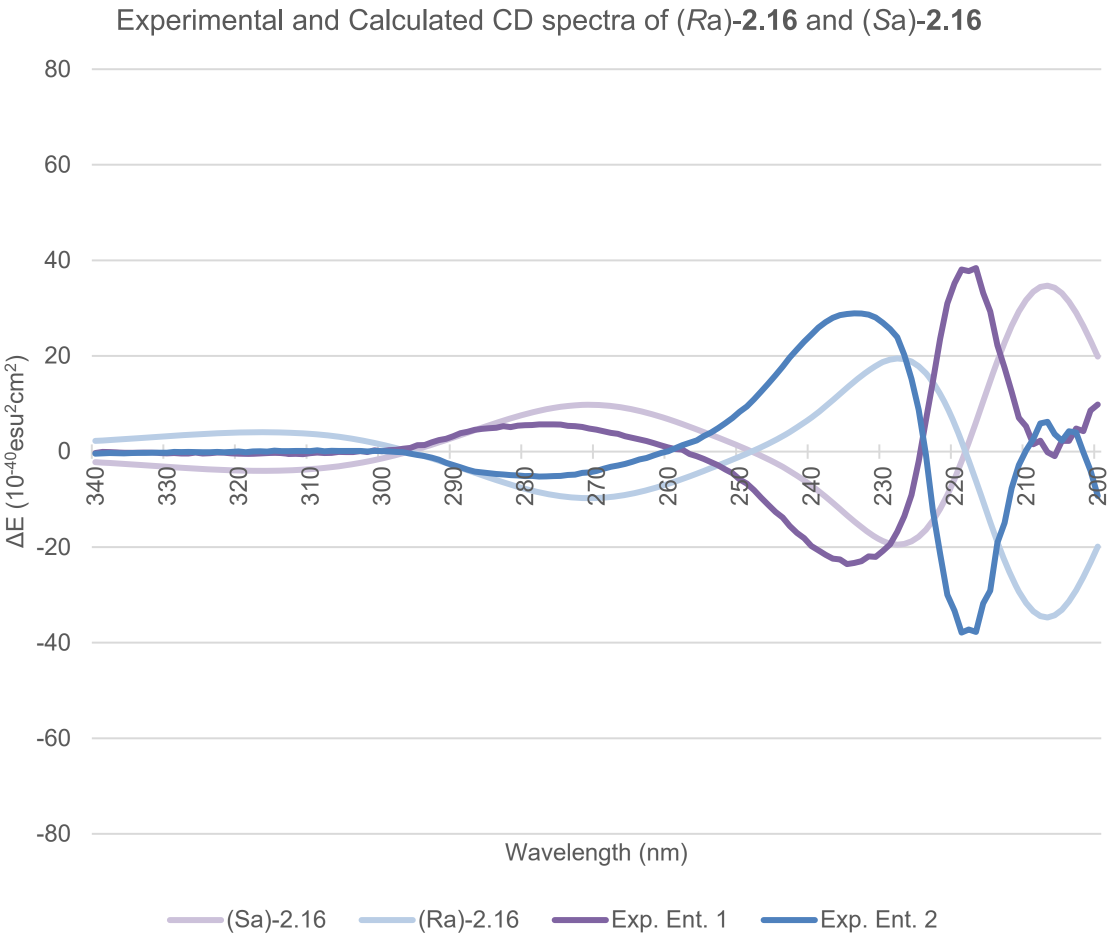

Shown in the graph above are the calculated CD spectra for (*R*a)-**3** minimized conformation with an -80° dihedral angle and (*S*a)-**2.16** minimized conformation with an 80° dihedral angle. The experimental spectra are labeled as "Ent. #", where the # is the order in which the atropisomers eluted off a Chiralpak IA HPLC column (50:50 Hexanes:EtOH). For scaffolds containing the isoquinoline off the *C*-3 position, enantiomer 2 (R_a) was the more biologically active inhibitor. Below are other calculated CD spectra for each (R_a)-**2.16** and (S_a)-**2.16** covering a range of low energy dihedral angles, -60° to -120° and 60° to 120°, respectively.

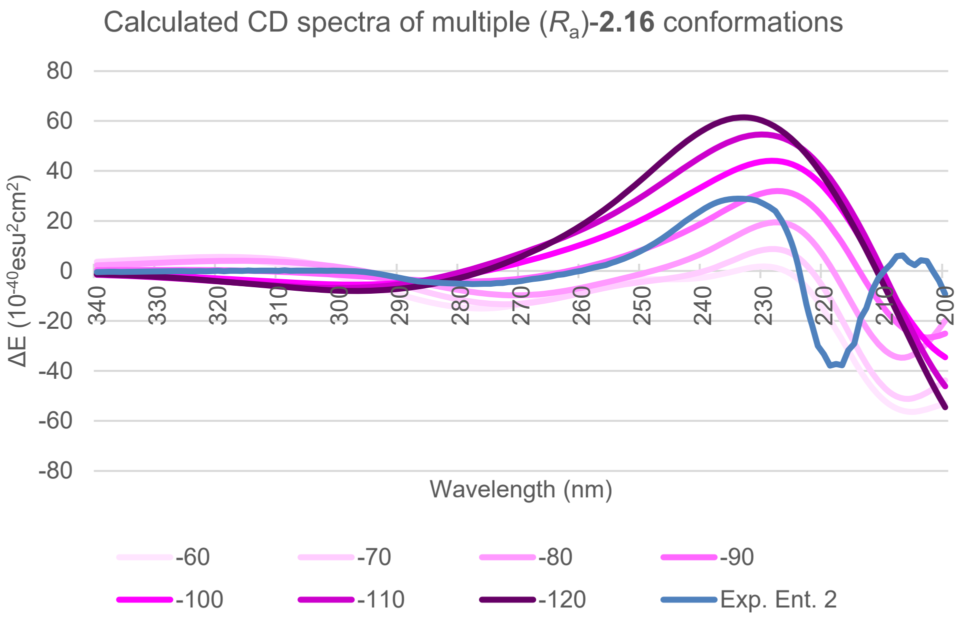
Calculated CD spectra of multiple (R_a)-**2.16** conformations

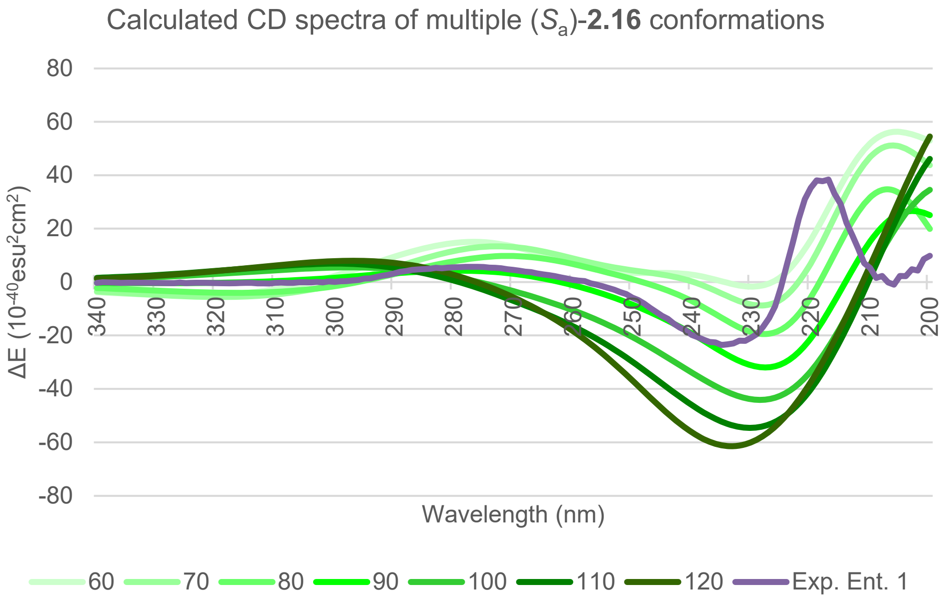
Calculated CD spectra of multiple (S_a)-**2.16** conformations

Racemization Kinetics

Enantiopure atropisomeric analogue of interest (3 mg) was dissolved in 1 mL of toluene or MeOH/PBS mixture. This solution was then heated at a constant temperature for a certain range of time (2-3 h, measured ~5 time points). At each time point, a 100-200 µL aliquot was isolated and quenched in an HPLC vial with ice cold 50:50 Hexanes:Isopropanol. Each sample was then injected into the chiral HPLC system containing an analytical column at 1ml/min and their ee% were measured. Each barrier to rotation measurement is determined from an average of two trials. The ee% vs. time (s) was plotted in order to determine the rate constant k_{obs} (i.e. the slope of the pseudo first-order kinetics) at this constant temperature using the following equation:

$$k_{obs} = \frac{\ln\left(\frac{1}{ee\%}\right)}{t}$$

From this, the racemization rate constant k_{rac} was determined using the following equation:

$$k_{rac} = \frac{k_{obs}}{2}$$

The average k_{rac} was determined by taking the average of the k_{rac} of each trial. From this, substitution into the Eyring equation was performed to determine the barrier to rotation:

$$\Delta G = RT \ln\left(\frac{Tk_b}{k_{rac}h}\right)$$

in which ΔG is the barrier to rotation measurement, R is the gas constant, T is the constant temperature, k_b is the Boltzmann distribution constant, and *h* is Planck's constant. To determine $t_{1/2}$ at 37 °C (physiological temperatures):

$$t_{1/2} = \frac{\left(\frac{k_b T e^{\frac{-\Delta G}{RT}}}{\ln 2}\right)}{\ln 2}$$

in which $t_{1/2}$ is the half-life to racemization in seconds. This unit can convert into hours, days, or years.

Barrier to Rotation Measurement of **2.16**

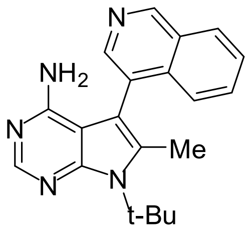

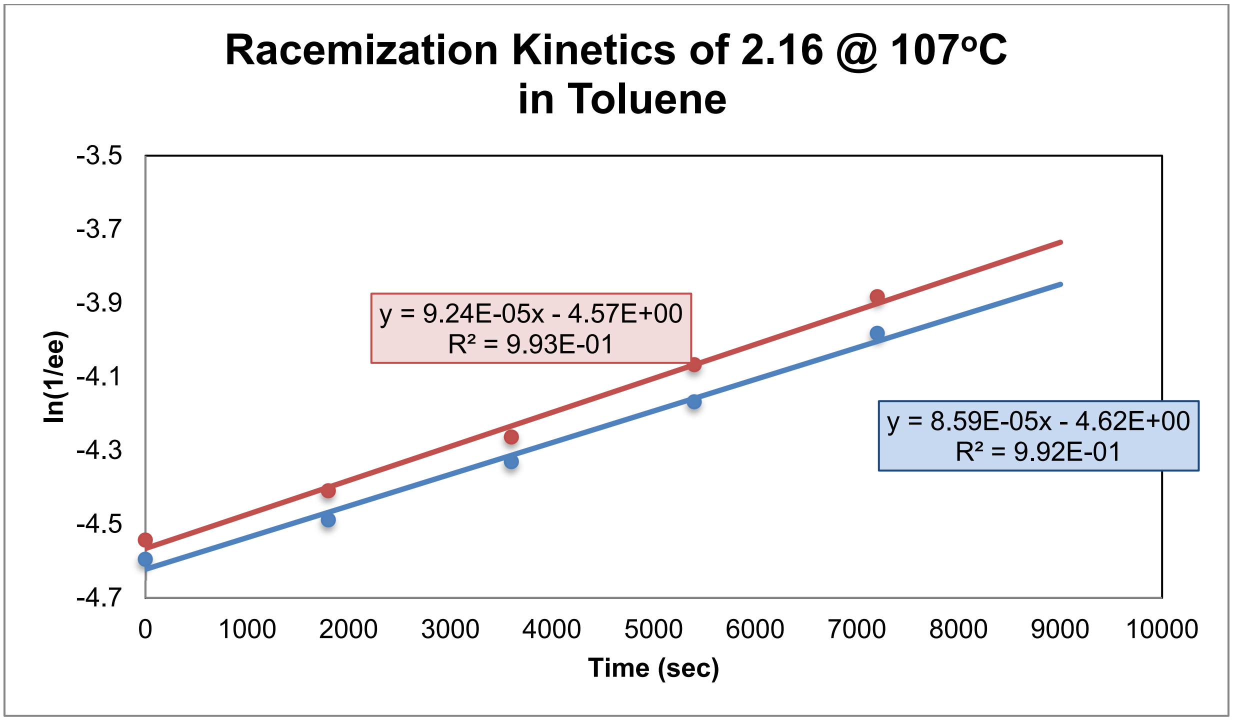

Time (s)	Trial Run 1 (ee%)	Trial 1 [ln(1/ee%)]	Trial Run 2 (ee%)	Trial 2 [ln(1/ee%)]
0	99	-4.59511985	94	-4.543295
1800	89	-4.48863637	82.218	-4.409374
3600	75.984	-4.33052279	71.082	-4.263834
5400	64.59	-4.1680596	58.412	-4.067521
7200	53.642	-3.98233234	48.572	-3.883047

Average k_{obs} = 8.92E-05, **Average k_{rac}** = 4.46E-05

Calculated Average ΔG = 30.04 kcal/mol

Calculated $t_{1/2}$ (37 °C) = 4.48 yr (or 1637 d)

Calculated t_{95} (37 °C) = 0.33 yr (or 121 d)

Barrier to Rotation Measurement of **2.16**

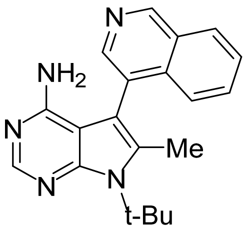

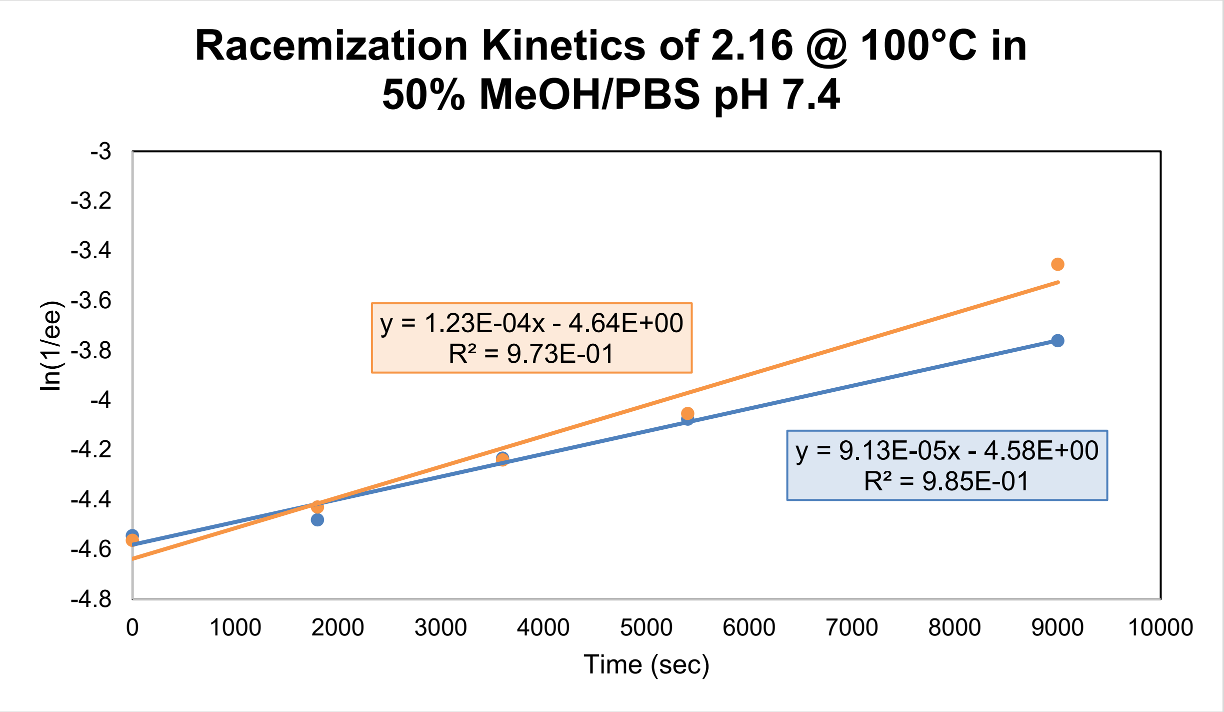

Time (s)	Trial Run 1 (ee%)	Trial 1 [ln(1/ee%)]	Trial Run 2 (ee%)	Trial 2 [ln(1/ee%)]
0	94.184	-4.54525	96.016	-4.56451484
1800	88.378	-4.481623	83.934	-4.43003078
3600	68.994	-4.23402	69.46	-4.24075105
5400	58.97	-4.077029	57.646	-4.05432086
9000	43.006	-3.76134	31.646	-3.45461176

Average k_{obs} = 2.39E-05, **Average k_{rac}** = 1.19E-05

Calculated Average ΔG = 29.93

Calculated $t_{1/2}$ (37 °C) = 4.017710622 yr (or 1466 d)

Calculated t_{100} (37 °C) = 0.0009 yr (or 8.07 h)

Barrier to Rotation Measurement of **2.9**

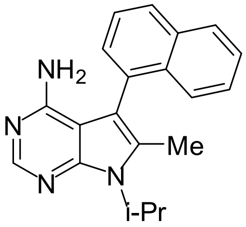

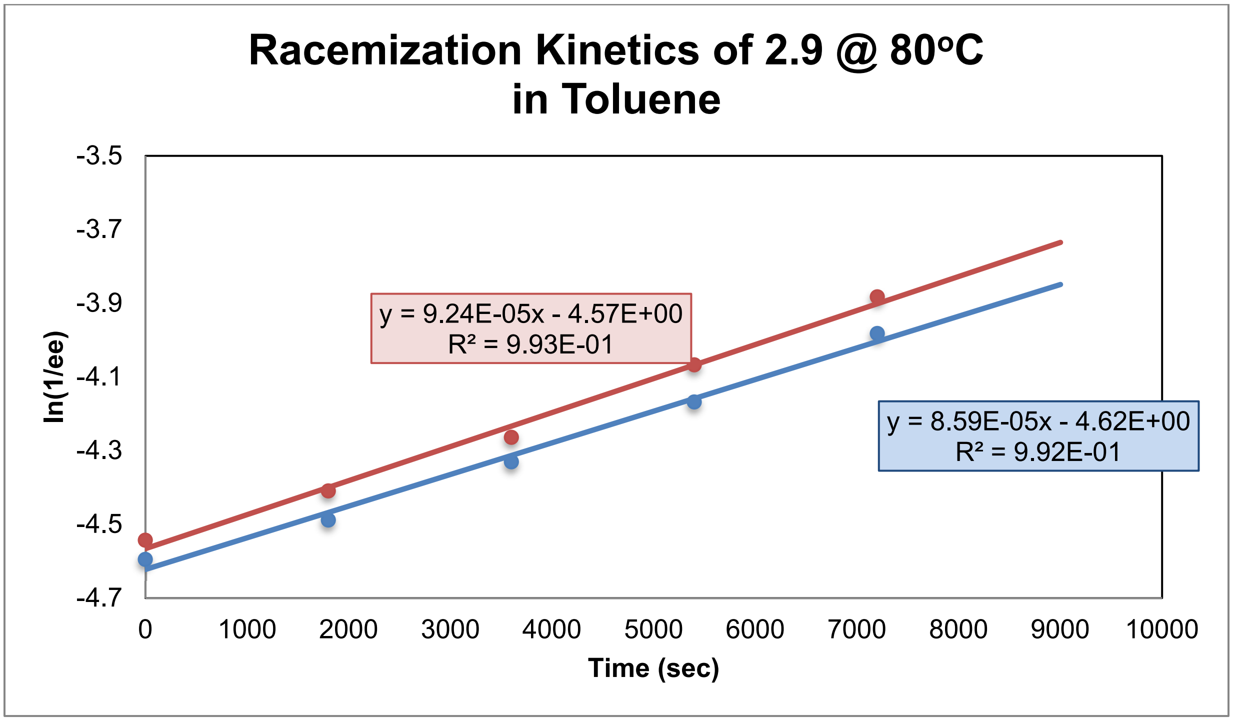

Time (s)	Trial Run 1 (ee%)	Trial 1 [ln(1/ee%)]	Trial Run 2 (ee%)	Trial 2 [ln(1/ee%)]
0	100	-4.60517019	100	-4.60517
1800	96.618	-4.57076506	96.294	-4.567406
3600	92.914	-4.53167433	92.14	-4.523309
5400	88.942	-4.48798447	87.716	-4.474104
7200	85.364	-4.44692447	83.546	-4.425397

Average k_{obs} = 2.42E-05, **Average k_{rac}** = 1.21E-05

Calculated Average ΔG = 28.77 kcal/mol

Calculated $t_{1/2}$ (37 °C) = 0.64 yr (or 234 d)

Calculated t_{95} (37 °C) = 0.04 yr (or 17 d)

A.2 Chapter 3 Experimental Section

Synthetic Scheme 1

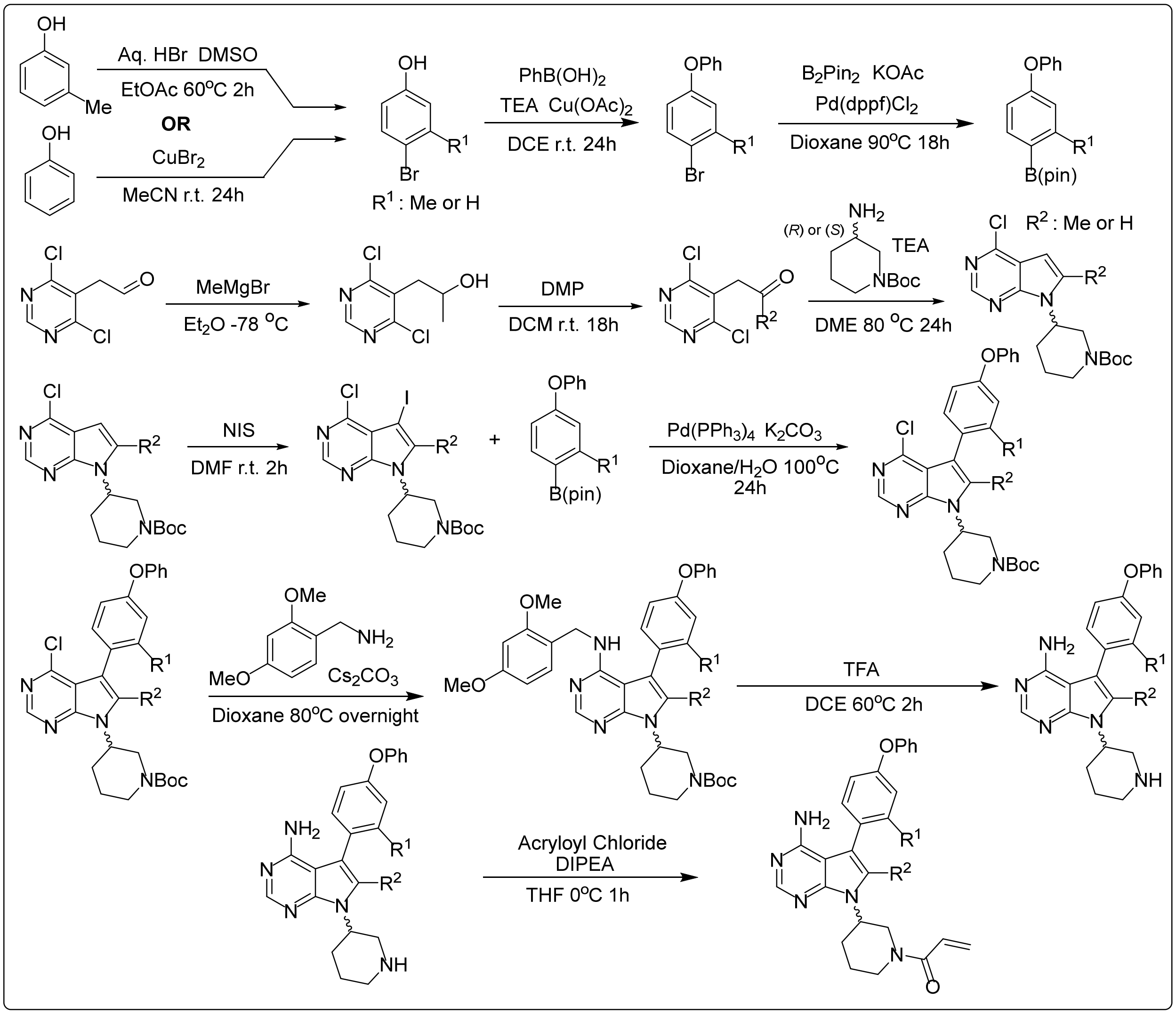

Aq. HBr DMSO
EtOAc 60°C 2h
OR
CuBr2
MeCN r.t. 24h
R1 : Me or H
PhB(OH)2
TEA Cu(OAc)2
DCE r.t. 24h
B2Pin2 KOAc
Pd(dppf)Cl2
Dioxane 90°C 18h
MeMgBr
Et2O -78 °C
DMP
DCM r.t. 18h
(R) or (S)
TEA
DME 80 °C 24h
R2 : Me or H
NIS
DMF r.t. 2h
Pd(PPh3)4 K2CO3
Dioxane/H2O 100°C 24h
Cs2CO3
Dioxane 80°C overnight
TFA
DCE 60°C 2h
Acryloyl Chloride
DIPEA
THF 0°C 1h

Synthetic Scheme 2

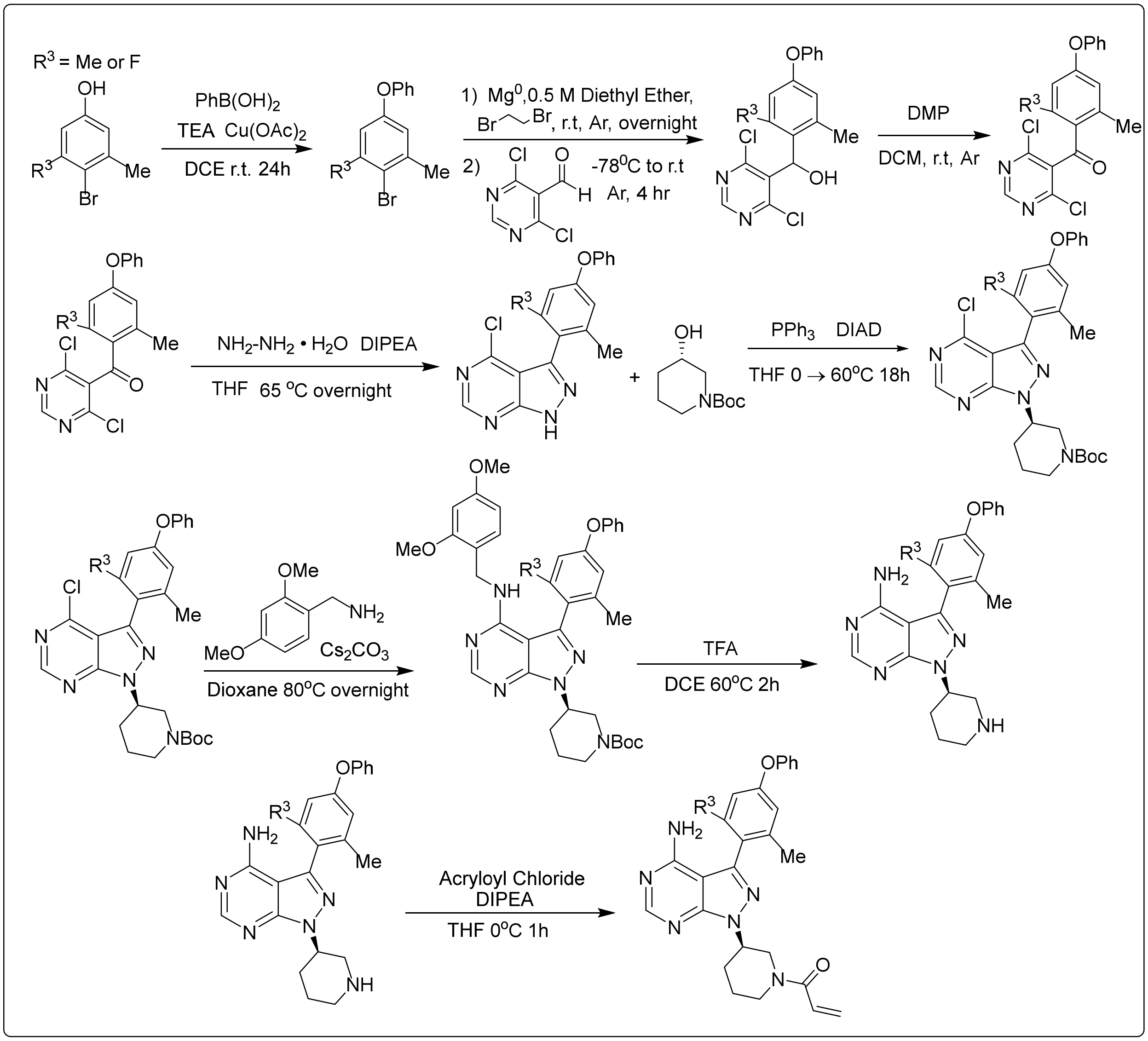
R3 = Me or F
PhB(OH)2
TEA Cu(OAc)2
DCE r.t. 24h
1) Mg0,0.5 M Diethyl Ether,
Br⁀Br, r.t, Ar, overnight
2)
-78°C to r.t
Ar, 4 hr
DMP
DCM, r.t, Ar
NH2-NH2 • H2O DIPEA
THF 65 °C overnight
PPh3 DIAD
THF 0 → 60°C 18h
Cs2CO3
Dioxane 80°C overnight
TFA
DCE 60°C 2h
Acryloyl Chloride
DIPEA
THF 0°C 1h
OH
OPh
Br
Me
Cl
N
H
OMe
MeO
NH2
NH
NBoc

Synthetic Scheme 3

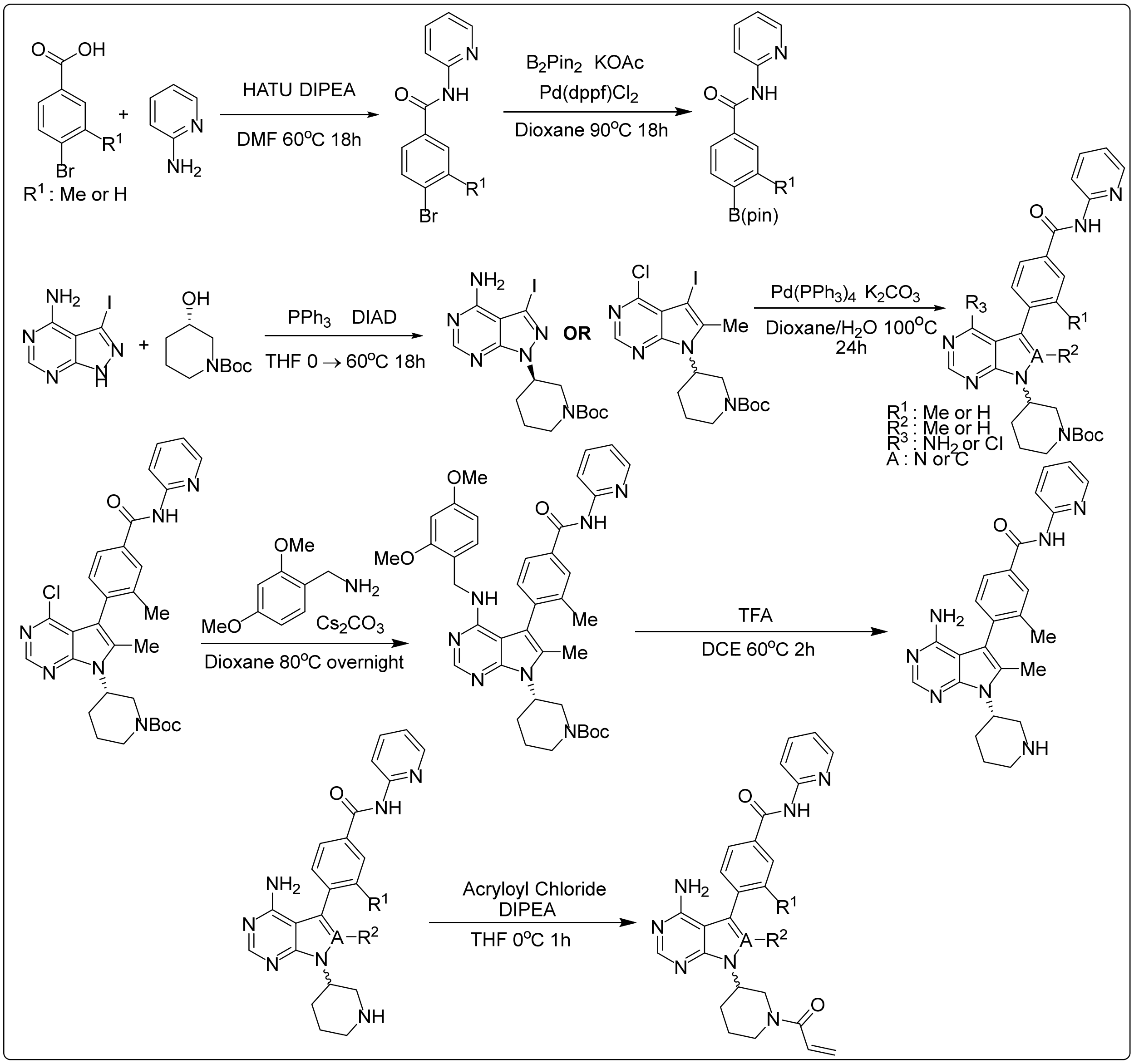

R¹ : Me or H
HATU DIPEA
DMF 60°C 18h
B₂Pin₂ KOAc
Pd(dppf)Cl₂
Dioxane 90°C 18h
B(pin)
PPh₃ DIAD
THF 0 → 60°C 18h
OR
Pd(PPh₃)₄ K₂CO₃
Dioxane/H₂O 100°C
24h
R¹ : Me or H
R² : Me or H
R³ : NH₂ or Cl
A : N or C
Cs₂CO₃
Dioxane 80°C overnight
TFA
DCE 60°C 2h
Acryloyl Chloride
DIPEA
THF 0°C 1h

Procedures for bromination of phenols

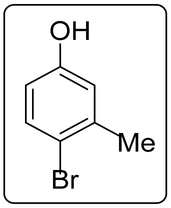

4-bromo-3-methylphenol:

M-cresol (4 g, 36.99 mmol, 1 eq.) and Dimethyl Sulfoxide (3.94 mL, 55.48 mmol, 1.5 eq.) was dissolved in ethyl acetate (.25M) at r.t.. Aqueous HBr 48% w/w (7.53 mL, 55.48 mmol, 1.5 eq.) was then added dropwise and the reaction was stirred for 1hr at 60°C. Saturated aqueous sodium bicarbonate was added to quench the reaction. The reaction mixture was partitioned in ethyl acetate and brine. The organic layer was dried over sodium sulfate and concentrated. The crude extract was purified via FCC with a gradient of hexanes/ethyl acetate (100:0 to 70:30) to yield 5.13 g of pure 4-bromo-3-methylphenol as a yellow oil (74.2% yield). The ^{1}H NMR matched those reported in the literature[174].

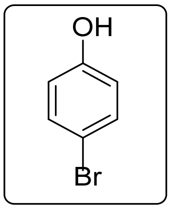

4-bromophenol

Phenol (5 g, 53.13 mmol, 1 eq.) and copper (II) bromide (26.11 g, 116.89 mmol, 2.2 eq.) were dissolved in acetonitrile (212 ml, .25M) and let stir at r.t. for 24 hours. The crude reaction mixture was vacuum filtered through celite and washed with ethyl acetate. The reaction mixture was partitioned in ethyl acetate and brine. The organic later was dried over sodium sulfate and concentrated. The crude extract was purified via FCC with a gradient of hexanes/dichloromethane

(50:50 to 0:100) to yield 5.12g of 4-bromophenol (56%). The ^{1}H NMR matched those reported in the literature[174].

General procedure for arylation of phenols

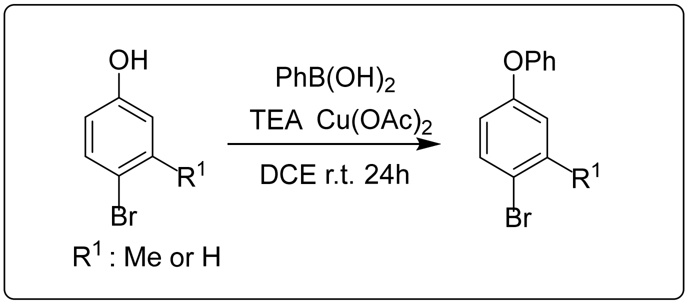

4Å powder molecular sieves (200mg/mmol of $PhB(OH)_2$) were added to a round bottom flask and flame dried under vacuum. 0.1 M of 1,2-dichloroethane was then added to the dried round bottom then opened to air. The functionalized phenol (1.0 eq.), Phenyl boronic acid (3.0 eq.), triethylamine (5.0 eq.), and copper (II) acetate anhydrous (2.0 eq.) were added and let stir overnight at r.t. The crude mixture was filtered through celite to remove sieves and washed with dichloromethane. The reaction mixture was partitioned between dichloromethane and brine and washed with aqueous 30% ammonium hydroxide. The organic layer was dried over sodium sulfate and concentrated. The crude extract was purified by FCC with a gradient of hexanes/ethyl acetate (100:0 to 75:25) to yield substituted diaryl ethers. (44% - 92.5%).

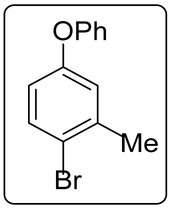

1-bromo-2-methyl-4-phenoxybenzene:

Following the general procedure, 4A powder molecular sieves (6.42 g, 200mg/mmol of $PhB(OH)_2$), 107 mL (0.1M) of 1,2-dichloroethane, 4-bromo-3methylphenol (2 g, 10.69 mmol, 1 eq.), $PhB(OH)_2$ (3.91 g, 32.08 mmol, 3.0 eq.), Triethylamine (7.45 mL, 53.45 mmol, 5.0 eq.), and copper (II) acetate anhydrous (3.88 g, 21.38 mmol, 2 eq.) were used. The crude mixture was worked up and purified following the procedure above yielding 2.59 g of 1-bromo-2-methyl-4-phenoxybenzene as a white solid (92.5%). The ^1H NMR matched those reported in the literature[175].

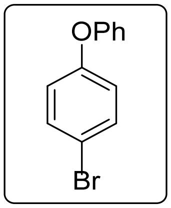

1-bromo-4-phenoxybenzene:

Following the general procedure, 4A powder molecular sieves (10.65 g, 200mg/mmol of $PhB(OH)_2$), 290 mL (0.1M) of 1,2-dichloroethane, 4-bromophenol (5.0 g, 29.06 mmol, 1.0 eq.), $PhB(OH)_2$ (10.65 g, 87.18 mmol, 3.0 eq.), Triethylamine (20.2 mL, 145.3 mmol, 5.0 eq.), and copper (II) acetate anhydrous (10.55 g, 58.12 mmol, 2 eq.) were used. The crude mixture was worked up and purified following the procedure above yielding 3.2 g of 1-bromo-4-phenoxybenzene (44%). The ^1H NMR spectra matched those reported in the literature[176].

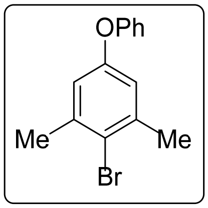

2-bromo-1,3-dimethyl-5-phenoxybenzene

Following the general procedure, 4A powder molecular sieves (15 g, 200mg/mmol of $PhB(OH)_2$), 250 mL (0.1M) of 1,2-dichloroethane, 4-bromo-3,5-dimethylphenol (5 g, 24.88 mmol, 1.0 eq.), $PhB(OH)_2$ (9.1 g, 74.63 mmol, 3.0 eq.), Triethylamine (17.3 mL, 124.4 mmol, 5.0 eq.), and copper (II) acetate anhydrous (9.04 g, 49.76 mmol, 2 eq.) were used. The crude mixture was worked up and purified following the procedure above yielding 3.3 g of 2-bromo-1,3-dimethyl-5-phenoxybenzene (48%). The ^1H NMR spectra matched those reported in the literature[177].

General procedure for amide coupling

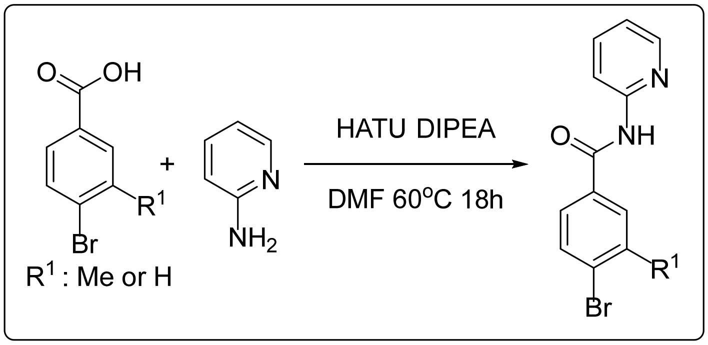

The brominated benzoic acid (1.0 eq.), HATU (1.2 eq.), diisopropylethylamine (5.0 eq.), and DMF (0.5 M) were added to a round bottom flask at room temperature open to air and stirred for 10 minutes. 2-aminopyridine (2.0 eq.) was then added to the reaction mixture and then heated to 60°C for 18 hours. Reaction progression was monitored by TLC and upon completion, the reaction was quenched with H2O and partitioned in a separatory funnel with EtOAc and sodium bicarbonate. The organic layer was then washed with 10% citric acid and then brine. The organic layer was dried over sodium sulfate and concentrated. The crude extract was purified by FCC with a gradient of hexanes/ethyl acetate (100:0 to 75:25) to yield amide coupled products (68% - 77%).

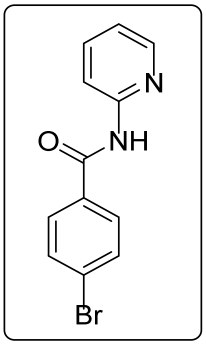

4-bromo-N-(pyridin-2-yl)benzamide

Following the general procedure, 4-bromobenzoic acid (2 g, 9.95 mmol, 1.0 eq.), 2-aminopyridine (1.87 g, 19.9 mmol, 2.0 eq.), HATU (4.53 g, 11.9 mmol, 1.2 eq.), diisopropylethylamine (8.65 ml, 49.75 mmol, 5.0 eq.), and DMF (20 ml, 0.5 M) were used. The crude mixture was worked up and purified following the procedure above yielding 1.874 g (68%) of 4-bromo-N-(pyridin-2-yl)benzamide.

^{1}H NMR (400 MHz, $CDCl_3$) δ 8.94 (s, 1H), 8.37 (d, J = 8.4 Hz, 1H), 8.21 (dd, J = 4.9, 1.0 Hz, 1H), 7.81 – 7.78 (m, 2H), 7.78 – 7.73 (m, 1H), 7.65 – 7.59 (m, 2H), 7.07 (ddd, J = 7.3, 4.9, 0.8 Hz, 1H).

MS (APCI) Calculated: $C_{12}H_{10}BrN_2O$ $[M+H]^+$ 277.0 **Found:** 277.1 m/z

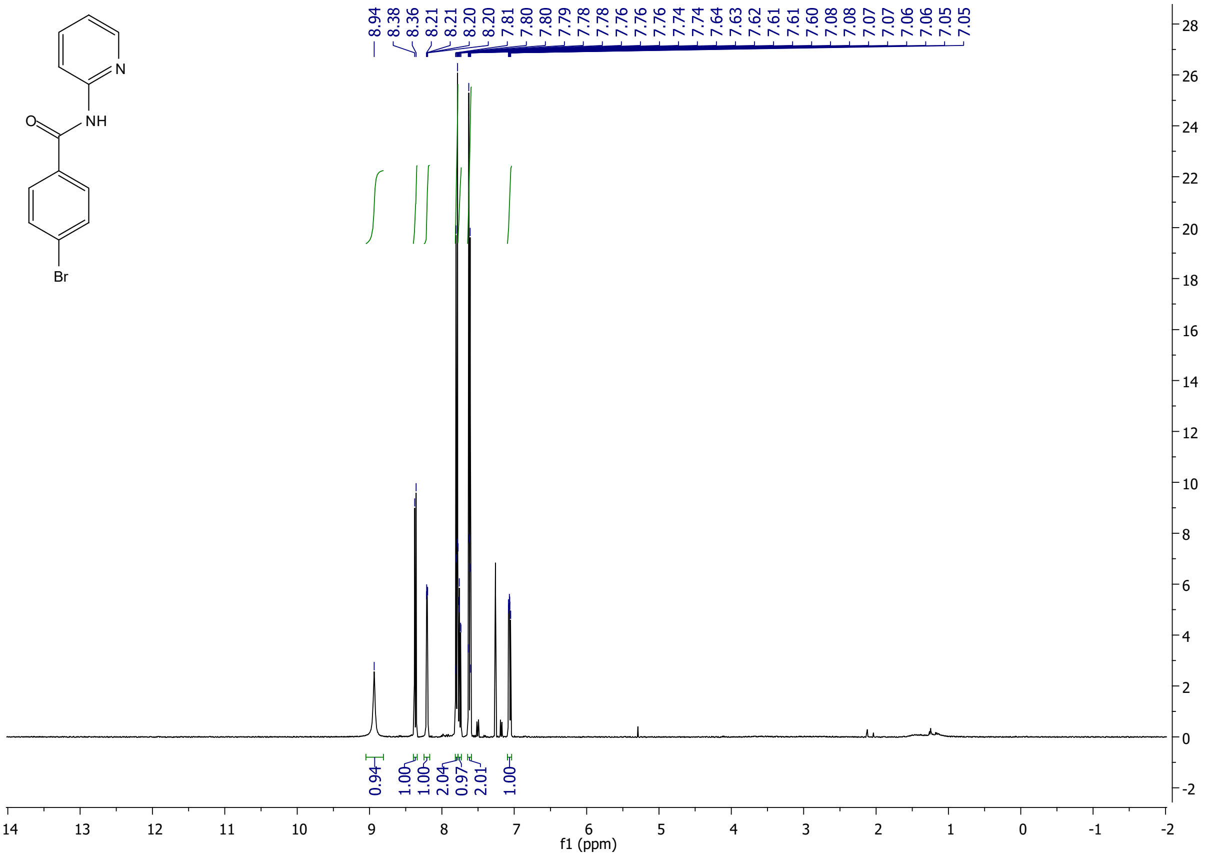

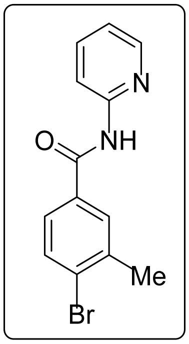

4-bromo-3-methyl-N-(pyridin-2-yl)benzamide

Following the general procedure, 4-bromo-3-methylbenzoic acid (1 g, 4.65 mmol, 1.0 eq.), 2-aminopyridine (0.875 g, 9.3 mmol, 2.0 eq.), HATU (2.12 g, 5.58 mmol, 1.2 eq.), diisopropylethylamine (4 ml, 23.25 mmol, 5.0 eq.), and DMF (9.5 ml, 0.5 M) were used. The crude mixture was worked up and purified following the procedure above yielding 1.04 g (77%) of 4-bromo-3-methyl-N-(pyridin-2-yl)benzamide. The ^{1}H matched those reported in the literature[178].

General procedure for aryl borylation

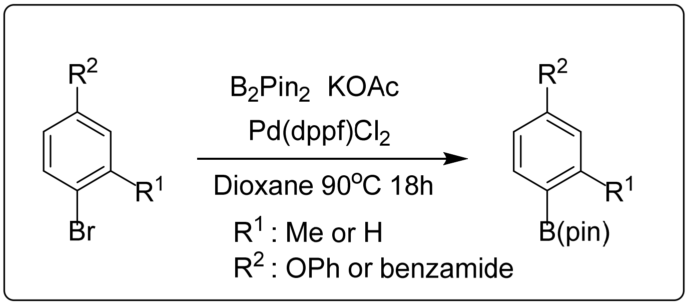

The brominated aryl (1.0 eq.), bis(pinacalato)diboron (2.0 eq.), $Pd(dppf)Cl_2$ (0.05 eq.) and potassium acetate (3.0 eq.) were added to a round bottom equipped with a stir bar. After purging reaction vessel with argon, degassed dioxane (0.3 M) was added and the reaction was refluxed at 90 °C for 18 hr. The crude reaction mixture was filtered through celite and washed with ethyl acetate. The reaction mixture was partitioned between ethyl acetate and brine. The organic layer was dried over sodium sulfate and concentrated. The crude extract was purified by FCC with a gradient of hexanes/ethyl acetate (100:0 to 85:15) to yield borylated aryl products (29% - 66%).

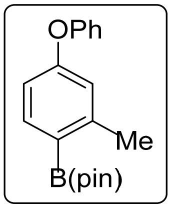

4,4,5,5-tetramethyl-2-(2-methyl-4-phenoxyphenyl)-1,3,2-dioxaborolane:

Following the general procedure, 1-bromo-2-methyl-4-phenoxybenzene (2.59g, 9.84 mmol, 1.0 eq.), bis(pinacalato)diboron (4.99 g, 19.69 mmol, 2.0 eq.), $Pd(dppf)Cl_2$ (402 mg, .492 mmol, 0.05 eq.), potassium acetate (2.89 g, 29.52 mmol, 3.0 eq.) and degassed dioxane (33 mL, 0.3M) were used. The crude mixture was worked up and purified following the procedure above yielding 2.0 g of 4,4,5,5-tetramethyl-2-(2-methyl-4-phenoxyphenyl)-1,3,2-dioxaborolane as a clear oil (66%). The ^1H matched those reported in the literature[179].

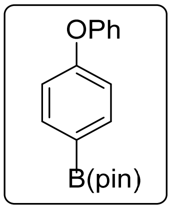

4,4,5,5-tetramethyl-2-(4-phenoxyphenyl)-1,3,2-dioxaborolane:

Following the general procedure, 1-bromo-4-phenoxybenzene (2.21 g, 8.92 mmol, 1.0 eq.), bis(pinacalato)diboron (3.40 g, 13.38 mmol, 1.5 eq.), Pd(dppf)Cl_2 (326 mg, .446 mmol, 0.05 eq.), potassium acetate (2.62 g, 26.76 mmol, 3.0 eq.) and degassed dioxane (29.7 mL, 0.3M) were used. The crude mixture was worked up and purified following the procedure above yielding 1.88 g of 4,4,5,5-tetramethyl-2-(4-phenoxyphenyl)-1,3,2-dioxaborolane (71%). The 1H matched those reported in the literature[180].

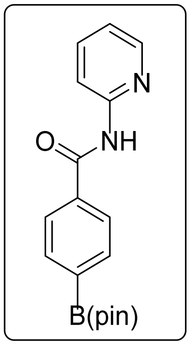

N-(pyridin-2-yl)-4-(4,4,5,5-tetramethyl-1,3,2-dioxaborolan-2-yl)benzamide

Following the general procedure, 4-bromo-N-(pyridin-2-yl)benzamide (1.874 g, 6.81 mmol, 1.0 eq.), bis(pinacalato)diboron (1.99 g, 7.84 mmol, 2.0 eq.), Pd(dppf)Cl_2 (556 mg, .681 mmol, 0.1 eq.), potassium acetate (1.67 g, 17.03 mmol, 2.5 eq.) and degassed dioxane (27 mL, 0.25M) were used. The crude mixture was worked up and purified following the procedure above yielding 0.870 g of N-(pyridin-2-yl)-4-(4,4,5,5-tetramethyl-1,3,2-dioxaborolan-2-yl)benzamide as a brown oil (29%). The ^{1}H matched those reported in the literature[181].

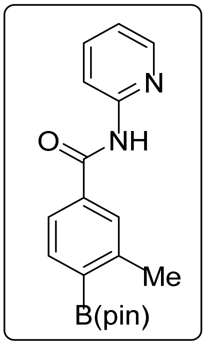

3-methyl-N-(pyridin-2-yl)-4-(4,4,5,5-tetramethyl-1,3,2-dioxaborolan-2-yl)benzamide

Following the general procedure, 4-bromo-3-methyl-N-(pyridin-2-yl)benzamide (1.0 g, 3.43 mmol, 1.0 eq.), bis(pinacalato)diboron (1.75 g, 6.87 mmol, 2.0 eq.), Pd(dppf)Cl_2 (250 mg, .343 mmol, 0.1 eq.), potassium acetate (1.01 g, 10.03 mmol, 3.0 eq.) and degassed dioxane (23 mL, 0.15M) were used. The crude mixture was worked up and purified following the procedure above yielding 0.518 g of 3-methyl-N-(pyridin-2-yl)-4-(4,4,5,5-tetramethyl-1,3,2-dioxaborolan-2-yl)benzamide as an orange oil (47%).

^{1}H NMR (400 MHz, $CDCl_3$) δ 8.69 (s, 1H), 8.40 (d, *J* = 8.4 Hz, 1H), 8.30 – 8.27 (m, 1H), 7.86 (d, *J* = 7.7 Hz, 1H), 7.78 – 7.74 (m, 1H), 7.73 – 7.71 (m, 1H), 7.68 (dd, *J* = 7.7, 1.8 Hz, 1H), 7.07 (ddd, *J* = 7.3, 4.9, 1.0 Hz, 1H), 2.60 (s, 3H), 1.36 (s, 12H).

MS (APCI) Calculated: $C_{19}H_{24}BN_2O_3$ $[M+H]^+$ 339.2 **Found:** 339.2 m/z

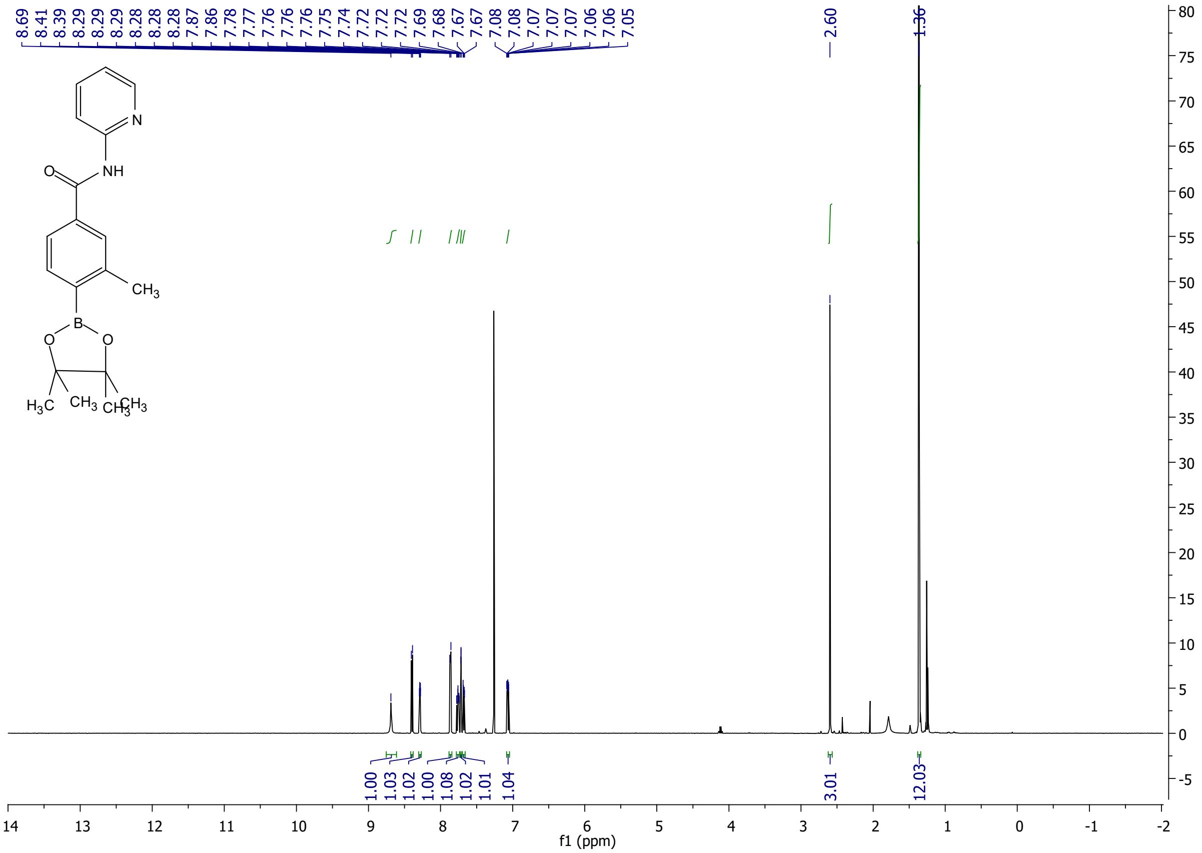
8.69
8.41
8.39
8.29
8.29
8.29
8.28
8.28
8.28
7.87
7.86
7.78
7.77
7.76
7.76
7.76
7.75
7.74
7.72
7.72
7.72
7.69
7.68
7.67
7.67
7.08
7.08
7.07
7.07
7.07
7.06
7.06
7.05
2.60
1.36
N
O
NH
CH3
B
O
O
H3C
CH3
CH3
CH3
1.00
1.03
1.02
1.00
1.08
1.02
1.01
1.04
3.01
12.03
80
75
70
65
60
55
50
45
40
35
30
25
20
15
10
5
0
-5
14
13
12
11
10
9
8
7
6
5
4
3
2
1
0
-1
-2
f1 (ppm)

Synthesis for 1-(4,6-dichloropyrimidin-5-yl)propan-2-one

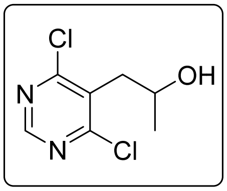

1-(4,6-dichloropyrimidin-5-yl)propan-2-ol:

2-(4,6-dichloropyrimidin-5-yl)acetaldehyde (3.0 g, 15.71 mmol, 1.0 eq) was dissolved into 52 mL of diethyl ether (0.3M) under Argon atmosphere. The reaction flask was cooled down to -78ºC. Methylmagnesiumbromide (3M solution in diethyl ether) (7.85 mL, 23.56 mmol, 1.5 eq.) was added dropwise and let stir for 0.5hr at -78ºC. The reaction was let warm to room temperature and stirred for an additional 3 hours, then quenched with water. The crude reaction mixture was filtered through celite and washed with ethyl acetate. The reaction mixture was partitioned in ethyl acetate and brine. The organic layer was dried over sodium sulfate and concentrated. The crude extract was purified via FCC (8:2 Hex:EtAc gradient) to yield 2.12 g of pure 1-(4,6-dichloropyrimidin-5-yl)propan-2-ol as a white solid (65% yield).

^{1}H NMR (400 MHz, $CDCl_3$) δ 8.58 (s, 1H), 4.24 – 4.17 (m, 1H), 3.10 (dd, J = 13.8, 8.4 Hz, 1H), 2.98 (dd, J = 13.7, 5.0 Hz, 1H), 2.11 (s, 1H), 1.31 (d, J = 6.2 Hz, 3H).

^{13}C NMR (101 MHz, $CDCl_3$) δ 162.43, 155.67, 130.71, 66.65, 39.30, 23.93.

MS (APCI) Calculated: $C_7H_9Cl_2N_2O$ $[M+H]^+$ 207.0 **Found:** 207.0 m/z

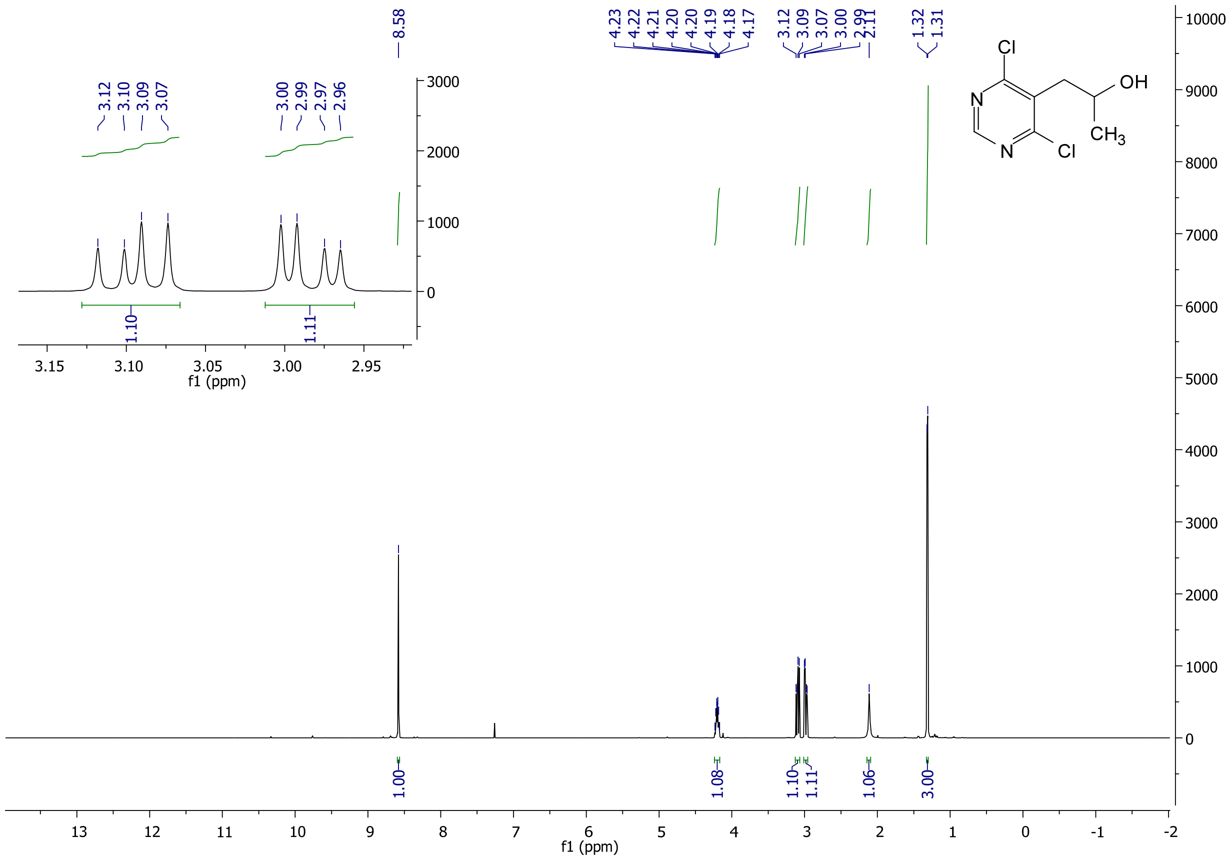

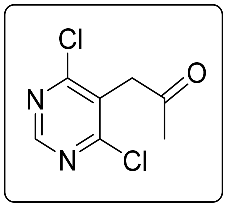

1-(4,6-dichloropyrimidin-5-yl)propan-2-one:

To 1-(4,6-dichloropyrimidin-5-yl)propan-2-ol (2.12 g, 10.24 mmol, 1.0 eq.) Dess-Martin periodinane (8.69 g, 20.48 mmol, 2.0 eq.) added and dissolved into 21 ml of DCM (0.5M). The reaction was left to stir overnight. The reaction mixture was partitioned in DCM, sodium thiosulfate (aq.) and sodium bicarbonate (aq.) The organic layer was dried over sodium sulfate and concentrated. The crude extract was purified via FCC (8:2 Hex:EtAc) to yield 1.72 g of pure 1-(4,6-dichloropyrimidin-5-yl)propan-2-one as a white solid (82% yield).

^{1}H NMR (400 MHz, $CDCl_3$) δ 8.67 (s, 1H), 4.07 (s, 2H), 2.32 (s, 3H).

MS (APCI) Calculated: $C_7H_7Cl_2N_2O$ $[M+H]^+$ 205.0 **Found:** 204.9 m/z

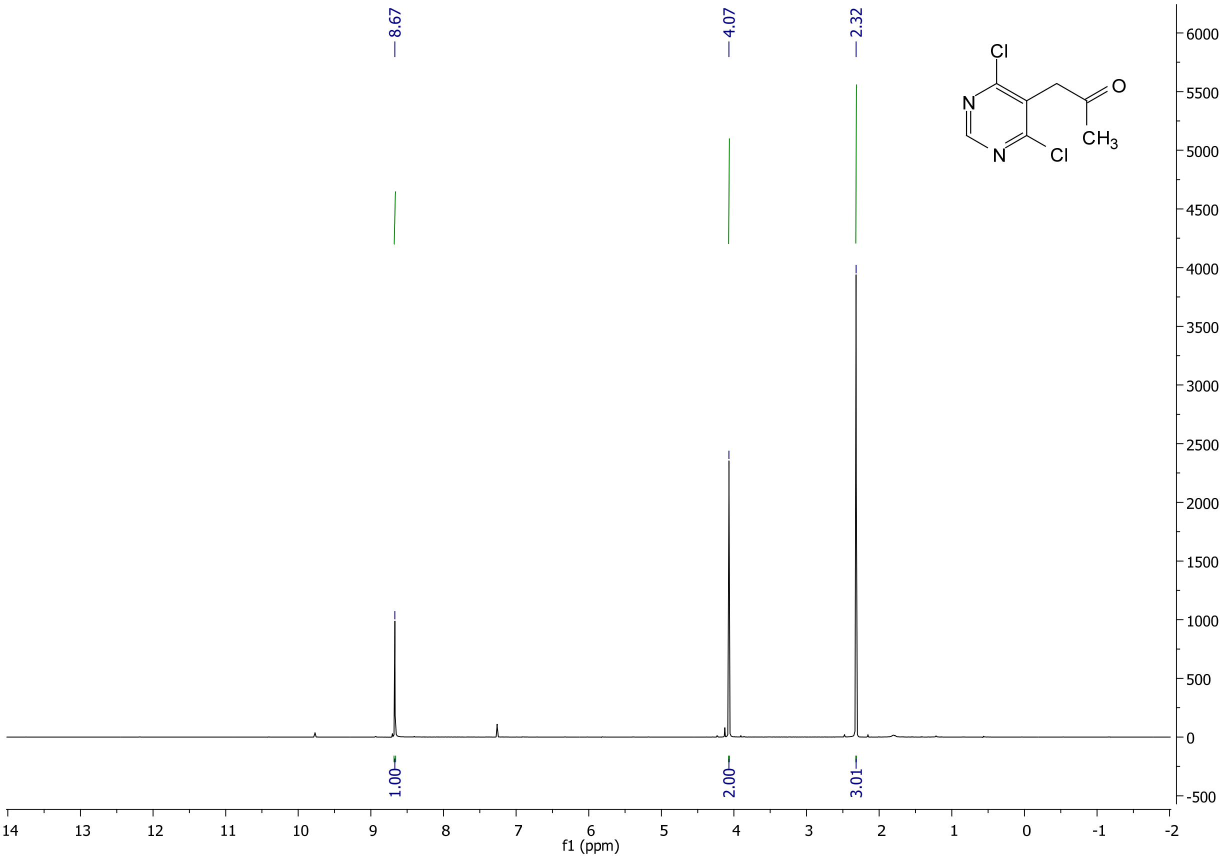

General procedure for amine cyclization to form pyrrolopyrimidines

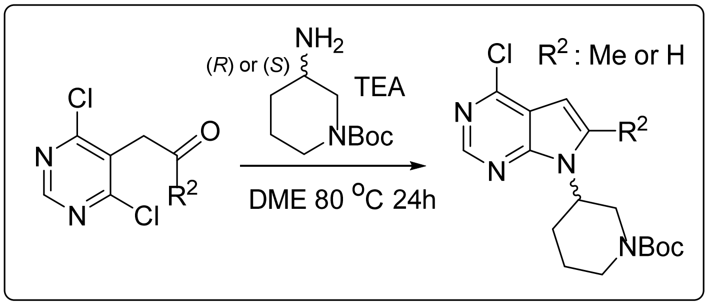

(R) or (S)
NH2
TEA
NBoc
DME 80 °C 24h
Cl
N
N
Cl
O
R2
Cl
R2 : Me or H
N
N
N
R2
NBoc

The functionalized pyrimidine (1.0 eq.), the boc-protected chiral amine (1.3 eq.), and Diisopropylethylamine (2 eq.) were dissolved in Dimethoxyethane (0.5M) and refluxed at 80 °C overnight. The crude reaction mixture was partitioned in ethyl acetate and brine. The organic layer was dried over sodium sulfate and concentrated. The crude mixture was purified with FCC with a slow hexanes/ethyl acetate gradient from 100:0 to 70:30 to yield various pyrrolopyrimidines (45% to 81% yields).

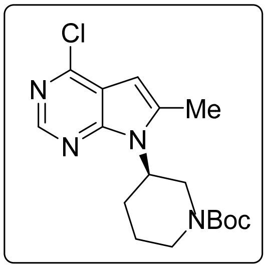

***tert*-butyl(*R*)-3-(4-chloro-6-methyl-7*H*-pyrrolo[2,3-*d*]pyrimidin-7-yl)piperidine-1-carboxylate:**

Following the general procedure: 1-(4,6-dichloropyrimidin-5-yl)propan-2-one (2.12 g, 10.44 mmol, 1.0 eq.) was cyclized with (R)-3-(Boc-amino)piperidine (2.72 g) along with diisopropylethylamine (3.64 mL) and dimethoxyethane as solvent (21 mL). Workup and purification follow the general procedure to yield 1.65 g of *tert*-butyl(*R*)-3-(4-chloro-6-methyl-7*H*-pyrrolo[2,3-*d*]pyrimidin-7-yl)piperidine-1-carboxylate as a yellow oil (45%).

^{1}H NMR: (400 MHz, Chloroform-*d*) δ 8.50 (s, 1H), 6.33 (s, 1H), 4.23 – 4.04 (m, 3H), 3.84 (t, *J* = 12.4 Hz, 1H), 2.89 (ddd, *J* = 25.3, 12.9, 4.2 Hz, 2H), 2.48 (s, 3H), 1.92 (dd, *J* = 26.7, 11.7 Hz, 2H), 1.62 (dd, *J* = 18.1, 6.9 Hz, 1H), 1.46 (s, 9H).

MS (APCI) Calculated: $C_{17}H_{24}ClN_4O_2$ $[M+H]^+$ 351.2 **Found:** 351.1 m/z

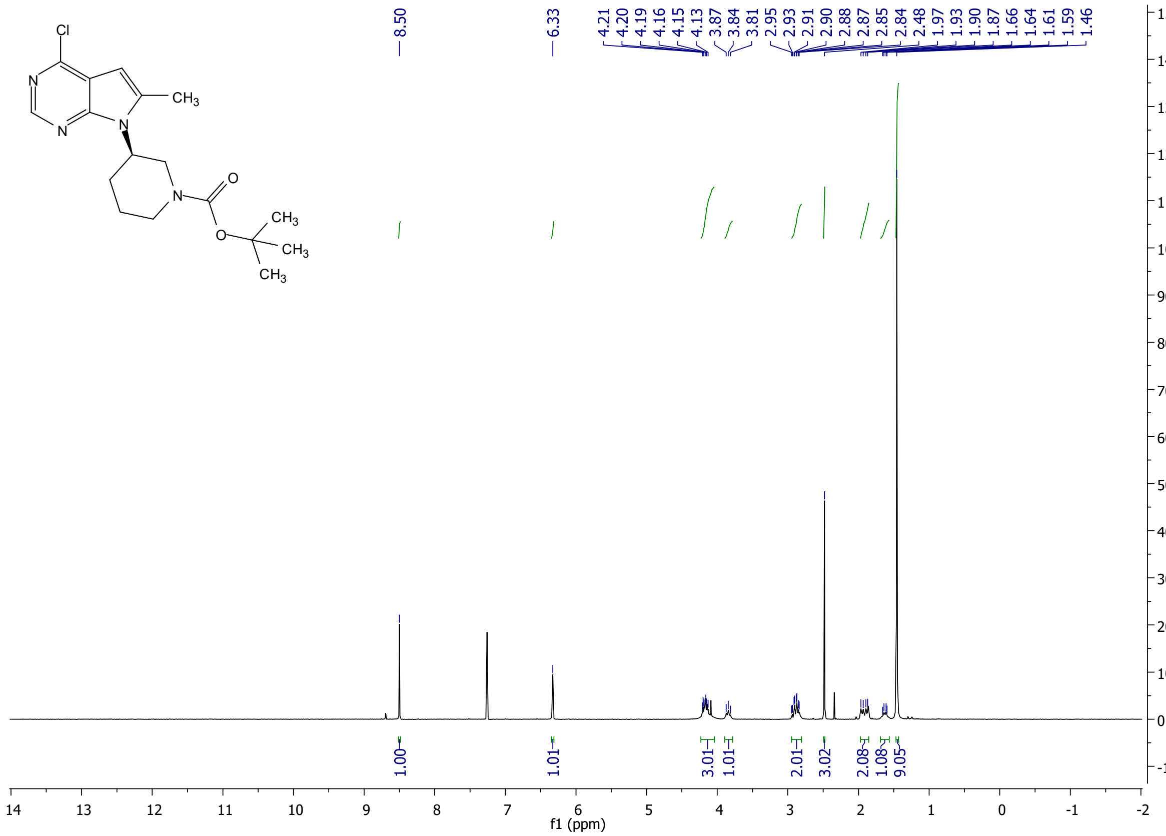

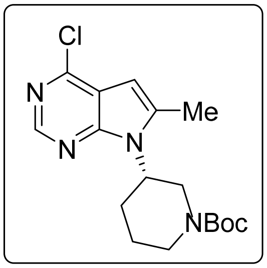

tert-butyl(_S_)-3-(4-chloro-6-methyl-7_H_-pyrrolo[2,3-_d_]pyrimidin-7-yl)piperidine-1-carboxylate:

Following the general procedure: 1-(4,6-dichloropyrimidin-5-yl)propan-2-one (1.72 g, 8.47 mmol, 1.0 eq.) was cyclized with (S)-3-(Boc-amino)piperidine (2.21 g) along with diisopropylethylamine (2.95 mL) and dimethoxyethane as solvent (17 mL). Workup and purification follow the general procedure to yield 2.40 g of _tert_-butyl(_S_)-3-(4-chloro-6-methyl-7_H_-pyrrolo[2,3-_d_]pyrimidin-7-yl)piperidine-1-carboxylate as a yellow oil (81%).

^{1}**H NMR**: (400 MHz, Chloroform-*d*) δ 8.48 (s, 1H), 6.31 (s, 1H), 4.27 – 4.03 (m, 3H), 3.83 (t, *J* = 10.5 Hz, 1H), 2.87 (ddd, *J* = 16.7, 12.8, 5.3 Hz, 2H), 2.46 (s, 3H), 1.89 (dd, *J* = 28.8, 12.9 Hz, 2H), 1.61 (q, *J* = 12.7 Hz, 1H), 1.44 (s, 9H).

MS (APCI) Calculated: $C_{17}H_{24}ClN_4O_2$ $[M+H]^+$ 351.2 **Found:** 351.2 m/z

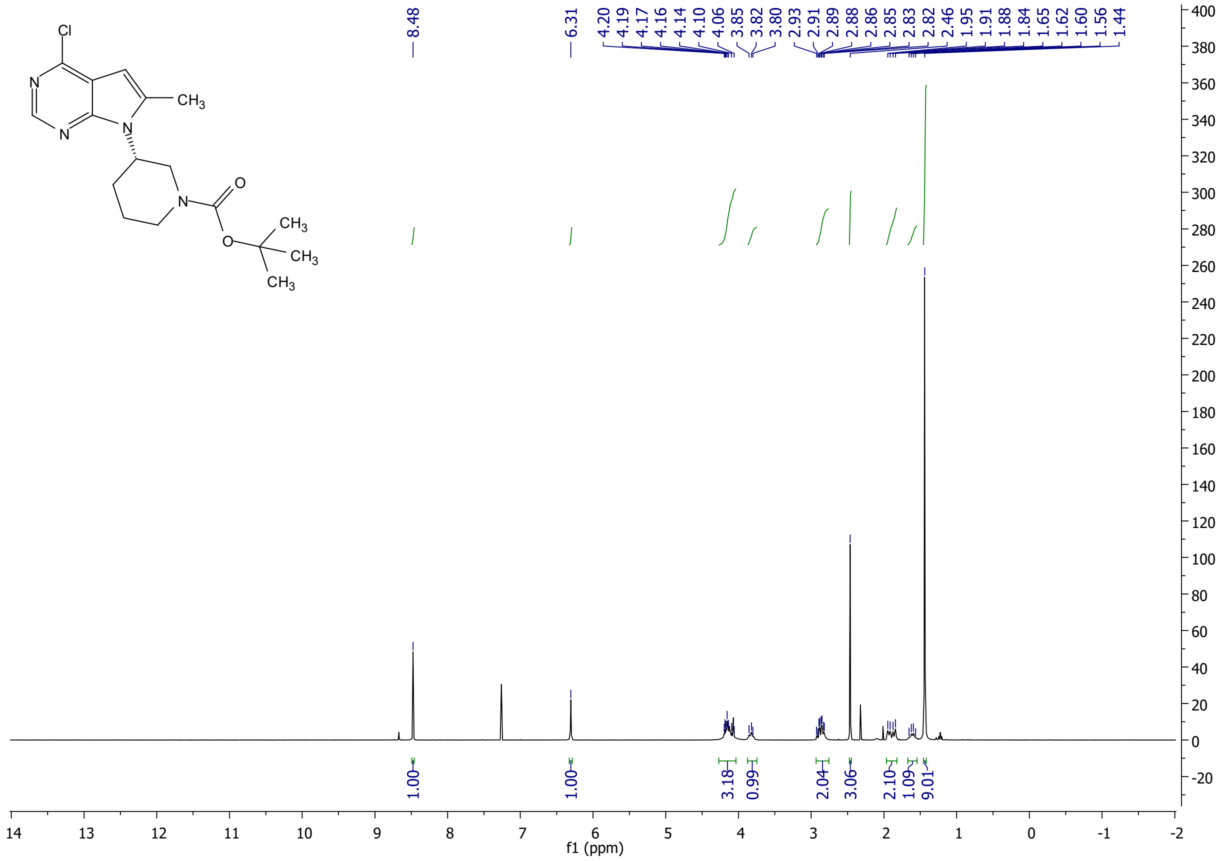

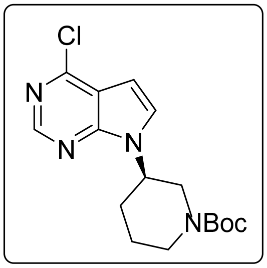

***tert*-butyl (*R*)-3-(4-chloro-7*H*-pyrrolo[2,3-*d*]pyrimidin-7-yl)piperidine-1-carboxylate:** Following the general procedure: 2-(4,6-dichloropyrimidin-5-yl)acetaldehyde (1 g, 5.24 mmol, 1.0 eq.) was cyclized with (R)-3-(Boc-amino)piperidine (1.54 mL) along with diisopropylethylamine

(1.83 mL) and dimethoxyethane as solvent (10.5 mL). Workup and purification follow the general procedure to yield 1.2 g of *tert*-butyl (*R*)-3-(4-chloro-7*H*-pyrrolo[2,3-*d*]pyrimidin-7-yl)piperidine-1-carboxylate as a yellow solid (68%).

^{1}**H NMR**: (400 MHz, Chloroform-*d*) 8.61 (s, 1H), 7.31 (d, *J* = 3.7 Hz, 1H), 6.60 (d, *J* = 3.6 Hz, 1H), 4.73 (ddd, *J* = 14.5, 10.1, 4.2 Hz, 1H), 4.23 (s, 1H), 4.00 (d, *J* = 11.4 Hz, 1H), 3.26 (dd, *J* = 12.9, 10.0 Hz, 1H), 3.00 – 2.89 (m, 1H), 2.16 (dd, *J* = 10.8, 6.2 Hz, 1H), 2.07 (d, *J* = 13.1 Hz, 1H), 1.83 (d, *J* = 13.2 Hz, 1H), 1.68 (dd, *J* = 23.2, 12.6 Hz, 1H), 1.44 (s, 9H).

MS (APCI) Calculated: $C_{16}H_{22}ClN_4O_2$ $[M+H]^+$ 337.1 **Found:** 337.1 m/z

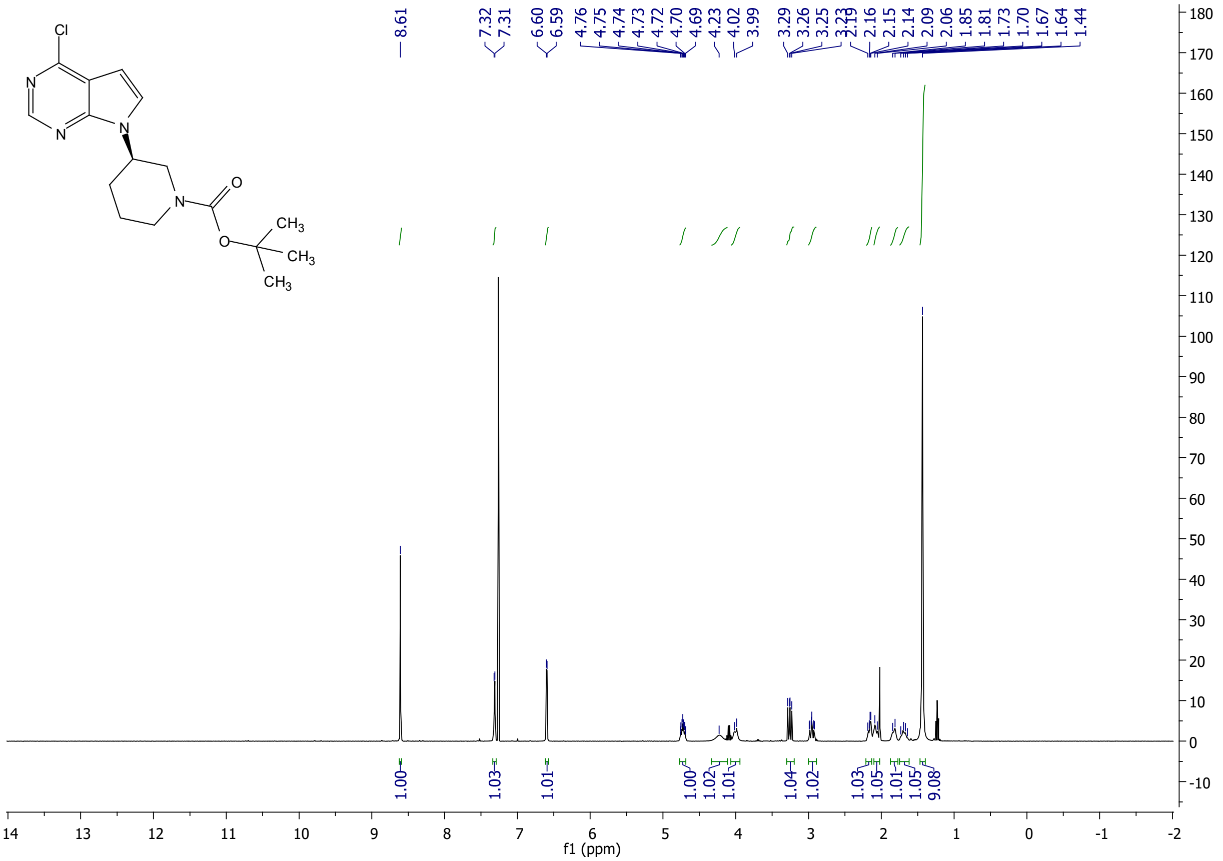

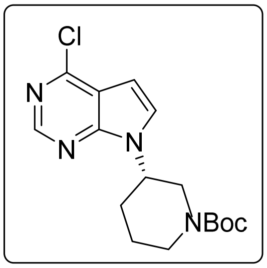

***tert*-butyl (*S*)-3-(4-chloro-7*H*-pyrrolo[2,3-*d*]pyrimidin-7-yl)piperidine-1-carboxylate**:

Following the general procedure: 2-(4,6-dichloropyrimidin-5-yl)acetaldehyde (2.0 g, 10.47 mmol, 1.0 eq.) was cyclized with (S)-3-(Boc-amino)piperidine (3.10 mL) along with diisopropylethylamine (3.65 mL) and dimethoxyethane as solvent (21 mL). Workup and purification follow the general procedure to yield 2.15 g of *tert*-butyl (*S*)-3-(4-chloro-7*H*-pyrrolo[2,3-*d*]pyrimidin-7-yl)piperidine-1-carboxylate as a yellow solid (58%)**.**

^{1}**H NMR**: (400 MHz, Chloroform-*d*) δ 8.61 (s, 1H), 7.32 (d, J = 3.7 Hz, 1H), 6.60 (d, J = 3.6 Hz, 1H), 4.73 (ddd, J = 14.4, 9.9, 4.2 Hz, 1H), 4.23 (s, 1H), 4.01 (d, J = 12.5 Hz, 1H), 3.26 (dd, J = 12.9, 10.0 Hz, 1H), 3.00 – 2.92 (m, 1H), 2.20 – 2.14 (m, 1H), 2.07 (dt, J = 12.8, 9.6 Hz, 1H), 1.84 (d, J = 16.2 Hz, 1H), 1.76 – 1.64 (m, 1H), 1.44 (s, 9H).

MS (APCI) Calculated: $C_{16}H_{22}ClN_4O_2$ $[M+H]^+$ 337.1 **Found:** 337.1 m/z

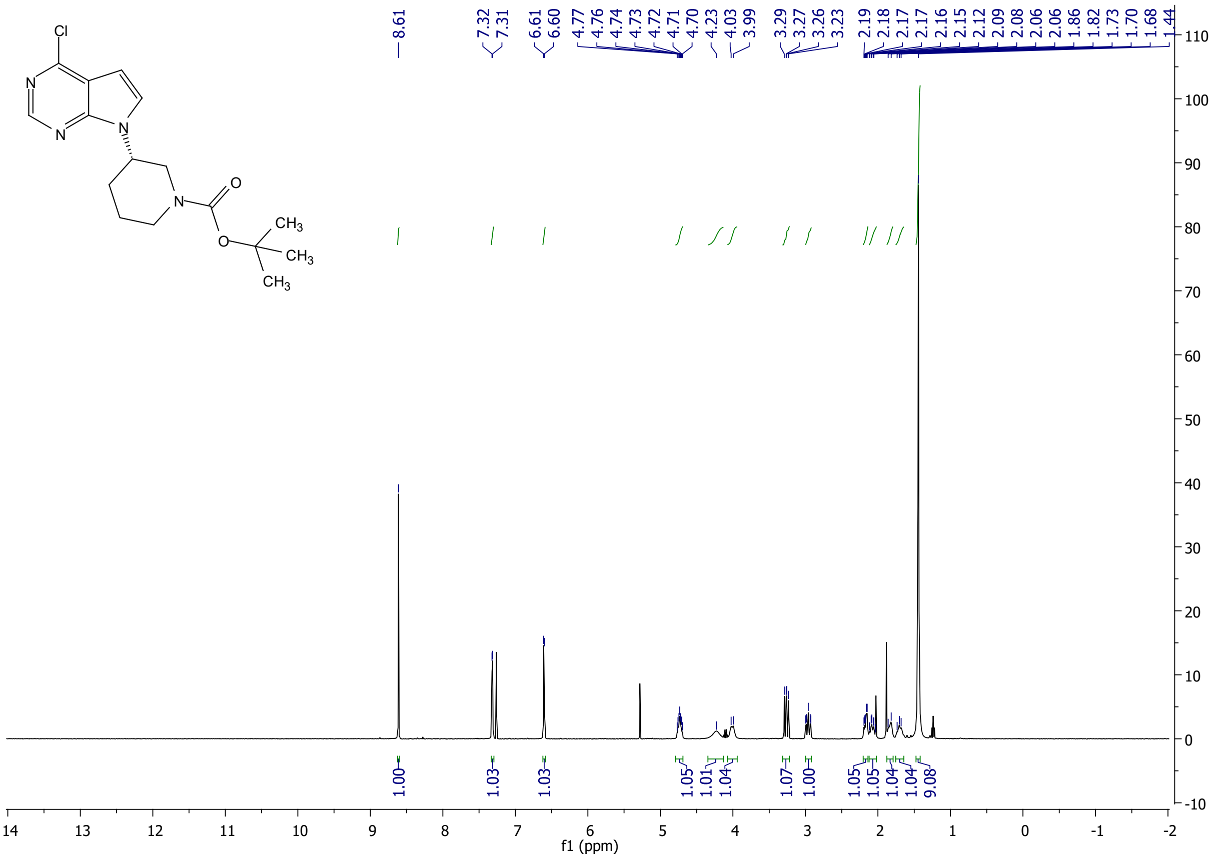
Cl
N
N
N
N
O
O
CH3
CH3
CH3
8.61
7.32
7.31
6.61
6.60
4.77
4.76
4.74
4.73
4.72
4.71
4.70
4.23
4.03
3.99
3.29
3.27
3.26
3.23
2.19
2.18
2.17
2.17
2.16
2.15
2.12
2.09
2.08
2.06
2.06
1.86
1.82
1.73
1.70
1.68
1.44
1.00
1.03
1.03
1.05
1.01
1.04
1.07
1.00
1.05
1.05
1.04
1.04
9.08
14
13
12
11
10
9
8
7
6
5
4
3
2
1
0
-1
-2
f1 (ppm)
110
100
90
80
70
60
50
40
30
20
10
0
-10

General procedure for iodination of pyrrolopyrimidines

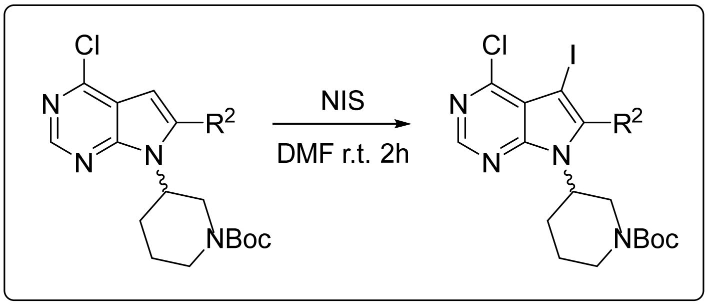

Pyrrolopyrimidine (1 eq.) and N-Iodosuccinimide (1.2 eq.) were dissolved in Dimethylformamide (DMF) (0.15 M) and let stir at r.t. for 2 hours. The crude reaction mixture was partitioned between ethyl acetate and brine and the organic layer washed with sodium thiosulfate. The organic layer was dried over sodium sulfate and concentrated to yield iodinated pyrrolopyrimidines**.**

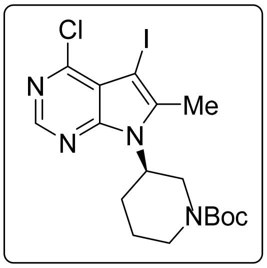

***tert*-butyl(*R*)-3-(4-chloro-5-iodo-6-methyl-7*H*-pyrrolo[2,3-*d*]pyrimidin-7-yl)piperidine-1-carboxylate**:

Following the general procedure, *tert*-butyl(*R*)-3-(4-chloro-6-methyl-7*H*-pyrrolo[2,3-*d*]pyrimidin-7-yl)piperidine-1-carboxylate (769 mg, 2.19 mmol, 1 eq.) was iodinated with N-Iodosuccinimide (592 mg) in DMF (14 mL). Workup was followed according to the general procedure yielding 872 mg of *tert*-butyl(*R*)-3-(4-chloro-5-iodo-6-methyl-7*H*-pyrrolo[2,3-*d*]pyrimidin-7-yl)piperidine-1-carboxylate as a white solid (82%).

^{1}**H NMR**: (400 MHz, Chloroform-*d*) δ 8.50 (s, 1H), 4.32 – 4.25 (m, 1H), 4.16 (s, 2H), 3.86 (t, *J* = 12.4 Hz, 1H), 2.94 – 2.77 (m, 2H), 2.56 (s, 3H), 1.97 – 1.84 (m, 2H), 1.68 – 1.58 (m, 1H), 1.46 (s, 9H).

MS (APCI) Calculated: $C_{17}H_{23}ClIN_4O_2$ $[M+H]^+$ 477.1 **Found:** 477.0 m/z

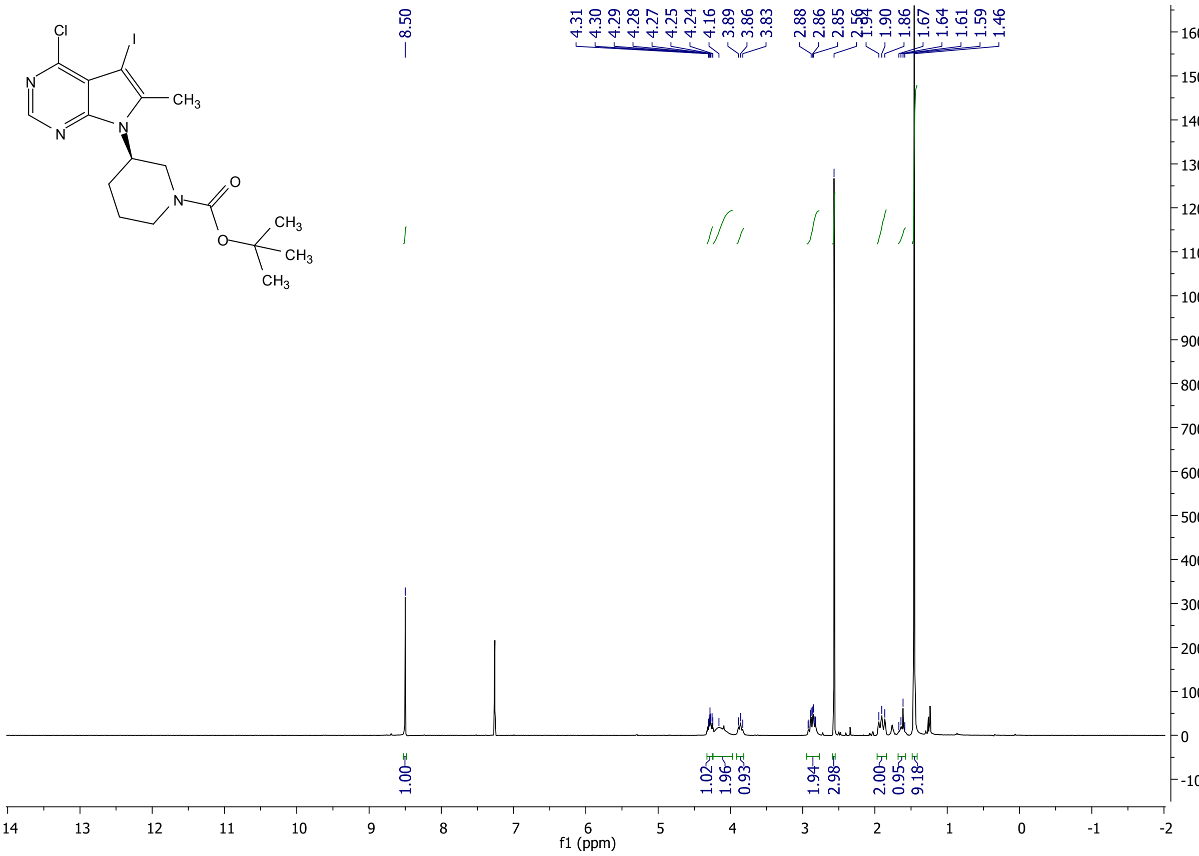

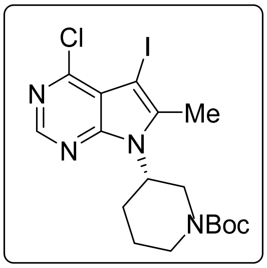

tert-butyl(R)-3-(4-chloro-5-iodo-6-methyl-7H-pyrrolo[2,3-d]pyrimidin-7-yl)piperidine-1-carboxylate:

Following the general procedure, *tert*-butyl(*S*)-3-(4-chloro-6-methyl-7*H*-pyrrolo[2,3-*d*]pyrimidin-7-yl)piperidine-1-carboxylate (2.40 g, 6.84 mmol, 1 eq.) was iodinated with N-Iodosuccinimide (1.85 g) in DMF (46 mL). Workup was followed according to the general procedure yielding 2.37 g of *tert*-butyl(*R*)-3-(4-chloro-5-iodo-6-methyl-7*H*-pyrrolo[2,3-*d*]pyrimidin-7-yl)piperidine-1-carboxylate as a white solid (73%).

^{1}**H NMR**: (400 MHz, Chloroform-*d*) δ 8.51 (s, 1H), 4.33 – 4.24 (m, 1H), 4.17 (s, 2H), 3.86 (t, *J* = 12.5 Hz, 1H), 2.96 – 2.76 (m, 2H), 2.57 (s, 3H), 1.97 – 1.85 (m, 2H), 1.68 – 1.61 (m, 1H), 1.46 (s, 9H).

MS (APCI) Calculated: $C_{17}H_{23}ClIN_4O_2$ $[M+H]^+$ 477.1 **Found:** 477.0 m/z

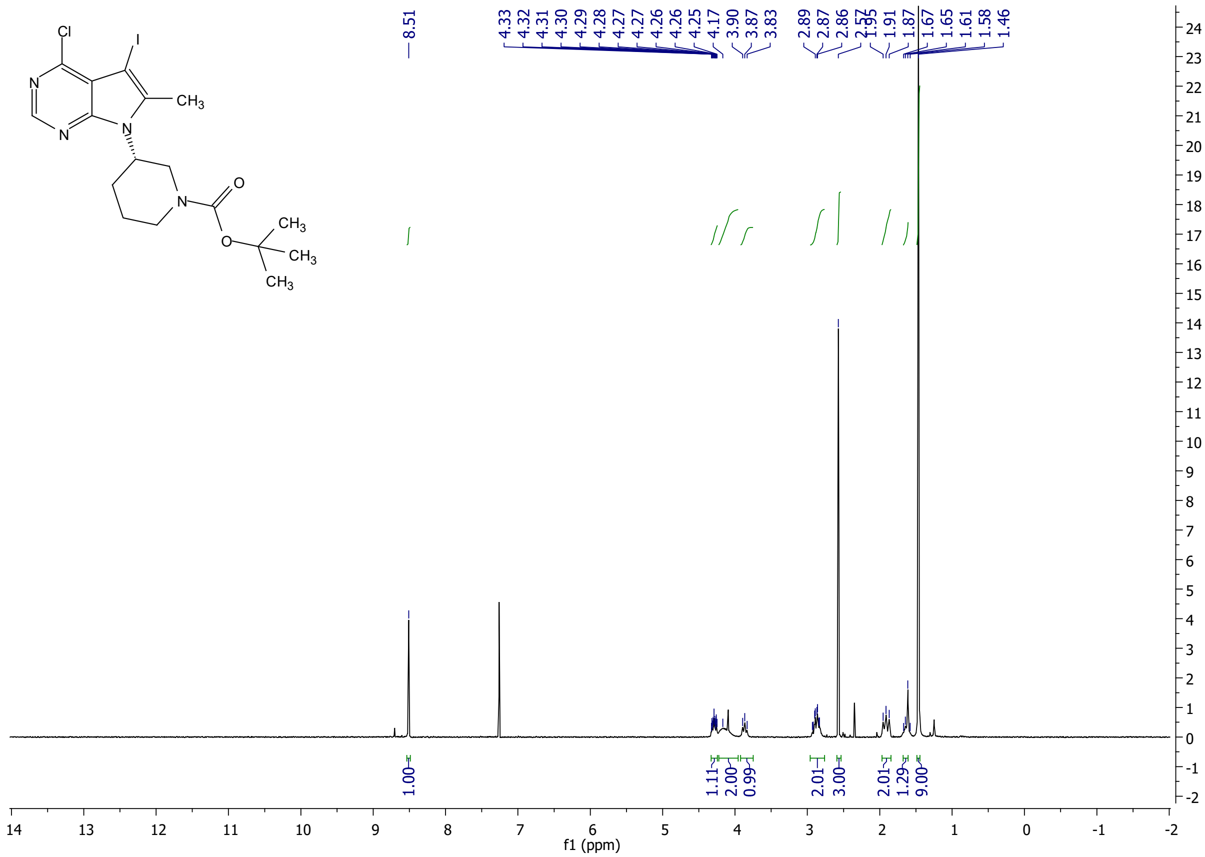

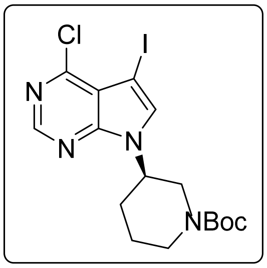

***tert*-butyl (*R*)-3-(4-chloro-5-iodo-7*H*-pyrrolo[2,3-*d*]pyrimidin-7-yl)piperidine-1-carboxylate**: Following the general procedure, *tert*-butyl (*R*)-3-(4-chloro-7*H*-pyrrolo[2,3-*d*]pyrimidin-7-yl)piperidine-1-carboxylate (800 mg, 2.36 mmol, 1 eq.), was iodinated with N-Iodosuccinimide (640 mg) in DMF (15 mL). Workup was followed according to the general procedure yielding 869 mg of *tert*-butyl (*R*)-3-(4-chloro-5-iodo-7*H*-pyrrolo[2,3-*d*]pyrimidin-7-yl)piperidine-1-carboxylate as a yellow-white solid (80%).

^{1}**H NMR**: (400 MHz, Chloroform-*d*) 8.61 (s, 1H), 7.47 (s, 1H), 4.82 – 4.71 (m, 1H), 4.18 (s, 1H), 3.95 (d, *J* = 12.8 Hz, 1H), 3.29 (t, *J* = 11.8 Hz, 1H), 3.03 (ddd, *J* = 13.5, 10.7, 3.2 Hz, 1H), 2.21 – 2.13 (m, 1H), 2.11 – 2.00 (m, 1H), 1.83 (d, *J* = 10.8 Hz, 1H), 1.74 – 1.66 (m, 1H), 1.46 (s, 9H).

MS (APCI) Calculated: $C_{16}H_{21}ClIN_4O_2$ $[M+H]^+$ 463.0 **Found:** 463.0 m/z

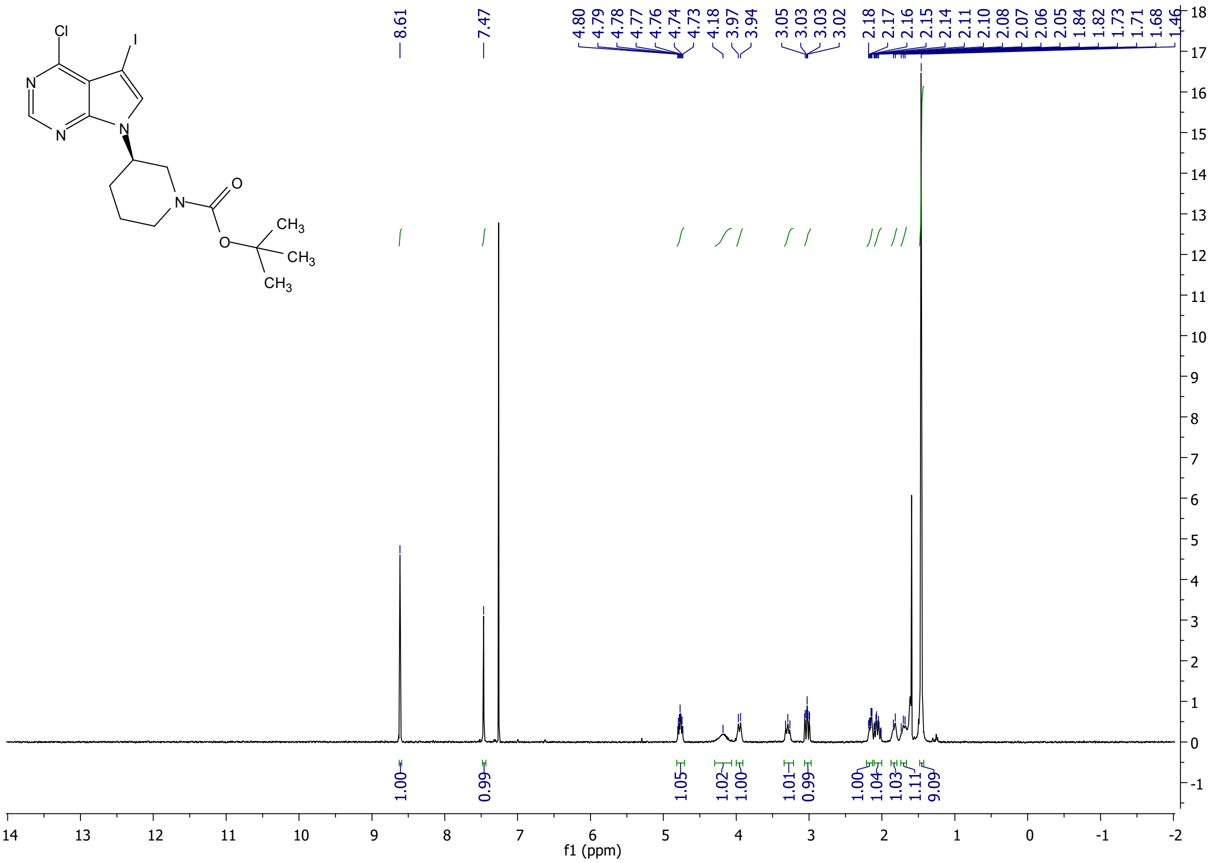
Cl
I
N
N
N
N
O
O
CH3
CH3
CH3
8.61
7.47
4.80
4.79
4.78
4.77
4.76
4.74
4.73
4.18
3.97
3.94
3.05
3.03
3.03
3.02
2.18
2.17
2.16
2.15
2.14
2.11
2.10
2.08
2.07
2.06
2.05
1.84
1.82
1.73
1.71
1.68
1.46
1.00
0.99
1.05
1.02
1.00
1.01
0.99
1.00
1.04
1.03
1.11
9.09
14
13
12
11
10
9
8
7
6
5
4
3
2
1
0
-1
-2
f1 (ppm)
18
17
16
15
14
13
12
11
10
9
8
7
6
5
4
3
2
1
0
-1

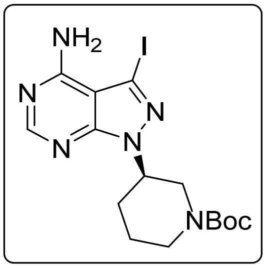

tert-butyl (R)-3-(4-amino-3-iodo-1H-pyrazolo[3,4-d]pyrimidin-1-yl)piperidine-1-carboxylate:

3-iodo-1H-pyrazolo[3,4-d]pyrimidin-4-amine (2 g, 7.66 mmol, 1 eq.), tert-butyl (S)-3-hydroxypiperidine-1-carboxylate (4.62 g, 23.0 mmol, 3 eq.), and triphenylphosphine (4.02 g, 15.32 mmol, 2 eq.) were added to anhydrous THF (77 ml, 0.1 M) in a dried round bottom flask. After cooling the mixture to 0 °C, DIAD (3 ml, 15.32 mmol, 2.0 eq.) was added and stirred for 10 minutes. The reaction mixture was then warmed to room temperature and stirred overnight. The reaction mixture was partitioned in ethyl acetate and brine. The organic layer was dried over sodium sulfate and concentrated. The crude extract was purified via FCC (96:4 DCM/MeOH) to yield 3.2 g of tert-butyl (R)-3-(4-amino-3-iodo-1H-pyrazolo[3,4-d]pyrimidin-1-yl)piperidine-1-carboxylate as a yellow solid (94% yield). The ^{1}H matched those reported in the literature[182].

General procedure for cross coupling of aryl boronic esters to pyrrolopyrimidines or pyrazolopyrimidines (3.1a-3.7a and 3.10a-3.12a):

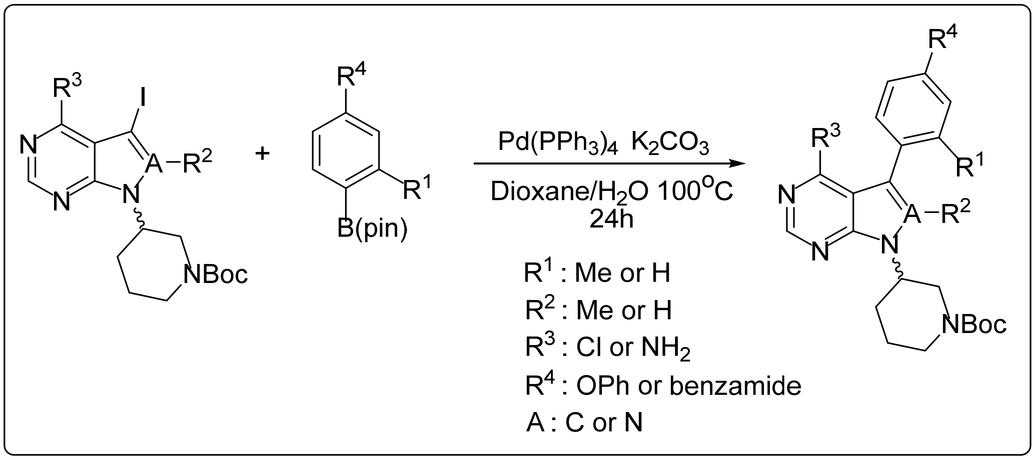
R3
I
N
N
A−R2
N
NBoc
+
R4
R1
B(pin)
Pd(PPh3)4 K2CO3
Dioxane/H2O 100°C
24h
R1 : Me or H
R2 : Me or H
R3 : Cl or NH2
R4 : OPh or benzamide
A : C or N
R4
R3
R1
A−R2
NBoc

Iodinated pyrrolopyrimidine or pyrazolopyrimidine (1 eq.) was combined with boronic ester (1.1 eq.), $Pd(PPh_3)_4$ (0.1 eq.), and K_2CO_3 (2.3 eq.). The reaction vessel was then purged with argon and a 3:1 mixture of dioxane (0.25 M)/ DI water was added. The reaction was then stirred at 100ºC for 18hr. The crude reaction mixture was filtered through celite and washed with ethyl acetate. The crude mixture was partitioned between ethyl acetate and brine. The organic later was dried over sodium sulfate and concentrated to yield crude **3.1a-3.7a** and **3.10a-3.12a**. The crude extract was then moved on to the next reaction with no further purification due to the similarity of polarity of product and dehalogenated starting material.

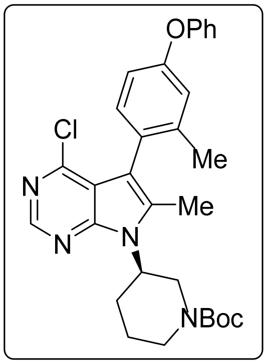

tert-butyl (R)-3-(4-chloro-6-methyl-5-(2-methyl-4-phenoxyphenyl)-7H-pyrrolo[2,3-d]pyrimidin-7-yl)piperidine-1-carboxylate (3.1a):

Following the general procedure, *tert*-butyl (*R*)-3-(4-chloro-5-iodo-6-methyl-7*H*-pyrrolo[2,3-*d*]pyrimidin-7-yl)piperidine-1-carboxylate (1.48 g, 3.10 mmol, 1 eq.) was coupled with 4,4,5,5-tetramethyl-2-(2-methyl-4-phenoxyphenyl)-1,3,2-dioxaborolane (1.06 g) to yield a crude mixture of **3.1a.** Workup and purification follow the general procedure.

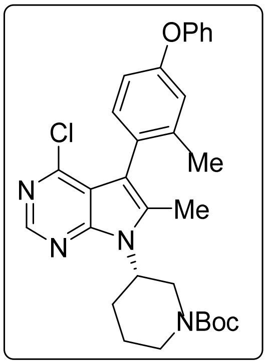

tert-butyl (S)-3-(4-chloro-6-methyl-5-(2-methyl-4-phenoxyphenyl)-7H-pyrrolo[2,3-d]pyrimidin-7-yl)piperidine-1-carboxylate (3.2a):

Following the general procedure, *tert*-butyl (*S*)-3-(4-chloro-5-iodo-6-methyl-7*H*-pyrrolo[2,3-*d*]pyrimidin-7-yl)piperidine-1-carboxylate (1.2 g, 2.52 mmol, 1 eq.) was coupled with 4,4,5,5-tetramethyl-2-(2-methyl-4-phenoxyphenyl)-1,3,2-dioxaborolane (859 mg) to yield a crude mixture of **3.2a.** Workup and purification follow the general procedure.

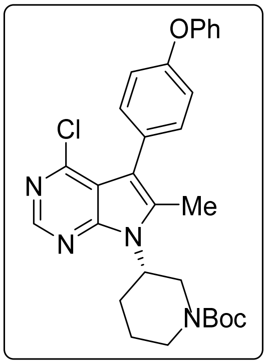

tert-butyl (S)-3-(4-chloro-6-methyl-5-(4-phenoxyphenyl)-7H-pyrrolo[2,3-d]pyrimidin-7-yl)piperidine-1-carboxylate (3.3a):

Following the general procedure, *tert*-butyl (S)-3-(4-chloro-6-methyl-5-iodo-7H-pyrrolo[2,3-d]pyrimidin-7-yl)piperidine-1-carboxylate (1.1 g, 2.31 mmol, 1 eq.) was coupled with 4,4,5,5-tetramethyl-2-(4-phenoxyphenyl)-1,3,2-dioxaborolane (753 mg) to yield a crude mixture of **3.3a.** Workup and purification follow the general procedure.

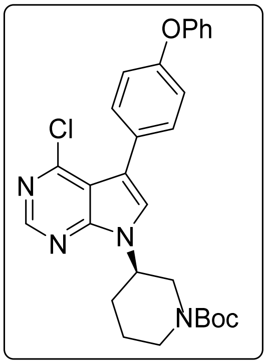

***tert*-butyl (*R*)-3-(4-chloro-5-(4-phenoxyphenyl)-7*H*-pyrrolo[2,3-*d*]pyrimidin-7-yl)piperidine-1-carboxylate (3.4a)**:

Following the general procedure, *tert*-butyl (*R*)-3-(4-chloro-5-iodo-7*H*-pyrrolo[2,3-*d*]pyrimidin-7-yl)piperidine-1-carboxylate (579 mg, 1.25 mmol, 1 eq.) was coupled with 4,4,5,5-tetramethyl-2-(4-phenoxyphenyl)-1,3,2-dioxaborolane (408 mg) to yield a crude mixture of **3.4a**. Workup and purification follow the general procedure.

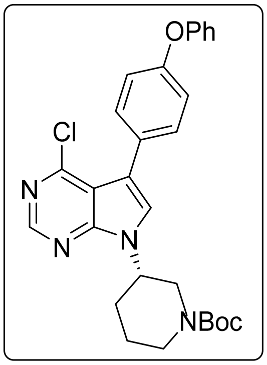

***tert*-butyl (*S*)-3-(4-chloro-5-(4-phenoxyphenyl)-7*H*-pyrrolo[2,3-*d*]pyrimidin-7-yl)piperidine-1-carboxylate (3.5a)**:

Following the general procedure, *tert*-butyl (*S*)-3-(4-chloro-5-iodo-7*H*-pyrrolo[2,3-*d*]pyrimidin-7-yl)piperidine-1-carboxylate (1.5 g, 3.24 mmol, 1 eq) was coupled with 4,4,5,5-tetramethyl-2-(4-phenoxyphenyl)-1,3,2-dioxaborolane (1.06g) to yield a crude mixture of **3.5a**. Workup and purification follow the general procedure.

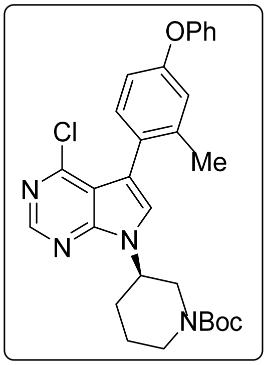

***tert-butyl* (R)-3-(4-chloro-5-(2-methyl-4-phenoxyphenyl)-7H-pyrrolo[2,3-d]pyrimidin-7-yl)piperidine-1-carboxylate (3.6a):**

Following the general procedure, *tert*-butyl (*R*)-3-(4-chloro-5-iodo-7*H*-pyrrolo[2,3-*d*]pyrimidin-7-yl)piperidine-1-carboxylate (1.1 g, 2.38 mmol, 1 eq.) was coupled with 4,4,5,5-tetramethyl-2-(2-methyl-4-phenoxyphenyl)-1,3,2-dioxaborolane (811 mg) to yield a crude mixture of **3.6a**. Workup and purification follow the general procedure.

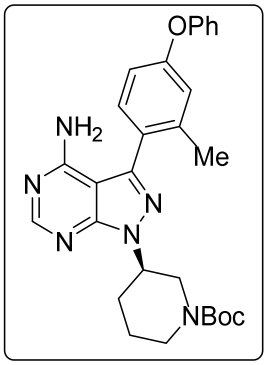

tert-butyl **(R)-3-(4-amino-3-(2-methyl-4-phenoxyphenyl)-1H-pyrazolo[3,4-d]pyrimidin-1-yl)piperidine-1-carboxylate (3.7a):**

Following the general procedure, tert-butyl (R)-3-(4-amino-3-iodo-1H-pyrazolo[3,4-d]pyrimidin-1-yl)piperidine-1-carboxylate (272 mg, 0,614 mml, 1 eq.) was coupled with 4,4,5,5-tetramethyl-2-(2-methyl-4-phenoxyphenyl)-1,3,2-dioxaborolane (200 mg) to yield a crude mixture of **3.7a**. Workup and purification follow the general procedure.

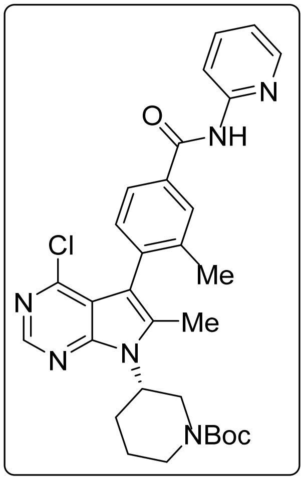

tert-butyl (S)-3-(4-chloro-6-methyl-5-(2-methyl-4-(pyridin-2-ylcarbamoyl)phenyl)-7H-pyrrolo[2,3-d]pyrimidin-7-yl)piperidine-1-carboxylate (3.10a):

Following the general procedure, *tert*-butyl (S)-3-(4-chloro-6-methyl-5-iodo-7H-pyrrolo[2,3-d]pyrimidin-7-yl)piperidine-1-carboxylate (1.2 g, 2.52 mmol, 1 eq.) was coupled with 3-methyl-

N-(pyridin-2-yl)-4-(4,4,5,5-tetramethyl-1,3,2-dioxaborolan-2-yl)benzamide (936 mg) to yield a crude mixture of **3.10a.** Workup and purification follow the general procedure.

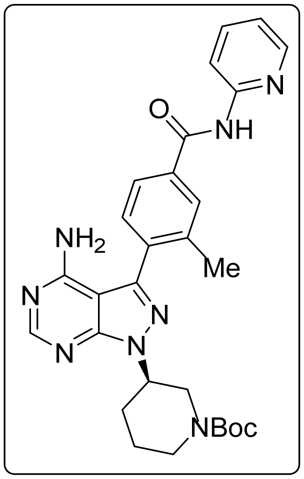

tert-butyl (R)-3-(4-amino-3-(2-methyl-4-(pyridin-2-ylcarbamoyl)phenyl)-1H-pyrazolo[3,4-d]pyrimidin-1-yl)piperidine-1-carboxylate (3.11a):

Following the general procedure, tert-butyl (R)-3-(4-amino-3-iodo-1H-pyrazolo[3,4-d]pyrimidin-1-yl)piperidine-1-carboxylate (300 mg, 0.675 mmol, 1 eq.) was coupled with 3-methyl-N-(pyridin-2-yl)-4-(4,4,5,5-tetramethyl-1,3,2-dioxaborolan-2-yl)benzamide (240 mg) to yield a crude mixture of **3.11a**. Workup and purification follow the general procedure.

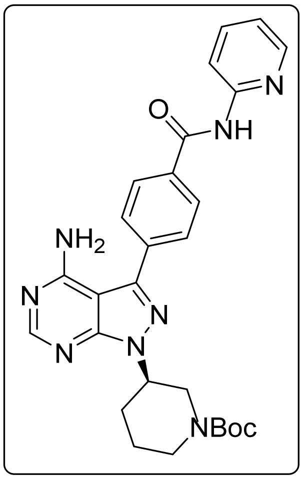

tert-butyl (R)-3-(4-amino-3-(4-(pyridin-2-ylcarbamoyl)phenyl)-1H-pyrazolo[3,4-d]pyrimidin-1-yl)piperidine-1-carboxylate (3.12a)

Following the general procedure, tert-butyl (R)-3-(4-amino-3-iodo-1H-pyrazolo[3,4-d]pyrimidin-1-yl)piperidine-1-carboxylate (870 mg, 1.96 mmol, 1 eq.) was coupled with N-(pyridin-2-yl)-4-(4,4,5,5-tetramethyl-1,3,2-dioxaborolan-2-yl)benzamide (762 mg) to yield a crude mixture of **3.12a**. Workup and purification follow the general procedure.

Synthesis for di-*ortho* substituted aryl pyrazolopyrimidines:

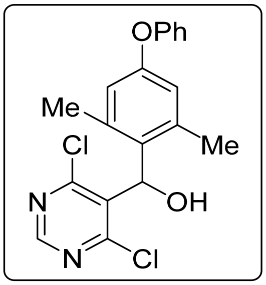

(4,6-dichloropyrimidin-5-yl)(2,6-dimethyl-4-phenoxyphenyl)methanol:

2-bromo-1,3-dimethyl-5-phenoxybenzene (1.58 g, 5.77 mmol, 1.5 eq.) was added to activated magnesium turnings (0.415 g, 17.31 mmol, 4.5 eq.) in dry diethyl (23 ml, .25 M) ether in a flame-dried round bottom under argon. The reaction was stirred at room temperature overnight. In a separate flame-dried round bottom flask 2-(4,6-dichloropyrimidin-5-yl)acetaldehyde (0.677 g, 3.85 mmol, 1.0 eq) was dissolved into 3.9 mL of diethyl ether (1 M) under argon atmosphere. The reaction flask was cooled down to -78°C. The magnesiumbromide aryl gringard (23 ml) was added dropwise and let stir for 0.5hr at -78°C. The reaction was let warm to room temperature and stirred for an additional 3 hours, then quenched with water. The reaction mixture was partitioned in ethyl acetate and brine. The organic layer was dried over sodium sulfate and concentrated. The crude extract was purified via FCC (8:2 Hex:EtAc gradient) to yield 0.760 g of pure (4,6-dichloropyrimidin-5-yl)(2,6-dimethyl-4-phenoxyphenyl)methanol as a white solid (53% yield).

^{1}H NMR: (400 MHz, Chloroform-*d*) δ 8.70 (s, 1H), 7.40 – 7.29 (m, 2H), 7.12 (t, J = 7.4 Hz, 1H), 7.01 (d, J = 7.7 Hz, 2H), 6.66 (s, 2H), 6.47 (d, J = 7.4 Hz, 1H), 2.57 (d, J = 7.4 Hz, 1H), 2.27 (s, 6H).

MS (APCI) Calculated: $C_{19}H_{17}Cl_2N_2O_2$ $[M+H]^+$ 375.1 **Found:** 375.0 m/z

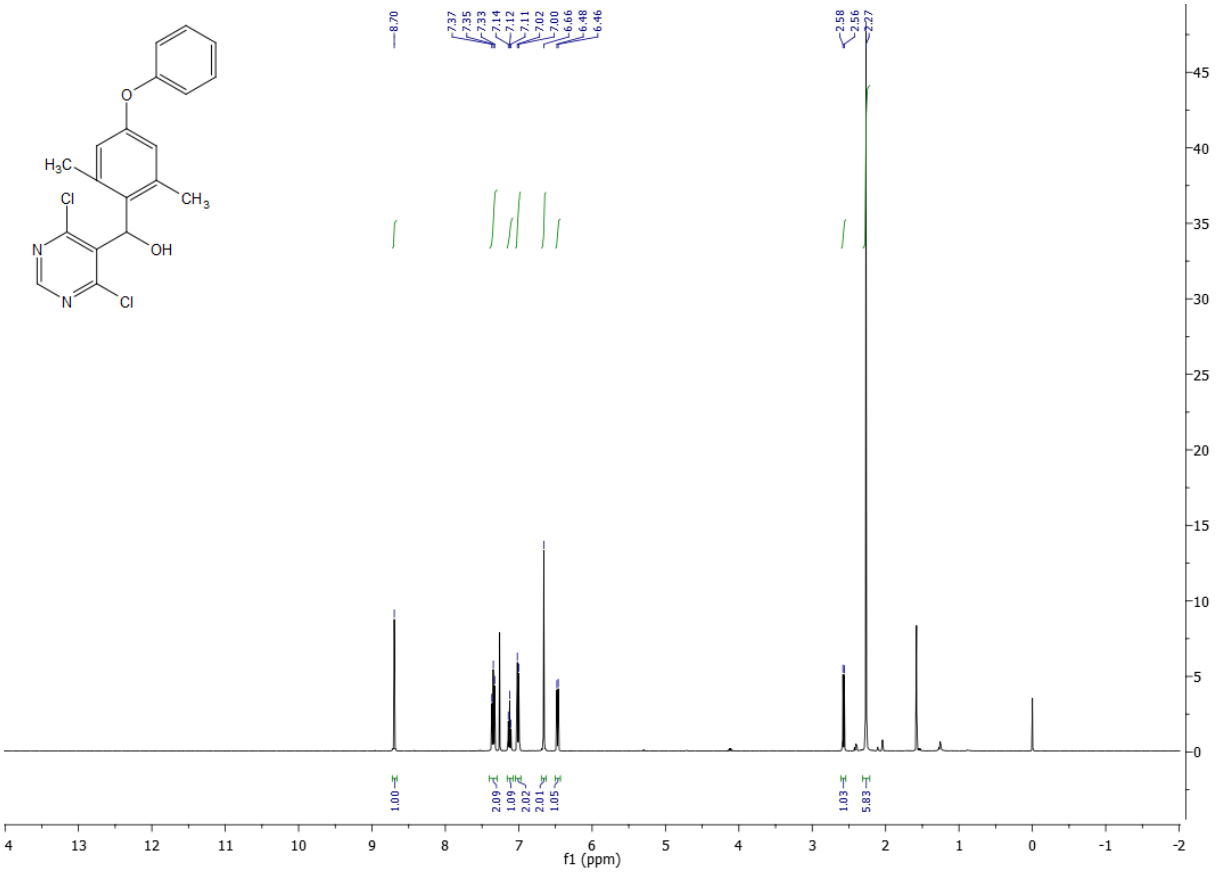

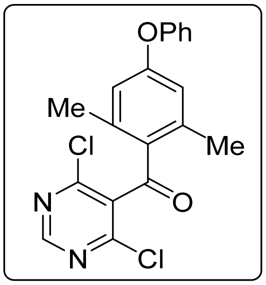

(4,6-dichloropyrimidin-5-yl)(2,6-dimethyl-4-phenoxyphenyl)methanone:

To (4,6-dichloropyrimidin-5-yl)(2,6-dimethyl-4-phenoxyphenyl)methanol (0.760 g, 2.025 mmol, 1.0 eq.) Dess-Martin periodinane (1.72 g, 4.05 mmol, 2.0 eq.) was added and dissolved into 4 ml of DCM (0.5M). The reaction was left to stir overnight. The reaction mixture was partitioned in DCM, sodium thiosulfate (aq.) and sodium bicarbonate (aq.) The organic layer was dried over sodium sulfate and concentrated. The crude extract was purified via FCC (8:2 Hex:EtAc) to yield

0.590 g of pure (4,6-dichloropyrimidin-5-yl)(2,6-dimethyl-4-phenoxyphenyl)methanone as a white solid (78% yield).

^{1}**H NMR**: (400 MHz, Chloroform-*d*) δ 8.82 (s, 1H), 7.40 (t, *J* = 8.0 Hz, 2H), 7.20 (t, *J* = 7.4 Hz, 1H), 7.07 (d, *J* = 7.6 Hz, 2H), 6.66 (s, 2H), 2.24 (s, 6H).

MS (APCI) Calculated: $C_{19}H_{15}Cl_2N_2O_2$ $[M+H]^+$ 373.1 **Found:** 373.1 m/z

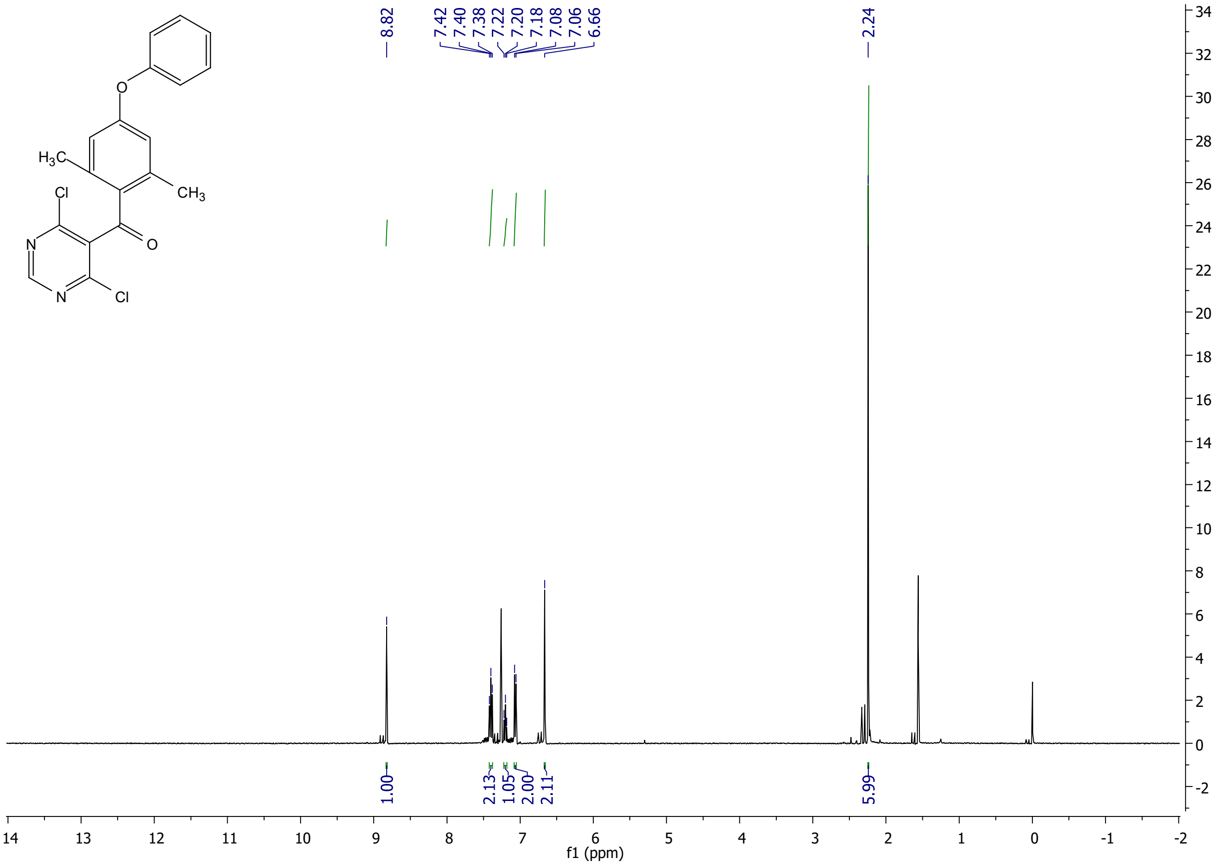

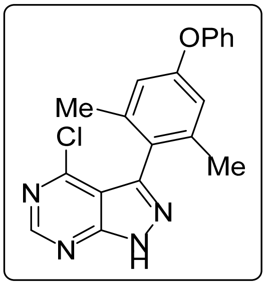

4-chloro-3-(2,6-dimethyl-4-phenoxyphenyl)-1H-pyrazolo[3,4-d]pyrimidine:

To (4,6-dichloropyrimidin-5-yl)(2,6-dimethyl-4-phenoxyphenyl)methanone (0.590 g, 1.58 mmol, 1 eq.) triethylamine (0.218 ml, 1.58 mmol, 1 eq.) and hydrazine monohydrate (0.083 ml, 1.74 mmol, 1.1 eq.) was dissolved into THF (8ml, .2 M) in a round bottom flask. After stirring for one hour at room temperature the reaction was heated to 65 °C and stirred overnight. The reaction mixture was partitioned in ethyl acetate and brine. The organic layer was dried over sodium sulfate and concentrated. The crude extract was purified via FCC (7:3 Hex:EtAc) to yield 0.298 g of 4-chloro-3-(2,6-dimethyl-4-phenoxyphenyl)-1H-pyrazolo[3,4-d]pyrimidine as a yellow solid (54% yield).

^{1}**H NMR**: (400 MHz, Chloroform-*d*) δ 11.72 (s, 1H), 8.89 (s, 1H), 7.43 – 7.33 (m, 2H), 7.15 (t, J = 7.4 Hz, 1H), 7.11 – 7.07 (m, 2H), 6.81 (s, 2H), 2.03 (s, 6H).

MS (APCI) Calculated: $C_{19}H_{16}ClN_4O$ $[M+H]^+$ 351.1 **Found:** 351.1 m/z

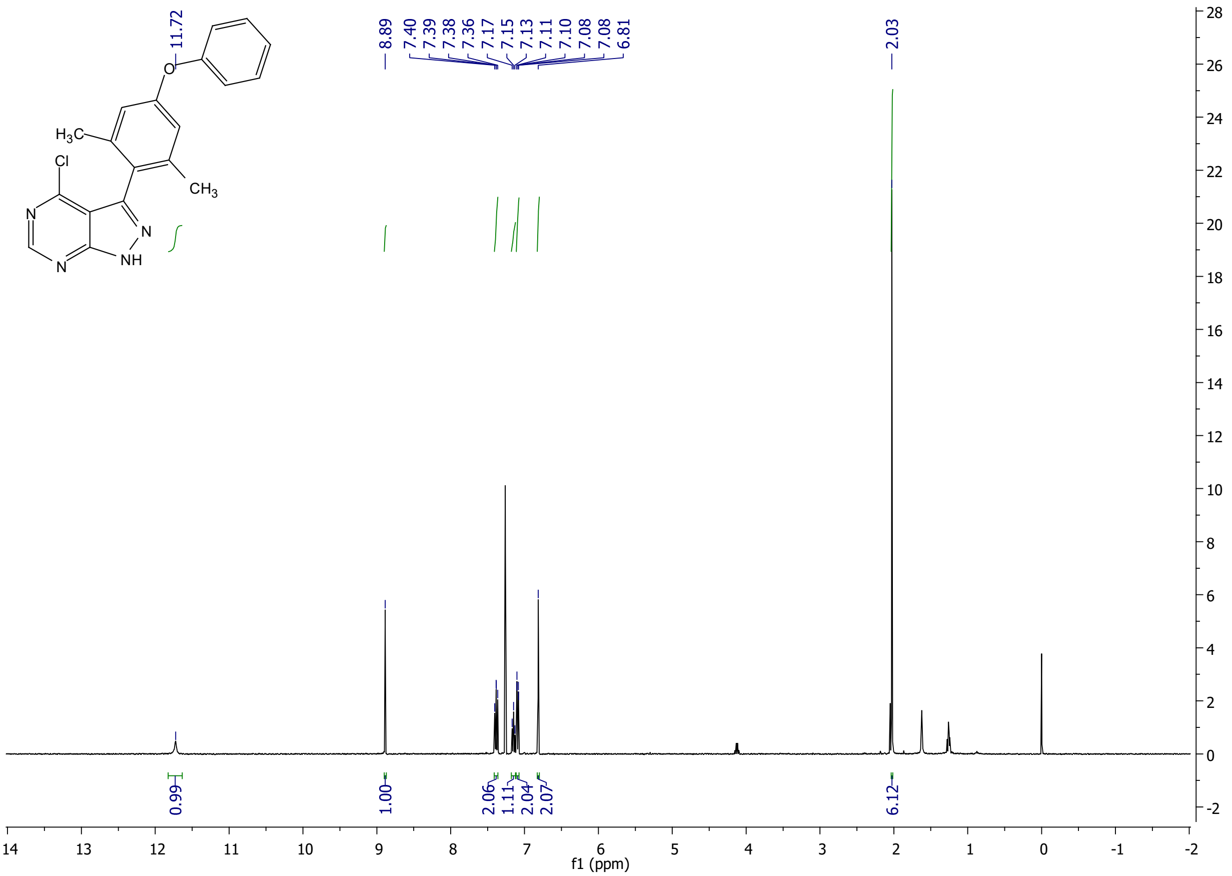

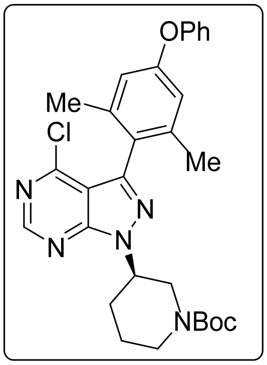

tert-butyl (R)-3-(4-chloro-3-(2,6-dimethyl-4-phenoxyphenyl)-1H-pyrazolo[3,4-d]pyrimidin-1-yl)piperidine-1-carboxylate (3.8a):

4-chloro-3-(2,6-dimethyl-4-phenoxyphenyl)-1H-pyrazolo[3,4-d]pyrimidine (0.178 g, 0.509 mmol, 1 eq.), tert-butyl (S)-3-hydroxypiperidine-1-carboxylate (0.307 g, 1.53 mmol, 3 eq.), and triphenylphosphine (0.267 g, 1.02 mmol, 2 eq.) were added to anhydrous THF (5 ml, 0.1 M) in a dried round bottom flask. After cooling the mixture to 0 °C, DIAD (0.200 ml, 1.02 mmol, 2 eq.) was added and stirred for 10 minutes. The reaction mixture was then warmed to room temperature and stirred overnight. The reaction mixture was partitioned in ethyl acetate and brine. The organic layer was dried over sodium sulfate and concentrated. The crude extract was purified via FCC (96:4 DCM/MeOH) to yield 0.171 g of **3.8a** as a yellow solid (63% yield).

^{1}**H NMR**: (400 MHz, Chloroform-*d*) δ 8.78 (s, 1H), 7.39 – 7.36 (m, 2H), 7.14 (t, *J* = 7.4 Hz, 1H), 7.07 (d, *J* = 7.6 Hz, 2H), 6.80 (s, 2H), 4.96 (s, 1H), 4.35 (s, 1H), 4.12 (s, 1H), 3.41 (s, 1H), 2.85 (t, *J* = 10.9 Hz, 1H), 2.30 (d, *J* = 7.5 Hz, 1H), 2.25 – 2.19 (m, 1H), 2.00 (s, 6H), 1.91 (d, *J* = 16.4 Hz, 1H), 1.77 – 1.70 (m, 1H), 1.47 (s, 9H).

MS (APCI) Calculated: $C_{29}H_{32}ClN_5O_3$ $[M+H]^+$ 533.2 **Found:** 533.2 m/z

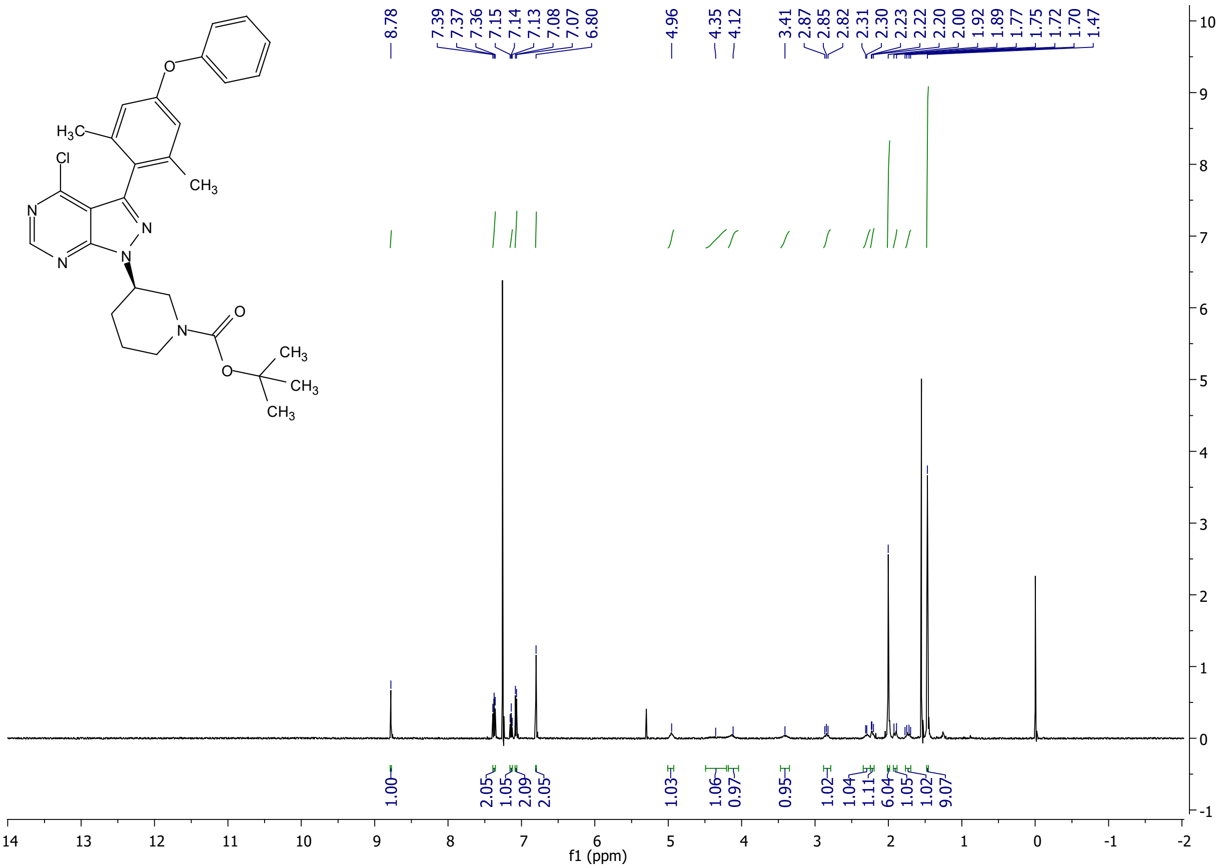
8.78
7.39
7.37
7.36
7.15
7.14
7.13
7.08
7.07
6.80
4.96
4.35
4.12
3.41
2.87
2.85
2.82
2.31
2.30
2.23
2.22
2.20
2.00
1.92
1.89
1.77
1.75
1.72
1.70
1.47
1.00
2.05
1.05
2.09
2.05
1.03
1.06
0.97
0.95
1.02
1.04
1.11
6.04
1.05
1.02
9.07
14
13
12
11
10
9
8
7
6
5
4
3
2
1
0
-1
-2
f1 (ppm)
10
9
8
7
6
5
4
3
2
1
0
-1
H3C
CH3
Cl
N
N
N
N
O
O
O
CH3
CH3
CH3

General procedure for benzylamination of pyrrolopyrimidines and pyrazolopyrimidines (3.1b-3.12b)

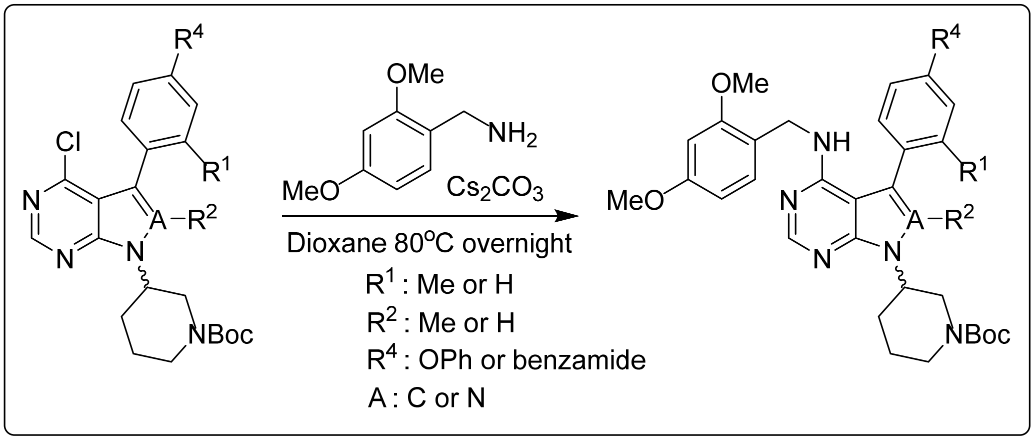
OMe
NH2
MeO
Cs2CO3
Dioxane 80°C overnight
R1 : Me or H
R2 : Me or H
R4 : OPh or benzamide
A : C or N
Cl
N
N
A−R2
NBoc
R4
R1
NH

Crude **3.1a-3.12a** (1.0 eq.) from cross coupling reaction, 2,4-Dimethoxybenzylamine (2.0 eq.) and Cs_2CO_3 (2.3 eq.) were dissolved in dioxane and refluxed at 80°C for 18hr. The crude mixture was partitioned in ethyl acetate and brine. The organic layer was dried over sodium sulfate and concentrated. The crude extract was purified by FCC with a hexanes/ethyl acetate gradient (80:20 to 0:100), to yield **3.1b – 3.12b** in moderate yields. At the time of this writing, characterization for some of the following compounds still need to be completed.

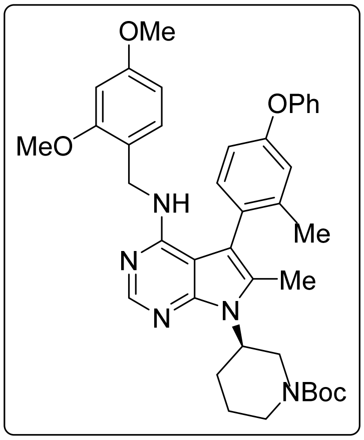
OMe
MeO
OPh
NH
Me
N
Me
N
N
NBoc

***tert*-butyl (*R*)-3-(4-((2,4-dimethoxybenzyl)amino)-6-methyl-5-(2-methyl-4-phenoxyphenyl)-7*H*-pyrrolo[2,3-*d*]pyrimidin-7-yl)piperidine-1-carboxylate (3.1b)**:

Following the general procedure, **3.1a** (crude 837 mg, 1.57 mmol, 1 eq.) was aminated with 2,4-dimethoxybenzylamine (330 ul) using Cs_2CO_3 (1.18 g) in dioxanes (7.85 ml). The workup and purification were followed according to the general procedure to yield 109 mg of **3.1b** as a light brown powder (10%).

^{1}H NMR: (400 MHz, Chloroform-*d*) δ 8.29 (s, 1H), 7.36 (t, *J* = 7.8 Hz, 2H), 7.15 - 7.12 (m, 3H), 7.02 (d, *J* = 8.0 Hz, 2H), 6.91 (s, 1H), 6.86 – 6.80 (m, 1H), 6.38 – 6.34 (m, 2H), 4.91 (s, 1H), 4.57 – 4.46 (m, 2H), 4.21 -4.11 (m, 3H), 3.87 (d, *J* = 7.9 Hz, 1H), 3.75 (s, 3H), 3.65 (s, 3H), 2.95 – 2.86 (m, 2H), 2.16 (s, 3H), 2.00 (s, 3H), 1.87 (d, *J* = 12.6 Hz, 1H), 1.61 (s, 1H), 1.46 (s, 9H), 1.40 (s, 1H).

MS (APCI) Calculated: $C_{39}H_{46}N_5O_5$ $[M+H]^+$ 664.4 **Found:** 664.4 m/z

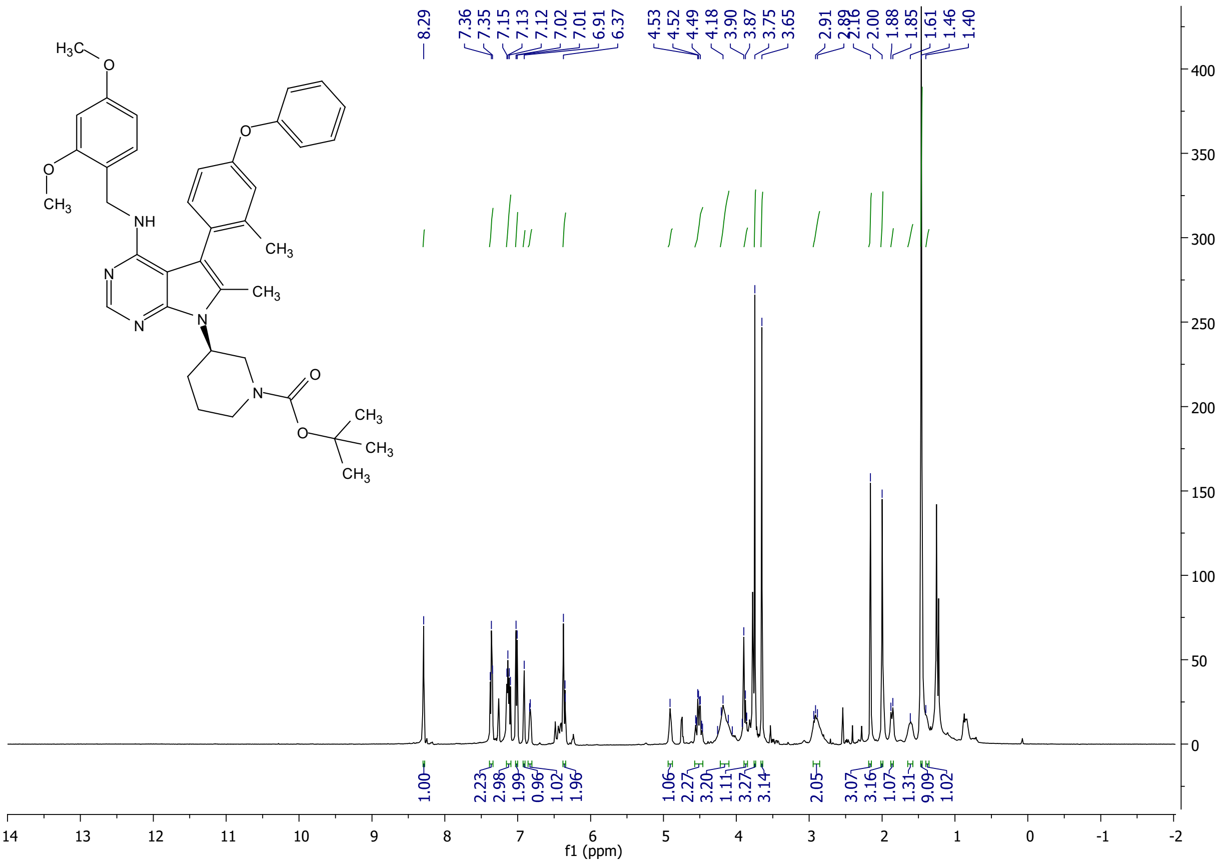

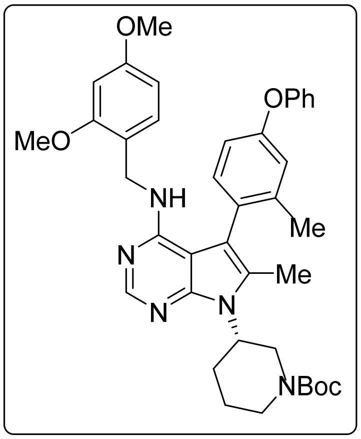

tert-butyl **(S)-3-(4-((2,4-dimethoxybenzyl)amino)-6-methyl-5-(2-methyl-4-phenoxyphenyl)-7H-pyrrolo[2,3-d]pyrimidin-7-yl)piperidine-1-carboxylate (3.2b):**

Following the general procedure, **3.2a** (1 eq.) was aminated with 2,4-dimethoxybenzylamine using Cs_2CO_3 in dioxanes. The workup and purification were followed according to the general procedure to yield **3.2b**.

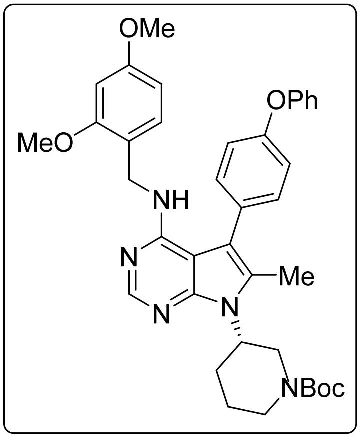

***tert*-butyl (S)-3-(4-((2,4-dimethoxybenzyl)amino)-6-methyl-5-(4-phenoxyphenyl)-7H-pyrrolo[2,3-d]pyrimidin-7-yl)piperidine-1-carboxylate (3.3b):**

Following the general procedure, **3.3a** (1 eq.) was aminated with 2,4-dimethoxybenzylamine using Cs_2CO_3 in dioxanes. The workup and purification were followed according to the general procedure to yield **3.3b**.

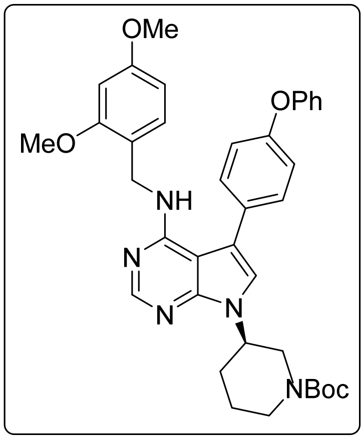

tert-butyl (R)-3-(4-((2,4-dimethoxybenzyl)amino)-5-(4-phenoxyphenyl)-7H-pyrrolo[2,3-d]pyrimidin-7-yl)piperidine-1-carboxylate (3.4b):

Following the general procedure, **3.4a** (1 eq.) was aminated with 2,4-dimethoxybenzylamine using Cs_2CO_3 in dioxanes. The workup and purification were followed according to the general procedure to yield **3.4b**.

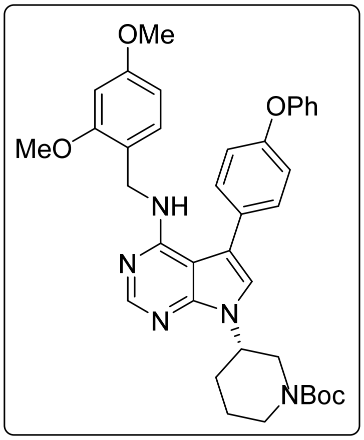

tert-butyl (S)-3-(4-((2,4-dimethoxybenzyl)amino)-5-(4-phenoxyphenyl)-7H-pyrrolo[2,3-d]pyrimidin-7-yl)piperidine-1-carboxylate (3.5b):

Following the general procedure, **3.5a** (1 eq.) was aminated with 2,4-dimethoxybenzylamine using Cs_2CO_3 in dioxanes. The workup and purification were followed according to the general procedure to yield **3.5b**.

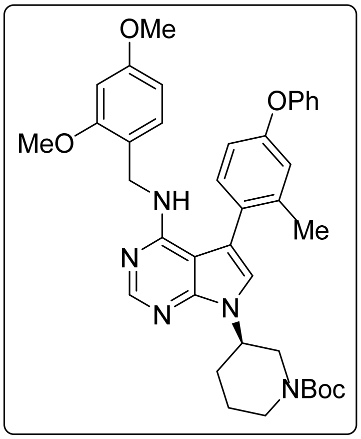

tert-butyl (R)-3-(4-((2,4-dimethoxybenzyl)amino)-5-(2-methyl-4-phenoxyphenyl)-7H-pyrrolo[2,3-d]pyrimidin-7-yl)piperidine-1-carboxylate (3.6b):

Following the general procedure, **3.6a** (1 eq.) was aminated with 2,4-dimethoxybenzylamine using Cs_2CO_3 in dioxanes. The workup and purification were followed according to the general procedure to yield **3.6b**.

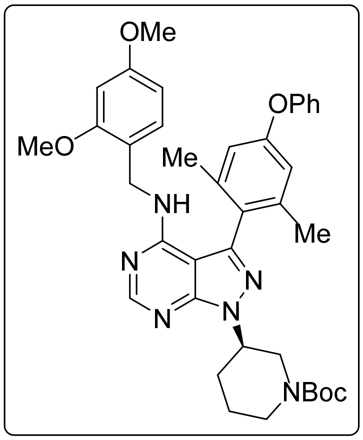

tert-butyl (R)-3-(4-((2,4-dimethoxybenzyl)amino)-3-(2,6-dimethyl-4-phenoxyphenyl)-1H-pyrazolo[3,4-d]pyrimidin-1-yl)piperidine-1-carboxylate (3.8b):

Following the general procedure, **3.8a** (171 mg, 0.32 mmol, 1 eq.) was aminated with 2,4-dimethoxybenzylamine (100 ul) using Cs_2CO_3 (240 mg) in dioxanes (1.6 ml). The workup and purification were followed according to the general procedure to yield 105 mg of **3.8b** as a yellow powder (49%).

^{1}H NMR: (400 MHz, Chloroform-*d*) δ 8.44 (s, 1H), 7.39 – 7.35 (m, 2H), 7.20 (s, 1H), 7.15 (t, J = 7.4 Hz, 1H), 7.01 (d, J = 7.7 Hz, 2H), 6.78 (s, 2H), 6.39 (dq, J = 4.9, 2.4 Hz, 2H), 5.44 (s, 1H), 4.81 (dt, J = 7.8, 6.1 Hz, 1H), 4.61 (s, 2H), 4.37 (s, 1H), 4.20 (s, 1H), 3.77 (s, 3H), 3.65 (s, 3H), 3.35 (s, 1H), 2.77 (t, J = 10.0 Hz, 1H), 2.24 – 2.12 (m, 2H), 1.97 (s, 6H), 1.88 – 1.81 (m, 1H), 1.73 – 1.65 (m, 1H), 1.45 (s, 9H).

MS (APCI) Calculated: $C_{38}H_{45}N_6O_5$ $[M+H]^+$ 665.3 **Found:** 665.4 m/z

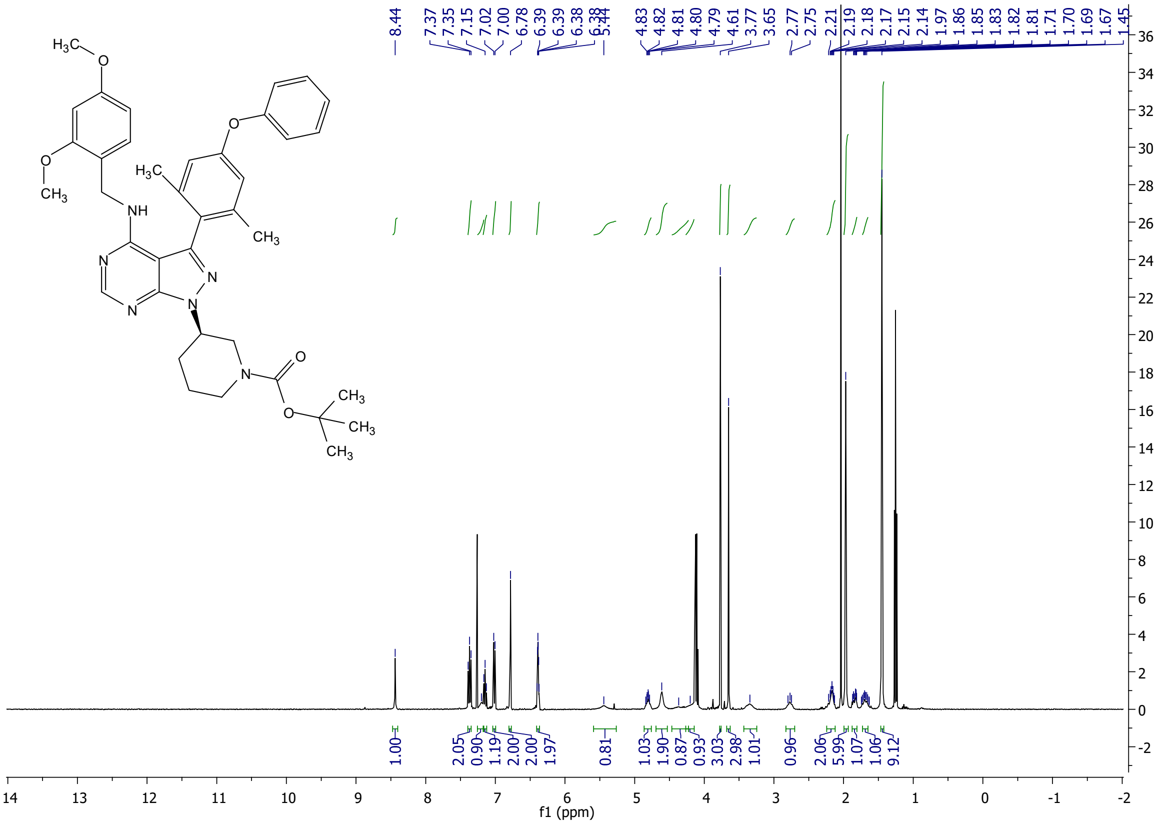

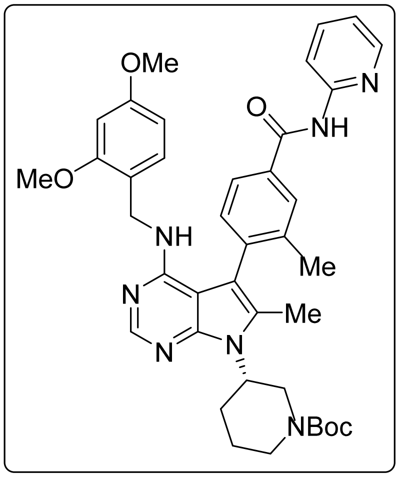

tert-butyl (S)-3-(4-((2,4-dimethoxybenzyl)amino)-6-methyl-5-(2-methyl-4-(pyridin-2-ylcarbamoyl)phenyl)-7H-pyrrolo[2,3-d]pyrimidin-7-yl)piperidine-1-carboxylate (3.10b): Following the general procedure, **3.10a** (1 eq.) was aminated with 2,4-dimethoxybenzylamine using Cs_2CO_3 in dioxanes. The workup and purification were followed according to the general procedure to yield **3.10b**.

General procedure for deprotection and addition of acryloyl chloride of pyrrolopyrimidines (3.1-3.12)

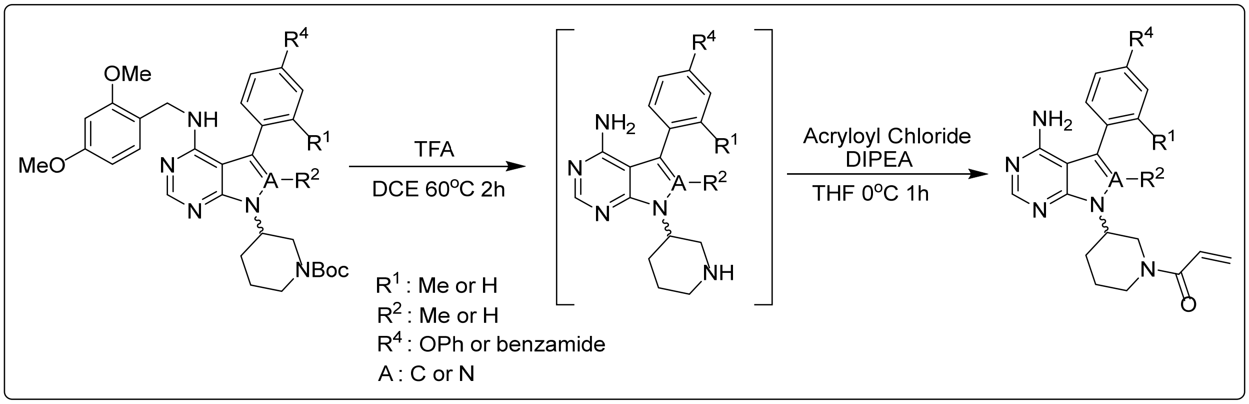

3.1b - 3.6b, 3.8b, 3.9b, 3.7a, 3.11a, 3.12a (1.0 eq.) and TFA (~ 0.15 M) were dissolved in DCE (~0.15 M) and heated at 60°C for 1.5hr. The crude mixture was partitioned in ethyl acetate and sodium bicarbonate. The organic layer was dried over sodium sulfate and concentrated. The crude extract was then dissolved in THF (0.05 M) followed by addition of DIPEA (6 eq.). After the reaction mixture was cooled to 0°C, acryloyl chloride (1.1 eq.) was added dropwise and stirred for 2 hours at 0°C. The crude mixture was partitioned in ethyl acetate and brine. The organic layer was dried over sodium sulfate and concentrated. The crude extract purified by FCC with a hexanes/ethyl acetate gradient (60:40 to 0:100) followed by DCM/MeOH (100:0 to 90:10) gradient, to yield **3.1** – **3.12**. At the time of this writing, characterization for some of the final compounds still need to be completed.

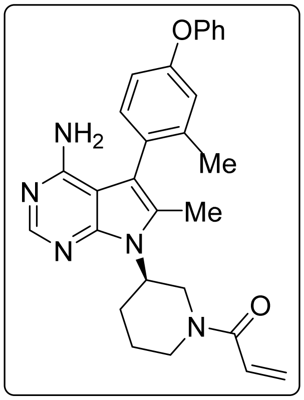

(R)-1-(3-(4-amino-6-methyl-5-(2-methyl-4-phenoxyphenyl)-7H-pyrrolo[2,3-d]pyrimidin-7-yl)piperidin-1-yl)prop-2-en-1-one (3.1):

Following the general procedure, **3.1b** (1 eq.) was deprotected with TFA in DCE. The workup was followed according to the general procedure to yield the deprotected intermediate which carried further without purification and reacted with acryloyl chloride and DIPEA in THF. Workup and purification yielded **3.1**.

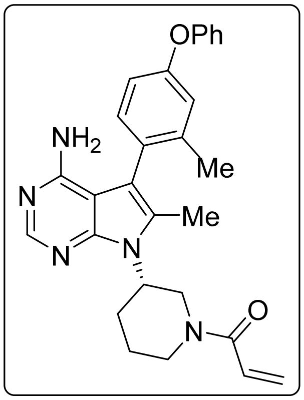

(S)-1-(3-(4-amino-6-methyl-5-(2-methyl-4-phenoxyphenyl)-7H-pyrrolo[2,3-d]pyrimidin-7-yl)piperidin-1-yl)prop-2-en-1-one (3.2):

Following the general procedure, **3.2b** (1 eq.) was deprotected with TFA in DCE. The workup was followed according to the general procedure to yield the deprotected intermediate which carried further without purification and reacted with acryloyl chloride and DIPEA in THF. Workup and purification yielded **3.2**.

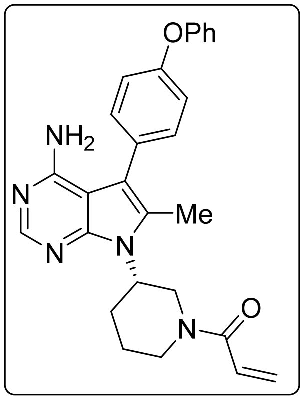

(S)-1-(3-(4-amino-6-methyl-5-(4-phenoxyphenyl)-7H-pyrrolo[2,3-d]pyrimidin-7-yl)piperidin-1-yl)prop-2-en-1-one (3.3):

Following the general procedure, **3.3b** (1 eq.) was deprotected with TFA in DCE. The workup was followed according to the general procedure to yield the deprotected intermediate which carried further without purification and reacted with acryloyl chloride and DIPEA in THF. Workup and purification yielded **3.3**.

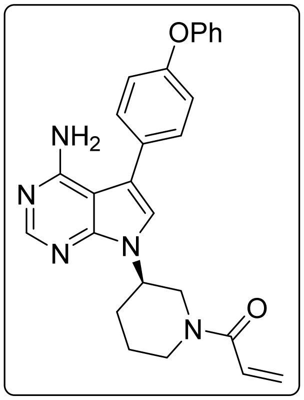

(R)-1-(3-(4-amino-5-(4-phenoxyphenyl)-7H-pyrrolo[2,3-d]pyrimidin-7-yl)piperidin-1-yl)prop-2-en-1-one (3.4):

Following the general procedure, **3.4b** (1 eq.) was deprotected with TFA in DCE. The workup was followed according to the general procedure to yield the deprotected intermediate which carried further without purification and reacted with acryloyl chloride and DIPEA in THF. Workup and purification yielded **3.4**.

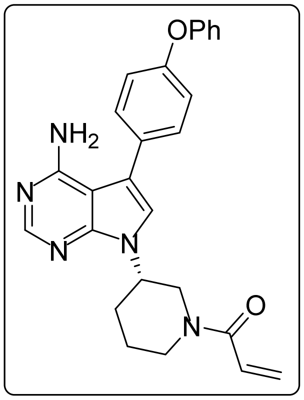

(S)-1-(3-(4-amino-5-(4-phenoxyphenyl)-7H-pyrrolo[2,3-d]pyrimidin-7-yl)piperidin-1-yl)prop-2-en-1-one (3.5):

Following the general procedure, **3.5b** (1 eq.) was deprotected with TFA in DCE. The workup was followed according to the general procedure to yield the deprotected intermediate which carried further without purification and reacted with acryloyl chloride and DIPEA in THF. Workup and purification yielded **3.5**.

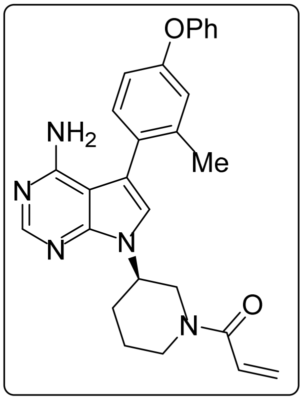

(R)-1-(3-(4-amino-5-(2-methyl-4-phenoxyphenyl)-7H-pyrrolo[2,3-d]pyrimidin-7-yl)piperidin-1-yl)prop-2-en-1-one (3.6):

Following the general procedure, **3.6b** (1 eq.) was deprotected with TFA in DCE. The workup was followed according to the general procedure to yield the deprotected intermediate which carried further without purification and reacted with acryloyl chloride and DIPEA in THF. Workup and purification yielded **3.6**.

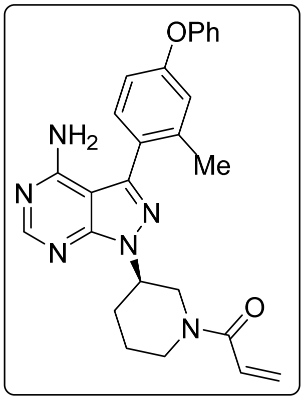

(R)-1-(3-(4-amino-3-(2-methyl-4-phenoxyphenyl)-1H-pyrazolo[3,4-d]pyrimidin-1-yl)piperidin-1-yl)prop-2-en-1-one (3.7):

Following the general procedure, **3.7a** (1 eq.) was deprotected with TFA in DCE. The workup was followed according to the general procedure to yield the deprotected intermediate which carried further without purification and reacted with acryloyl chloride and DIPEA in THF. Workup and purification yielded **3.7**.

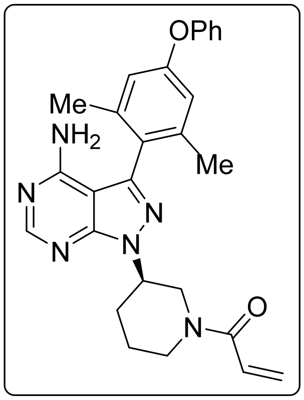

(R)-1-(3-(4-amino-3-(2,6-dimethyl-4-phenoxyphenyl)-1H-pyrazolo[3,4-d]pyrimidin-1-yl)piperidin-1-yl)prop-2-en-1-one (3.8):

Following the general procedure, **3.8b** (105 mg, 0.158 mmol, 1 eq.) was deprotected with TFA (1.1 mL) in DCE (1.1 mL). The workup was followed according to the general procedure to yield the deprotected intermediate (80 mg) which carried further without purification and reacted with acryloyl chloride (19 ul) and DIPEA (200 ul) in THF (2 ml). Workup and purification yielded 32 mg of **3.8** as a white powder (43%).

^{1}H NMR: (400 MHz, Chloroform-*d*) δ 8.32 (s, 1H), 7.40 – 7.35 (m, 2H), 7.15 (t, *J* = 7.4 Hz, 1H), 7.06 (d, *J* = 7.6 Hz, 2H), 6.81 (s, 2H), 6.64 – 6.55 (m, 1H), 6.29 (dd, *J* = 16.8, 1.8 Hz, 1H), 5.69 (dd, *J* = 13.0, 10.8 Hz, 1H), 4.89 (s, 1H), 4.72 (dd, *J* = 84.8, 10.3 Hz, 1H), 4.12 (dd, *J* = 64.1, 13.3 Hz, 1H), 3.73 – 3.30 (m, 1H), 2.99 (dt, *J* = 121.9, 10.8 Hz, 1H), 2.32 – 2.18 (m, 2H), 2.05 (s, 6H), 2.02 – 1.95 (m, 2H), 1.79 – 1.67 (m, 1H).

^{13}C NMR: (101 MHz, Chloroform-*d*) δ 166.12, 163.02, 162.64, 159.27, 155.79, 153.50, 151.13, 146.10, 145.57, 139.75, 139.44, 130.01, 128.99, 127.02, 124.29, 123.00, 119.94, 117.69, 114.24, 98.39, 53.25, 46.14, 45.92, 30.18, 24.95, 20.24, 20.21.

MS (APCI) Calculated: $C_{27}H_{29}N_6O_2$ $[M+H]^+$ 469.2 **Found:** 469.2 m/z

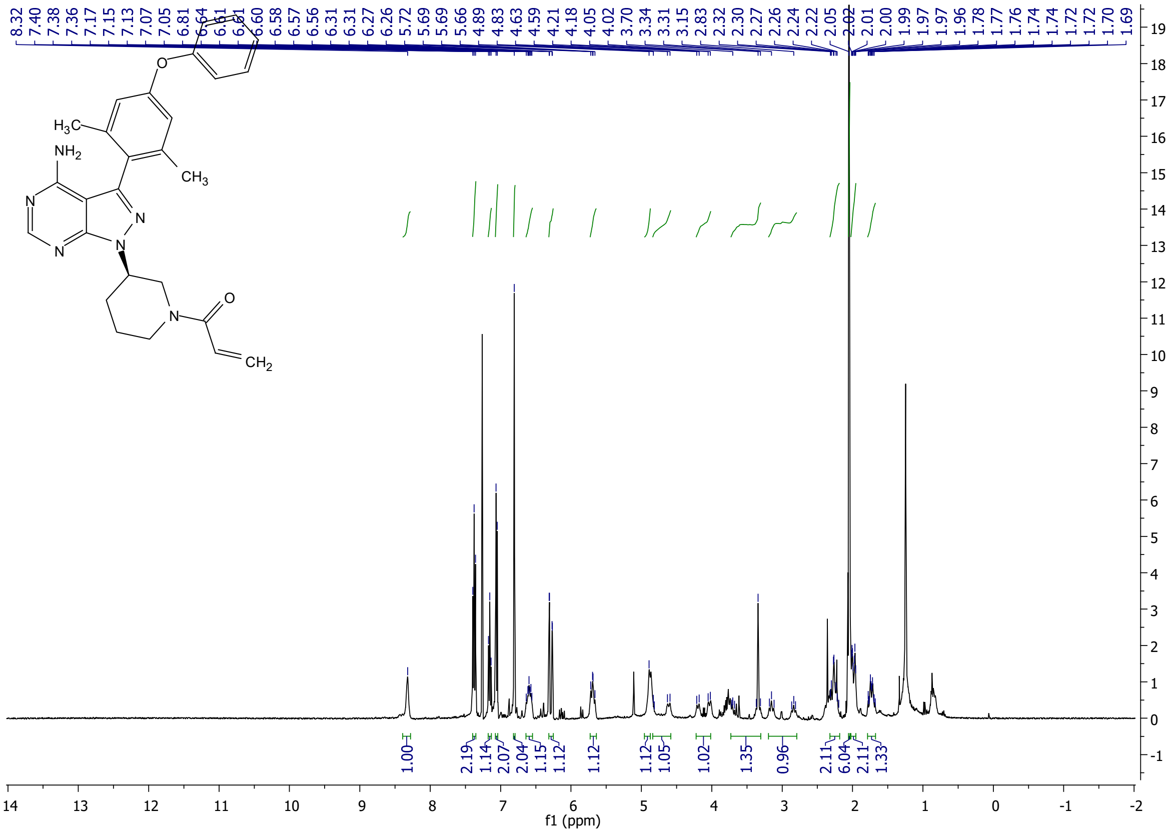

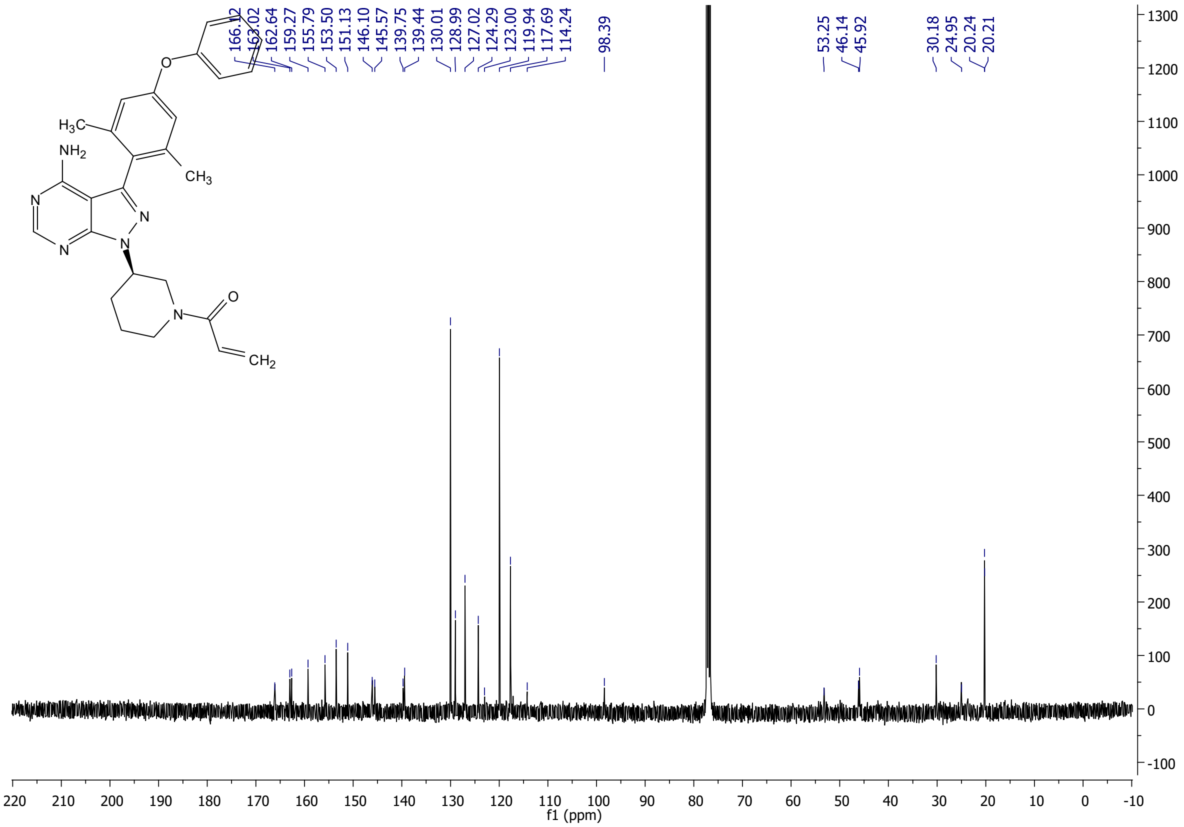

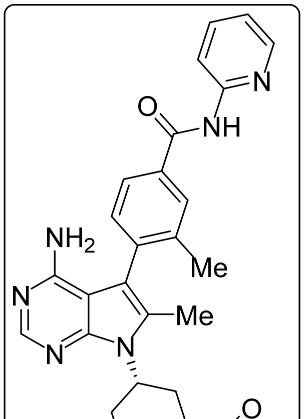

(S)-4-(7-(1-acryloylpiperidin-3-yl)-4-amino-6-methyl-7H-pyrrolo[2,3-d]pyrimidin-5-yl)-3-methyl-N-(pyridin-2-yl)benzamide (3.10):

Following the general procedure, **3.10b** (1 eq.) was deprotected with TFA in DCE. The workup was followed according to the general procedure to yield the deprotected intermediate which carried further without purification and reacted with acryloyl chloride and DIPEA in THF. Workup and purification yielded **3.10**.

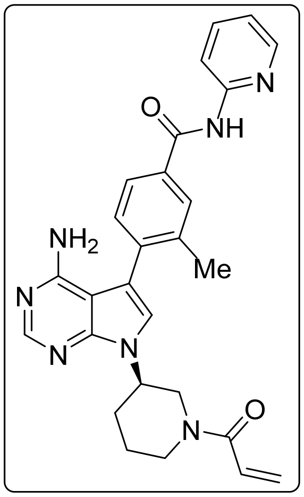

(R)-4-(7-(1-acryloylpiperidin-3-yl)-4-amino-7H-pyrrolo[2,3-d]pyrimidin-5-yl)-3-methyl-N-(pyridin-2-yl)benzamide (3.11):

Following the general procedure, **3.11a** (1 eq.) was deprotected with TFA in DCE. The workup was followed according to the general procedure to yield the deprotected intermediate which carried further without purification and reacted with acryloyl chloride and DIPEA in THF. Workup and purification yielded **3.11**.

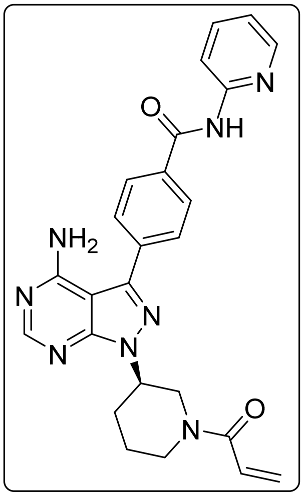

(R)-4-(1-(1-acryloylpiperidin-3-yl)-4-amino-1H-pyrazolo[3,4-d]pyrimidin-3-yl)-N-(pyridin-2-yl)benzamide (3.12):

Following the general procedure, **3.12a** (100 mg, 0.194 mmol, 1 eq.) was deprotected with TFA (0.32 mL, 0.6 M) in DCE (1.2 mL). The workup was followed according to the general procedure to yield the deprotected intermediate (30 mg) which carried further without purification and reacted with acryloyl chloride (7 ul) and DIPEA (75 ul) in THF (720 ul). Workup and purification yielded 8 mg of **3.12** as a white powder (9%).

^{1}H NMR: (400 MHz, Chloroform-*d*) δ 8.81 (s, 1H), 8.41 (d, *J* = 8.4 Hz, 1H), 8.32 (d, *J* = 3.2 Hz, 1H), 8.11 (d, *J* = 8.2 Hz, 2H), 7.85 (d, *J* = 8.1 Hz, 2H), 7.82 – 7.77 (m, 1H), 7.11 (dd, *J* = 7.3, 4.9 Hz, 1H), 6.66 – 6.52 (m, 1H), 6.30 (t, *J* = 16.0 Hz, 1H), 5.69 (dd, *J* = 25.7, 12.0 Hz, 2H), 4.91 (s, 1H), 4.72 (dd, *J* = 102.1, 11.3 Hz, 1H), 4.12 (dd, *J* = 70.1, 12.2 Hz, 1H), 3.59 (dt, *J* = 146.8, 10.7 Hz, 1H), 3.07 (dt, *J* = 119.9, 11.2 Hz, 1H), 2.47 – 2.31 (m, 1H), 2.27 (dd, *J* = 15.6, 4.0 Hz, 1H), 2.05 – 1.97 (m, 1H), 1.84 – 1.70 (m, 2H).

^{13}C NMR: (126 MHz, Chloroform-*d*) δ 165.31, 164.54, 157.28, 155.79, 155.52, 154.11, 150.95, 147.53, 142.64, 138.22, 136.55, 134.32, 128.46, 127.85, 127.76, 127.66, 127.22, 119.82, 113.86, 98.23, 53.27, 49.53, 45.70, 29.68, 24.84.

MS (APCI) Calculated: $C_{25}H_{25}N_8O_2$ $[M+H]^+$ 469.2 **Found:** 469.2 m/z

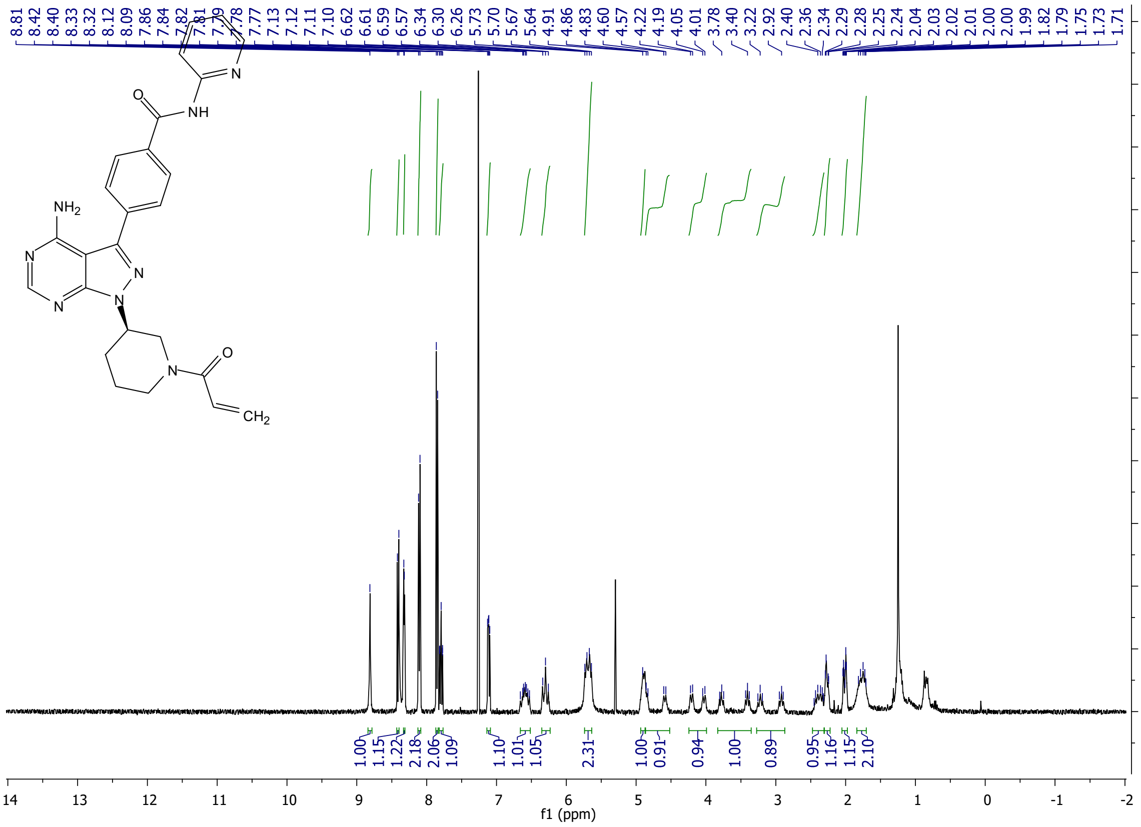
8.81 8.42 8.40 8.33 8.32 8.12 8.09 7.86 7.84 7.82 7.81 7.79 7.78 7.77 7.13 7.12 7.11 7.10 6.62 6.61 6.59 6.57 6.34 6.30 6.26 5.73 5.70 5.67 5.64 4.91 4.86 4.83 4.60 4.57 4.22 4.19 4.05 4.01 3.78 3.40 3.22 2.92 2.40 2.36 2.34 2.29 2.28 2.25 2.24 2.04 2.03 2.02 2.01 2.00 2.00 1.99 1.82 1.79 1.75 1.73 1.71
1.00 1.15 1.22 2.18 2.06 1.09 1.10 1.01 1.05 2.31 1.00 0.91 0.94 1.00 0.89 0.95 1.16 1.15 2.10
NH2
N
N
N
N
O
NH
N
O
N
CH2
5.5
5.0
4.5
4.0
3.5
3.0
2.5
2.0
1.5
1.0
0.5
0.0
14 13 12 11 10 9 8 7 6 5 4 3 2 1 0 -1 -2
f1 (ppm)

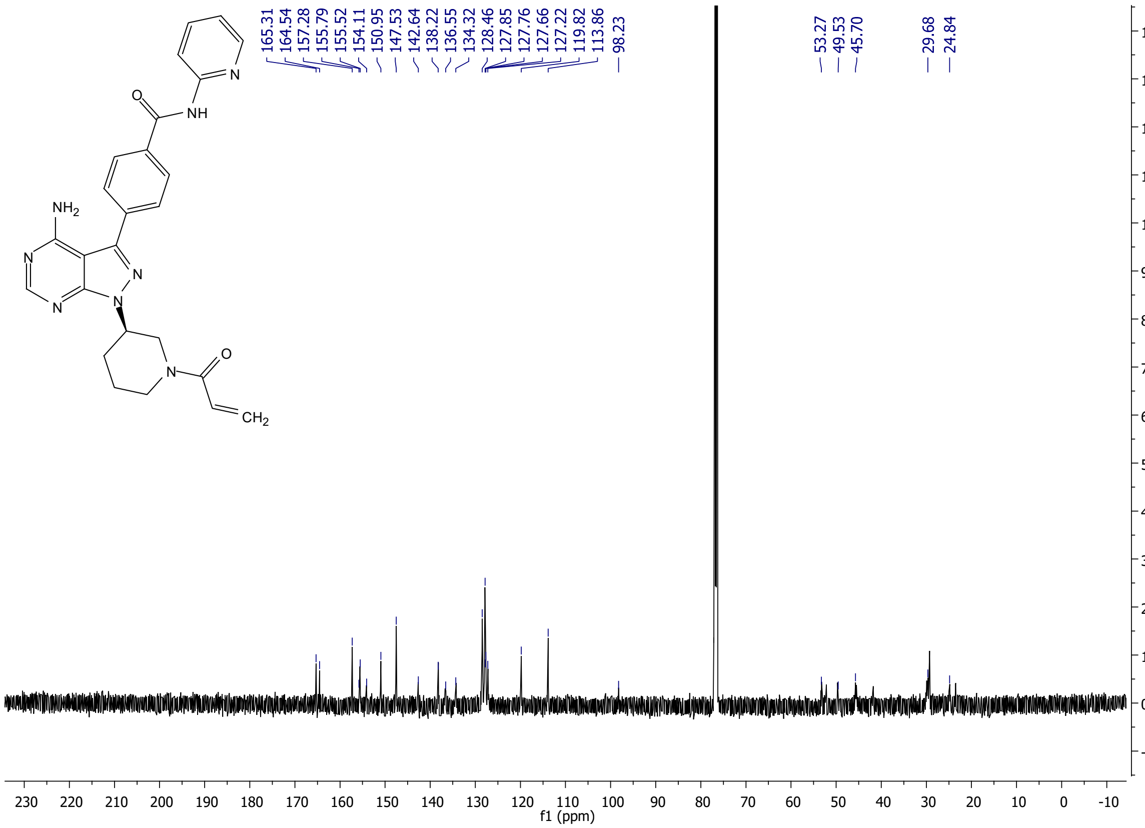
165.31 164.54 157.28 155.79 155.52 154.11 150.95 147.53 142.64 138.22 136.55 134.32 128.46 127.85 127.76 127.66 127.22 119.82 113.86 98.23
53.27 49.53 45.70
29.68 24.84
NH2
N
N
N
N
O
NH
N
O
N
CH2
140
130
120
110
100
90
80
70
60
50
40
30
20
10
0
-10
230 220 210 200 190 180 170 160 150 140 130 120 110 100 90 80 70 60 50 40 30 20 10 0 -10
f1 (ppm)

Racemization Kinetics

Enantiopure atropisomeric analogue of interest (3 mg) was dissolved in 1 mL of toluene. This solution was then heated at a constant temperature for a certain range of time (2.5 hours, measured 6 time points). At each time point, a 100 µL aliquot was isolated and quenched in an HPLC vial with ice cold 50:50 Hexanes:Isopropanol. Each sample was then injected into the chiral HPLC system containing an analytical column at 1ml/min and their ee% were measured.

Each barrier to rotation measurement is determined from an average of two trials.

The ee% vs. time (s) was plotted in order to determine the rate constant k_{obs} (i.e. the slope of the pseudo first-order kinetics) at this constant temperature using the following equation:

$$k_{obs} = \frac{\ln\left(\frac{1}{ee\%}\right)}{t}$$

From this, the racemization rate constant k_{rac} was determined using the following equation:

$$k_{rac} = \frac{k_{obs}}{2}$$

The average k_{rac} was determined by taking the average of the k_{rac} of each trial. From this, substitution into the Eyring equation was performed to determine the barrier to rotation:

$$\Delta G = RT \ln\left(\frac{Tk_b}{k_{rac}h}\right)$$

in which ΔG is the barrier to rotation measurement, R is the gas constant, T is the constant temperature, k_b is the Boltzmann distribution constant, and *h* is Planck's constant.

To determine $t_{1/2}$ at 37 °C (physiological temperatures):

$$t_{1/2} = \frac{\left(\frac{k_b T e^{\frac{-\Delta G}{RT}}}{\ln 2}\right)}{\ln 2}$$

in which $t_{1/2}$ is the half-life to racemization in seconds. This unit can convert into hours, days, or years.

Barrier to Rotation Measurement of **3.1**

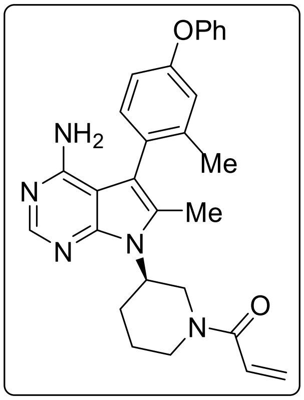

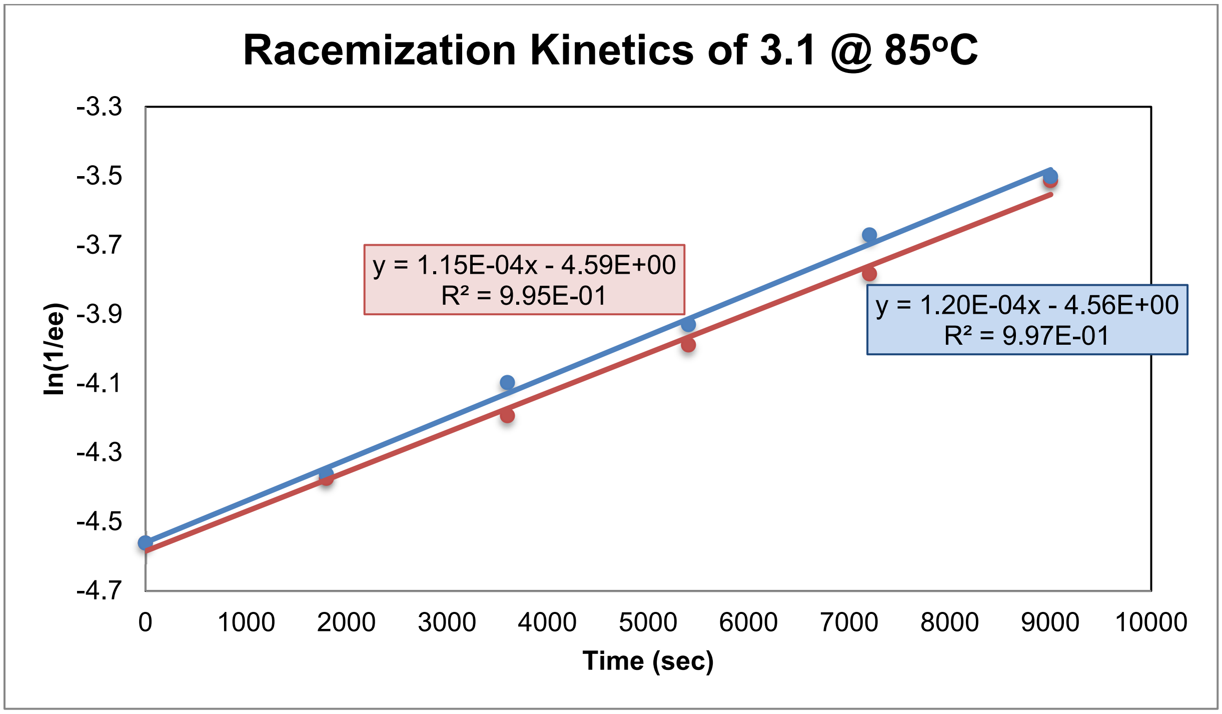

Time (s)	Trial Run 1 (ee%)	Trial 1 [ln(1/ee%)]	Trial Run 2 (ee%)	Trial 2 [ln(1/ee%)]
0	95.75	-4.56174063	95.75	-4.561741
1800	78.54	-4.36360805	79.42	-4.37475
3600	60.2	-4.09767235	66.26	-4.193586
5400	50.92	-3.93025577	54	-3.988984
7200	39.28	-3.67071548	43.95	-3.783053
9000	33.17	-3.50164585	33.56	-3.513335

Average k_{obs} = 1.20E-04, Average k_{rac} = 5.88E-05
Calculated Average ΔG = 28.06 kcal/mol
Calculated $t_{1/2}$ (37 °C) = 0.20 yr (or 73 d)
Calculated t_{95} (37 °C) = 0.01 yr (or 5 d)

References

(1) Law, V.; Knox, C.; Djoumbou, Y.; Jewison, T.; Guo, A. C.; Liu, Y.; Maciejewski, A.; Arndt, D.; Wilson, M.; Neveu, V.; Tang, A.; Gabriel, G.; Ly, C.; Adamjee, S.; Dame, Z. T.; Han, B.; Zhou, Y.; Wishart, D. S. DrugBank 4.0: Shedding New Light on Drug Metabolism. *Nucleic Acids Res.* **2014**, *42*, 1091–1097.

(2) Wu, P.; Nielsen, T. E.; Clausen, M. H. FDA-Approved Small-Molecule Kinase Inhibitors. *Trends Pharmacol. Sci.* **2015**, *36*, 422–439.

(3) Laplante, S. R.; Edwards, P. J.; Fader, L. D.; Jakalian, A.; Hucke, O. Revealing Atropisomer Axial Chirality in Drug Discovery. *ChemMedChem* **2011**, *6*, 505–513.

(4) Clayden, J.; Moran, W. J.; Edwards, P. J.; LaPlante, S. R. The Challenge of Atropisomerism in Drug Discovery. *Angew. Chemie - Int. Ed.* **2009**, *48*, 6398–6401.

(5) Zask, A.; Murphy, J.; Ellestad, G. A. Biological Stereoselectivity of Atropisomeric Natural Products and Drugs. *Chirality* **2013**, *25*, 265–274.

(6) Smith, D. E.; Marquez, I.; Lokensgard, M. E.; Rheingold, A. L.; Hecht, D. A.; Gustafson, J. L. Exploiting Atropisomerism to Increase the Target Selectivity of Kinase Inhibitors. *Angew. Chemie - Int. Ed.* **2015**, *54*, 11754–11759.

(7) LaPlante, S. R.; D. Fader, L.; Fandrick, K. R.; Fandrick, D. R.; Hucke, O.; Kemper, R.; Miller, S. P. F.; Edwards, P. J. Assessing Atropisomer Axial Chirality in Drug Discovery and Development. *J. Med. Chem.* **2011**, *54*, 7005–7022.

(8) Eveleigh, P.; Hulme, E. C.; Schudt, C.; Birdsall, N. J. The Existence of Stable Enantiomers of Telenzepine and Their Stereoselective Interaction with Muscarinic Receptor Subtypes. *Mol. Phamacology* **1989**, *35*, 477–483.

(9) Bringmann, G.; Price Mortimer, A. J.; Keller, P. A.; Gresser, M. J.; Garner, J.; Breuning, M. Atroposelective Synthesis of Axially Chiral Biaryl Compounds. *Angew. Chemie - Int. Ed.* **2005**, *44*, 5384–5427.

(10) Bringmann, G.; Gulder, T.; Gulder, T. A. M.; Breuning, M. Atroposelective Total Synthesis of Axially Chiral Biaryl Natural Products. *Chem. Rev.* **2011**, *111*, 563–639.

(11) Pietra, F. Why Colchicine Does Not Show Mutarotation. With M05-2X Density Functional in the Realm of Tricky Natural Products. *J. Phys. Org. Chem.* **2007**, *20*, 1102–1107.

(12) Berg, U.; Deinum, J.; Lincoln, P.; Kvassman, J. Stereochemistry of Colchicinoids. Enantiomeric Stability and Binding to Tubulin of Desacetamidocolchicine and Desacetamidoisocolchicine. *Bioorg. Chem.* **1991**, *19*, 53–65.

(13) Wang, J.; Zeng, W.; Li, S.; Shen, L.; Gu, Z.; Zhang, Y.; Li, J. Discovery and Assessment of Atropisomers of (±)-Lesinurad. *ACS Med. Chem. Lett.* **2017**, *8*, 299–303.

(14) Dodou, K.; Anderson, R. J.; Lough, W. J.; Small, D. A. P.; Shelley, M. D.; Groundwater, P. W. Synthesis of Gossypol Atropisomers and Derivatives and Evaluation of Their Anti-Proliferative and Anti-Oxidant Activity. *Bioorg. Med. Chem.* **2005**, *13*, 4228–4237.

(15) Kang, M. H.; Reynolds, C. P. Bcl-2 Inhibitors: Targeting Mitochondrial Apoptotic

Pathways in Cancer Therapy. *Clin. Cancer Res.* **2009**, *15*, 1126–1132.

(16) Matlin, S. A.; Zhou, R. (-)-GOSSYPOL: AN ACTIVE MALE ANTIFERTILITY AGENT. *Contraception* **1985**, *31*, 141–149.

(17) Stipanovic, R.; Puckhaber, L.; Liu, J.; Bell, A. Total and Percent Atropisomers of Gossypol and Gossypol-6-Methyl Ether in Seeds from Pima Cottons and Accessions of Gossypium Barbadense L. *J. Agric. Food Chem.* **2009**, *57*, 566–571.

(18) Porter, J.; Payne, A.; Whitcombe, I.; de Candole, B.; Ford, D.; Garlish, R.; Hold, A.; Hutchinson, B.; Trevitt, G.; Turner, J.; Edwards, C.; Watkins, C.; Davis, J.; Stubberfield, C. Atropisomeric Small Molecule Bcl-2 Ligands: Determination of Bioactive Conformation. *Bioorganic Med. Chem. Lett.* **2009**, *19*, 1767–1772.

(19) Porter, J.; Payne, A.; de Candole, B.; Ford, D.; Hutchinson, B.; Trevitt, G.; Turner, J.; Edwards, C.; Watkins, C.; Whitcombe, I.; Davis, J.; Stubberfield, C. Tetrahydroisoquinoline Amide Substituted Phenyl Pyrazoles as Selective Bcl-2 Inhibitors. *Bioorganic Med. Chem. Lett.* **2009**, *19*, 230–233.

(20) Takahashi, H.; Wakamatsu, S.; Tabata, H.; Oshitari, T.; Harada, A.; Inoue, K.; Natsugari, H. Atropisomerism Observed in Indometacin Derivatives. *Org. Lett.* **2011**, *13*, 760–763.

(21) O'Connor, S. P.; Wang, Y.; Simpkins, L. M.; Brigance, R. P.; Meng, W.; Wang, A.; Kirby, M. S.; Weigelt, C. A.; Hamann, L. G. Synthesis, SAR, and Atropisomerism of Imidazolopyrimidine DPP4 Inhibitors. *Bioorganic Med. Chem. Lett.* **2010**, *20*, 6273–6276.

(22) Ichikawa, M.; Yokomizo, A.; Itoh, M.; Haginoya, N.; Sugita, K.; Usui, H.; Terayama, K.; Kanda, A. Discovery of Atrop Fixed Alkoxy-Aminobenzhydrol Derivatives: Novel, Highly Potent and Orally Efficacious Squalene Synthase Inhibitors. *Bioorganic Med. Chem.* **2011**, *19*, 5207–5224.

(23) LaPlante, S. R.; Forgione, P.; Boucher, C.; Coulombe, R.; Gillard, J.; Hucke, O.; Jakalian, A.; Joly, M.-A. A.; Kukolj, G.; Lemke, C.; McCollum, R.; Titolo, S.; Beaulieu, P. L.; Stammers, T. Enantiomeric Atropisomers Inhibit HCV Polymerase and/or HIV Matrix: Characterizing Hindered Bond Rotations and Target Selectivity. *J. Med. Chem.* **2014**, *57*, 1944–1951.

(24) Yoshida, K.; Itoyama, R.; Yamahira, M.; Tanaka, J.; Loaëc, N.; Lozach, O.; Durieu, E.; Fukuda, T.; Ishibashi, F.; Meijer, L.; Iwao, M. Synthesis, Resolution, and Biological Evaluation of Atropisomeric (AR)- and (aS)-16-Methyllamellarins N: Unique Effects of the Axial Chirality on the Selectivity of Protein Kinases Inhibition. *J. Med. Chem.* **2013**, *56*, 7289–7301.

(25) Leivers, A. L.; Tallant, M.; Shotwell, J. B.; Dickerson, S.; Leivers, M. R.; Mcdonald, O. B.; Gobel, J.; Creech, K. L.; Strum, S. L.; Mathis, A.; Rogers, S.; Moore, C. B.; Botyanszki, J. Discovery of Selective Small Molecule Type III Phosphatidylinositol 4 - Kinase Alpha (PI4KIII α) Inhibitors as Anti Hepatitis C (HCV) Agents. *J. Med. Chem.* **2014**, *57*, 2091–2106.

(26) Clapham, K. M.; Rennison, T.; Jones, G.; Craven, F.; Bardos, J.; Golding, B. T.; Griffin, R. J.; Haggerty, K.; Hardcastle, I. R.; Thommes, P.; Ting, A.; Cano, C. Potent Enantioselective Inhibition of DNA-Dependent Protein Kinase (DNA-PK) by Atropisomeric Chromenone Derivatives. *Org. Biomol. Chem.* **2012**, *10*, 6747–6757.

(27) Brown, D. G.; Boström, J. Analysis of Past and Present Synthetic Methodologies on Medicinal Chemistry: Where Have All the New Reactions Gone? *J. Med. Chem.* **2016**, *59*, 4443–4458.

(28) Roughley, S. D.; Jordan, A. M. The Medicinal Chemist's Toolbox: An Analysis of Reactions Used in the Pursuit of Drug Candidates. *J. Med. Chem.* **2011**, *54*, 3451–3479.

(29) Foster, S. A.; Whalen, D. M.; Ozen, A.; Wongchenko, M. J.; Yin, J. P.; Yen, I.; Schaefer, G.; Mayfield, J. D.; Chmielecki, J.; Stephens, P. J.; Albacker, L. A.; Yan, Y.; Song, K.; Hatzivassiliou, G.; Eigenbrot, C.; Yu, C.; Shaw, A. S.; Manning, G.; Skelton, N. J.; Hymowitz, S. G.; Malek, S. Activation Mechanism of Oncogenic Deletion Mutations in BRAF, EGFR, and HER2. *Cancer Cell* **2016**, *29*, 477–493.

(30) Wang, H.; Liu, Y.; Huai, Q.; Cai, J.; Zoraghi, R.; Francis, S. H.; Corbin, J. D.; Robinson, H.; Xin, Z.; Lin, G.; Ke, H. Multiple Conformations of Phosphodiesterase-5: Implications for Enzyme Function and Drug Development. *J. Biol. Chem.* **2006**, *281*, 21469–21479.

(31) Hanson, S. M.; Morlock, E. V; Satyshur, K. A.; Czajkowski, C. Structural Requirements for Eszopiclone and Zolpidem Binding to the GABAA Receptor Are Different. *J. Med. Chem.* **2008**, *51*, 7243–7252.

(32) Bracegirdle, A.; Clayden, J.; Lai, L. W. Asymmetric Synthesis of Biaryl Atropisomers by Dynamic Resolution on Condensation of Biaryl Aldehydes with (-)-Ephedrine or a Proline-Derived Diamine. *Beilstein J. Org. Chem.* **2008**, *4*, 47.

(33) Betson, M. S.; Clayden, J.; Worrall, C. P.; Peace, S. Three Groups Good, Four Groups Bad? Atropisomerism in Ortho-Substituted Diaryl Ethers. *Angew. Chemie - Int. Ed.* **2006**, *45*, 5803–5807.

(34) Clayden, J.; Worrall, C. P.; Moran, W. J.; Helliwell, M. Enantioselective Synthesis of an Atropisomeric Diaryl Ether. *Angew. Chemie - Int. Ed.* **2008**, *47*, 3234–3237.

(35) Fuji, K.; Oka, T.; Kawabata, T.; Kinoshita, T. The First Synthesis of an Optically Active Molecular Bevel Gear with Only Two Cogs on Each Wheel. *Tetrahedron Lett.* **1998**, *39*, 1373–1376.

(36) Stjepanovic, N.; Capdevila, J. Multikinase Inhibitors in the Treatment of Thyroid Cancer: Specific Role of Lenvatinib. *Biologics* **2014**, *8*, 129–139.

(37) Okamoto, K.; Ikemori-Kawada, M.; Jestel, A.; Von Konig, K.; Funahashi, Y.; Matsushima, T.; Tsuruoka, A.; Inoue, A.; Matsui, J. Distinct Binding Mode of Multikinase Inhibitor Lenvatinib Revealed by Biochemical Characterization. *ACS Med. Chem. Lett.* **2015**, *6*, 89–94.

(38) Kawabata, T.; Jiang, C.; Hayashi, K.; Tsubaki, K.; Yoshimura, T.; Majumdar, S.; Sasamori, T.; Tokitoh, N. Axially Chiral Binaphthyl Surrogates with an Inner N-H-N Hydrogen Bond. *J. Am. Chem. Soc.* **2009**, *131*, 54–55.

(39) Hayashi, K.; Matubayasi, N.; Jiang, C.; Yoshimura, T.; Majumdar, S.; Sasamori, T.; Tokitoh, N.; Kawabata, T. Insights into the Origins of Configurational Stability of Axially Chiral Biaryl Amines with an Intramolecular N-H-N Hydrogen Bond. *J. Org. Chem.* **2010**, *75*, 5031–5036.

(40) Vaidya, S. D.; Toenjes, S. T.; Yamamoto, N.; Maddox, S. M.; Gustafson, J. L. Catalytic

Atroposelective Synthesis of N-Aryl Quinoid Compounds. *J. Am. Chem. Soc.* **2020**, *142*, 2198–2203.

(41) Knowles, P. P.; Murray-Rust, J.; Kjaer, S.; Scott, R. P.; Hanrahan, S.; Santoro, M.; Ibanez, C. F.; McDonald, N. Q.; Ibanez, C. F.; McDonald, N. Q. Structure and Chemical Inhibition of the RET Tyrosine Kinase Domain. *J. Biol. Chem.* **2006**, *281*, 33577–33587.

(42) Levinson, N. M.; Boxer, S. G. Structural and Spectroscopic Analysis of the Kinase Inhibitor Bosutinib and an Isomer of Bosutinib Binding to the Abl Tyrosine Kinase Domain. *PLoS One* **2012**, *7*, e29828.

(43) Solca, F.; Dahl, G.; Zoephel, A.; Bader, G.; Sanderson, M.; Klein, C.; Kraemer, O.; Himmelsbach, F.; Haaksma, E.; Adolf, G. R. Target Binding Properties and Cellular Activity of Afatinib (BIBW 2992), an Irreversible ErbB Family Blocker. *J. Pharmacol. Exp. Ther.* **2012**, *343*, 342 LP – 350.

(44) Jacques, V.; Czarnik, A. W.; Judge, T. M.; Van Der Ploeg, L. H.; Dewitt, S. H. Differentiation of Antiinflammatory and Antitumorigenic Properties of Stabilized Enantiomers of Thalidomide Analogs. *Proc. Natl. Acad. Sci.* **2015**, *112*, 1471–1479.

(45) Arrowsmith, C. H.; Audia, J. E.; Austin, C.; Baell, J.; Bennett, J.; Blagg, J.; Bountra, C.; Brennan, P. E.; Brown, P. J.; Bunnage, M. E.; Buser-Doepner, C.; Campbell, R. M.; Carter, A. J.; Cohen, P.; Copeland, R. a; Cravatt, B.; Dahlin, J. L.; Dhanak, D.; Edwards, A. M.; Frye, S. V; Gray, N.; Grimshaw, C. E.; Hepworth, D.; Howe, T.; Huber, K. V. M.; Jin, J.; Knapp, S.; Kotz, J. D.; Kruger, R. G.; Lowe, D.; Mader, M. M.; Marsden, B.; Mueller-Fahrnow, A.; Müller, S.; O'Hagan, R. C.; Overington, J. P.; Owen, D. R.; Rosenberg, S. H.; Roth, B.; Ross, R.; Schapira, M.; Schreiber, S. L.; Shoichet, B.; Sundström, M.; Superti-Furga, G.; Taunton, J.; Toledo-Sherman, L.; Walpole, C.; Walters, M. a; Willson, T. M.; Workman, P.; Young, R. N.; Zuercher, W. J. The Promise and Peril of Chemical Probes. *Nat. Chem. Biol.* **2015**, *11*, 536–541.

(46) Bain, J.; Plater, L.; Elliott, M.; Shpiro, N.; Hastie, C. J.; Mclauchlan, H.; Klevernic, I.; Arthur, J. S. C.; Alessi, D. R.; Cohen, P. The Selectivity of Protein Kinase Inhibitors: A Further Update. *Biochem. J.* **2007**, *408*, 297–315.

(47) Manning, G.; Whyte, D. B.; Martinez, R.; Hunter, T.; Sudarsanam, S. The Protein Kinase Complement of the Human Genome. *Science* **2002**, *298*, 1912–1934.

(48) Cohen, P.; Alessi, D. R. Kinase Drug Discovery - What's Next in the Field? *ACS Chem. Biol.* **2012**, *8*, 96–104.

(49) Cohen, P. Protein Kinases--the Major Drug Targets of the Twenty-First Century? *Nat. Rev. Drug Discov.* **2002**, *1*, 309–315.

(50) Davis, M. I.; Hunt, J. P.; Herrgard, S.; Ciceri, P.; Wodicka, L. M.; Pallares, G.; Hocker, M.; Treiber, D. K.; Zarrinkar, P. P. Comprehensive Analysis of Kinase Inhibitor Selectivity. *Nat Biotech* **2011**, *29*, 1046–1051.

(51) Cornelison, M.; Jabbour, E. J.; Welch, M. A. Managing Side Effects of Tyrosine Kinase Inhibitor Therapy to Optimize Adherence in Patients with Chronic Myeloid Leukemia: The Role of the Midlevel Practitioner. *J. Support. Oncol.* **2012**, *10*, 14–23.

(52) Mellor, H. R.; Bell, A. R.; Valentin, J.-P.; Roberts, R. R. A. Cardiotoxicity Associated with

Targeting Kinase Pathways in Cancer. *Toxicol. Sci.* **2011**, *120*, 14–32.

(53) Laufer, S.; Bajorath, J. New Frontiers in Kinases: Second Generation Inhibitors. *J. Med. Chem.* **2014**, *57*, 2167–2168.

(54) Murray, A. J. Pharmacological PKA Inhibition: All May Not Be What It Seems. *Sci. Signal.* **2008**, *1*, re4.

(55) Barf, T.; Kaptein, A. Irreversible Protein Kinase Inhibitors: Balancing the Benefits and Risks. *J. Med. Chem.* **2012**, *55*, 6243–6262.

(56) Liu, Q.; Sabnis, Y.; Zhao, Z.; Zhang, T.; Buhrlage, S. J.; Jones, L. H.; Gray, N. S. Developing Irreversible Inhibitors of the Protein Kinase Cysteinome. *Cell* **2013**, *20*, 146–159.

(57) Cohen, M. S.; Zhang, C.; Shokat, K. M.; Taunton, J. Structural Bioinformatics-Based Design of Selective, Irreversible Kinase Inhibitors. *Science* **2005**, *308*, 1318–1321.

(58) Liu, Y.; Gray, N. S. Rational Design of Inhibitors That Bind to Inactive Kinase Conformations. *Nat. Chem. Biol.* **2006**, *2*, 358–364.

(59) Knight, Z. A.; Shokat, K. M. Chemical Genetics: Where Genetics and Pharmacology Meet. *Cell* **2007**, *128*, 425–430.

(60) Singh, J.; Petter, R. C.; Kluge, A. F. Targeted Covalent Drugs of the Kinase Family. *Curr. Opin. Chem. Biol.* **2010**, *14*, 475–480.

(61) Liu, Y.; Bishop, A.; Witucki, L.; Kraybill, B.; Shimizu, E.; Tsien, J.; Ubersax, J.; Blethrow, J.; Morgan, D. O.; Shokat, K. M. Structural Basis for Selective Inhibition of Src Family Kinases by PP1. *Chem. Biol.* **1999**, *6*, 671–678.

(62) Schönherr, H.; Cernak, T. Profound Methyl Effects in Drug Discovery and a Call for New C-H Methylation Reactions. *Angew. Chemie - Int. Ed.* **2013**, *52*, 12256–12267.

(63) Leung, C. S.; Leung, S. S. F.; Tirado-Rives, J.; Jorgensen, W. L. Methyl Effects on Protein-Ligand Binding. *J. Med. Chem.* **2012**, *55*, 4489–4500.

(64) Driggers, E. M.; Hale, S. P.; Lee, J.; Terrett, N. K. The Exploration of Macrocycles for Drug Discovery - an Underexploited Structural Class. *Nat. Rev. Drug Discov.* **2008**, *7*, 608–624.

(65) Cisar, J. S.; Ferreras, J. A.; Soni, R. K.; Quadri, L. E. N.; Tan, D. S. Exploiting Ligand Conformation in Selective Inhibition of Non-Ribosomal Peptide Synthetase Amino Acid Adenylation with Designed Macrocyclic Small Molecules. *J. Am. Chem. Soc.* **2007**, *129*, 7752–7753.

(66) Dinsmore, C. J.; Bogusky, M. J.; Culberson, J. C.; Bergman, J. M.; Homnick, C. F.; Zartman, C. B.; Mosser, S. D.; Schaber, M. D.; Robinson, R. G.; Koblan, K. S.; Huber, H. E.; Graham, S. L.; Hartman, G. D.; Huff, J. R.; Williams, T. M. Conformational Restriction of Flexible Ligands Guided by the Transferred NOE Experiment: Potent Macrocyclic Inhibitors of Farnesyltransferase. *J. Am. Chem. Soc.* **2001**, *123*, 2107–2108.

(67) Bott, G.; Field, L. D.; Sternhell, S. Steric Effects. A Study of a Rationally Designed System. *J. Am. Chem. Soc.* **1980**, *102*, 5618–5626.

(68) Watterson, S. H.; De Lucca, G. V.; Shi, Q.; Langevine, C. M.; Liu, Q.; Batt, D. G.; Beaudoin Bertrand, M.; Gong, H.; Dai, J.; Yip, S.; Li, P.; Sun, D.; Wu, D. R.; Wang, C.; Zhang, Y.;

Traeger, S. C.; Pattoli, M. A.; Skala, S.; Cheng, L.; Obermeier, M. T.; Vickery, R.; Discenza, L. N.; D'Arienzo, C. J.; Zhang, Y.; Heimrich, E.; Gillooly, K. M.; Taylor, T. L.; Pulicicchio, C.; McIntyre, K. W.; Galella, M. A.; Tebben, A. J.; Muckelbauer, J. K.; Chang, C.; Rampulla, R.; Mathur, A.; Salter-Cid, L.; Barrish, J. C.; Carter, P. H.; Fura, A.; Burke, J. R.; Tino, J. A. Discovery of 6-Fluoro-5-(R)-(3-(S)-(8-Fluoro-1-Methyl-2,4-Dioxo-1,2-Dihydroquinazolin-3(4H)-Yl)-2-Methylphenyl)-2-(S)-(2-Hydroxypropan-2-Yl)-2,3,4,9-Tetrahydro-1H-Carbazole-8-Carboxamide (BMS-986142): A Reversible Inhibitor of Bruton's Tyrosine Kinase. *J. Med. Chem.* **2016**, *59*, 9173–9200.

(69) Bhat, V.; Wang, S.; Stoltz, B. M.; Virgil, S. C. Asymmetric Synthesis of QUINAP via Dynamic Kinetic Resolution. *J. Am. Chem. Soc.* **2013**, *135*, 16829–16832.

(70) Gustafson, J. L.; Lim, D.; Miller, S. J. Dynamic Kinetic Resolution of Biaryl Atropisomers via Peptide-Catalyzed Asymmetric Bromination. *Science (80-.).* **2010**, *328*, 1251–1255.

(71) Tanaka, K.; Takeishi, K.; Noguchi, K. Enantioselective Synthesis of Axially Chiral Anilides through Rhodium-Catalyzed [2+2+2] Cycloaddition of 1,6-Diynes with Trimethylsilylynamides. *J. Am. Chem. Soc.* **2006**, *128*, 4586–4587.

(72) Chen, Y.-H.; Cheng, D.-J.; Zhang, J.; Wang, Y.; Liu, X.-Y.; Tan, B. Atroposelective Synthesis of Axially Chiral Biaryldiols via Organocatalytic Arylation of 2-Naphthols. *J. Am. Chem. Soc.* **2015**, *137*, 15062–15065.

(73) Fandrick, K. R.; Li, W.; Zhang, Y.; Tang, W.; Gao, J.; Rodriguez, S.; Patel, N. D.; Reeves, D. C.; Wu, J.-P.; Sanyal, S.; Gonnella, N.; Qu, B.; Haddad, N.; Lorenz, J. C.; Sidhu, K.; Wang, J.; Ma, S.; Grinberg, N.; Lee, H.; Tsantrizos, Y.; Poupart, M.-A.; Busacca, C. A.; Yee, N. K.; Lu, B. Z.; Senanayake, C. H. Concise and Practical Asymmetric Synthesis of a Challenging Atropisomeric HIV Integrase Inhibitor. *Angew. Chemie - Int. Ed.* **2015**, *54*, 7144–7148.

(74) Diener, M. E.; Metrano, A. J.; Kusano, S.; Miller, S. J. Enantioselective Synthesis of 3-Arylquinazolin-4(3H)-Ones via Peptide-Catalyzed Atroposelective Bromination. *J. Am. Chem. Soc.* **2015**, *137*, 12369–12377.

(75) Barrett, K. T.; Miller, S. J. Enantioselective Synthesis of Atropisomeric Benzamides Through. *J. Am. Chem. Soc.* **2013**, *135*, 2963–2966.

(76) Yuan, B.; Page, A.; Worrall, C. P.; Escalettes, F.; Willies, S. C.; McDouall, J. J. W.; Turner, N. J.; Clayden, J. Biocatalytic Desymmetrization of an Atropisomer with Both an Enantioselective Oxidase and Ketoreductases. *Angew. Chemie - Int. Ed.* **2010**, *49*, 7010–7013.

(77) Armstrong, R. J.; Smith, M. D. Catalytic Enantioselective Synthesis of Atropisomeric Biaryls: A Cation-Directed Nucleophilic Aromatic Substitution Reaction. *Angew. Chemie - Int. Ed.* **2014**, *53*, 12822–12826.

(78) Kumarasamy, E.; Raghunathan, R.; Sibi, M. P.; Sivaguru, J. Nonbiaryl and Heterobiaryl Atropisomers: Molecular Templates with Promise for Atropselective Chemical Transformations. *Chem. Rev.* **2015**, *115*, 11239–11300.

(79) Fleuren, E. D. G.; Zhang, L.; Wu, J.; Daly, R. J. The Kinome "at Large" in Cancer. *Nat. Rev. Cancer* **2016**, *16*, 83–98.

(80) Zhang, J.; Yang, P. L.; Gray, N. S. Targeting Cancer with Small Molecule Kinase Inhibitors. *Nat. Rev. Cancer* **2009**, *9*, 28–39.

(81) Ferguson, F. M.; Gray, N. S. Kinase Inhibitors: The Road Ahead. *Nat. Rev. Drug Discov.* **2018**, *17*, 353–376.

(82) Karaman, M. W.; Herrgard, S.; Treiber, D. K.; Gallant, P.; Atteridge, C. E.; Campbell, B. T.; Chan, K. W.; Ciceri, P.; Davis, M. I.; Edeen, P. T.; Faraoni, R.; Floyd, M.; Hunt, J. P.; Lockhart, D. J.; Milanov, Z. V; Morrison, M. J.; Pallares, G.; Patel, H. K.; Pritchard, S.; Wodicka, L. M.; Zarrinkar, P. P. A Quantitative Analysis of Kinase Inhibitor Selectivity. *Nat. Biotechnol.* **2008**, *26*, 127–132.

(83) Barouch-Bentov, R.; Sauer, K. Mechanisms of Drug Resistance in Kinases. *Expert Opin. Investig. Drugs* **2011**, *20*, 153–208.

(84) Thress, K. S.; Paweletz, C. P.; Felip, E.; Cho, B. C.; Stetson, D.; Dougherty, B.; Lai, Z.; Markovets, A.; Vivancos, A.; Kuang, Y.; Ercan, D.; Matthews, S. E.; Cantarini, M.; Barrett, J. C.; Jänne, P. A.; Oxnard, G. R. Acquired EGFR C797S Mutation Mediates Resistance to AZD9291 in Non-Small Cell Lung Cancer Harboring EGFR T790M. *Nat. Med.* **2015**, *21*, 560–562.

(85) Mulligan, L. M. RET Revisited: Expanding the Oncogenic Portfolio. *Nat. Rev. Cancer* **2014**, *14*, 173–186.

(86) Eng, C.; Clayton, D.; Schuffenecker, I.; Lenoir, G.; Cote, G.; Gagel, R. F.; Ploos Van Amstel, H. K.; Lips, C. J. M.; Nishisho, I.; Takai, S. I.; Marsh, D. J.; Robinson, B. G.; Frank-Raue, K.; Raue, F.; Xue, F.; Noll, W. W.; Romei, C.; Pacini, F.; Fink, M.; Niederle, B.; Zedenius, J.; Nordenskjöld, M.; Komminoth, P.; Hendy, G. N.; Gharib, H.; Thibodeau, S. N.; Lacroix, A.; Frilling, A.; Ponder, B. A. J.; Mulligan, L. M. The Relationship between Specific Ret Proto-Oncogene Mutations and Disease Phenotype in Multiple Endocrine Neoplasia Type 2: International RET Mutation Consortium Analysis. *J. Am. Med. Assoc.* **1996**, *276*, 1575–1579.

(87) Mulligan, L. M.; Eng, C.; Healey, C. S.; Clayton, D.; Kwok, J. B. J.; Gardner, E.; Ponder, M. A.; Frilling, A.; Hendrik, C. E. J.; Neumann, H. P. H.; Thibodeau, S. N.; Ponder, B. A. J. Specific Mutations of the RET Proto-Oncogene Are Related to Disease Phenotype in MEN 2A and FMTC. *Nat. Genet.* **1994**, *6*, 70–74.

(88) Grieco, M.; Santoro, M.; Berlingieri, M. T.; Melillo, R. M.; Donghi, R.; Bongarzone, I.; Pierotti, M. A.; Della Ports, G.; Fusco, A.; Vecchiot, G. PTC Is a Novel Rearranged Form of the Ret Proto-Oncogene and Is Frequently Detected in Vivo in Human Thyroid Papillary Carcinomas. *Cell* **1990**, *60*, 557–563.

(89) Li, F.; Feng, Y.; Fang, R.; Fang, Z.; Xia, J.; Han, X.; Liu, X. Y.; Chen, H.; Liu, H.; Ji, H. Identification of RET Gene Fusion by Exon Array Analyses in "Pan-Negative" Lung Cancer from Never Smokers. *Cell Res.* **2012**, *22*, 928–931.

(90) Piotrowska, Z.; Isozaki, H.; Lennerz, J. K.; Gainor, J. F.; Lennes, I. T.; Zhu, V. W.; Marcoux, N.; Banwait, M. K.; Digumarthy, S. R.; Su, W.; Yoda, S.; Riley, A. K.; Nangia, V.; Lin, J. J.; Nagy, R. J.; Lanman, R. B.; Dias-Santagata, D.; Mino-Kenudson, M.; Iafrate, A. J.; Heist, R. S.; Shaw, A. T.; Evans, E. K.; Clifford, C.; Ou, S.-H. I.; Wolf, B.; Hata, A. N.; Sequist, L. V. Landscape of Acquired Resistance to Osimertinib in EGFR-Mutant

NSCLC and Clinical Validation of Combined EGFR and RET Inhibition with Osimertinib and BLU-667 for Acquired RET Fusion. *Cancer Discov.* **2018**, *8*, 1529–1539.

(91) Lipson, D.; Capelletti, M.; Yelensky, R.; Otto, G.; Parker, A.; Jarosz, M.; Curran, J. A.; Balasubramanian, S.; Bloom, T.; Brennan, K. W.; Donahue, A.; Downing, S. R.; Frampton, G. M.; Garcia, L.; Juhn, F.; Mitchell, K. C.; White, E.; White, J.; Zwirko, Z.; Peretz, T.; Nechushtan, H.; Soussan-Gutman, L.; Kim, J.; Sasaki, H.; Kim, H. R.; Park, S. Il; Ercan, D.; Sheehan, C. E.; Ross, J. S.; Cronin, M. T.; Jänne, P. A.; Stephens, P. J. Identification of New ALK and RET Gene Fusions from Colorectal and Lung Cancer Biopsies. *Nat. Med.* **2012**, *18*, 382–384.

(92) Boulay, A.; Breuleux, M.; Stephan, C.; Fux, C.; Brisken, C.; Fiche, M.; Wartmann, M.; Stumm, M.; Lane, H. a.; Hynes, N. E. The Ret Receptor Tyrosine Kinase Pathway Functionally Interacts with the ERa Pathway in Breast Cancer. *Cancer Res.* **2008**, *68*, 3743–3751.

(93) Maxwell, J. E.; Sherman, S. K.; O'Dorisio, T. M.; Howe, J. R. Medical Management of Metastatic Medullary Thyroid Cancer. *Cancer* **2014**, *120*, 3287–3301.

(94) US Department of Health and Human Services, National Institutes of Health, N. C. I. Common Terminology Criteria for Adverse Events (CTCAE) Version 5.0. **2017**.

(95) Fallahi, P.; Ferrari, S. M.; Vita, R.; Domenicantonio, A. Di; Corrado, A.; Benvenga, S.; Antonelli, A. Thyroid Dysfunctions Induced by Tyrosine Kinase Inhibitors. *Expert Opin. Drug Saf.* **2014**, *13*, 723–733.

(96) Kiura, K.; Nakagawa, K.; Shinkai, T.; Eguchi, K.; Ohe, Y.; Yamamoto, N.; Tsuboi, M.; Yokota, S.; Seto, T.; Jiang, H.; Nishio, K.; Saijo, N.; Fukuoka, M. A Randomized, Double-Blind, Phase IIa Dose-Finding Study of Vandetanib (ZD6474) in Japanese Patients with Non-Small Cell Lung Cancer. *J. Thorac. Oncol.* **2008**, *3*, 386–393.

(97) Morabito, A.; Piccirillo, M. C.; Falasconi, F.; De Feo, G.; Del Giudice, A.; Bryce, J.; Di Maio, M.; De Maio, E.; Normanno, N.; Perrone, F. Vandetanib (ZD6474), a Dual Inhibitor of Vascular Endothelial Growth Factor Receptor (VEGFR) and Epidermal Growth Factor Receptor (EGFR) Tyrosine Kinases: Current Status and Future Directions. *Oncologist* **2009**, *14*, 378–390.

(98) Mendoza, L. Clinical Development of RET Inhibitors in RET-Rearranged Non-Small Cell Lung Cancer: Update. *Oncol. Rev.* **2018**, *12*, 69–73.

(99) Kamba, T.; McDonald, D. M. Mechanisms of Adverse Effects of Anti-VEGF Therapy for Cancer. *Br. J. Cancer* **2007**, *96*, 1788–1795.

(100) Lacouture, M. E. Mechanisms of Cutaneous Toxicities to EGFR Inhibitors. *Nat. Rev. Cancer* **2006**, *6*, 803–812.

(101) Subbiah, V.; Gainor, J. F.; Rahal, R.; Brubaker, J. D.; Kim, J. L.; Maynard, M.; Hu, W.; Cao, Q.; Sheets, M. P.; Wilson, D.; Wilson, K. J.; Dipietro, L.; Fleming, P.; Palmer, M.; Hu, M. I.; Wirth, L.; Brose, M. S.; Ou, S. H. I.; Taylor, M.; Garralda, E.; Miller, S.; Wolf, B.; Lengauer, C.; Guzi, T.; Evans, E. K. Precision Targeted Therapy with BLU-667 for RET-Driven Cancers. *Cancer Discov.* **2018**, *8*, 836–849.

(102) Zhou, W.; Ercan, D.; Chen, L.; Yun, C. H.; Li, D.; Capelletti, M.; Cortot, A. B.; Chirieac,

L.; Iacob, R. E.; Padera, R.; Engen, J. R.; Wong, K. K.; Eck, M. J.; Gray, N. S.; Jänne, P. A. Novel Mutant-Selective EGFR Kinase Inhibitors against EGFR T790M. *Nature* **2009**, *462*, 1070–1074.

(103) Cross, D. A. E.; Ashton, S. E.; Ghiorghiu, S.; Eberlein, C.; Nebhan, C. A.; Spitzler, P. J.; Orme, J. P.; Finlay, M. R. V.; Ward, R. A.; Mellor, M. J.; Hughes, G.; Rahi, A.; Jacobs, V. N.; Brewer, M. R.; Ichihara, E.; Sun, J.; Jin, H.; Ballard, P.; Al-Kadhimi, K.; Rowlinson, R.; Klinowska, T.; Richmond, G. H. P.; Cantarini, M.; Kim, D. W.; Ranson, M. R.; Pao, W. AZD9291, an Irreversible EGFR TKI, Overcomes T790M-Mediated Resistance to EGFR Inhibitors in Lung Cancer. *Cancer Discov.* **2014**, *4*, 1046–1061.

(104) Sequist, L. V.; Soria, J.-C.; Gadgeel, S. M.; Wakelee, H. A.; Camidge, D. R.; Varga, A.; Solomon, B. J.; Papadimitrakopoulou, V.; Jaw-Tsai, S. S.; Caunt, L.; Kaur, P.; Rolfe, L.; Allen, A. R.; Goldman, J. W. First-in-Human Evaluation of CO-1686, an Irreversible, Highly Selective Tyrosine Kinase Inhibitor of Mutations of EGFR (Activating and T790M). *J. Clin. Oncol.* **2014**, *32*, 8010–8010.

(105) Chen, L.; Fu, W.; Zheng, L.; Liu, Z.; Liang, G. Recent Progress of Small-Molecule Epidermal Growth Factor Receptor (EGFR) Inhibitors against C797S Resistance in Non-Small- Cell Lung Cancer Miniperspective. *J. Med. Chem.* **2017**, *61*, 4290–4300.

(106) Grabe, T.; Lategahn, J.; Rauh, D. C797S Resistance: The Undruggable EGFR Mutation in Non-Small Cell Lung Cancer? *ACS Med. Chem. Lett.* **2018**, *9*, 779–782.

(107) Jia, Y.; Yun, C. H.; Park, E.; Ercan, D.; Manuia, M.; Juarez, J.; Xu, C.; Rhee, K.; Chen, T.; Zhang, H.; Palakurthi, S.; Jang, J.; Lelais, G.; DiDonato, M.; Bursulaya, B.; Michellys, P. Y.; Epple, R.; Marsilje, T. H.; McNeill, M.; Lu, W.; Harris, J.; Bender, S.; Wong, K. K.; Jänne, P. A.; Eck, M. J. Overcoming EGFR(T790M) and EGFR(C797S) Resistance with Mutant-Selective Allosteric Inhibitors. *Nature* **2016**, *534*, 129–132.

(108) To, C.; Jang, J.; Chen, T.; Park, E.; Mushajiang, M.; Clercq, D. J. H. De; Xu, M.; Wang, S.; Cameron, M. D.; Heppner, D. E.; Shin, B. H.; Gero, T. W.; Yang, A.; Dahlberg, S. E.; Wong, K.; Eck, M. J.; Gray, N. S.; Jänne, P. A. Single and Dual Targeting of Mutant EGFR with an Allosteric Inhibitor. *Cancer Discov.* **2019**, *9*, 927–943.

(109) Zhu, S.-J.; Zhao, P.; Yang, J.-W.; Ma, R.; Yan, X.-E.; Yang, S.-Y.; Yang, J.-W.; Yun, C.-H. Structural Insights into Drug Development Strategy Targeting EGFR T790M/C797S. *Oncotarget* **2018**, *9*, 13652–13665.

(110) Gu, M.; Lategahn, J.; Juchum, M.; Do, E.; Keul, M.; Engel, J.; Tumbrink, H. L.; Rauh, D.; Laufer, S. Trisubstituted Pyridinylimidazoles as Potent Inhibitors of the Clinically Resistant L858R/T790M/C797S EGFR Mutant: Targeting of Both Hydrophobic Regions and the Phosphate Binding Site. *J. Med. Chem.* **2017**, *60*, 4636–4656.

(111) Lu, X.; Zhang, T.; Zhu, S. J.; Xun, Q.; Tong, L.; Hu, X.; Li, Y.; Chan, S.; Su, Y.; Sun, Y.; Chen, Y.; Ding, J.; Yun, C. H.; Xie, H.; Ding, K. Discovery of JND3229 as a New EGFRC797S Mutant Inhibitor with in Vivo Monodrug Efficacy. *ACS Med. Chem. Lett.* **2018**, *9*, 1123–1127.

(112) Park, H.; Jung, H. Y.; Mah, S.; Hong, S. Discovery of EGF Receptor Inhibitors That Are Selective for the D746-750/T790M/C797S Mutant through Structure-Based de Novo Design. *Angew. Chemie - Int. Ed.* **2017**, *56*, 7634–7638.

(113) Engel, J.; Becker, C.; Lategahn, J.; Keul, M.; Ketzer, J.; Mühlenberg, T.; Kollipara, L.; Schultz-fademrecht, C.; Zahedi, R. P.; Bauer, S.; Rauh, D. Insight into the Inhibition of Drug-Resistant Mutants of the Receptor Tyrosine Kinase EGFR. *Angew. Chemie - Int. Ed.* **2016**, *55*, 10909–10912.

(114) Günther, M.; Juchum, M.; Kelter, G.; Fiebig, H.; Laufer, S. Lung Cancer: EGFR Inhibitors with Low Nanomolar Activity against a Therapy-Resistant L858R/T790M/C797S Mutant. *Angew. Chemie - Int. Ed.* **2016**, *55*, 10890–10894.

(115) Uchibori, K.; Inase, N.; Araki, M.; Kamada, M.; Sato, S.; Okuno, Y.; Fujita, N.; Katayama, R. Brigatinib Combined with Anti-EGFR Antibody Overcomes Osimertinib Resistance in EGFR-Mutated Non-Small-Cell Lung Cancer. *Nat. Commun.* **2017**, *8*, 1–16.

(116) Toenjes, S. T.; Gustafson, J. L. Atropisomerism in Medicinal Chemistry : Challenges and Opportunities. *Future Med. Chem.* **2018**, *10*, 409–422.

(117) Zhang, C.; Lopez, M. S.; Dar, A. C.; LaDow, E.; Finkbeiner, S.; Yun, C.-H.; Eck, M. J.; Shokat, K. M. Structure-Guided Inhibitor Design Expands the Scope of Analog-Sensitive Kinase Technology. *ACS Chem. Biol.* **2013**, *8*, 1931–1338.

(118) Dong, J.; Krasnova, L.; Finn, M. G.; Sharpless, K. B. Sulfur (VI) Fluoride Exchange (SuFEx): Another Good Reaction for Click Chemistry. *Angew. Chemie - Int. Ed.* **2014**, *53*, 9430–9448.

(119) Sanfeliciano Guteirrez, S. M.; Schaus, J. M. Rapid Assessment of Conformational Preferences in Biaryl and Aryl Carbonyl Fragments. *PLoS One* **2018**, *13*, 1–21.

(120) Carlomagno, F.; Vitagliano, D.; Guida, T.; Napolitano, M.; Vecchio, G.; Fusco, A.; Gazit, A.; Levitzki, A.; Santoro, M. The Kinase Inhibitor PP1 Blocks Tumorigenesis Induced by RET Oncogenes. *Cancer Res.* **2002**, *62*, 1077–1082.

(121) Rho, J. K.; Lee, I. Y.; Choi, Y. J.; Choi, C.; Hur, J.; Koh, J. S.; Lee, J. J. J. J. C.; Suh, B.; Song, H.; Salgaonkar, P.; Lee, J. J. J. J. C.; Lee, J. J. J. J. C.; Jung, D. S.; Kim, S.; Woo, D.; Baek, I.; Lee, J. J. J. J. C.; Ha, C. H.; Sung, Y. H.; Kim, J. K.; Kim, W. S.; Song, J. S.; Kim, C. H.; Bivona, T. G.; Lee, J. J. J. J. C. Superior Efficacy and Selectivity of Novel Small-Molecule Kinase Inhibitors of T790M-Mutant EGFR in Preclinical Models of Lung Cancer. *Cancer Res.* **2017**, *77*, 1200–1212.

(122) Zhang, S.; Anjum, R.; Squillace, R.; Nadworny, S.; Zhou, T.; Keats, J.; Ning, Y.; Wardwell, S. D.; Miller, D.; Song, Y.; Eichinger, L.; Moran, L.; Huang, W.; Liu, S.; Zou, D.; Wang, Y.; Mohemmad, Q.; Jang, H. G.; Ye, E.; Narasimhan, N.; Wang, F.; Miret, J.; Zhu, X.; Clackson, T.; Dalgarno, D.; Shakespeare, W. C.; Rivera, V. M. The Potent ALK Inhibitor Brigatinib (AP26113) Overcomes Mechanisms of Resistance to First- and Second-Generation ALK Inhibitors in Preclinical Models. *Clin. Cancer Res.* **2016**, *22*, 1–13.

(123) Juchum, M.; Günther, M.; Döring, E.; Sievers-Engler, A.; Lämmerhofer, M.; Laufer, S. Trisubstituted Imidazoles with a Rigidized Hinge Binding Motif Act As Single Digit NM Inhibitors of Clinically Relevant EGFR L858R/T790M and L858R/T790M/C797S Mutants: An Example of Target Hopping. *J. Med. Chem.* **2017**, *60*, 4636–4656.

(124) Assadieskandar, A.; Yu, C.; Maisonneuve, P.; Liu, X.; Chen, Y. C.; Prakash, G. K. S.; Kurinov, I.; Sicheri, F.; Zhang, C. Effects of Rigidity on the Selectivity of Protein Kinase Inhibitors. *Eur. J. Med. Chem.* **2018**, *146*, 519–528.

(125) Bradshaw, J. M. The Src, Syk, and Tec Family Kinases: Distinct Types of Molecular Switches. *Cell. Signal.* **2010**, *22*, 1175–1184.

(126) Qiu, Y.; Kung, H. J. Signaling Network of the Btk Family Kinases. *Oncogene* **2000**, *19*, 5651–5661.

(127) Favas, C.; Isenberg, D. A. B-Cell-Depletion Therapy in SLE - What Are the Current Prospects for Its Acceptance? *Nat. Rev. Rheumatol.* **2009**, *5*, 711–716.

(128) Davis, R. E.; Ngo, V. N.; Lenz, G.; Tolar, P.; Young, R. M.; Romesser, P. B.; Kohlhammer, H.; Lamy, L.; Zhao, H.; Yang, Y.; Xu, W.; Shaffer, A. L.; Wright, G.; Xiao, W.; Powell, J.; Jiang, J. K.; Thomas, C. J.; Rosenwald, A.; Ott, G.; Muller-Hermelink, H. K.; Gascoyne, R. D.; Connors, J. M.; Johnson, N. A.; Rimsza, L. M.; Campo, E.; Jaffe, E. S.; Wilson, W. H.; Delabie, J.; Smeland, E. B.; Fisher, R. I.; Braziel, R. M.; Tubbs, R. R.; Cook, J. R.; Weisenburger, D. D.; Chan, W. C.; Pierce, S. K.; Staudt, L. M. Chronic Active B-Cell-Receptor Signalling in Diffuse Large B-Cell Lymphoma. *Nature* **2010**, *463*, 88–92.

(129) Haselmayer, P.; Camps, M.; Liu-Bujalski, L.; Nguyen, N.; Morandi, F.; Head, J.; O'Mahony, A.; Zimmerli, S. C.; Bruns, L.; Bender, A. T.; Schroeder, P.; Grenningloh, R. Efficacy and Pharmacodynamic Modeling of the BTK Inhibitor Evobrutinib in Autoimmune Disease Models. *J. Immunol.* **2019**, *202*, 2888–2906.

(130) Honigberg, L. A.; Smith, A. M.; Sirisawad, M.; Verner, E.; Loury, D.; Chang, B.; Li, S. The Bruton Tyrosine Kinase Inhibitor PCI-32765 Blocks B-Cell Activation and Is Efficacious in Models of Autoimmune Disease and B-Cell Malignancy. *Proc. Natl. Acad. Sci.* **2010**, *107*, 13075–13080.

(131) Barf, T.; Covey, T.; Izumi, R.; van de Kar, B.; Gulrajani, M.; van Lith, B.; van Hoek, M.; de Zwart, E.; Mittag, D.; Demont, D.; Verkaik, S.; Krantz, F.; Pearson, P. G.; Ulrich, R.; Kaptein, A. Acalabrutinib (ACP-196): A Covalent Bruton Tyrosine Kinase Inhibitor with a Differentiated Selectivity and In Vivo Potency Profile. *J. Pharmacol. Exp. Ther.* **2017**, *363*, 240–252.

(132) Tam, C.; Grigg, A. P.; Opat, S.; Ku, M.; Gilbertson, M.; Anderson, M. A.; Seymour, J. F.; Ritchie, D. S.; Dicorleto, C.; Dimovski, B.; Hedrick, E.; Yang, J.; Wang, L.; Luo, L.; Xue, L.; Roberts, A. W. The BTK Inhibitor, Bgb-3111, Is Safe, Tolerable, and Highly Active in Patients with Relapsed/ Refractory B-Cell Malignancies: Initial Report of a Phase 1 First-in-Human Trial. *Blood* **2015**, *126*, 832.

(133) Byrd, J. C.; Harrington, B.; O'Brien, S.; Jones, J. A.; Schuh, A.; Devereux, S.; Chaves, J.; Wierda, W. G.; Awan, F. T.; Brown, J. R.; Hillmen, P.; Stephens, D. M.; Ghia, P.; Barrientos, J. C.; Pagel, J. M.; Woyach, J.; Johnson, D.; Huang, J.; Wang, X.; Kaptein, A.; Lannutti, B. J.; Covey, T.; Fardis, M.; McGreivy, J.; Hamdy, A.; Rothbaum, W.; Izumi, R.; Diacovo, T. G.; Johnson, A. J.; Furman, R. R. Acalabrutinib (ACP-196) in Relapsed Chronic Lymphocytic Leukemia. *N. Engl. J. Med.* **2016**, *374*, 323–332.

(134) Byrd, J. C.; Furman, R. R.; Coutre, S. E.; Flinn, I. W.; Burger, J. A.; Blum, K. A.; Grant, B.; Sharman, J. P.; Coleman, M.; Wierda, W. G.; Jones, J. A.; Zhao, W.; Heerema, N. A.; Johnson, A. J.; Sukbuntherng, J.; Chang, B. Y.; Clow, F.; Hedrick, E.; Buggy, J. J.; James, D. F.; O'Brien, S. Targeting BTK with Ibrutinib in Relapsed Chronic Lymphocytic Leukemia. *N. Engl. J. Med.* **2013**, *369*, 32–42.

(135) Byrd, J. C.; Brown, J. R.; O'Brien, S.; Barrientos, J. C.; Kay, N. E.; Reddy, N. M.; Coutre, S.; Tam, C. S.; Mulligan, S. P.; Jaeger, U.; Devereux, S.; Barr, P. M.; Furman, R. R.; Kipps, T. J.; Cymbalista, F.; Pocock, C.; Thornton, P.; Caligaris-Cappio, F.; Robak, T.; Delgado, J.; Schuster, S. J.; Montillo, M.; Schuh, A.; De Vos, S.; Gill, D.; Bloor, A.; Dearden, C.; Moreno, C.; Jones, J. J.; Chu, A. D.; Fardis, M.; McGreivy, J.; Clow, F.; James, D. F.; Hillmen, P. Ibrutinib versus Ofatumumab in Previously Treated Chronic Lymphoid Leukemia. *N. Engl. J. Med.* **2014**, *371*, 213–223.

(136) O'Brien, S.; Furman, R. R.; Coutre, S. E.; Sharman, J. P.; Burger, J. A.; Blum, K. A.; Grant, B.; Richards, D. A.; Coleman, M.; Wierda, W. G.; Jones, J. A.; Zhao, W.; Heerema, N. A.; Johnson, A. J.; Izumi, R.; Hamdy, A.; Chang, B. Y.; Graef, T.; Clow, F.; Buggy, J. J.; James, D. F.; Byrd, J. C. Ibrutinib as Initial Therapy for Elderly Patients with Chronic Lymphocytic Leukaemia or Small Lymphocytic Lymphoma: An Open-Label, Multicentre, Phase 1b/2 Trial. *Lancet Oncol.* **2014**, *15*, 48–58.

(137) Toenjes, S. T.; Garcia, V.; Maddox, S. M.; Dawson, G. A.; Ortiz, M. A.; Piedrafita, F. J.; Gustafson, J. L. Leveraging Atropisomerism to Obtain a Selective Inhibitor of RET Kinase with Secondary Activities toward EGFR Mutants. *ACS Chem. Biol.* **2019**, *14*, 1930–1939.

(138) Cardenas, M. M.; Toenjes, S. T.; Nalbandian, C. J.; Gustafson, J. L. Enantioselective Synthesis of Pyrrolopyrimidine Scaffolds through Cation-Directed Nucleophilic Aromatic Substitution. *Org. Lett.* **2018**, *20*, 2037–2041.

(139) Nalbandian, C. J.; Hecht, D. E.; Gustafson, J. L. The Preorganization of Atropisomers to Increase Target Selectivity. *Synlett* **2016**, *27*, 977–983.

(140) Peluso, P.; Mamane, V.; Aubert, E.; Cossu, S. Recent Trends and Applications in Liquid-Phase Chromatography Enantioseparation of Atropisomers. *Electrophoresis* **2017**, *38*, 1830–1850.

(141) Dai, J.; Wang, C.; Traeger, S. C.; Discenza, L.; Obermeier, M. T.; Tymiak, A. A.; Zhang, Y. The Role of Chromatographic and Chiroptical Spectroscopic Techniques and Methodologies in Support of Drug Discovery for Atropisomeric Drug Inhibitors of Bruton's Tyrosine Kinase. *J. Chromatogr. A* **2017**, *1487*, 116–128.

(142) Barrett, K. T.; Miller, S. J. Regioselective Derivatizations of a Tribrominated Atropisomeric Benzamide Scaffold. *Org. Lett.* **2015**, *17*, 580–583.

(143) Bella, M.; Kobbelgaard, S.; Jørgensen, K. A. Organocatalytic Regio- and Asymmetric C -Selective SNAr Reactions-Stereoselective Synthesis of Optically Active Spiro-Pyrrolidone-3,3′-Oxoindoles. *J. Am. Chem. Soc.* **2005**, *127*, 3670–3671.

(144) Islas-Gonzalez, G.; Bois-Choussy, M.; Zhu, J. From Central to Planar Chirality, the First Example of Atropenantioselective Cycloetherification. *Org. Biomol. Chem.* **2003**, *1*, 30–32.

(145) Shirakawa, S.; Koga, K.; Tokuda, T.; Yamamoto, K.; Maruoka, K. Catalytic Asymmetric Synthesis of 3,3′-Diaryloxindoles as Triarylmethanes with a Chiral All-Carbon Quaternary Center: Phase-Transfer-Catalyzed SNAr Reaction. *Angew. Chemie* **2014**, *126*, 6334–6337.

(146) Liu, J.; Robins, M. J. SNAr Displacements with 6-(Fluoro, Chloro, Bromo, Iodo, and Alkylsulfonyl)Purine Nucleosides: Synthesis, Kinetics, and Mechanism1. *J. Am. Chem. Soc.* **2007**, *129*, 5962–5968.

(147) Organ, M. G.; Abdel-Hadi, M.; Avola, S.; Hadei, N.; Nasielski, J.; O'Brien, C. J.; Valente, C. Biaryls Made Easy: PEPPSI and the Kumada-Tamao-Corriu Reaction. *Chem. - A Eur. J.* **2007**, *13*, 150–157.

(148) Kalvet, I.; Sperger, T.; Scattolin, T.; Magnin, G.; Schoenebeck, F. Palladium(I) Dimer Enabled Extremely Rapid and Chemoselective Alkylation of Aryl Bromides over Triflates and Chlorides in Air. *Angew. Chemie - Int. Ed.* **2017**, *56*, 7078–7082.

(149) Bruno, N. C.; Tudge, M. T.; Buchwald, S. L. Design and Preparation of New Palladium Precatalysts for C–C and C–N Cross-Coupling Reactions. *Chem. Sci.* **2013**, *4*, 916–920.

(150) Brandvold, R.; Ste, M. E.; Fox, C. C.; Soellner, M. B. Development of a Highly Selective C-Src Kinase Inhibitor. *ACS Chem. Biol.* **2012**, *7*, 1393–1398.

(151) Jiang, J.; Gui, F.; He, Z.; Li, L.; Li, Y.; Li, S.; Wu, X.; Deng, Z.; Sun, X.; Huang, X.; Huang, W.; Han, S.; Zhang, T.; Wang, Z.; Jiao, B.; Song, S.; Wang, H.; Chen, L.; Zhou, D.; Liu, Q.; Ren, R.; Zhang, J.; Deng, X. Targeting BRK-Positive Breast Cancers with Small-Molecule Kinase Inhibitors. *Cancer Res.* **2017**, *77*, 175–186.

(152) Zeng, H.; Belanger, D. B.; Curran, P. J.; Shipps, G. W.; Miao, H.; Bracken, J. B.; Arshad Siddiqui, M.; Malkowski, M.; Wang, Y. Discovery of Novel Imidazo[1,2-a]Pyrazin-8-Amines as Brk/PTK6 Inhibitors. *Bioorganic Med. Chem. Lett.* **2011**, *21*, 5870–5875.

(153) Nicolaou, K. C.; Boddy, C. N. C. Atropselective Macrocyclization of Diaryl Ether Ring Systems: Application to the Synthesis of Vancomycin Model Systems. *J. Am. Chem. Soc.* **2002**, *124*, 10451–10455.

(154) Clayden, J.; Kubinski, P. M.; Sammiceli, F.; Diorazio, L. Sulfoxides as ' Traceless ' Resolving Agents for the Synthesis of Atropisomers by Dynamic or Classical Resolution. **2004**, *60*, 4387–4397.

(155) Staniland, S.; Adams, R. W.; McDouall, J. J. W.; Maffucci, I.; Contini, A.; Grainger, D. M.; Turner, N. J.; Clayden, J. Biocatalytic Dynamic Kinetic Resolution for the Synthesis of Atropisomeric Biaryl N-Oxide Lewis Base Catalysts. *Angew. Chemie - Int. Ed.* **2016**, *55*, 10755–10759.

(156) Manna, M. S.; Mukherjee, S. Organocatalytic Enantioselective Formal C(Sp2)-H Alkylation. *J. Am. Chem. Soc.* **2015**, *137*, 130–133.

(157) Sarkar, R.; Mukherjee, S. Catalytic Enantioselective Desymmetrization of Norbornenoquinones via C(Sp2)–H Alkylation. *Org. Lett.* **2016**, *18*, 6160–6163.

(158) Diedrich, C.; Grimme, S. Systematic Investigation of Modern Quantum Chemical Methods to Predict Electronic Circular Dichroism Spectra. *J. Phys. Chem. A* **2003**, *107*, 2524–2539.

(159) Berova, N.; Bari, L. Di; Pescitelli, G. Application of Electronic Circular Dichroism in Configurational and Conformational Analysis of Organic Compounds. *Chem. Soc. Rev.* **2007**, *36*, 914.

(160) Li, X.-C.; Ferreira, D.; Ding, Y. Determination of Absolute Configuration of Natural Products: Theoretical Calculation of Electronic Circular Dichroism as a Tool. *Curr. Org. Chem.* **2010**, *14*, 1678–1697.

(161) Koelblinger, P.; Dornbierer, J.; Dummer, R. A Review of Binimetinib for the Treatment of

Mutant Cutaneous Melanoma. *Futur. Oncol.* **2017**, *13*, 1–12.

(162) Costil, R.; Dale, H. J. A.; Fey, N.; Whitcombe, G.; Matlock, J. V.; Clayden, J. Heavily Substituted Atropisomeric Diarylamines by Unactivated Smiles Rearrangement of N-Aryl Anthranilamides. *Angew. Chemie - Int. Ed.* **2017**, *56*, 12533–12537.

(163) Dinh, A. N.; Noorbehesht, R. R.; Toenjes, S. T.; Jackson, A. C.; Saputra, M. A.; Maddox, S. M.; Gustafson, J. L. Toward a Catalytic Atroposelective Synthesis of Diaryl Ethers Through C(Sp 2)-H Alkylation with Nitroalkanes. *Synlett* **2018**, *29*, 2155–2160.

(164) Akiyama, T. Stronger Brønsted Acids. *Chem. Rev.* **2007**, *107*, 5744–5758.

(165) Kashikura, W.; Itoh, J.; Mori, K.; Akiyama, T. Enantioselective Friedel-Crafts Alkylation of Indoles, Pyrroles, and Furans with Trifluoropyruvate Catalyzed by Chiral Phosphoric Acid. *Chem. - An Asian J.* **2010**, *5*, 470–472.

(166) Akiyama, T.; Itoh, J.; Yokota, K.; Fuchibe, K. Enantioselective Mannich-Type Reaction Catalyzed by a Chiral Brønsted Acid. *Angew. Chemie* **2004**, *116*, 1592–1594.

(167) Mori, K.; Ichikawa, Y.; Kobayashi, M.; Shibata, Y.; Yamanaka, M.; Akiyama, T. Enantioselective Synthesis of Multisubstituted Biaryl Skeleton by Chiral Phosphoric Acid Catalyzed Desymmetrization/Kinetic Resolution Sequence. *J. Am. Chem. Soc.* **2013**, *135*, 3964–3970.

(168) Merad, J.; Lalli, C.; Bernadat, G.; Maury, J.; Masson, G. Enantioselective Brønsted Acid Catalysis as a Tool for the Synthesis of Natural Products and Pharmaceuticals. *Chem. - A Eur. J.* **2018**, *24*, 3925–3943.

(169) Parmar, D.; Sugiono, E.; Raja, S.; Rueping, M. Complete Field Guide to Asymmetric BINOL-Phosphate Derived Brønsted Acid and Metal Catalysis: History and Classification by Mode of Activation; Brønsted Acidity, Hydrogen Bonding, Ion Pairing, and Metal Phosphates. *Chem. Rev.* **2014**, *114*, 9047–9153.

(170) Maddox, S. M.; Dinh, A. N.; Armenta, F.; Um, J.; Gustafson, J. L. The Catalyst-Controlled Regiodivergent Chlorination of Phenols. *Org. Lett.* **2016**, *18*, 5476–5479.

(171) Maddox, S. M.; Nalbandian, C. J.; Smith, D. E.; Gustafson, J. L. A Practical Lewis Base Catalyzed Electrophilic Chlorination of Arenes and Heterocycles. *Org. Lett.* **2015**, *17*, 1042–1045.

(172) Frisch, M. J.; Trucks, G. W.; Schlegel, H. B.; Scuseria, G. E.; Robb, M. A.; Cheeseman, J. R.; Scalmani, G.; Barone, V.; Mennucci, B.; Petersson, G. A.; Nakatsuji, H.; Caricato, M.; Li, X.; Hratchian, H. P.; Izmaylov, A. F.; Bloino, J.; Zheng, G.; Sonnenb, D. J. . *Gaussian 09, Revis. E.01* Gaussian Inc.: Wallingford, CT, 2009.

(173) Andrews, M. D.; Bagal, S. K.; Gibson, K. R.; Omoto, K.; Ryckmans, T.; Skerratt, S. E.; Stupple, P. A. PYRROLO [2, 3 -D] PYRIMIDINE DERIVATIVES AS INHIBITORS OF TROPOMYOSIN- RELATED KINASES. WO 2012/137089 A1, 2012.

(174) Kavala, V.; Naik, S.; Patel, B. K. A New Recyclable Ditribromide Reagent for Efficient Bromination under Solvent Free Condition. *J. Org. Chem.* **2005**, *70*, 4267–4271.

(175) Bourbeau, M. P.; Siegmund, A.; Allen, J. G.; Shu, H.; Fotsch, C.; Bartberger, M. D.; Kim, K.; Komorowski, R.; Graham, M.; Busby, J.; Wang, M.; Meyer, J.; Xu, Y.; Salyers, K.;

Fielden, M.; Ve, M. M.; Gu, W. Piperazine Oxadiazole Inhibitors of Acetyl-CoA Carboxylase. *J. Med. Chem.* **2013**, *56*, 10132–10141.

(176) Mills, L. R.; Graham, J. M.; Patel, P.; Rousseaux, S. A. L. Ni-Catalyzed Reductive Cyanation of Aryl Halides and Phenol Derivatives via Transnitrilation. *J. Am. Chem. Soc.* **2019**, *141*, 19257–19262.

(177) Lee, M.; Hesek, D.; Shi, Q.; Noll, B. C.; Fisher, J. F.; Chang, M.; Mobashery, S. Conformational Analyses of Thiirane-Based Gelatinase Inhibitors. *Bioorg. Med. Chem. Lett.* **2008**, *18*, 3064–3067.

(178) Ferrins, L.; Gazdik, M.; Rahmani, R.; Varghese, S.; Sykes, M. L.; Jones, A. J.; Avery, V. M.; White, K. L.; Ryan, E.; Charman, S. A.; Kaiser, M.; Bergstro, C. A. S.; Baell, J. B. Pyridyl Benzamides as a Novel Class of Potent Inhibitors for the Kinetoplastid Trypanosoma Brucei. *J. Med. Chem.* **2014**, *57*, 6393–6402.

(179) Hirst, G. C.; Calderwood, D.; Munschaer, R.; Arnold, L. D.; Johnston, D. N.; Rafferty, P. Pyrrolopyrimidines as Tyrosine Kinase Inhibitors. WO 01/72751 A1, 2001.

(180) Malapit, C. A.; Bour, J. R.; Laursen, S. R.; Sanford, M. S. Mechanism and Scope of Nickel-Catalyzed Decarbonylative Borylation of Carboxylic Acid Fluorides. *J. Am. Chem. Soc.* **2019**, *141*, 17322–17330.

(181) Ma, Y.; Leng, T.; Qu, Y.; Wang, C.; Shen, Y.; Zhu, W. A Dual Chemosensor for Cu2+ and Fe3+ Based on Pi-Extend Tetrathiafulvalene Derivative. *Tetrahedron* **2017**, *73*, 14–20.

(182) Zapf, C. W.; Gerstenberger, B. S.; Xing, L.; Limburg, D. C.; Anderson, D. R.; Caspers, N.; Han, S.; Aulabaugh, A.; Kurumbail, R.; Shakya, S.; Li, X.; Spaulding, V.; Czerwinski, R. M.; Seth, N.; Medley, Q. G. Covalent Inhibitors of Interleukin-2 Inducible T Cell Kinase (Itk) with Nanomolar Potency in a Whole-Blood Assay. *J. Med. Chem.* **2012**, *55*, 10047–10063.